Journal of Applied Mechanics

(*Contributions of the ASME Applied Mechanics Division*)

Stresses Due to Tangential and Normal Loads on an Elastic Solid . . *J. O. Smith and C. K. Liu* 157
Forced Lateral Vibration of Beams on Damped Flexible End Supports . . . . . *D. F. Miller* 167
Frequencies of Longitudinal Vibration in Variable Section Rod . . *J. L. Lubkin and Y. L. Luke* 173
An Invariant Membrane Stress Function for Shells . . . . . *H. L. Langhaar* 178
On the Plastic Strains in Slabs With Cutouts . . . . . *P. G. Hodge, Jr.* 183
Response of a Cylindrical Shell to a Shock Wave . . . . . *R. D. Mindlin and H. H. Bleich* 189
The Origin of Damping in High-Strength Ferromagnetic Alloys . . . . . *A. W. Cochardt* 196
Damping Constants and Stress Distribution in Resonance Response . . . . . *B. J. Lazan* 201
Unsteady Radial Flow of Gas Through Porous Media . . . . *R. Jenkins and J. S. Aronofsky* 210
Pure Bending of an Incomplete Torus . . . . . *M. A. Sadowsky and E. Sternberg* 215
Circular Beams on Elastic Foundations . . . . . *Enrico Volterra* 227
On the Application of the Impedance Method to Continuous Systems . . . . *P. F. Chenea* 233
On an Iterative Method for Nonlinear Vibrations . . . . . *R. E. Roberson* 237
Natural Frequencies of Twisted Cantilever Beams . . . . . *D. D. Rosard* 241
An Analytical Theory of the Creep Deformation of Materials . . *Yoh-Han Pao and Joseph Marin* 245
Influence of Viscous Effects on Impact Tubes . . . *C. W. Hurd, K. P. Chesky, and A. H. Shapiro* 253
Axisymmetric Flexural Temperature Stresses in Circular Plates. . . . . *J. E. Goldberg* 257
Transient Thermal Stresses in Slabs and Circular Pressure Vessels . . . . . *M. P. Heisler* 261
The Shearing of a Rectangular Block Between Rough Plates . . . . . *J. W. Craggs* 270
The Torsion of Spiral Rods. . . . . *H. Ōkubo* 273
Reinforced Circular Holes in Bending With Shear . . . . . *S. R. Heller, Jr.* 279
Some New Types of Orthotropic Plates Laminated of Orthotropic Material. . . . *C. B. Smith* 286
High-Temperature Compression Testing of Graphite. . . . . *Leon Green, Jr.* 289
Discussion on previously published papers by *J. E. Brock; H. J. Fletcher and C. J. Thorne; C. A. Gongwer; L. S. Jacobsen; M. K. Huang and H. D. Conway; E. Sternberg and F. Rosenthal; D. S. Wood; M. H. L. Wu; W. F. Z. Lee and Edward Saibel; Yoh-Han Pao and Joseph Marin; and A. E. Abramson* 295
Book Reviews 312

JUNE, 1953

VOL. 20, NO. 2

Transactions of The American Society of Mechanical Engineers

Journal of Applied Mechanics

Papers Contributed to the Transactions by the ASME Applied Mechanics Division

EXECUTIVE COMMITTEE OF THE APPLIED MECHANICS DIVISION

Dana Young, *Chairman* N. M. Newmark, *Secretary*

James M. Lessells, *Technical Editor*

Published Quarterly by

The American Society of Mechanical Engineers

Publication Office, 20th and Northampton Streets, Easton, Pa.
Editorial Department at the Headquarters of the Society, 29 West Thirty-Ninth Street, New York 18, N. Y.

OFFICERS OF THE SOCIETY

Frederick S. Blackall, jr., *President*

James L. Kopf, *Treasurer* C. E. Davies, *Secretary*
E. J. Kates, *Assistant Treasurer*

PUBLICATIONS COMMITTEE

Gaetano E. Beltz, *Chairman* Gaetano A. Stimson, *Editor*
K. W. Cissonnetto, *Mgr. Editor*

By-Laws: The Society shall not be responsible for statements or opinions advanced in papers or . . . printed in its publications (B13, Par. 4).

Published quarterly by The American Society of Mechanical Engineers. Publication office at 20th and Northampton Streets, Easton, Pa. The editorial department is located at the headquarters of the Society, 29 West Thirty-Ninth Street, New York 18, N. Y. Cable address, "Dynamic," New York. Price $1.50 a copy, $5.00 a year; to members $2.50 a year, single copy price to members, $1.00. Changes of address must be received at Society headquarters four weeks before they are to be effective on the mailing list. Please send old as well as new address. . . . By-Law: The Society shall not be responsible for statements or opinions advanced in papers or . . . printed in its publications (B13, Par. 4). . . . Entered as second-class matter March 14, 1953, at the Post Office at Easton, Pa., under the act of August 24, 1912. . . . Copyright, 1953, by The American Society of Mechanical Engineers. Reprints from this publication may be made on condition that full credit be given the JOURNAL OF APPLIED MECHANICS and the author, and that date of publication be stated.

Stresses Due to Tangential and Normal Loads on an Elastic Solid With Application to Some Contact Stress Problems

By J. O. SMITH[1] and CHANG KENG LIU,[2] URBANA, ILL.

The results of two-dimensional approach using real variable method to Hertz's problem of contact of elastic bodies are presented. Both normal and tangential loads are assumed to be distributed in Hertzian fashion over the area of contact. The magnitude of the intensity of the tangential load is assumed to be linearly proportional to that of the normal load when sliding motion of the body is impending. The stresses in the elastic body due to the application of these loads on its boundary are presented in closed form for both plane-stress and plane-strain cases. A numerical value of $f = 1/3$ is assumed for the linear proportionality (coefficient of friction) between the tangential and normal loads in order that the distribution of stresses may be illustrated. The significance of the stress distribution, across the contact area and in the body, is also discussed. It is shown that when the combination of loads considered in the paper are applied at the contact area of bodies in contact the maximum shearing stress may be at the surface instead of beneath the surface. For example, for plane strain, if the coefficient of friction is $f = 1/3$, the maximum shearing stress is at the surface and is 43 per cent larger than the maximum shearing stress, which would be below the surface, that occurs when the normal force acts alone. The effect of range of normal stress and of shearing stress on the plane of maximum shear and on the plane of maximum octahedral shear on failure by progressive fracture (fatigue) is discussed.

Introduction

THE problem of the contact of elastic bodies under normal loading was first investigated by H. Hertz (1)[3] in 1881. He computed and verified with experiment the load distribution over the contact area, and solved for the stresses in the body in terms of a Newtonian potential function. S. Fuchs (2) in 1913, performed a laborious arithmetical integration to obtain the stresses. Eight years later, W. B. Morton and L. J. Close (3), using zonal harmonics, calculated the stresses in a half space on which a spherical ball is pressed by a normal load. At about the same time (as Morton and Close) Coker and Ahmed (4) studied analytically and experimentally a plane-stress problem where a portion of the boundary of a half plane is loaded with normal pressure. In 1930, H. R. Thomas and V. A. Hoersch (5) transformed the Hertzian solution for the stresses on the axis of symmetry into standard elliptical integrals and discovered that the shearing stress on the axis of symmetry is maximum at some distance underneath the center of the contact area. Their computation of the stresses is checked by agreement with experiment. Independently, Belajef (6) calculated the stresses at any point in the half space by the use of elliptical co-ordinates. His solution gives similar results on the axis of symmetry to those obtained by Thomas and Hoersch. L. Foeppl (7), in 1936, also obtained a similar solution for the problem of a cylinder and a spherical ball pressed on a flat plate, and verified the results by a photoelastic experiment.

The effect on the stresses due to the presence of a tangential load, however, was not taken into consideration by investigators until 1939, when G. Lundberg (8) developed a general theory of elastic contact between two semi-infinite bodies. In his theory, he introduced three potential functions which correspond to three components of the load along three axes of a Cartesian co-ordinate. The components of the load tangent to the contact area presumably are regarded as frictional forces between the contact surfaces. He made no attempt to find the stresses caused by the frictional forces in addition to the normal load.

R. D. Mindlin (9), in 1949, investigated the distribution of tangential load across the area of contact when one elastic body slides over the other. He found that the stress on the bounding curve of the contact area due to the tangential load is infinite and consequently a state of impending slipping prevails. Corresponding to this condition the intensity of tangential force at a point in the contact area cannot usually exceed the product of the coefficient of friction between the sliding surfaces and the normal pressure at the same point. In this paper, a value of $1/3$ is used for the coefficient of friction, in order to show the stress distributions due to the tangential load superimposed on the normal load acting over the same area of contact.

In December, 1949, not long after the authors completed their solution of this problem, H. Poritsky (10) presented a solution of the same problem (he uses a coefficient of friction of 0.3) by means of an Airy's function. The results, independently obtained by two different methods, agree. In this paper the authors have extended the results of the solution to include an interpretation of the significance of these stresses in causing failure by inelastic yielding and by fatigue.

Equations for Stresses

Plane-Stress Problem: Concentrated Forces—Normal or Tangential. From elasticity theory, the stresses in a half plane due to a concentrated force p, acting either normally or tangentially to its boundary as shown in Figs. 1(*a*) and (*b*), respectively, are

[1] Professor of Theoretical and Applied Mechanics, University of Illinois. Mem. ASME.

[2] Formerly, Associate of Theoretical and Applied Mechanics, University of Illinois. Jun. ASME.

[3] Numbers in parentheses refer to the Bibliography at the end of the paper.

Contributed by the Applied Mechanics Division and presented at the Annual Meeting, New York, N. Y., November 30 December 5, 1952, of The American Society of Mechanical Engineers.

Discussion of this paper should be addressed to the Secretary, ASME, 29 West 39th Street, New York, N. Y., and will be accepted until July 10, 1953, for publication at a later date. Discussion received after closing date will be returned.

Note: Statements and opinions advanced in papers are to be understood as individual expressions of their authors and not those of the Society. Manuscript received by ASME Applied Mechanics Division, April 21, 1952. Paper No. 52—A-13.

FIG. 1 CONCENTRATED NORMAL LOAD AND TANGENTIAL LOAD ON BOUNDARY

$$\left.\begin{aligned}\sigma_x &= -\frac{2p}{\pi z}\cos^2\theta\sin^2\theta\\ \sigma_z &= -\frac{2p}{\pi z}\cos^4\theta\\ \tau_{xz} &= -\frac{2p}{\pi z}\sin\theta\cos^3\theta\end{aligned}\right\}\quad\ldots\ldots\ldots[1]$$

$$\left.\begin{aligned}\sigma_x &= -\frac{2q}{\pi z}\cos^3\theta'\sin\theta'\\ \sigma_z &= -\frac{2q}{\pi z}\cos\theta'\sin^3\theta'\\ \tau_{xz} &= -\frac{2q}{\pi z}\sin^2\theta'\cos^2\theta'\end{aligned}\right\}\quad\ldots\ldots\ldots[2]$$

in which

$$\theta = \text{arc cos}\frac{z}{\sqrt{z^2+x^2}},\ \text{and}\ \theta' = \text{arc cos}\frac{x}{\sqrt{x^2+z^2}}$$

Stresses Due to Distributed Normal Forces.[4] If the normal forces as just discussed are distributed along a portion of the boundary of the half plane, as shown in Fig. 2, the stresses in the

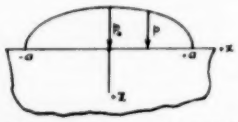

FIG. 2 ELLIPTICAL DISTRIBUTION OF NORMAL LOAD ON BOUNDARY

half plane are

$$\left.\begin{aligned}\sigma_{zn} &= -\frac{p_0}{\pi}z\left[\frac{a^2+2x^2+2z^2}{a}\bar{\Psi}-\frac{2\pi}{a}-3x\Psi\right]\\ \sigma_{xn} &= -\frac{p_0 z}{\pi}\left[a\bar{\Psi}-x\Psi\right]\\ \tau_{xzn} &= -\frac{p_0}{\pi}z^2\Psi\end{aligned}\right\}\quad\ldots[3]$$

[4] If the normal load per unit of length in the y-direction applied on the boundary is P, then $p_0 = \frac{2P}{\pi a}$, Fig. 2. The value of a, the half width of the contact area, may be found for two cylindrical cylinders whose longitudinal axes are parallel, that are in contact along a line, from the equation $a = \sqrt{\frac{2P\Delta}{\pi}}$ in which

$$\Delta = \frac{1}{\frac{1}{2}\left(\frac{1}{R_1}+\frac{1}{R_2}\right)}\left[\frac{1-\mu_1^2}{E_1}+\frac{1-\mu_2^2}{E_2}\right]$$

The symbols R_1, μ_1, and E_1 represent the radius, Poisson's ratio, and modulus of elasticity, respectively, for one cylinder, and R_2, μ_2, and E_2 have similar meaning for the second cylinder.

in which

$$\left.\begin{aligned}\Psi &= \frac{\pi}{K_1}\frac{1-\sqrt{\frac{K_2}{K_1}}}{\sqrt{\frac{K_2}{K_1}}\sqrt{2\sqrt{\frac{K_2}{K_1}}+\left(\frac{K_1+K_2-4a^2}{K_1}\right)}}\\ \bar{\Psi} &= \frac{\pi}{K_1}\frac{1+\sqrt{\frac{K_2}{K_1}}}{\sqrt{\frac{K_2}{K_1}}\sqrt{2\sqrt{\frac{K_2}{K_1}}+\left(\frac{K_1+K_2-4a^2}{K_1}\right)}}\\ K_1 &= (a+x)^2+z^2\\ K_2 &= (a-x)^2+z^2\end{aligned}\right\}\quad\ldots[4]^5$$

Stresses Due to Distributed Tangential Forces. In a similar manner, the stresses in a half plane due to a tangential force dis-

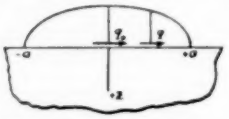

FIG. 3 (*left*) ELLIPTICAL DISTRIBUTION OF TANGENTIAL LOAD ON BOUNDARY

tributed along a portion of its boundary as shown by the ordinates to the ellipse in Fig. 3 are given by the following equations

$$\left.\begin{aligned}\sigma_{xt} &= -\frac{q_0}{\pi}\left[(2x^2-2a^2-3z^2)\Psi+2\pi\frac{x}{a}+2(a^2-x^2-z^2)\frac{x}{a}\bar{\Psi}\right]\\ \sigma_{zt} &= -\frac{q_0}{\pi}z^2\Psi\\ \tau_{xzt} &= -\frac{q_0}{\pi}\left[(a^2+2x^2+2z^2)\frac{z}{a}\bar{\Psi}-2\pi\frac{z}{a}-3xz\Psi\right]\end{aligned}\right\}\quad\ldots[5]$$

in which Ψ and $\bar{\Psi}$ denote the same quantities as expressed by Equations [4].

An examination of Equations [3] and [5] reveals that, except for a constant multiplier, σ_{zt} and τ_{xzn} have identical form, and so do τ_{xzt} and σ_{xn}.

In order to facilitate the plotting of the stresses against x while z is taken as a parameter, the values of Ψ and $\bar{\Psi}$ are first computed from Equations [4]. Table 1 shows the values of Ψ and $\bar{\Psi}$ for various values of x and z where z is taken as $0.125a$, $0.25a$, $0.375a$, $0.50a$, $0.75a$, $1.00a$, $1.50a$, and $2.00a$. It is seen that $\bar{\Psi}$ is symmetrical to x, whereas Ψ is symmetrical to the origin.

Stresses on Boundary Due to Distributed Normal and Tangential Forces. Special consideration is given to the computation of the stresses in the area of contact. They can be shown to be expressed, respectively, by the following equations:

(*A*) For distributed tangential load on boundary

$$\text{i}\quad \sigma_{xt} = \left\{\begin{aligned}&-2q_0\left[\frac{x}{a}-\sqrt{\frac{x^2}{a^2}-1}\right] && \text{for } x \geqslant a\\ &-2q_0\left[\frac{x}{a}+\sqrt{\frac{x^2}{a^2}-1}\right] && \text{for } x \leqslant -a\\ &-2q_0\frac{x}{a} && \text{for } |x| \leqslant -a\end{aligned}\right\}\quad\ldots[6]$$

[5] The derivation of Equations [4] can be found in reference (11).

TABLE 1 VALUES OF ψ AND Ψ

$\frac{x}{a}$	$z = 0.125a$		$z = 0.25a$		$z = 0.375a$		$z = 0.50a$	
	ψ	Ψ	ψ	Ψ	ψ	Ψ	ψ	Ψ
±4	±0.017175	+0.068769	±0.017059	+0.068520	±0.016869	+0.068109	±0.016609	+0.067542
±3	±0.043995	+0.132244	±0.043408	+0.131239	±0.042456	+0.129603	±0.041181	+0.127390
±2	±0.189648	+0.381269	±0.181679	+0.370867	±0.169666	+0.355007	±0.155094	+0.335404
±1.5	±0.681510	+1.034918	±0.596645	+0.938128	±0.494131	+0.818711	±0.397638	+0.702863
±1	±10.281792	+11.649856	±3.286846	+4.224414	±1.618003	+2.349094	±0.946560	+1.552699
±0.75	±8.125376	+11.204954	±3.200000	+4.800000	±1.644113	+2.750869	±0.962013	+1.814951
±0.5	±4.434819	+9.053184	±1.983798	+4.290146	±1.128147	+2.639019	±0.703155	+1.840884
±0.375	±3.136568	+8.515818	±1.435473	+4.103299	±0.837865	+2.591848	±0.533935	+1.823685
±0.25	±2.011807	+8.181206	±0.932308	+3.976819	±0.552732	+2.539731	±0.357433	+1.805773
±0.125	±0.984018	+7.997064	±0.458916	+3.904208	±0.274341	+2.507644	±0.178875	+1.793268
0	0	+7.938238	0	+3.880572	0	+2.496877	0	+1.788855

$\frac{x}{a}$	$z = 0.75a$		$z = 1.00a$		$z = 1.50a$		$z = 2.00a$	
	ψ	Ψ	ψ	Ψ	ψ	Ψ	ψ	Ψ
±4	±0.015900	+0.065979	±0.014985	+0.063919	±0.012783	+0.058734	±0.010456	+0.052826
±3	±0.037866	+0.121520	±0.033907	+0.114263	±0.025644	+0.098004	±0.018508	+0.082202
±2	±0.123658	+0.291460	±0.094958	+0.248603	±0.053975	+0.179423	±0.030949	+0.132013
±1.5	±0.251632	+0.517119	±0.161253	+0.390254	±0.071873	+0.242207	±0.035479	+0.163798
±1	±0.415822	+0.865845	±0.217287	+0.568865	±0.076980	+0.307921	±0.033323	+0.194222
±0.75	±0.409649	+0.991404	±0.206280	+0.638105	±0.068606	+0.334686	±0.028377	+0.206565
±0.5	±0.315303	+1.048121	±0.159598	+0.680775	±0.051689	+0.354278	±0.020750	+0.215885
±0.375	±0.245772	+1.059185	±0.125429	+0.693299	±0.040439	+0.361111	±0.016079	+0.219237
±0.25	±0.167802	+1.064253	±0.086294	+0.701305	±0.027778	+0.365955	±0.010973	+0.221656
±0.125	±0.084988	+1.066196	±0.043935	+0.705709	±0.014139	+0.368842	±0.005564	+0.223118
0	0	+1.066667	0	+0.707107	0	+0.369800	0	+0.223607

NOTE: Entries in this table are to be multiplied by z/a^2, where a is the half length of the loading region on the boundary.

ii $$\tau_{zxt} = \begin{cases} -q_0\sqrt{1-\frac{x^2}{a^2}} & \text{for } |x| \leqslant a \\ 0 & \text{for } x \geqslant a, \text{ and } x \leqslant -a \end{cases} \quad \ldots [7]$$

iii $$\sigma_{zt} = 0 \qquad \text{for all points on boundary.} \quad \ldots [8]$$

(*B*) For distributed normal load on boundary

i $$\sigma_{zn} = \begin{cases} -p_0\sqrt{1-\frac{x^2}{a^2}} & \text{for } |x| \leqslant a \\ 0 & \text{for } x \geqslant a, \text{ and } x \leqslant -a \end{cases} \quad \ldots [9]$$

ii $$\sigma_{zn} = \begin{cases} -p_0\sqrt{1-\frac{x^2}{a^2}} & \text{for } |x| \leqslant a \\ 0 & \text{for } x \geqslant a, \text{ and } x \leqslant -a \end{cases} \quad \ldots [10]$$

iii $$\tau_{zzn} = 0 \qquad \text{for all points on boundary.} \quad \ldots [11]$$

A complete picture of stresses in the half plane is plotted from Equations [3], [5], and [6] through [11]. They are shown in Figs. 4 to 7.

In reality, any presence of tangential load must be associated with that of normal load. Hence the stresses from Equations [3] and [5] (plotted in Figs. 4 to 7), should be superimposed upon each other, provided the quantities p_0 and q_0 are related by some law. According to Mindlin (9), $q_0 = fp_0$, where f denotes the coefficient of friction of the surfaces of contact; f can vary in a wide range in accordance with the surface conditions of the bodies in contact. For the purpose of illustration, f is assumed to be equal to $1/2$. Thus the stresses due to combined application of distributed normal and tangential loads, as expressed in terms of p_0 when $f = 1/3$, become

$$\left.\begin{aligned} \sigma_x^* &= -\frac{p_0}{\pi}\left\{(a^2 + 2x^2 + xz^2)\frac{z}{a}\Psi - 2\pi\frac{z}{a} \right.\\ &\quad - 3xz\psi + \frac{1}{3}\left[(2x^2 - 2a^2 - 3z^2)\psi + 2\pi\frac{x}{a}\right.\\ &\quad \left.\left. + 2(a^2 - x^2 - z^2)\frac{x}{a}\Psi\right]\right\} \\ \sigma_z^* &= -\frac{p_0}{\pi}z\left[a\Psi - x\psi + \frac{z}{3}\psi\right] \end{aligned}\right\} \quad \ldots [12]$$

$$\left.\begin{aligned} \tau_{xz}^* &= -\frac{p_0}{\pi}\left\{z^2\psi + \frac{1}{3}\left[(a^2 + 2x^2 + 2z^2)\frac{z}{a}\Psi \right.\right.\\ &\quad \left.\left. - 2\pi\frac{z}{a} - 3xz\psi\right]\right\} \end{aligned}\right\} \quad [12] \text{ (Continued)}$$

in which z is always greater than zero, i.e., for the points in the half plane. For the points on the boundary the stresses become

$$\sigma_{x/z=0}^* = \begin{cases} -\frac{2}{3}p_0\left[\frac{x}{a} - \sqrt{\frac{x^2}{a^2} - 1}\right] & \text{for } x \geqslant a \\ -p_0\left[\sqrt{1-\frac{x^2}{a^2}} + \frac{2}{3}\frac{x}{a}\right] & \text{for } |x| \leqslant a \\ -\frac{2}{3}p_0\left[\frac{x}{a} + \sqrt{\frac{x^2}{a^2} - 1}\right] & \text{for } x \leqslant -a \end{cases} \quad [12a]$$

$$\sigma_{z/z=0}^* = \begin{bmatrix} -p_0\sqrt{1-\frac{x^2}{a^2}} & \text{for } |x| \leqslant a \\ 0 & \text{for } x \geqslant a \text{ and } x \leqslant -a \end{bmatrix}$$

$$\tau_{xz/z=0}^* = \begin{bmatrix} -\frac{1}{3}p_0\sqrt{1-\frac{x^2}{a^2}} & \text{for } |x| \leqslant a \\ 0 & \text{for } x \geqslant a \text{ and } x \leqslant -a \end{bmatrix}$$

PLANE-STRAIN PROBLEM

In the preceding section the stresses have been found for a state of plane stress. For a state of plane strain two principal stresses are the same as for plane stress, but the third principal stress σ_y, is not zero as in the case for plane stress. The stress σ_y in the y-direction (perpendicular to the xz-plane) for the case of plane strain (contact of long cylinders) due to combined application of distributed tangential and normal loads is

$$\sigma_y^* = \nu(\sigma_x^* + \sigma_z^*) \quad \ldots [13]$$

where ν is the Poisson's ratio of the material.

When Equations [12] are substituted into Equation [13], the following is obtained

$$\sigma_y^* = -\frac{2\nu}{\pi}p_0\left\{\left[(a^2 + x^2 + z^2)\frac{z}{a}\Psi - \frac{\pi z}{a} - 2xz\psi\right] + \frac{1}{3}\left[(x^2 - a^2 - z^2)\psi + \frac{\pi x}{a} + (a^2 - x^2 - z^2)\frac{x}{a}\Psi\right]\right\} \quad [14]$$

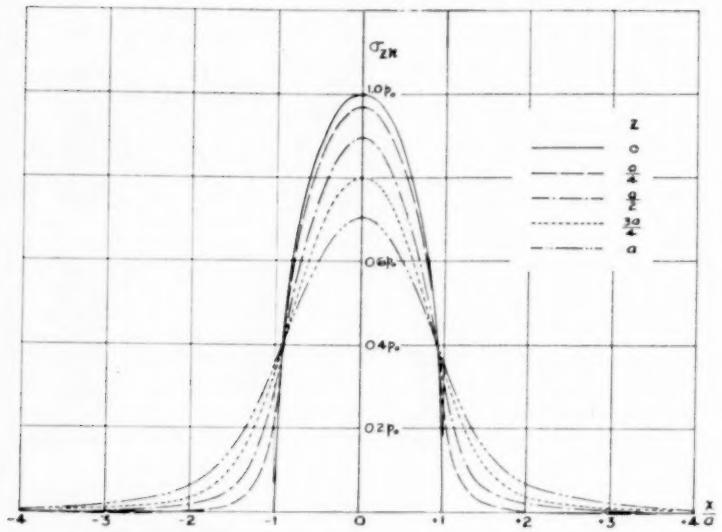

FIG. 4 CURVES SHOWING VALUES OF STRESS σ_{zx} FOR VARIOUS VALUES OF x, AT SURFACE AND AT VARIOUS DEPTHS BELOW SURFACE
(See Fig. 2, for loading.)

Consequently, on the boundary, the stress in y-direction is expressed by the following equations corresponding to their respective regions

$$\sigma_{y/z=0}^{*} = \begin{cases} -\nu p_0 \dfrac{2}{3}\left[\dfrac{x}{a} - \sqrt{\dfrac{x^2}{a^2} - 1}\right] & \text{for } x \geqslant a \\ -\nu p_0 \left[2\sqrt{1 - \dfrac{x^2}{a^2}} + \dfrac{2}{3}\dfrac{x}{a}\right] & \text{for } |x| \leqslant a \\ -\nu p_0 \dfrac{2}{3}\left[\dfrac{x}{a} + \sqrt{\dfrac{x^2}{a^2} - 1}\right] & \text{for } x \leqslant -a \end{cases} \quad \ldots [15]$$

In later calculations, ν is assumed to be equal to $1/4$.

MAXIMUM STRESSES AND THEIR SIGNIFICANCE

Introduction. The results of the preceding sections may be used to solve certain problems involving contact stresses, for example, for computing the stresses in two cylindrical rollers of the same material whose longitudinal axes are parallel, that are pressed against each other, Fig. 8(*a*), while one or both cylinders are rotated about a longitudinal axis causing a sliding friction force between the rollers, as shown in Fig. 8(*b*). The normal and tangential loads are distributed over the area of contact as shown in Fig. 8(*c*). In this section the results of computations of the stresses in the cylinders in this example will be given, but before this is done, it should be noted that the significance of the maximum values of stress cannot be determined apart from a knowledge of what action constitutes failure of the roller.

While it is not possible here to describe all types of failure of such rollers it can be said that failure generally occurs in one of two main types. The term failure is used to mean any action which will destroy the load-carrying capacity. Failure from contact stresses starts as a localized inelastic deformation (yielding or distortion) and by fracture, especially fracture by progressive spreading of a crack (fatigue). Usually it is assumed that the inelastic deformation type of failure is associated with the maximum shearing stress or with the maximum octahedral

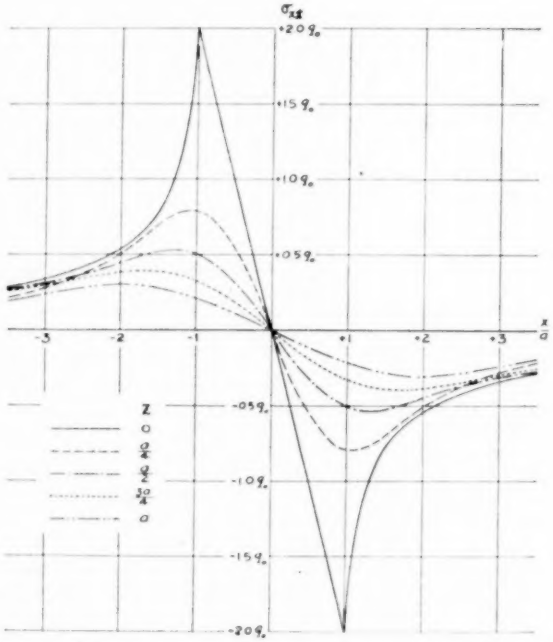

FIG. 5 CURVES SHOWING VALUES OF STRESS σ_{xz} FOR VARIOUS VALUES OF x, AT SURFACE AND AT VARIOUS DEPTHS BELOW SURFACE
(See Fig. 3, for loading.)

shearing stress. The maximum shearing stress is given by the equation

$$\tau_{max} = \frac{1}{2}(\sigma_1 - \sigma_3) \quad \ldots [16]$$

in which σ_1 and σ_3 are the maximum and minimum values of the principal stresses at the point. The maximum octahedral shearing stress is given by the equation

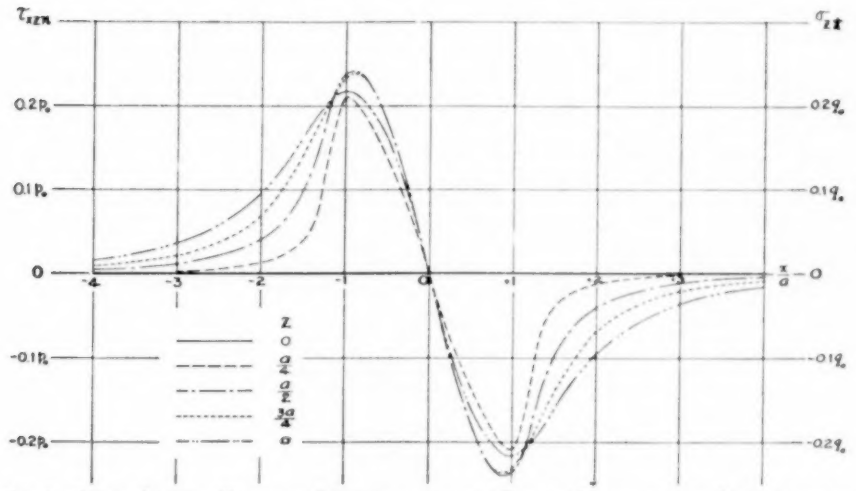

FIG. 6 CURVES SHOWING VALUES OF STRESSES τ_{xzn}, σ_{zz} FOR VARIOUS VALUES OF z, AT SURFACE AND AT VARIOUS DEPTHS BELOW SURFACE
(See Figs. 2 and 3, respectively, for loading.)

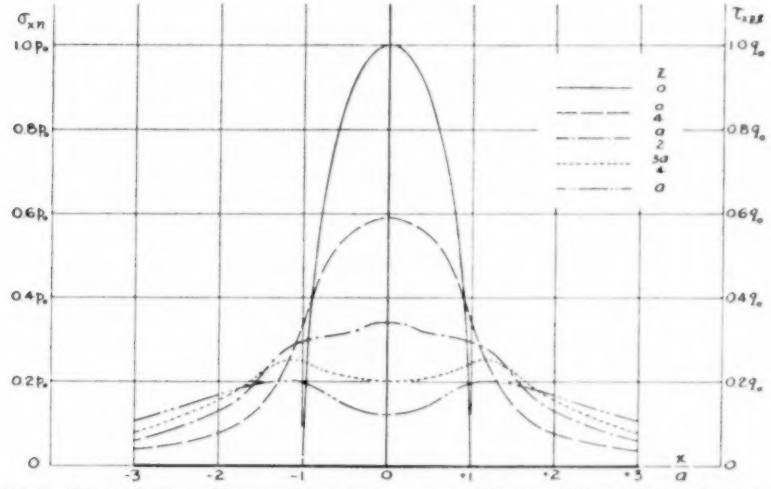

FIG. 7 CURVES SHOWING VALUES OF STRESSES σ_{xn}, τ_{zzt} FOR VARIOUS VALUES OF x, AT SURFACE AND AT VARIOUS DEPTHS BELOW SURFACE
(See Figs. 2 and 3, respectively, for loading.)

$$\tau_{G\,\max} = \frac{1}{3}\sqrt{(\sigma_1 - \sigma_2)^2 + (\sigma_2 - \sigma_3)^2 + (\sigma_3 - \sigma_1)^2} \quad [17]$$

in which σ_1 and σ_3 are defined as before and σ_2 is the third (intermediate value) principal stress.

The second type of failure is associated with many repeated applications of the loads and is characterized by a (fatigue) fracture that starts as a localized crack with very little visual evidence of inelastic deformation. The crack starts either at the surface or underneath the surface and grows progressively as the stress is repeated until some of the metal breaks out of the surface thereby causing pitting, shelling, or other damaging effects to the surface which constitutes failure. In the type of failure known as fatigue we must know the "range" of stress. This means that we must determine for the roller the magnitude, direction (line of action through point) and sense, that is, whether positive or negative, of the stress at a given point on a given plane

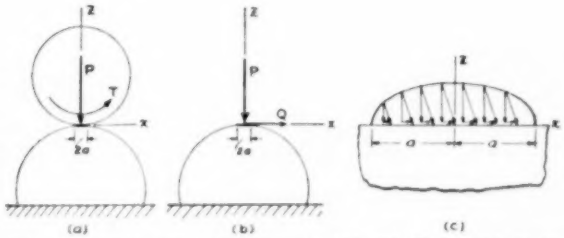

FIG. 8 NORMAL AND TANGENTIAL LOADS FOR TWO ROLLERS IN CONTACT

throughout one cycle of application and release of the load. This will be done later in this paper.

In this section of the paper the values of σ_1, σ_2, and σ_3 are given for a sufficient number of points in the cross sections of the

rollers near the contact area so that the maximum value of τ_{max} and $\tau_{0\ max}$ may be determined from Equations [16] and [17].

Maximum Stresses. By making use of Equations [12] [12*a*], [13], [14], and [15], the stresses σ_x^*, σ_z^*, σ_θ^*, and τ_{xz}^* have been found at points whose x and z-co-ordinates are given in Table 1. By making use of Mohr's circle the three principal stresses, σ_1^*, σ_2^*, and σ_3^* were determined at each point described in Table 1. From these results contour lines that represent constant values of principal stress, σ_1^*, σ_2^*, and σ_3^* are plotted in Figs. 9, 10, and 11. It is found that at the point $A(z = 0, x = +0.3a)$ in Fig. 9, 10, or 11, the maximum values of the three principal stresses occur. These values at the point A are

$$\sigma_{1\ max}^* = -1.39p_0,\ \sigma_{2\ max}^* = -0.72p_0,\ \text{and}\ \sigma_{3\ max}^* = -0.53p_0 \quad \ldots\ldots\ldots [18]$$

See footnote[4] for a method of obtaining the values of p_0 and a. Fig. 12 shows the directions of $\sigma_{1\ max}^*$ and $\sigma_{2\ max}^*$. The third stress $\sigma_{3\ max}^*$ is perpendicular to the plane of the other two.

It is found from Equation [16] by the substitution of the values of stresses from Figs. 9, 10, or 11 that the maximum value of τ_{max} also occurs at the point A and has a value

$$\tau_{max} = 0.43\ p_0 \quad \ldots\ldots\ldots [19]$$

In a similar manner by making use of Equation [17] it is found

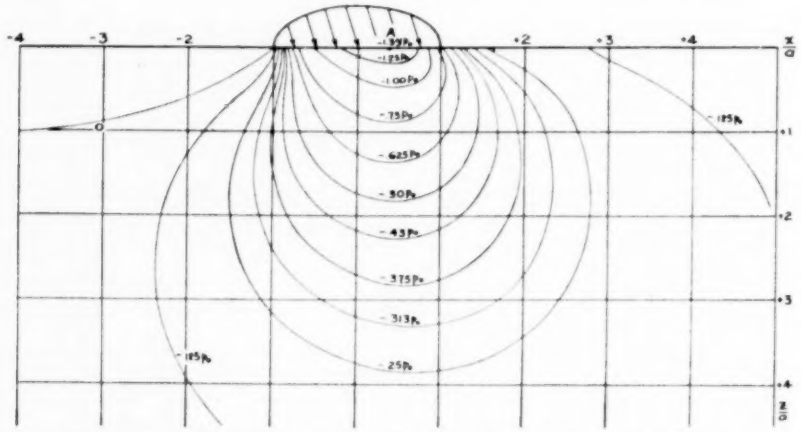

FIG. 9 CONTOURS FOR ONE OF TWO PRINCIPAL STRESSES LYING IN xz-PLANE

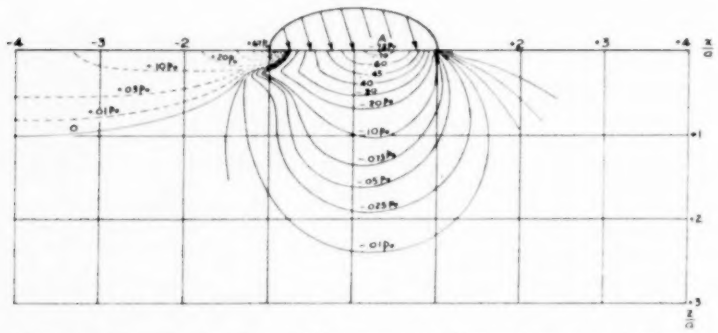

FIG. 10 CONTOURS FOR ONE OF TWO PRINCIPAL STRESSES LYING IN xz-PLANE

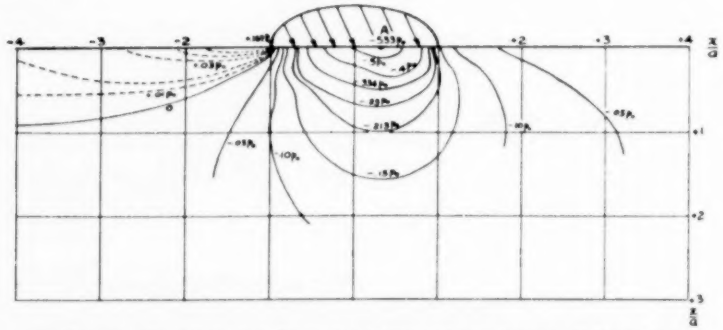

FIG. 11 CONTOURS FOR PRINCIPAL STRESS WHICH ACTS IN Y-DIRECTION

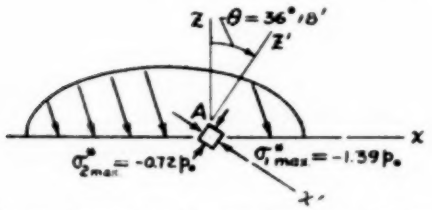

FIG. 12 LOCATION OF MAXIMUM PRINCIPAL STRESSES

that the maximum value of $\tau_{G\max}$ also occurs at the point A and has the value

$$\tau_{G\max} = 0.37\ p_0 \quad [20]$$

It should be noted that if the normal forces act alone, that is, the friction coefficient is assumed to be zero, the stresses as given in Equations [18], [19], and [20] would be, respectively,

$$\sigma_{1\max} = -p_0,\ \sigma_{2\max} = -p_0,\ \sigma_{3\max} = -0.5\ p_0 \quad [21]$$

$$\tau_{\max} = 0.30\ p_0 \quad [22]$$

$$\tau_{G\max} = 0.27\ p_0 \quad [23]$$

and these values of $\tau_{\max}$ and $\tau_{G\max}$ occur[6] on the z-axis at a distance $z = 0.78a$ underneath the surface. Therefore the tangential force caused by the coefficient of friction of $^1/_3$ increases the maximum principal stress 39 per cent, the maximum shearing stress by 43 per cent, and the maximum octahedral shearing stress by 37 per cent. Furthermore, the location of these maximum shearing stresses is changed by the addition of the tangential force from beneath the surface to the point A in the surface. Investigation shows that when the coefficient of friction becomes greater than $f = {}^1/_3$ the maximum shearing stress occurs at a point in the surface, but when f is less than $^1/_3$ this stress is underneath the surface.

Range of Stress for One Load Cycle. In order to determine the range of stress it is necessary to compute the stresses at a given point for several positions of the loads relative to the location of the given point. To state the idea differently, the loads applied to the rollers are assumed to remain constant while the movement of the roller surfaces changes the location at which the loads are applied. At a point located a relatively large distance from the loads the stresses due to these loads are approximately zero. As the loads move nearer to the point the stresses at the point increase. Moreover, as the loads begin to pass over the point the magnitude, line of action, and sense of the stresses change. From a study of these changes in the stresses the range of stress is established.

In Figs. (*a*) through (*i*) of Table 2, the point O represents a fixed point in the surface of one of the rollers (the dimensions a are greatly magnified) as the load approaches and passes over the point O. The figures in the second column show the magnitude, direction, and sense (sense here means whether tensile or compressive stress) of the three principal stresses at the point O for each position of the load. In Table 2 the symbol $\sigma_1{}^*$ is always given to the principal stress having the largest magnitude, $\sigma_2{}^*$ to the principal stress of least magnitude and $\sigma_3{}^*$ to the principal stress whose magnitude is intermediate. From Table 2 it is noted that the directions of the two principal stresses that lie in the xz-plane rotate through 90 deg during each load cycle. This fact makes the range of stress more difficult to determine because in most members that are subjected to repeated loads the direction of each of the principal stresses remains fixed during the load

[6] Reference (5), p. 29.

TABLE 2 TABLE SHOWING CHANGES IN MAGNITUDE, SENSE AND DIRECTION OF PRINCIPAL STRESSES AT A FIXED POINT O IN SURFACE, AS LOAD MOVES PAST IT

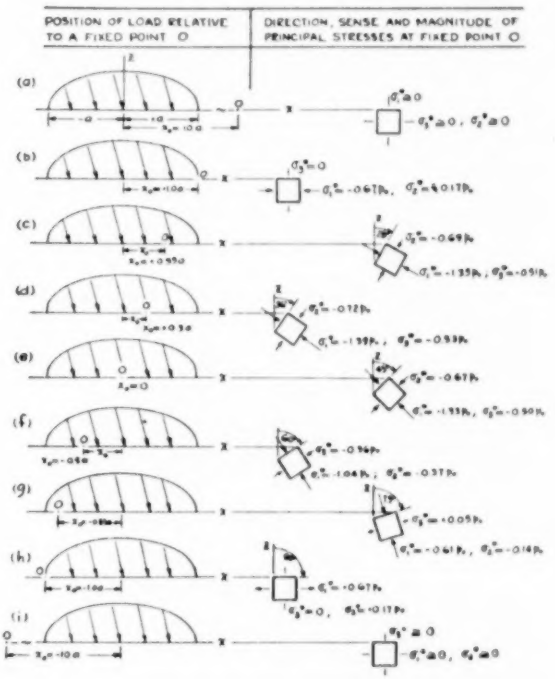

cycle so that only the magnitude and sense of the stress changes. Therefore, in order to make use in this paper of the methods usually employed in describing the effect of range of stress (14), the changes in the stress on a fixed plane through a point O in the surface of the roller will be considered. Three different fixed planes are selected here for this purpose, as discussed in the following paragraphs.

Range of Normal Stress $\sigma_x{}^*$. From the first of Equations [12*a*] the values of $\sigma_x{}^*$ have been computed at points on the surface for various values of x relative to one position of the load. The results are plotted in Fig. 13 in which the ordinates represent values of $\sigma_x{}^*$ at each value of x. If the load in Fig. 13 is allowed to move along the surface, then the stress $\sigma_x{}^*$ at a fixed point O will have in turn each of the values shown in Fig. 13. Fig. 13 shows that the stress $\sigma_x{}^*$ changes from a maximum compression of $-1.20\ p_0$ to a maximum tension of $+0.67\ p_0$, or, that is, a maximum range of stress of $1.87\ p_0$. The stress $\sigma_x{}^*$ has been chosen here because it has a greater change in magnitude than the normal stress on any other fixed plane through a fixed point on the surface or underneath the surface. Two important facts about this range of stress should be noted: (*a*) When this range of normal stress is compared with the range that occurs when there

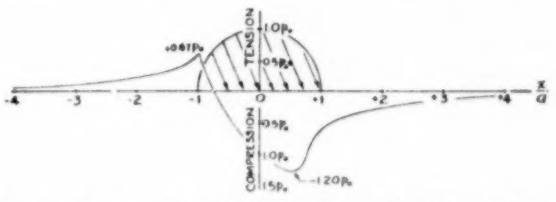

FIG. 13 RANGE OF VALUES OF $\sigma_x{}^*$ AT A POINT O (FIXED) AS LOAD MOVES PAST POINT

is no friction force, which is from zero to $-1.0\ p_0$ in compression, it is noted that there is an 87 per cent increase in magnitude (coefficient of friction $^1/_3$). (*b*) There is a change in the sense of the stress from tension to compression; that is, there is some reversal of stress, a fact that is of considerable importance in explaining how a progressive crack starts and propagates when the stresses are predominantly in compression.

Range of Shearing Stress on Plane of Maximum Shear. The magnitude and direction of the shearing stress on the plane of the maximum shearing stress (plane bisecting angle between σ_1^* and σ_3^* in Fig. *d*, Table 2) have been computed at the point *O* for each position of the load as shown in Table 2. In Fig. 14 the vectors

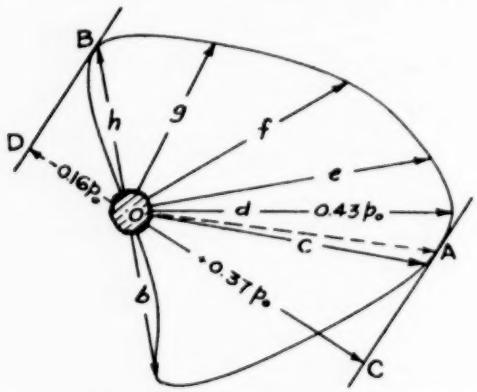

FIG. 14 DIAGRAM SHOWING MANNER IN WHICH MAGNITUDE, SENSE, AND DIRECTION OF SHEARING STRESS VARY ON PLANE OF MAXIMUM SHEAR
($f = {}^1/_3$, $\mu = {}^1/_4$, $E = 30{,}000{,}000$ psi.)

through the point *O* marked *b*, *c*, and so on through *h*, respectively, represent these values of the stress. A smooth curve *O-A-B* is drawn and a vector from *O* to this curve represents the shearing stress on this particular plane through *O* for some position of the load. The magnitude of the maximum shearing stress on this plane, therefore, varies from zero to 0.43 p_0. However, it is seen from Fig. 14 that the changes in direction of the shearing stress are such that along certain lines in the plane there is a change in sense, that is, a reversal of the shearing stress. For example, the vectors marked *b* and *h* represent equal and opposite shearing stresses, that is, a complete reversal of stress, each being equal to 0.23 p_0 or a total range of 0.46 p_0. But the line *C-O-D*, where *DO* is a component of the stress *OB* and *OC* is a component of the stress *OA*, represents the largest range of the shearing stress along all lines that can be drawn in this plane through *O*. The vectors $OD = -0.16\ p_0$ and $OC = +0.37\ p_0$ give a total range of 0.53 p_0 which is 23 per cent greater than the range from zero to 0.43 p_0 along the vector *d* in Fig. 14. Furthermore, a comparison of this range of stress of 0.53 p_0 with the maximum shearing stress[7] of 0.30 p_0 when the coefficient of friction is assumed to be zero (Equation [22]) shows an increase of 77 per cent in range of shearing stress due to the addition of the tangential force caused by a friction coefficient of $^1/_3$.

Range of Shearing Stress on Plane of Maximum Octahedral Shearing Stress. It will now be shown that on the plane of maximum octahedral shearing stress a greater range of shearing stress occurs than that on the plane of maximum shear. In Fig. 15

[7] E. I. Radzimovsky in reference (13) has shown that when the coefficient of friction is zero the maximum range of shearing stress occurs at a point below the surface on a plane parallel to the *x* and *y*-axes, Fig. 8, and this range of stress is from $-0.25p_0$ to $+0.25p_0$.

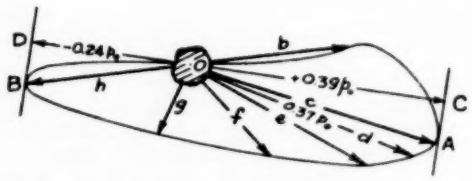

FIG. 15 DIAGRAM SHOWING MANNER IN WHICH MAGNITUDE, SENSE, AND DIRECTION OF SHEARING STRESS VARY ON PLANE OF MAXIMUM OCTAHEDRAL SHEARING STRESS
($f = {}^1/_3$, $\mu = {}^1/_4$, $E = 30{,}000{,}000$ psi.)

the vectors marked *b*, *c*, *d*, and so on, respectively, represent the shearing stresses on a plane making equal angles with σ_1^*, σ_2^*, and σ_3^* in Fig. *d* of Table 2, for the corresponding positions of the load in Table 2 and the smooth curve *O-A-B* is drawn so that any vector from *O* to the curve represents the shearing stress in this plane through *O* for some position of the load. The line *C-O-D*, as was the case in Fig. 14, represents the direction in this plane along which occurs the greatest range of shearing stress. This range consists of $OD = -0.24\ p_0$ and $OC = +0.39\ p_0$ or a total range of 0.63 p_0 which is 61 per cent greater than the range[8] of 0.39 p_0. The range of shearing stress on the octahedral plane is from zero to 0.27 p_0 when the coefficient of friction is assumed to be zero (Equation [23]). Thus by comparing 0.63 p_0 with 0.27 p_0 it is noted that the tangential force caused by a coefficient of friction of $^1/_3$ produces an increase of 122 per cent in range of shearing stress.

SIGNIFICANCE OF CONTACT STRESS IN SHELLING FAILURES OF RAILROAD RAILS

Many examples involving the stresses described in the foregoing sections could be given to illustrate the relationship of these stresses with failure, such as pitting failures, bearing races, gear teeth, rolls for rolling steel or other metals, and the like. One such example, namely, the wheel of a locomotive rolling on the rail of a railroad, is chosen for showing the relation of contact stresses with failure of the rail.

In Fig. 16 are shown the forces of a locomotive wheel on rails of straight and curved railway. The force *P* is due to the weight of the locomotive, *F* is a frictional force that, on straight rail, is due to the driving or braking forces applied through the wheel. For a rail on curved track *F* also includes frictional forces caused by wheel slippage because the wheels are rigidly attached to the axle. The force *T* is the thrust on the outside rail of a curve due to the centrifugal forces on the train. Both of the forces *P* and *F* that occur on curved rail, Fig. 16(*b*), therefore may be considerably larger than on straight rail, Fig. 16(*a*).

It might be expected from the foregoing analysis of the forces on the wheels and railway rails that rail failures are more severe on curved rail, where contact stresses due to both normal or tangential forces occur, than on straight rail. Reports contained in the Proceedings of the American Railway Association show that this is the case. R. E. Cramer (15) has described several types of shelly failures of railway rails that frequently occur on curved rail, usually in the outside rail on the curve. Most of these failures are of a progressive fracture type. First phase of the failure is characterized by inelastic strains in the surface layer on top of the rail head and on the rail-head edge in contact with the wheel flange, Fig. 16(*b*). These inelastic strains probably are caused by the high shearing

[8] The reason for omitting the use of distortion energy, which is usually found in discussions of fatigue failure, is shown by these facts. Distortion energy is a scalar quantity that is proportional to the square of the magnitude of the maximum octahedral shearing stress. Hence the range of distortion energy will not have increases corresponding to those shown in Figs. 14 and 15.

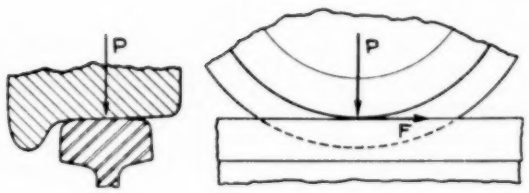

(a) FORCES ON RAILWAY RAIL FROM LOCOMOTIVE WHEEL ON STRAIGHT RAIL.

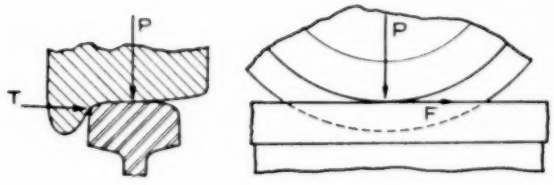

(b) FORCES ON RAILWAY RAIL FROM LOCOMOTIVE WHEEL ON CURVED RAIL.

FIG. 16 CONTACT FORCES ON RAILWAY RAIL

FIG. 17 FATIGUE FAILURE OF RAIL HEAD DUE TO COMBINATION OF NORMAL AND TANGENTIAL LOADING

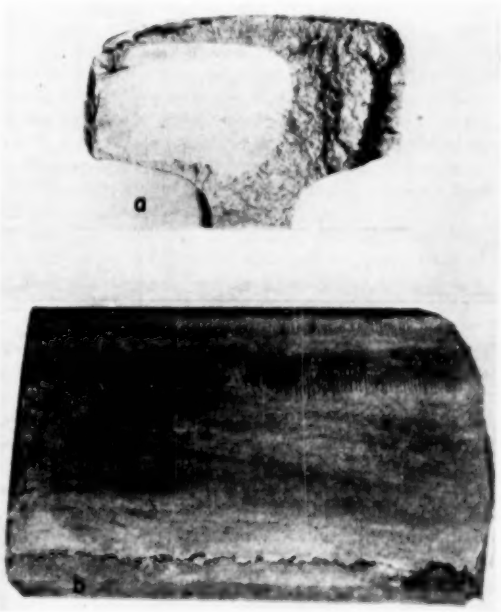

FIG. 18 FATIGUE FAILURE OF RAIL HEAD DUE TO COMBINATION OF NORMAL AND TANGENTIAL LOADING

stresses that occur when the combined normal and tangential forces act on the rail head. After many applications of such combinations of normal and tangential contact loads, cracks in the rail head will form and progress either horizontally or transversely (or both) across the rail head. Figs. 17 and 18 illustrate two of these failures of railway rail probably caused by these stresses.

The theoretical stresses, such as given in this paper, are an important factor in determining the cause of failure, but in actual materials, discontinuities, particularly when they occur at points of high stress, may have a large influence on failure.

Railway Wheels. The foregoing remarks apply also to shelly failures in the rims of wheels used on diesel locomotives. These wheel surfaces are subjected to heavy normal forces due to the weight of the locomotive and to tangential forces due to the driving torque applied through these wheels.

BIBLIOGRAPHY

1 "Gesammelte Werke," by H. Hertz, Leipzig, Germany, vol. 1, 1895; English translation in Miscellaneous Papers, 1896.

2 "Hauptspannungstrajekorie bei der Beruehrung einer Kugel mit einer Platte," by S. Fuchs, *Physikalische Zeitschrift*, vol. 14, 1913, p. 1282.

3 "Notes on Hertz's Theory of the Contact of Elastic Bodies," by W. B. Morton and L. J. Close, *Philosophical Magazine*, series 6, vol. 43, 1922, p. 320.

4 "Contact Pressures and Stresses," by E. G. Coker and M. S. Ahmed, The Institution of Mechanical Engineers, London, England, vol. 1, July, 1921, p. 365.

5 "Stresses Due to the Pressure of One Elastic Solid on Another," by H. R. Thomas and V. A. Hoersch, Bulletin of Engineering Experiment Station No. 212, University of Illinois, 1930.

6 "Bulletin of Engineers' Ways and Communications," by N. M. Belajef, Leningrad, USSR, 1917; also see "Pitting Due to Rolling Contact," by Stewart Way, JOURNAL OF APPLIED MECHANICS, Trans. ASME, vol. 57, 1935, pp. A-49–A-58.

7 "Der Spannungszustand und die Austrengung des Werk-Stoffes bei der Beruehrung Zweier Korper," by L. Foeppl, *Forschung auf dem Gebiete des Ingenieurwesens, Ausgabe A*, vol. 7, September-October, 1936, pp. 209–221.

8 "Elastische Beruehrung Zweier Halbraeume," by G. Lundberg, *Forschung auf dem Gebiete des Ingenieurwesens, Ausgabe A*, vol. 10, September-October, 1939, pp. 201–211.

9 "Compliance of Elastic Bodies in Contact," by R. D. Mindlin, JOURNAL OF APPLIED MECHANICS, Trans. ASME, vol. 71, 1949, pp. 259–268.

10 "Stresses and Deflections of Cylindrical Bodies in Contact With Application to Contact of Gears and of Locomotive Wheels," by H. Poritsky, JOURNAL OF APPLIED MECHANICS, Trans. ASME, vol. 72, 1950, pp. 191–201.

11 "Stress and Deformations Due to Tangential and Normal Loads on an Elastic Solid With Applications to Contact Stress," by C. K. Liu, PhD thesis, University of Illinois, June, 1950.

12 "The Effect of Range of Stress on the Torsional Fatigue

Strength of Steel," by J. O. Smith, Bulletin No. 316 of Engineering Experiment Station, University of Illinois, 1939.

13 "Stress Distribution and Strength Condition of Two Rolling Cylinders Pressed Together," by E. I. Radzimovsky; Bulletin No. 408, Engineering Experiment Station, University of Illinois, 1953.

14 "The Effect of Range of Stress on the Fatigue Strength of Metals," by J. O. Smith, Bulletin No. 334, Engineering Experiment Station, University of Illinois, 1942.

15 "Fifth Progress Report of the Shelly Rail Studies at the University of Illinois," by R. E. Cramer, Proceedings of the American Railway Engineering Association, vol. 48, 1947, pp. 756–766.

Forced Lateral Vibration of Beams on Damped Flexible End Supports

By D. F. MILLER,[1] EAST PITTSBURGH, PA.

The steady-state forced-vibration problem, for a beam or rotating shaft on damped, flexible end supports, is completely solved by the procedure described. The analysis is an extension of a Holzer-type iteration method applied to beams by Myklestad and others. Resonant frequencies of any mode, forced amplitudes, shears, and moments at any point on the beam, and phase effects introduced by the damping, are all evaluated. The damped problem is handled conveniently using complex notation with its vector interpretation. Vector diagrams, which give a physical idea of the vibration, are shown for the two numerical examples of the paper.

Nomenclature

The following nomenclature is used in the paper:

M_i = moment at position i, lb-in.
θ_i = slope at i, radians
y_i = deflection at i, in.
S_i = shear just to right of position i, lb
$\alpha_i, \beta_i, \gamma_i$ = stiffness coefficients of beam section
m_i = concentrated mass at i, lb sec^2/in.
ω = circular frequency, radians/sec
l_i = length of section i, in.
k = spring constant of end support, lb/in.
c = damping constant of beam end damper, lb sec/in.
P = forcing function amplitude, lb
U, V, Z = co-ordinate axes
ϕ = phase angle between amplitude vector for mass point at forcing function and forcing-function vector
E, I_i = section flexural rigidity, lb-in.^{2}

Introduction

In the study of rotor critical speeds, it is becoming necessary to consider the effect of damping, as well as flexibility, in the bearing oil films and supports. These effects may be studied by considering the forced vibration of a beam supported by a spring and damper in parallel at each end as shown in Fig. 1. Problems in which damping exists in a boundary condition, as in this practical example, are called forced, damped-end beam vibration problems. Internal damping of the beam is not considered. The analysis covers the steady-state forced vibration of the beam. As far as is known, a method of solving forced, damped-end beam problems has not been given previously. The method of handling these problems is similar to the Holzer method for forced, damped torsional vibrations[2] but four equations, instead of two, are necessary for lateral beam vibration solutions.

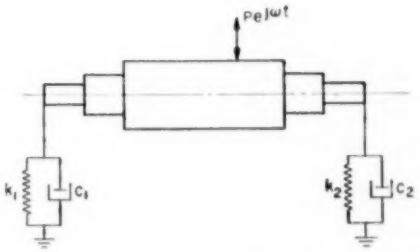

Fig. 1 Forced Vibration of Beam With Damping in End Supports

A beam may be approximated by a system consisting of a number of concentrated masses connected by massless beams.[3,4,5] Any desired accuracy is obtained by taking a large enough number of mass points. Complex notation, with a vector interpretation, is used for forced damped-end beam vibration problems. The procedure is quite general. It may be used for any mode, giving the forced amplitudes of vibration, the phase angles between the forcing function and the motion of points of the beam, and the shear and moment at any point of the beam. The resonant frequencies are found by calculating forced amplitudes at a number of forcing frequencies and plotting a resonance curve. In this paper, resonant frequency shall always mean a frequency for a peak amplitude of vibration.

It is the purpose of this discussion to show how calculations are performed using complex notation and to give a clear physical picture of the vibration of forced, damped-end beams.

Method

The distributed mass of a beam must be concentrated at a number of points. This may be done by dividing the beam into a number of lengths, and concentrating a part of the mass of the length at each end, in such a way that its center of gravity remains unchanged.[4] The flexural rigidity between mass points is that which exists in the beam between these points. Therefore the beam is approximated by this system of concentrated masses connected by massless beams. A section of this approximate system is defined as a massless beam with a concentrated mass at one end as shown in Fig. 2.

Formulation of the problem is based on the fact that each section of the beam is in dynamic equilibrium. By use of an inertia

[1] Westinghouse Research Laboratories. Jun. ASME.

Contributed by the Applied Mechanics Division and presented at the Annual Meeting, New York, N. Y., November 30–December 5, 1952, of The American Society of Mechanical Engineers.

Discussion of this paper should be addressed to the Secretary, ASME, 29 West 39th Street, New York, N. Y., and will be accepted until July 10, 1953, for publication at a later date. Discussion received after the closing date will be returned.

Note: Statements and opinions advanced in papers are to be understood as individual expressions of their authors and not those of the Society. Manuscript received by ASME Applied Mechanics Division, June 30, 1952. Paper No. 52—A-23.

[2] "Holzer Method for Forced-Damped Torsional Vibrations," by T. W. Spaetgens, Trans. ASME, vol. 72, 1950, p. 59.

[3] "A New Method of Calculating Natural Models of Uncoupled Bending Vibrations of Airplane Wings and Other Types of Beams," by N. O. Myklestad, *Journal of the Aeronautical Sciences*, vol. 11, 1944, p. 153.

[4] "A General Method for Calculating Critical Speeds of Flexible Rotors," by M. A. Prohl, Journal of Applied Mechanics, Trans. ASME, vol. 67, 1945, p. A-142.

[5] "Matrix Solution for the Vibration of Nonuniform Beams," by W. T. Thomson, Journal of Applied Mechanics, Trans. ASME, vol. 72, 1950, p. 337.

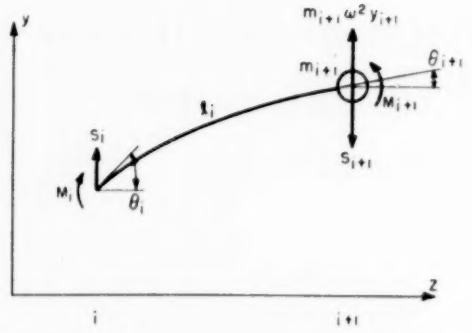

FIG. 2 DYNAMIC EQUILIBRIUM OF BEAM SECTION SHOWING SIGN CONVENTIONS

force, $m\omega^2 y$, along with the other forces and moments acting on a section, the usual static-equilibrium equations apply (D'Alembert's principle). Referring to Fig. 2, which shows the positive directions of the forces and moments acting on a section,[6] the basic beam equations may be written[4]

$$M_{i+1} = l_i S_i + M_i \quad [1]$$

$$\theta_{i+1} = -\beta_i S_i - \alpha_i M_i + \theta_i \quad [2]$$

$$y_{i+1} = -\gamma_i S_i - \beta_i M_i - l_i \theta_{i+1} + y_i \quad [3]$$

$$S_{i+1} = S_i + m_{i+1}\omega^2 y_{i+1} \quad [4]$$

The stiffness coefficients α_i, β_i, γ_i may be simply expressed for a section of constant flexural rigidity, a uniform section

$$\alpha_i = \frac{l_i}{E_i I_i} \quad [5]$$

$$\beta_i = \frac{l_i^2}{2E_i I_i} \quad [6]$$

$$\gamma_i = \frac{l_i^3}{3E_i I_i} \quad [7]$$

For a nonuniform section, the stiffness coefficients may be found by the area-moment principle

$$\alpha_i = \int_0^{l_i} \frac{d\xi}{EI} \quad [8]$$

$$\beta_i = \int_0^{l_i} \frac{\xi d\xi}{EI} \quad [9]$$

$$\gamma_i = \int_0^{l_i} \frac{\xi^2 d\xi}{EI} \quad [10]$$

These equations are applied to each section successively, using an assumed frequency, ω. The two known boundary conditions at each end permit the final calculation of shear, moment, slope, and deflection at each mass point. In an undamped free vibration, all four boundary conditions are satisfied only if the assumed frequency corresponds to a natural frequency. For forced, damped vibration, it is possible to solve the equations at any forced frequency. A force P is present at every frequency, including the resonant frequency, to supply the energy loss of the dampers.

For a damped-end beam in which the damping force opposes the motion, the shear force may be represented in complex form, since the damping force is 90 deg out of phase with the spring force.

Therefore

$$S = (k + jc\omega)y$$

In general, a beam problem is unsymmetrical about the forcing function, as is the beam of Fig. 1. For a problem to be symmetrical, there must be symmetry of the beam, boundary conditions, and forcing functions.

To illustrate the method for forced, damped-end beam vibration problems, two examples are shown:

1 A uniform beam, symmetrical problem, System I, Fig. 3(*a*)

2 A nonuniform beam, nonsymmetrical problem, System II, Fig. 7.

SYSTEM I

As a simple introduction to the method, a uniform beam mounted on identical parallel spring-damper supports at each end with the forcing function at the center as shown in Fig. 3(*a*) will be discussed. This is a symmetrical problem, and consequently it is necessary to apply the method to only one half of the beam.

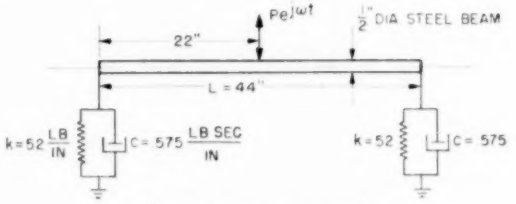

FIG. 3(*a*) ACTUAL SYSTEM I
(Uniform beam, symmetrical problem.)

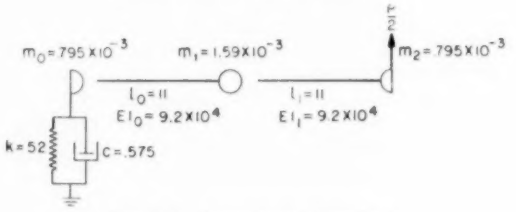

FIG. 3(*b*) APPROXIMATE SYSTEM I

The half-beam was divided into two equal lengths; the mass of each then split in half and concentrated at each end of the length, resulting in the approximate system in Fig. 3(*b*). For illustrative purposes the small number of sections is sufficient. The boundary conditions for the half-beam are

$$\text{At } m_0 \begin{cases} M_0 = 0 & [11] \\ S_0 = -(k - m_0\omega^2 + jc\omega)y_0 & [12] \end{cases}$$

$$\text{At } m_2 \begin{cases} \theta_2 = 0 & [13] \\ S_2 = -P/2 & [14] \end{cases}$$

The inertia force of m_0 must be subtracted from the spring force to obtain the shear on the left end of the massless beam of the first section. The negative signs for shear are due to the sign conventions used, Fig. 2.

In Table 1 the results of the calculation for a forced frequency of 16 cycles per sec (cps) are tabulated. This frequency is near the first resonant frequency of the beam. The table is divided into four parts.

(*A*) Constants of the problem.

(*B*) Results of the iteration calculation containing unknown, θ_0.

[4] Secondary rotary inertia and shear effects not considered.

TABLE 1 FORCED VIBRATION OF SYSTEM I, FIG. 3, AT 16.0 CPS

$k = 52$ lb/in., $c = 0.575$ lb-sec/in., $\omega = 100.5$ rad/sec, $\omega^2 = 10100$, $c\omega = 57.88$

Position	m_i lb-sec²/in.	l_i in.	α_i 1/lb-in.	β_i 1/lb	γ_i in/lb	$m_i\omega^2$ lb/in.
(A) 0	0.795×10^{-3}	11	1.196×10^{-4}	6.576×10^{-4}	48.224×10^{-4}	8.0295
1	1.59×10^{-3}	11	1.196×10^{-4}	6.576×10^{-4}	48.224×10^{-4}	16.0590
2	0.795×10^{-3}					8.0295

Position	M_i	θ_i	y_i	S_i	$m_i\omega^2 y_i$
(B) 0	0	θ_0	1.0	$-43.98 - j57.88$	
1	$-483.78 - j636.68$	$0.0289212 + j0.0380620 + \theta_0$	$0.893955 - j0.139560 - 11\theta_0$	$-29.62397 - j60.121199 - 176.6490\theta_0$	
2	$-809.64367 - j1298.013 - 1943.1398\theta_0$	$0.106262 + j0.153744 + 1.116164\theta_0$	$0.186065 - j1.122141 - 22.425948\theta_0$	$-28.12996 - j69.13143 - 356.7186\theta_0$	
(C) 0	0	$-0.09520 - j0.13774$	1.0	$-43.98 - j57.88$	
1	$-483.78 - j636.68$	$-0.066282 - j0.099682$	$1.94119 + j1.37562$	$-12.80649 - j35.7889$	
2	$-624.651 - j1030.36$	0	$2.32108 + j1.96689$	$5.8306 - j19.9958$	
(D) 0			1.0/0°	59.9/232.8°	8.03/0°
1			2.38/35.3°	38.1/250.3°	38.22/35.3°
2			3.05/40.2°	20.85/286.25°	24.49/40.2°

$\phi = 66.05°$ $\quad P/2 = 20.85/106.25°$ $\quad \frac{y_2}{P/2} = \frac{3.05}{41.70} = 0.073$ in/lb

Energy balance:

Forcing energy $= (20.85 \sin 66.05)(3.05) = 58.12$ in-lb/rad
Damping energy $= c\omega = 57.88$ in-lb/rad

(*C*) Results in complex form after application of the terminal boundary conditions and the elimination of the unknowns.

(*D*) Vector form for shear, deflection, and inertia forces (slide-rule accuracy).

Part (*B*) shows the two boundary conditions, $S_0 = -43.98 - j57.88$ (Equation [12]) and $M_0 = 0$, entered in the first row. The initial deflection y_0, and slope θ_0, are unknowns in the calculation. It is possible to set y_0 equal to unity for simplicity. The forcing function P will then be the force necessary to give the beam ends a unit amplitude at 16 cps. The iteration calculations, corresponding to part (*B*) of Table 1, are shown in the Appendix. The unknown slope θ_0 is found by applying the boundary condition $\theta_2 = 0$. The slope θ_0 is then eliminated from all quantities and the results tabulated in Table 1, part (*C*). The solution for a forced frequency of 16 cps has been completed; however, a physical interpretation of the complex moments, slopes, deflections and shears has not been given.

Consider the forced vibration, in a plane, of the simple damped system in Fig. 4(*a*). The sinusoidal variation as well as the phase

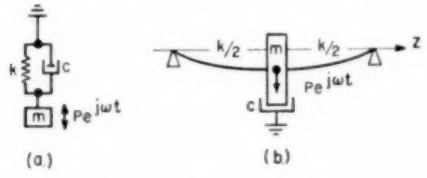

EQUIVALENT SIMPLE SYSTEMS.

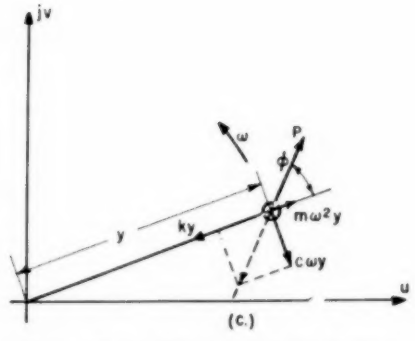

FIG. 4 VECTOR DIAGRAM OF SIMPLE SYSTEM

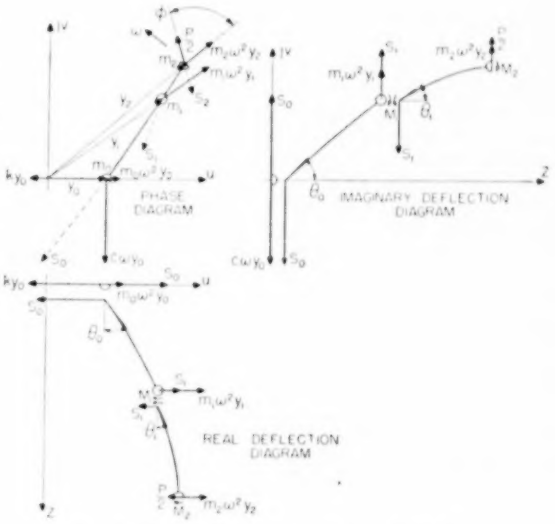

FIG. 5 VECTOR DIAGRAM FOR SYSTEM I, 16 CPS

relationships of all the forces and the motions may be shown by rotating vectors in the complex plane, as shown in Fig. 4(*c*). The diagram is drawn for a constant forcing frequency ω. If the forcing frequency is changed, all the vectors change in magnitude, but only the phase angle ϕ changes. The inertia force is always in phase with the motion, the damping force lags by 90 deg, and the spring force lags by 180 deg. The variation of the amplitude vector y is usually shown by a resonance curve. The diagram is also a representation of the damped vibration of the shaft center of a disk on a massless shaft, as shown in Fig. 4(*b*). For the plane vibration of the system in Fig. 4(*a*), either the u or the v-component of each vector shows the sinusoidal variation of the quantity. The motion of the mass point itself is an end view of the rotating-shaft vibration of the system in Fig. 4(*b*). With this vector diagram in mind, the results of our complex iteration procedure are very simply explained.

If the shears and deflections for System I, as given in Table 1, part (*C*), are plotted in the complex plane, the phase diagram in Fig. 5 is obtained. The diagram is similar to that for the simple systems in Fig. 4, but there are a number of mass points, one for each concentrated mass of the beam. The diagram clearly shows

the phase angles between the amplitude vectors y_s of each mass point. The forces acting on m_0 are exactly as given for the simple system. Although the damping does not act directly on the other mass points m_1 and m_2, the damping effect is felt by all the masses. The greatest effect, however, is felt by those masses closest to the damper, as shown by the angles of the lines joining mass points in the phase diagram. It is interesting to note that in the phase diagram the shear forces do not lie on the lines joining the mass points. In the special case, the undamped beam, the mass points all lie in a straight line on the real axis. All forces and motions are either in or out of phase and the calculations are all real. Dynamic equilibrium of each section of the beam is best illustrated by deflection diagrams, which are the projections of the real and imaginary parts of the phase diagram, plotted against the beam length (shown as the Z-direction, Fig. 5). Both the real and the imaginary deflection diagrams are in dynamic equilibrium. It would have been possible to solve the problem in the real and imaginary plane independently, each as an ordinary beam problem.

The real and imaginary parts of the complex slopes and moments are seen in the real and imaginary deflection diagrams. They do not appear in the phase diagram, because both depend upon beam length, which is not shown in the phase diagram. The vibration of a damped-end beam may be said to consist of two standing waves, 90 deg out of phase with each other,[7] as represented by the deflection diagrams; however, a more physically satisfying concept may be given by the analogy of beam vibrations with those of a rotating shaft.

The phase diagram represents an end view of the vibration of a rotating shaft. The force P is an unbalance force in the shaft. The shaft must have identical flexural rigidity in two perpendicular directions equal to that of the beam. Then, with this analogy, the vibration of the shaft in the UZ-plane or the VZ-plane is that of the vibration of the beam. The forcing function seems to rotate the shaft in the ω-direction. The sections of the shaft do not lie in a plane; that is, the shaft is bent in a space curve.

A very useful method of checking calculations is given by an energy balance. The energy balance holds at any frequency, for the energy put into the system by the forcing function must be equal to that dissipated in the dampers. The energy balance is

$$\left(\frac{P}{2}\sin\phi\right)y_3 = c\omega y_3^2 \quad \ldots\ldots\ldots\ldots\ldots\ldots\ldots\ldots [15]$$

An energy balance for System I, which is within $^1/_2$ per cent, is shown at the end of Table 1.

The forced vibration at a given forcing frequency has been discussed. In an actual problem, the resonant frequencies would be of particular interest. To find them, the procedure is repeated for a number of forcing frequencies. For each, the amplitude at the center for a unit force $|y_2|/|P|$ is calculated. From these values a resonance curve is drawn, the peaks giving the values of resonant frequency. This has been done for System I and the resonance curve near the first resonant frequency has been plotted in Fig. 6. The phase angle ϕ also has been shown. The resonant frequency is less than that for a 90 deg phase angle, as in a simple system. The phase angle does provide a convenient way of locating the resonant frequencies, since it tells whether we are far above or below the resonant frequency.

Higher resonant frequencies are obtained as easily in the same manner. Since, in System I, the forcing function is at the exact center of the beam, the even order modes will not be excited. It is interesting to compare the first resonant frequency of 16.8 cps with the natural frequency of 15 cps for the first mode of the beam on the springs, but without the damping at the ends. Damping has raised the frequency, since it has a "stiffening" effect at the ends.

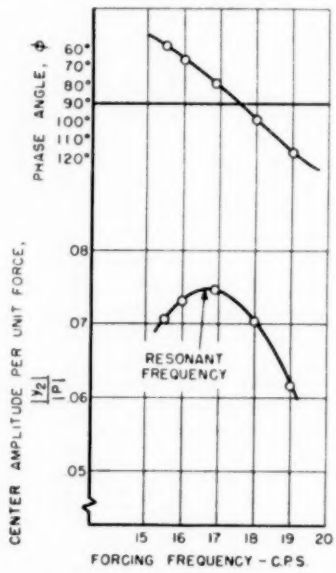

Fig. 6 Resonance and Phase-Angle Curves for System I

System II

The previous method always can be used when the system is identical on both sides of the forcing function. This is a very restrictive case, and, in general, the calculation must include the whole beam. The forcing functions must be included as unknowns in the calculation. To show this, the system in Fig. 7 has been solved. The calculation is illustrative of the type which would be carried out for any nonuniform beam, nonsymmetrical problem. The procedure is the same as for System I up to the forcing function. An extra term P is added to the shear force at position 2 to represent the forcing function. It is carried through the calculations as an unknown, as is θ_0. The boundary conditions at position 4 are

$$\text{At } m_4 \begin{cases} M_4 = 0 \quad \ldots\ldots\ldots\ldots\ldots\ldots\ldots\ldots [16] \\ S_4 = +(k + jc_4\omega)y_4 \quad \ldots\ldots\ldots\ldots [17] \end{cases}$$

Notice the plus sign for the shear at the right end of the beam due to sign conventions used. The two resulting simultaneous equations are solved for P and θ_0, and these unknowns are eliminated from all quantities.

The results are shown in Table 2 for a forcing frequency of 19.3 cps. The phase diagram for this frequency is plotted to scale in Fig. 8. The angles in the phase diagram are not as pronounced as they were for System I. This is expected, for a lower value of damping has been chosen for this example. The higher the damping at the initial end, the steeper the slope of the line connecting the first two mass points. Since the beam is not symmetrical, the mass points all appear in different positions. The resonance and phase-angle curves for the first mode are shown in Fig. 9. Because of the lower damping of this system, the resonance curve is sharper and of greater amplitude and the phase angle curve has a more abrupt change than for System I.

[7] "Free Lateral Vibration of a Cantilever Beam With a Terminal Dashpot," by E. J. McBride, Journal of Applied Mechanics, Trans. ASME, vol. 65, 1943, p. A-168.

TABLE 2 FORCED VIBRATION OF SYSTEM II, FIG. 7, AT 19.3 CPS

$k_0 = 150$ lb/in., $c_0 = 0.25$ lb-sec/in., $\omega = 121.26545$ rad/sec, $c_0\omega = 30.316369$
$k_4 = 200$ lb/in., $c_4 = 0.4$ lb-sec/in., $\omega^2 = 14705.309$, $c_4\omega = 48.506180$

PART (A)

Position	m_i, lb-sec²/in.	l_i, in.	α_i, 1/lb-in.	β_i, 1/lb	γ_i, in/lb	$m_i\omega^2$, lb/in.
0	0.8×10^{-3}	10	1.25×10^{-4}	6.25×10^{-4}	41.666667×10^{-4}	11.764253
1	1.6×10^{-3}	13	1.3×10^{-4}	8.45×10^{-4}	73.233333×10^{-4}	23.528494
2	1.3×10^{-3}	11	1.2222222×10^{-4}	6.7222222×10^{-4}	49.296296×10^{-4}	19.116902
3	1.9×10^{-3}	10	1.25×10^{-4}	6.25×10^{-4}	41.666667×10^{-4}	27.940087
4	1.0×10^{-3}					14.705309

PART (B)

Position	M_i	θ_i	y_i	S_i
0	0	θ_0	1.0	$-138.23575 - j30.316369$
1	$-1382.3575 - j303.16369$	$0.086397342 + j0.018947731 + \theta_0$	$0.71200887 - j0.06315910 - 10\theta_0$	$-121.48324 - j31.802408$ $-235.28505\theta_0$
2	$-2961.6396 - j716.59499$ $-3058.70576\theta_0 + P$	$0.36875715 + j0.085232045$ $+1.1988159\theta_0$	$-2.0240798 - j0.68210274$ $-23.861535\theta_0$	$-160.17740 - j44.842106$ $-691.443906\theta_0$
3	$-4723.5910 - j1209.8582$ $-10664.5886\theta_0 + 11P$	$0.83840948 + j0.20295958$ $+2.0374609\theta_0 - 6.722222 \times 10^{-4}P$	$-8.4660888 - j2.2118021$ $-40.808914\theta_0 + 24.648149 \times 10^{-4}P$	$-396.72076 - j106.64259$ $-1831.6490\theta_0 + 1.0688072P$
4	$-8690.7986 - j2276.2841$ $-28081.0796\theta_0 + 21.0867P$	$1.6768088 + j0.42084347$ $4.5153152\theta_0 - 2.7152642 \times 10^{-4}P$	$-20.628930 - j5.2198212$ $-71.664826\theta_0 + 0.018288844P$	$-700.0757 - j183.4017$ $-2885.5029\theta_0 + 1.3378104P$

PART (C)

Position	M_i	θ_i	y_i	S_i
0	0	$-0.29883650 - j0.069201900$	1.0	$-138.23575 - j30.316369$
1	$-1382.3574 - j30.316369$	$-0.21243916 - j0.050254169$	$3.7003739 + j0.62885990$	$-51.171482 - j15.520236$
2	$-2047.5867 - j304.92675$	$+0.01507215 + j0.02271710$	$5.1066179 + j0.96916085$	$+47.843379 + j15.489926$
3	$-1521.3096 - j334.53757$	$+0.22860598 + j0.053572195$	$3.7325353 + j0.64293009$	$+152.13079 + j33.453457$
4	0	$+0.32368793 + j0.074480980$	$0.81259621 - j0.03218313$	$+164.08027 + j32.980194$

PART (D)

Position	y_i	S_i	$m_i\omega^2 y_i$
0	1.0/0°	141.5/192.38	11.76/0°
1	3.78/9.63°	53.4/196.9°	89./9.63°
2	5.19/10.74°	49.5/14.93°	98.2/10.74°
3	3.79/9.77°	156./12.4°	105.8/9.77°
4	0.813/−2.27°	167.5/11.35°	11.95/2.27°

$\phi = 72.89°$ $\quad P = 1.3921734 + j12.482862 = 12.56/83.63°$

$$\frac{y_2}{P} = \frac{5.19}{12.56} = 0.413$$

Energy balance:

Forcing energy $= (P \sin \phi)y_2 = 62.39596$ in-lb/rad
Damping energy $= \omega(c_0 + c_4y_4^2) = 62.3958$ in-lb/rad

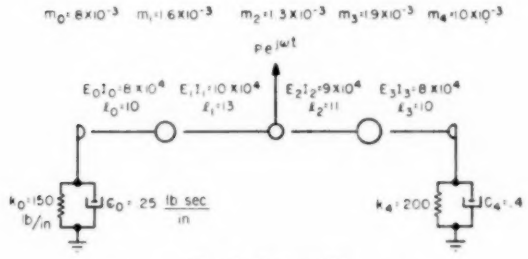

FIG. 7 SYSTEM II
(Nonuniform beam, nonsymmetrical problem.)

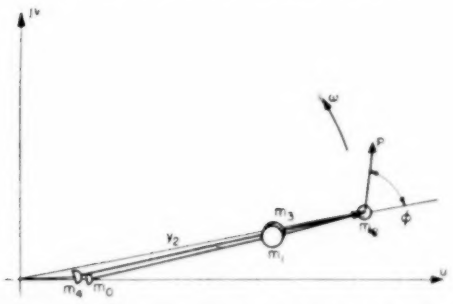

FIG. 8 PHASE DIAGRAM FOR SYSTEM II, 19.3 CPS

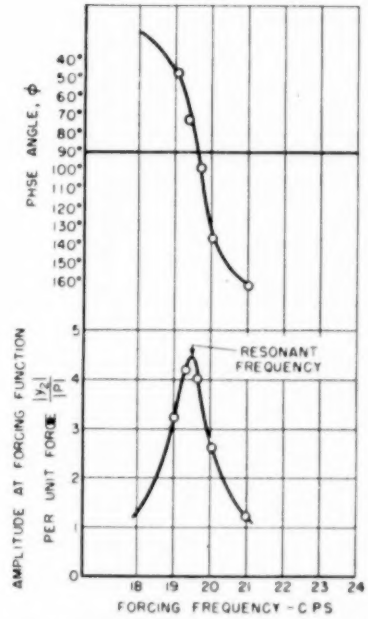
PHSE ANGLE, ϕ
40° 50° 60° 70° 80° 90° 100° 110° 120° 130° 140° 150° 160°
RESONANT FREQUENCY
AMPLITUDE AT FORCING FUNCTION PER UNIT FORCE $\frac{|y_2|}{|P|}$
0 1 2 3 4 5
18 19 20 21 22 23 24
FORCING FREQUENCY - CPS

FIG. 9 RESONANCE AND PHASE-ANGLE CURVES FOR SYSTEM II

Other End Conditions

The procedure has been illustrated for parallel spring-damper end conditions, but many other types of boundary conditions can be handled. For the transmission-line type of boundary condition, consisting of series sections of masses and parallel springs and dampers, the Equations [1], [2], [3], [4] are applied successively to initial boundary sections, beam sections, and terminal boundary sections. For these boundary sections the moments and slopes are zero and the equations become

$$y_{i+1} = -\gamma_i S_i + y_i \quad [18]$$

$$S_{i+1} = S_i + m_{i+1}\omega^2 y_{i+1} \quad [19]$$

where

$$\gamma_i = \frac{1}{k_i + jc_i\omega} \quad [20]$$

If the damping at the end is a torque opposing the end rotation the boundary condition is

$$M = jc\omega\theta$$

Boundary moments and gyroscopic moments also can be included. Beams on many supports are handled in the usual manner, using the complex iteration procedure. For problems with numerous forcing functions, of the same frequency, acting at different points on the beam, the amplitude and phase relations of the forcing functions must be known. Each forcing function is then treated as was done in System II.

Conclusions

Formulation of the forced, damped-end beam vibration problem could have been given in matrix or finite difference form, but some of the simplicity of the method would have been sacrificed. The procedure described is applicable to most problems of forced vibration of beams and critical speeds of shafts, in which boundary damping is present. The calculations and formulas have been kept as simple as possible. The method has not been obscured by long tabular procedures. If a tabular method is desired, it may be based on an existing one.[4]

The task is tedious for the general forced, damped-vibration problem when done by hand-calculating machines. Slide-rule calculation is, in general, unsuitable, as more digits must be carried. Punched-card computing machines are the best way to solve these problems and should be used whenever possible. An energy balance should be calculated for each forced frequency, as it forms a valuable check on the accuracy of the iteration calculations.

Acknowledgment

The author wishes to thank Mr. A. C. Hagg of the Westinghouse Research Laboratories for his generous support and assistance throughout this problem and Mr. D. B. Breedon of the Westinghouse Computing Laboratories for the punched-card solution of System II.

Appendix

System I:

Section 0

$M_0 = 0$

$\theta_0 = \theta_0$

$y_0 = 1.0$

$S_0 = -(52 - 8.0295 + j57.88) = -43.98 - j57.88$ (from Equation [12])

Section 1

$M_1 = 11(-43.98 - j57.88) = -483.78 - j636.68$ (from Equation [1])

$\theta_1 = -6.576 \times 10^{-4}(-43.98 - j57.88) + \theta_0$

$= 0.0289212 + j0.0380620 + \theta_0$ (from Equation [2])

$y_1 = -48.224 \times 10^{-4}(-43.98 - j57.88) - 11(0.0289212 + j0.0380620 + \theta_0) + 1.0$

$= 0.893955 - j0.139560 - 11\theta_0$ (from Equation [3])

$S_1 = -43.98 - j57.88 + 16.0590(0.893955 - j0.139560 - 11\theta_0)$

$= 29.62397 - j60.121199 - 176.649\theta_0$ (from Equation [4])

Section 2

$M_2 = 11(-29.62397 - j60.121199 - 176.649\theta_0) - 483.78 - j636.68$

$= -809.64367 - j1298.013 - 1943.139\theta_0$

$\theta_2 = -6.576 \times 10^{-4}(-29.62397 - j60.121199 - 176.649\theta_0) - 1.196 \times 10^{-4}(-483.78 - j636.68) + 0.0289212 + j0.0380620 + \theta_0$

$= 0.106262 + j0.153744 + 1.116164\theta_0$

$y_2 = -48.224 \times 10^{-4}(-29.62397 - j60.121199 - 176.649\theta_0) - 6.576 \times 10^{-4}(-483.78 - j636.68) - 11(0.106262 + j0.153744 + 1.116164\theta_0) + 0.893955 + j0.139560 - 11\theta_0$

$= 0.186065 - j1.122141 - 22.42594\theta_0$

$S_2 = -29.62397 - j60.121199 - 176.649\theta_0 + 8.0295(0.186065 - j1.122141 - 22.42594\theta_0)$

$= -28.12996 - j69.13143 - 356.718\theta_0$

Application of boundary condition

$\theta_2 = 0, \quad \theta_0 = -0.0952028 - j0.1377436$

Frequencies of Longitudinal Vibration for a Slender Rod of Variable Section

By JAMES L. LUBKIN[1] and YUDELL L. LUKE[2]

The natural frequencies of a slender, homogeneous, fixed-free rod of variable section are studied in a one-dimensional theory. The rod is uniform at the fixed end for a certain distance L_1, and then tapers for a distance L_2 so that the cross-sectional area varies linearly. The frequency equation is derived and its first five zeros are tabulated for several ratios of L_1 to L_2, and various tapers. The first few terms of asymptotic expansions for the roots of the frequency equation are presented and discussed.

Nomenclature

The following nomenclature is used in the paper:

t = time
x = axial co-ordinate; zero at fixed end
$u = u(x, t)$ = displacement
L_1 = length of uniform section of rod
L_2 = length of tapered portion
$A = A(x)$ = cross-sectional area
A_0 = area of uniform section of rod
ϵ = taper parameter
E = Young's modulus
ρ = mass density
$c = \sqrt{E/\rho}$
p_n = nth natural circular frequency
$\nu_n = p_n/c$
$X_n = X_n(x)$ = nth eigenfunction (mode-shape) for rod

Additional symbols are defined as introduced.

Introduction and Mathematical Statement of Problem

The purpose of this paper is to study the longitudinal natural frequencies of a slender rod of continuously variable cross section, in terms of a one-dimensional theory. The rod is assumed to be fixed at one end and free at the other, and possesses the following sectional characteristics. Immediately adjacent to the fixed end, the rod is uniform for a certain distance L_1. For the remainder, L_2, of the rod's length, the cross-sectional area A is taken to vary linearly with distance along the rod.[3]

The results of this investigation should prove useful in a number of technical fields, because a composite rod that is partly uniform and partly tapered is not uncommon in practice. Application appears possible to certain types of phonograph needle, and other transducers; variable-speed mechanisms involving uniform shafts attached to tapered pulleys; other shafts and spindles encountered in mechanical design; and rifles. In addition, the frequency equation whose roots are tabulated may offer a solution to useful problems in acoustics and in wave-guide propagation.

Taking the x-axis along the rod with $x = 0$ at the fixed end, the equation governing free vibrations is derived from a consideration of the forces acting upon an elementary length of the rod. If $u(x, t)$ be the displacement, $A(x)$ the area of the section, E Young's modulus, and ρ the mass density

$$\partial^2 u/\partial t^2 = [c^2/A(x)]\ \partial[A(x)\ \partial u/\partial x]/\partial x \quad [1]$$

$$c^2 = E/\rho \quad [2]$$

Unless $A(x)$ is constant, the system is dispersive, and the shape of a wave propagated along the rod is altered as it progresses. In dealing with Equation [1], consideration of reflections is necessary at points of discontinuity or very rapid variation of section. In the present study the taper is assumed to be gradual, as is required if one-dimensional theory is to apply, and the area function is assumed to be continuous. The latter is taken to be

$$A(x) = A_0 \qquad : 0 \le x \le L_1$$
$$= A_0\,[1 + \epsilon(x - L_1)/L_2] : L_1 \le x \le L_1 + L_2 \quad [3]$$

where A_0 is the area of the uniform section of length L_1, and ϵ is a taper parameter, governing the change of section of the tapered portion (length L_2).

In addition to the boundary conditions, which are

$$u(0, t) = 0,\ \partial u(L_1 + L_2, t)/\partial x = 0 \quad [4]$$

we require continuity of displacement and strain at $x = L_1$.

Frequency Equation

The usual substitution is made in Equation [1]

$$u = e^{ip_n t}\ X_n(x) \quad [5]$$

Here p_n is the nth natural circular frequency and $X_n(x)$ is the corresponding mode shape or eigenfunction; the result of the substitution is

$$X_n'' + A'X_n'/A + \nu_n^2 X_n = 0 \quad [6]$$

$$\nu_n = p_n/c \quad [7]$$

primes denoting differentiation with respect to x.

The solution of Equation [6] for the general class of area variations $A(x) = (h + kx)^\mu$, μ any real number, is well known and expressible in terms of cylinder functions (1, 2).[4] For the present case $\mu = 1$, and the solution of Equation [6], subject to Equations [3], the first of Equations [4], and the two conditions of continuity at $x = L_1$, is as follows

---

[1] Research Engineer, Midwest Research Institute, Kansas City, Mo. Jun. ASME.

[2] Research Mathematician, Midwest Research Institute, Kansas City, Mo.

[3] Essentially the same theory as that developed in the paper governs the torsional vibration of a rod having a uniform and then a linearly varying second polar moment of area. Note, however, that in a given rod, a linear variation of area generally indicates that the second moment of area will not be linear (and vice versa), except for certain types of rod having a very gentle taper.

Contributed by the Applied Mechanics Division and presented at the Annual Meeting, New York N. Y., Nov. 30–Dec. 5, 1952, of The American Society of Mechanical Engineers.

Discussion of this paper should be addressed to the Secretary, ASME, 29 West 39th Street, New York, N. Y., and will be accepted until July 10, 1953, for publication at a later date. Discussion received after the closing date will be returned.

Note: Statements and opinions advanced in papers are to be understood as individual expressions of their authors and not those of the Society. Manuscript received by ASME Applied Mechanics Division, July 2, 1952. Paper No. 52—A-27.

[4] Numbers in parentheses refer to the Bibliography at the end of the paper.

TABLE 1 VALUES OF $\nu_n(L_1 + L_2)$

Root	ϵ	$\lambda = 0$	0.125	0.25	0.375	0.5	0.625	0.75	0.875	1.0
First,	-1	2.40483	2.38325	2.31244	2.19853	2.06229	1.92341	1.79303	1.67531	$\pi/2$
	-2/3	1.91914	1.93533	1.92998	1.89981	1.84975	1.78208	1.71036	1.63875	$\pi/2$
$\nu_1(L_1+L_2)$	-1/3	1.70146	1.71176	1.71419	1.70721	1.69079	1.66643	1.63658	1.60393	$\pi/2$
	0	$\pi/2$	$\pi/2$	$\pi/2$	$\pi/2$	$\pi/2$	$\pi/2$	$\pi/2$	$\pi/2$	$\pi/2$
	1/3	1.48074	1.47044	1.46573	1.46726	1.47543	1.49039	1.51193	1.53929	$\pi/2$
	2/3	1.41355	1.39368	1.38388	1.38484	1.39719	1.42166	1.45899	1.50932	$\pi/2$
	1	1.36078	1.33213	1.31743	1.31696	1.33138	1.36206	1.41113	1.48081	$\pi/2$
Second,	-1	5.52008	5.47730	5.40683	5.42883	5.52241	5.52288	5.32432	5.02095	$3\pi/2$
	-2/3	4.87433	4.86743	4.83956	4.85970	4.95693	5.06301	5.05257	4.90804	$3\pi/2$
$\nu_2(L_1+L_2)$	-1/3	4.76032	4.75402	4.73527	4.73620	4.77656	4.83459	4.85454	4.80492	$3\pi/2$
	0	$3\pi/2$	$3\pi/2$	$3\pi/2$	$3\pi/2$	$3\pi/2$	$3\pi/2$	$3\pi/2$	$3\pi/2$	$3\pi/2$
	1/3	4.68352	4.69128	4.71326	4.72154	4.69358	4.64201	4.60805	4.62999	$3\pi/2$
	2/3	4.66263	4.67813	4.72260	4.74376	4.69564	4.59969	4.52934	4.55679	$3\pi/2$
	1	4.64590	4.66866	4.73507	4.77146	4.70821	4.57383	4.46847	4.49172	$3\pi/2$
Third,	-1	8.65373	8.60241	8.60798	8.66063	8.56650	8.59352	8.67626	8.35090	$5\pi/2$
	-2/3	7.95636	7.93573	7.94347	8.01108	7.99640	8.00525	8.18498	8.15199	$5\pi/2$
$\nu_3(L_1+L_2)$	-1/3	7.88301	7.87010	7.86908	7.89924	7.88898	7.87800	7.95979	7.98626	$5\pi/2$
	0	$5\pi/2$	$5\pi/2$	$5\pi/2$	$5\pi/2$	$5\pi/2$	$5\pi/2$	$5\pi/2$	$5\pi/2$	$5\pi/2$
	1/3	7.83671	7.85071	7.85552	7.82790	7.83955	7.86310	7.80191	7.74934	$5\pi/2$
	2/3	7.82422	7.85225	7.86399	7.80998	7.83282	7.88522	7.77662	7.66613	$5\pi/2$
	1	7.81416	7.85594	7.87603	7.79645	7.82943	7.91283	7.76584	7.59925	$5\pi/2$
Fourth,	-1	11.79153	11.74478	11.79325	11.73468	11.79138	11.71857	11.77928	11.65243	$7\pi/2$
	-2/3	11.06993	11.04692	11.08881	11.07668	11.11446	11.14705	11.17697	11.35263	$7\pi/2$
$\nu_4(L_1+L_2)$	-1/3	11.01636	11.00262	11.02277	11.01162	11.02277	11.03662	11.02921	11.13887	$7\pi/2$
	0	$7\pi/2$	$7\pi/2$	$7\pi/2$	$7\pi/2$	$7\pi/2$	$7\pi/2$	$7\pi/2$	$7\pi/2$	$7\pi/2$
	1/3	10.98324	10.99808	10.98225	10.99229	10.98671	10.97414	10.99963	10.89866	$7\pi/2$
	2/3	10.97433	11.00429	10.97374	10.99385	10.98564	10.96023	11.01877	10.83138	$7\pi/2$
	1	10.96714	11.01223	10.96777	10.99757	10.98872	10.94979	11.04448	10.78336	$7\pi/2$
Fifth,	-1	14.93092	14.89759	14.91921	14.91548	14.88103	14.94422	14.82936	14.91016	$9\pi/2$
	-2/3	14.19542	14.17812	14.20912	14.20504	14.22454	14.27250	14.26307	14.49566	$9\pi/2$
$\nu_5(L_1+L_2)$	-1/3	14.15335	14.14277	14.15632	14.15031	14.15720	14.17143	14.15978	14.26183	$9\pi/2$
	0	$9\pi/2$	$9\pi/2$	$9\pi/2$	$9\pi/2$	$9\pi/2$	$9\pi/2$	$9\pi/2$	$9\pi/2$	$9\pi/2$
	1/3	14.12758	14.13923	14.12661	14.13509	14.12943	14.12199	14.13806	14.06829	$9\pi/2$
	2/3	14.12065	14.14440	14.11944	14.13761	14.12642	14.11498	14.14777	14.02902	$9\pi/2$
	1	14.11506	14.15114	14.11394	14.14253	14.12556	14.11233	14.16119	14.00649	$9\pi/2$

$$X_n(x) = \sin \nu_n x \ : \ 0 \le x \le L_1 \quad \ldots\ldots\ldots\ldots [8]$$

$$X_n(x) = C_n J_0\left[\frac{\nu_n L_2}{|\epsilon|}\frac{A(x)}{A_0}\right] + D_n Y_0\left[\frac{\nu_n L_2}{|\epsilon|}\frac{A(x)}{A_0}\right] : L_1 \le x \le L_1 + L_2 \quad [9]$$

where J_m and Y_m, respectively, are the mth order Bessel functions of the first and second kinds. The absolute value of ϵ is required for a single formula to accommodate both positive and negative values of ϵ. The constants C_n and D_n are given by

$$\left.\begin{aligned} -2C_n/\pi\beta &= \sin\gamma\ Y_1(\beta) + \cos\gamma\ Y_0(\beta)\ |\epsilon|/\epsilon \\ 2D_n/\pi\beta &= \sin\gamma\ J_1(\beta) + \cos\gamma\ J_0(\beta)\ |\epsilon|/\epsilon \end{aligned}\right\} \quad \ldots [10]$$

$$\beta = \nu_n L_2/|\epsilon|, \qquad \gamma = \nu_n L_1 \quad \ldots\ldots\ldots [11]$$

except when $\epsilon = -1$, in which case $D_n = 0$ and $C_n = \sin\gamma/J_0(\beta)$. In deriving Equations [10], we have used the well-known relations

$$\left.\begin{aligned} J_0'(z) &= -J_1(z), \qquad Y_0'(z) = -Y_1(z) \\ J_1(z)Y_0(z) - J_0(z)Y_1(z) &= 2/\pi z \end{aligned}\right\} \quad \ldots\ldots [12]$$

Finally, using the second of the boundary conditions, Equations [4], the frequency equation is obtained

$$0 = \sin\gamma\{J_1[\beta(1+\epsilon)]Y_1(\beta) - Y_1[\beta(1+\epsilon)]J_1(\beta)\} + (\epsilon/\epsilon)\cos\gamma\{J_1[\beta(1+\epsilon)]Y_0(\beta) - Y_1[\beta(1+\epsilon)]J_0(\beta)\} \quad [13]$$

It is seen that $\nu_n(L_1 + L_2)$, for any given n, constitutes a two-parameter family, depending upon the proportion of the rod that is tapered (L_1/L_2) and the degree of taper (ϵ). The latter are therefore the principal variables in treating the frequency equation.

Discussion of Frequency Equation

Equation [13] simplifies considerably for certain values of L_1/L_2 and/or ϵ. When $L_1 = 0$, only the tapered portion of the rod remains, and we obtain

$$J_0(\beta)Y_1[\beta(1+\epsilon)] - Y_0(\beta)J_1[\beta(1+\epsilon)] = 0 \quad [14]$$

Equation [14] is encountered frequently in physical problems, and its roots have been studied by a number of authors (3, 4, 5).

When ϵ assumes its smallest value of -1, the rod tapers to zero area at its free end, and Equation [13] reduces to

$$\cos\gamma J_0(\beta) - \sin\gamma J_1(\beta) = 0 \quad \ldots\ldots\ldots [15]$$

For a rod which both "tapers to a point" and has no uniform region ($\epsilon = -1$, $L_1 = 0$), this reduces further to

$$J_0(\beta) = 0 \quad \ldots\ldots\ldots\ldots [16]$$

the zeros of which are tabulated extensively (6).

In the degenerate case of $\epsilon = 0$, i.e., a uniform rod of length $L_1 + L_2$, the frequency equation of course becomes

$$\cos\nu_n(L_1 + L_2) = 0 \quad \ldots\ldots\ldots [17]$$

If the tapered portion had been taken as of length L_1 at the fixed end and the uniform section as of length L_2 at the free end, it is found that a very similar frequency equation obtains; the lengths L_1 and L_2 are interchanged in Equation [13], and the functions J_1, Y_1 in the first pair of braces are replaced by J_0, Y_0, respectively.[5] It is easy to see, however, that the frequency equation becomes exceedingly complex for a composite rod consisting of more than two sections, even when the area variation is a linear function.

[5] This presupposes $A(x) = A_0(1 + \epsilon x/L_1)$: $0 \le x \le L_1$, and $A(x) = A_0(1+\epsilon)$ thereafter.

Roots of Frequency Equation

In tabulating these quantities, it is convenient to introduce as the length variable

$$\lambda = \frac{L_1/L_2}{1 + L_1/L_2} \quad \ldots\ldots\ldots [18]$$

i.e., the fraction of the total rod length that is uniform. Thus the ratios $L_1/L_2 = 0$, $1/7$, $1/3$, $3/5$, 1, $5/3$, 3, 7, ∞ become $\lambda = 0(0.125)1$,[6] respectively. For these values of λ, Table 1 gives to five decimals the values of $\nu_n(L_1 + L_2)$ corresponding to the first five zeros of Equation [13]. The parameter ϵ, the net increase in cross-sectional area up to the free end of the rod, expressed as a fraction of that of the uniform portion of the rod, is given the values $-1(1/8)1$.

These zeros are computed by tabulating the frequency equation near the desired roots, using standard tables of Bessel and circular functions (6, 7). The entries are then subtabulated (8) at sufficiently close intervals for the first differences to be essentially constant. The zero is found by linear inverse interpolation. Seven or eight decimals are carried in the computations, sufficient to insure that only occasional entries, if any, are in error by as much as one unit in the fifth place.

Because of the comparatively few entries in Table 1, interpolation is generally not good, especially λ-wise, although probably adequate for most engineering purposes. Intermediate values in λ-wise interpolation probably can be obtained to 1 per cent or better, either graphically or by formulas. However, considerably greater precision may be obtained in some portions of Table 1, and it is recommended that any user interested in accurate intermediate values investigate local tabular differences. It has been found that ϵ-wise interpolation may be substantially improved by the device of first multiplying the entries of Table 1 by a factor $a_{n,\lambda} + \epsilon$ and then interpolating for the auxiliary function $(a_{n,\lambda} + \epsilon)\ \nu_n(L_1 + L_2)$. Table 2 suggests appropriate "smoothing factors" $a_{n,\lambda}$ and indicates an approximation for the maximum error to be expected in five-point interpolation.

Natural frequencies for composite and uniform rods may be compared simply by reference to Table 1. Fig. 1 illustrates for a typical case the effect of rod geometry on the shapes of the natural modes of vibration. Curves are presented for the first three modes of a rod which is $^3/_8$ uniform and $^5/_8$ tapered. A mode shape is given for $\epsilon = -1$, 1, and 0, corresponding, respectively, to rods whose area varies linearly to zero, linearly to double that of the uniform section, or remains constant for the entire rod length.

Asymptotic Expansions

The first few terms of asymptotic expansions for the roots of Equations [13] to [15] have been obtained. Because of the complexity of these equations, the terms are lengthy and no attempt will be made to write down a single explicit expression. An equivalent procedure is outlined instead.

At least in the range of ϵ, λ of Table 1, these expansions always give an approximation, however poor, for the gravest natural frequency.[7] The higher roots of the frequency equation are larger and therefore better approximated, for given ϵ and λ. However, as λ approaches unity (rod tends to uniformity of section), all asymptotic expansions offer an increasingly poor representation of the desired zeros. Essentially, this appears to be because the sinusoidal functions do not possess asymptotic expansions. Again, as ϵ approaches -1, the general expansion

[6] The notation 0(0.125)1 means from zero to unity by eighths.

[7] In some applications, asymptotic expansions have been found to miss the early zeros of functions similar to that of the frequency equation (9).

TABLE 2 SMOOTHING FACTORS $a_{n,\lambda}$ AND CORRESPONDING MAXIMUM ERRORS IN FIVE-POINT ϵ-WISE INTERPOLATION

(Figure in parentheses after each $a_{n,\lambda}$ is approximate maximum error, in thousandths of a per cent.)

λ	$n = 1$	$n = 2$	$n = 3$	$n = 4$	$n = 5$
0	1.440(3.4)	1.155(6.8)	1.080(4.6)	1.055(3.6)	1.040(2.6)
0.125	1.583(4.2)	1.190(6.4)	1.099(4.5)	1.065(3.7)	1.045(4.3)
0.25	1.768(1.8)	1.256(5.5)	1.120(5.2)	1.075(5.7)	1.060(5.9)
0.375	2.125(2.8)	1.340(4.9)	1.156(5.4)	1.100(4.1)	1.070(3.7)
0.5	2.859(3.3)	1.500(3.5)	1.210(4.6)	1.130(4.8)	1.100(5.0)
0.625	4.537(1.6)	2.120(3.3)	1.340(4.5)	1.200(3.5)	1.140(3.9)
0.75	9.292(0.3)	4.116(5.3)	2.250(4.0)	1.450(4.0)	1.230(5.5)
0.875	34.800(0.0)	2.106(0.1)	1.555(2.0)	5.500(3.4)	5.500(4.0)

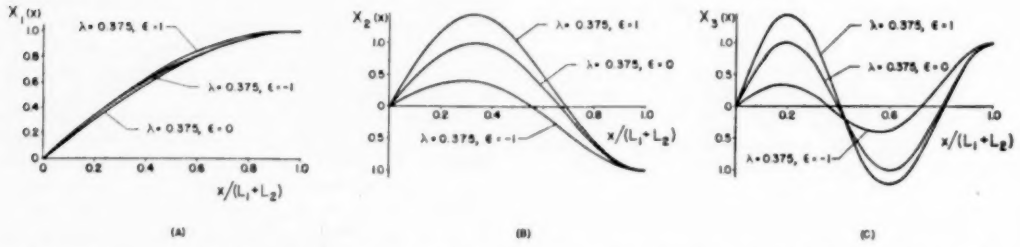

FIG. 1 COMPARISON OF FIRST THREE MODE-SHAPE FUNCTIONS FOR A ROD HAVING $\lambda = 0.375$ AND $\epsilon = 1, 0$ AND -1

(A, First mode; B, second mode; C, third mode.)

corresponding to Equation [13] loses its usefulness, even for higher roots. When $\epsilon = -1$, Equation [15] obtains, and a special expansion is presented in this case.

For brevity, Equation [13] is rewritten with the notation

$$y = \beta(1 + \epsilon),\ ay = \beta,\ by = \gamma\ \epsilon/|\epsilon| \quad \ldots\ldots [19]$$

and becomes

$$f(y) \equiv \sin by\ [J_1(y)\ Y_1(ay) - J_1(ay)\ Y_1(y)] + \cos by\ [J_1(y)\ Y_0(ay) - J_0(ay)\ Y_1(y)] = 0 \quad \ldots [20]$$

Substituting the asymptotic expansions for the various Bessel functions into Equation [20], for n sufficiently large the limiting values of the zeros, say y_n, are found to be

$$R\ y_n = (2n - 1)\ \pi\epsilon/2|\epsilon| \quad \ldots\ldots [21]$$

$$R = b - a + 1 \quad \ldots\ldots [22]$$

Equation [21] is easily proved equivalent to

$$\nu_n(L_1 + L_2) = (2n - 1)\ \pi/2\text{:}\quad n \text{ large} \quad \ldots\ldots [23]$$

which bears the physical interpretation that the higher rod frequencies tend to be independent of the taper, and to depend only on total rod length.

If z_n be the nth zero of Equation [20], it may be shown that

$$z_n \sim y_n + \mu_1/y_n + \mu_2/y_n^2 + \mu_3/y_n^3 + \ldots\ldots [24]$$

To calculate the μ_i, let $z_n = y_n + h$. By Taylor's theorem

$$f(y_n + h) = \sum_{k=0}^{\infty} \frac{h^k}{k!} f^{(k)}(y_n) \quad \ldots\ldots [25]$$

Equating this expression to zero, the value of h is determined by reversion (10)

$$h = -f/f' - f''f^2/2f'^3 + [f'''/6f' - f''^2/2f'^2]f^3/f'^3 + \ldots\ldots [26]$$

whence the coefficients μ_i may be evaluated. However, to derive these μ_i explicitly involves considerable manipulation. It appears to be simpler merely to give the necessary asymptotic expansions of $f(y)$ and its derivatives, all evaluated at $y = y_n$. Defining

$$S = b + a - 1,\ \theta_n = Sy_n \quad \ldots\ldots [27]$$

it is found that

$$\left.\begin{aligned} \pi\sqrt{a}\ y_n f(y_n)/2 &= \sum_{k=1}^{4} A_k y_n^{-k} + \ldots \\ \pi\sqrt{a}\ y_n f'(y_n)/2 &= \sum_{k=1}^{4} B_k y_n^{1-k} + \ldots \\ \pi\sqrt{a}\ y_n f''(y_n)/2 &= C_1/y_n + C_2/y_n^2 + \ldots \\ \pi\sqrt{a}\ y_n f'''(y_n)/2 &= D_1 + D_2/y_n + \ldots \end{aligned}\right\} \quad \ldots\ldots [28]$$

where

$$\left.\begin{aligned} 8aA_1 &= (-)^n(3a - 1) + 2\sin\theta_n \\ 32a^2A_2 &= -3(a + 1)\cos\theta_n \\ 1024a^3A_3/3 &= 2(5a^2 - 6a - 15)\sin\theta_n \\ &\quad - (-)^n(35a^3 + 5a^2 - 3a - 5) \\ (8a)^4A_4/15 &= (7a^3 - 3a^2 + 9a + 35)\cos\theta_n \end{aligned}\right\} \quad \ldots [29]$$

$$\left.\begin{aligned} B_1 &= (-)^n R,\ 4aB_2 = S\cos\theta_n \\ 128a^2B_3 &= 3(-)^n R(5a^2 + 2a + 1) \\ &\quad + 12(a + 1)S\sin\theta_n - 64a\sin\theta_n + 32a(-)^n(1 - 3a) \\ 512a^3B_4 &= 144a(a + 1)\cos\theta_n \\ &\quad + 3(5a^2 - 6a - 15)S\cos\theta_n \end{aligned}\right\} \quad \ldots [30]$$

$$\left.\begin{aligned} 8aC_1 &= (-)^{n-1}16aR + (-)^n(1 - 3a)R^2 - 2S^2\sin\theta_n \\ 32a^2C_2 &= 3(a + 1)S^2\cos\theta_n - 32aS\cos\theta_n \end{aligned}\right\} \quad \ldots [31]$$

$$D_1 = (-)^{n-1}R^3,\ 4aD_2 = -S^2\cos\theta_n \quad \ldots\ldots [32]$$

Substituting Equations [28] in [26] assures the inclusion in the expansion for z_n of terms of order y_n^{-4}, but all higher orders are neglected. The factor involving $(f''/f')^2$ introduces a term of order y_n^{-6}, and for consistency the latter should be neglected.

As noted previously, this expansion is useful away from $\epsilon = -1$, where $a = (1 + \epsilon)^{-1}$ is infinite, and away from $\lambda = 1$, where

no asymptotic expansion exists. Two-way interpolation in Table 1, with the assistance of Table 2, is recommended for intermediate values for the first five roots. Thereafter, the expansion must be used.

When $b = 0$ the algebra simplifies considerably, and it is found that

$$z_n \sim y_n - \frac{3a+1}{8a(1-a)y_n} - \frac{63a^4 - 9a^3 + 36a^2 + 31a - 25}{384a^3(1-a)^2y_n^3} + \quad \ldots [33]$$

a result deducible from earlier studies (3, 4).

Equation [15] obtains when $\epsilon = -1$, and must be treated separately. Let

$$\nu_n L_2 = w, \qquad L_1/L_2 = q \ldots\ldots\ldots\ldots [34]$$

$$g(w) \equiv \sin qw\ J_1(w) - \cos qw\ J_0(w) \ldots\ldots\ldots [35]$$

For n sufficiently large, the limiting values of the zeros are given by

$$(q+1)w_n = \nu_n(L_1 + L_2) = (4n-1)\,\pi/4 \ldots\ldots [36]$$

Define

$$\left.\begin{aligned} \varphi_n = (q-1)w_n = \nu_n(L_1 - L_2), \quad r &= \cos\varphi_n + \sin\varphi_n \\ s &= \cos\varphi_n - \sin\varphi_n \end{aligned}\right\} \ldots [37]$$

Proceeding as before, it is found that the left-hand members of the system equivalent to Equations [28] should read $2\sqrt{\pi w_n}\,g^{(k)}(w_n)$, and the coefficients in the right-hand members become

$$\left.\begin{aligned} 8A_1 &= 2r - (-)^n\sqrt{2},\ 32A_2 = 3s \\ 1024A_3/15 &= (-)^n\sqrt{2} - 6r,\ 4096A_4 = -525s \end{aligned}\right\} \ldots [38]$$

$$\left.\begin{aligned} B_1 &= (-)^{n-1}\sqrt{2}\,(1+q),\ 4B_2 = (q-1)\,s \\ 128B_3 &= -12r(q+3) + 3(-)^n\sqrt{2}\,(7-q), \\ 512B_4 &= -15(3q+5)\,s \end{aligned}\right\} \ldots [39]$$

$$\left.\begin{aligned} 8C_1 &= -2(q-1)^2\,r + (-)^n\sqrt{2}\,(q+1)(q+9) \\ 32C_2 &= 3(1-q)(7+q)\,s \end{aligned}\right\} \ldots [40]$$

$$D_1 = (-)^n\sqrt{2}\,(1+q)^3,\ 4D_2 = (1-q)^3\,s \ldots\ldots [41]$$

Again, Equations [38] to [41] include the terms of order w_n^{-4}, and again the w_n^{-5} term introduced by the factor $(g''/g')^2$ should be omitted. As a check on Equations [38] to [41], q may be set equal to zero, and using Equation [26], the well-known asymptotic expansion for the zeros of $J_0(w)$ is readily obtainable.

For sixth and higher roots, the expansion must be used; as usual, its usefulness is destroyed as L_2 approaches zero (λ approaches unity).

BIBLIOGRAPHY

1 "Applied Bessel Functions," by F. E. Relton, Blackie and Son Ltd., London, England, 1946, article 6.7, pp. 85–87; particularly, ex. 3.

2 "Bessel Functions for Engineers," by N. W. McLachlan, Oxford University Press, London, England, reprint of 1946, pp. 73–76; particularly, equation [86].

3 S. Sasaki, *Tôhoku Mathematical Journal*, vol. 5, 1914, pp. 45–47.

4 "Abkühlung und Erwärmung zylindrischer Rohre und Geschichteter Zylinder," by J. Fischer, *Ingenieur-Archiv*, vol. 10, 1939, pp. 95–112.

5 "Some Roots of an Equation Involving Bessel Functions," by B. P. Bogert, *Journal of Mathematics and Physics*, vol. 30, July, 1951, pp. 102–105; additional references are given in this paper.

6 "Bessel Functions," Mathematical Tables, vol. 6, part 1, BAAS, Cambridge University Press, London, England, 1950.

7 "Tables of Circular and Hyperbolic Sines and Cosines for Radian Arguments," U. S. National Bureau of Standards, U. S. Government Printing Office, 1940.

8 "Tables of Lagrangian Interpolation Coefficients," Mathematical Tables Project, U. S. National Bureau of Standards, Columbia University Press, New York, N. Y., 1944.

9 "Table of Roots for Natural Frequencies in Coaxial Type Cavities," by H. B. Dwight, *Journal of Mathematics and Physics*, vol. 27, April, 1948, pp. 84–89.

10 "Formula for Solution of an Arbitrary Analytic Equation," by D. R. Blaskett and H. Schwertfeger, *Quarterly of Applied Mathematics*, vol. 3, 1945, pp. 266–268.

An Invariant Membrane Stress Function for Shells

By H. L. LANGHAAR,[1] URBANA, ILL.

Inextensional shells that have no thickness are idealized representations of real shells that have small bending stresses and small deformations. With certain restrictions, the stresses in these shells are derivable from a generalized Airy function. For shells of constant Gaussian curvature, the stress function is unrestricted, but, for other shells, it is expressed as a function of the Gaussian curvature. Although, in this respect, t is less general than Pucher's stress function, it has t'e advantage that it may be used with any surface co-or.inates.

Introduction

If (x, y) are any orthogonal co-ordinates on the surface of a shell, the square of the line element is

$$ds^2 = A^2\,dx^2 + B^2\,dy^2 \qquad [1]$$

where

$$A = A(x, y), \quad B = B(x, y)$$

Let (R_1, R_2) be the principal radii of curvature of the surface. The positive side of the surface may be designated arbitrarily. A principal radius of curvature will be defined to be positive if the corresponding center of curvature lies on the negative side of the tangent plane. With this definition, the radii of curvature of a convex surface are positive, if the positive surface normal is directed outward.

The Gaussian curvature K (subsequently called the "curvature of the shell") is defined by

$$K = \frac{1}{R_1 R_2} \qquad [2]$$

This quantity is expressed in terms of A and B by the Gauss equation[2]

$$\frac{\partial}{\partial x}\left(\frac{1}{A}\frac{\partial B}{\partial x}\right) + \frac{\partial}{\partial y}\left(\frac{1}{B}\frac{\partial A}{\partial y}\right) = -KAB \qquad [3]$$

The curvature K is a bending invariant, i.e., it is not changed by any deformation of the shell that is compatible with the condition of inextensibility. Consequently, there are many surfaces for which K is constant. Any developable surface has zero curvature. Any surface of revolution with constant positive curvature can be obtained by inextensional bending of a segment of a spherical shell. Rotation of a tractrix about an axis generates a surface with constant negative curvature, called a "pseudosphere".[4] Any surface of revolution with constant negative curvature can be obtained by inextensional bending of a segment of a pseudospherical shell.

Any point P on a surface of negative curvature is the intersection of two curves that lie in the surface and that have contact of at least second order with the tangent plane at P. These curves are called the "asymptotic lines" of the surface. For a developable surface, the two families of asymptotic lines coalesce with the generators. The asymptotic lines on a surface of positive curvature are imaginary. If the co-ordinate lines are the lines of principal curvature, the differential equation of the asymptotic lines is

$$\frac{A^2}{R_1}\,dx^2 + \frac{B^2}{R_2}\,dy^2 = 0 \qquad [4]$$

Equilibrium Equations

Consider a differential surface element that is bounded by orthogonal co-ordinate lines, Fig. 1. The equilibrium equations for tangential forces on the element may be derived with the assumption that the element is plane, since the curvature is a second-order effect.

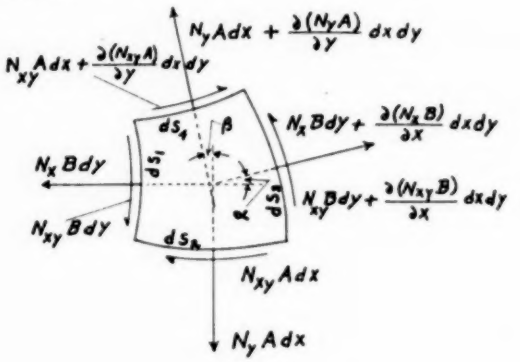

Fig. 1

The lengths of the sides of the element are

$$ds_1 = B\,dy, \quad ds_2 = A\,dx$$
$$ds_3 = \left(B + \frac{\partial B}{\partial x}\,dx\right)dy$$
$$ds_4 = \left(A + \frac{\partial A}{\partial y}\,dy\right)dx$$

Consequently, the angles α and β, Fig. 1, are

$$\left.\begin{aligned} \alpha &= \frac{ds_2 - ds_4}{ds_1} = -\frac{1}{B}\frac{\partial A}{\partial y}\,dx \\ \beta &= \frac{ds_3 - ds_1}{ds_2} = \frac{1}{A}\frac{\partial B}{\partial x}\,dy \end{aligned}\right\} \qquad [a]$$

[1] Professor of Theoretical and Applied Mechanics, University of Illinois. Mem. ASME.

[2] Reference (1),[3] p. 138.

[3] Numbers in parentheses refer to the Bibliography at the end of the paper.

Contributed by the Applied Mechanics Division and presented at the Annual Meeting, New York, N. Y., November 30–December 5, 1952, of The American Society of Mechanical Engineers.

Discussion of this paper should be addressed to the Secretary, ASME, 29 West 39th Street, New York, N. Y., and will be accepted until July 10, 1953, for publication at a later date. Discussion received after the closing date will be returned.

Note: Statements and opinions advanced in papers are to be understood as individual expressions of their authors and not those of the Society. Manuscript received by ASME Applied Mechanics Division, May 22, 1952. Paper No. 52—A-18.

[4] Reference (2), p. 149.

With the same stress notations as in the theory of plates,[5] the forces on the edges of the element are as shown in Fig. 1. Resolution of forces in the direction of the line element ds_2 yields

$$-N_x B\,dy + N_x B\,dy + \frac{\partial(N_x B)}{\partial x}\,dx\,dy - N_{xy} A\,dx + N_{xy} A\,dx + \frac{\partial(N_{xy} A)}{\partial y}\,dx\,dy - N_{xy}\,\alpha\,B\,dy - N_y\,\beta\,A\,dx = 0$$

A similar equation is obtained for equilibrium of forces in the direction of the line element ds_1. Elimination of α and β by means of Equation [a], and simplification of the results, yields the following equilibrium equations for tangential forces

$$\left.\begin{aligned} B\frac{\partial N_x}{\partial x} + A\frac{\partial N_{xy}}{\partial y} + N_x\frac{\partial B}{\partial x} + 2N_{xy}\frac{\partial A}{\partial y} - N_y\frac{\partial B}{\partial x} &= 0 \\ B\frac{\partial N_{xy}}{\partial x} + A\frac{\partial N_y}{\partial y} - N_x\frac{\partial A}{\partial y} + 2N_{xy}\frac{\partial B}{\partial x} + N_y\frac{\partial A}{\partial y} &= 0 \end{aligned}\right\} \quad \ldots [5]$$

If the co-ordinate lines are the lines of principal curvature, the equilibrium equation for the normal forces takes the following well-known form

$$\frac{N_x}{R_1} + \frac{N_y}{R_2} = p \quad \ldots [6]$$

The function $p(x, y)$ is the external normal pressure (positive if it acts in the direction of the positive surface normal).

Stress Function

Under certain conditions, Equations [5] are satisfied identically[6] if the stresses are derived from a single function $F(x, y)$, as follows

$$\left.\begin{aligned} N_x &= \frac{1}{B^2}\frac{\partial^2 F}{\partial y^2} + \frac{1}{A^2 B}\frac{\partial B}{\partial x}\frac{\partial F}{\partial x} - \frac{1}{B^3}\frac{\partial B}{\partial y}\frac{\partial F}{\partial y} + KF - \int F\,dK \\ N_y &= \frac{1}{A^2}\frac{\partial^2 F}{\partial x^2} - \frac{1}{A^3}\frac{\partial A}{\partial x}\frac{\partial F}{\partial x} + \frac{1}{AB^2}\frac{\partial A}{\partial y}\frac{\partial F}{\partial y} + KF - \int F\,dK \\ N_{xy} &= -\frac{1}{AB}\frac{\partial^2 F}{\partial x\,\partial y} + \frac{1}{A^2 B}\frac{\partial A}{\partial y}\frac{\partial F}{\partial x} + \frac{1}{AB^2}\frac{\partial B}{\partial x}\frac{\partial F}{\partial y} \end{aligned}\right\} \quad \ldots [7]$$

For shells of constant curvature, $\int F\,dK = 0$, and, with some restrictions on continuity and differentiability, the function $F(x, y)$ is arbitrary. Accordingly, for shells of constant curvature, Equations [7] give the general solution of Equations [5]. For flat plates, F is the well-known Airy stress function.

Prof. Harry Levy showed the author that the term $\int F\,dK$ generalizes the solution, so that a class of stresses is obtained for shells of variable curvature. However, Equations [7] are not the most general solution of Equations [5], for, if K is variable, F must be a function of K, rather than an arbitrary function of x and y.

[5] Reference (3), p. 299.

[6] See Appendix.

The function F is useful for inverse solutions of membrane problems, for, if F is a given function, the pressure $p(x, y)$ that causes the prescribed stresses is determined by Equation [6].

A. Pucher (4) employed a different type of stress function that relates to extrinsic quantities, for the shell is projected orthogonally on a plane, and rectangular or polar co-ordinates in the plane are adopted as surface co-ordinates. Pucher derived the stresses from a scalar function, in conjunction with certain angles that depend on the orientation of the tangent plane with respect to the plane of projection. Seemingly, Pucher's relations cannot be expressed in an invariant intrinsic form.

Differential Equation for Stress Function

Attention is tentatively restricted to shells of constant curvature. If the co-ordinate lines are the lines of principal curvature, and if the pressure $p(x, y)$ is given, Equations [6] and [7] provide a second-order linear differential equation of the following form

$$\frac{1}{A^2 R_2}\frac{\partial^2 F}{\partial x^2} + \frac{1}{B^2 R_1}\frac{\partial^2 F}{\partial y^2} + f\left(x, y, F, \frac{\partial F}{\partial x}, \frac{\partial F}{\partial y}\right) = 0 \quad \ldots [8]$$

Evidently, this equation is elliptic, parabolic, or hyperbolic, according as K is positive, zero, or negative. If the shell is a flat plate, Equation [6] degenerates to $p = 0$, and the compatibility equation of plane elasticity supersedes Equation [8].

The stress function F is a point function on the surface of the shell. Consequently, the characteristics of Equation [8] may be regarded as two families of curves on the shell. The equation of characteristics is the same as Equation [4]. Accordingly, *the characteristics of Equation [8] are the asymptotic lines on the shell.*

Discontinuities of Stress

In view of Equation [6], at least one component of stress is discontinuous wherever p is discontinuous. Lines of discontinuity of stress also may originate from boundary conditions. Two types of discontinuity may occur; stepwise discontinuity, and points of infinite stress.

If C is a line of stepwise discontinuity, the co-ordinates may be chosen so that C is the line $x = 0$. Then, from statical requirements, N_x and N_{xy} are continuous, i.e., the discontinuity exists only in the component N_y. For shells of constant curvature, these conditions are satisfied if the discontinuity exists in $\partial^2 F/\partial x^2$, while the remaining derivatives, and F itself, are continuous. Because of the invariance of F, and an arbitrariness in the functions A and B, which stems from the freedom of choice of co-ordinates, these properties of the function F are also necessary. Consequently, in general, F, $\partial F/\partial x$, and $\partial F/\partial y$ are continuous at a line C of stepwise discontinuity of stress, but the second directional derivative of F, in the direction normal to the line C, is discontinuous.

By virtue of a well-known property of characteristics, many different solutions of Equation [8] may be stitched together along an asymptotic line, in such a way that F, $\partial F/\partial x$, and $\partial F/\partial y$ are continuous. The union of appropriate integral surfaces on characteristic lines is a fundamental procedure in the solving of boundary-value problems in hyperbolic differential equations. In general, the stitching does not preserve continuity of second derivatives, and therefore certain asymptotic lines on shells of constant curvature may be lines of discontinuity of stress. This condition arises if the boundary stresses are discontinuous.

For example, let (x, θ) be cylindrical co-ordinates on a circular cylindrical shell with radius a. If there is no normal external pressure, Equation [6] reduces to $N_\theta = 0$. Since $A = 1$, $B = a$, and $K = 0$, Equations [7] yield $\partial^2 F/\partial x^2 = 0$, whence $F = mx + n$, where $m = m(\theta)$, $n = n(\theta)$. Furthermore, by Equations [7]

$$a^2 N_x = m'' x + n'', \quad a N_{x\theta} = -m' \ldots\ldots [a]$$

Equations [a] show that discontinuities of N_x or $N_{x\theta}$ at the end section of the shell are propagated along the generators. For example, if a concentrated axial load acts at the end of a cylindrical shell, the stresses are infinite at all points of the generator on which the force is applied. W. Flügge (5) has questioned the significance of this conclusion. Perhaps a small amount of flexural stiffness causes rapid dissipation of the stresses in the neighborhood of a concentrated tangential load.

Shells of Revolution With Constant Curvature

W. Flügge (6) and C. Truesdell (7, 8) have treated the membrane theory of shells of revolution extensively. Truesdell employed stress functions in connection with Fourier analyses of the stresses, but they are not directly related to the function F.

For a shell of revolution, the arc length x on a meridian and the longitude θ may be adopted as co-ordinates. Then the co-ordinate lines are also the lines of principal curvature. The coefficients A and B in Equation [1] are

$$A = 1, \quad B = r(x) \ldots\ldots [9]$$

where r is the radius of the cross section at co-ordinate x.

Equation [3] yields

$$r'' + K r = 0 \ldots\ldots [10]$$

If K is constant, there are three general solutions of Equation [10], depending on whether K is positive, negative, or zero. These solutions determine all shells of revolution with constant curvature.[7] For these shells, Equations [7] reduce to

$$N_x = \frac{1}{r^2}\frac{\partial^2 F}{\partial \theta^2} + \frac{r'}{r}\frac{\partial F}{\partial x} + KF \ldots\ldots [11a]$$

$$N_\theta = \frac{\partial^2 F}{\partial x^2} + KF \ldots\ldots [11b]$$

$$N_{x\theta} = -\frac{\partial^2}{\partial x \partial \theta}\left(\frac{F}{r}\right) \ldots\ldots [11c]$$

If the shell is closed circumferentially, N_x, N_θ, and $N_{x\theta}$ must have period 2π in θ. This condition imposes a restriction on F, but it does not necessarily signify that F is periodic. Rather, F may be a multiple-valued point function on the shell, such that a circuit of the shell leads to a new branch of the function.

Attention is restricted to cases in which the stresses are continuous. Then $N_{x\theta}$ may be represented by a uniformly convergent Fourier series in θ. Equating this series to the expression for $N_{x\theta}$ in Equation [11c], and integrating, one obtains a relation of the following form

$$F = r f(\theta) + \theta g(x) + \phi(x, \theta) \ldots\ldots [a]$$

where $\phi(x, \theta)$ is a function with continuois second derivatives that has period 2π in θ. The functions $f(\theta)$ and $g(x)$ also have continuous second derivatives. Equation [a] is necessary and sufficient for periodicity of $N_{x\theta}$.

In view of Equation [10], Equation [11b] now yields

$$g'' + K g = 0 \ldots\ldots [b]$$

Equations [a] and [b] are necessary and sufficient for periodicity of N_θ and $N_{x\theta}$.

Equation [11a] now shows that the following expression must be periodic in θ

$$f'' + (r'^2 + K r^2) f + (r' g' + K r g)\theta \ldots\ldots [c]$$

[7] Reference (2), p. 147.

The following notations are introduced

$$r'^2 + K r^2 = \alpha, \quad r' g' + K r g = \beta \ldots\ldots [d]$$

Then Equation [c] becomes

$$f'' + \alpha f + \beta\theta \ldots\ldots [e]$$

Equations [10], [b], and [d] yield $d\alpha/dx = d\beta/dx = 0$. Consequently, the coefficients α and β are constants.

Since Expression [e] is continuous and periodic, it may be represented by a uniformly convergent Fourier series, i.e.

$$f'' + \alpha f + \beta\theta = \frac{1}{2} a_0 + \sum_{n=1}^{\infty} a_n \cos n\theta + b_n \sin n\theta \ldots [f]$$

Several distinct cases arise in the integration of Equation [f].

Case 1. $\alpha \neq 0$.

If α is a positive number, but not the square of an integer, integration of Equation [f] yields

$$f(\theta) = C_1 \sin \sqrt{\alpha}\,\theta + C_2 \cos \sqrt{\alpha}\,\theta - \frac{\beta}{\alpha}\theta + \psi(\theta)$$

where $\psi(\theta)$ is periodic. The sine and cosine terms contribute nothing to the stresses. Consequently, they may be discarded. Then, when the expressions for α and β are introduced

$$F = \frac{r'(r' g - r g')\theta}{\alpha} + \phi(x, \theta) \ldots\ldots [g]$$

By Equations [10] and [b]

$$\frac{d}{dx}(r' g - r g') = 0$$

Consequently, Equation [g] reduces to

$$F = C r'\theta + \phi(x, \theta) \ldots\ldots [12]$$

where C is a constant.

Equation [12] remains valid if α is any negative number, for then exponentials occur in the integral of Equation [f], but they contribute nothing to the stresses. Consequently, if α is not the square of an integer, Equation [12] is the most general form of the stress function that yields continuous stresses with period 2π in θ. The term $C r'\theta$ represents pure torsion.

If $\alpha = n^2$, where n is a positive integer, Equation [12] may be augmented by the term

$$r\theta(C_1 \sin n\theta + C_2 \cos n\theta)$$

Case 2. *Circular Cylindrical Shells.* For circular cylindrical shells, $K = 0$ and $r' = 0$. Consequently, $\alpha = \beta = 0$. The general solution of Equation [b] is then $g = A_1 x + A_2$, where A_1 and A_2 are constants. Equation [f] yields

$$f(\theta) = \frac{1}{4} a_0 \theta^2 + A_3\theta + \psi(\theta)$$

where A_3 is a constant, and $\psi(\theta)$ is periodic. Consequently, neglecting terms that do not contribute to the stresses, one obtains from Equation [a]

$$F = C_1\theta^2 + C_2\theta x + \phi(x, \theta) \ldots\ldots [13]$$

where C_1 and C_2 are constants. Equation [13] is the most general stress function that insures continuous periodic stresses in a circular cylindrical shell. The term $C_1\theta^2$ represents simple tension, and the term $C_2\theta x$ represents pure torsion.

Case 3. *Noncylindrical Shells With* $\alpha = 0$. The most gen-

eral surface of revolution with constant curvature that satisfies the condition $\alpha = 0$ is defined by

$$r = a\, e^{kx} \qquad [14]$$

where a is a positive constant, and k is any real constant. If $k = 0$, the surface is a cylinder. The curvature of the surface is $K = -k^2$. Consequently, if the surface is not a cylinder, it has negative curvature.

If $k \neq 0$, the general solution of Equation [b] is

$$g = A_1\, e^{kx} + A_2\, e^{-kx}$$

where A_1 and A_2 are constants. Also, $\beta = -2\, a\, k^2\, A_2$.

Since $\alpha = 0$, integration of Equation [f] yields

$$f(\theta) = -\frac{1}{6}\,\beta\theta^3 + \frac{1}{4}\,a_0\,\theta^2 + A_3\theta + \psi(\theta)$$

where A_3 is a constant, and $\psi(\theta)$ is periodic. Consequently, neglecting terms that do not contribute to the stresses, one obtains from Equation [a]

$$F = C_1\theta^2\, e^{kx} + C_2\left(\frac{1}{3}\,a^2\,k^2\,\theta^3\, e^{kx} + \theta e^{-kx}\right) + \phi(x, \theta) \qquad [15]$$

where C_1 and C_2 are constants. Equation [15] is the most general stress function that yields continuous periodic stresses in the shell defined by Equation [14], if $k \neq 0$. The term $C_1\,\theta^2\, e^{kx}$ yields stresses of the form, $N_x = \text{const}/r$, $N_\theta = N_{x\theta} = 0$. In view of Equation [6], this stress distribution cannot be realized without external pressure. The second term in Equation [15] is the stress function for pure torsion.

Shells of Revolution With Variable Curvature

For any shell of revolution, $K = K(x)$. In an interval where $dK/dx \neq 0$, this relation may be inverted, i.e., $x = x(K)$. Consequently, if F is any function of x, it is likewise a function of K. Then, by Equations [7] and [9]

$$N_x = \frac{r'\,F'}{r} + \int KF'\,dx,\quad N_\theta = F'' + \int KF'\,dx,\quad N_{x\theta} = 0 \qquad [16]$$

If F is any function of x, Equations [16] define an axially symmetrical state of stress. Equations [16] remain valid for shells of constant curvature.

Appendix

Derivation of Stress Function

For shells of constant curvature, one may derive Equations [7] by writing expressions[8] of the following form for the stresses, and substituting these expressions into Equations [5] to determine the unknown coefficients a_1, a_2, etc.

$$\left.\begin{aligned} N_x &= a_1\frac{\partial^2 F}{\partial x^2} + a_2\frac{\partial^2 F}{\partial x\,\partial y} + a_3\frac{\partial^2 F}{\partial y^2} + a_4\frac{\partial F}{\partial x} \\ &\qquad + a_5\frac{\partial F}{\partial y} + a_6 F \\ N_{xy} &= b_1\frac{\partial^2 F}{\partial x^2} + \ldots\ldots,\quad N_y = c_1\frac{\partial^2 F}{\partial x^2} + \ldots\ldots \end{aligned}\right\} \qquad [a]$$

Equation [3] serves to simplify the results. It is found that, when K is not constant, the coefficients in Equations [a] cannot be chosen so that Equations [5] are satisfied identically in F, when A and B conform to Equation [3]. The demonstration of this fact is facilitated by the use of isometric co-ordinates, i.e., orthogonal co-ordinates for which $A = B$. Such co-ordinates exist on any surface.[9] Possibly the general solution of Equations [5] can be obtained if Equations [a] are augmented by higher derivatives of F, but the algebra becomes very complicated.

Tensor principles seem to afford the most promising means for deriving the general solution of Equations [5]. These principles also permit the theory to be extended to nonorthogonal co-ordinates. If (x^1, x^2) are any surface co-ordinates on a shell, and if T^{ij} is the stress tensor, the stress vector on a section of the surface with unit normal n_j is $T^{ij}\,n_j$. The component of this vector in the direction of a unit vector m_i is $T^{ij}\,m_i\,n_j$. Consequently, if the co-ordinates are orthogonal, the physical stress components are

$$N_x = A^2\,T^{11},\quad N_y = B^2\,T^{22},\quad N_{xy} = ABT^{12}$$

In tensor form, Equations [5] are

$$T^{ij}{}_{,ij} = 0 \qquad [17]$$

Since this is a tensor equation, it remains valid when the co-ordinates are not orthogonal. Equation [17] is a special case of the general equilibrium equations of Chien (9).

Let g_{ij} be the metric tensor of the surface, and let g be the determinant of the matrix (g_{ij}). Absolute antisymmetric tensors, e^{ij} and e_{ij}, are defined as follows

$$e^{11} = e^{22} = 0,\quad e^{12} = \frac{1}{\sqrt{g}},\quad e^{21} = \frac{-1}{\sqrt{g}}$$

$$e_{11} = e_{22} = 0,\quad e_{12} = \sqrt{g},\quad e_{21} = -\sqrt{g}$$

The Riemann tensor of the surface[10] is

$$R_{ijmn} = K\,e_{ij}\,e_{mn}$$

where K is the Gaussian curvature. Accordingly, if P_i is a covariant vector, the Ricci identity[11] is

$$P_{i,jk} - P_{i,kj} = K\,P_h\,g^{hm}\,e_{mi}\,e_{jk} \qquad [18]$$

Let F be an invariant, and let a symmetric tensor be defined by

$$A^{ij} = e^{im}\,e^{jn}\,F_{,mn} \qquad [19]$$

Then, by the Ricci identity

$$A^{ij}{}_{,j} = -K\,g^{ij}\,F_{,j} \qquad [20]$$

Equation [20] suggests that a class of solutions of Equation [17] can be obtained by setting

$$T^{ij} = e^{im}\,e^{jn}\,F_{,mn} + G\,g^{ij} \qquad [21]$$

where G is an invariant. Then

$$T^{ij}{}_{,j} = g^{ij}\,(G_{,j} - K\,F_{,j})$$

Equation [17] is satisfied if $G_{,j} - K\,F_{,j} = 0$. If K is constant, this is satisfied by $G = K\,F$. If F is a function of K, it is satisfied by

$$G = K\,F - \int F\,dK$$

Thus the solution is found for the case $K = \text{const}$, and for the case $F = F(K)$. It seems probable that the general solution of Equation [17] is a linear expression containing third or fourth

[8] No generality is gained by adding terms to Equations [a] that are independent of F.

[9] Reference (1), p. 131.

[10] Reference (10), p. 183.

[11] Reference (11), p. 30.

covariant derivatives of F, but the author has not succeeded in finding this generalization.

W. Zerna (12) neatly generalized Pucher's results by use of tensor calculus, but, like Pucher, he treats the equilibrium conditions for a flat projection of the shell.

Acknowledgment

Prof. Harry Levy helpfully extended the results to include the case in which F is a function of the Gaussian curvature.

BIBLIOGRAPHY

1 "Differential Geometry," by W. C. Graustein, The Macmillan Company, New York, N. Y., 1935.

2 "Differential Geometry," by D. J. Struik, Addison-Wesley Press, Inc., Cambridge, Mass., 1950.

3 "Theory of Plates and Shells," by S. Timoshenko, McGraw-Hill Book Company, Inc., New York, N. Y., 1940.

4 "Über den Spannungszustand in gekrümmten Flächen," by A. Pucher, *Beton and Eisen*, vol. 33, 1934, pp. 298–304.

5 "Recent Trends in the Theories of Plates and Shells," by W. Flügge, *Applied Mechanics Reviews*, vol. 4, September, 1951, pp. 489–491.

6 "Statik und Dynamik der Schalen," by W. Flügge, Edwards Bros., Inc., Ann Arbor, Mich., 1943.

7 "On the Reliability of the Membrane Theory of Shells of Revolution," by C. Truesdell, Bulletin, of the American Mathematical Society, vol. 54, October, 1948, pp. 994–1008.

8 "The Membrane Theory of Shells of Revolution," by C. Truesdell, Trans. of the American Mathematical Society, vol. 58, July, 1945, pp. 96–166.

9 "The Intrinsic Theory of Thin Shells and Plates," by W. Z. Chien, *Quarterly of Applied Mathematics*, vol. 1, January, 1944, pp. 297–327.

10 "Applications of the Absolute Differential Calculus," by A. J. McConnell, Blackie and Son, Ltd., Glasgow, Scotland, 1931.

11 "Riemannian Geometry," by L. P. Eisenhart, Princeton University Press, Princeton, N. J., 1926.

12 "Zur Spannungsfunktion bei Membranschalen," W. Zerna, Zeitschrift für angewandte Mathematik und Mechanik, vol. 31, 1951, p. 272.

On the Plastic Strains in Slabs With Cutouts[1]

By P. G. HODGE, JR.,[2] LOS ANGELES, CALIF.

The complete elastic-plastic problem is set up for a circular slab with a central circular cutout, subjected to uniform external tension. The analysis is carried out under the assumption of generalized plane stress but with possibly finite deformations. The material is assumed to be isotropic, homogeneous, and incompressible, to yield according to the Tresca yield condition, and to satisfy Hooke's law in the elastic domain and the plastic potential law in the plastic domain. The equations are solved by a perturbation method based on the ratio of the maximum shear stress to the shear modulus, in which each of the significant quantities, stress, displacement, and slab thickness, is expanded in a power series in this ratio. A similar technique is employed to solve the fully plastic flow problem. It is shown that for cutout radii greater than 1 per cent of the radius of the slab, the "first approximations" obtained by neglecting all but the leading term in each series are satisfactory, up to loads at which the slab becomes wholly plastic. The ratio of the maximum strain in the just fully plastic slab to that in the completely elastic slab is computed. It is found that this ratio is less than about 6 if the cutout radius is at least 1 per cent of the radius of the slab. Some observations are advanced on the case where the cutout is very small compared to the slab.

1 Introduction

RECENT papers by the author and others (1, 2)[3] have been concerned with the limit analysis of slabs with cutouts, and with the design of reinforcements to bring the slabs back to full strength. One weakness of the limit-analysis approach is that no information about the strains is obtained. From a practical design viewpoint, it may be that the structure has not "collapsed" in the sense of limit analysis, and yet has undergone such deformation as to make it unserviceable nonetheless. In the bending of beams, for example, it is known that this phenomenon can, in fact, occur (3).

The present paper, then, is concerned with a complete elastic-plastic analysis for the simplest type of problem previously considered. It will be shown that for this problem the strains at full yield are still sufficiently small so that they will not make the slab unserviceable. While this does not by any means constitute a proof that the same results would be valid for more complicated loadings, it seems intuitively reasonable to expect this to be the case. The fact that in this case at least the strains are small, provides a partial justification of a fundamental assumption of the limit-analysis approach, namely, that motion of the boundaries may be neglected under loads less than the yield loads.

In section 2 we shall define the functions which serve to express the solution of this problem, and enumerate the equations and boundary conditions available for the determination of these functions. The equations are found to be nonlinear, and in section 3 a perturbation method for obtaining a solution will be outlined. The elastic solution will be obtained in section 4, the elastic-plastic solution in section 5, and the fully plastic solution in section 6. In section 7 we shall define and compute a measure of the plastic strain, and show that for the slabs considered it is not unduly large. The changes necessary in the solution when the cutout radius tends to zero will be discussed in section 8. Finally, the results obtained will be summarized in section 9.

2 Statement of the Problem

We consider a thin slab in the shape of an annulus, Fig. 1.[4] Let

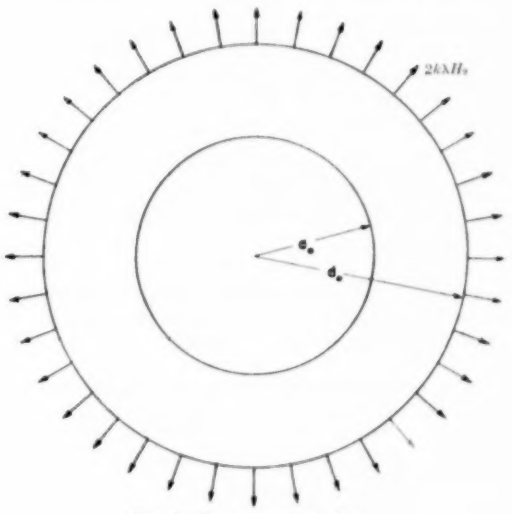

Fig. 1 Dimensions of Slab

the initial values of the inner and outer radii be denoted by a_0 and d_0, respectively, and let H_0 denote the initial thickness. A uniform radial force of magnitude $2k\lambda H_0$ per unit length is applied to the outer edge; the inner edge is stress-free.

In accord with the theory of generalized plane stress, we shall define the problem in terms of quantities averaged over the thickness of the slab h. Since the problem is radially symmetric, the resulting quantities will be functions only of the distance r from the center of the plate, and of the time t. Thus the solution of the problem may be specified entirely by the following functions of a distance and time:

[1] The results presented in this paper were obtained in the course of research conducted under Contract N7onr-35810 between the Office of Naval Research and Brown University.

[2] Department of Mathematics, University of California. Jun. ASME.

[3] Numbers in parentheses refer to the Bibliography at the end of the paper.

Contributed by the Applied Mechanics Division and presented at the Annual Meeting, New York, N. Y., November 30–December 5, 1952, of The American Society of Mechanical Engineers.

Discussion of this paper should be addressed to the Secretary, ASME, 29 West 39th Street, New York, N. Y., and will be accepted until July 10, 1953, for publication at a later date. Discussion received after the closing date will be returned.

Note: Statements and opinions advanced in papers are to be understood as individual expressions of their authors and not those of the Society. Manuscript received by ASME Applied Mechanics Division, June 30, 1952. Paper No. 52—A-22.

[4] In the limit-analysis case (1) a square slab with a circular cutout was considered. It is intuitively obvious that the additional material in the corners will not increase the strains, so that the results obtained for the annulus may be taken as upper bounds for the hollow square.

$h(r, t)$ = thickness of slab
$u(r, t)$ = radial displacement averaged over thickness of slab } ....[1a]

$\sigma_r(r, t)$ = radial normal stress averaged over thickness of slab
$\sigma_\theta(r, t)$ = tangential normal stress averaged over thickness of slab

It is convenient to define the new quantities

$$\left.\begin{aligned} \sigma(r, t) &= \sigma_r/2G \\ s(r, t) &= \sigma_\theta/2G \end{aligned}\right\} \quad \ldots\ldots\ldots\ldots\ldots\ldots [1b]$$

where G is the modulus of elasticity in shear.

The functions defined in Equations [1] must satisfy the equations of equilibrium, the condition of incompressibility, and the appropriate stress-strain relations. Since the thickness of the slab is one of the unknowns, the equations of equilibrium must be written in terms of the total tractions across the thickness. Thus in the present problem the only equation of equilibrium which is not satisfied identically is

$$\frac{1}{2G}\left[\frac{\partial}{\partial r}(rh\sigma_r) - h\sigma_\theta\right] = \frac{\partial}{\partial r}(rh\sigma) - hs = 0 \ldots\ldots [2]$$

The condition of incompressibility also must be expressed in terms of averaged quantities, and must be stated as a function of the deformed positions of the particles. Thus (4)

$$\frac{\partial h}{\partial t} + \frac{\partial}{\partial r}\left(h\frac{\partial u}{\partial t}\right) + \frac{h}{r}\frac{\partial u}{\partial t} = 0 \ldots\ldots\ldots\ldots [3]$$

Equations [2] and [3] must be satisfied at all times throughout the slab, regardless of whether the material is elastic or plastic. The same remark applies to the yield restriction which we take to be that of Tresca (maxima shearing stress)

$$F(\sigma_r, \sigma_\theta) \equiv \max\left[|\sigma_r|, \quad |\sigma_\theta|, \quad |\sigma_r - \sigma_\theta|\right] - 2k \leq 0$$

For the problem under consideration it may be verified a posteriori that the absolutely largest principal stress is always σ_θ. Therefore, and in view of Equations [1], the yield restriction may be written

$$s \leq k/G \ldots\ldots\ldots\ldots\ldots\ldots\ldots [4]$$

Where the strict Inequality [4] holds, the material is elastic, and two stress-strain relations are furnished by Hooke's law. Where $s = k/G$, the material is plastic, and there will be one stress-strain relation.

Since we are concerned with the possibility of large displacements, it is necessary to satisfy the boundary conditions on the deformed boundaries. Thus if $a(t)$ and $d(t)$ represent the radii of the inner and outer edge of the slab, respectively

$$\sigma[a(t), t] = 0 \ldots\ldots\ldots\ldots\ldots\ldots [5a]$$

$$h[d(t), t]\sigma[d(t), t] = (k/G)\lambda(t)H_0 \ldots\ldots\ldots [5b]$$

In addition, all stresses, displacements, and strains[5] must be continuous at the elastic-plastic boundary $r = \rho$

$$\left.\begin{aligned} u(\rho^+, t) &= u(\rho^-, t), \qquad \frac{\partial u}{\partial r}(\rho^+, t) = \frac{\partial u}{\partial r}(\rho^-, t) \\ \sigma(\rho^+, t) &= \sigma(\rho^-, t), \qquad s(\rho^+, t) = s(\rho^-, t) \end{aligned}\right\} \ldots [6]$$

The equilibrium Equation [2], condition of incompressibility Equation [3], Yield Restriction [4], together with the stress-strain laws and the boundary conditions Equations [5] and [6], are sufficient to determine the four unknown functions σ, s, u, h, and the position of the elastic-plastic boundary corresponding to any given load. In sections 4 and 5 we shall determine these quantities. First, however, we shall define a perturbation method by means of which the equations can be linearized.

3 Method of Solution

The problem defined in the preceding section is a nonlinear one, and a solution in closed form does not appear to be available. However, an approximate solution can be obtained by a perturbation method based on the small parameter[6] $\mu = k/G$. To see the physical meaning of μ, imagine a sequence of slabs, each with the same yield stress k, but with indefinitely increasing shear modulus G. The limiting case $G = \infty$ corresponds to a rigid plastic material.

Expanding each unknown function Equation [1] as a power series in μ we obtain

$$\left.\begin{aligned} \sigma &= \sigma_0 + \mu\sigma_1 + \mu^2\sigma_2 + \ldots; & s &= s_0 + \mu s_1 + \mu^2 s_2 + \ldots \\ u &= u_0 + \mu u_1 + \mu^2 u_2 + \ldots; & h &= h_0 + \mu h_1 + \mu^2 h_2 + \ldots \end{aligned}\right\} \ldots [7]$$

The quantities $\sigma_0, \sigma_1, \ldots, h_2, \ldots$ on the right-hand sides of Equations [7] are functions of r and t but are independent of the parameter μ.

We assume that at least part of the slab is elastic, postponing a consideration of the fully plastic case until section 6. In the elastic domain, $\mu = 0$ corresponds to $G = \infty$, i.e., to a rigid material, so that $u_0 = 0$. We shall show in section 6, that the same result holds in the plastic domain of the elastic-plastic slab. Therefore, in terms of the quantities defined by the last two Equations [7], the condition of incompressibility Equation [3] becomes

$$\frac{\partial h_0}{\partial t} + \mu\left[\frac{\partial h_1}{\partial t} + \frac{\partial}{\partial r}\left(h_0\frac{\partial u_1}{\partial t}\right) + \frac{h_0}{r}\frac{\partial u_1}{\partial t}\right] + \ldots = 0 \ldots [8]$$

Equation [8] must be identically satisfied in μ, so that the coefficient of each power of μ must vanish. From the first such relation we see that h_0 is independent of the time. Since at time $t = 0$, $h_0 = H_0$, it follows that

$$h_0 = H_0 = \text{const} \ldots\ldots\ldots\ldots\ldots [9]$$

at all times throughout the slab. Substituting Equation [9] into the coefficient of μ in Equation [8] and integrating the resulting equation, we obtain

$$h_1 = -H_0\left(\frac{\partial u_1}{\partial r} + \frac{u_1}{r}\right) \ldots\ldots\ldots\ldots [10]$$

It follows from the Yield Restriction [4] that the dimensionless stresses σ and s must be of order μ, so that $\sigma_0 = s_0 = 0$. Substituting this result, together with Equations [10] and [7] into the equilibrium Equation [2], collecting like powers of μ and setting the coefficients equal to zero, we obtain

$$\left.\begin{aligned} &\frac{\partial}{\partial r}(r\sigma_1) = s_1 \\ &\frac{\partial}{\partial r}\left\{r\left[\sigma_2 - \left(\frac{\partial u_1}{\partial r} + \frac{u_1}{r}\right)\sigma_1\right]\right\} = s_2 \\ &\qquad - \left(\frac{\partial u_1}{\partial r} + \frac{u_1}{r}\right)s_1, \ldots. \end{aligned}\right\} \ldots [11]$$

Since the displacement u is of order μ and hence a small quan-

[5] From a strictly geometric viewpoint, there is no reason why ϵ_r should be continuous. However, if there is a discontinuity across the elastic-plastic boundary, it must be consistent with the plastic stress-strain law. It can be shown that under this restriction there can be no discontinuity. Likewise, although equilibrium alone does not demand continuity of σ_θ, the fact that a continuous solution can be found shows that there is no reason to introduce such a discontinuity.

[6] The ratio μ is of the order of magnitude of 0.1 per cent (reference 5, p. 59).

tity, the boundary conditions may be expressed in terms of the initial positions of the boundary by expansion in a Taylor's series. Thus, to within second-order terms in μ, and at all times t

$$\left.\begin{aligned}\sigma(a) &= \mu\sigma_1(a) + \mu^2\sigma_2(a)\\ &= \mu\sigma_1[a_0 + u(a)] + \mu^2\sigma_2(a_0)\\ &= \mu\sigma_1(a_0) + \mu^2\left[\sigma_2(a_0) + u_1(a_0)\frac{\partial\sigma_1}{\partial r}(a_0)\right] = 0\end{aligned}\right\}\ldots[12]$$

Similarly, it follows from Equation [5b] that

$$\mu\sigma_1(d_0) + \mu^2\left\{\sigma_2(d_0) + u_1(d_0)\frac{\partial\sigma_1}{\partial r}(d_0) - \sigma_1(d_0)\left[\frac{\partial u_1}{\partial r}(d_0) + \frac{u_1(d_0)}{d_0}\right]\right\} = \mu\lambda\ldots[13]$$

4 Elastic Solution

At any point where $s < \mu$ we shall assume that the strains are sufficiently small to justify the linear form of Hooke's law.[7] Thus

$$\sigma = 2\,\partial u/\partial r + u/r, \quad s = \partial u/\partial r + 2\,u/r\ldots\ldots[14]$$

Since Equation [14] is linear, exactly the same form of relationship will subsist between the corresponding terms of σ, s, and u in Equations [7]. Thus Equations [11] are readily converted into linear equations for u_1 and u_2, respectively. The solutions are easily found to be

$$u_1 = A_1 r + B_1/r, \quad u_2 = A_2 r + B_2/r\ldots\ldots[15]$$

The substitution of Equations [15] into [14] yields

$$\sigma_i = 3A_i - B_i/r^2, \quad s_i = 3A_i + B_i/r^2, \quad i = 1, 2\ldots[16]$$

For sufficiently small values of λ, the slab will be fully elastic so that Equations [15] and [16] apply throughout. In this case the constants A_i and B_i are determined from Equations [12] and [13]. In applying Equation [13], we note that the load is prescribed independently of the parameter μ, so that the coefficient of μ^2 on the left-hand side of Equation [13] must vanish. After some computation, the constants are seen to be

$$\left.\begin{aligned}A_1 &= \frac{1}{3}\frac{\lambda}{1 - a_0^2/d_0^2}, \qquad B_1 = \frac{\lambda a_0^2}{1 - a_0^2/d_0^2}\\ A_2 &= \frac{2}{9}\left(1 + 3\frac{a_0^2}{d_0^2}\right)\left(\frac{\lambda}{1 - a_0^2/d_0^2}\right)^2\\ B_2 &= \frac{2}{3}a_0^2\left(5 + 3\frac{a_0^2}{d_0^2}\right)\left(\frac{\lambda}{1 - a_0^2/d_0^2}\right)^2\end{aligned}\right\}\ldots[17]$$

The fully elastic solution to second-order terms is then

$$\left.\begin{aligned}\sigma &= \mu(3A_1 - B_1/r^2) + \mu^2(3A_2 - B_2/r^2)\\ s &= \mu(3A_1 + B_1/r^2) + \mu^2(3A_2 + B_2/r^2)\\ u &= \mu r(A_1 + B_1/r^2) + \mu^2 r(A_2 + B_2/r^2)\end{aligned}\right\}\ldots[18]$$

where A_1, B_1, A_2, B_2 are given by Equations [17].

Equations [18] are valid as long as the load λ is sufficiently small so that the Yield Restriction [4] is nowhere violated. As λ is slowly increased, let λ^* denote the value of λ for which s first equals μ at any point in the slab. Since this value may be expected to depend upon the shear modulus and yield stress, we must write

$$\lambda^* = \lambda_0^* + \mu\lambda_1^*\ldots\ldots[19]$$

[7] It may be verified readily that the error made by neglecting nonlinear terms is of order μ^3 and hence does not affect our results.

Obviously the slab will first become plastic at the inner boundary, so that in analogy with Equations [12] and [13] we may determine λ^* from

$$s(a) = \mu s_1(a_0) + \mu^2\left[u_1(a_0)\frac{\partial s_1}{\partial r}(a_0) + s_2(a_0)\right] = \mu\ldots[20]$$

In view of Equations [17] through [20], it is readily verified that to second-order terms

$$\lambda^* = \frac{1}{2}\left(1 - \frac{a_0^2}{d_0^2}\right)\left[1 - \frac{1}{3}\mu\left(1 + 3\frac{a_0^2}{d_0^2}\right)\right]\ldots\ldots[21]$$

As λ is increased beyond the value λ^*, a plastic zone will form at the edge of the cutout and extend into the slab. Thus the slab will be plastic for $a \le r \le \rho$ and elastic for $\rho \le r \le d$. In the elastic domain, Equations [18] are still valid, but new expressions must be found for the A_i and B_i.

It proves convenient to regard ρ as the independent quantity, rather than λ. The boundary condition, Equation [13], then serves to determine λ (which must now be expressed as a series in μ) as a function of ρ, once σ is completely known. Since at $r = \rho$, $s = \mu$, the second Equation [18] yields

$$s_1 = 3A_1 + B_1/\rho^2 = 1, \quad s_2 = 3A_2 + B_2/\rho^2 = 0\ldots[22]$$

Thus B_1 and B_2 may be eliminated and the elastic solution written as

$$\left.\begin{aligned}\left.\begin{matrix}\sigma_1\\ s_1\end{matrix}\right\} &= 3A_1 \mp (1 - 3A_1)\rho^2/r^2,\\ \left.\begin{matrix}\sigma_2\\ s_2\end{matrix}\right\} &= 3A_2(1 \pm \rho^2/r^2)\\ \left.\begin{matrix}u_1/r\\ \partial u_1/\partial r\end{matrix}\right\} &= A_1 \pm (1 - 3A_1)\rho^2/r^2,\\ \left.\begin{matrix}u_2/r\\ \partial u_2/\partial r\end{matrix}\right\} &= A_2(1 \mp 3\rho^2/r^2\end{aligned}\right\}\ldots[23]$$

5 Plastic Solution

In the plastic domain, the yield equality must be satisfied, so that

$$s_1 = 1, \quad s_2 = 0\ldots\ldots[24]$$

Substituting this into the first equation furnished by Equations [11], integrating, and applying the boundary condition Equation [12] at $r = a$, we obtain

$$\sigma_1 = 1 - a_0/r\ldots\ldots[25]$$

Continuity of σ_1 at $r = \rho$, then demands that

$$A_1 = \frac{1}{6}(2 - a_0/\rho)\ldots\ldots[26]$$

in the elastic domain. The substitution of Equations [26] and [23] into Equation [13] then yields

$$\lambda_0 = 1 - a_0/2\rho - a_0\rho/2d_0^2\ldots\ldots[27]$$

Thus the first approximation to the stress distribution has been found with no reference to the plastic stress-strain law. However, to find the plastic displacements, or the second stress approximations, a stress-strain relation is needed. We shall here adopt the "plastic potential" law (6), which states that the plastic strain-rate vector must be normal to the yield surface. In the present case, the restricting part of the yield surface is $\sigma_\theta = 2k$, so that there must be no component of plastic strain rate in the direction of σ_θ. It follows that the strain-rate component $d\epsilon_\theta/dt$ is entirely elastic and hence may be expressed in terms of the

stress-rate components by Hooke's law. From Equations [14], then

$$\partial \dot{u}/\partial r = (2\dot{\sigma} - \dot{s})/3 = (2/3)\dot{\sigma} \quad [28]$$

where the last step follows from Equations [24].

In Equation [28], the "dot" is customarily interpreted to mean differentiation with respect to time. However, it is fundamental in the static theory of perfectly plastic solids to neglect any inertia effects. Therefore we can always replace time by any convenient monotonic function of time.[8] In the present case, the radius of the elastic-plastic boundary is such a function, so that we shall consistently replace the time t by the radius ρ wherever it occurs in the present section.

Integrating Equation [28] with respect to ρ, and using the power series expansions, Equations [7], we obtain

$$\frac{\partial u_i}{\partial r} = \frac{2}{3}[\sigma_i - f_i(r)], \qquad i = 1, 2 \quad [29]$$

To determine $f_1(r)$, we set $r = \rho$ in Equation [29] and equate the result to the elastic strain at $r = \rho$. The result yields

$$f_1(\rho) = 1/2$$

Since this must be true for all positions of the elastic-plastic boundary, $f_1(r) \equiv 1/2$, hence

$$\frac{\partial u_1}{\partial r} = \frac{2}{3}\left(\sigma_1 - \frac{1}{2}\right) = \frac{1}{3}\left(1 - 2\frac{a_0}{r}\right) \quad [30]$$

where the last step follows from Equation [25].

The displacement is now found by integrating Equation [30] with respect to r, and evaluating the arbitrary function of ρ by the continuity of u_1 at $r = \rho$. The resulting expression is

$$u_1 = \frac{r}{3}\left(1 + \frac{a_0}{r} + 2\frac{a_0}{r}\log\frac{\rho}{r}\right) \quad [31]$$

The second approximations are now found by repeating the foregoing process. In the equilibrium equation (the second Equation [11]) everything is now known except σ_2. The second boundary condition, Equation [12], determines the integration function, and A_2 is determined from the continuity of σ_2 at $r = \rho$. The stress-strain law is then integrated, first with respect to ρ and then with respect to r to yield $\partial u_2/\partial r$ and u_2, respectively. In each case the arbitrary functions introduced by integration are determined by the condition of continuity at $r = \rho$. The resulting solution is given as follows:

Elastic ($\rho \leq r \leq d$)

$$\left.\begin{matrix}\sigma \\ s\end{matrix}\right\} = \mu\left[1 - \frac{a_0}{2\rho} \mp \frac{a_0\rho}{2r^2}\right] - \frac{\mu^2 a_0}{6\rho}\left[2 + 3\log\frac{\rho}{a_0} + \left(\log\frac{\rho}{a_0}\right)^2\right]\left(1 \pm \frac{\rho^2}{r^2}\right) \quad [32a, b]$$

$$\left.\begin{matrix}u/r \\ \partial u/\partial r\end{matrix}\right\} = \mu\left[\frac{1}{3} - \frac{a_0}{6\rho} \pm \frac{a_0\rho}{2r^2}\right] - \frac{\mu^2 a_0}{18\rho}\left[2 + 3\log\frac{\rho}{a_0} + \left(\log\frac{\rho}{a_0}\right)^2\right]\left(1 \mp 3\frac{\rho^2}{r^2}\right) \quad [32c, d]$$

Plastic ($a \leq r \leq \rho$)

$$\sigma = \mu\left[1 - \frac{a_0}{r}\right] - \frac{\mu^2 a_0}{3\rho}\left[2 + \log\frac{\rho^2 r}{a_0^3} + \log\frac{\rho^2}{a_0 r}\log\frac{r}{a_0}\right] \quad [32e]$$

$$s = \mu \quad [32f]$$

$$\frac{u}{r} = \frac{\mu}{3}\left[1 + \frac{a_0}{r} + 2\frac{a_0}{r}\log\frac{\rho}{r}\right] + \frac{\mu^2 a_0}{9r}\left[2 + \log\frac{\rho^4 r^3}{a_0^7} - \left(\log\frac{\rho^2 r}{a_0^3}\right)^2 + 10\left(\log\frac{\rho}{a_0}\right)^2 - 2\log\frac{\rho}{a_0}\left(\log\frac{r}{a_0}\right)^2 + \frac{4}{3}\left(\log\frac{\rho}{a_0}\right)^3 + \frac{2}{3}\left(\log\frac{r}{a_0}\right)^3\right] \quad [32g]$$

$$\frac{\partial u}{\partial r} = \frac{\mu}{3}\left[1 - 2\frac{a_0}{r}\right] - \frac{2\mu^2 a_0}{9r}\left[2 + \log\frac{\rho^2 r}{a_0^3} + \log\frac{\rho^2}{a_0 r}\log\frac{r}{a_0}\right] \quad [32h]$$

Load

$$\lambda = 1 - \frac{a_0}{2\rho} - \frac{a_0\rho}{2d_0^2} - \frac{\mu}{6}\left[4 - 2\frac{a_0}{\rho} + \frac{a_0^2}{\rho^2} + 2\frac{a_0^2}{d_0^2} - 2\frac{a_0\rho}{d_0^2} - 3\frac{a_0^2\rho^2}{d_0^4} - \frac{a_0}{\rho}\left(1 + \frac{\rho^2}{d_0^2}\right)\log\frac{\rho}{a_0}\left(3 + \log\frac{\rho}{a_0}\right)\right] \quad [32i]$$

6 Fully Plastic Solution

The results presented in Equations [32] are valid so long as at least part of the slab is elastic, i.e., so long as $\rho < d$. Since the displacement is of first order in μ, we may find the first approximation to the yield load by setting $\rho = d_0$ in Equation [32i]

$$\lambda_0^{**} = 1 - a_0/d_0 \quad [33]$$

If $\lambda = \lambda^{**}$, the slab will be plastic throughout and will flow. The question arises as to the value of λ necessary to maintain this fully plastic state, and the resulting stress and displacement distributions if it is so maintained.

It will be convenient to formulate this problem in terms of the velocity $v = \partial u/\partial t$, rather than the displacement. Further, we shall now take the radius of the cutout a as the time variable, there being no elastic-plastic boundary. Since the material is plastic throughout, we may set $s = \mu$ to satisfy the yield condition. The equilibrium equation, incompressibility condition, and stress-strain relation then become

$$\left.\begin{matrix}\partial(rh\sigma)/\partial r = \mu h \\ \partial h/\partial a + \partial(hv)/\partial r + hv/r = 0 \\ \partial\sigma/\partial a = (3/2)(\partial v/\partial r)\end{matrix}\right\} \quad [34]$$

As in section 3 we may expand the three unknown functions as power series in μ, and find successive terms by solving linear equations. However, in the present problem the resulting equations become quite complex, so that, for the sake of brevity, we shall restrict our attention to the leading term in each series. The leading terms turn out to be

$$\sigma = \mu\sigma_1, \quad v = v_0, \quad h = h_0 \quad [35]$$

so that Equations [34] become, to a first approximation in μ

$$\frac{\partial}{\partial r}(rh_0\sigma_1) = h_0 \quad [36]$$

$$\frac{\partial h_0}{\partial a} + \frac{\partial}{\partial r}(h_0 v_0) + \frac{h_0 v_0}{r} = 0 \quad [37]$$

$$\frac{\partial v_0}{\partial r} = 0 \quad [38]$$

From Equation [38] we see that v_0 is a function of a only. This justifies the assertion made in section 3 that u_0 was zero in the plastic domain of the elastic-plastic slab. For, since v_0 is zero in the elastic domain, continuity demands it be zero in the plastic

[8] Reference (7), p. 99.

domain at $r = \rho$. Then, since it is independent of r, it is zero throughout the plastic domain. Finally, if the velocity v_0 is always zero, the displacement u_0 is also zero.

However, once the slab becomes entirely plastic, there is no longer any boundary condition at $r = \rho$. Instead, it follows from our definition of "time" as the radius of the cutout that the velocity at the cutout $r = a$ must be 1, and hence

$$v_0 = 1 \quad [39]$$

throughout the slab.

The displacements in the slab will be defined if we know the instantaneous position of each particle as a function of the initial position of that particle and the time a. Since the velocity is the time derivative of position[9]

$$v_0 = \frac{dr}{da} \quad [40]$$

Combining Equations [40] and [39], and integrating, we obtain

$$r = R_0 + a - a_0 \quad [41]$$

where R_0 is the initial position of the particle.

The substitution of Equation [39] into [37] yields a first-order equation for h_0, the solution to which is

$$h_0 = \varphi(a - r)/r \quad [42]$$

Here φ is an arbitrary function of one variable which is determined from the relation

$$h_0(r, a_0) = \varphi(a_0 - r)/r = H_0 \quad [43]$$

Thus

$$\varphi(a - r) = (a_0 - a + r)H_0$$

and

$$h_0(r, a) = \frac{r - a + a_0}{r} H_0 = \frac{R_0}{r} H_0 \quad [44]$$

Substituting Equation [44] into the equilibrium Equation [36] and integrating, we obtain the dimensionless radial stress

$$\sigma_1 = \frac{r - a - (a - a_0)\log(r/a)}{r - a + a_0} \quad [45]$$

It can be shown that σ_1 always lies between 0 and 1, so that the yield condition $s = \mu$ is the correct one throughout the plastic flow.

The load λ necessary to maintain plastic flow at a given displacement a is found from the boundary condition Equation [5b] and the values of σ_1, d, and h_0 given by Equations [45], [41], and [44], respectively

$$\lambda_0 = h[d(a), a]\,\sigma_1[d(a), a]$$

$$= \left[d_0 - a_0 - (a - a_0)\log\frac{a - a_0 + d_0}{a}\right] \Big/ (a - a_0 + d_0) \quad [46]$$

In Fig. 2 we have plotted λ as a function of a/d_0 for selected values of a_0/d_0.

7 Analysis of Strains

Equations [32] express the complete solution of the elastic-plastic problem to second-order terms in the small parameter $\mu = k/G$. In terms of the quantities given in Equations [32], the averaged normal strain components are

[9] For a further discussion of this point, see reference (7), section 18.

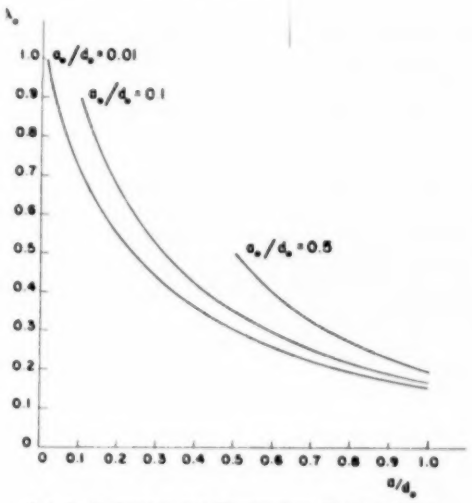

Fig. 2 Pressure for Continuing Plastic Flow

$$\epsilon_r = \frac{\partial u}{\partial r}, \qquad \epsilon_\theta = \frac{u}{r}, \qquad \epsilon_z = \frac{\text{change in thickness}}{\text{current thickness}} = \frac{h - H_0}{h} = 1 - H_0/h \quad [47]$$

while the shearing strains, of course, vanish. For $a_0/d_0 > 0.01$, and μ of order 0.001, it is readily verified that the second term is small compared to the first for each one of the stress and strain components, and for all values of r and ρ. Further, it is apparent that the absolutely largest principal strain is the circumferential strain ϵ_θ. For a given value of ρ, the maximum value of this function occurs at the inner boundary. To first-order terms in μ, it follows from Equation [32g] that this strain is

$$\epsilon_\theta(a_0, \rho) = (2\mu/3)\left(1 + \log\frac{\rho}{a_0}\right) \quad [48]$$

This is obviously an increasing function of ρ, so that the absolutely largest principal strain which occurs in the slab in the course of loading is

$$\epsilon^p = \epsilon_\theta(a_0, d_0) = (2\mu/3)\left(1 + \log\frac{d_0}{a_0}\right) \quad [49]$$

To obtain a criterion of strain independent of the particular material, let the absolutely largest strain in the fully elastic slab be denoted by ϵ^e, and define the plastic-elastic strain ratio η by $\eta = \epsilon^p/\epsilon^e$. Since, to first-order terms

$$\epsilon^e = \epsilon_\theta(a_0, a_0) = 2\mu/3 \quad [50]$$

it follows from Equation [49] that

$$\eta = 1 + \log d_0/a_0 \quad [51]$$

In Fig. 3 we have plotted η as a function of a_0/d_0. It is seen that for a_0/d_0 greater than 0.01, η is less than 6. Therefore, for the slabs thus far considered, we may conclude that the maximum strain for any load less than the yield load is not so large as to make the slab unserviceable.

8 Analysis of Small Cutouts

Let us consider a sequence of slabs of the same initial thick-

ness and outer radius, but with inner radius a_0 tending to zero. To discuss qualitatively the relation of the solution Equations [32] to this problem, let us consider the behavior of $\epsilon_\theta = u/r$, as given by Equations [32*c*, *g*]. Since the maximum value of strain occurs at the inner radius, let

$$r = a \simeq a_0 + u_1(a_0)$$

in Equation [32*g*], and then let a_0 tend to zero. It is readily seen that not only does the leading coefficient u_1/a_0 tend to infinity, but the ratio of the second term to the leading term, u_2/u_1 tends to infinity. Therefore it is most unlikely that the series expression for ϵ_θ would converge, and hence the entire method of solution breaks down.

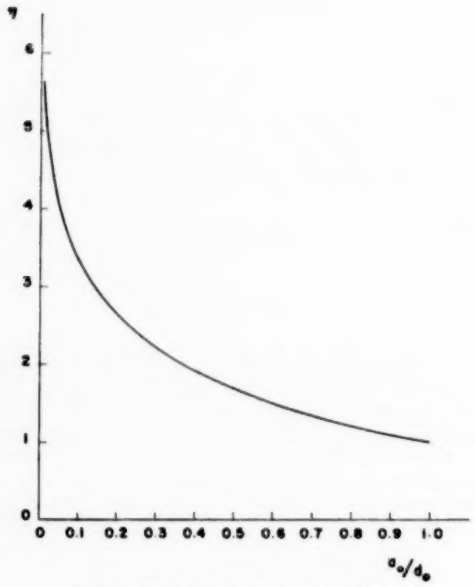

FIG. 3 PLASTIC-ELASTIC STRAIN RATIO

Let us now view the problem somewhat differently. Assign to r a fixed but arbitrarily small value in each slab of the sequence, and then let a_0 tend to zero. The limits are easily computed, and we find that $\epsilon_\theta = \mu/3 + \mu^2 \cdot 0$ independently of r and ρ and in both the elastic and plastic domains.

To deduce a reasonable hypothesis to account for the preceding results, let us postulate a Saint Venant's principle (8) for our elastic-plastic material. Thus we assume that any actual set of tractions may be replaced by any other statically equivalent set of tractions without appreciable change except in the immediate neighborhood of the points of application. A possible explanation of the divergence of the power series in the immediate neighborhood of the cutout is that the stresses will produce displacements of such a nature that the resulting configuration is no longer well represented by plane stress. In any event, since at any finite distance from the cutout the series does appear to converge rapidly, it follows from the Saint Venant's principle that the solution there is still valid.

Further support for this viewpoint is obtained from an analysis of the load λ. The first approximation to the load λ^* at which the inner boundary first becomes plastic is (see Equation [21])

$$\lambda_0^* = \frac{1}{2}(1 - a_0^2/d_0^2) \quad [52]$$

As a_0 tends to zero, we see that even for an infinitesimal hole, the maximum fully elastic load is only 1/2, while (see Equation [33]) the maximum load without yielding is 1. Thus the slab is partially plastic during approximately half of its loading history.

On the other hand, let ρ have a fixed, but arbitrarily small value for each slab. Then, as a_0 tends to zero, it follows from Equation [32*i*] that, to a first approximation, λ tends to 1. In other words, although the slab becomes plastic at the inner boundary for a load 1/2, the plastic zone is purely local until the yield load $\lambda = 1$ is reached.

9 CONCLUSIONS

The fully elastic, elastic-plastic, and fully plastic solutions to the problem of an annular slab under uniform radial tension on its outer edge have been obtained. It has been shown that except for a purely local phenomenon in the vicinity of very small cutouts ($a_0/d_0 < 0.01$), the plastic strains at collapse are not excessively large compared to the elastic strains.

It was shown that as the load increases, a plastic zone will begin to form at a load considerably less than the final yield load. However, the plastic zone grows slowly at first, and the strains remain small. This result is consistent with a result obtained by Southwell (9) for the torsion of a hollow rectangular prism, where small strains were found sufficient to relieve a large stress concentration.

It was also shown that once the load reaches the yield load, unrestricted plastic flow will take place, and a continually smaller load will be necessary to maintain the plastic flow. The primary reason is that the thickness of the slab decreases as the flow progresses, and hence cannot support the original load. This is in marked contrast to the case of internally applied pressure (4) where the slab thickens near the hole and hence can support an increasingly large traction.

BIBLIOGRAPHY

1 "Limit Design of Reinforcements of Cutouts in Slabs," by P. G. Hodge, Jr., and W. Prager, Tech. Rep. B11-2, Contract N7onr-35810, Brown University, Providence, R. I., 1951.

"Upper and Lower Bounds on the Yield Load of a Square Slab With a Centered Circular Cutout," by P. G. Hodge, Jr., Tech. Rep. B11-7, N7onr-35810, Brown University, 1952.

2 "Limit Design of Full Reinforcement of Circular Cutout in Uniform Slab," by H. J. Weiss, W. Prager, and P. G. Hodge, Jr., JOURNAL OF APPLIED MECHANICS, Trans. ASME, vol. 74, 1952, pp. 397–401.

3 "The Interpretation of Failure Loads in the Plastic Theory of Continuous Frames and Beams," by P. S. Symonds and B. G. Neal, *Journal of the Aeronautical Sciences*, vol. 19, 1952, pp. 15–22.

4 "Plastic Distortion of Non-Uniform Sheets," by R. Hill, *Philosophical Magazine*, series 7, vol. 40, 1949, pp. 971–983.

5 "Mathematical Theory of Elasticity," by I. S. Sokolnikoff, McGraw-Hill Book Company, Inc., New York, N. Y., 1946.

6 "Mechanik der Plastischen Formaenderung von Kristallen," by R. von Mises, *Zeitschrift angewandte Mathematik und Mechanik*, vol. 8, 1928, pp. 161–185.

7 "Theory of Perfectly Plastic Solids," by W. Prager and P. G. Hodge, Jr., John Wiley and Sons, Inc., New York, N. Y., 1951.

8 "Mémoires sur la torsion des prism avec des configuration sur leur flexions, ainsi que sur l'équilivre interieur des solides élastique en générale," by B. de Saint Venant, Mémoires présentés par divers savants à l'Académie des sciences de l'Institut de France, vol. 14, 1856, p. 345.

9 "On the Computation of Strain and Displacement in a Prism Plastically Strained by Torsion," by R. V. Southwell, *Quarterly Journal of Mechanics and Applied Mathematics*, vol. 2, 1949, pp. 385–397.

Response of an Elastic Cylindrical Shell to a Transverse, Step Shock Wave

By R. D. MINDLIN[1] and H. H. BLEICH,[2] NEW YORK, N. Y.

A plane shock wave in an acoustic medium encounters a long cylindrical shell whose axis is parallel to the wave front. An approximate mathematical solution is obtained for the elastic response of the shell.

Introduction

In this paper there is described a mathematical study of the response of a cylindrical shell to a shock wave. The shell is elastic, circular in cross section, homogeneous, and infinitely long. Its motions are restricted to dilatational, translational, and inextensional-flexural modes. The shell is submerged in an acoustic fluid, i. e., one whose motions conform to the linear theory of waves of expansion. The shock wave is assumed to be plane, with its wave front parallel to the axis of the shell.

By means of an approximation, which is valid for the early stages, the potential of the diffraction and radiation is eliminated between the simultaneous equations which couple the generalized co-ordinates of the shell and the fluid. As a result, a simple differential equation is obtained for each generalized co-ordinate describing the motion of the shell. The solution is reduced to a definite integral during the time of transit of the shock-wave front across the shell and, for the case of the step shock wave, is expressed in terms of tabulated functions thereafter. Explicit formulas are given for the displacement, velocity, acceleration, and pressure associated with each mode of motion of the shell.

Equations Governing Interaction Between Shell and Fluid

Let w be the radial displacement of the shell and Z the pressure on it, both positive inward, Fig. 1. Let

$$w = \sum_{n=0}^{\infty} q_n(t) \cos n\theta \quad [1]$$

$$Z = \sum_{n=0}^{\infty} Q_n(t) \cos n\theta \quad [2]$$

Then, one form of the equation of cylindrical motion of a shell may be written

$$\ddot{q}_n + \omega_n^2 q_n = Q_n/m_n \quad [3]$$

where ω_n are the natural frequencies of cylindrical vibration of the shell under a uniform pressure (but not submerged) and

$$m_n = m(n^2 + 1)/n^2, \ n > 0 \quad [4]$$

$$m_0 = m, \ n = 0 \quad [5]$$

where m is the mass per unit of surface area of the shell.

The mode $n = 0$ is purely dilatational; $n = 1$ is translational, parallel to $\theta = 0$; $n > 1$ are inextensional, flexural modes. Extensional deformations in $n > 0$ are neglected.

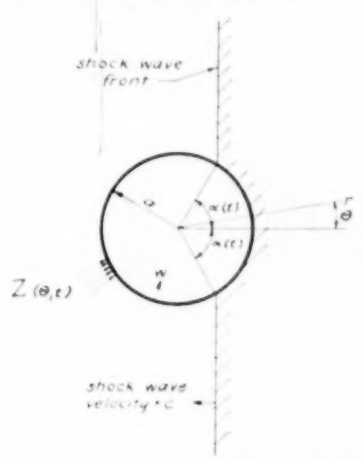

Fig. 1 Geometry of Problem Considered

The pressure on the shell is due to the shock wave and to the waves reflected and radiated from the vibrating shell:

$$Z = p(\theta, t) + \rho\dot{\varphi}(a, \theta, t) \quad [6]$$

where $p(\theta, t)$ is the shock-wave pressure at the surface of the shell ($r = a$), ρ is the density of the fluid, and $\varphi(r, \theta, t)$ is the velocity potential of the reflected and radiated waves, governed by the equation

$$c^2\nabla^2\varphi = \ddot{\varphi} \quad [7]$$

where c is the velocity of sound in the fluid.

Let

$$p(\theta, t) = \sum_{n=0}^{\infty} P_n(t) \cos n\theta \quad [8]$$

$$\varphi(r, \theta, t) = \sum_{n=0}^{\infty} \psi_n(r, t) \cos n\theta \quad [9]$$

Then

$$Q_n(t) = P_n(t) + \rho\dot{\psi}_n(a, t) \quad [10]$$

so that, from Equation [3], on $r = a$

$$\ddot{q}_n + \omega_n^2 q_n = (P_n + \rho\dot{\psi}_n)/m_n \quad [11]$$

This is the first of the two equations controlling the interaction between the shell and the fluid.

---

[1] Professor of Civil Engineering, Columbia University. Member ASME.

[2] Professor of Civil Engineering, Columbia University.

Contributed by the Applied Mechanics Division and presented at the Annual Meeting, New York, N. Y., November 30–December 5, 1952, of The American Society of Mechanical Engineers.

Discussion of this paper should be addressed to the Secretary, ASME, 29 West 39th Street, New York, N. Y., and will be accepted until July 10, 1953, for publication at a later date. Discussion received after the closing date will be returned.

Note: Statements and opinions advanced in papers are to be understood as individual expressions of their authors and not those of the Society. Manuscript received by ASME Applied Mechanics Division, July 14, 1952. Paper No. 52—A-19.

The radial velocity of a point on the shell must equal the sum of the radial components of the particle velocities of the shock wave and the diffracted wave. Thus

$$\dot{w} = v(\theta, t) + \frac{\partial \varphi(a, \theta, t)}{\partial a} \quad [12]$$

where $v(\theta, t)$ is the radial component of the particle velocity in the shock wave at $r = a$. Let

$$\rho c v(\theta, t) = \sum_{n=0}^{\infty} V_n(t) \cos n\theta \quad [13]$$

Then, on $r = a$

$$\dot{q}_n = \frac{V_n}{\rho c} + \frac{\partial \psi_n}{\partial a} \quad [14]$$

This is the second of the two equations governing the interaction between the shell and the fluid.

The essential difficulty, in finding the response of the shell, is the awkwardness involved in the process and result of eliminating ψ_n between Equations [11] and [14].

Approximate Equation of Motion During Early Stages

The process of eliminating ψ_n is begun by expanding it in Fourier series over a time interval as yet unspecified

$$\psi_n(r, t) = \sum_{s=1}^{\infty} \chi_{ns}(r) e^{i\xi_s ct/a} \quad [15]$$

where

$$\xi_s = ks\pi/2, \quad s = 1,2, \ldots, \quad [16]$$

and k is a number which fixes the interval of expansion. Then, from Equations [7], [9] and [15]

$$\frac{d^2\chi_{ns}}{dr^2} + \frac{1}{r}\frac{d\chi_{ns}}{dr} + \left(\frac{\xi_s^2}{a^2} - \frac{n^2}{r^2}\right)\chi_{ns} = 0 \quad [17]$$

The solution of Equation [17] for diverging waves is

$$\chi_{ns} = A_{ns} H_n(\xi_s r/a) \quad [18]$$

where H_n is the Hankel function of the second kind (ordinarily written $H_n^{(2)}$). Hence, during $0 \leqq t \leqq 2a/kc$

$$\psi_n(a, t) = \sum_{s=1}^{\infty} A_{ns} H_n(\xi_s) e^{i\xi_s ct/a} \quad [19]$$

$$\dot{\psi}_n(a, t) = i(c/a) \sum_{s=1}^{\infty} A_{ns}\xi_s H_n(\xi_s) e^{i\xi_s ct/a} \quad [20]$$

$$\frac{\partial \psi_n(a, t)}{\partial a} = \frac{1}{a} \sum_{s=1}^{\infty} A_{ns}\xi_s H_n'(\xi_s) e^{i\xi_s ct/a} \quad [21]$$

where $H_n'(\xi_s) = \partial H_n(\xi_s)/\partial \xi_s$.

The approximation is now made that ξ_s is large enough so that

$$H_n(\xi_s) \approx iH_n'(\xi_s), \quad (\xi_s \gg 1). \quad [22]$$

For the later terms ($s \gg 1$) of the expansion, Equation [15], the approximation is very good. For the early terms, the value of k, which determines the interval of expansion, plays an important role. The larger the value of k the shorter is the interval of expansion and the better is the approximation. Thus the solution to be obtained may be expected to be good at the early stages of envelopment and to become progressively poorer at later times.

To this approximation, then, from Equations [20] and [21]

$$\frac{\partial \psi_n}{\partial a} = -\frac{1}{c}\frac{\partial \psi_n}{\partial t} \quad [23]$$

Thus the main effect of the approximation is to give the reflection and radiation, associated with each mode of the shell, the propagation characteristics of plane waves rather than cylindrical waves.

From Equations [10], [14], and [23]

$$Q_n = P_n + V_n - \rho c \dot{q}_n \quad [24]$$

and hence from Equation [3]

$$\ddot{q}_n + \frac{\rho c}{m_n}\dot{q}_n + \omega_n^2 q_n = \frac{P_n + V_n}{m_n} \quad [25]$$

Thus the response of the shell to a given shock wave is obtained simply by integrating Equation [25] with the appropriate $P_n + V_n$. The fluid pressure on the shell is then obtained from Equation [24].

There is no difficulty in solving Equation [25] for quite general shock-wave properties, since only one integration is involved. However, a minimum of computations is required for a step wave.

Form of $P_n + V_n$ for a Step Shock Wave

The pressure in a step shock wave, at the periphery of the shell, is

$$p(\theta, t) = \left\{ \begin{array}{l} p, \ -\alpha \leqq \theta \leqq \alpha \\ 0, \ \alpha \leqq \theta \leqq 2\pi - \alpha \end{array} \right\}, \ 0 \leqq t \leqq 2a/c \quad [26]$$

$$p(\theta, t) = p, \quad -\pi \leqq \theta \leqq \pi, \quad t \geqq 2a/c$$

where p is the constant peak pressure and

$$\alpha = \alpha(t) = \cos^{-1}(1 - ct/a) \quad [27]$$

The particle velocity at $r = a$ is

$$v(\theta, t) = p(\theta, t) \cos\theta/\rho c \quad [28]$$

Inserting Equations [26] and [28] into [8] and [13], the usual methods of expansion in series lead to the following:

(*a*) During $0 \leqq t \leqq 2a/c$

$$P_n = \left\{ \begin{array}{ll} \dfrac{p\alpha}{\pi}, & n = 0 \\ \dfrac{2p}{n\pi} \sin n\alpha, & n > 0 \end{array} \right\} \quad [29]$$

$$V_n = \left\{ \begin{array}{ll} \dfrac{p}{\pi} \sin\alpha, & n = 0 \\ \dfrac{p}{\pi}(\alpha + \sin\alpha\cos\alpha), & n = 1 \\ \dfrac{p}{\pi}\left[\dfrac{\sin(n-1)\alpha}{n-1} + \dfrac{\sin(n+1)\alpha}{n+1}\right], & n > 1 \end{array} \right\} \quad [30]$$

(*b*) During $t \geqq 2a/c$

$$P_n = \left\{ \begin{array}{l} p, \ n = 0 \\ 0, \ n > 0 \end{array} \right\} \quad [31]$$

$$V_n = \left\{ \begin{array}{l} 0, \ n = 0 \\ p, \ n = 1 \\ 0, \ n > 1 \end{array} \right\} \quad [32]$$

It is interesting to observe that the impulse delivered to each mode contains a factor

$$\int_0^{2a/c} (P_n + V_n)dt = \left\{ \begin{array}{ll} 3pa/2c, & n = 0 \\ 2pa/c, & n = 1 \\ pa/2c, & n = 2 \\ 0, & n \geq 3 \end{array} \right\} \quad [33]$$

DILATATIONAL MODE ($n = 0$)

In Equation [25] let $n = 0$ and

$$\beta_0 = \rho c/2m\omega_0 \quad [34]$$

Then the equation of motion of the dilatational mode becomes

$$\ddot{q}_0 + 2\beta_0\omega_0\dot{q}_0 + \omega_0^2 q_0 = (P_0 + V_0)/m \quad [35]$$

Now, β_0 is the fraction of critical damping. This is greater than unity in the applications contemplated. Hence an appropriate form of the solution of Equation [35] is

$$m\omega_0\sqrt{\beta_0^2 - 1}\; q_0 = \int_0^t [P_0(\lambda) + V_0(\lambda)]e^{-\beta_0\omega_0(t-\lambda)} \sinh[\omega_0\sqrt{\beta_0^2 - 1}\,(t - \lambda)]d\lambda \quad [36]$$

Let

$$\gamma = \cos^{-1}(1 - c\lambda/a) \quad [37]$$

$$S_0(\gamma) = P_0(\lambda) + V_0(\lambda) = \left\{ \begin{array}{ll} \dfrac{p}{\pi}(\gamma + \sin\gamma), & 0 \leq \gamma \leq \pi \\ p, & \gamma \geq \pi \end{array} \right\} \quad [38]$$

Then

$$cd\lambda = a \sin\gamma d\gamma \quad [39]$$

$$c(t - \lambda) = a(\cos\gamma - \cos\alpha) \quad [40]$$

and Equation [36] takes the form

$$2cm\omega_0\sqrt{\beta_0^2 - 1}\; q_0 = ae^{z_0\cos\alpha}\int_0^\alpha S_0(\gamma)\sin\gamma e^{-z_0\cos\gamma}d\gamma - ae^{z_0\cos\alpha}\int_0^\alpha S_0(\gamma)\sin\gamma e^{-z_0\cos\gamma}d\gamma \quad [41]$$

where

$$\left. \begin{array}{l} z_0 = \dfrac{\omega_0 a}{c}(\beta_0 + \sqrt{\beta_0^2 - 1}), \\ \hat{z}_0 = \dfrac{\omega_0 a}{c}(\beta_0 - \sqrt{\beta_0^2 - 1}), \end{array} \right\} \quad [42]$$

During the time of transit ($0 \leq \alpha \leq \pi$, i.e., $0 \leq t \leq 2a/c$) of the shock-wave front across the shell, the integrals in Equation [41] are incomplete modified Bessel functions of the first kind. These functions do not appear to be tabulated, but the integrations are performed numerically without difficulty. Upon and after full envelopment ($\alpha \geq \pi$, i. e., $t \geq 2a/c$) the integrals have the forms

$$\left. \begin{array}{l} \displaystyle\int_0^\pi \gamma \sin\gamma e^{-z\cos\gamma}d\gamma = \pi z^{-1}[e^z - I_0(z)] \\ \displaystyle\int_0^\pi \sin^2\gamma e^{-z\cos\gamma}d\gamma = \pi z^{-1}I_1(z) \\ \displaystyle\int_\pi^\alpha \sin\gamma e^{-z\cos\gamma}d\gamma = z^{-1}(e^{-z\cos\alpha} - e^z) \end{array} \right\} \quad [43]$$

where $I_n(z)$ is the modified Bessel function of the first kind.

The solution of Equation [35] after envelopment is then

$$\frac{2cm\omega_0\sqrt{\beta_0^2 - 1}}{ap}\; q_0 = \frac{1}{\hat{z}_0} - \frac{1}{z_0} - \frac{e^{z_0\cos\alpha}}{z_0}[I_0(\hat{z}_0) - I_1(\hat{z}_0)] + \frac{e^{z_0\cos\alpha}}{z_0}[I_0(z_0) - I_1(z_0)] \quad [44]$$

where

$$\cos\alpha = 1 - ct/a \quad [45]$$

Noting that

$$\left. \begin{array}{l} z_0 - \hat{z}_0 = \dfrac{2\omega_0 a}{c}\sqrt{\beta_0^2 - 1} \\ z_0\hat{z}_0 = \left(\dfrac{\omega_0 a}{c}\right)^2 \end{array} \right\} \quad [46]$$

and, also, setting

$$q_0^* = p/m\omega_0^2 \quad [47]$$

i.e., q_0^* is the static displacement of the shell under a uniform pressure p, the solution after envelopment may be written

$$\frac{q_0}{q_0^*} = 1 - \frac{z_0 e^{\hat{z}_0\cos\alpha}}{z_0 - \hat{z}_0}[I_0(\hat{z}_0) - I_1(\hat{z}_0)] + \frac{\hat{z}_0 e^{z_0\cos\alpha}}{z_0 - \hat{z}_0}[I_0(z_0) - I_1(z_0)] \quad [48]$$

In typical applications $z_0 \gg \hat{z}_0$ and $z_0 \gg 1$. Then $I_0(z_0) - I_1(z_0) \ll 1$ and $z_0\cos\alpha$ is large and negative. Hence the second line of Equation [48] is small and vanishes rapidly. Since $I_0(\hat{z}_0) > I_1(\hat{z}_0)$, the displacement (and therefore the strain) at the instant of complete envelopment is less than the static displacement under the same pressure, but is increasing; and the difference $q_0 - q_0^*$ diminishes essentially exponentially with time constant $a/c\hat{z}_0$.

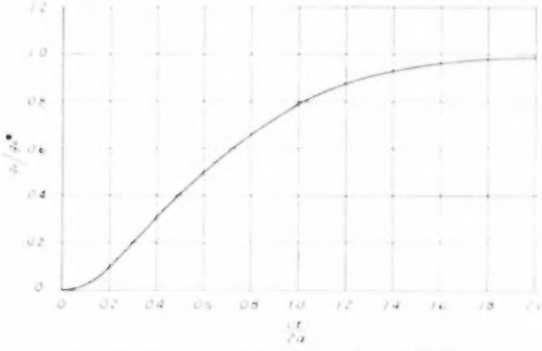

FIG. 2 DISPLACEMENT OF DILATATIONAL MODE
(q_0^* = displacement under static pressure p.)

A typical displacement response (q_0) is illustrated in Fig. 2 for $z_0 = 8.40$, $\hat{z}_0 = 1.33$. The displacement increases almost linearly with time up to 80 per cent of the static displacement at the time of full envelopment. Thereafter the displacement approaches the static displacement with a time constant of about 40 per cent of the transit time.

The ratio of the velocity ($\dot{q}_0$) of the dilatational mode to the particle velocity ($p/\rho c$) in the shock wave is readily found to be, during the transit time

$$\frac{\rho c\dot{q}_0}{p} = \frac{z_0 + \hat{z}_0}{p(z_0 - \hat{z}_0)}\left[-\hat{z}_0 e^{\hat{z}_0\cos\alpha}\int_0^\alpha S_0(\gamma)e^{-\hat{z}_0\cos\gamma}\sin\gamma d\gamma + z_0 e^{z_0\cos\alpha}\int_0^\alpha S_0(\gamma)e^{-z_0\cos\gamma}\sin\gamma d\gamma\right] \quad [49]$$

and, after the transit time

$$\frac{\rho c\dot{q}_0}{p} = \frac{z_0 + \hat{z}_0}{z_0 - \hat{z}_0}\{e^{\hat{z}_0\cos\alpha}[I_0(\hat{z}_0) - I_1(\hat{z}_0)] - e^{z_0\cos\alpha}[I_0(z_0) - I_1(z_0)]\} \quad [50]$$

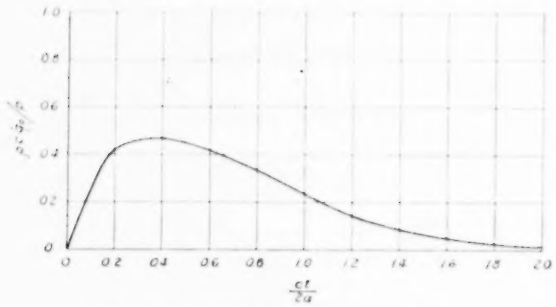

FIG. 3 VELOCITY OF DILATATIONAL MODE
($p/\rho c$ = particle velocity in shock wave.)

This is illustrated in Fig. 3.

The pressure in the dilatational mode is simply

$$Q_0 = P_0 + V_0 - \rho c \dot{q}_0 \quad \ldots\ldots [51]$$

and the acceleration is given by

$$\frac{2a\rho\ddot{q}_0}{p} = 2(z_0 + \bar{z}_0)\left(\frac{Q_0}{p} - \frac{q_0}{q_0^*}\right) \quad \ldots\ldots [52]$$

These are illustrated in Figs. 4 and 5.

It may be seen that, despite the apparent limitation of the validity of the solution to short times, all the results for the dilatational mode approach the correct limits for large t.

TRANSLATIONAL MODE ($n = 1$)

In Equation [25] set $n = 1$ and note that $m_1 = 2m$ and $\omega_1 = 0$. Thus the equation of motion of the translational mode is

$$\ddot{q}_1 + \frac{\rho c}{2m}\dot{q}_1 = \frac{P_1 + V_1}{2m} \quad \ldots\ldots [53]$$

Hence the velocity is given by

$$\rho c \dot{q}_1 = z_1 e^{z_1 \cos\alpha} \int_0^\alpha S_1(\gamma) \sin\gamma e^{-z_1\cos\gamma}\, d\gamma \quad \ldots [54]$$

where

$$z_1 = \rho a/2m \quad \ldots\ldots [55]$$

$$S_1(\gamma) = \begin{cases} \dfrac{p}{\pi}(\gamma + 2\sin\gamma + \sin\gamma\cos\gamma), & 0 \leq \gamma \leq \pi \\ p, & \gamma \geq \pi \end{cases} \quad \ldots [56]$$

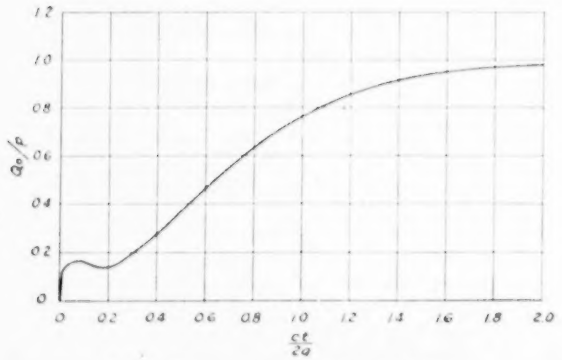

FIG. 4 PRESSURE IN DILATATIONAL MODE

During the transit time the integral in Equation [54] is again composed of incomplete Bessel functions, but it can easily be integrated numerically, especially since $z_1 = 1$ for a body in neutral buoyancy; i.e., only one integration has to be performed for all floating shells.

For the period $t \geq 2a/c$ there are four integrals in Equation [54]. Three of them are identical with Equations [43] and the fourth is

$$\int_0^\pi \sin 2\gamma \sin\gamma e^{-z_1\cos\gamma}\, d\gamma = -2\pi z_1^{-1} I_2(z_1) \quad \ldots [57]$$

Hence, for $t \geq 2a/c$

$$\rho c\dot{q}_1/p = 1 - e^{z_1\cos\alpha}[I_0(z_1) - 2I_1(z_1) + I_2(z_1)] \quad \ldots [58]$$

For the neutrally buoyant body ($z_1 = 1$) the quantity in brackets in Equation [58] is 0.1. Thus the shell as a whole reaches $^9/_{10}$ of the particle velocity in the shock wave at the instant of complete envelopment and thereafter approaches the particle velocity exponentially, with time constant a/c, i.e., half the transit time. (The translational velocity during and after envelopment is shown in Fig. 6.)

The displacement of the shell at the end of the transit time is found to be

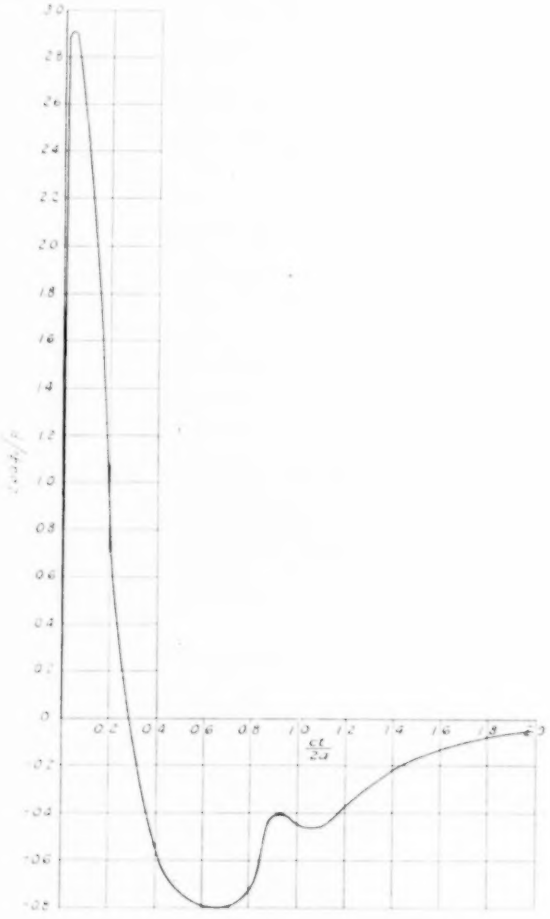

FIG. 5 ACCELERATION IN DILATATIONAL MODE
($p/2\rho a$ = uniform acceleration which would produce particle velocity in time $2a/c$.)

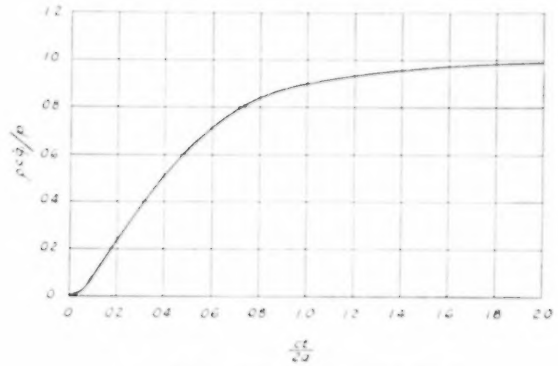

FIG. 6 VELOCITY IN TRANSLATIONAL MODE
($p/\rho c$ = particle velocity in shock wave.)

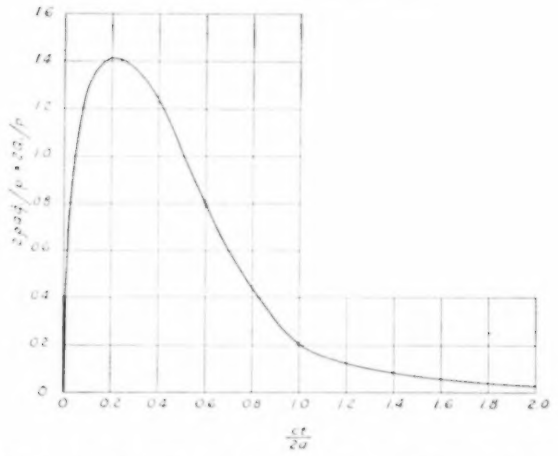

FIG. 7 ACCELERATION AND PRESSURE IN TRANSLATIONAL MODE

$$q_1 = 1.1\,\frac{pa}{\rho c^2}, \qquad t = 2a/c \qquad [59]$$

The translational acceleration is found by substituting Equations [54] and [58] into [53] and is plotted in Fig. 7 as a ratio to

$$\ddot{q}_1^* = p/2\rho a \qquad [60]$$

i.e., to the constant acceleration, during the transit time, that would produce a shell velocity equal to the particle velocity in the shock wave.

The generalized pressure in the translational mode is given by

$$Q_1 = m_1\ddot{q}_1 = 2m\ddot{q}_1 \qquad [61]$$

corresponding to a real pressure distribution

$$Z_1 = Q_1 \cos\theta \qquad [62]$$

Thus for a shell in neutral buoyancy

$$\frac{Q_1}{p} = \frac{1}{2}\,\frac{\ddot{q}_1}{\ddot{q}_1^*} \qquad [63]$$

i.e., the ordinates in Fig. 7 are also equal to $2Q_1/p$.

As in the case of the dilatational mode, the solution for the translational mode also approaches the correct limit for large t, despite the approximation.

FLEXURAL MODES ($n \geq 2$)

The solution of Equation [25] for $n \geq 2$ may be written

$$q_n = \frac{ap}{2\pi c m_n \omega_n \sqrt{\beta_n^2 - 1}}\,(B_n e^{z_n \cos\alpha} - B_n e^{\bar{z}_n \cos\alpha}) \qquad [64]$$

where

$$\beta_n = \rho c/2m_n\omega_n \qquad [65]$$

$$\left.\begin{aligned} z_n &= \frac{\omega_n a}{c}\,(\beta_n + \sqrt{\beta_n^2 - 1}) \\ \bar{z}_n &= \frac{\omega_n a}{c}\,(\beta_n - \sqrt{\beta_n^2 - 1}) \end{aligned}\right\} \qquad [66]$$

$$B_n = \left\{\begin{aligned} &\frac{\pi}{p}\int_0^{\alpha} (P_n + V_n)\sin\gamma e^{-z_n\cos\gamma}\,d\gamma, \quad 0 \leq \alpha \leq \pi \\ &\frac{2\pi(-1)^n}{z_n}\,[I_n'(z_n) - I_n(z_n)], \qquad \alpha \geq \pi \end{aligned}\right\} \qquad [67]$$

and B_n is the same as B_n except that z_n is replaced by $\bar{z}_n$.

A comparison of the displacement in a flexural mode with that in the dilatational mode has little significance, but it is interesting to compare the maximum stress σ_n, in the flexural mode with the stress σ_0^* in the dilatational mode under constant pressure p. The former is

$$\sigma = Ed/R_n \qquad [68]$$

where

$$\frac{1}{R_n} = \frac{n^2 - 1}{a^2}\,q_n \qquad [69]$$

is the change of curvature, E is the appropriate modulus of elasticity, and d is the distance from the neutral axis to the extreme fiber. Also

$$\sigma_0^* = pa/h \qquad [70]$$

where h is the shell thickness. Hence, after some rearrangement

$$\frac{\sigma_n}{\sigma_0^*} = \frac{dhE(n^2 - 1)(z_n + \bar{z}_n)}{\pi a^2 \kappa (z_n - \bar{z}_n)}\,(B_n e^{z_n\cos\alpha} - B_n e^{\bar{z}_n\cos\alpha}) \qquad [71]$$

where $\kappa = \rho c^2$ is the bulk modulus of the fluid. This ratio is plotted in Fig. 8 for the mode $n = 2$ and $\bar{z}_2 = 0.01$, $z_2 = 7.0$.

The later portion of the curve in Fig. 8 is dashed to indicate that it is unreliable as a result of the approximation.

The velocity in $n \geq 2$ is given by

$$\frac{\rho c\dot{q}_n}{p} = \frac{z_n + \bar{z}_n}{\pi(z_n - \bar{z}_n)}\,(z_n B_n e^{z_n\cos\alpha} - \bar{z}_n B_n e^{\bar{z}_n\cos\alpha}) \qquad [72]$$

This is plotted in Fig. 9 for $n = 2$.

The pressure is computed from

$$\frac{Q_n}{p} = \frac{P_n + V_n}{p} - \frac{\rho c\dot{q}_n}{p} \qquad [73]$$

and, finally, the acceleration, calculated from the preceding results is

$$\frac{\ddot{q}_n}{\ddot{q}_1^*} = 2(z_n + \bar{z}_n)\,\frac{Q_n}{p} + \frac{2z_n\bar{z}_n(z_n + \bar{z}_n)}{\pi(z_n - \bar{z}_n)}\,(B_n e^{z_n\cos\alpha} - \bar{B}_n e^{\bar{z}_n\cos\alpha}) \qquad [74]$$

The pressure and acceleration are plotted in Figs. 10 and 11 for $n = 2$.

Flexural Instability

After the diffraction effects are over, the flexural modes are

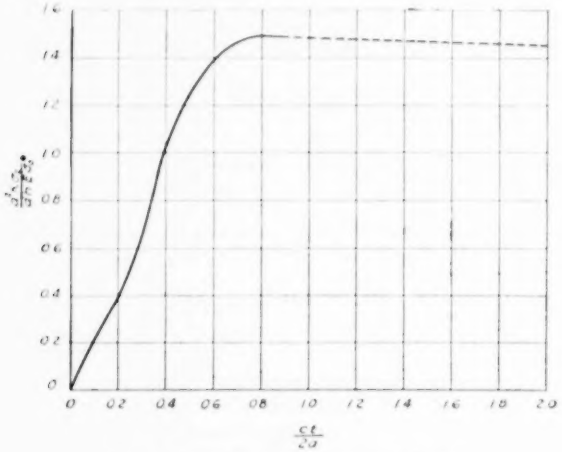

Fig. 8 Stress in First Flexural Mode

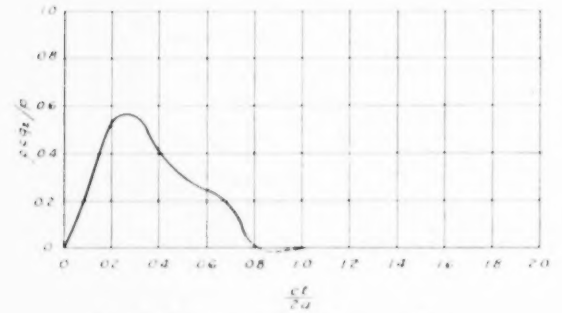

Fig. 9 Velocity in First Flexural Mode

essentially in a state of free vibration. In this case the solution takes a different form. Returning to Equation [15], let

$$\psi_n = \chi_n(r)e^{i\Omega_n t} \quad [75]$$

where Ω_n are the natural frequencies of the shell immersed in the fluid. Then the equation on χ_n becomes

$$\frac{d^2\chi_n}{dr^2} + \frac{1}{r}\frac{d\chi_n}{dr} + \left(\frac{\Omega_n^2}{c^2} - \frac{n^2}{r^2}\right)\chi_n = 0 \quad [76]$$

whence

$$\left.\begin{aligned} \psi_n(a, t) &= A_n H_n(\eta_n)e^{i\Omega_n t} \\ \dot{\psi}_n(a, t) &= i(c/a)A_n\eta_n H_n(\eta_n)e^{i\Omega_n t} \\ \frac{\partial\psi_n(a, t)}{\partial a} &= \frac{1}{a}A_n\eta_n H_n'(\eta_n)e^{i\Omega_n t} \end{aligned}\right\} \quad [77]$$

where $\eta_n = \Omega_n a/c$.

Noting that, for $n \geqq 2$, $P_n = V_n = 0$ in this interval, Equation [11] becomes

$$\ddot{q}_n + \omega_n^2 q_n = \rho\dot{\psi}_n/m_n \quad [78]$$

and Equation [14] may be written as

$$\ddot{q}_n = \partial\dot{\psi}_n/\partial a \quad [79]$$

But, from Equations [77]

$$\dot{\psi}_n = \frac{aH_n(\eta_n)}{\eta_n H_n'(\eta_n)}\frac{\partial\dot{\psi}_n}{\partial a} \quad [80]$$

Hence

$$\left[1 - \frac{\rho a H_n(\eta_n)}{m_n\eta_n H_n'(\eta_n)}\right]\ddot{q}_n + \omega_n^2 q_n = 0 \quad [81]$$

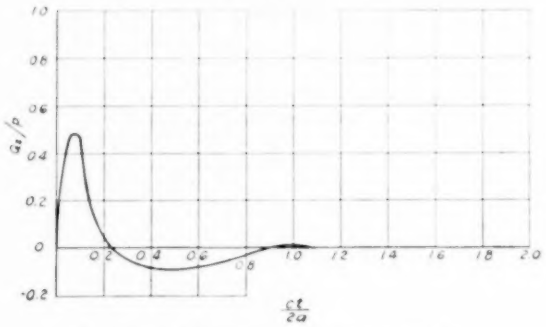

Fig. 10 Pressure in First Flexural Mode

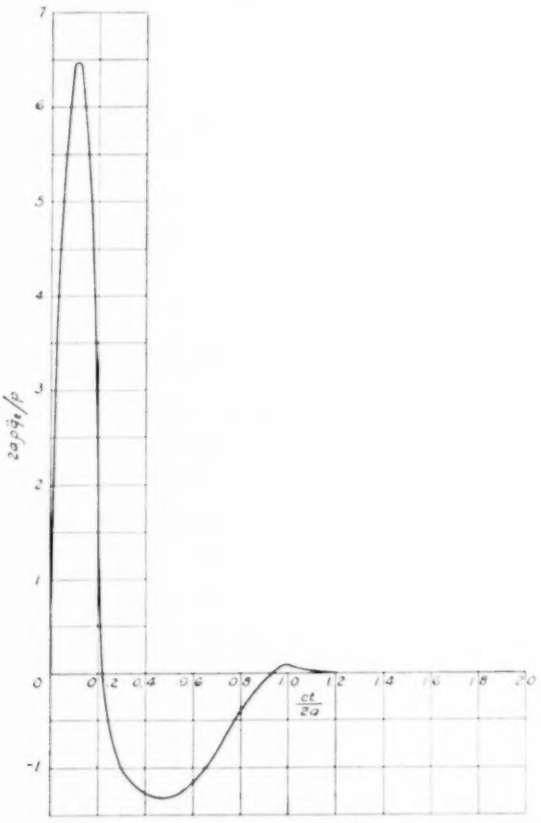

Fig. 11 Acceleration in First Flexural Mode

is the equation governing the free vibrations. This also gives the transcendental equation

$$\Omega_n^2\left[1-\frac{\rho a H_n(\eta_n)}{m_n \eta_n H_n'(\eta_n)}\right]=\omega_n^2 \quad \ldots\ldots\ldots [82]$$

whose roots determine the natural frequencies Ω_n of the submerged shell when the frequencies ω_n under a uniform pressure are known.

The flexural modes of greatest interest are the lower ones and for these η_n is small. But

$$\frac{H_n(\eta_n)}{\eta_n H_n'(\eta_n)} \backsimeq -\frac{1}{n}, \qquad \eta_n \ll 1 \quad \ldots\ldots\ldots [83]$$

Hence

$$\Omega_n^2 \approx \omega_n^2/(1+\rho a/n m_n) \quad \ldots\ldots\ldots [84]$$

Thus Ω_n is essentially real as long as the ratio of the pressure to the stiffness is small enough for ω_n to be real. In this case the solution of Equation [81] is oscillatory. If the pressure increases sufficiently ω_n, and hence Ω_n can become imaginary. Then the solution of Equation [81] becomes nonoscillatory and buckling ensues.

Acknowledgment

This investigation was supported by the Office of Naval Research under Contracts Nonr-266 (08 and 09) with Columbia University.

The Origin of Damping in High-Strength Ferromagnetic Alloys

By A. W. COCHARDT,[1] EAST PITTSBURGH, PA.

A theoretical analysis and test data are presented which explain the damping capacity of standard high-strength alloys in terms of the magnetostrictive effect. Conditions for obtaining maximum damping are described and the results of experiments are reported which provide a firm basis for the development of high-strength high-damping alloys.

Nomenclature

The following nomenclature is used in the paper:

δ = logarithmic decrement
U = elastic energy
V = volume
σ = normal stress
σ_m = maximum normal stress of cantilever beam
τ = shear stress
τ_m = maximum shear stress
E = Young's modulus
G = shear modulus
z = distance from neutral axis of cantilever beam
x = distance from clamped end of cantilever beam
y = deflection of cantilever beam
y_m = maximum deflection of cantilever beam
I = moment of inertia of rectangular cross section
m = mass per unit length
ω = circular frequency
M = bending moment
l = length
h = height
b = width
R = radius of cross section

Introduction

The significance of the damping capacity as an engineering property of materials has received widespread recognition in recent years. Wherever vibrational stresses are encountered (as in turbine, compressor, and propeller blades, shafts of various kinds, transmission cables, and so on) the damping capacity of a material may prove to be of more importance than such properties as fatigue strength (1, 2).[2] Despite the importance of damping capacity as a criterion for the selection of materials for machine and structural parts, relatively little work so far has been reported on the damping capacities of engineering alloys. The purpose of this paper is to describe the outcome of an investigation of magnetostrictive damping in high-strength ferromagnetic alloys.

During the last few decades, the origin of damping in metals has been traced to four sources; plastic flow (3), the thermoelastic effect (4), the magnetoelastic effect (5), and atomic diffusion (6). Plastic flow is certainly the most common cause of damping; in high-strength alloys, however, plastic flow occurs noticeably only at stress levels beyond those for which the structure is designed. Damping due to the thermoelastic effect becomes noticeable only at a critical frequency (7) whereas the damping attributed to interstitial diffusion of atoms is important only at low stress levels and is also associated with a critical frequency (8). Consequently, only the magneto-mechanical effect contributes significantly to the large damping capacity in high-strength alloys; and this effect, of course, is limited to ferromagnetic materials.

The energy dissipated during a stress-strain cycle as a result of the magneto-mechanical effect is generally caused by the irreversible magnetostrictive strain (9). Every ferromagnetic material consists of so-called domains which are more or less randomly oriented in an unmagnetized material. However, on the application of a magnetic field, or a stress, these domains tend to align themselves in the direction of the field, or in the direction of the tension strain. This movement of the domains then results in an irreversible change of the dimensions of the material which is called "magnetostriction." Accordingly, when a stress-strain curve for an unmagnetized ferromagnetic material is recorded, more strain is measured than postulated by Hooke's law. This is illustrated in Fig. 1 where a loading curve of a 50 per cent CoFe

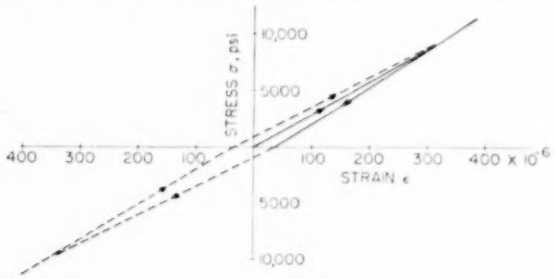

Fig. 1 Stress-Strain Diagram of a 50 Per Cent CoFe Strip Under Static Load

(Solid line represents measured data; dashed curve is schematic completion of hysteresis loop.)

strip is presented. It is seen that the irreversible strain is of the order of 40×10^{-6} at 10,000 psi. At this stress level (hereafter called the critical stress σ_c) all domains appear to be aligned in one direction, inasmuch as the slope of the loading curve changes beyond this point.[3] On relieving the load, the elastic strain reverts to zero, assuming plastic strain is negligible, but the magnetostrictive strain remains almost constant; in other words, the curve follows a hysteresis loop which is indicated by the dashed line in Fig. 1. The greater the area of the loop the larger the damping capacity of the material, from which it is inferred that the damping capacities of high-strength alloys are functions only of the magnetostriction and critical stress. The critical stress σ_c

[1] Westinghouse Research Laboratories.

[2] Numbers in parentheses refer to the Bibliography at the end of the paper.

Contributed by the Applied Mechanics Division and presented at the Annual Meeting, New York, N. Y., November 30–December 5, 1952, of The American Society of Mechanical Engineers.

Discussion of this paper should be addressed to the Secretary, ASME, 29 West 39th Street, New York, N. Y., and will be accepted until July 10, 1953, for publication at a later date. Discussion received after the closing date will be returned.

Note: Statements and opinions advanced in papers are to be understood as individual expressions of their authors and not those of the Society. Manuscript received by ASME Applied Mechanics Division, July 7, 1952. Paper No. 52—A-21.

[3] This phenomenon has also been described as ΔE-effect; see (10), for example.

is the stress level above which the area of the hysteresis loop remains constant.

Experimental Results

Of all materials which must withstand large vibrational stresses, turbine-blading alloys probably have received most attention. A large number of alloys have been tested and a 12 per cent chrome steel has been found to be superior to all other turbine-blading materials, mainly because of its large damping capacity. Fig. 2 gives some of the results of previous damping measurements conducted on torsion specimens with the Föppl-Pertz apparatus by T. Hengstenberg.[4] Also shown, Fig. 3, are data obtained with

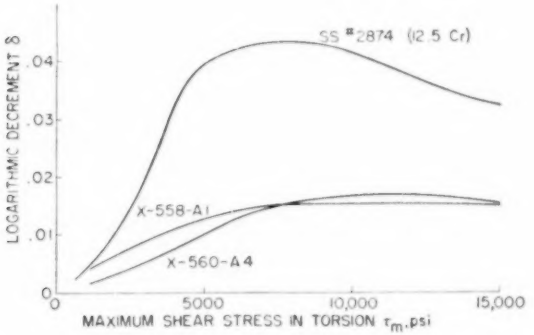

Fig. 2 Damping Curves of Circular Bars of Turbine-Blade Materials in Torsional Vibration According to Hengstenberg

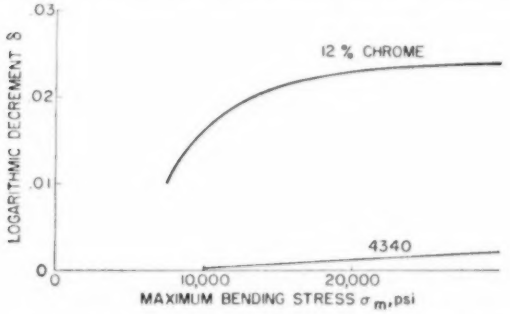

Fig. 3 Damping Curves of Two Steels in Bending Vibration According to Rosard

tuning forks by Rosard;[5] the large damping capacity of the chrome steel is evident. The difference in shape between the torsion and tuning-fork curves measured on the chrome steel, requires particular mention. In torsion the logarithmic decrement reaches a maximum while the decrement recorded with the tuning fork increases continuously as the stress level is raised. The maximum value of the decrement is greater in torsion. This phenomenon which might seem puzzling at first sight will be explained later.

First, however, it will be demonstrated experimentally that the high damping capacity of standard turbine-blading materials is indeed caused by the magnetostrictive effect. The oscillogram of torsional vibration for a hollow specimen $^1/_2$ in. diam and $^1/_{16}$ in. wall thickness was recorded with the Föppl-Pertz unit. Under the particular test conditions employed, the stress is approximately constant along the entire length of the tube. Theory then predicts a linear rise of the logarithmic decrement for small stresses, according to Rayleigh's law (11) and a quadratic decrease of the decrement when the critical stress is exceeded (12).

The results of measurements performed on a hollow chrome-steel specimen are presented in Fig. 4; the decrement is indeed found to increase linearly with stress almost up to the maximum, and to diminish nearly as the inverse square of the stress beyond the critical value; or in other words, since the logarithmic decrement is proportional to the energy dissipated divided by the square of the stress, the energy loss during the vibration was found to increase in proportion to the third power of the stress almost up to the critical stress and to remain essentially constant thereafter.

A second experiment consisted in testing the same specimen under essentially the same conditions, only this time in a strong magnetic field. Now the domains are aligned in the direction of the applied field and are not able to move under the influence of an alternating stress; thus energy cannot be dissipated and the damping capacity therefore must be small. This has been confirmed by the measurements as seen from Fig. 4. The high damping capacity of the chrome steel has vanished as a consequence of the magnetic field. The small residual damping is due to relatively large background losses.

In order to show that this effect is not restricted to a torsion vibration, tuning forks also were tested both with and without a magnetic field. The result was the same; the chrome steel exhibited practically no damping in a strong magnetic field, other than the damping attributable to the eddy currents set up by the test conditions.

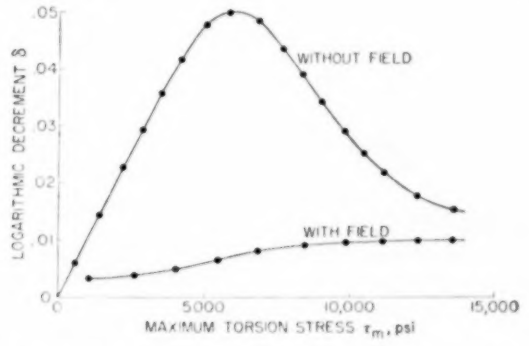

Fig. 4 Effect of Magnetic Field on Damping of Hollow Chrome-Steel Specimen in Torsion

Theoretical Analysis

An attempt will now be made to determine the precise relationships which exist between damping capacity, magnetostriction, critical stress, and maximum stress, first for torsion and then for the tuning fork. The damping capacity is to be expressed by the logarithmic decrement which is given by

$$\delta = \frac{1}{2}\frac{\Delta U}{U} \qquad [1]$$

where U is the mean elastic energy of the specimen

$$U = \frac{1}{V}\frac{1}{2}\int\frac{\sigma^2}{E}dV \qquad [2]$$

ΔU is the energy dissipated in the entire specimen per cycle per unit volume

$$\Delta U = \frac{1}{V}\int dU\,dV \qquad [3]$$

[4] Westinghouse Research Laboratories, East Pittsburgh, Pa.
[5] Westinghouse South Philadelphia Works, Philadelphia, Pa.

and dU is the energy loss per cycle and unit volume at the volume element dV. Term dU therefore represents the area of the observed hysteresis loop due to the magneto-mechanical effect, Fig. 1. For small stresses the area of the loop is given by

$$dU = D\sigma^3$$

according to Rayleigh's law (11), where D is a constant; for stresses larger than the critical stress the area of the hysteresis loop remains the same, no matter how large the alternating stress may be. For this case dU is equal to a constant and may be expressed by

$$dU = K\lambda\sigma_c$$

where K is a factor which depends on the shape of the hysteresis loop. $K = 4$ for an ideal, parallelogram-shaped loop and will be of the order of 1 in most practical cases as is evident[6] from other measurements (13). Term λ is the saturation magnetostriction in the easy direction of magnetization. The assumption is now made that Rayleigh's law is valid up to the critical stress. Term dU may then be written as

$$\left.\begin{aligned} dU &= D\sigma^3; \quad 0 < \sigma < \sigma_c \\ dU &= K\lambda\sigma_c; \quad \sigma_c < \sigma < \sigma_m \end{aligned}\right\} \quad \ldots\ldots\ldots\ldots [4]$$

from which it follows that

$$D = \frac{K\lambda}{\sigma_c^2}$$

Substituting Equations [4] into [3] and replacing

$$dV \text{ by } \frac{dV}{d\sigma}\,d\sigma$$

the logarithmic decrement becomes

$$\delta = \frac{1}{V}\,\frac{K\lambda}{2f}\left[\int_0^{\sigma_c} \frac{\sigma^3}{\sigma_c^2}\,\frac{dV}{d\sigma}\,d\sigma + \int_{\sigma_c}^{\sigma_m} \sigma_c\,\frac{dV}{d\sigma}\,d\sigma\right] \quad \ldots [5]$$

This expression can be evaluated if the stress-distribution function $dV/d\sigma$ is known.

$dV/d\tau$ is easily derived for simple torsion; the stress at any distance r from the center line of a circular bar is

$$\tau = \frac{r}{R}\,\tau_m$$

The volume which is subjected to a stress lower than τ is then

$$V(\tau) = \pi r^2\,\frac{R^2}{\tau_m^2}\,l$$

and the stress-distribution function then becomes

$$\frac{dV}{d\tau} = 2V\,\frac{\tau}{\tau_m^2} \quad \ldots\ldots\ldots\ldots\ldots\ldots [6]$$

Since Equations [4] hold for shear stresses as well as for tensile stresses, Equation [5] can now be modified by substituting τ for σ. Performing the indicated integration, and noting that the average energy in torsion is

$$\frac{1}{4}\,\frac{\tau_m^2}{G}$$

leads to the expression

$$\delta = 2GK\,\lambda_T\,\frac{\tau_c}{\tau_m^2}\left(1 - \frac{3}{5}\,\frac{\tau_c^2}{\tau_m^2}\right); \quad \tau_c < \tau_m \quad \ldots\ldots [7]$$

[6] This can also be seen from Fig. 1.

where λ_T is the torsion magnetostriction in the easy direction.

In order to evaluate Equation [7] numerically, it is assumed that the work in aligning the ferromagnetic domains should be the same whether the applied stress is tensile or shear so that $\lambda\sigma_c = \lambda_T\tau_c$. Furthermore, it can be shown on the basis of considerations of magnetostriction and crystal anisotropy that the critical stress in tension is almost twice the critical stress in torsion. Since it is not possible to compute the relation between both stresses precisely, $\tau_c = 0.5\sigma_c$ is used for the calculation. The constants in Equation [7] are thus known for the 12 per cent chrome steel; τ_c is seen from Fig. 4 to be 6000 psi, $G = 12 \times 10^6$ psi, λ_T is 25×10^{-6}, and K is approximately 1 as mentioned before. Using these values, (with $K = 1$) the decrement calculated according to Equation [7] is plotted in Fig. 5 and compared

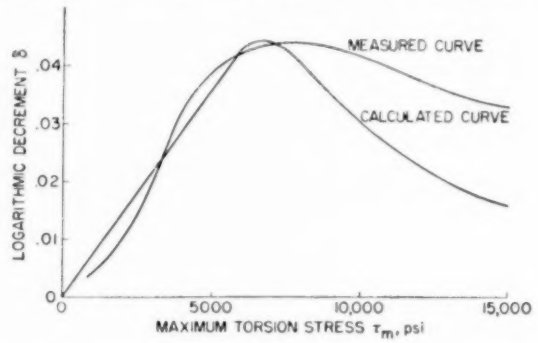

FIG. 5 COMPARISON BETWEEN OBSERVED AND CALCULATED DAMPING CURVES OF 12 PER CENT CHROME STEEL IN TORSION

with the experimental torsion curve. The close agreement between both curves is evident. Although a slightly greater deviation is observed at higher stress levels, this is probably due to the beginning of plastic flow, which has not been considered in these calculations, and to the relatively large background damping at higher stress levels. The component of the decrement due to plastic flow can be estimated from the curve obtained in a magnetic field, Fig. 4.

The evaluation of the stress-distribution function for the tuning fork is more complicated and is obtainable only by making certain approximations. It is assumed that the stress conditions in a tuning fork can be approximated by those in a cantilever beam. The stress for any point may then be written as $\sigma = Mz/I$. The bending moment of the inertia forces is

$$M = \int_x^l m\omega^2 y\,(x' - x)dx' \quad \ldots\ldots\ldots\ldots [8]$$

where x' is an integration variable; y is the solution of a differential equation of the fourth order and has been evaluated in textbooks (14). In order to simplify the integration of Equation [8], y is taken as

$$y = 2y_m\left[\left(\frac{x}{l}\right)^2 - \frac{2}{3}\left(\frac{x}{l}\right)^3 + \frac{1}{6}\left(\frac{x}{l}\right)^4\right] \quad \ldots\ldots [9]$$

This expression satisfies all four boundary conditions and agrees with the precise solution within a few per cent. Substituting Equation [9] into [8], the moment is found to be

$$M = m\omega^2 y_m l^2\left[\frac{13}{45} - \frac{2}{5}\,\frac{x}{l} + \frac{1}{6}\left(\frac{x}{l}\right)^4 - \frac{1}{15}\left(\frac{x}{l}\right)^5 + \frac{1}{90}\left(\frac{x}{l}\right)^6\right]$$

This expression for M is very nearly linear for all values of x with

$0 < x < 0.6l$. Since the error introduced by assuming a linear change in bending moment is small, M may be approximated by

$$M = \frac{1}{4} m w^2 y_m l (l - x)$$

The calculation of $dV/d\sigma$ can be carried out in a manner analogous to that for torsion. First, the volume which is at a stress lower than σ, becomes

$$V(\sigma) = V - hl \int_{\frac{\sigma h}{2\sigma_m}}^{h} 2 \left(1 - \frac{\sigma}{\sigma_m} \frac{h}{2} \frac{1}{z}\right) dz$$

and from this the stress distribution may be written as

$$\frac{dV}{d\sigma} = -\frac{V}{\sigma_m} \ln \frac{\sigma}{\sigma_m} \quad \ldots\ldots\ldots\ldots\ldots\ldots [10]$$

Inserting this value into Equation [5] and considering that the average elastic energy in a cantilever beam is

$$\frac{1}{18} \frac{\sigma_m^2}{E}$$

the logarithmic decrement for the case of the cantilever beam may finally be expressed in the form

$$\delta = 9K\lambda E \frac{\sigma_c}{\sigma_m^2} \left(1 - \frac{\sigma_c}{\sigma_m} \left(\frac{3}{4} \ln \frac{\sigma_m}{\sigma_c} + \frac{15}{16}\right)\right); \quad \sigma_c < \sigma_m \ldots [11]$$

With $K = 1$ and $\lambda = 12.5 \times 10^{-6}$ as before, $E = 30 \times 10^6$ and $\sigma_c = 12{,}000$ psi (twice the critical shear stress in torsion); this expression is plotted in Fig. 6. A comparison of the curve calculated in this way and the curve measured on the tuning fork shows good agreement despite the approximations made. As before, the recorded curve exhibits a little more damping at larger stresses.

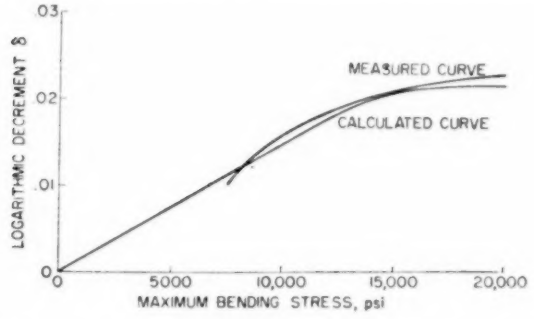

FIG. 6 COMPARISON BETWEEN OBSERVED AND CALCULATED DAMPING CURVES OF CHROME-STEEL TUNING FORKS

The difference in shape between the torsion and tuning-fork curves measured on the chrome steel is due to the entirely different stress distributions which occur. This can be seen by a comparison of Equations [6] and [10]. In torsion, a larger fraction of the specimen is subjected to higher stresses for a given maximum stress while the contrary is true for the tuning fork where the stress distribution function[7] approaches zero at the maximum stress. This is the reason why several investigators observed peaks in damping curves of torsional vibration and not in damping curves of bending vibration.

[7] By stress distribution function is meant fractional volume of the specimen for which the stress lies within a unit interval at a given stress.

The experiments and calculations which have been described make it appear highly probable that the high damping capacity of the 12 per cent chrome steel is associated with its magnetostriction. Virtually the same results have also been obtained with other high-strength steels, such as X-560-Ar (1.6 per cent Ni, 0.7 per cent Cr, 0.9 per cent Mo) and X-558-Ai (12 per cent Cr, 3 per cent W, 0.05 per cent C) although these steels exhibit only a medium damping capacity, Fig. 2. It seems reasonable to conclude therefore that damping caused by magnetostrictive effects is a general phenomenon in high-strength ferromagnetic alloys.

CONDITIONS FOR MAXIMUM DAMPING

The conditions under which maximum damping is obtained in high-strength alloys will be discussed briefly for the case of the cantilever beam where the stress conditions closely correspond to those in vibrating blades, shafts, and so forth. A large damping capacity indicates a large energy loss ΔU during a stress-strain cycle; for the cantilever beam, ΔU, derived from Equations [1], [2], and [10] is

$$\Delta U = K\lambda\sigma_c \left[1 - \frac{\sigma_c}{\sigma_m} \left(\frac{3}{4} \ln \frac{\sigma_m}{\sigma_c} + \frac{15}{16}\right)\right]$$

On plotting this expression as a function of σ_c, a maximum is found at about $\sigma_c = 0.4\sigma_m$; furthermore, it is noticed that ΔU falls to zero both at small and large critical stresses. Accordingly, the highest damping capacity is obtained when λ is as large as possible and when $\sigma_c = 0.4\sigma_m$. This prediction that the critical stress must fall within a certain range of stress also has been verified experimentally by measuring damping capacities of materials with different values of magnetostriction and critical stress. The magnetostriction in the easy direction of magnetization of a Co-30 per cent Fe alloy, for example, can be estimated from data available to be more than twice that of the 12 per cent chrome steel; the critical stress was found to be approximately $\sigma_c = 4500$ psi when the material was air cooled from 850° C. According to Equation [7] the logarithmic decrement of such an alloy would then be about 0.09 at the maximum which is more than twice the value for the high-damping chrome steel. The recorded curve measured on such an alloy is presented in Fig. 7, and it is noted that the decrement does approach the theoretical value. The second curve in Fig. 7, measured in a strong magnetic field, again shows that the extremely high damping is practically entirely due to magnetostriction.

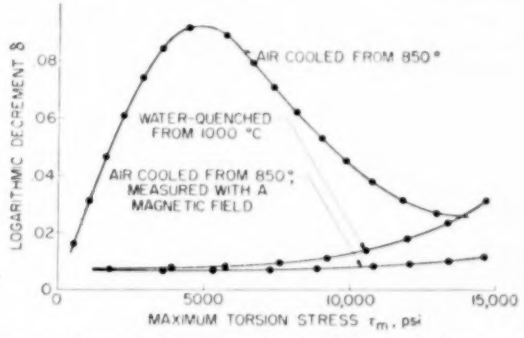

FIG. 7 DAMPING CURVES OF CO-30 PER CENT FE ALLOYS IN TORSION

Critical stresses may be estimated from coercive-force measurements since the areas of the magnetic and mechanical hysteresis loops are proportional to each other as a consequence of the magneto-mechanical effect. Approximating the area of the mag-

netic hysteresis loop by the product of saturation induction B_s and the coercive force H_c, the following relation holds

$$H_c B_s \propto \lambda \sigma_c$$

The saturation induction is constant for a given alloy. Furthermore, in the alloy under consideration for which the crystal anisotropy energy is large and internal stresses are relatively small,[8] the magnetostriction in the easy direction is virtually constant. Hence in this case H_c is approximately proportional to σ_c. On quenching the Co-30 per cent Fe alloy from 1000 C in water, the coercive force was found to be about three times larger than when the alloy was air-cooled from 850 C. Tripling the critical stress should reduce the decrement according to Equation [7] approximately to 0.1 at 5000, to 0.02 at 10,000, and to 0.03 at 15,000 psi. The data Fig. 8 again confirm the theoretical

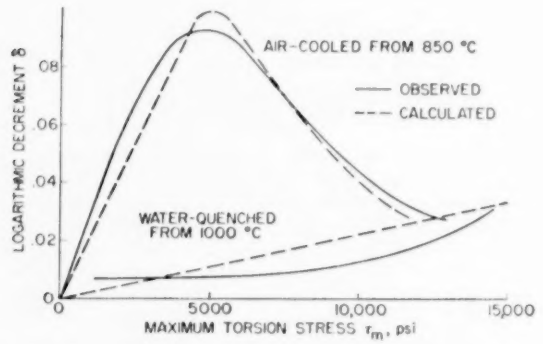

FIG. 8 COMPARISON BETWEEN OBSERVED AND CALCULATED DAMPING CURVES OF CO-30 PER CENT FE ALLOY

prediction. The calculated curve is drawn with $G = 11 \times 10^6$ psi and $\lambda_T = 50 \times 10^{-6}$.

CONCLUSIONS

That the magnetostrictive effect represents the principal source of damping in high-strength ferromagnetic alloys is shown by the following observations:

1 The energy dissipated, when test conditions are such that the stress is virtually constant in all parts of the material, is found to increase in proportion to the third power of the stress almost up to some critical value and to remain essentially constant thereafter.

2 It is observed that alloys with extremely large damping capacities do not exhibit appreciable damping when tested in a strong magnetic field.

3 For a given material the logarithmic decrement measured after various heat-treatments is shown to be dependent upon the magnitude of the critical stress; heat-treatments which raise the stress value lower the decrement and vice versa.

A theoretical analysis has been presented which is in quantitative agreement with these and previous damping measurements employing either torsional vibrations or tuning forks. According to this analysis the energy loss during the vibration of high-strength ferromagnetic alloys is proportional to the magnetostriction in the easy direction of magnetization and is a function of both the critical and maximum stress.

[8] As known from magnetic measurements.

ACKNOWLEDGMENT

The author wishes to express his great appreciation to Dr. C. Zener, Associate Director of the Westinghouse Research Laboratories, for suggesting this problem and for guidance in its solution and to Dr. S. B. Batdorf for demonstrating how to perform some aspects of the theoretical analysis.

BIBLIOGRAPHY

1 "Damping Capacities of Metals," by E. V. Potter, Report of Investigation R.I. 4194, Bureau of Mines, March, 1948, p. 41.

2 "Turbine-Blade Vibration Due to Partial Admission," by R. P. Kroon, JOURNAL OF APPLIED MECHANICS, Trans. ASME, vol. 62, 1940, p. A-161.

3 "Wartenberg," Verhandlung der Deutschen Physikalischen Gesellschaft, vol. 20, 1918, p. 113.

4 "Internal Friction in Solids," by C. Zener, *Physical Review*, vol. 52, 1937, p. 230.

5 "Ferromagnetismus," by R. Becker and W. Doering, Springer-Verlag, Berlin, Germany, 1939, p. 357.

6 "Theorie der Elastischen Nachwirkung in ungeordneten Mischkristallen," by W. S. Gorsky, *Physikalische Zeitschrift der Sowjetunion*, vol. 8, 1935, p. 457.

7 "Ueber die inners Reibung fester Koerper," by K. Bennewitz and H. Roetger, *Physikalische Zeitschrift*, vol. 39, 1938, p. 835.

8 "Interstitial Atomic Diffusion Coefficients," by C. Wert and C. Zener, *Physical Review*, vol. 76, 1949, p. 1169.

9 "Ferromagnetismus," Ibid., p. 364.

10 "Ueber die Abhaengigkeit des Elastizitaetsmoduls und der Daempfung transversal schwingender Metallstaebe von der Amplitude," by F. Foerster and W. Koester, *Naturwissenschaften*, vol. 25, 1937, p. 436.

11 "Ferromagnetism," by R. M. Bozorth, D. Van Nostrand Company, Inc., New York, N. Y., 1951, p. 708.

12 "Ferromagnetismus," Ibid., p. 366.

13 "Ferromagnetismus," Ibid., p. 338.

14 "Theory of Sound," by Lord Rayleigh, Dover Publications, New York, N. Y., vol. 1, 1945, p. 285.

Effect of Damping Constants and Stress Distribution on the Resonance Response of Members

By B. J. LAZAN,[1] MINNEAPOLIS, MINN.

The amplitude of vibration of a member at resonance, as defined by its resonance amplification factor, is analyzed in relationship to the damping properties of materials. Data are presented on damping energy to indicate the effect of stress magnitude, stress history, and temperature. Based on the mathematical relationship found to exist between damping and stress magnitude the resonance amplification factors are determined for a variety of direct stress members and beams. It is shown that the amplification in vibration caused by resonance may be considered to be the product of three basic factors, i.e., (*a*) the material factor, (*b*) the cross-sectional shape factor, and (*c*) the longitudinal stress-distribution factor. The first of these factors may be calculated from the damping and dynamic modulus properties of the material and the last two from the shape and loading characteristics of the member. Diagrams are presented to show these basic factors as functions of the damping exponent and other variables for members commonly encountered in engineering practice. Experimental data are presented to confirm the equations derived for resonance amplification factor of members having various shapes and stress distribution.

Introduction

NEAR-resonance vibration is generally considered to be a common cause for fatigue and other types of service failures in many and diverse fields of engineering. Even if actual failure can be avoided, the rough and noisy operation associated with the near-resonance condition frequently necessitates correction. Current trends toward higher speeds and decreased factor of safety have increased the importance of resonance vibration as a factor in design.

Considerable work has been done on the fatigue and other properties of materials which define their ability to withstand cyclic stress produced by resonance or other vibration conditions. However, relatively little has been done on the analysis of the properties of materials and other factors which govern the amplification in vibration that is caused by the near-resonance condition. Hence this paper is concerned with an analysis of factors which govern the relationship of the external force which excites a vibration (hereafter called the exciting force) to the internal force excited in the member at resonance (hereafter called the resonance excited force). The ratio of excited to exciting force shall be called (1)[2] the resonance amplification factor A_r, in this paper.

The general nature of the viscous damped resonance curve is well known (2) and will not be discussed here. Although the internal hysteresis damping of a material is fundamentally different in nature from viscous damping (3), and the resonance curves may be quite unsymmetrical (4), the resonance amplification factor nevertheless provides a convenient measure of the severity of the resonant condition. Consequently, this factor shall be used in this paper as a basis for analysis.

Variables Which Affect Magnitude of Damping Energy in Materials and Parts

The energy absorption by an actual part, or its damping, may be due to several factors, among which are: (*a*) The inelastic behavior of the material as indicated by its damping capacity, (*b*) slippage and other structural or joint factors, and (*c*) aerodynamic effects. In general, there is very little data on the relative magnitude and importance of each of these three absorbers of damping energy. It is likely that in many applications the primary absorber of damping energy is the structure or joint factor and the contributions offered by the material damping are insignificant. However, there is little doubt that to generalize this statement, which is sometimes done, is highly misleading. In many applications subjected to resonance vibrations it is difficult to include significant structural damping and one must rely on material damping. Even where significant structural and aerodynamic damping may be present it is shown by recent work (5) that material damping may still be sufficiently large to be highly significant as a limiter of resonance vibrations.

Since this paper is concerned primarily with the dynamic properties of materials, structural and aerodynamic damping shall not be discussed further and only the material damping factor will be analyzed in detail.

With this as background let us now discuss, as an indication of the variables which affect the magnitude of damping in materials, the dynamic properties of one particular material. For this discussion, data on the temperature-resistant material S-816 at three temperatures will be presented so as to illustrate a variety of trends and patterns of significance in resonance-vibration studies.

For brevity, the recently developed damping, elasticity, and fatigue testing machines (3, 6) used to procure the data on S-816 will not be described in this paper. Also, for brevity, diagrams showing the variation in damping energy absorbed by the material at various stress magnitudes as a function of a number of cycles of fatigue stress (5) are omitted. However, in order to establish mathematical relationships for later analysis, damping energy is plotted as a function of stress magnitude in Fig. 1, the different curves indicating the relationship for different stress histories and temperatures. The significance of the right-hand

[1] Professor of Materials Engineering, University of Minnesota. Mem. ASME.

Contributed by the Applied Mechanics Division and presented at the Annual Meeting, New York, N. Y., November 30–December 5, 1952, of The American Society of Mechanical Engineers.

Discussion of this paper should be addressed to the Secretary, ASME, 29 West 39th Street, New York, N. Y., and will be accepted until July 10, 1953, for publication at a later date. Discussion received after the closing date will be returned.

Note: Statements and opinions advanced in papers are to be understood as individual expressions of their authors and not those of the Society. Manuscript received by ASME Applied Mechanics Division, February 3, 1952. Paper No. 52—A-8.

[2] Numbers in parentheses refer to the Bibliography at the end of the paper.

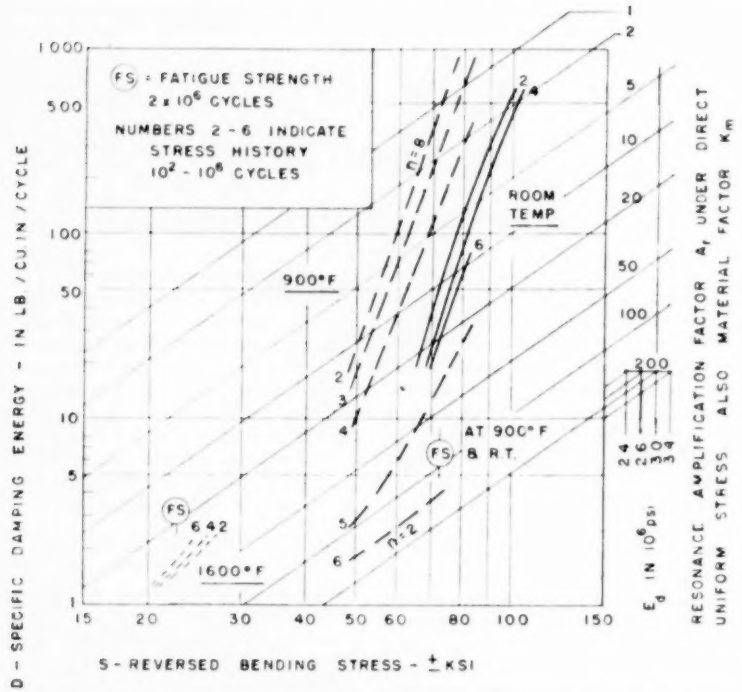

FIG. 1 D-S-N-A_r DIAGRAM FOR ALLOY S-816 INDICATING EFFECT OF STRESS MAGNITUDE AND STRESS HISTORY ON DAMPING ENERGY

ordinate of this figure will be discussed later. The series of curves shown at each temperature (solid lines represent room temperature, long dash 900 F, and short dash 1600 F) are identified with the numbers 2, 3, 4, 5, and 6 to indicate the damping values after 10^2, 10^3, 10^4, 10^5, and 10^6 cycles of stress. The stress level during the imposition of the stress history was the same as during the damping measurement. The flags enclosing the letters F.S. indicate the fatigue strengths of the material.

Due to space limitations, data for S-816 only are presented in this paper. It should be pointed out, however, that the damping values do not always decrease with an increase in number of cycles at room temperature as shown in Fig. 1. Many different patterns of behavior have been observed; for example, the damping of some powdered metals increases continuously with an increase in the number of cycles; 403 stainless displays an initial decrease followed by an increase to a peak after which the values decrease if the specimen does not previously fracture. The data for some metals show damping values that decrease to a minimum, followed by a steady increase to fracture; other materials display practically no change in damping with number of cycles; and Inconel X has high initial damping followed by a period of practically no change, after which the damping increases sharply preceding failure. The general trends for a given material may be the same at elevated temperature as at room temperature or they may be reversed, as in the case of S-816 at room temperature and 1600 F. In most cases studied to date, however, the plot of log damping versus log stress (at constant stress history and constant temperature) may be represented by reasonably straight lines.

Mathematical Relationship Between Damping and Stress Magnitude

It is desirable at this point to determine the mathematical relationships between damping and stress magnitude, stress history, and temperature. As indicated previously, stress history affects different materials in pronouncedly different manners. It is therefore impossible to generalize stress-history effects at this time and express such effects mathematically. It is also impossible to generalize temperature effects at this time. However, there are sufficient data (7, 8, 5) to indicate that for many materials the effect of stress magnitude (at constant temperature and stress history) may be expressed by the equation

$$D = J S^n \qquad [1]$$

where

D = specific damping energy, in-lb/cu in/cycle
S = stress, psi
J, n = const

Referring to Fig. 1, it may be seen that the log D versus log S is reasonably straight with slopes ranging from 2 to 8. Thus for S-816, exponent n varies between 2 and 8 depending on stress history, magnitude, and temperature.

In some of the earlier work (4, 8) exponent n was found to be approximately 3 for several materials at room temperature. However, most of the materials now under study at the University of Minnesota display exponents n which generally are greater than 3, particularly if various stress histories are included. An exponent n as large as 30 has been observed for one material at high stress.

In future work more careful analyses will be undertaken of stress history and temperature effects. For a given material it may be possible to handle these variables mathematically by considering J and n as functions of stress history and temperature, rather than as constants as assumed in the foregoing.

Resonance Amplification Factor Under Uniform Direct Stress

So far basic data only have been presented on the damping energy. Now what does such data mean in terms of vibration amplification of actual parts at resonance?

The effect of damping energy on the resonant behavior of a part may be specified in terms of the resonance amplification factor A_r, as briefly discussed previously. This factor is the ratio of the force which is excited during resonance vibration to the force exciting the vibration. Thus A_r is a measure of the severity of a resonant condition. For most applications in which linearity may be assumed with reasonable accuracy this factor generally may be computed (1) from the equation

$$A_r = 2\pi W_0 / D_0 \quad [2]$$

where

W_0 = elastic energy in member at maximum stress, in-lb
D_0 = total damping energy in in-lb/cycle, VD
V = volume of material at stress

Therefore, for the special case of direct uniform stress for which the elastic energy $W_0 = VS^2/2E_d$

$$A_r = \pi S^2 / E_d D = \pi / E_d J S^{n-2} \quad [3]$$

where E_d = dynamic modulus of elasticity (5), psi.

If the modulus of elasticity E_d is assumed to be reasonably constant, then A_r is a function of the variables S and D only, and for this simplified case of direct uniform stress only, a grid of lines may be drawn in Fig. 1 as shown (see right-hand ordinate) to indicate the values of A_r. However, as shown in a previous publication (5) the modulus of elasticity does not remain constant but varies between 21 and 34 $\times$ 10^6 psi, depending on temperature, stress magnitude, and stress history. Therefore the right-hand scale in Fig. 3 includes provisions for determining A_r for various values of E_d as indicated at the lower end of this scale.

The wide range of A_r values observed for S-816, as revealed by Fig. 1, is of considerable engineering significance. Depending upon stress magnitude and stress history, A_r under direct uniform stress may be insignificantly small or as large as 150. At 900 F, for example, stress history alone may increase A_r to over 100 times its virgin value. It is therefore apparent that the specification of A_r for a given material and its comparison with other materials cannot be done in a simple manner, since two variables other than material and temperature are involved.

It is desirable to review for future reference the relationship between damping exponent n and change in A_r under increasing stress. As indicated previously, if $n = 2$ then A_r is independent of stress magnitude since both elastic and damping energy increase as the square of stress. If, however, n is larger than 2, which is the usual case, the damping energy increases more rapidly with stress than does the elastic energy resulting in an A_r which decreases with increasing stress. These observations will be amplified in the analysis of cross-section shape and longitudinal stress-distribution effects in later sections.

Resonance Amplification Factor Under Nonuniform Direct Stress

All discussion to this point has been concerned primarily with the basic damping, elasticity, and fatigue properties of materials and the interpretation of these properties in terms of behavior of a resonant member under uniform direct stress only. In practice this rather desirable state of uniform stress is, of course, quite rare. Generally speaking, critical members are almost always stressed nonuniformly, in which case the equation $A_r = \pi S^2/E_d D$ does not hold. Therefore, in the interest of providing wider engineering applicability for the type of data presented previously, this section is concerned with an analysis of the resonance amplification factor A_r under nonuniform direct stress. Bending members are analyzed in the next section. Other types of members, such as those subjected to torsional stress, are not included in this paper for reasons of brevity, but may be analyzed in a similar manner.

Analyses of members under resonant vibrations have been made in the past (9, 8, 1) to indicate that fatigue strength is not the sole criterion for indicating resonance durability. However, an attempt is made in this section to undertake a more thorough treatment of the important variables and to generalize the equations expressing the resonance amplification factor of members. This type of analysis is also given in reference (10) published after the completion of this paper.

The general case of direct stress vibration covered in this section considers the inertia forces produced by and within the vibrating member. The force on a section of a member with internal inertia forces will be, of course, a function of the longitudinal location of the section. Although the member may have variable cross section as shown in the diagram in Table 1, it is assumed that the stress at a given cross section is uniformly distributed (although the total force on the section and the resultant stress may vary along the length of the member).

As indicated in Equation [2] the resonance amplification factor A_r for a member generally may be computed from the equation $A_r = 2\pi W_0/D_0$.

Referring to the figure and symbol definitions in Table 1 the total elastic energy

$$W_0 = \int dW_0 = \int W_x \, dV = \int_0^a \frac{S_x^2}{2E_d} A_x \, dx \quad [4]$$

where W_x is the unit elastic energy at any location and dV is a small differential volume having thickness dx.

As indicated (5), some materials display sufficiently large variation in E_d to necessitate considering this modulus a function of stress level and stress history. However, for most materials and stress ranges, E_d may be assumed to be a constant for most engineering calculations. Therefore E_d may be moved from within the integral sign as indicated

$$W_0 = \frac{1}{2E_d} \int_0^a S_x^2 \, A_x \, dx \quad [5]$$

Again, referring to the figure and symbols in Table 1, the total damping energy

$$D_0 = \int dD_0 = \int D_x \, dV = J \int_0^a S_x^n \, A_x \, dx \quad [6]$$

Combining Equations [2], [5], and [6]

$$A_r = \frac{\pi}{E_d J} \frac{\int_0^a S_x^2 \, A_x \, dx}{\int_0^a S_x^n \, A_x \, dx} = \frac{\pi}{E_d J S_m^{n-2}} \frac{\int_0^a \left(\frac{S_x}{S_m}\right)^2 A_x \, dx}{\int_0^a \left(\frac{S_x}{S_m}\right)^n A_x \, dx} \quad [7]$$

In the foregoing equation, S_m is the stress at the section of maximum stress, as defined in Table 1.

For convenience in analysis and interpretation, it is desirable to define the following factors (justification for these definitions will appear later)

$$\text{Material factor, } K_m = \frac{\pi}{E_d J S_m^{n-2}} \quad [8]$$

$$\text{Longitudinal stress-distribution factor, } K_s = \frac{\int_0^a \left(\frac{S_x}{S_m}\right)^2 A_x \, dx}{\int_0^a \left(\frac{S_x}{S_m}\right)^n A_x \, dx} \quad [9]$$

TABLE I:- SUMMARY OF VALUES FOR RESONANCE AMPLIFICATION FACTOR A_f UNDER DIRECT STRESS $A_f = K_m K_c K_s$, WHERE $K_m = \pi / E_d J S_m^{n-2}$, $K_c = 1$, AND K_s GIVEN BELOW IN SEVERAL CASES

	LONGITUDINAL SHAPE AND STRESS DISTRIBUTION IN MEMBER	VALUES OF K_s	DEFINITION OF SYMBOLS
I	GENERAL CASE OF DIRECT STRESS FOR EITHER (1) CONTINUOUS MEMBERS OR (2) MEMBERS WITH DISCONTINUITIES CONSIDERING INTERNAL INERTIA FORCES.	$\dfrac{\int_0^a (S_x/S_m)^2 A_x dx}{\int_0^a (S_x/S_m)^n A_x dx}$	RESONANCE EXCITING FORCE = P_0 EXCITED FORCE AT SECTION A_m OF MAX. STRESS $S_m = P_m = P_0 A_f$
IA	CONTINUOUS MEMBERS HAVING CONSTANT CROSS-SECTIONAL AREA. $A_x = A_m$ IN GENERAL, $S_x \neq P_m/A_x$ IF INTERNAL INERTIA FORCES ARE SIGNIFICANT	$\dfrac{\int_0^a (S_x/S_m)^2 dx}{\int_0^a (S_x/S_m)^n dx}$	
IA1	INTERNAL INERTIA FORCES NEGLIGIBLE $S_x = P_m/A_m = S_m$	$K_s = 1$	
IA2	INTERNAL INERTIA FORCES SUCH THAT: $S_x = (x/a) S_m$	$(n+1)/3$	
IA3	INTERNAL INERTIA FORCES SUCH THAT: $S_x = (x/a)^m S_m$	$(mn+1)/(2m+1)$	
IA4	INTERNAL INERTIA FORCES SUCH THAT $S_x = S_m \sin(\pi x/2a)$ (LONG. VIB. IN CANTILEVER ROD)	$\pi \Big/ 4\int_0^{\pi/2} \sin^n \theta \, d\theta$	
IB	CONTINUOUS MEMBERS HAVING VARIABLE AREA	USE EQUATION I	
IB1	INTERNAL INERTIA FORCES NEGLIGIBLE $S_x = P_m/A_x$	$A_m^{2-n} \dfrac{\int_0^a A_x^{-1} dx}{\int_0^a A_x^{1-n} dx}$	
IB1a	ROD HAVING TAPER "s" $A_x = A_m\left[1+(x/a)(s-1)\right]$	$\dfrac{(n-2)\log s}{(1-s^{2-n})}$	
IB2	INTERNAL INERTIA FORCES SUCH THAT: $S = S_m(x/a), S_m \sin(\pi x/2a)$, ETC.	USE EQUATION I	
IC	DISCONTINUOUS MEMBER HAVING CONSTANT CROSS-SECTION BETWEEN DISCONTINUITIES. A_1 a_1 | A_2 a_2	$\dfrac{A_1\int_0^{a_1} (S_x/S_m)^2 dx + A_2\int_{a_1}^{a_2+a_1} (S_x/S_m)^2 dx + \cdots}{A_1\int_0^{a_1} (S_x/S_m)^n dx + A_2\int_{a_1}^{a_2+a_1} (S_x/S_m)^n dx + \cdots}$	
IC1	INTERNAL FORCES NEGLIGIBLE $S_x = P_m/A_x$	$\dfrac{(a_1/a_2)+(A_1+A_2)}{(a_1/a_2)+(A_1+A_2)^{n-1}}$	FOR TWO SECTION MEMBER (ONE DISCONTINUITY) $A_m = A_1$ & $a_m = a_1$
IC2	INT. INERTIA FORCES NOT NEGLIGIBLE.	USE EQUATION IC.	
ID	DISCONTINUOUS MEMBERS WITH VARIABLE SECTION BETWEEN DISCONTINUITIES.	USE EQUATION I.	

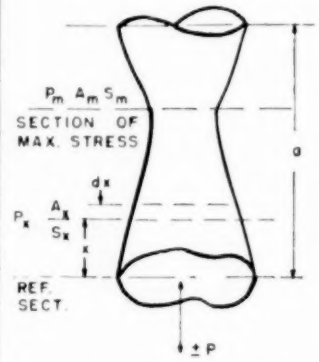

FORCE ON REFERENCE SECTION

IF INTERNAL INERTIA FORCES ARE NEGLIGIBLE: THEN $P = P_m$

IF EXTERNAL INERTIA FORCES ARE NEGLIGIBLE: THEN $P = P_0$

In accordance with these definitions, the resonance amplification factor for the general case of direct stress may be written as

$$A_r = K_m K_s \quad \ldots\ldots [10]$$

The material factor K_m is, of course, independent of cross-sectional shape and stress distribution of the member; it depends only on the properties of the material E_d, J, and n, and the operating stress S_m. Referring to Equation [3], it may be seen that the material factor is identical to the resonance amplification factor A_r under direct uniform stress. This relationship will be discussed again in connection with bending members.

The longitudinal stress distribution factor K_s, separated from K_m as shown in Equations [7], [9], and [10], is a function of member shape (as specified by A_z), longitudinal stress distribution S_z, member length a, and damping exponent n, and it is independent of damping constant J.

In the analysis of bending members in a later section it will be observed that A_r also may be separated into material and longitudinal stress-distribution factors K_m and K_s, with an additional K_c-factor required to account for cross-sectional stress distribution. In the interest of generalizing, this K_c-factor is included in the summary for direct stress members given in Table 1, K_c being equal to 1 for this case since a uniform stress distribution at a given cross section is assumed.

Referring to Table 1, the first row lists the general case of direct stress and subsequent rows cover various special direct-stress cases encountered in engineering practice. For each of the general, semigeneral, and special cases listed, the values of K_s are given in the second column. For conciseness, the derivations for the K_s-equations listed in this table are not shown in this paper. In general, these equations are rather simple mathematical reductions of the equation for general case I with appropriate substitutions for S_z and A_z. The trends revealed by these K_s-equations will be discussed later.

Resonance Amplification Factor Under Bending Stress

An analysis of the resonance amplification factor of beams, a structural component in which resonant vibrations are often of critical importance, is given in the following.

Referring to the figures in Table 2, the elastic and damping energy of a beam of general shape may be expressed as indicated in the following

$$\text{Total elastic energy, } W_e = \int 1/2\ M_z\, d\theta = \frac{1}{2}\int_0^a \frac{M_z^2\, dx}{E_d I_z}$$

and assuming E_d is constant as discussed previously

$$W_0 = \frac{1}{2E_d}\int_0^a \frac{S_z^2 I_z\, dx}{t_z^2} \quad \ldots\ldots [11]$$

$$\text{Total damping energy} = D_0 = \int D\, dv = \int\int DZ\, dy\, dx$$

but

$$D = J S^n \text{ and } S = \frac{y}{t_z} S_z$$

where S = stress at any point, S_z = maximum stress (at outer fibers) at any position x, and t_z = maximum distance from neutral axis to outer fibers at any position x.

Thus, since t_z and S_z are not functions of y

$$D_0 = \int\int J \frac{y^n}{t_z^n} S_z^n Z\, dy\, dx$$

$$= J \int_{x=0}^{a} \left[\int_{y=-t'(x)}^{y=t(x)} y^n Z\, dy\right] \frac{S_z^n}{t_z^n}\, dx \quad \ldots [12]$$

where $t(x)$ and $t'(x)$ are functions of x which define the location of the fibers most distant from neutral axis of the beam.

Combining Equations [2], [11], and [12]

$$A_r = \frac{2\pi}{2E_d J} \frac{\displaystyle\int_0^a S_z^2 \frac{I_z}{t_z^2}\, dx}{\displaystyle\int_{x=0}^{a}\left[\int_{y=-t'(x)}^{t(x)} y^n Z\, dy\right]\frac{S_z^n}{t_z^n}\, dx}$$

$$= \frac{\pi}{E_d J S_m^{n-2}} \frac{\displaystyle\int_0^a \left(\frac{S_z}{S_m}\right)^2 \frac{I_z}{t_z^2}\, dx}{\displaystyle\int_{x=0}^{a}\left[\int_{y=-t'(x)}^{t(x)} y^n Z\, dy\right]\left(\frac{S_z}{S_m}\right)^n t_z^{-n}\, dx} \quad \ldots\ldots [13]$$

Inspecting Equation [13], it is apparent that the first factor $\pi/E_d J S_m^{n-2}$ is the material factor K_m discussed previously. It will be shown that, in general, the remaining part of this equation may be considered to be the product of two other factors: (*a*) The longitudinal stress distribution factor K_s, as discussed previously, and (*b*) the cross-sectional shape factor K_c to be discussed later.

In the foregoing general case these two factors cannot be separated conveniently and only their product $(K_s K_c)$ is specified. However, in most special cases discussed below, K_s and K_c can be separated.

Consider now the special case of beams having constant cross-sectional moment of inertia I and neutral-axis distance t and t' within the length of the beam under consideration. Under these conditions the integral

$$\int_{y=t'(x)}^{t(x)} y^n Z\, dy$$

reduces to

$$\int_{-t'}^{t} y^n Z\, dy$$

which is not a function of x and may therefore be removed from within the $\int_{x=0}^{a} dx$ integral. Thus Equation [13] reduces to

$$A_r = \frac{\pi}{E_d J S_m^{n-2}} \frac{\displaystyle\int_0^a \left(\frac{S_z}{S_m}\right)^2 dx}{\displaystyle\int_0^a \left(\frac{S_z}{S_m}\right)^n dx} \frac{I t^{n-2}}{\displaystyle\int_{-t'}^{t} y^n Z\, dy} \quad \ldots [14]$$

Comparing Equation [14] with direct-stress Equation [7] (with A_z = const), it may be seen that the material factor

$$K_m = \frac{\pi}{E_d J S_m^{n-2}}$$

and the longitudinal stress-distribution factor

$$K_s = \frac{\displaystyle\int_0^a \left(\frac{S_z}{S_m}\right)^2 dx}{\displaystyle\int_0^a \left(\frac{S_z}{S_m}\right)^n dx}$$

are identical to those defined in Equations [8] and [9]. All that remains to be accounted for in Equation [14] is therefore the last factor, which may be defined as follows

$$\text{Cross-sectional shape factor } K_c = \frac{I t^{n-2}}{\displaystyle\int_{-t'}^{t} y^n Z\, dy} \quad \ldots [15]$$

TABLE II.- SUMMARY OF VALUES FOR RESONANCE AMPLIFICATION FACTOR A_r FOR BEAMS $A_r = K_m \cdot K_c \cdot K_s$, WHERE $K_m = \pi / E_d J S_m^{n-2}$, AND K_c AND K_s ARE GIVEN BELOW FOR SEVERAL CASES

	LONGITUDINAL SHAPE AND STRESS DISTRIBUTION	VALUES FOR K_c, K_s OR $K_s \cdot K_c$		
II	GENERAL CASE OF BENDING STRESS FOR EITHER (1) CONTINUOUS BEAMS OR (2) BEAMS WITH DISCONT. WITH SIGNIFICANT INTERNAL INERTIA FORCES CONSIDERED.	$K_c \cdot K_s = \dfrac{\int_0^a (S_x/S_m)^2 (I_x/t_x^2)\, dx}{\int_{x=0}^{a}\int_{y=t'(x)}^{t(x)} y^n Z\, dy \dfrac{(S_x/S_m)^n}{t_x^n}\, dx}$		
IIA	CONTINUOUS BEAM HAVING CONSTANT CROSS-SECTION. $I_x = I$, $t_x = t$	$K_c = \dfrac{I t^{n-2}}{\int_{-t'}^{t} y^n Z\, dy}$ $\quad K_s = \dfrac{\int_0^a (S_x/S_m)^2\, dx}{\int_0^a (S_x/S_m)^n\, dx}$		
	SPECIAL CROSS-SECTIONAL SHAPE CONSIDERED	RECTANGLE	CIRCLE	DIAMOND
	VALUES OF K_s K_c	$K_c = 0.33(n+1)$	$K_c = \dfrac{0.196(n+2)}{\int_0^{\pi/2} \sin^n\theta\, d\theta}$	$K_c = 0.083(n+1)(n+2)$
IIA1	CONSTANT MOMENT $S_x = S_m$; $K_s = 1$	$0.33(n+1)$	$\dfrac{0.196(n+2)}{\int_0^{\pi/2} \sin^n\theta\, d\theta}$	$0.083(n+1)(n+2)$
IIA2	VARIABLE MOMENT SUCH THAT $S_x = (x/a) S_m$, $K_s = (n+1)/3$	$0.111(n+1)^2$	$\dfrac{0.065(n+1)(n+2)}{\int_0^{\pi/2} \sin^n\theta\, d\theta}$	$0.028(n+1)^2(n+2)$
IIA3	VARIABLE MOMENT SUCH THAT $S_x = (x/a)^m S_m$, $K_s = (mn+1)/(2m+1)$	$\dfrac{0.33(n+1)(mn+1)}{2m+1}$	$\dfrac{0.196(mn+1)(n+2)}{(2m+1)\int_0^{\pi/2} \sin^n\theta\, d\theta}$	$\dfrac{0.083(n+1)(n+2)(mn+1)}{(2m+1)}$
IIA4	VARIABLE MOMENT SUCH THAT $S_x = S_m \sin(\pi x/2a)$, $K_s = \pi/4 \int_0^{\pi/2} \sin^n\theta\, d\theta$	$\dfrac{0.26(n+1)}{\int_0^{\pi/2} \sin^n\theta\, d\theta}$	$\dfrac{0.154(n+2)}{\left[\int_0^{\pi/2} \sin^n\theta\, d\theta\right]^2}$	$\dfrac{0.065(n+1)(n+2)}{\int_0^{\pi/2} \sin^n\theta\, d\theta}$
IIB	DISCONTINUOUS BEAMS HAVING CONSTANT CROSS-SECTION BETWEEN DISCONTINUITIES	$K_c = \dfrac{I_1 t_1^{n-2}}{\int_{-t_1'}^{t_1} Z y^n dy}$ $\quad K_s = \dfrac{1 + \left[\frac{t_1}{t_2}\right]^2 \left[\frac{a_1}{a_2}\right] \left[\frac{s_2}{s_1}\right]^2 \left[\frac{I_2}{I_1}\right] + \cdots + \left[\frac{t_1}{t_g}\right]^2 \left[\frac{a_g}{a_1}\right] \left[\frac{s_g}{s_1}\right]^2 \left[\frac{I_g}{I_1}\right]}{1 + \left[\frac{t_1}{t_2}\right]^n \left[\frac{a_1}{a_2}\right] \left[\frac{s_2}{s_1}\right]^n \int_{-t_2'}^{t_2} z y^n dy \Big/ \int_{-t_1'}^{t_1} z y^n dy + \cdots}$		
IIB1	CONSTANT MOMENT ON TWO SECTION MEMBER (1 SIMILAR TO 2) $K_s = \dfrac{a_1}{a_2} + \dfrac{I_1}{I_2} \Big/ \dfrac{a_1}{a_2} + \left[\dfrac{I_1}{I_2}\right]^{\frac{3n-2}{4}}$	$0.33(n+1)\left[\dfrac{a_1}{a_2} + \dfrac{I_1}{I_2}\right] \Big/ \dfrac{a_1}{a_2} + \left[\dfrac{I_1}{I_2}\right]^{\frac{3n-2}{4}}$	$0.196(n+2)\left[\dfrac{a_1}{a_2} + \dfrac{I_1}{I_2}\right] \Big/ \int_0^{\pi/2} \sin^n\theta\, d\theta \left\{\dfrac{a_1}{a_2} + \left[\dfrac{I_1}{I_2}\right]^{\frac{3n-2}{4}}\right\}$	$(n+1)(n+2)\left[\dfrac{a_1}{a_2} + \dfrac{I_1}{I_2}\right] \Big/ 12 \left\{\dfrac{a_1}{a_2} + \left[\dfrac{I_1}{I_2}\right]^{\frac{3n-2}{4}}\right\}$

Inspection of Equation [15] will show that the name assigned to this factor is descriptive of its nature.

Therefore it appears to be possible to define the resonance amplification factor of beam by the equation

$$A_r = K_m K_s K_c \quad \ldots\ldots\ldots\ldots\ldots\ldots [16]$$

In all cases K_m appears as a separate factor. Although for the case of beams of uniform cross section and other special cases it may be possible to separate the K_s and K_c-factors as shown; in the most general case only the product $K_c K_s$ can be specified.

Table 2 is a summary of values for the resonance amplification factor A_r for various general and special types of beams encountered in engineering practice. The arrangement of this table is similar to that of Table 1 and is self-explanatory. It should be noted that three cross-sectional shapes frequently encountered in engineering practice (the rectangle or square, circle, and diamond) are analyzed merely to indicate trends to be discussed later. Other shapes can, of course, also be analyzed by the same methods.

From Table 2 it may be noted that the equation for a vibrating beam (case IIA2) of rectangular cross section is

$$A_r = \frac{\pi}{E_d S^{n-2}} \left(\frac{n+1}{3} \right)^2$$

If this equation is used to compute the allowable force P_0 at resonance and if a value of 3 is substituted for n, then the resultant equation is in exact agreement with Marin's Equation [14] in reference (9).

Referring to Equation [14] of this paper, it may be seen that both the K_s and K_c-factors are functions of damping exponent n. Since this exponent is widely different for different materials, a range from 2 to 30 having been observed to date, it is desirable to diagram these factors as a function of n as shown in Figs. 2 and 3. These diagrams also reveal trends which provide a basis for discussing the interpretation of damping data in terms of resonance amplification factor as used in engineering design.

Fig. 2 diagrams the longitudinal stress-distribution factor K_s, as a function of damping exponent n for various common shapes of members and types of loading. Members without discontinuities are shown in solid lines and members with one discontinuity (two section members) are shown in broken lines.

For all the cases referred to in Fig. 2, factor K_s equals 1 at $n = 2$, and, except for uniform direct stress, increases with increasing values of n. The rate of increase in K_s with n is greatly dependent on the type of member and loading.

For example, for a freely vibrating cantilever member of constant cross section under either tension or bending stress (stress distribution assumed to be $S_x = S_m \sin[\pi x/2a]$ as indicated for cases IA4 and IIA4) K_s increases from 1 to only 3.5 as damping exponent n increases from 1 to 30. As a second example, K_s for a tapered tension member (case IB1a) having a taper s of 4 displays the much larger increase from 1 to 40 in the same range of n-values.

In the case of discontinuous members (broken lines), it is of course possible to have an infinite number of ratios of section area, and so on, at the discontinuities. For simplicity, members with one discontinuity only are considered, and for further simplification only a few ratios q of areas A_1 to A_2 and only a few ratios p of lengths a_1 to a_2 between discontinuities are included. Small values of ratio p were selected to indicate the characteristics of members with notches and other stress-concentration effects. For example, a member with a small notch (which allows relatively low working stress in the rest of the member) can attain K_s-values as high as 80. This means that at the same nominal working stress a notched member may have 80 times the

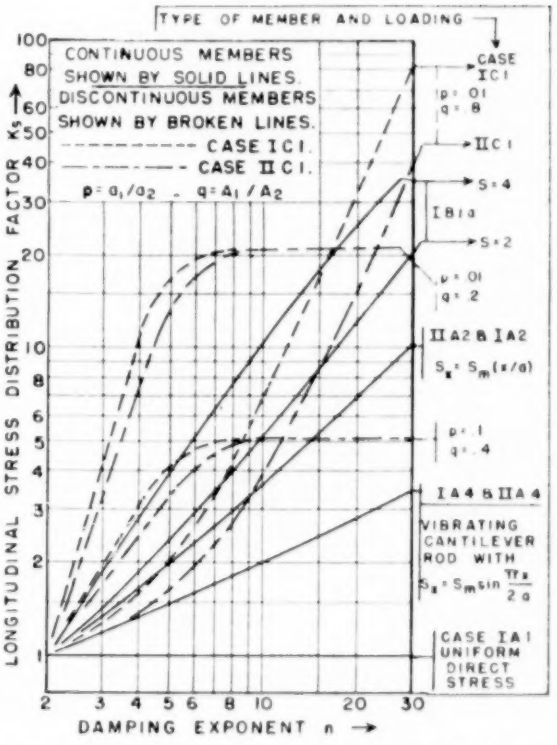

Fig. 2 Longitudinal Stress-Distribution Factor K_s for Various Common Types of Members and Loadings as a Function of Damping Exponent n

resonance amplification factor A_r of the unnotched member, if other factors remain constant.

To illustrate the effect of damping exponent n on the cross-sectional shape factor K_c, three common sections were analyzed and diagrammed as shown in Fig. 3. The equations used to plot the characteristics of the diamond, circle, and rectangle are given in Table 2. The broken lines indicate the general trend for a modified diamond shape (with sharp upper and lower edges) and an I-beam. Since the exact shape of these sections governs the exact locations of the corresponding curves, these curves are qualitative indications only of the general trends.

It is significant to note from the curves that merely changing the cross-sectional shape of a beam from a diamond to an I-section (all other factors remaining constant) may decrease its resonance amplification factor very significantly, as much as 20 times under certain conditions. It is sometimes possible to make such shapes in cross-sectional shape in vacuum-tube components, structural beams, and other parts to reduce resonance amplification vibrations and increase service life without affecting functional behavior.

Referring again to the five shapes diagrammed in Fig. 3, it is apparent that the smaller the percentage volume at near peak stress, the larger is the K_c-factor, particularly at large values of damping exponent n. The physical reason for this mathematical observation may be explained on the basis of the ratio of the elastic energy to damping energy. In general, it may be stated that if either the cross-sectional shape or longitudinal stress distribution are such as to cause a large percentage of the material to be at stress low enough as to dissipate negligible damping energy, and yet at a stress high enough to store significant elastic

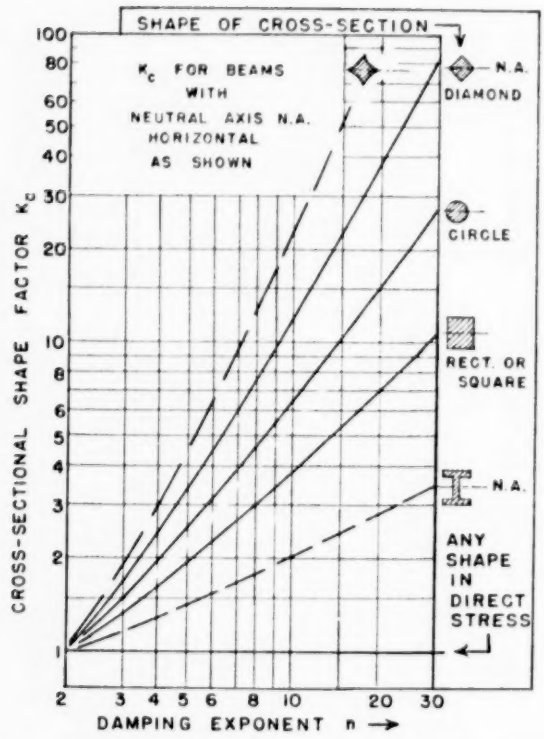

FIG. 3 CROSS-SECTIONAL SHAPE FACTOR K_c FOR VARIOUS COMMON SECTIONS AS A FUNCTION OF DAMPING EXPONENT n

energy, then relatively large A_r-factor will result. This is so for diamond-shaped cross section (as compared to I-beams), for tapered members at constant force (as compared to constant section members), for cantilever beams (as compared to constant moment beams), and for stepped or notched (discontinuous) members (as compared to continuous members). In general, as much volume as possible should be exposed to near peak stress if A_r is to be kept small.

An example of the method of using the three factors which govern the amplification in vibration caused by resonance is given in the following. The example considered is a cantilever beam of constant diamond cross-sectional shape made of S-816, vibrated at 900 F, and exposed to a maximum stress of 60,000 psi (virgin material assumed).

From Equation [16]

$$A_r = K_m K_s K_c$$

From Fig. 1, $K_m = 19$ for virgin material at 900 F, at 60,000 psi and damping exponent $n = 8$

From Fig. 2, $K_s = 1.7$ for a vibrating cantilever beam (case IIA4) with a damping exponent of 8

From Fig. 3, $K_c = 7.8$ for a diamond cross section of a material with a damping exponent of 8

$$A_r = 19 \times 1.7 \times 718 = 252$$

If this resonance amplification factor is too large for the application under consideration, a change in cross section from diamond to I-section could be considered. The resultant reduction in K_c-factor from 7.8 to 1.7 would result in a reduction in resonance amplification from 252 to 55. Needless to say, the resultant reduction in fatigue stress at resonance may be sufficient to eliminate service-failure difficulties in critically stressed members.

EXPERIMENTAL VERIFICATION FOR A_r-EQUATIONS

In order to procure at least partial experimental confirmation of the A_r equations derived in the previous sections a series of tests was undertaken with a newly developed resonance-vibration testing machine described in reference (4). With this machine it is possible to excite resonant vibrations in various types of systems and at the same time maintain the desired excited force by controlling the magnitude of the exciting force. Automatic controls maintain (*a*) a state of resonance and (*b*) the desired excited force, even under conditions of changing damping and dynamic stiffness in the system. The value of the resonance amplification factor A_r may then be computed from the ratio of the excited force (indicated by an accelerometer output) to the exciting force (determined from a tachometer and a counter which indicate unbalance in a revolving eccentric).

Tests were undertaken in this machine to determine A_r for a beam-type specimen made of alloy TP-2-B,[3] this alloy being selected because its large damping exponent n of 13 provides a more critical test of the theory than a material with a small damping exponent. In these tests, made at a stress of 80,000 psi and a stress history of approximately 1000 cycles, three cross-sectional shapes were used, i.e., a square with the neutral axis parallel to one side, a circle, and a diamond shape (actually the same specimen as used for the square cross-section test, except that it was oriented so that the neutral axis was diagonally across two opposite corners). The experimental A_r-values so determined and the theoretical A_r-values calculated by means of the equations presented previously are indicated in Table 3.

It might appear from Table 3 that the check between the theoretical and experimental values of A_r is rather poor. However, considering that in alloy TP-2-B (with a damping exponent n of 13) a 3 per cent error in stress magnitude will result in a 29 per cent error in K_m and A_r, and that the number of other variables which affect damping (such as variability of stress history and rest, cyclic stress frequency, machining stress, and others discussed in reference 3), the check between theory and experiment is considered adequate.

GENERAL OBSERVATIONS, SUMMARY, AND CONCLUSIONS

In many machines and structures, it is highly desirable, if not essential, that the amplitude of near-resonance vibration encountered in service be reduced. In general, the most satisfactory approach is, of course, to reduce the magnitude of the exciting force or change its frequency so as to avoid the resonant conditions. However, this cannot always be accomplished, in which case it becomes necessary either to make the machine more vibration-resistant or to increase the damping of the system in order to reduce the magnitude of the near-resonance vibrations. Frequently, the methods for increasing the fatigue and dynamic strength of a part are exhausted without a satisfactory solution, in which case one must resort to increasing damping.

Sometimes it is possible to increase the damping of a vibrating system through more effective use of joint, aerodynamic, and other damping not directly related to the material, shape, and stress distribution in the members. However, this too may be quite difficult to accomplish, in which case it becomes necessary to increase the damping of the actual part. It is this last type of damping which is the subject of this paper.

It was shown in this paper that the amplification A_r in vibration of a part at resonance is the product of three factors; (*a*) material factor K_m, (*b*) longitudinal stress-distribution factor K_s,

[3] See reference (5) for details on this material, including data on its damping, elasticity, and fatigue properties.

TABLE 3 COMPARISON OF THEORETICAL AND EXPERIMENTAL VALUES FOR FACTOR A_r FOR TP-2-B AT A STRESS OF 80,000 PSI AND A STRESS HISTORY OF 1000 CYCLES
($D = 6.2 \times 10^{-41} S^{13}$; therefore, $J = 6.2 \times 10^{-41}$, and $n = 13$)

Cross-sectional shape	Theoretically computed values				Experimental
	K_m see Eq. [8]	K_s see Eq. [9][a]	K_c see Fig. 3	A_r see Eq. [16]	A_r from resonance test
Square	14	2.2	4.8	150	170
Circle	14	2.2	9	280	340
Diamond	14	2.2	18	550	950

[a] Tapered-beam specimens of the type used in rotating-beam damping work (see reference 3) to produce uniform stress distribution longitudinally also were used in these resonance tests. However, in the resonance tests the longitudinal stress distribution was not uniform. Therefore the K_s-factor for these specimens lies between 1 (for the case IIA1 having uniform longitudinal stress) and $(n + 1)/3 = 4.7$ (for case IIA2 having cantilever-beam-type stress). For the beam used K_s was computed to be very approximately 2.2.

and (*c*) cross-sectional shape factor K_c. The critical relationships of these factors to damping exponent n and other variables were derived and analyzed. Methods of decreasing the resonance amplification factor, based on the equations derived, were suggested and demonstrated. Experimental data were presented to verify the theory.

It is desirable at this point to generalize and interpret physically some of the mathematically derived K_s and K_c-relationships discussed in the previous sections. This is done to provide a guide for those who find it necessary to reduce the resonance amplification factor of parts which encounter troublesome resonance vibration.

Probably the most important generalizations and conclusions apparent from Tables 1 and 2, and Figs. 2 and 3, are as follows:

(*a*) For materials with low damping exponent, say, values of n near 2, the cross-sectional shape and longitudinal stress distribution in the members is relatively unimportant compared to the general level of material damping as defined by constant J.

(*b*) For materials with high damping exponent n, and many of the temperature-resistant materials may be so classified, the cross-sectional shape and longitudinal stress-distribution factors are extremely important. Relatively small changes in member shape and loading, which can sometimes be made through design without affecting functional behavior, cost, and so on, may greatly improve the ability of a part to withstand resonant conditions.

(*c*) As a guide for decreasing the K_s and K_c-factors for a part having large damping exponent n, an attempt should be made to design the part so that the percentage of material at peak or near-peak stress is as large as possible. Material at relatively low stress contributes a relatively large ratio of elastic energy to damping energy which tends to increase the resonance amplification factor.

The above observations and conclusions are of course based on the assumption that damping is related to stress exponentially as indicated by Equation [1]. Although most materials seem to follow this relationship, some, notably a few temperature resistant alloys, possess high magneto-mechanical or other types of damping which may cause significant deviation from this relationship. The analysis of members made of such materials must of course consider the significance of the deviation from the exponential relationship.

It is felt that the analyses and observations discussed in this paper should provide the design engineer with improved perspective in dealing with problems involving resonant vibrations.

Acknowledgments

Most of the data on the damping and elasticity properties of S-816 were taken from a paper coauthored by L. J. Demer.

The author is also grateful to J. Klumpp for checking the manuscript and procuring some of the experimental data.

The work reported in this paper was performed as part of a project sponsored by the Office of Naval Research and the U. S. Air Force, whose fine co-operation is gratefully acknowledged.

BIBLIOGRAPHY

1 "Some Mechanical Properties of Plastics and Metals Under Sustained Vibrations," by B. J. Lazan, Trans. ASME, vol. 65, 1943, pp. 87–102.

2 "Mechanical Vibrations," by J. P. Den Hartog, McGraw-Hill Book Company, Inc., New York, N. Y., 1940.

3 "A Study With New Equipment of the Effects of Fatigue Stress in the Damping Capacity and Elasticity of Mild Steel," by B. J. Lazan, Trans. of the American Society for Metals, vol. 92, 1950, pp. 499–548.

4 "A New Resonance Vibration Exciter and Controller for Testing Materials and Structures," by B. J. Lazan, J. Brown, A. Gannett, P. Kirmser, and J. Klumpp; presented before the American Society for Testing Materials in June, 1952.

5 "The Damping, Elasticity, and Fatigue Properties of Temperature Resistant Materials," by B. J. Lazan and L. J. Demer, Proceedings of the American Society for Testing Materials," vol. 51, 1951, pp. 611–648.

6 "Damping, Fatigue and Dynamic Stress-Strain Properties of Mild Steel," by B. J. Lazan and T. Wu, Proceedings of the American Society for Testing Materials, vol. 51, 1951, pp. 649–681.

7 "Internal Friction in Engineering Materials," by J. M. Robertson and A. J. Yorgiadis, Journal of Applied Mechanics, Trans. ASME, vol. 68, 1946, p. A-173.

8 "Plywood Characteristics Disclosed by Vibration Tests," by A. J. Yorgiadis and J. M. Robertson, *Aero Digest*, vol. 45, April 1, 1944, pp. 76–77, 80–82, 196, 198, 201, 202, 204.

9 "A New Fatigue Strength-Damping Criterion for the Design of Resonance Members," by J. Marin and F. B. Stulen, Journal of Applied Mechanics, Trans. ASME, vol. 69, 1947, p. A-269.

10 "Technische Schwingungslehre," by Karl Klotter, Springer-Verlag, Berlin, Germany, 1951, pp. 237–246.

Unsteady Radial Flow of Gas Through Porous Media

By R. JENKINS[1] and J. S. ARONOFSKY[1]

This paper presents a numerical method for describing the transient flow of gases radially inward or outward through a porous medium in which the initial and terminal pressures and/or rates are specified. Specific examples are worked out which have application in the study of natural-gas reservoirs. The computations were carried out by means of punch-card machines. The pressure distribution as a function of time has been calculated for various ratios of reservoir diameter to well diameter and for various dimensionless flow rates for a well penetrating the center of a homogeneous disk-shaped reservoir. A simple means of predicting the well pressure at any time in the history of such an idealized field has been developed. Flow rates and pressure distributions within the radial reservoir also have been calculated for the case in which the well pressure is suddenly lowered from its initial static value, and then held constant.

Nomenclature

The following nomenclature is used in the paper:

h = formation thickness, cm
k = permeability, darcys
N = P_w/P_0
P = pressure within reservoir, atm
P_a = bulk average pressure in reservoir, atm
P_0 = initial pressure within reservoir, atm
P_w = well pressure, atm
Q = flow rate from or into well, standard cc per sec (measured at 60 F and 1 atm)
r = radial distance from center of well, cm
r_d = effective drainage radius, cm
r_e = radius of reservoir, cm
r_w = well radius, cm
t = time, sec
ξ = $\ln \frac{r}{r_w}$
μ = viscosity, centipoises
ϕ = porosity, fraction
τ = dimensionless time parameter

Introduction

The unsteady flow of compressible liquids through porous media has been investigated in many different geometrical forms (1, 2, 3),[2] and is directly analogous to the unsteady conduction of heat, which has been investigated at great length (4). The pressure-density relationship of gases has different characteristics from that of liquids, such that the differential equation for unsteady flow of gases is nonlinear, and has not been solved by analytical methods. A numerical solution of the case of one-dimensional gas flow through porous media has previously been presented as the initial stage of this investigation (5). This paper presents numerical solutions of the problem of unsteady flow of gas radially inward to (or outward from) a well bore from a reservoir having an impervious, circular outer boundary. These numerical solutions were obtained with the aid of IBM punch-card calculators, which were found to be quite effective for this type of problem.

The principal application of these calculations is believed to be to flow in natural-gas fields, in the interpretation of pressure drawdown tests, in the estimation of reserves, and in calculation of injection pressures required in gas-injection and cycling operations. The belief has existed for many years that transients in reservoirs producing only gas were of minor importance. This study has shown this assumption to be true in some cases, but not in others, and has delineated the conditions where transient behavior is important.

Flow Characteristics

Visualize a well passing through the center of a sand body of uniform thickness and circular cross section, such as is shown in Fig. 1, containing gas at a uniform pressure P_0. The top, bottom, and outer boundary of this sand are impervious to the gas, which can escape only through the well. Suppose that at time $t=0$, withdrawal of gas through this well is begun and maintained thereafter at a constant rate, in standard cubic feet per hour. The pressure at the well P_w will then fall below its original pressure P_0, as a result of flow of the gas through the sand. This pressure drop can be calculated from the equation for steady-state laminar, radial flow of gas through porous media, as given, for example, by Muskat (1)

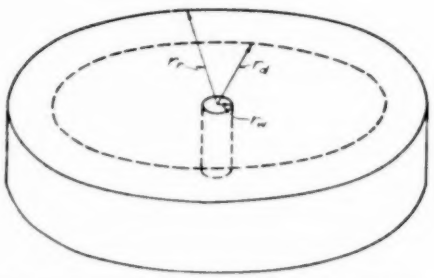

Fig. 1 Schematic Section of Radial Reservoir

$$P_0^2 - P_w^2 = \frac{Q\mu \ln r_d/r_w}{\pi kh} \quad \ldots\ldots\ldots\ldots [1]$$

if the proper drainage radius is used.

[1] Magnolia Petroleum Company, Field Research Laboratories, Dallas, Tex.

[2] Numbers in parentheses refer to the Bibliography at the end of the paper.

Contributed by the Applied Mechanics Division and presented at the Annual Meeting New York, N. Y., Nov. 30–Dec. 5, 1952, of The American Society of Mechanical Engineers.

Discussion of this paper should be addressed to the Secretary, ASME, 29 West 39th Street, New York, N. Y., and will be accepted until July 10, 1953, for publication at a later date. Discussion received after the closing date will be returned.

Note: Statements and opinions advanced in papers are to be understood as individual expressions of their authors and not those of the Society. Manuscript received by ASME Applied Mechanics Division, July 3, 1952. Paper No. 52—A-26.

In the first instant of time after withdrawal of gas begins, the gas removed originates very close to the well itself, so that the effective radius of drainage is practically the same as the radius of the well. Therefore the logarithmic term in Equation [1] is zero, indicating the absence of pressure drop. As time passes, and as additional gas is withdrawn from the sand, the effective radius of drainage will move away from the well into the interior of the reservoir, and a corresponding drop in the well pressure will be observed. As the reservoir becomes depleted, the average pressure in the reservoir, P_a (bulk average)[3] at the time in question should be used, rather than the initial reservoir pressure in Equation [1]; thus

$$P_a^2 - P_w^2 = \frac{Q\mu \ln r_d/r_w}{\pi kh} \quad [2]$$

We shall use Equation [2] to define the effective drainage radius. Thus, when P_a, P_w, k, h, Q, and μ are known, we may calculate the effective radius of drainage from Equation [2]. It should be observed that r_d is a variable representing a fictitious radius, and that fluid may move toward the well from points further away than r_d. Obviously, the recession of the effective drainage radius cannot continue indefinitely; the upper limit for the effective radius of drainage is the radius of the reservoir itself. It was found in this study that after approximately 5 per cent of the gas originally in the reservoir has been withdrawn, the drainage radius, as defined by Equation [2], stops receding, and becomes constant at a value equal to one half the distance from the well to the outer boundary of the sand body, or reservoir.

The characteristics obtained in injection of gas into a well are similar to those described in the foregoing.

Equations of Gas Flow

The basic differential equation which describes the flow of gas through a porous medium has been described in the literature (1). This equation for isothermal flow is

$$\nabla^2(P/P_0)^2 = \frac{2\phi\mu}{P_0 k}\frac{\partial}{\partial t}(P/P_0) \quad [3]$$

For radial flow, this equation reduces to

$$\frac{\partial^2(P/P_0)^2}{\partial r^2} + \frac{1}{r}\frac{\partial(P/P_0)^2}{\partial r} = \frac{2\phi\mu}{P_0 k}\frac{\partial(P/P_0)}{\partial t} \quad [4]$$

The assumptions involved in using Equation [4] are as follows:

1 The reservoir has the shape of a horizontal disk with its center at the well bore; its top, bottom, and outer radius are impervious.

2 The permeability to gas within the reservoir is constant and uniform.

3 The only phase flowing is a gas of constant composition.

4 The density of this gas is directly proportional to the pressure (Boyle's law).

5 The viscosity of the gas is constant.

6 The flow follows Darcy's law; i.e., is in the viscous range.

7 Gravitational forces are neglected.

A field developed in a square or staggered pattern would approximately satisfy the first assumption. A free gas field or an oil field producing at a high gas-oil ratio would satisfy the third requirement. In the fourth assumption, where deviations from Boyle's law are severe, PVT measurements may be used to select an appropriate correction factor for these calculations. Assumptions 5 and 6 may be relaxed sufficiently to handle many cases which would be encountered in the field.

[3] At any time, P_a is the pressure which would be found if flow at the well were stopped, and pressure in the reservoir allowed to equalize.

Equations [3] and [4] would be linear, and easily solved by analytical methods, if P/P_0 appeared as the first power on the left-hand side of these equations. Instead, this ratio is squared and it was necessary to reduce Equation [4] to a "difference" equation, which was then solved numerically, as described in the literature (6, 7, 8). The procedure used is described in the following section.

Methods of Calculation

All the calculations of pressures and rates shown in this paper are the result of solving the differential equation for radial gas flow. These solutions were found by calculating the changes in pressure at a series of points in the reservoir after small intervals of time, and repeating this process a large number of times by means of IBM electronic punch-card calculating machines to obtain the complete curves. Equation [4], the differential equation for radial gas flow, has been simplified by introducing a new variable

$$\xi = \ln\left(\frac{r}{r_w}\right) \quad [5]$$

The differential equation, written in terms of this new variable and the dimensionless pressure P/P_0, becomes

$$\frac{\partial^2(P/P_0)^2}{\partial\xi^2} = \frac{2\phi\mu r_w^2\left(\frac{r}{r_w}\right)^2}{kP_0}\frac{\partial(P/P_0)}{\partial t} \quad [6]$$

The step-by-step calculations of the pressure change have been performed on the finite-difference form of this equation, which is

$$(P/P_0)_{\xi,t+\Delta t} = \frac{\Delta t P_0 k}{2\phi\mu r_w^2\left(\frac{r}{r_w}\right)^2\Delta\xi^2}\left[(P/P_0)^2_{\xi+\Delta\xi,t} + (P/P_0)^2_{\xi-\Delta\xi,t} - 2(P/P_0)^2_{\xi,t}\right] + (P/P_0)_{\xi,t} \quad [7]$$

where

$(P/P_0)_{\xi,t}$ = dimensionless pressure at distance ξ and time t

$(P/P_0)_{\xi+\Delta\xi,t}$ = dimensionless pressure at next larger radial position, $\xi + \Delta\xi$, and time t

It was found convenient in the calculation to choose time increment Δt, such that

$$\frac{\Delta t P_0 k}{2(\Delta\xi)^2 r_w^2 \mu\phi} = 1 \quad [8]$$

These time increments are sufficiently small to insure the convergence of the step-by-step calculation, as shown by Frankel (9). Equation [7] now becomes

$$(P/P_0)_{\xi+\Delta\xi,t} = \frac{1}{\left(\frac{r}{r_w}\right)^2}\left[(P/P_0)^2_{\xi+\Delta\xi,t} + (P/P_0)^2_{\xi-\Delta\xi,t} - 2(P/P_0)^2_{\xi,t}\right] + (P/P_0)_{\xi,t} \quad [9]$$

Radial positions were selected such that the radius at each point was twice that at the preceding point, starting with the well radius, out to a maximum of 1024 times the well radius. This selection of radius values yields equal values of $\Delta\xi$.

While the arithmetic process of calculating successive, step-by-step pressure values from Equation [9] is quite simple, the equation cannot be used as it stands because of the very small size of the time increment. To avoid this obstacle, Equation [9] has been used with a fictitious well radius, 8, or 64 times the actual well radius. From Equation [8] it can be seen that these ficti-

tious well radii increase the time increment represented by each step by 64, and 4096, respectively.

In calculating the pressure values at the fictitious well radius (for the next succeeding time step), it has been assumed that the steady-state flow equation can be applied between this radius and the actual well bore. This is equivalent to neglecting the time required for the gas originally inside the fictitious well radius to flow out through the actual well. Correction for this time has been made by making additional calculations using the true well radius that overlap those made with the fictitious radius, and fitting the curves together. The time correction was found to be very small.

Well-Pressure Variation

A generalized correlation of the well-bore pressure in an infinite reservoir is presented in Fig. 2. This figure applies to injection as well as production, and shows in dimensionless form a variation in the results with the flow rate during gas injection, but very little change in the curves with flow rate for gas withdrawal. More than one curve is obtained in Fig. 2 because of the nonlinearity of the differential equation for gas flow. At very small flow rates, the nonlinearity becomes negligible and the differential equation of gas flow approaches, as the limiting case, the classical diffusion equation. A curve for the limiting case of the flow rate (either injection or production) approaching zero has been calculated independently by Carslaw and Jaeger (4), using an analytical method and is shown as the dashed curve in Fig. 2. The agreement between this curve and those calculated numerically is quite satisfactory, and illustrates the continuous trend of the curves from injection to withdrawal.

A similar generalized correlation of the well-bore pressure for finite reservoirs of several radii is presented in Fig. 3. The curves shown are for the two withdrawal rates shown in Fig. 2 but they can be applied to any withdrawal rate with very little error. Fig. 3 shows the early transient period clearly, with a relatively sharp transition as the effective radius of drainage ceases to move outward, into the later period where the entire reservoir is being depleted.

In order to give a clearer physical meaning to these results, a plot of the radius of drainage versus dimensionless time is presented in Fig. 4. This plot emphasizes the fact that, initially, the effective drainage radius is independent of the reservoir radius,

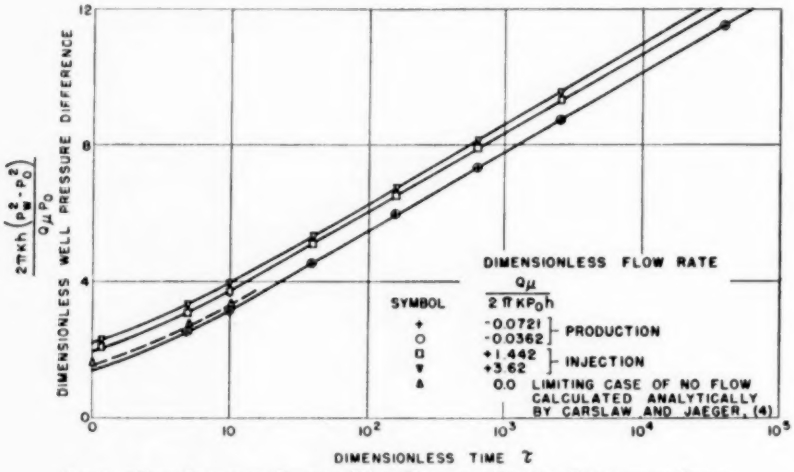

Fig. 2 Well-Pressure Change With Time for Various Production Rates

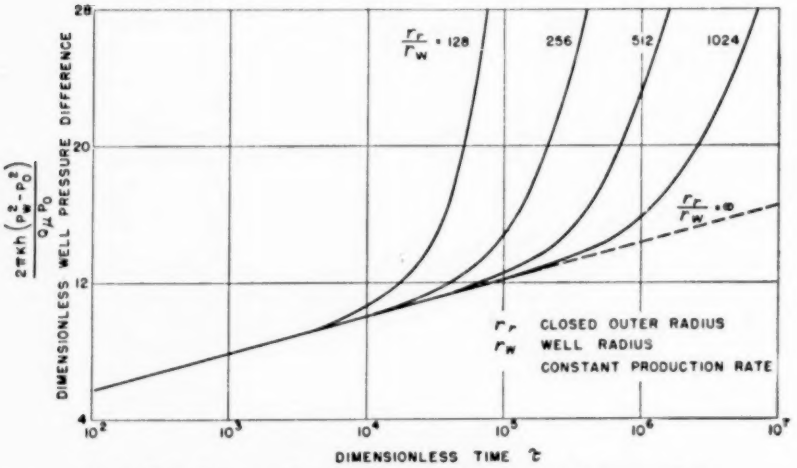

Fig 3 Well-Pressure Change With Time for Various Reservoir Radii

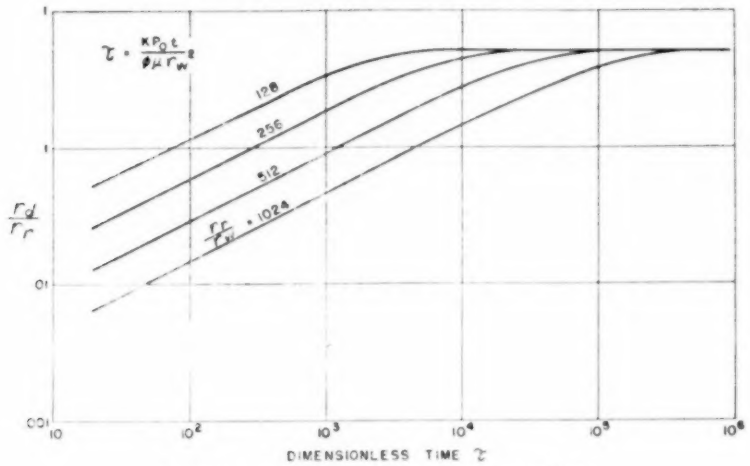

FIG. 4(a) DRAINAGE RADIUS AS A FUNCTION OF TIME

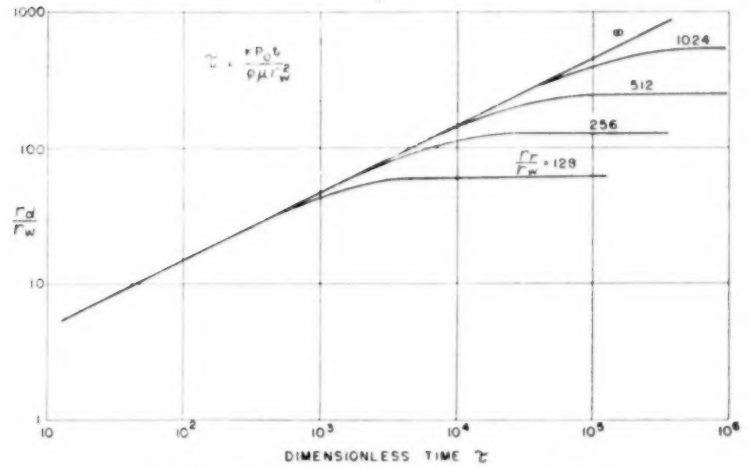

FIG. 4(b) DRAINAGE RADIUS AS A FUNCTION OF TIME

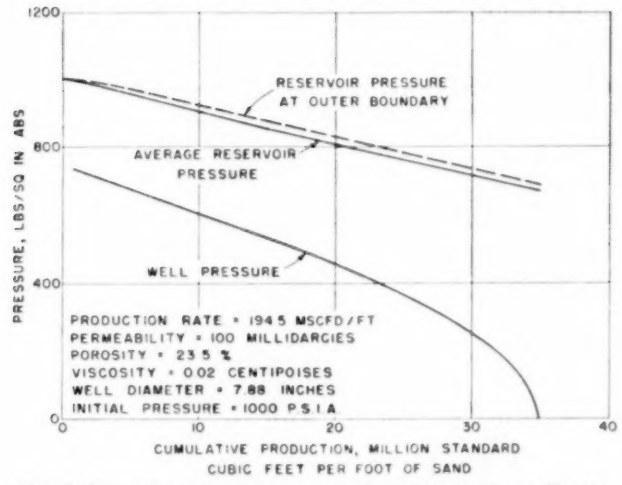

FIG. 5 WELL PRESSURE AND AVERAGE RESERVOIR PRESSURE VERSUS CUMULATIVE GAS PRODUCTION

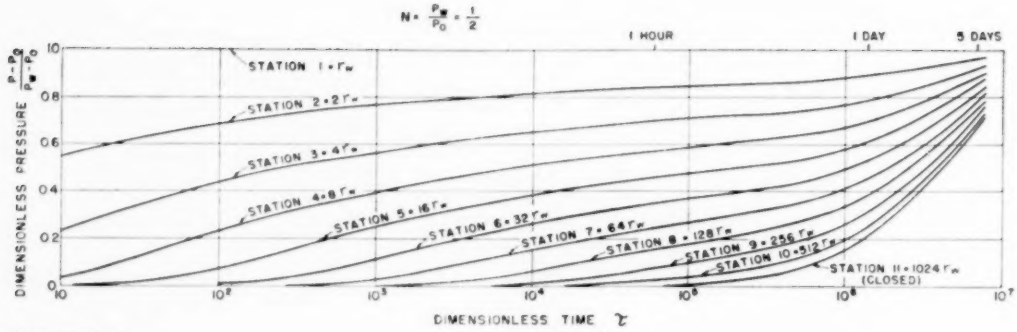

μ = 0.02 centipoise
K = 100 millidarcies
P_0 = 100 atm (initial press)
P_w = 50 atm (well press)
r_w = 10 cm
ϕ = 0.3
n = incremental time advance

$(\Delta\xi)^2 = \ln 2$

$\tau = \dfrac{KP_0 t}{\mu\phi r_w^2}$

$\tau = 2n\,(\Delta\xi)^2 = 2n \ln 2$

$N = \dfrac{P_w}{P_0} = {}^1/_2$

FIG. 6 DIMENSIONLESS PRESSURE DISTRIBUTION IN A FREE GAS RESERVOIR AFTER A SUDDEN PRESSURE CHANGE AT WELL

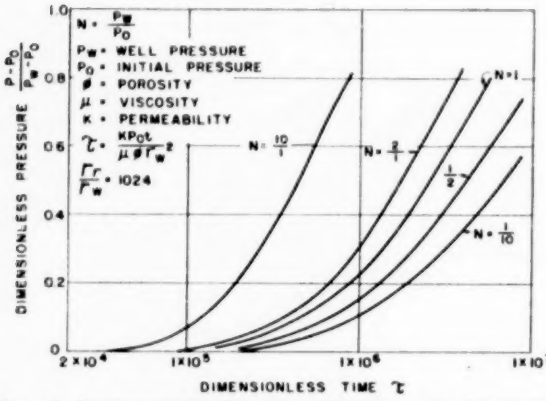

FIG. 7 DIMENSIONLESS PRESSURE VARIATION AT RESERVOIR BOUNDARY FOR SEVERAL VALUES OF N

but that later the situation is reversed, and the drainage radius is independent of the well radius, varying directly with the reservoir radius.

The well-pressure variation for conditions chosen to represent a typical natural-gas well has been calculated, using an effective drainage radius equal to one half the reservoir radius, and is shown in Fig. 5.

CONSTANT WELL PRESSURE

Solutions of the differential equation for radial gas flow, Equation [4], also have been obtained for the case in which the flowing pressure at the well bore is held constant, and the outer boundary of the reservoir is assumed to be impervious, as in the constant-rate problem. The variation of the pressure at several points inside the reservoir with time is shown in Fig. 6 for $N = P_w/P_0 = {}^1/_2$. At first, before the pressure at the outer radius of the reservoir has changed, the curves for different radial positions are parallel. Then, as the outer portion of the reservoir is drained, all the curves converge toward the well pressure

$$\left(\frac{P - P_0}{P_w - P_0} = 1\right)$$

Different sets of curves would be obtained for different values of $N = P_w/P_0$. The effect of this pressure ratio N, on the character of these curves is shown in Fig. 7 in a plot of dimensionless pressure, $(P - P_0)/(P_w - P_0)$ at the outer boundary, or reservoir radius, versus dimensionless time τ, for values of N from 10/1 to 1/10. The curve for $N = 1$ corresponds to the limiting case of a very small pressure change and falls between the curves for $N > 1$ (injection) and $N < 1$ (withdrawal). The more rapid pressure changes found at the higher values of N are very similar to those reported for linear gas flow in a previous paper (5). Similar plots could be prepared from calculations already completed for many other positions within a radial reservoir system.

ACKNOWLEDGMENT

Grateful acknowledgment is made to the management of the Magnolia Petroleum Company for permission to publish the results of this investigation. The authors are particularly indebted to Messrs. A. C. Buchanan and G. L. Hamilton of the Magnolia Petroleum Company's Comptroller's Department, for their energetic co-operation in the punch-card operations.

BIBLIOGRAPHY

1 "Flow of Homogeneous Fluids," by M. Muskat, second printing, J. Edwards, Inc. Ann Arbor, Mich., 1946.

2 "Physical Principles of Oil Production," by M. Muskat, McGraw-Hill Book Company, New York, N. Y., 1949.

3 "The Application of the LaPlace Transformation to Flow Problems in Reservoirs," by A. F. Van Everdingen and W. Hurst, *Journal of Petroleum Technology*, AIME, vol. 1, no. 12, December, 1949, pp. 305-326.

4 "Conduction of Heat in Solids," by H. Carslaw and J. Jaeger, Oxford Clarendon Press, London, England, 1947.

5 "Unsteady Flow of Gas Through Porous Media: One-Dimensional Case," by J. S. Aronofsky and R. Jenkins, presented at the First U. S. National Congress of Applied Mechanics, Chicago, Ill., June, 1951.

6 "Relaxation Methods in Theoretical Physics," by R. V. Southwell, Oxford Clarendon Press, London, England, 1946.

7 "Numerical Methods of Analysis in Engineering," by L. Grinter, The Macmillan Company, New York, N. Y., 1949.

8 "Numerical Analysis of Heat Flow," by G. M. Dusinberre, McGraw-Hill Book Company, New York, N. Y., 1949.

9 "Convergence Rates of Iterative Treatment of Partial Differential Equations," by S. P. Frankel, "Mathematical Tables and Aids to Computation," April, 1950

Pure Bending of an Incomplete Torus[1]

By M. A. SADOWSKY[2] and E. STERNBERG,[3] CHICAGO, ILL.

An exact solution in series form is presented for the stresses and displacements in an incomplete torus of circular center line and circular cross section under conditions of pure bending. The solution is preceded by a formal treatment of the case in which the shape of the cross section is arbitrary. This more general problem is reduced to one of axisymmetry, which is in turn attacked by a modification of the stress-function approach of Timpe to rotationally symmetric problems in elasticity theory. The modified stress-function approach, which may be of interest beyond the present application, is referred to general orthogonal axisymmetric co-ordinates, and the solution of the specific problem considered here is based on the use of toroidal co-ordinates. The normal stresses acting on the circular cross sections of the torus are evaluated numerically in an illustrative example and are compared with the results of previous approximate solutions of the same problem. The adaptation of the present solution to the determination of the initial stresses in a complete torus from which a wedge-shaped portion has been removed is indicated.

Introduction—Statement of Problem

THE extension of the problem of Saint Venant to curved beams with a circular center line has received repeated previous attention in the literature. The generalized problem consists in determining, within the classical theory of elasticity, the stresses and displacements in an incomplete circular torus of arbitrary uniform cross section under the following loading conditions: The lateral surface of the torus is free from stress; the terminal cross sections are acted upon by a system of normal and shearing tractions, the stress resultant of which is prescribed arbitrarily subject to the requirement of equilibrium of the body as a whole. Two special cases are of particular significance: (*a*) the case in which the tractions applied to each of the terminal sections are statically equivalent to a single force whose line of action coincides with the axis of revolution of the torus ("pure torsion"). (*b*) The case in which the resultant of the loading on either terminal section is a couple whose axis is parallel to the axis of revolution of the torus ("pure bending").

The case of pure torsion, which is important in connection with the theory of helical springs of small pitch, was treated by Michell (1)[4] and Fubini (2) on the basis of a semi-inverse approach, starting with the displacement equations of equilibrium. Southwell (4) derived Michell's general results by aid of the stress equations of equilibrium and compatibility. With reference to circular cylindrical co-ordinates (ρ, γ, z) the problem is reducible to the determination of a single stress function $\phi(\rho, z)$ which is characterized by

$$\left.\begin{aligned} \phi_{\rho\rho} - \frac{3}{\rho}\phi_\rho + \phi_{zz} &= 1 \text{ in } D \\ \phi(\rho, z) &= 0 \text{ on } \Gamma \end{aligned}\right\} \quad \ldots\ldots\ldots [1][5]$$

where the z-axis is assumed to coincide with the axis of the torus, D designates the cross-sectional region, and Γ is the boundary of D, Fig. 1.

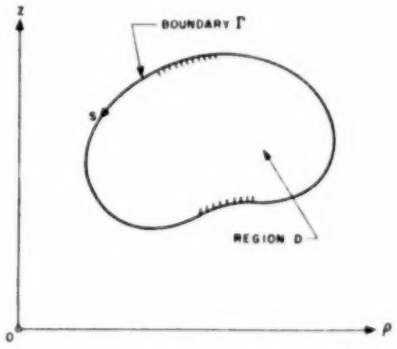

Fig. 1 Meridional Cross Section of Torus

Exact solutions, based on Equations [1], for a torus of nearly circular and of rectangular cross section were given by Michell (1). The rectangular cross section was reconsidered in greater detail by Tricomi (3) and Langhaar (11). In a recent paper, Freiberger (5), with the aid of toroidal co-ordinates, obtained an exact series solution corresponding to the circular cross section. Göhner (7, 8, 10) arrived at approximate results for the circular, elliptic, and rectangular cross section by a method of successive approximations; he employed the known solutions to the corresponding problem of Saint Venant-torsion of a straight beam as a first approximation, and deduced higher approximations through a perturbation scheme applied to Equations [1].

The case of pure bending, with which we are concerned, presents considerably greater analytical difficulties. Here, again, the first contribution is due to Michell (1). Guided by considerations of symmetry, Michell made certain restrictive assumptions regarding the displacement field and reduced the problem to the determination of a stress function $\phi(\rho, z)$ which obeys

$$\left.\begin{aligned} \Lambda^4\phi &= 1 \text{ in } D \\ \Lambda^2 &\equiv \frac{\partial^2}{\partial\rho^2} - \frac{1}{\rho}\frac{\partial}{\partial\rho} + \frac{\partial^2}{\partial z^2} \\ L_i[\phi(\rho, z)] &= 0\ (i = 1, 2) \text{ on } \Gamma \end{aligned}\right\} \quad \ldots\ldots\ldots [2]$$

[1] The results presented in this paper were obtained in the course of an investigation conducted under contract N7onr-32906 with the Office of Naval Research, Department of the Navy, Washington, D. C.

[2] Associate Professor of Mathematics, Illinois Institute of Technology. Mem. ASME.

[3] Professor of Mechanics, Illinois Institute of Technology. Jun. ASME.

[4] Numbers in parentheses refer to the Bibliography at the end of the paper.

Contributed by the Applied Mechanics Division and presented at the Annual Meeting, New York, N. Y., November 30–December 5, 1952, of The American Society of Mechanical Engineers.

Discussion of this paper should be addressed to the Secretary, ASME, 29 West 39th Street, New York, N. Y., and will be accepted until July 10, 1953, for publication at a later date. Discussion received after the closing date will be returned.

Note: Statements and opinions advanced in papers are to be understood as individual expressions of their authors and not those of the Society. Manuscript received by ASME Applied Mechanics Division, June 12, 1952. Paper No. 52—A-17.

[5] Subscripts attached to functions which originally bear no subscript denote partial differentiation with respect to the argument indicated.

where L_1 and L_2 are linear operators involving partial derivatives up to the third order. Essentially the same result was established by Southwell (4), whose derivation rests on the stress equations of equilibrium and compatibility. Fubini (2) and, more recently, Freiberger and Smith (6), arrived at alternative reductions of the problem on the basis of displacement approaches. Thus the formal solution presented in (6) necessitates the determination of two harmonic functions $\phi_0(\rho, z)$ and $\phi_1(\rho, z)$, which are subject to a pair of interlocking boundary conditions, each involving partial derivatives up to the second order.

The specific applications of these general solutions apparently have been confined to the trivial case of a narrow rectangular cross section for which the well-known generalized plane-stress solution[6] was re-established (4, 6). Göhner (9, 10) treated the case of a circular cross section by a method of successive approximations analogous to that described previously with reference to the problem of pure torsion. His perturbation process here rests on the stress equations of equilibrium in conjunction with the Beltrami-Michell conditions of compatibility, and the solution appropriate to pure Saint Venant-bending of a straight beam is used as a first approximation. Reference is also made to the elementary treatment of the problem by means of the approximate theory of curved beams, originated by Winkler.[7] Finally, we mention the available shell-theoretic investigations of the bending of thin-walled toroidal shells; a pertinent bibliography is given in the most recent study of this kind, by Clark, Gilroy, and E. Reissner (22). One of the objectives of the current investigation is to examine the limitations of the existing approximate solutions in connection with the solid circular cross section. Furthermore, the exact solution presented here lends itself to the rigorous study of certain dislocations and initial stresses in a complete torus.

In connection with the foregoing formal solutions to the problem of pure bending for a torus of arbitrary cross section, we note that Michell's work (1) clearly implies a reduction of the problem to one of torsion-free axisymmetry, which is characterized by prescribed surface tractions on the lateral boundary of the torus. Moreover, it should be emphasized that this reduction is by no means unique, and that the axisymmetric residual problem so arising is amenable to any one of the various available stress-function approaches[8] to rotationally symmetric problems in elasticity theory, such as those of Boussinesq-Papkovich-Neuber, Michell, Love-Galerkin, Föppl, Timpe, or Weber. The essential feature of the present treatment is twofold; (*a*) the particular reduction to an axisymmetric problem adopted here seems to yield a more tractable form of the residual problem; (*b*) the residual problem is attacked by means of a modification of Timpe's approach (15, 16) with an apparent gain in facility. We now turn to a discussion of this modified stress-function approach which is preliminary to the consideration of the problem to be dealt with subsequently.

Modification of Timpe's Stress-Function Approach

A solution of the basic field equations is said to possess torsion-free rotational symmetry with respect to the z-axis if its displacement field conforms to the conditions

$$u_\gamma = 0, \quad \frac{\partial u_\rho}{\partial \gamma} = 0, \quad \frac{\partial u_z}{\partial \gamma} = 0 \ldots\ldots [3]$$

where (u_ρ, u_γ, u_z) are the cylindrical components of displacement. According to Timpe (15, 16) the general solution of the displacement equations of equilibrium subject to the restrictions, Equations [3], and in the absence of body forces, is representable as the sum of the two displacement fields

$$[T_1]: \quad 2Gu_\rho = \phi_{\rho}, \qquad 2Gu_z = \phi_z \ldots\ldots [4]$$

$$[T_2]: \quad 2Gu_\rho = \Psi_\rho - \frac{4(1-\nu)}{\rho}\Psi, \quad 2Gu_z = \Psi_z \ldots\ldots [5]$$

where

$$\nabla^2\phi(\rho, z) = 0, \quad \Lambda^2\Psi(\rho, z) = 0 \ldots\ldots [6]$$

Here ∇^2 is the Laplacian, the operator Λ^2 is defined as in Equations [2]; whereas G and ν designate the shear modulus and Poisson's ratio, respectively. The displacement fields given by Equations [4] and [5], together with their associated fields of stress, constitute the first and second Timpe solution, and are denoted by $[T_1]$ and $[T_2]$, respectively.[9]

The stress function Ψ, which generates $[T_2]$, satisfies the partial differential equation characterizing the stream function in axisymmetric potential flows of an ideal incompressible fluid, and we shall find it convenient to refer to any solution of the equation $\Lambda^2\Psi = 0$ as a "stream function." In analogy to the velocity potential of such rotationally symmetric flows, we may associate with every stream function Ψ a conjugate potential function Φ defined by

$$\Phi_\rho = -\frac{1}{\rho}\Psi_z, \quad \Phi_z = \frac{1}{\rho}\Psi_\rho \ldots\ldots [7]$$

or, alternatively, by the line integral

$$\Phi(\rho, z) = \int_{(\rho_0, z_0)}^{(\rho, z)} \left[-\frac{1}{\rho}\Psi_z d\rho + \frac{1}{\rho}\Psi_\rho dz\right] \ldots\ldots [8]$$

where (ρ_0, z_0) is an arbitrary fixed point of the meridional half plane $\rho \geq 0$. Since $\Lambda^2\Psi = 0$, the line integral, Equation [8], is independent of the path and $\Phi(\rho, z)$ is single-valued in any simply connected domain throughout which $\Psi(\rho, z)$ is regular; moreover, $\nabla^2\Phi = 0$. In the same manner we may use Equations [7] to associate with any given harmonic function $\Phi(\rho, z)$ a conjugate stream function $\Psi(\rho, z)$. A potential function and a stream function satisfying Equations [7] will be called conjugate with respect to each other.

If ψ denotes the stream function conjugate with regard to ϕ, the displacements of $[T_1]$, Equations [4], may be written as

$$2Gu_\rho = -\frac{1}{\rho}\psi_z, \quad 2Gu_z = \phi_z \ldots\ldots [9]$$

Now, let a new conjugate pair of potential and stream functions be defined by

$$\bar{\phi}(\rho, z) = -\phi_z, \quad \bar{\psi} = -\psi_z \ldots\ldots [10]$$

and the first Timpe solution becomes

$$2Gu_\rho = \frac{1}{\rho}\bar{\psi}, \quad 2Gu_z = -\bar{\phi} \ldots\ldots [11]$$

This solution henceforth will be referred to as basic solution $[A]$. Next, we define a second and independent basic solution $[B]$ by means of

$$[B] = 4(1-\nu)[A] + [T_2] \ldots\ldots [12]$$

---

[6] See, for example, (13), p. 61. This solution is here attributed to Golovin.

[7] See (14), p. 65.

[8] See (16) for references.

[9] Throughout this paper, capital letters in brackets denote either the displacement vector-field or the stress tensor-field of the corresponding solution, and equality, addition, as well as multiplication by a scalar, are to be interpreted accordingly.

with the provision that [A] in Equation [12] is generated by $\overline{\phi} = \Phi(\rho, z)$ and $\overline{\psi} = \Psi(\rho, z)$. Since the Timpe solutions [T_1], [T_2] will be abandoned in favor of the new basic solutions [A], [B], we may, without risk of ambiguity, omit the bars over the stress functions appearing in Equations [11]. With this understanding, and by virtue of Equations [12], [11], and [5], we reach

$$[A]: \quad 2Gu_\rho = \frac{1}{\rho}\psi, \quad 2Gu_z = -\phi \qquad [13]$$

$$[B]: \quad 2Gu_\rho = \Psi_\rho, \quad 2Gu_z = -4(1-\nu)\Phi + \Psi_z \qquad [14]$$

where

$$\nabla^2\phi = \nabla^2\Phi = 0, \quad \Lambda^2\psi = \Lambda^2\Psi = 0 \qquad [15]$$

and $\{\phi, \psi\}$ as well as $\{\Phi, \Psi\}$ are conjugate pairs in the sense of Equations [7]. It follows from the generality of the Timpe solutions that any torsion-free axisymmetric solution of the displacement equations of equilibrium is also representable as the sum of basic solutions [A] and [B], provided the generating stress functions are chosen appropriately.

Comparing Equations [13], [14] with Equations [4], [5], we observe that each of the displacements of [A] and [B], in contrast to those of [T_1] and [T_2], involves potential as well as stream functions. In the corresponding formulas for the stresses this mixed representation is no longer necessary, and the potential functions may be eliminated entirely with the aid of Equations [7].[10] The displacements of [A] contain only the generating stress functions, and hence the associated field of stress is found to involve no derivatives higher than the first of ϕ or ψ with respect to the co-ordinates; the stresses of [T_1], on the other hand, contain the second derivatives of ϕ. Similarly, the stress formulas belonging to [B] are less unwieldy than those appropriate to [T_2].[11] These simplifications may become appreciable in applications requiring the use of more general curvilinear co-ordinates. More significant analytical gains, however, have been encountered in connection with curvilinear co-ordinate systems which are not separable in the strict sense, such as spherical dipolar or toroidal co-ordinates. Here, as will become apparent, a single-term stream function may give rise to a conjugate potential function in series form, and the corresponding benefits derived from the modification of Timpe's approach are nontrivial.[12]

We now introduce general axisymmetric curvilinear co-ordinates (α, β, γ) through the transformation

$$x = \rho(\alpha, \beta)\cos\gamma, \quad y = \rho(\alpha, \beta)\sin\gamma, \quad z = z(\alpha, \beta) \qquad [16]$$[13]

which is assumed to satisfy the orthogonality condition

$$\rho_\alpha\rho_\beta + z_\alpha z_\beta = 0 \qquad [17]$$

The differential of arc length is given by

$$ds^2 = \left(\frac{d\alpha}{h_1}\right)^2 + \left(\frac{d\beta}{h_2}\right)^2 + \left(\frac{d\gamma}{h_3}\right)^2 \qquad [18]$$

and the metric coefficients h_1, h_2, h_3 become

$$h_1 = (\rho_\alpha^2 + z_\alpha^2)^{-1/2}, \quad h_2 = (\rho_\beta^2 + z_\beta^2)^{-1/2}, \quad h_3 = \rho^{-1} \qquad [19]$$

Basic solution [A] may be referred to the curvilinear co-ordinates (α, β, γ) by the usual transformation methods;[14] once this is accomplished, the curvilinear components of displacement and stress for [B] are readily obtained from Equations [16], [17] of reference (16) and the current Equation [12]. The results of these computations follow:

Solution [A]

$$2Gu_\alpha = h_1\left(\frac{\psi\rho_\alpha}{\rho} - \phi z_\alpha\right), \quad 2Gu_\beta = h_2\left(\frac{\psi\rho_\beta}{\rho} - \phi z_\beta\right) \qquad [20]$$

$$\left.\begin{aligned}
\sigma_\alpha &= \frac{h_1^2\rho_\alpha}{\rho}\psi_\alpha - \frac{h_2^2\rho_\beta}{\rho}\psi_\beta - \frac{h_1^2\rho_\alpha^2}{\rho^2}\psi \\
\sigma_\beta &= \frac{h_2^2\rho_\beta}{\rho}\psi_\beta - \frac{h_1^2\rho_\alpha}{\rho}\psi_\alpha - \frac{h_2^2\rho_\beta^2}{\rho^2}\psi \\
\sigma_\gamma &= \frac{\psi}{\rho^2} \\
\tau_{\alpha\beta} &= \frac{h_1h_2}{\rho}\left(\rho_\beta\psi_\alpha + \rho_\alpha\psi_\beta - \frac{\rho_\alpha\rho_\beta}{\rho}\psi\right)
\end{aligned}\right\} \qquad [21]$$

Solution [B]

$$\left.\begin{aligned}
2Gu_\alpha &= h_1[\Psi_\alpha - 4(1-\nu)z_\alpha\Phi] \\
2Gu_\beta &= h_2[\Psi_\beta - 4(1-\nu)z_\beta\Phi]
\end{aligned}\right\} \qquad [22]$$

$$\left.\begin{aligned}
\sigma_\alpha &= h_1^2\Psi_{\alpha\alpha} + h_1\left(\frac{\partial h_1}{\partial\alpha} - 2\nu h_1\frac{\rho_\alpha}{\rho}\right)\Psi_\alpha \\
&\quad - h_2^2\left[2(2-\nu)\frac{\rho_\beta}{\rho} + \frac{1}{h_1}\frac{\partial h_1}{\partial\beta}\right]\Psi_\beta \\
\sigma_\beta &= h_2^2\Psi_{\beta\beta} + h_2\left(\frac{\partial h_2}{\partial\beta} - 2\nu h_2\frac{\rho_\beta}{\rho}\right)\Psi_\beta \\
&\quad - h_1^2\left[2(2-\nu)\frac{\rho_\alpha}{\rho} + \frac{1}{h_2}\frac{\partial h_2}{\partial\alpha}\right]\Psi_\alpha \\
\sigma_\gamma &= \frac{1-2\nu}{\rho}\left[h_1^2\rho_\alpha\Psi_\alpha + h_2^2\rho_\beta\Psi_\beta\right] \\
\tau_{\alpha\beta} &= h_1h_2\left[\Psi_{\alpha\beta} + \frac{2(1-\nu)}{\rho}(\rho_\beta\Psi_\alpha + \rho_\alpha\Psi_\beta)\right] \\
&\quad + h_2\frac{\partial h_1}{\partial\beta}\Psi_\alpha + h_1\frac{\partial h_2}{\partial\alpha}\Psi_\beta
\end{aligned}\right\} \qquad [23]$$

In the preceding equations (u_α, u_β) and $(\sigma_\alpha, \ldots \tau_{\alpha\beta}, \ldots)$ are the curvilinear components of displacement and stress, respectively; the displacement u_γ and the stresses $\tau_{\gamma\alpha}, \tau_{\gamma\beta}$, which vanish by virtue of the rotational symmetry, have been omitted altogether.

For future reference we recall that Laplace's equation assumes the form

$$\frac{\partial}{\partial\alpha}\left(\frac{\rho h_1}{h_2}\Phi_\alpha\right) + \frac{\partial}{\partial\beta}\left(\frac{\rho h_2}{h_1}\Phi_\beta\right) = 0 \qquad [24]$$

whereas the curvilinear transform of the stream-function equation is given by

$$\frac{\partial}{\partial\alpha}\left(\frac{h_1}{\rho h_2}\Psi_\alpha\right) + \frac{\partial}{\partial\beta}\left(\frac{h_2}{\rho h_1}\Psi_\beta\right) = 0 \qquad [25]$$

Finally, Equations [7] become

[10] The general curvilinear components of stress will be given later in terms of the stream functions exclusively.

[11] Compare the general curvilinear transforms of [A] and [B], which are recorded subsequently, with those of [T_1] and [T_2], presented in reference (16).

[12] The authors find that their work in (17), which rests on the use of dipolar co-ordinates, could have been simplified essentially by means of the present stress-function approach.

[13] Let the Jacobian determinant of the transformation be negative so that the (α, β)-system in the meridional half plane $\rho \geq 0$ is right-handed.

[14] See reference (12), art. 19–22C.

$$\Phi_\alpha = -\frac{h_2}{\rho h_1}\Psi_\beta, \quad \Phi_\beta = \frac{h_1}{\rho h_2}\Psi_\alpha \quad \ldots\ldots [26]$$

Basic Solutions in Cylindrical and Toroidal Co-Ordinates

In what follows we shall have occasion to refer in particular to circular cylindrical and to toroidal co-ordinates. For this reason we cite here the corresponding special forms assumed by basic solutions [*A*] and [*B*], Equations [20] to [23]. The cylindrical representations of the two displacement fields were given in Equations [13], [14]. For the stresses we obtain

$$\left.\begin{aligned} [A]: \quad \sigma_\rho &= \frac{\Psi_\rho}{\rho} - \frac{\Psi}{\rho^2}, \qquad \sigma_z = -\frac{\Psi_\rho}{\rho} \\ \sigma_\gamma &= \frac{\Psi}{\rho^2}, \qquad \tau_{\rho z} = \frac{\Psi_z}{\rho} \end{aligned}\right\} \quad \ldots\ldots [27]$$

$$\left.\begin{aligned} [B]: \quad \sigma_\rho &= \Psi_{\rho\rho} - \frac{2\nu}{\rho}\Psi_\rho, \quad \sigma_z = \Psi_{zz} - \frac{2(2-\nu)}{\rho}\Psi_\rho \\ \sigma_\gamma &= \frac{(1-2\nu)}{\rho}\Psi_\rho, \quad \tau_{\rho z} = \Psi_{\rho z} + \frac{2(1-\nu)}{\rho}\Psi_z \end{aligned}\right\} \quad \ldots [28]$$

Toroidal co-ordinates[15] (α, β, γ) are introduced by setting in Equations [16]

$$\rho(\alpha, \beta) = \frac{\bar{q}}{q-p}, \qquad z(\alpha, \beta) = \frac{\bar{p}}{q-p} \quad \ldots\ldots [29]$$

where

$$p = \cos\alpha, \quad \bar{p} = \sin\alpha, \quad q = \cosh\beta, \quad \bar{q} = \sinh\beta \quad \ldots [30]$$

and the curvilinear co-ordinates are confined to the ranges

$$0 \leq \alpha \leq 2\pi, \quad 0 \leq \beta < \infty, \quad 0 \leq \gamma \leq 2\pi \quad \ldots\ldots [31]$$

so that

$$-1 \leq p, \quad \bar{p} \leq 1, \quad 1 \leq q < \infty, \quad 0 \leq \bar{q} < \infty \quad \ldots\ldots [32]$$

Equations [29], [16] imply

$$\left(\rho - \frac{q}{\bar{q}}\right)^2 + z^2 = \frac{1}{\bar{q}^2}, \qquad \rho^2 + \left(z - \frac{p}{\bar{p}}\right)^2 = \frac{1}{\bar{p}^2} \quad \ldots [33]$$

The co-ordinate surfaces α = const are thus spherical bowls of radius $|\bar{p}|^{-1}$ centered on the z-axis at $z = p/\bar{p}$. The surfaces β = const are tori, the meridional cross sections of which are the circles of radius $\bar{q}^{-1}$ centered on the ρ-axis at $\rho = q/\bar{q}$. As $\beta \to \infty$ the tori degenerate into the circle[16] $\rho = 1$, which lies in the plane $z = 0$. Fig. 2 shows the traces of the foregoing two mutually orthogonal families of co-ordinate surfaces upon the meridional half planes γ = const.

According to Equations [19] and [29], the metric coefficients here become

$$h_1 = h_2 = q - p, \qquad h_3 = \frac{q-p}{\bar{q}} \quad \ldots\ldots [34]$$

With the auxiliary notations

$$\mu = (q-p)^{1/2}, \quad \omega = 1 - pq \quad \ldots\ldots [35]$$

[15] See references (19, 5) and also the closely related discussions of spherical dipolar co-ordinates in references (19, 17).

[16] This normalization of the co-ordinate transformation Equations [29] is, of course, inessential.

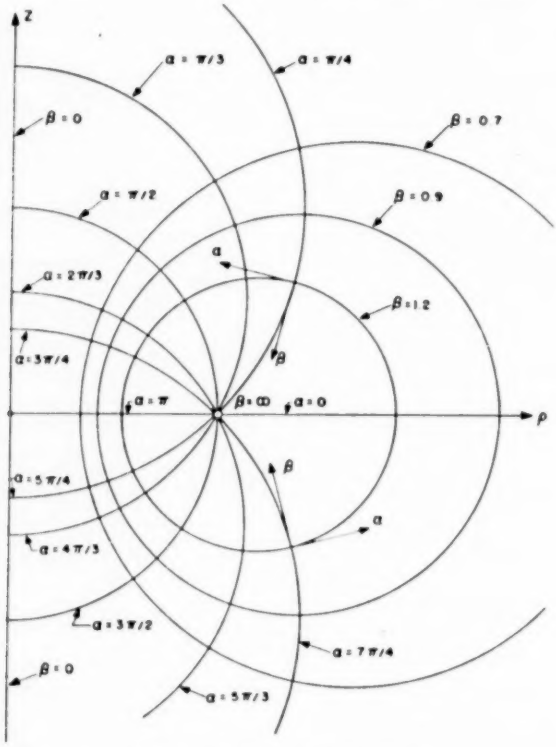

Fig. 2 Toroidal Co-Ordinates
(Traces of surfaces α = const and β = const on a half plane γ = const.)

substitution of Equations [29], [34] into [20] to [23] finally yields the following:

Solution [A]

$$2Gu_\alpha = \frac{\omega}{\mu^2}\phi - \bar{p}\psi, \qquad 2Gu_\beta = \frac{\bar{p}\,\bar{q}}{\mu^2}\phi + \frac{\omega}{\bar{q}}\psi \quad \ldots [36]$$

$$\left.\begin{aligned}
\sigma_\alpha &= -\frac{\mu^2}{\bar{q}}(\bar{p}\bar{q}\,\psi_\alpha + \omega\psi_\beta) - \bar{p}^2\psi \\
\sigma_\beta &= \frac{\mu^2}{\bar{q}}(\bar{p}\bar{q}\psi_\alpha + \omega\psi_\beta) - \frac{\omega^2}{\bar{q}^2}\psi \\
\sigma_\gamma &= \frac{\mu^4}{\bar{q}^2}\psi \\
\tau_{\alpha\beta} &= \frac{\mu^2}{\bar{q}}(\omega\psi_\alpha - \bar{p}\bar{q}\,\psi_\beta) + \frac{\omega\bar{p}}{\bar{q}}\psi
\end{aligned}\right\} \quad \ldots [37]$$

Solution [B]

$$\left.\begin{aligned}
2Gu_\alpha &= 4(1-\nu)\frac{\omega}{\mu^2}\Phi + \mu^2\Psi_\alpha \\
2Gu_\beta &= 4(1-\nu)\frac{\bar{p}\bar{q}}{\mu^2}\Phi + \mu^2\Psi_\beta
\end{aligned}\right\} \quad \ldots [38]$$

$$\left.\begin{aligned}
\sigma_\alpha &= \mu^2\Psi_{\alpha\alpha} + (1+2\nu)\mu^2\bar{p}\Psi_\alpha \\
&\quad - \frac{\mu^2}{\bar{q}}[(4-2\nu)\omega + \bar{q}^2]\Psi_\beta \\
\sigma_\beta &= \mu^2\Psi_{\beta\beta} + (3-2\nu)\mu^2\bar{p}\Psi_\alpha - \frac{\mu^2}{\bar{q}}(2\nu\omega - \bar{q}^2)\Psi_\beta \\
\sigma_\gamma &= -(1-2\nu)\mu^2(\bar{p}\Psi_\alpha - \frac{\omega}{\bar{q}}\Psi_\beta) \\
\tau_{\alpha\beta} &= \mu^2\Psi_{\alpha\beta} + \frac{\mu^2}{\bar{q}}[\bar{q}^2 + (2-2\nu)\omega]\Psi_\alpha - \\
&\quad (1-2\nu)\mu^2\bar{p}\Psi_\beta
\end{aligned}\right\} \quad \ldots [39]$$

Laplace's Equation [24] appears as

$$\mu^2\bar{q}(\Phi_{\alpha\alpha} + \Phi_{\beta\beta}) - \bar{p}\bar{q}\Phi_\alpha + \omega\Phi_\beta = 0 \quad \ldots [40]$$

whereas the toroidal form of the stream Equation [25] is given by

$$\mu^2\bar{q}(\Psi_{\alpha\alpha} + \Psi_{\beta\beta}) + \bar{p}\bar{q}\Psi_\alpha - \omega\Psi_\beta = 0 \quad \ldots [41]$$

Finally, we obtain for Equations [26]

$$\Phi_\alpha = -\frac{\mu^2}{\bar{q}}\Psi_\beta, \qquad \Phi_\beta = \frac{\mu^2}{\bar{q}}\Psi_\alpha \quad \ldots [42]$$

Pure Bending of a Torus of Arbitrary Cross Section

We return here to the main problem of this investigation, and consider first a torus of arbitrary cross section, Fig. 1. As stated previously, we are concerned with the case of pure bending in which the lateral surface is traction-free and the tractions on either terminal cross section are statically equivalent to a couple of moment M whose axis is parallel to the z-axis. Following Michell (1), we assume the displacement field in the form

$$u_\rho = u_\rho(\rho, z), \qquad u_z = u_z(\rho, z), \qquad u_\gamma = \frac{c\rho\gamma}{2G} \quad \ldots [43]$$

where c is an initially arbitrary constant.[17] Equations [43] yield

$$\tau_{\gamma\rho} = \tau_{\gamma z} \equiv 0 \quad \ldots [44]$$

and the remaining stress components are independent of γ. The lateral surface of the torus will therefore be free from stress if

$$\sigma_\rho\frac{dz}{ds} - \tau_{\rho z}\frac{d\rho}{ds} = 0, \qquad \tau_{\rho z}\frac{dz}{ds} - \sigma_z\frac{d\rho}{ds} = 0 \text{ on } \Gamma \quad \ldots [45]$$

and the boundary conditions for the terminal sections are met provided

$$\left.\begin{aligned}
&\int_D\!\!\int \sigma_\gamma\, d\rho\, dz = 0, \qquad \int_D\!\!\int z\sigma_\gamma\, d\rho\, dz = 0, \\
&\int_D\!\!\int \rho\sigma_\gamma\, d\rho\, dz = M
\end{aligned}\right\} \quad \ldots [46]$$

It is easy to see (1, 2, 4, 6) that Equations [43], [45] automatically assure the satisfaction of the first two of Equations [46]. Indeed,[18] by virtue of Equations [43], the stress equations of equilibrium[19] reduce to

$$\left.\begin{aligned}
\frac{\partial\sigma_\rho}{\partial\rho} + \frac{\partial\tau_{\rho z}}{\partial z} + \frac{\sigma_\rho - \sigma_\gamma}{\rho} &= 0 \\
\frac{\partial\sigma_z}{\partial z} + \frac{\partial\tau_{\rho z}}{\partial\rho} + \frac{\tau_{\rho z}}{\rho} &= 0
\end{aligned}\right\} \quad \ldots [47]$$

and imply the identities

$$\left.\begin{aligned}
&\int_D\!\!\int \sigma_\gamma\, d\rho\, dz \\
&\quad = \int_D\!\!\int\left[\frac{\partial}{\partial\rho}(\rho\sigma_\rho) + \frac{\partial}{\partial z}(\rho\tau_{\rho z})\right]d\rho\, dz \\
&\int_D\!\!\int z\sigma_\gamma\, d\rho\, dz = \int_D\!\!\int\left[\frac{\partial}{\partial\rho}(\rho z\sigma_\rho - \rho^2\tau_{\rho z})\right. \\
&\quad \left. + \frac{\partial}{\partial z}(\rho z\tau_{\rho z} - \rho^2\sigma_z)\right]d\rho\, dz
\end{aligned}\right\} \quad [48]$$

The right-hand members of Equations [48] are found to vanish with the aid of Green's theorem and by virtue of Equations [45].

We now assume the solution $[S]$ to the problem governed by the boundary conditions, Equations [45], and the third of conditions, Equations [46], in the form

$$[S] = [S_0] + [R] \quad \ldots [49]$$

where $[S_0]$ is a particular solution of the field equations which conforms to Equations [43], and $[R]$ is the solution to a "residual problem," the characterization of which follows from Equation [49]. Moreover, $[R]$ clearly possesses torsion-free rotational symmetry.[20]

With a view toward arriving at $[S_0]$, we note[21] that the displacement equations of equilibrium, in accordance with Equations [43], here reduce to

$$\left.\begin{aligned}
\nabla^2 u_\rho + \frac{1}{1-2\nu}\frac{\partial e}{\partial\rho} - \frac{u_\rho}{\rho^2} &= \frac{c}{\rho G} \\
\nabla^2 u_z + \frac{1}{1-2\nu}\frac{\partial e}{\partial z} &= 0
\end{aligned}\right\} \quad \ldots [50]$$

where

[17] The coefficient $\frac{1}{2G}$ is introduced for later convenience.

[18] The argument is reproduced here briefly for the convenience of the reader.

[19] See, for example, reference (12), p. 90.

[20] See Equations [3]. This general reduction of the problem to one of axisymmetry is already implicit in Michell's work (1); see also (6).

[21] See reference (12), p. 288.

$$e = \frac{\partial u_\rho}{\partial \rho} + \frac{u_\rho}{\rho} + \frac{\partial u_z}{\partial z}, \qquad \nabla^2 = \frac{\partial^2}{\partial \rho^2} + \frac{1}{\rho}\frac{\partial}{\partial \rho} + \frac{\partial^2}{\partial z^2} \quad [51]$$

It is readily verified by direct substitution that

$$\left.\begin{aligned} [S_0]: \quad 2Gu_\rho &= \frac{cz^2}{\rho}, \qquad 2Gu_z = -cz, \qquad 2Gu_\gamma = c\rho\gamma \\ \sigma_\rho &= -\frac{cz^2}{\rho^2}, \qquad \sigma_z = -c, \qquad \sigma_\gamma = c\left(1 + \frac{z^2}{\rho^2}\right), \\ & \qquad\qquad \tau_{\rho z} = \frac{cz}{\rho} \end{aligned}\right\} \quad [52]$$

is a particular integral of Equations [50], and is consistent with the stress-displacement relations. This specific choice of $[S_0]$ is, of course, not unique. Thus Freiberger and Smith (6) define $[S_0]$ through

$$2Gu_\rho = \frac{c(1-2\nu)}{2(1-\nu)}\rho \log \rho, \qquad u_z = 0, \qquad 2Gu_\gamma = c\rho\gamma \quad [53]$$

Different choices of $[S_0]$ give rise to alternative forms of the residual problem; in the subsequent application to the torus of circular cross section, the choice adopted in Equations [52] was found to be especially advantageous.

Next, we may set

$$[R] = [A] + [B] \quad [54]$$

where $[A]$ and $[B]$ are the basic axisymmetric solutions defined by Equations [13], [14], and [15]. It follows from Equations [54], [49], and the stresses listed in Equations [52], [27], [28] that the boundary conditions Equations [45] now become

$$\left.\begin{aligned} &\left[\frac{\Psi_\rho}{\rho} - \frac{\Psi}{\rho^2} + \Psi_{\rho\rho} - \frac{2\nu}{\rho}\Psi_\rho\right]dz \\ &\quad - \left[\frac{\Psi_z}{\rho} + \Psi_{\rho z} + \frac{2(1-\nu)}{\rho}\Psi_z\right]d\rho \\ &\qquad = c\left[\frac{z^2}{\rho^2}\frac{dz}{ds} + \frac{z}{\rho}\frac{d\rho}{ds}\right] \\ &\left[\frac{\Psi_z}{\rho} + \Psi_{\rho z} + \frac{2(1-\nu)}{\rho}\Psi_z\right]dz \\ &\quad + \left[\frac{\Psi_\rho}{\rho} - \Psi_{zz} + \frac{2(2-\nu)}{\rho}\Psi_\rho\right]d\rho \\ &\qquad = -c\left[\frac{z}{\rho}\frac{dz}{ds} + \frac{d\rho}{ds}\right] \text{ on } \Gamma \end{aligned}\right\} \quad [55]$$

The problem thus ultimately reduces to the determination of the two stress functions Ψ and Ψ which satisfy $A^2\Psi = 0$, $A^2\Psi = 0$ in D, and obey the boundary conditions, Equations [55], on Γ. Once this is accomplished, the parameter c is determined from the third of conditions, Equations [46], which presently yields

$$c\int_D\int\left(\rho + \frac{z^2}{\rho}\right)d\rho\,dz = M - \int_D\int\left[\frac{\Psi}{\rho} + (1-2\nu)\Psi_\rho\right]d\rho\,dz \quad [56]$$

Torus of Circular Cross Section, Toroidal Potential and Stream Functions

Turning to the special case in which Γ is a circle, we observe that the unwieldy character of the boundary conditions, Equations [55], necessitates the introduction of toroidal co-ordinates defined in Equations [29]. Let the lateral surface of the torus coincide with the parametric surface $\beta = \beta_0$, Fig. 2. Then, according to Equations [33]

$$\Delta = \frac{b}{a} = q^0 \equiv \cosh \beta_0 \quad [57]^{22}$$

where a and b are the radii of the cross section and of the center line, respectively, and Δ will be called the "shape-ratio."

Upon transformation into toroidal co-ordinates, we obtain from Equations [52]

$$\left.\begin{aligned} [S_0]: \quad 2Gu_\alpha &= -\frac{cp\bar{p}}{\mu^2}, \qquad 2Gu_\beta = \frac{c\bar{p}^2 q}{\bar{q}\mu^2}, \qquad 2Gu_\gamma = \frac{c\bar{q}\gamma}{\mu^2} \\ \sigma_\alpha &= -cp^2, \qquad \sigma_\beta = -\frac{c\bar{p}^2q^2}{\bar{q}^2}, \\ & \qquad\qquad \sigma_\gamma = c\left(1 + \frac{\bar{p}^2}{\bar{q}^2}\right), \qquad \tau_{\alpha\beta} = \frac{cp\bar{p}q}{\bar{q}} \end{aligned}\right\} \quad [58]$$

By Equations [49] and [58], the solution $[R]$ to the residual problem here obeys the boundary conditions

$$\mu^0\sigma_\beta(\alpha, \beta_0) = \frac{c\mu^0\bar{p}^2(q^0)^2}{(\bar{q}^0)^2}, \qquad \frac{\mu^0}{q^0}\tau_{\alpha\beta}(\alpha, \beta_0) = -\frac{c\mu^0 p\bar{p}q^0}{(\bar{q}^0)^2} \quad [59]^{23}$$

which assure a traction-free lateral surface, and are equivalent to Equations [45] or [55].

Our next task consists in constructing a doubly infinite aggregate of component solutions, in terms of which the desired solution $[R]$ may be expanded. With a view toward securing the necessary supply of generating stress functions, we recall Equations [40], [41], and observe that neither the potential equation nor the stream equation is strictly separable in toroidal co-ordinates. There do exist, however, pseudo-product solutions of the form

$$\Phi(\alpha, \beta) = \mu A(\alpha)B(\beta) \quad [60]^{24}$$

to Laplace's equation, and of the form

$$\Psi(\alpha, \beta) = \frac{q^2}{\mu}A(\alpha)B(\beta) \quad [61]$$

to the stream equation. Substitution of Equations [60], [61] into Equations [40], [41], subsequent separation of variables, and adherence to the requirement that the stress functions sought have periodicity 2π in α, ultimately yield the solutions

$$\left.\begin{aligned} \Phi(\alpha, \beta) &= \mu[\cos n\alpha \text{ or } \sin n\alpha] \\ & \qquad [P_{n-1/2}(q) \text{ or } Q_{n-1/2}(q)] \\ \Psi(\alpha, \beta) &= \frac{q^2}{\mu}[\cos n\alpha \text{ or } \sin n\alpha] \\ & \qquad [P_{n-1/2}'(q) \text{ or } Q_{n-1/2}'(q)] \\ & \qquad (n = 0, 1, 2, \ldots) \end{aligned}\right\} \quad [62]^{25}$$

where $P_{n-1/2}$ and $Q_{n-1/2}$ are Legendre functions of the first and second kind, respectively.

The functions $P_{n-1/2}(q)$ become singular as $q \to \infty$, and thus violate the regularity requirements inherent in the problem under consideration. Moreover, as is apparent from Equations [52],

[22] The superscript zero attached to any function of β, henceforth will designate its evaluation for $\beta = \beta_0$.

[23] The introduction of the artificial factors μ^0 and μ^0/q^0 will be accounted for later.

[24] See reference (19), chapter X.

[25] The primes denote differentiation with respect to the argument q.

solution $[S_0]$ is symmetric with respect to the plane $z = 0$, and hence $[R]$ must have the same symmetry. This limits the supply of stream functions available from Equations [62], and admissible as stress-functions in conjunction with basic solutions $[A]$ and $[B]$ to

$$\left.\begin{aligned}\psi_n(\alpha,\beta) \equiv \Psi_n(\alpha,\beta) &= \frac{4\bar{q}^2}{(4n^2-1)\mu}\, Q_{n-1/2}'(q)\cos n\alpha \\ &(n = 0, 1, 2, \ldots)\end{aligned}\right\} \quad [63]^{28}$$

The solutions generated by $\psi_n(\alpha, \beta)$ and $\Psi_n(\alpha, \beta)$ will be designated by $[A_n]$ and $[B_n]$, respectively, and consistent with Equation [54], we put

$$[R] = \sum_{n=0}^{\infty} a_n[A_n] + b_n\,[B_n] \quad \ldots\ldots\ldots\ldots [64]$$

in which the coefficients of superposition a_n, b_n are eventually to be determined from the boundary conditions, Equations [59].[27]

Before we pursue the residual problem further, we need to attend to certain analytical preliminaries. For future reference, we record Legendre's equation

$$(1-q^2)\,Q_{n-1/2}'' - 2qQ_{n-1/2}' + \left(n^2 - \frac{1}{4}\right)Q_{n-1/2} = 0 \quad [65]^{29}$$

and recall the recursion formulas

$$\left.\begin{aligned} Q_{-n-1/2} &= Q_{n-1/2} \\ 4nqQ_{n-1/2} &= (2n+1)\,Q_{n+1/2} + (2n-1)\,Q_{n-3/2} \\ 2\bar{q}^2 Q_{n-1/2}' &= (2n-1)\,(qQ_{n-1/2} - Q_{n-3/2}) \end{aligned}\right\} \quad [66]$$

which are valid for all integral values of n. Furthermore, we cite the Fourier series[29]

$$\frac{1}{\mu} = \frac{\sqrt{2}}{\pi}\,Q_{-1/2} + \frac{2\sqrt{2}}{\pi}\sum_{n=1}^{\infty} Q_{n-1/2}\cos n\alpha \quad \ldots\ldots [67]$$

which gives rise to the identity

$$Q_{n-1/2} = \frac{1}{\sqrt{2}}\int_0^{\pi} \frac{\cos n\alpha}{\mu}\, d\alpha \quad \ldots\ldots\ldots [68]$$

and note the representation of $Q_{n-1/2}$ through the Laurent series,[30] convergent for $1 < q < \infty$

$$\left.\begin{aligned} Q_{n-1/2} = \frac{\pi}{2^{3n+1/2}}\frac{|2n}{(|n)^2}\left[\frac{1}{q^{n+1/2}} + \frac{(2n+1)(2n+3)}{2^4\cdot 1(n+1)q^{n+3/2}}\right. \\ \left. + \frac{(2n+1)(2n+3)(2n+5)(2n+7)}{2^8\cdot 1\cdot 2(n+1)(n+2)q^{n+5/2}} + \ldots\right] \end{aligned}\right\} \quad [69]$$

The explicit determination of the displacements belonging to solutions $[A_n]$ and $[B_n]$, defined by Equations [63], as evidenced by Equations [36], [38], necessitates a knowledge of the potential function $\phi_n(\alpha, \beta) \equiv \Phi_n(\alpha, \beta)$ conjugate to the stream function $\psi_n(\alpha, \beta) \equiv \Psi_n(\alpha, \beta)$. According to relations, Equations [42], the equations to be integrated presently are

$$\frac{\partial\Phi_n}{\partial\alpha} = -\frac{\mu^2}{\bar{q}}\frac{\partial\Psi_n}{\partial\beta}, \qquad \frac{\partial\Phi_n}{\partial\beta} = \frac{\mu^2}{\bar{q}}\frac{\partial\Psi_n}{\partial\alpha} \quad \ldots\ldots [70]$$

where $\Psi_n(\alpha, \beta)$ is given by Equations [63]. It is readily confirmed with the aid of Equations [70] that

$$\frac{2n-1}{2}\,\Phi_n - \frac{2n+3}{2}\,\Phi_{n+1} = \mu\,[Q_{n+1/2}\sin(n+1)\alpha - Q_{n-1/2}\sin n\alpha] \quad [71]$$

This recursion formula yields Φ_n once Φ_0 is known. In order to establish Φ_0, we observe that letting

$$k = \sqrt{\frac{2}{q+1}} \equiv \frac{1}{\cosh\beta/2}, \qquad \theta = \frac{\pi-\alpha}{2} \quad \ldots\ldots [72]$$

Equation [68] implies the alternative representation

$$Q_{-1/2} = k\int_0^{\pi/2} \frac{d\theta}{\sqrt{1-k^2\sin^2\theta}} = kK \quad \ldots [73]^{31}$$

and thus

$$\Psi_0 = -\frac{4\bar{q}^2}{\mu}\,Q_{-1/2}' = \frac{4E}{k\mu} \quad \ldots\ldots\ldots\ldots [74]$$

where K and E are the complete elliptic integrals[32] of the first and second kind, respectively, for the modulus k. Now let t be defined by

$$\mathrm{am}(t, k) = \theta \equiv \frac{\pi-\alpha}{2} \quad \ldots\ldots\ldots\ldots [75]$$

am being the amplitude function, then Equations [70], with $n = 0$, after some computation lead to

$$\frac{\partial\Phi_0}{\partial\alpha} = \sqrt{2}\left(\frac{E}{\mathrm{dnt}} - K\,\mathrm{dnt}\right), \qquad \frac{\partial\Phi_0}{\partial\beta} = -\frac{\sqrt{2}\,k^2}{k'}\frac{E\,\mathrm{snt\,cnt}}{\mathrm{dnt}} \quad [76]$$

in which sn, cn, dn designate the Jacobian elliptic functions referred to the modulus k, and k' is the complementary modulus. Equations [76] are explicitly integrable, and yield

$$\phi_0 = \Phi_0 = 2\sqrt{2}[KE(t) - tE] \quad \ldots\ldots\ldots [77]$$

where $E(t)$ is the incomplete elliptic integral of the second kind for the modulus k. We conclude from Equations [71], [77] that

$$\phi_n(\alpha,\beta) = \Phi_n(\alpha,\beta) = \frac{2}{4n^2-1}\left\{\sqrt{2}[tE - KE(t)] - (2n+1)\mu Q_{n-1/2}\sin n\alpha + 2\mu\sum_{i=0}^{n} Q_{i-1/2}\sin i\alpha\right\} \quad [78]$$

It is important to observe[33] on the basis of Equation [78] that the toroidal pseudo-product solutions of the potential and stream equations, listed in Equations [62], do not constitute conjugate pairs. Indeed, a single pseudo-product stream function gives rise to a conjugate potential function whose representation requires an infinite series of pseudo-product potential functions; the closed representation, Equation [78], was made possible only through the introduction of elliptic functions and integrals.

[28] The unessential coefficient $(4/4n^2-1)$ is a matter of convenience only.

[27] It will become apparent later that b_0 is exceptional, and must vanish by virtue of regularity considerations.

[28] The argument of $Q_{n-1/2}$ is henceforth assumed to be q.

[29] See reference (19), p. 443.

[30] See reference (18), p. 317. The present series is obtained by replacing n with $n - 1/2$ and using the hypergeometric series given on p. 281 of reference (18).

[31] See also reference (20).

[32] See reference (18), chapter XXII, for a discussion of Jacobian elliptic functions and elliptic integrals.

[33] Cf. the remarks preceding Equations [16].

Solution of Residual Problem for Torus of Circular Cross Section

We are now in a position to return to the residual problem for the circular cross section, the solution of which was assumed in the form of Equations [64]. The displacements and stresses of the component solutions $[A_n]$, $[B_n]$ result from substitution of Equations [63] into Equations [36] to [39]. In this manner, by aid of Equations [65], [66], and with the auxiliary notations $c_n = \cos n\alpha$ and $s_n = \sin n\alpha$, we finally obtain the following formulas:

Solution $[A_n]$

$$\left.\begin{aligned} 2Gu_\alpha &= \frac{4}{(4n^2-1)\mu}\left[\frac{\omega\phi_n}{\mu} - \bar{p}\bar{q}^2\, Q_{n-1/2}'\, c_n\right] \\ 2Gu_\beta &= \frac{4\bar{q}}{(4n^2-1)\mu}\left[\frac{\bar{p}}{\mu}\,\phi_n + \omega Q_{n-1/2}' c_n\right] \end{aligned}\right\} \quad \ldots [79]$$

$$\left.\begin{aligned} \sigma_\alpha &= -\mu\omega Q_{n-1/2}\, c_n + \frac{2\mu\bar{q}^2}{4n^2-1}\, Q_{n-1/2}'(2n\bar{p}s_n - pc_n) \\ \sigma_\beta &= \mu\omega Q_{n-1/2} c_n \\ &\quad - \frac{2\mu}{4n^2-1}\, Q_{n-1/2}'\,[(\omega q + \mu^2)c_n + 2n\bar{p}\bar{q}^2 s_n] \\ \sigma_\gamma &= \frac{4\mu^3}{4n^2-1}\, Q_{n-1/2}'\, c_n \\ \tau_{\alpha\beta} &= -\mu\bar{p}\bar{q} Q_{n-1/2}\, c_n \\ &\quad - \frac{2\mu\bar{q}}{4n^2-1}\, Q_{n-1/2}'\,[2n\omega s_n - q\bar{p}c_n] \end{aligned}\right\} \quad \ldots [80]$$

Solution $[B_n]$

$$\left.\begin{aligned} 2Gu_\alpha &= \frac{2}{4n^2-1}\left[\frac{8}{\mu^2}(1-\nu)\omega\Phi_n \right. \\ &\quad \left. - \bar{q}^2\, Q_{n-1/2}'\left(2n\mu s_n + \frac{\bar{p}}{\mu}\, c_n\right)\right] \\ 2Gu_\beta &= \frac{1}{4n^2-1}\left\{\frac{16}{\mu^2}(1-\nu)\bar{p}\bar{q}\Phi_n \right. \\ &\quad \left. + \left[(4n^2-1)\mu Q_{n-1/2} - \frac{2\bar{q}^2}{\mu}\, Q_{n-1/2}'\right]\bar{q}c_n\right\} \end{aligned}\right\} \quad \ldots [81]$$

$$\left.\begin{aligned} \sigma_\alpha &= -\mu Q_{n-1/2}\,[(4-2\nu)\,\omega + \bar{q}^2]\, c_n \\ &\quad + \frac{\bar{q}^2}{4n^2-1}\, Q_{n-1/2}'\left\{\left[-4n^2\mu^3 + (2q - 8p + 4\nu p)\mu \right.\right. \\ &\quad \left.\left. + (7-8\nu)\,\frac{\bar{p}^2}{\mu}\right] c_n - 8n\nu\mu\bar{p}s_n\right\} \\ \sigma_\beta &= \mu Q_{n-1/2}\,[(1-2\nu)\omega + \bar{q}^2]c_n \\ &\quad + \frac{\bar{q}^2}{4n^2-1}\, Q_{n-1/2}'\left\{\left[(4n^2-2)\mu^3 - 4\nu\mu p \right.\right. \\ &\quad \left.\left. - \frac{(7-8\nu)}{\mu}\,\bar{p}^2\right] c_n - 4n(3-2\nu)\mu\bar{p}s_n\right\} \\ \sigma_\gamma &= (1-2\nu)\mu\left[\omega Q_{n-1/2}\, c_n \right. \\ &\quad \left. + \frac{2\bar{q}^2}{4n^2+1}\, Q_{n-1/2}'\,(2n\bar{p}s_n + pc_n)\right] \end{aligned}\right\} \quad \ldots [82]$$

$$\left.\begin{aligned} \tau_{\alpha\beta} &= -\frac{\bar{q}\mu}{2}\, Q_{n-1/2}\,[(3-4\nu)\bar{p}c_n + 2n\mu^2 s_n] \\ &\quad - \frac{\bar{q}Q_{n-1/2}'}{4n^2-1}\left\{[\bar{q}^2 + 4(1-\nu)\omega]\, 2n\mu s_n \right. \\ &\quad \left. + \left[4(1-\nu)q\mu - (7-8\nu)\,\frac{\bar{q}^2}{\mu}\right]\bar{p}c_n\right\} \end{aligned}\right\} \quad \ldots [82]\ (cont.)$$

The function $\phi_n \equiv \Phi_n$, appearing in Equations [79], [81], was given in Equation [78], and the auxiliary parameters μ, ω were defined in Equations [35]. The series, Equation [69], enable us to examine the regularity of the preceding solutions. Such an examination reveals that all components of stress of solutions $[A_n]$ and $[B_n]$ for $n = 0, 1, 2, \ldots$ remain finite as $q \to \infty$. The same is found to apply to the displacements,[34] with the exception of those belonging to $[B_0]$ which have poles of the first order at $q = \infty$. For this reason $[B_0]$ must be deleted or, equivalently, b_0 must vanish in Equation [64].

Next, we approach the determination of the remaining coefficients of superposition a_n, b_n in Equation [64] from the boundary conditions Equations [59]. To this end, we expand the right-hand members of Equations [59] as a Fourier series so that the boundary conditions assume the form

$$\left.\begin{aligned} \mu^0\sigma_\alpha(\alpha, \beta_0) &= c\sum_{n=0}^{\infty} \xi_n \cos n\alpha \\ \frac{\mu^0}{\bar{q}^0}\,\tau_{\alpha\beta}(\alpha, \beta_0) &= c\sum_{n=1}^{\infty} \eta_n \sin n\alpha \end{aligned}\right\} \quad \ldots\ldots [83]$$

where σ_α, $\tau_{\alpha\beta}$ are again stresses of solution $[R]$. With the aid of Equations [67], [66], as well as the addition formulas for trigonometric functions, we arrive at the Fourier coefficients

$$\left.\begin{aligned} \xi_n &= -\frac{\sqrt{2}\,q^2}{\pi(1+\delta_{n0})}\left[\frac{Q_{n-1/2}'}{(2n-5)(2n-3)} - \frac{2Q_{n-1/2}'}{4n^2-1} \right. \\ &\quad \left. + \frac{Q_{n+1/2}'}{(2n+3)(2n+5)}\right] (n = 0, 1, 2, \ldots) \\ \eta_n &= \frac{\sqrt{2}\,q}{\pi}\left[\frac{Q_{n+1/2}'}{(2n+3)(2n+5)} \right. \\ &\quad \left. - \frac{Q_{n-1/2}'}{(2n-5)(2n-3)}\right] (n = 1, 2, \ldots) \end{aligned}\right\} \quad [84][35]$$

where δ_{n0} is the Kronecker-delta. At this point we represent $\mu\sigma_\alpha$ and $\mu\tau_{\alpha\beta}/\bar{q}$ of solutions $[A_n]$ and $[B_n]$, Equations [80] and [82], as Fourier cosine and sine series. Subsequently, in accordance with Equations [83], we equate to $c\xi_n$ and $c\eta_n$ the coefficients of $\cos n\alpha$ and $\sin n\alpha$ in $\mu^0\sigma_\alpha(\alpha, \beta_0)$ and $\mu^0\tau_{\alpha\beta}(\alpha, \beta_0)/\bar{q}^0$ of solution $[R]$, Equation [64]. This results in an infinite system of linear equations characterizing the unknown coefficients of superposition a_n $(n = 0, 1, 2, \ldots)$ and b_n $(n = 1, 2, \ldots)$. The trivial, though tedious, computation just outlined yields

[34] $\phi_n(\alpha, \beta)$ is analytic in the domain under consideration.

[35] The superscripts zero, which all functions of β ought to bear in these equations, have been suppressed.

$$\frac{1}{1+\delta_{n0}}\Big\{(a_{n-2}+a_{-n+2})\left[\frac{q}{4}\,Q_{n-3/2}-\frac{2q^2+(2n-5)\bar{q}^2}{2(2n-5)\,(2n-3)}\,Q_{n-3/2}'\right]$$
$$+(a_{n-1}+a_{-n+1})\left[-\frac{q^2+1}{2}\,Q_{n-3/2}+\frac{4+(2n-1)\bar{q}^2}{(2n-3)\,(2n-1)}\,qQ_{n-3/2}'\right]$$
$$+(a_n+a_{-n})\left[\frac{3q}{2}\,Q_{n-1/2}-\frac{5\bar{q}^2+6}{4n^2-1}\,Q_{n-1/2}'\right]$$
$$+a_{n+1}\left[-\frac{q^2+1}{2}\,Q_{n+1/2}+\frac{4-(2n+1)\bar{q}^2}{(2n+1)(2n+3)}\,qQ_{n+1/2}'\right]$$
$$+a_{n+2}\left[\frac{q}{4}\,Q_{n+1/2}-\frac{2q^2-(2n+5)\,\bar{q}^2}{2(2n+3)(2n+5)}\,Q_{n+3/2}'\right]$$
$$+(b_{n-2}+b_{-n+2})\left[\frac{(1-2\nu)}{4}\,qQ_{n-3/2}+\frac{(2n-9+4\nu)\bar{q}^2}{4(2n-3)}\,Q_{n-3/2}'\right]$$
$$+(b_{n-1}+b_{-n+1})\left[[(-1+\nu)\bar{q}^2-1+2\nu]\,Q_{n-1/2}\right.$$
$$\left.+\frac{(2n-2)\,(-2n+5-2\nu)+2-2\nu}{(2n-3)(2n-1)}\,q\bar{q}^2Q_{n-3/2}'\right]$$
$$+b_n\left[(2\bar{q}^2+3-6\nu)\,\frac{q}{2}\,Q_{n-1/2}+\frac{4(2n^2-1)q^2+4n^2-9+12\nu}{2(4n^2-1)}\right.$$
$$\left.\times\,\bar{q}^2Q_{n-1/2}'\right]+b_{n+1}\left[[(-1+\nu)\bar{q}^2-1+2\nu]\,Q_{n+1/2}\right.$$
$$\left.+\frac{-(2n+2)\,(2n+5-2\nu)+2-2\nu}{(2n+1)(2n+3)}\,q\bar{q}^2Q_{n+1/2}'\right]$$
$$+b_{n+2}\left[\frac{(1-2\nu)}{4}\,qQ_{n+3/2}+\frac{(2n+9-4\nu)}{4(2n+3)}\,\bar{q}^2Q_{n+3/2}'\right]\Big\}=c\xi_n \qquad \text{..[85]}$$
$$(n=0,1,2,\ldots),\ a_i=0 \text{ for } i<0,\ b_i=0 \text{ for } i\leq 0$$

$$(a_{n-2}+a_{-n+2})\left[\frac{1}{4}\,Q_{n-3/2}-\frac{q}{2(2n-5)}\,Q_{n-3/2}'\right]$$
$$+(a_{n-1}+a_{-n+1})\left[-\frac{q}{2}\,Q_{n-3/2}+\frac{(2n-1)q^2+2n-2}{(2n-3)\,(2n-1)}\,Q_{n-3/2}'\right]$$
$$+a_n\left[-\frac{6n}{4n^2-1}\,qQ_{n-1/2}'\right]$$
$$+a_{n+1}\left[\frac{q}{2}\,Q_{n+1/2}+\frac{(2n+1)q^2+2n+2}{(2n+1)\,(2n+3)}\,Q_{n+1/2}'\right]$$
$$+a_{n+2}\left[-\frac{1}{4}\,Q_{n+3/2}-\frac{q}{2(2n+5)}\,Q_{n+3/2}'\right]$$
$$+(b_{n-2}+b_{-n+2})\left[\frac{(-2n+7-4\nu)}{8}\,Q_{n-3/2}-\frac{(1-\nu)}{2n-3}\,qQ_{n-3/2}'\right]$$
$$+b_{n-1}\left[(4n-7+4\nu)\,\frac{q}{4}\,Q_{n-1/2}\right.$$
$$\left.+\frac{(3-4\nu)\,(q^2+2n-2)+(5-4\nu)\,(2n-2)q^2-7+8\nu}{2(2n-3)\,(2n-1)}\,Q_{n-3/2}'\right]$$
$$+b_n\left[-\frac{n}{2}\,(2q^2+1)Q_{n-1/2}-\frac{2n(q^2+5-6\nu)q}{4n^2-1}\,Q_{n-1/2}'\right]$$
$$+b_{n+1}\left[(4n+7-4\nu)\,\frac{q}{4}\,Q_{n+1/2}\right.$$
$$\left.+\frac{(-3+4\nu)(q^2-2n-2)+(5-4\nu)(2n+2)q^2+7-8\nu}{2(2n+1)\,(2n+3)}\,Q_{n+1/2}'\right]$$
$$+b_{n+2}\left[\frac{(-2n-7+4\nu)}{8}\,Q_{n+3/2}-\frac{(1-\nu)q}{2n+3}\,Q_{n+3/2}'\right]=c\eta_n \qquad \text{..[86]}^{36}$$
$$(n=1,2,3,\ldots),\ a_i=0 \text{ for } i<0,\ b_i=0 \text{ for } i\leq 0$$

[36] In these equations, the superscript zero, appropriate to all functions of β, again was omitted.

The structure of the foregoing system of equations is apparent from the matrix scheme shown later, in which the asterisks denote nonvanishing coefficients. The first equation is seen to involve five unknowns, whereas each additional pair of equations successively involves two additional unknowns. The maximum number of unknowns entering any one equation is ten. This is a consequence of the fact that $\mu\sigma_\alpha$ and $\mu\tau_{\alpha\beta}/\bar{q}$ of solutions $[A_n]$, $[B_n]$, Equations [80], [82], are even and odd trigonometric polynomials in α, so that the corresponding Fourier series terminate. The stresses σ_α and $\tau_{\alpha\beta}$ of these solutions, without prior multiplication by μ, are irrational functions of $\cos\alpha$ and $\sin\alpha$, which give rise to infinite Fourier expansions. The artificial factors μ^0 in Equations [59] were introduced for the purpose of avoiding a doubly infinite system of equations in place of the simply infinite system, Equation [87].

$$\left.\begin{bmatrix} * & * & * & * & * & 0 & 0 & 0 & 0 & 0 & 0 & 0 & 0 & 0 & 0 & \cdot & \cdot \\ * & * & * & * & * & * & 0 & 0 & 0 & 0 & 0 & 0 & 0 & 0 & 0 & \cdot & \cdot \\ * & * & * & * & * & * & * & 0 & 0 & 0 & 0 & 0 & 0 & 0 & 0 & \cdot & \cdot \\ * & * & * & * & * & * & * & * & 0 & 0 & 0 & 0 & 0 & 0 & 0 & \cdot & \cdot \\ * & * & * & * & * & * & * & * & * & 0 & 0 & 0 & 0 & 0 & 0 & \cdot & \cdot \\ 0 & * & * & * & * & * & * & * & * & * & 0 & 0 & 0 & 0 & 0 & \cdot & \cdot \\ 0 & * & * & * & * & * & * & * & * & * & * & 0 & 0 & 0 & 0 & \cdot & \cdot \\ 0 & 0 & 0 & * & * & * & * & * & * & * & * & * & 0 & 0 & 0 & \cdot & \cdot \\ 0 & 0 & 0 & * & * & * & * & * & * & * & * & * & * & 0 & 0 & \cdot & \cdot \\ \cdot & \cdot & \cdot & \cdot & \cdot & \cdot & \cdot & \cdot & \cdot & \cdot & \cdot & \cdot & \cdot & \cdot & \cdot & \cdot & \cdot \\ \cdot & \cdot & \cdot & \cdot & \cdot & \cdot & \cdot & \cdot & \cdot & \cdot & \cdot & \cdot & \cdot & \cdot & \cdot & \cdot & \cdot \\ \cdot & \cdot & \cdot & \cdot & \cdot & \cdot & \cdot & \cdot & \cdot & \cdot & \cdot & \cdot & \cdot & \cdot & \cdot & \cdot & \cdot \\ \cdot & \cdot & \cdot & \cdot & \cdot & \cdot & \cdot & \cdot & \cdot & \cdot & \cdot & \cdot & \cdot & \cdot & \cdot & \cdot & \cdot \end{bmatrix}\right\} \left.\begin{bmatrix} a_0 \\ b_1 \\ a_1 \\ b_2 \\ a_2 \\ b_3 \\ a_3 \\ b_4 \\ a_4 \\ b_5 \\ a_5 \\ \cdot \\ \cdot \\ \cdot \end{bmatrix}\right\} = c \left.\begin{bmatrix} \xi_0 \\ \eta_1 \\ \xi_1 \\ \eta_2 \\ \xi_2 \\ \eta_3 \\ \xi_3 \\ \eta_4 \\ \xi_4 \\ \eta_5 \\ \cdot \\ \cdot \\ \cdot \end{bmatrix}\right\} \quad \ldots [87]$$

Equations [85], [86] cannot be decomposed into an infinite number of determinate finite systems; their solution may be accomplished by the usual sectionalization process. Once the values of a_n/c and b_n/c have been established, the parameter c is determined from the moment-condition, Equation [56], or, equivalently, from the third of Equations [46]. By virtue of Equations [29], [30], [34], and [35]

$$M = \int_0^{2\pi}\int_{\beta_0}^{\infty} \frac{\rho\,\sigma_\gamma}{h_1 h_2}\,d\alpha\,d\beta = \int_0^{2\pi}\int_{q_0}^{\infty} \frac{\sigma_\gamma}{\mu^6}\,d\alpha\,dq \quad \ldots [88]$$

where σ_γ belongs to the complete solution $[S]$ which, by Equations [64], [49], now appears as

$$[S] = [S_0] + \sum_{n=0}^{\infty} a_n[A_n] + \sum_{n=1}^{\infty} b_n[B_n] \quad \ldots [89][37]$$

We substitute for σ_γ in Equation [88], the value consistent with Equation [89] as well as the stress formulas, Equations [58], [80], [82], and carry out the two successive integrations indicated. In the integration with respect to α the identity, Equation [68], is needed, the remaining integrals so encountered being elementary. The subsequent integration with respect to q requires the use of the identities

$$\left.\begin{aligned} \int_q^\infty \frac{Q_{n-1/2}\,Q_{n-1/2}'}{\bar{q}}\,dq &= -\frac{4n^2-1}{4}\,\bar{q}Q^2_{n-1/2} \\ &\quad + q\bar{q}Q_{n-1/2}\,Q_{n-1/2}' + \bar{q}^2 Q_{n-1/2}'^2 \\ \int_q^\infty Q_{n-1/2}'^2 dq &= \frac{q\bar{q}^2}{2}\,Q_{n-1/2}'^2 \\ &\quad + \frac{\bar{q}^2}{2}\,Q_{n-1/2}\,Q_{n-1/2}' - \frac{4n^2-1}{8}\,qQ_{n-1/2}^2 \end{aligned}\right\} \quad \ldots [90]$$

which are subject to direct verification with recourse to the recurrence relations, Equations [66]. In this manner one obtains ultimately

$$\left.\begin{aligned} \frac{2\,[2q-2(q-\bar{q})\bar{q}^2]}{3\bar{q}^3}\,\pi c &= M + 8\sqrt{2}\sum_{n=0}^{\infty} a_n \\ &\quad \times \left[\bar{q}^2\,\frac{(qQ_{n-1/2}'^2 + Q_{n-1/2}Q_{n-1/2}')}{4n^2-1} - \frac{q}{4}\,Q_{n-1/2}^2\right] \\ &\quad - \frac{8\sqrt{2}}{3}(1-2\nu)\bar{q}^2 \sum_{n=1}^{\infty} b_n Q_{n-1/2}' \left[Q_{n-1/2} - \frac{2q}{4n^2-1}\,Q_{n-1/2}'\right] \end{aligned}\right\} \quad \ldots [91][38]$$

The complete solution $[S]$ to the problem of pure bending of a torus of circular cross section is given by Equation [89], with reference to the stresses and displacements of the component solutions $[S_0]$, $[A_n]$, and $[B_n]$, recorded in Equations [58], [79], [80], and [81], [82], respectively. The coefficients of superposition a_n ($n = 0, 1, 2, \ldots$) and b_n ($n = 1, 2, 3, \ldots$) are uniquely determined by the system of Equations [85], [86], and the moment condition, Equation [91].

Numerical Example, Comparison With Approximate Solutions; Initial Stresses in a Complete Torus

In specific applications of the preceding solution, the values of the normal stress acting on the circular cross section, along the diameter perpendicular to the axis of the torus, are of foremost interest. For this reason we cite here, in particular, the formulas for σ_γ of $[S]$ at $z = 0$, and observe that the two segments $\alpha = 0$ and $\alpha = \pi$ of the ρ-axis, Fig. 2, require separate treatment. By means of the equations defining the solution $[S]$, and through elementary geometric considerations based on Equations [29], [33], and [59], we obtain, for $\alpha = 0$

$$\left.\begin{aligned} &\sqrt{\Delta^2-1} \le \rho/a \le \Delta + 1 \\ \sigma_\gamma &= c + 4(q-1)^{3/2} \sum_{n=0}^{\infty} \frac{a_n Q_{n-1/2}'}{4n^2-1} \\ &\quad + (1-2\nu)\sqrt{q-1} \sum_{n=1}^{\infty} b_n \left[(1-q)Q_{n-1/2} + \frac{2\bar{q}^2 Q_{n-1/2}'}{4n^2-1}\right] \end{aligned}\right\} \quad \ldots [92]$$

and for $\alpha = \pi$

$$\left.\begin{aligned} &\Delta - 1 \le \rho/a \le \sqrt{\Delta^2-1} \\ \sigma_\gamma &= c + 4(q+1)^{3/2} \sum_{n=0}^{\infty} \frac{a_n(-1)^n Q_{n-1/2}'}{4n^2-1} \\ &\quad + (1-2\nu)\sqrt{q+1} \sum_{n=1}^{\infty} b_n(-1)^n \left[(1+q)Q_{n-1/2}' - \frac{2\bar{q}^2 Q_{n-1/2}'}{4n^2-1}\right] \end{aligned}\right\} \quad \ldots [93]$$

where $\Delta = b/a$ is the shape ratio first introduced in Equation [57]. Furthermore, along the ρ-axis

$$q = \pm\,\frac{(\rho/a)^2 + \Delta^2 - 1}{(\rho/a)^2 - \Delta^2 + 1} \quad \ldots [94]$$

[37] Recall that $b_0 = 0$.

[38] See footnote 36.

in which the plus and minus signs apply to $\alpha = 0$ and $\alpha = \pi$, respectively. Finally

$$\lim_{q \to \infty} \rho/a = \sqrt{\Delta^2 - 1} \quad \ldots\ldots\ldots\ldots\ldots [95]$$

and proceeding to the limit as $q \to \infty$ in Equation [92] or [93], there results, with the aid of the expansion, Equation [69]

$$\lim_{q \to \infty} \sigma_\gamma = c + \pi \sqrt{2} \left[a_0 - \frac{(1 - 2\nu)}{4} b_1 \right] \quad \ldots\ldots [96]$$

We now turn to a numerical example and assume $\Delta = b/a = 5$, $\nu = 0.3$. For these values of the shape ratio and of Poisson's ratio, the infinite system of Equations [85] and [86], or [87], yields[39] the numerical values listed in Table 1.

TABLE 1 NUMERICAL VALUES OF a_n/c AND b_n/c FOR $\Delta = 5$, $\nu = 0.3$

n	a_n/c	b_n/c
0	−0.22976	
1	0.02371	−0.01266
2	−3.297	1.79746
3	−7.6	4.096
4	−10	6.28
5		8

The values given in Table 1 are stabilized in the sense that the results of the last two successive approximations used in the sectionalization process applied to Equation [87] coincided within the number of digits shown. A total of no more than 11 simultaneous equations had to be solved in order to establish the listed values, and these values in turn sufficed to stabilize the desired stress values up to four significant figures. This indicates the unusually favorable convergence of the solution for the shape ratio chosen here. The convergence is, of course, bound to deteriorate as Δ approaches the limiting value of unity. In this connection it should be kept in mind, however, that values of Δ of the order of less than 3 are no longer apt to possess any physical interest in view of the appeal to Saint Venant's principle which underlies the present formulation of the problem.

Substitution of the numerical data of Table 1 into the moment condition, Equation [91] leads to the dimensionless value

$$M/a^3c = 0.1939 \quad \ldots\ldots\ldots\ldots\ldots [97][40]$$

The values of σ_γ now follow readily from Equation [97], Table 1, and the stress formulas, Equations [92], [93], and [96]. They are plotted in dimensionless form in Fig. 3 which also contains the corresponding curves obtained on the basis of the elementary beam theory for straight beams, the approximate theory of curved beams of Winkler,[41] and the second approximation in Göhner's perturbation scheme.[42] The maximum and minimum values of σ_γ, which occur at the end points of the diameter $z = 0$, for the current solution and for the foregoing three approximate solutions, are recorded in Table 2. As a check on the accuracy of the present solution, the stress component σ_β at $z = 0$ and $\rho/a = 4$, which ought to vanish, was computed also. The ratio of this stress to the value of σ_γ at the same point is found to be 0.000, which indicates a violation of the boundary conditions of less than 0.1 per cent.

The comparison with the approximate solutions reveals that both Göhner's and Winkler's results are within 10 per cent of the correct values for $\Delta = b/a = 5$. It is interesting to note, however, that Göhner's maximum value of σ_γ is slightly more in error than that which stems from the much cruder approximations of Winkler.

TABLE 2 EXTREME VALUES OF $\pi a^3 \sigma_\gamma / 4M$ FOR $\Delta = 5$, $\nu = 0.3$

ρ/a	Current solution	Göhner	Winkler	Elementary beam theory
4	−1.273	−1.200	−1.175	−1
6	0.8909	0.8514	0.8666	1

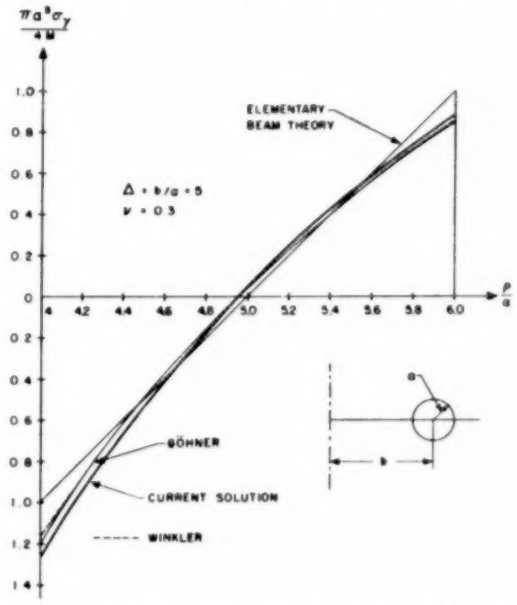

FIG. 3 VARIATION OF σ_γ ALONG TRANSVERSE DIAMETER OF CROSS SECTION

Solution [S] to the problem of pure bending of an incomplete torus is readily adapted to the determination of the initial stresses in a complete torus from which a wedge-shaped portion has been removed, the two free end sections having been joined subsequently.[43] If γ_* is the opening angle[44] of the wedge, the dislocation condition becomes

$$u_\gamma (\gamma = 2\pi) - u_\gamma (\gamma = 0) = \rho\gamma_* \quad \ldots\ldots\ldots [98]$$

In view of Equations [43], this implies

$$c = \frac{\gamma_* G}{\pi} \quad \ldots\ldots\ldots\ldots\ldots [99]$$

With c known, Equation [56] yields the bending moment M, provided the associated problem of pure bending for the incomplete torus has otherwise been solved. In particular, in case of the circular cross section, the value of M follows from Equation [91], once the solution to the system of Equation [87] is available. In the numerical example considered previously, we conclude from Equations [97], [99] that for $\Delta = b/a = 5$, $\nu = 0.3$

$$\frac{M}{Ga^3} = \frac{0.1939}{\pi} \gamma_* \quad \ldots\ldots\ldots\ldots [100]$$

ACKNOWLEDGMENT

The authors are indebted to Mr. R. A. Eubanks, Assistant Research Engineer at Illinois Institute of Technology, and to Mr. W. F. Darsow, Project Computer, for their valuable assistance

[39] The required numerical values of the functions $Q_{n-1/2}$ are available in reference (21).

[40] Note that for the normalized form [29] of the toroidal co-ordinate transformation, $a = 1/\bar{q}^0$, and that in the present instance $q^0 = \Delta = 5$.

[41] See reference (14), pp. 74, 75.

[42] See references (9), p. 407, and (10), p. 356.

[43] See reference (13), p. 68, for a discussion of the analogous plane problem.

[44] This angle is, of course, assumed to be sufficiently small.

in connection with the numerical work underlying this investigation.

BIBLIOGRAPHY

1 "The Uniform Torsion and Flexure of Incomplete Tores, With Application to Helical Springs," by J. H. Michell, Proceedings of the London Mathematical Society, London, England, vol. 31, 1899, p. 130.

2 "Sulla teoria della trave ad asse curvo," by Guido Fubini, Atti, Reale Accademia delle Scienze di Torino, vol. 72, part 1, 1937, p. 386.

3 "Su di un notevole caso di deformazione di una trave curva," by Francesco Tricomi, Atti, Reale Accademia delle Scienze di Torino, vol. 73, part 1, 1937, p. 79.

4 "Some Practically Important Stress-Systems in Solids of Revolution," by R. V. Southwell, Proceedings of the Royal Society of London, series A, vol. 180, 1942, p. 367.

5 "The Uniform Torsion of Incomplete Tore," by W. Freiberger, *Australian Journal of Scientific Research*, series A, vol. 2, 1949, p. 354.

6 "The Uniform Flexure of an Incomplete Tore," by W. Freiberger and R. C. T. Smith, *Australian Journal of Scientific Research*, series A, vol. 2, 1949, p. 469.

7 "Schubspannungsverteilung im Querschnitt einer Schraubenfeder," by O. Göhner, *Ingenieur Archiv*, vol. 1, 1930, p. 619.

8 "Schubspannungsverteilung im Querschnitt eines gedrillten Ringstabs mit Anwendung auf Schraubenfedern," by O. Göhner, *Ingenieur Archiv*, vol. 2, 1931, p. 1.

9 "Spannungsverteilung in einem an den Endquerschnitten belasteten Ringstabsektor," by O. Göhner, *Ingenieur Archiv*, vol. 2, 1931, p. 381.

10 "Zur Berechnung des gebogenen oder gedrillten Ringstabs mit Kreisquerschnitt und der zylindrischen Schraubenfeder," by O. Göhner, *Ingenieur Archiv*, vol. 9, 1938, p. 365.

11 "Torsion of Curved Beams of Rectangular Cross Section," by H. L. Langhaar, JOURNAL OF APPLIED MECHANICS, Trans. ASME, vol. 74, March, 1952, pp. 49–53.

12 "A Treatise on the Mathematical Theory of Elasticity," by A. E. H. Love, fourth edition, Dover Publications, New York, N. Y., 1944.

13 "Theory of Elasticity," by S. Timoshenko and J. N. Goodier, second edition, McGraw-Hill Book Company, Inc., New York, N. Y., 1951.

14 "Strength of Materials," by S. Timshenko, part 2, second edition, D. Van Nostrand Company, Inc., New York, N. Y., 1941.

15 "Achsensymmetrische Deformation von Umdrehungskörpern," by A. Timpe, *Zeitschrift für angewandte Mathematik und Mechanik*, vol. 4, 1924, p. 361.

16 "On the Stress-Function Approaches of Boussinesq and Timpe to the Axisymmetric Problem of Elasticity Theory," by E. Sternberg, R. A. Eubanks, and M. A. Sadowsky, *Journal of Applied Physics*, vol. 22, no. 9, 1951, pp. 1121–1124.

17 "On the Axisymmetric Problem of the Theory of Elasticity for an Infinite Region Containing Two Spherical Cavities," by E. Sternberg and M. A. Sadowsky, JOURNAL OF APPLIED MECHANICS, Trans. ASME, vol. 74, March, 1952, pp. 19–27.

18 "A Course of Modern Analysis," by E. T. Whittaker and G. N. Watson, fourth edition, University Press, Cambridge, England, 1931.

19 "The Theory of Spherical and Ellipsoidal Harmonics," by E. W. Hobson, University Press, Cambridge, England, 1931.

20 "Dipolare Koordinaten und Kugelfunktionen," by Walter Fouquet, *Zeitschrift für angewandte Mathematik und Mechanik*, vol. 17, 1937, p. 51.

21 "Tables of the Associated Legendre Functions," Mathematical Tables Project, Columbia University Press, New York, N. Y., 1945.

22 "Stresses and Deformations of Toroidal Shells of Elliptical Cross Section," by R. A. Clark, T. I. Gilroy, and E. Reissner, JOURNAL OF APPLIED MECHANICS, Trans. ASME, vol. 74, March, 1952, pp. 37–48.

Deflections of Circular Beams Resting on Elastic Foundations Obtained by Methods of Harmonic Analysis

By ENRICO VOLTERRA,[1] TROY, N. Y.

Solutions in form of Fourier series are given for the problem of circular beams resting on elastic foundations on the assumption that the foundation reacts according to the classical Winkler-Zimmermann hypothesis. The case of an arbitrary load distribution is disposed of by separate treatment of the symmetric and antisymmetric load components. Numerical tables of the coefficients of the trigonometric series expressing deflections, angles of twist, bending and twisting moments are presented for both symmetric and antisymmetric loadings.

Nomenclature

The following nomenclature is used in the paper:

M_z = bending moment
M_s = twisting moment
v = displacement of axis of beam in direction perpendicular to plane of beam
β = angle of twist
$1/R$ = initial curvature of center line of beam
I_z = moment of inertia of cross section of beam with respect to z-axis
C = torsional rigidity of beam
E = Young's modulus of beam
$y = v/R$
$\mu = C/EI_z$
$a = EI_z/R$
P = concentrated load
p = distributed load
k = elastic constant of foundation
$\lambda = (kR^4)/(EI_z)$
$\nu = (R^3P)/(EI_z)$

Introduction

In a previous paper (1)[2] the problem of a circular beam resting on an elastic foundation and loaded by concentrated forces, arranged symmetrically with respect to the center and perpendicular to the plane of the original curvature of the beam, was solved in closed form under the assumption that the foundation reacts following the classical Winkler-Zimmermann hypothesis. This problem has a practical application in civil engineering in the calculation of circular beams used as a foundation of reinforced-concrete water tanks, Fig. 1. In this instance, not only the case of symmetric loading, Fig. 2, has to be taken into consideration, but also the case of antisymmetric loading, Fig. 3, which is induced by the wind action on the water tank.[3]

In the present paper a solution in terms of trigonometric series for the problem in the absence of symmetry restrictions is given.

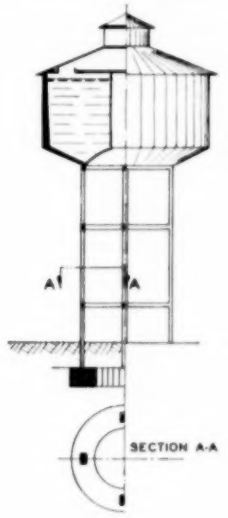

Fig. 1

This solution offers a simple approximate method of evaluating deflections, angles of twist, bending and twisting moments for any case of external loading. In order to facilitate the necessary computations, numerical tables giving the first 24 terms in the required series development for different beam characteristics are presented.

The following assumptions will be made: (*a*) The beam has constant inertia characteristics EI_z, and its axis is a circle of radius R. (*b*) The reaction forces due to the foundation are proportional at every point to the deflection of the beam at that point (2, 3, 4).

Particular Solution by Trigonometric Series of the Problem of a Circular Beam Resting on an Elastic Foundation

The beam will be referred to a system of rectangular co-ordinates O-X-Y-Z, Fig. 4, with the origin O at the centroid of the cross section, the axis X and Y coinciding with the principal axes of inertia of the cross section, and the axis Z with the tangent to

[1] Professor of Mechanics, Rensselaer Polytechnic Institute. Mem. ASME.

[2] Numbers in parentheses refer to the Bibliography at the end of the paper.

Contributed by the Applied Mechanics Division and presented at the Annual Meeting, New York, N. Y., November 30–December 5, 1952, of The American Society of Mechanical Engineers.

Discussion of this paper should be addressed to the Secretary, ASME, 29 West 39th Street, New York, N. Y., and will be accepted until July 10, 1953, for publication at a later date. Discussion received after the closing date will be returned.

Note: Statements and opinions advanced in papers are to be understood as individual expressions of their authors and not those of the Society. Manuscript received by ASME Applied Mechanics Division, May 5, 1952. Paper No. 52—A-16.

[3] This was pointed out in the discussion which followed the presentation of the previous paper (1) before the 1951 Annual Meeting of the Society by Prof. R. M. Mindlin of Columbia University and by Prof. F. S. Shaw of Brooklyn Polytechnic Institute.

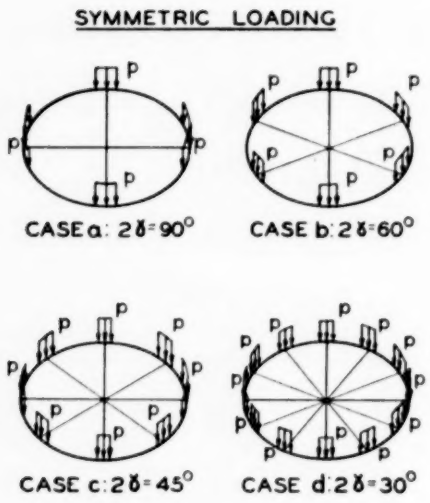

FIG. 2

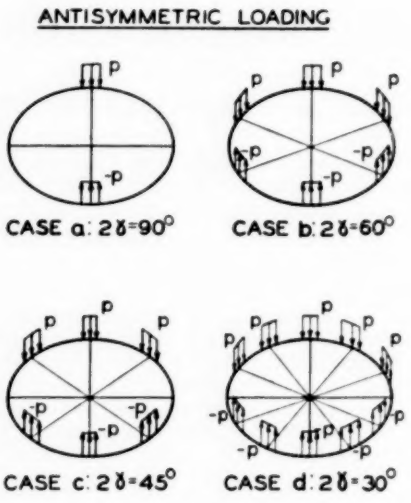

FIG. 3

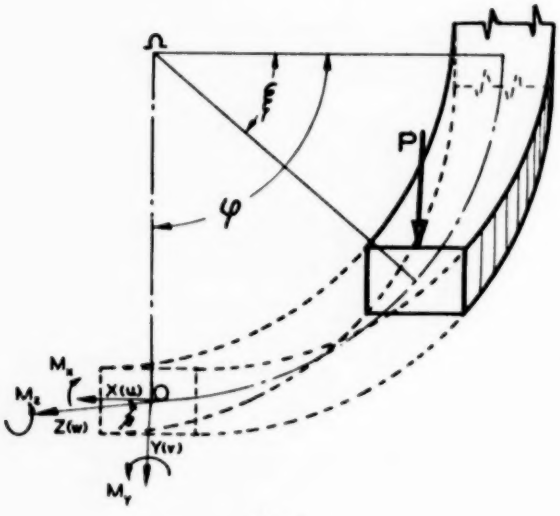

FIG. 4

the center line at O. The plane X-Z coincides with the horizontal plane of the initial curvature of the beam, the positive direction of X being toward the center of curvature; Y is positive downward, Z is taken positive in the direction in which the rotation from X to Y is clockwise, the length s of the center line being measured in the same direction as Z.

The displacement of the centroid O during bending is resolved into three components, u, v, w, in the directions of the X, Y, and Z-axes, respectively.

The angle of twist β of the cross section about the Z-axis is taken positive when the rotation is counterclockwise with respect to the Z-axis. The deformation of an element of the curved bar, bounded by two adjacent cross sections, consists of bending in the principal planes X-Z and Y-Z and of a twist about the Z-axis. If M_x, M_y, M_z are the moments on the cross section at O about the X, Y, Z-axes (their positive directions are shown in Fig. 4), EI_x, EI_y the two principal flexural rigidities, C the torsional rigidity, $1/R$ the initial curvature of the center line of the bar, the following Equations arise (5, 6, 7)

$$\left.\begin{aligned} EI_x\left(\frac{\beta}{R} - \frac{d^2v}{ds^2}\right) &= M_x \\ EI_y\left(-\frac{u}{R^2} + \frac{d^2u}{ds^2}\right) &= M_y \\ C\left(\frac{d\beta}{ds} + \frac{1}{R}\frac{dv}{ds}\right) &= M_z \\ \frac{dw}{ds} - \frac{u}{R} &= 0 \end{aligned}\right\} \quad \ldots\ldots [1]$$

In the case of a circular beam resting on an elastic foundation, the displacements u and w can be neglected (1) and Equations [1] reduced to

$$\left.\begin{aligned} EI_x\left(\frac{\beta}{R} - \frac{d^2v}{ds^2}\right) &= M_x \\ C\left(\frac{d\beta}{ds} + \frac{1}{R}\frac{dv}{ds}\right) &= M_z \end{aligned}\right\} \quad \ldots\ldots [2]$$

If k is the elastic constant of the foundation, $y = v/R$, $a = EI_x/R$ $\mu = C/(EI_x)$ Equations [2] become

$$\left.\begin{aligned} a\left(\beta - \frac{d^2y}{d\varphi^2}\right) &= M_x \\ \mu a\left(\frac{d\beta}{d\varphi} + \frac{dy}{d\varphi}\right) &= M_z \end{aligned}\right\} \quad \ldots\ldots [3]$$

while, for equilibrium, if $p(\varphi)$ represents the external distributed force, Fig. 5

$$\left.\begin{aligned} \frac{dM_z}{d\varphi} - M_x &= 0 \\ \frac{d^2M_x}{d\varphi^2} + \frac{dM_z}{d\varphi} + R^2[p(\varphi) - Rky(\varphi)] &= 0 \end{aligned}\right\} \quad \ldots\ldots [4]$$

From Equations [3] and [4] we conclude that

$$\left.\begin{aligned} &-\beta + \mu\frac{d^2\beta}{d\varphi^2} + (1+\mu)\frac{d^2y}{d\varphi^2} = 0 \\ &\frac{d^2\beta}{d\varphi^2}(1+\mu) + \mu\frac{d^2y}{d\varphi^2} - \frac{d^4y}{d\varphi^4} \\ &\qquad + \frac{R^2}{a}[p(\varphi) - kRy(\varphi)] = 0 \end{aligned}\right\} \quad \ldots [5]$$

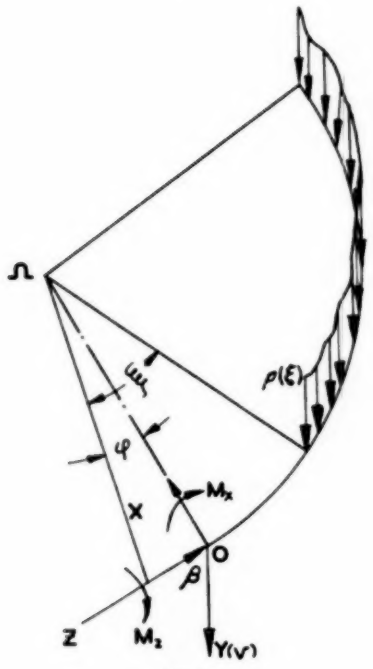

FIG. 5

Combining Equations [5], there follows

$$\left.\begin{aligned} \beta &= \frac{1+2\mu}{1+\mu}\frac{d^2y}{d\varphi^2} + \frac{\mu}{1+\mu}\frac{d^4y}{d\varphi^4} \\ &\qquad - \frac{\mu R^2}{a(1+\mu)}[p(\varphi) - kRy(\varphi)] \\ \frac{d^6y}{d\varphi^6} &+ 2\frac{d^4y}{d\varphi^4} + \frac{d^2y}{d\varphi^2}\left(1 + \frac{kR^3}{a}\right) - \frac{R^2}{a\mu}ky \\ &= -\frac{R^2}{a\mu}p(\varphi) + \frac{R^2}{a}\frac{d^2p(\varphi)}{d\varphi^2} \end{aligned}\right\} \quad \ldots [6]$$

the periodicity conditions are

$$\left.\begin{aligned} &\beta(0) = \beta(2\pi);\ \left(\frac{d\beta}{d\varphi}\right)_0 = \left(\frac{d\beta}{d\varphi}\right)_{2\pi};\ y(0) = y(2\pi) \\ &\left(\frac{dy}{d\varphi}\right)_0 = \left(\frac{dy}{d\varphi}\right)_{2\pi};\ \left(\frac{d^2y}{d\varphi^2}\right)_0 = \left(\frac{d^2y}{d\varphi^2}\right)_{2\pi}; \\ &\qquad \left(\frac{d^3y}{d\varphi^3}\right)_0 = \left(\frac{d^3y}{d\varphi^3}\right)_{2\pi} \end{aligned}\right\} \quad \ldots [7]$$

If a concentrate load P is acting on the section $\varphi = \xi$, then

$$p(\varphi) = \frac{P}{2\pi R}\left\{1 + 2\sum_{n=1}^{\infty}\cos n(\xi - \varphi)\right\} \quad \ldots [8]^4$$

the solutions of Equations [3], [6] are expressed by

$$y(\varphi) = \frac{P}{2\pi R^3 k} + \frac{PR}{a\mu\pi}\sum_{n=1}^{\infty} Y_n \cos n(\xi - \varphi) \quad \ldots [9]$$

where

$$Y_n = \frac{\mu n^2 - 1}{n^6 - 2n^4 + n^2(1+\lambda) + \dfrac{\lambda}{\mu}} \quad \ldots [10]$$

$$\beta(\varphi) = \frac{PR}{a\mu\pi}\sum_{n=1}^{\infty} B_n \cos n(\xi - \varphi) \quad \ldots [11]$$

where

$$B_n = -\frac{(1+\mu)n^2}{1+\mu n^2} Y_n \quad \ldots [12]$$

$$M_x(\varphi) = \frac{PR}{\mu\pi}\sum_{n=1}^{\infty} M_{xn}\cos n(\xi - \varphi) \quad \ldots [13]$$

where

$$M_{xn} = B_n + n^2 Y_n \quad \ldots [14]$$

$$M_z(\varphi) = \frac{PR}{\mu\pi}\sum_{n=1}^{\infty} M_{zn}\cos n(\xi - \varphi) \quad \ldots [15]$$

where

$$M_{zn} = -\frac{M_{xn}}{n} \quad \ldots [16]$$

Now, if $P(\xi)$ is the intensity of a distributed load at the section $\varphi = \xi$, by applying the principle of superposition, the following expressions are obtained

$$y(\varphi) = \frac{1}{2\pi k R^3}\int_0^{2\pi} P(\xi)d\xi + \frac{R}{a\mu\pi}\sum_{n=1}^{\infty} Y_n \left[\cos n\varphi \int_0^{2\pi} P(\xi)\cos n\xi\, d\xi + \sin n\varphi \int_0^{2\pi} P(\xi)\sin n\xi d\xi\right] \quad \ldots [17]$$

$$\beta(\varphi) = \frac{R}{a\mu\pi}\sum_{n=1}^{\infty} B_n\left[\cos n\varphi \int_0^{2\pi} P(\xi)\cos n\xi d\xi + \sin n\varphi \int_0^{2\pi} P(\xi)\sin n\xi d\xi\right] \quad \ldots [18]$$

$$M_x(\varphi) = \frac{R}{\mu\pi}\sum_{n=1}^{\infty} M_{xn}\left[\cos n\varphi \int_0^{2\pi} P(\xi)\cos n\xi d\xi + \sin n\varphi \int_0^{2\pi} P(\xi)\sin n\xi d\xi\right] \quad \ldots [19]$$

[4] It should be noted that Series [8], as the trigonometric expansion used for representing concentrated loads in the case of simply supported beams, is not a convergent series (8); but, as in the case of simply supported beams, this will not interfere with the legitimacy of the harmonic process which is to be used for determining deflections.

$$M_x(\varphi) = \frac{R}{\mu\pi}\sum_{n=1}^{\infty} M_{xn}\left[\sin n\varphi \int_0^{2\pi} P(\xi)\cos n\xi d\xi - \cos n\varphi \int_0^{2\pi} P(\xi)\sin n\xi d\xi\right] \quad [20]$$

Symmetric Case of Loading

If the loads are symmetric, Fig. 2, so that $P(\xi)$ is an even function of ξ through obvious reductions, the coefficients of $\sin\varphi$ in Equations [17], [18], [19] and of $\cos\varphi$ in Equation [20] vanish, and we obtain

$$y(\varphi) = \frac{2}{\pi k R^3}\int_0^{\pi/2} P(\xi)d\xi + \frac{4R}{a\mu\pi}\sum_{n=2,4,6,\cdots}^{\infty} Y_n \cos n\varphi \int_0^{\pi/2} P(\xi)\cos n\xi d\xi \quad [21]$$

$$\beta(\varphi) = \frac{4R}{a\mu\pi}\sum_{n=2,4,6,\cdots}^{\infty} B_n \cos n\varphi \int_0^{\pi/2} P(\xi)\cos n\xi d\xi \quad [22]$$

$$M_x(\varphi) = \frac{4R}{\mu\pi}\sum_{n=2,4,6,\cdots}^{\infty} M_{xn}\cos n\varphi \int_0^{\pi/2} P(\xi)\cos n\xi d\xi \quad [23]$$

$$M_z(\varphi) = \frac{4R}{\mu\pi}\sum_{n=2,4,6,\cdots}^{\infty} M_{zn}\sin n\varphi \int_0^{\pi/2} P(\xi)\cos n\xi d\xi \quad [24]$$

Tables 1 and 2 contain the first 24 coefficients of the series expressing the functions $y(\varphi)$, $\beta(\varphi)$, $M_x(\varphi)$ and $M_z(\varphi)$ for $\mu = 1$, $\lambda = 100$; $\mu = 0.7$, $\lambda = 60$.

Antisymmetric Case of Loading

If the loads are antisymmetric, Fig. 3, so that $P(\xi)$ is an odd function of ξ, analogous reductions lead to

$$y(\varphi) = \frac{4R}{a\mu\pi}\sum_{n=1,3,5,\cdots}^{\infty} Y_n \sin n\varphi \int_0^{\pi/2} P(\xi)\sin n\xi d\xi \quad [25]$$

$$\beta(\varphi) = \frac{4R}{a\mu\pi}\sum_{n=1,3,5,\cdots}^{\infty} B_n \sin n\varphi \int_0^{\pi/2} P(\xi)\sin n\xi d\xi \quad [26]$$

$$M_x(\varphi) = \frac{4R}{\mu\pi}\sum_{n=1,3,5,\cdots}^{\infty} M_{xn}\sin n\varphi \int_0^{\pi/2} P(\xi)\sin n\xi d\xi \quad [27]$$

$$M_z(\varphi) = \frac{4R}{\mu\pi}\sum_{n=1,3,5,\cdots}^{\infty} M_{zn}\cos n\varphi \int_0^{\pi/2} P(\xi)\sin n\xi d\xi \quad [28]$$

Tables 3 and 4 contain the first 24 coefficients of the series expressing the functions $y(\varphi)$, $\beta(\varphi)$, $M_x(\varphi)$ and $M_z(\varphi)$ for $\mu = 1$, $\lambda = 100$; $\mu = 0.7$, $\lambda = 60$.

Numerical Example. Suppose a circular beam of radius R = 25 ft in reinforced concrete [$E = 3(10^6)$ psi] of square cross section (depth 30 in., width 30 in.) with eight concentrated loads P =

TABLE 1 COEFFICIENTS FOR SYMMETRIC LOADING; $\mu = 1$; $\lambda = 100$

n	Y_n	B_n	M_{xn}	M_{zn}
2	$0.0^{3}559701$	$-0.0^{3}895522$	0.0134328	$-0.0^{3}671640$
4	$0.0^{3}283019$	$-0.0^{3}532742$	0.0399556	$-0.0^{3}998890$
6	$0.0^{3}732217$	$-0.0^{4}142485$	0.0249350	$-0.0^{4}415583$
8	$0.0^{3}241828$	$-0.0^{4}476215$	0.0150000	$-0.0^{4}187500$
10	$0.0^{4}981948$	$-0.0^{3}194445$	$0.0^{3}962504$	$-0.0^{3}962504$
12	$0.0^{4}483262$	$-0.0^{4}959858$	$0.0^{4}886299$	$-0.0^{4}571916$
14	$0.0^{4}260953$	$-0.0^{4}519257$	$0.0^{4}506275$	$-0.0^{4}361625$
16	$0.0^{4}152950$	$-0.0^{4}304710$	$0.0^{4}388505$	$-0.0^{4}242816$
18	$0.0^{4}954489$	$-0.0^{4}190310$	$0.0^{4}307351$	$-0.0^{4}170750$
20	$0.0^{4}626128$	$-0.0^{4}124913$	$0.0^{4}249202$	$-0.0^{4}124601$
22	$0.0^{4}427583$	$-0.0^{4}853403$	$0.0^{4}206097$	$-0.0^{4}936804$
24	$0.0^{4}301841$	$-0.0^{4}602636$	$0.0^{4}173257$	$-0.0^{4}721904$

TABLE 2 COEFFICIENTS FOR SYMMETRIC LOADING; $\mu = 0.70$; $\lambda = 60$

n	Y_n	B_n	M_{xn}	M_{zn}
2	$0.0^{3}497630$	$-0.0^{3}890496$	0.0110002	$-0.0^{3}550010$
4	$0.0^{3}219557$	$-0.0^{3}489504$	0.0302341	$-0.0^{3}755852$
6	$0.0^{3}522163$	$-0.0^{4}121971$	0.0175782	$-0.0^{4}292970$
8	$0.0^{4}169806$	$-0.0^{3}403382$	0.0104643	$-0.0^{4}130804$
10	$0.0^{4}699665$	$-0.0^{4}167525$	$0.0^{4}672913$	$-0.0^{4}672913$
12	$0.0^{4}338250$	$-0.0^{4}813395$	$0.0^{4}478946$	$-0.0^{4}399122$
14	$0.0^{4}182458$	$-0.0^{4}439906$	$0.0^{4}353219$	$-0.0^{4}252299$
16	$0.0^{4}106951$	$-0.0^{4}258297$	$0.0^{4}271212$	$-0.0^{4}169507$
18	$0.0^{4}667610$	$-0.0^{4}161422$	$0.0^{4}214692$	$-0.0^{4}119273$
20	$0.0^{4}437960$	$-0.0^{4}105983$	$0.0^{4}174124$	$-0.0^{4}870620$
22	$0.0^{4}299094$	$-0.0^{4}724233$	$0.0^{4}144037$	$-0.0^{4}654714$
24	$0.0^{4}211157$	$-0.0^{4}511541$	$0.0^{4}121115$	$-0.0^{4}504646$

TABLE 3 COEFFICIENTS FOR ANTISYMMETRIC LOADING; $\mu = 1$; $\lambda = 100$

n	Y_n	B_n	M_{xn}	M_{zn}
1	0	0	0	0
3	0.0^{5}507614	−0.0^{3}913705	0.0365483	−0.0121828
5	0.0^{5}141176	−0.0^{3}271492	0.0365483	−0.0^{4}651582
7	0.0^{5}407138	−0.0^{3}797990	0.0191518	−0.0^{4}273597
9	0.0^{5}151918	−0.0^{3}300131	0.0120053	−0.0^{4}133392
11	0.0^{5}683916	−0.0^{3}135662	0.0^{4}813972	−0.0^{4}739974
13	0.0^{5}350981	−0.0^{4}697793	0.0^{5}586146	−0.0^{4}450882
15	0.0^{5}198018	−0.0^{4}394283	0.0^{4}441597	−0.0^{4}294398
17	0.0^{5}120001	−0.0^{5}239174	0.0^{5}344411	−0.0^{4}202595
19	0.0^{5}768873	−0.0^{5}153350	0.0^{4}276030	−0.0^{4}145279
21	0.0^{5}515091	−0.0^{5}102785	0.0^{5}226127	−0.0^{5}107679
23	0.0^{5}357894	−0.0^{5}714437	0.0^{5}188612	−0.0^{5}820052

TABLE 4 COEFFICIENTS FOR ANTISYMMETRIC LOADING; $\mu = 0.70$; $\lambda = 60$

n	Y_n	B_n	M_{xn}	M_{zn}
1	−0.0^{5}205882	0.0^{5}205882	0	0
3	0.0^{5}441037	−0.0^{5}924365	0.0304497	−0.0101499
5	0.0^{5}103217	−0.0^{5}237120	0.0234330	−0.0^{4}468660
7	0.0^{5}287263	−0.0^{5}677875	0.0133980	−0.0^{4}191400
9	0.0^{5}106431	−0.0^{5}253996	0.0^{4}836692	−0.0^{4}929658
11	0.0^{5}478355	−0.0^{5}114816	0.0^{4}566327	−0.0^{4}514843
13	0.0^{5}245393	−0.0^{5}590959	0.0^{4}408805	−0.0^{4}314465
15	0.0^{5}137393	−0.0^{5}331564	0.0^{5}305818	−0.0^{5}203879
17	0.0^{5}839161	−0.0^{5}202794	0.0^{5}240489	−0.0^{5}141464
19	0.0^{5}537736	−0.0^{5}130078	0.0^{5}192822	−0.0^{5}101485
21	0.0^{5}360291	−0.0^{5}872167	0.0^{5}158016	−0.0^{5}752957
23	0.0^{5}250358	−0.0^{5}606375	0.0^{5}131833	−0.0^{5}573187

50 tons each ($2\gamma = 45$ deg), Fig. 6. The constant of the foundation is supposed to be $k = 1500$ lb per in. per in. It follows

$I_x = 6.75(10^4)$ in.^{4}

$\lambda = 60$

$\mu = 0.7$

$$Y = \frac{R^2P}{EI_x} = 0.04444$$

$$a = \frac{EI_x}{R} = 28{,}125 \text{ ft-tons}$$

$a\gamma = 1250$ ft-tons

From Equations [21], [22], [23], and [24] one obtains, in this particular case

$$v(\varphi) = \frac{4P}{\pi kR} + \frac{8R^2P}{a\mu\pi} \sum_{n=8,16,24,\cdots}^{\infty} Y_n \cos n\varphi \cos n(22^\circ\ 30') \quad \ldots\ldots\ldots\ldots [29]$$

$$\beta(\varphi) = \frac{8RP}{a\mu\pi} \sum_{n=8,16,24,\cdots}^{\infty} B_n \cos n\varphi \cos n(22^\circ\ 30') \ldots [30]$$

$$M_x(\varphi) = \frac{8RP}{\mu\pi} \sum_{n=8,16,24,\cdots}^{\infty} M_{xn} \cos n\varphi \cos n\ (22^\circ\ 30') \ldots [31]$$

$$M_z(\varphi) = \frac{8RP}{\mu\pi} \sum_{n=8,16,24,\cdots}^{\infty} M_{zn} \sin n\varphi \cos n\ (22^\circ\ 30') \ldots [32]$$

In Table 5 the results obtained by using the first three terms of the series given by the approximate Equations [29], [30], [31], and [32] are presented.

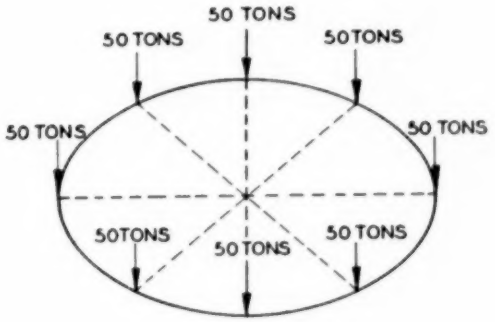

CASE c: $2\gamma = 45^0$

FIG. 6

In Table 6 the results obtained using the solution in closed form developed in the previous paper (1) are given.

As should be expected and should be seen by inspection from Tables 1, 2, 3, and 4, the convergence of the bending-moment series is less favorable than the convergence of the series of the deflections, angles of twist, and twisting moments.

BIBLIOGRAPHY

1 "Bending of a Circular Beam Resting on an Elastic Founda-

TABLE 5

φ	r, in.	β, radians	M_x, ft-tons	M_z, ft-tons
0°	0.2751	0.0°6187	—40.7586	0
5°	0.2766	0.0°4964	—31.7226	—3.2630
10°	0.2809	0.0°1483	—16.8080	—5.3952
15°	0.2867	—0.0°4586	12.1185	—5.8185
20°	0.2910	—0.0°6489	57.1428	—2.7282
22° 30′	0.2917	—0.0°7022	65.4239	0

TABLE 6

φ	r, in.	β, radians	M_x, ft-tons	M_z, ft-tons
0°	0.2748	0.0°6444	—40.9000	0
5°	0.2764	0.0°5111	—34.850	—3.3875
10°	0.2811	0.0°1529	—16.700	—5.7250
15°	0.2869	—0.0°3111	13.6125	—5.9500
20°	0.2915	—0.0°6755	56.1125	—3.0000
22° 30′	0.2923	—0.0°7377	81.8875	0

tion," by E. Volterra, JOURNAL OF APPLIED MECHANICS, Trans. ASME, vol. 74, March, 1952, pp. 1–4.

2 "Beams on Elastic Foundation," by M. Hetényi, The University of Michigan Press, Ann Arbor, Mich., 1946.

3 "Die Lehre von der Elastizität und Festigkeit," by E. Winkler, Prague, Czechoslovakia, 1867, p. 182.

4 "Die Berechnung des Eisenbahnoberbaues," by H. Zimmermann, second edition, Berlin, Germany, 1888, 1930.

5 "The Mathematical Theory of Elasticity," by A. E. H. Love, fourth edition, Dover Publications, New York, N. Y., October, 1944.

6 "Memoire sur le calcul de la resistance et de la fléxion des pièces solides à simple ou à double courbure, en prenant simultanément en considération les divers efforts auxquels elles peuvent être soumises dans tous les sens," by Barré De Saint Venant, *Comptes Rendus* de l'Academie des Sciences de Paris, France, vol. 17, 1843, pp. 942–954 and 1020–1031.

7 "Strength of Materials—Part II Advanced Theory and Problems," by S. Timoshenko, The Macmillan Company, New York, N. Y., 1936, pp. 467–473.

8 "A Mathematical Treatise on Vibrations in Railway Bridges," by C. E. Inglis, Cambridge University Press, Cambridge, England, 1934, chapter1: "Deflections of Beams Obtained by Methods of Harmonic Analysis."

On the Application of the Impedance Method to Continuous Systems

By P. F. CHENEA,[1] LAFAYETTE, IND.

It is shown how the concept of impedance may be extended to apply to those continuous systems whose vibratory behavior leads to the wave equation. The use of the method is demonstrated by three examples which include the free and forced vibration of an elastic bar in longitudinal oscillation and torsional oscillation of a tapered shaft.

Nomenclature

The following nomenclature is used in the paper:

- σ = longitudinal stress
- A, J = cross-sectional area, and polar moment of inertia of cross section
- M_t = external torque
- ρ = density of medium
- u = longitudinal displacement
- θ = angle of twist
- z = impedance
- x = co-ordinate along length of bar
- ω = circular frequency
- f = natural frequency
- $j = \sqrt{-1}$
- E, G = Young's and shear modulus of elasticity
- ν = Poisson's ratio

Introduction

The solution to free and forced vibrations of systems which are linear in character is generally made more systematic by the introduction of the impedance concept. This method has received wide recognition in the treatment of vibratory systems which have discrete physical elements. Although the concept of impedance has been used in the problems of electrical circuits and acoustics, it has not received attention in the treatment of continuous vibratory systems whose formulations lead, in general, to the wave equation. It is the purpose of the present paper to show how the impedance concept may be applied readily to this general class of problems such as the free and forced-vibration problems for the longitudinal oscillation of an elastic bar, the lateral vibration of a string, and the torsional oscillation of a shaft.

Analysis

Consider an elastic bar whose cross-sectional area, as well as the physical properties of its medium (such as elastic moduli, damping constants, and density) vary with the co-ordinate x in the longitudinal direction. It is assumed that the variation in the cross-sectional area is gradual, a requirement which is essential in one-dimensional treatment of the problem. The damping may be both internal and external but it must, of course, be linear.

The equation of motion for an element of the bar, shown in Fig. 1(*a*), is

$$\frac{\partial}{\partial x}\left[\sigma A(x)\right] = \rho(x)\, A(x)\, \frac{\partial^2 u}{\partial t^2} + c'(x)\, \frac{\partial u}{\partial t} \qquad [1]$$

where $c'(x)$ is the damping coefficient.

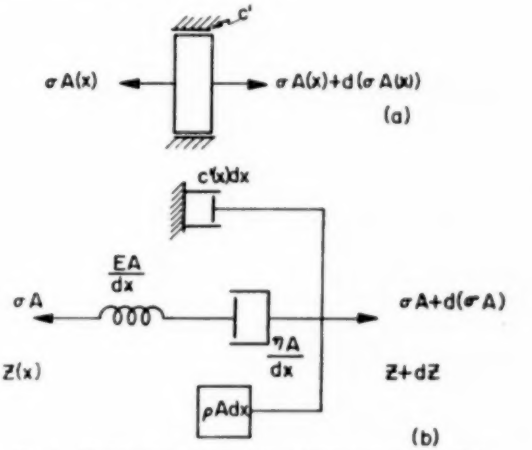

Fig. 1 Model for Longitudinal Oscillation of a Bar

The stress-strain relation modified to include internal viscous damping η is

$$\frac{\partial^2 u}{\partial x \partial t} = \frac{1}{E(x)}\, \frac{\partial \sigma}{\partial t} + \frac{\sigma}{\eta(x)} \qquad [2]$$

The model which exhibits the properties of the infinitesimal element of the bar is shown in Fig. 1(*b*). It consists of a spring and dashpot in series, this combination in parallel with another dashpot, and a mass. Since the model is linear, the solution to Equations [1] and [2] may be written as

$$\left.\begin{aligned} \sigma(x,t)\, A(x) &= S e^{j\omega t} \\ u(x,t) &= U e^{j\omega t} \end{aligned}\right\} \qquad [3]$$

where the force and displacement amplitudes $S(x)$ and $U(x)$ are, in general, complex, indicating a phase difference. The impedance is then defined as

$$z(x) = \frac{\sigma A}{u} = \frac{S(x)}{U(x)} \qquad [4]$$

The change in the impedance dz across the infinitesimal element in Fig. 1(*a*) may be obtained in the usual fashion,[2] namely

[1] Professor of Engineering Mechanics, Purdue University.

Contributed by the Applied Mechanics Division and presented at the Annual Meeting, New York, N. Y., November 30–December 5, 1952, of The American Society of Mechanical Engineers.

Discussion of this paper should be addressed to the Secretary, ASME, 29 West 39th Street, New York, N. Y., and will be accepted until July 10, 1953, for publication at a later date. Discussion received after the closing date will be returned.

Note: Statements advanced in papers are to be understood as individual expressions of their authors and not those of the Society. Manuscript received by ASME Applied Mechanics Division, April 29, 1952. Paper No. 52—A-28.

[2] See, for example, "Mechanics of Vibration," by H. M. Hansen and P. F. Chenea, John Wiley & Sons, New York, N. Y., 1952.

$$z + dz = \frac{1}{\frac{1}{z} + \frac{dx}{EA} + \frac{dx}{j\omega\eta A}} + j\omega c' dx - \rho\omega^2 A dx$$

This equation is now simplified to read

$$\frac{dz}{dx} + z^2 g(x) + h(x) = 0 \quad \ldots\ldots [5]$$

where

$$g(x) = \frac{1}{A(x)}\left[\frac{1}{E(x)} + \frac{1}{j\omega\eta(x)}\right]$$

and

$$h(x) = -j\omega c'(x) + \omega^2 \rho(x) A(x)$$

Equation [5] is of the Ricatti type[3] which, in many cases, can be integrated directly. However, the introduction of a new variable ξ defined by the relation

$$z = \frac{1}{g(x)} \frac{1}{\xi} \frac{d\xi}{dx} \quad \ldots\ldots [6]$$

transforms Equation [5] into the linear second-order equation

$$\frac{d}{dx}\left[\frac{1}{g(x)} \frac{d\xi}{dx}\right] + \omega^2 \xi\, h(x) = 0 \quad \ldots\ldots [7]$$

which may be more tractable. The solution of Equation [5] provides the impedance $z(x)$ containing one arbitrary constant. The constant of integration may be evaluated from the boundary conditions in question which are easily expressed in terms of the impedance, as follows:

For free end: $\sigma = 0, \quad z = 0$
For fixed end: $u = 0, \quad z = \infty$
For end which is elastically restrained: $\sigma A = ku, \quad z = k$

The results of the foregoing analysis, particularly Equations [5] and [7], are valid for all problems in which their formulations lead to the wave equation. For instance, when the continuous system is subjected to torsional oscillation, the quantities σA, u, $\rho A dx$, and EA/dx in Fig. 1(b) and Equations [1] and [2] must be replaced by M_t, θ, $\rho J dx$, and GJ/dx, respectively. The impedance in this case is defined as

$$z = \frac{M_t}{\theta} = \frac{T}{\Theta}$$

where T and (Θ) are the torque and twist amplitudes, respectively.

Likewise, for a vibrating string, the only alteration required is to replace the spring constant EA/dx by F/dx (F being the tension in the string) and, of course, to remove both of the dashpots in Fig. 1(b).

Examples

Uniform Elastic Bar Without Damping. Assuming E, A, and ρ to be constants and taking $c' = 0$, $\eta = \infty$, then for a longitudinal oscillation of an elastic bar without damping

$$g = 1/EA \qquad h = \omega^2 \rho A$$

and Equation [5] may be integrated directly to yield

$$x = -\frac{c}{\omega} \tan^{-1}\left(\frac{z}{\omega A \sqrt{E\rho}}\right) + C \quad \ldots\ldots [8]$$

[3] "A Treatise on Differential Equations," by A. R. Forsyth, MacMillan & Co., New York, N. Y., 1943, p. 191.

where $c = \sqrt{E/\rho}$ is the velocity of sound in the bar and $\bar{z} = \omega A \sqrt{E\rho}$ may be called the specific impedance of the bar. If the impedance at the end $x = 0$ of the bar is z_0, then the constant C is

$$C = \frac{c}{\omega} \tan^{-1}\left(\frac{z_0}{\bar{z}}\right)$$

and Equation [8] becomes

$$x = \frac{c}{\omega} \tan^{-1}\left[\frac{\frac{z_0}{\bar{z}} - \frac{z}{\bar{z}}}{1 - \frac{zz_0}{\bar{z}^2}}\right]$$

from which

$$z = \frac{z_0 - \bar{z} \tan \frac{\omega x}{c}}{1 + \frac{z_0}{\bar{z}} \tan \frac{\omega x}{c}} \quad \ldots\ldots [9]$$

At the end $x = L$ of the bar, the impedance is

$$z_L = \frac{z_0 - \bar{z} \tan \frac{\omega L}{c}}{1 + \frac{z_0}{\bar{z}} \tan \frac{\omega L}{c}}$$

It is clear that the frequency equation can now be obtained by specifying the appropriate values of z_0 and z_L.

If both ends are free, then $z_0 = z_L = 0$ and it follows that

$$\tan \frac{\omega L}{c} = 0$$

and thus the natural frequencies of the system are

$$f = nc/2L \quad (n = 1, 2, \ldots)$$

For fixed ends, $z_0 = z_L = \infty$ and the natural frequencies are identical with those of the free-free ends.

When one end is free ($z_L = 0$) and the other end fixed ($z_0 = \infty$), then

$$\tan \frac{\omega L}{c} = \infty$$

and the natural frequencies of the system are

$$f = (2n - 1)c/4L \quad (n = 1, 2, \ldots)$$

If one end of the bar (say, the end $x = L$) is forced so that

$$(\sigma A)_{x=L} = S_L e^{j\omega t}$$

then, by Equation [4]

$$U_L = \frac{1 + \frac{z_0}{\bar{z}} \tan \frac{\omega L}{c}}{z_0 - \bar{z} \tan \frac{\omega L}{c}} S_L$$

It will now be shown how the force and displacement amplitudes S and U can be obtained at any section of the bar. Since $c' = 0$, it follows from Equations [1] and [3] that

$$dS/S = \frac{\omega^2 \rho A\, dx}{\bar{z} \tan \frac{\omega}{c}(x - C)}$$

from which

$$S = B \sin \frac{\omega}{c}(x - C)$$

The constant C has been determined previously and the constant $B = S_L/\sin(\omega/c)(x - C)$ is evaluated at the end $x = L$ of the bar. Hence the expressions for the force and displacement amplitudes at any section x of the bar are

$$S = S_L \left[\frac{\frac{z_0}{\hat{z}} - \tan \frac{\omega x}{c}}{\frac{z_0}{\hat{z}} - \tan \frac{\omega L}{c}} \right] \frac{\cos \frac{\omega x}{c}}{\cos \frac{\omega L}{c}}$$

and

$$U = \frac{S_L}{\hat{z}} \left[\frac{1 + \frac{z_0}{\hat{z}} \tan \frac{\omega x}{c}}{\frac{z_0}{\hat{z}} - \tan \frac{\omega L}{c}} \right] \frac{\cos \frac{\omega x}{c}}{\cos \frac{\omega L}{c}}$$

Torsional Vibration of a Stepped Shaft. Consider the shaft shown in Fig. 2 which has two sections of different cross-sectional

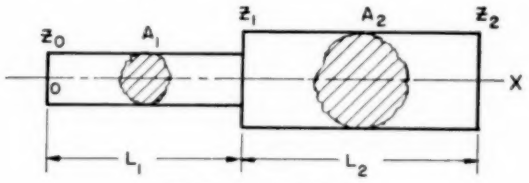

FIG. 2 STEPPED SHAFT

area and length. In this case

$$g(x) = 1/GJ, \quad h(x) = \omega^2 \rho J$$

and by Equation [5]

$$\frac{dz}{dx} + \frac{z^2}{GJ} + \omega^2 \rho J = 0$$

The impedance for each section of the shaft is readily obtained as in the preceding example. They are

$$z_1 = \frac{z_0 - \hat{z}_1 \tan \frac{\omega L_1}{a}}{1 + \frac{z_0}{\hat{z}_1} \tan \frac{\omega L_1}{a}}$$

and

$$z_2 = \frac{z_1 - \hat{z}_2 \tan \frac{\omega L_2}{a}}{1 + \frac{z_1}{\hat{z}_2} \tan \frac{\omega L_2}{a}}$$

where

$$a^2 = \frac{G}{\rho}, \qquad \hat{z}_1 = \omega \rho a J_1, \qquad \hat{z}_2 = \omega \rho a J_2$$

If the end $x = 0$ is free, $z_0 = 0$ and z_1 becomes

$$z_1 = -\omega \rho a J_1 \tan \frac{\omega L_1}{a}$$

Hence

$$z_2 = -\frac{\frac{J_1}{J_2} \tan \frac{\omega L_1}{a} + \tan \frac{\omega L_2}{a}}{1 - \frac{J_1}{J_2} \tan \frac{\omega L_1}{a} \tan \frac{\omega L_2}{a}}$$

If the end $x = L_1 + L_2$ is also free, then $z_2 = 0$ and the frequency equation is

$$\frac{J_1}{J_2} \tan \frac{\omega L_1}{a} + \tan \frac{\omega L_2}{a} = 0$$

It is clear that the foregoing procedure may be applied to shafts of n steps.

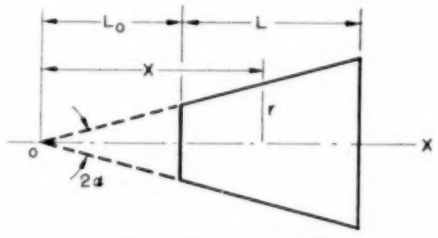

FIG. 3 TAPERED SHAFT

Torsional Oscillation of a Tapered Shaft. It is seen from the geometry of Fig. 3 that

$$r = x \tan \alpha \quad \text{and} \quad J = J_0 x^4$$

where

$$J_0 = \frac{\pi \tan^4 \alpha}{2}$$

In this case

$$g(x) = 1/GJ_0x^4 \quad \text{and} \quad h(x) = \omega^2 \rho J_0 x^4$$

and Equation [5] becomes

$$\frac{dz}{dx} + \frac{z^2}{GJ_0x^4} + \omega^2 \rho J_0 x^4 = 0 \qquad [10]$$

A change of variable in accordance with Equation [6], namely

$$z = GJ_0x^4 \frac{1}{\xi} \frac{d\xi}{dx} \qquad [11]$$

reduces Equation [10] to

$$\frac{d^2\xi}{dx^2} + \frac{4}{x} \frac{d\xi}{dx} + \frac{\omega^2 \rho}{G} \xi = 0$$

which may be reduced to Bessel's standard form whose solution is

$$\xi = x^{-3/2} \left[B_1 J_{3/2}\left(\sqrt{\frac{\rho}{G}}\, \omega x \right) + B_2 J_{-3/2}\left(\sqrt{\frac{\rho}{G}}\, \omega x \right) \right]$$

where

$$J_{3/2}(\varphi) = \sqrt{\frac{2}{\pi \varphi}} \left(\frac{\sin \varphi}{\varphi} - \cos \varphi \right)$$

$$J_{-3/2}(\varphi) = -\sqrt{\frac{2}{\pi \varphi}} \left(\sin \varphi + \frac{\cos \varphi}{\varphi} \right)$$

Thus by Equation [11]

$$z = GJ_0^\circ x^4 \left[\frac{-DJ_{5/3}(\varphi) + J_{-5/3}(\varphi)}{DJ_{3/3}(\varphi) + J_{-3/3}(\varphi)} \right] \left(\sqrt{\frac{\rho}{G}}\, \omega \right)$$

where

$$D = B_1/B_2, \qquad \varphi = \frac{\omega x}{a}, \qquad a^2 = \frac{G}{\rho} = \frac{c^2}{2(1+\nu)}$$

The constant D is evaluated from the condition of the end $x = L_0$ for which we may denote the impedance by z_0. Thus

$$D = \frac{GJ_0 L_0^4 \dfrac{\omega}{a} J_{-5/3}(\varphi_0) - z_0 J_{-5/3}(\varphi_0)}{GJ_0 L_0^4 \dfrac{\omega}{a} J_{3/3}(\varphi_0) + z_0 J_{3/3}(\varphi_0)}; \qquad \varphi_0 = \omega \frac{L_0}{a}$$

If the end $x = L_0$ is free, then $z_0 = 0$ and

$$D = \frac{J_{-5/3}(\varphi_0)}{J_{3/3}(\varphi_0)}$$

and finally, the impedance z of the shaft is

$$z = GJ_0 x^4 \frac{\omega}{a} \left[\frac{J_{3/3}(\varphi_0) J_{-5/3}(\varphi) - J_{-5/3}(\varphi_0) J_{3/3}(\varphi)}{J_{3/3}(\varphi_0) J_{-3/3}(\varphi) + J_{-3/3}(\varphi_0) J_{3/3}(\varphi)} \right]$$

If the end $x = L_0 + L$ is also free so that $z_{L_0+L} = 0$, the frequency equation is

$$J_{3/3}(\varphi_0) J_{-5/3}(\varphi_1) - J_{-5/3}(\varphi_0) J_{3/3}(\varphi_1) = 0$$

If one end of the bar, say, $x = L + L_0$, is forced with an oscillating torque

$$(M_t)_{x=L_0+L} = T_0 e^{j\omega t}$$

and the end $x = L_0$ is free, then as in the previous example

$$(\Theta)_{L_0+L} = \frac{T_0}{(z)_{\varphi=\varphi_1}} = \frac{T_0 a}{GJ_0 x^4 \omega} \left[\frac{J_{3/3}(\varphi_0) J_{-5/3}(\varphi_1) + J_{-5/3}(\varphi_0) J_{3/3}(\varphi_1)}{J_{3/3}(\varphi_0) J_{-3/3}(\varphi_1) - J_{-3/3}(\varphi_0) J_{3/3}(\varphi_1)} \right]$$

The twist and torque amplitudes at any section x may be found as in the first example.

The above solution is in agreement with that of Conway[4] who obtained the solution to torsional vibration of a truncated cone via the wave equation.

[4] "The Calculation of Frequencies of Vibration of a Truncated Cone," by H. D. Conway, *Aircraft Engineering*, vol. 18, 1946, pp. 235–236.

On an Iterative Method for Nonlinear Vibrations

By R. E. ROBERSON,[1] DOWNEY, CALIF.

An iterative method for nonlinear vibrations, previously discussed by Brock,[2] is treated from a primarily analytic point of view. In this light, it is a modification of a Picard-like process for two-point boundary conditions mentioned by Gwoh-Fan Djang.[3] It is generalized from previous treatments to systems with more than one degree of freedom and to dissipative systems. Despite its quite different rationale, the results are only slight modifications of those obtained by the application of Duffing's method, indicating that the two are facets of the same fundamental process.

Introduction

BROCK[2] recently proposed an iterative numerical method for solving certain problems in nonlinear vibrations. It adapts a Stodola process of numerical integration to an iteration method of a modified Picard type. As proposed, the method is convenient and of fairly wide applicability. However, it is considered as a primarily numerical method, and with the kind of numerical integration which is used, it is limited to nondissipative systems. Actually, the method can be quite useful from a purely analytic point of view, aside from the numerical procedure involved.

The essential feature of this iteration method is the enforcement of a condition in excess of the usual pair of initial conditions, and the use of this excess condition to determine an unknown parameter of the problem. Thus certain intervals of integration in the iteration involve a parameter, rather than always being the interval $(0, t)$ as in the classical Picard iteration. Seen in this light, the rationale of Brock's method is similar to that described by Djang[3] for two-point boundary conditions.

The purpose of this paper is to unify the points of view represented by these two works and to consider the extension of the method to dissipative systems and systems with more than one degree of freedom. We wish to emphasize that the basis for the method is independent of the particular process of numerical integration that one might be led to use.

Review of the Method

Consider the equation

$$\ddot{x} = f(x, \dot{x}, t) \quad \ldots\ldots [1]$$

For our purposes, the most convenient initial conditions are $x(0) = a$, $\dot{x}(0) = 0$, with the supplementary condition $x(T) = 0$.[4] The first two are conditions which maintain at a relative maximum or minimum of the solution curve, so that if the response is oscillatory and periodic, a has the interpretation of solution amplitude. The third condition is a statement that there exists a time $t = T$ at which the solution becomes zero (for the first time), and is particularly important for periodic solutions. This condition will not generally be true, of course, for arbitrary functions f. Write Equation [1] in normal form with $x_1 = x$, $x_2 = \dot{x}$, and put the result into a form for iteration

$$\left.\begin{aligned} \dot{x}_1^{(m+1)} &= x_2^{(m)} \\ \dot{x}_2^{(m+1)} &= f\,[x_1^{(m)}, x_2^{(m)}, t] \end{aligned}\right\} \quad \ldots\ldots [2]$$

Here superscripts in parentheses are iteration numbers.

Now assume approximate solutions $x_1^{(0)}(t)$ and $x_2^{(0)}(t)$, such that $x_1^{(0)}(0) = a$ and $x_1^{(0)}(T) = 0$, T being the first zero. We may consider that $x_1^{(0)}$ contains both a and T as parameters, and may denote it as $x_1^{(0)}(t;\ a;\ T)$. Any other parameters relating to initial conditions, as in a system with more than one degree of freedom, would be included with a between semicolons. Integrating Equation [2b]

$$x_2^{(1)}(t;\ a;\ T) = \int_0^t f\,[x_1^{(0)}(\tau;\ a;\ T), x_2^{(0)}(\tau), \tau]\, d\tau \quad \ldots [3]$$

In continuing by the Picard iteration, one would next integrate Equation [2a] to obtain

$$x_1^{(1)}(t;\ a) = a + \int_0^t x_2^{(0)}(\tau) d\tau$$

However, in Djang's method this would be changed to

$$x_1^{(1)}(t;\ a;\ T) = a + \int_0^t x_2^{(1)}(\tau;\ a;\ T) d\tau \quad \ldots\ldots [4]$$

since $x_2^{(1)}$ already has been obtained from Equation [3]. In Brock's procedure, one goes a step further and uses the $x_1(T)$ condition rather than the $x_1(0)$ condition. This gives

$$x_1^{(1)}(t;\ a;\ T) = -\int_t^T x_2^{(1)}(\tau;\ a;\ T) d\tau \quad \ldots\ldots [5]$$

The importance of avoiding the additive term a which appears in Equation [4] is related to the process of numerical integration which is used. With an integral of the form of Equation [5], the necessary double integration can be performed very easily. One continues in the same way to find higher approximations.

If we now use the remaining initial condition, insisting that $x(0) = a$ for each approximate solution, we have an algebraic relationship between the initial amplitude and the time which it takes for the solution to reach its first zero. This is

---

[1] Electro-Mechanical Engineering Department, North American Aviation. Jun. ASME.

[2] "An Iterative Numerical Method for Nonlinear Vibrations," by J. E. Brock, JOURNAL OF APPLIED MECHANICS, Trans. ASME, vol. 73, 1951, pp. 1–11.

[3] "A Modified Method of Iteration of the Picard Type in the Solution of Differential Equations," by Gwoh-Fan Djang, *Journal of The Franklin Institute*, vol. 246, 1948, pp. 453–457. This merely touches upon the question of two-point boundary conditions. Djang's main efforts were to show how the Picard method can be made to converge more rapidly by using the new approximation for each variable, immediately as it is obtained, in the iterations for the remaining variables.

Contributed by the Applied Mechanics Division and presented at the Annual Meeting, New York, N. Y., November 30–December 5, 1952, of THE AMERICAN SOCIETY OF MECHANICAL ENGINEERS.

Discussion of this paper should be addressed to the Secretary, ASME, 29 West 39th Street, New York, N. Y., and will be accepted until July 10, 1953, for publication at a later date. Discussion received after the closing date will be returned.

NOTE: Statements and opinions advanced in papers are to be understood as individual expressions of their authors and not those of the Society. Manuscript received by ASME Applied Mechanics Division, July 7, 1952. Paper No. 52—A-20.

[4] Brock adequately illustrates a case in which the second and third conditions are modified, while leaving the first unchanged.

$$a = -\int_0^T d\sigma \int_0^\sigma f\,[x_1^{(m)}(\tau; a; T), x_2^{(m)}(\tau; a; T), \tau]\,d\tau \quad [6]$$

(When the integrations are numerical, it is important to change the variables of integration so that the parameter T does not appear in the limits of integration.) The process may be continued, of course, without using Equation [6] until convergence is complete. This equation may be considered as giving the time T when an initial value a is known. But alternately, desiring a solution with the period or first crossing time T, one can use Equation [6] to find the initial value compatible with this time requirement.

The general nature of the method is as outlined, but there are modifications and deviations to suit various specific problems, some of which are treated in the following.

It is appropriate to remark briefly on the question of the convergence of this method. There are really two aspects of convergence to be considered. The first of these relates to the convergence of the iteration when all integrations are exact. The second relates to the convergence when there are errors at each step due to approximate numerical integrations. Brock has shown by example that there are systems for which there is convergence even in the presence of such errors. The difficulty, of course, is that there is no way of stating how closely the function reached by such a convergent process approximates the true solution of the differential equation. The answer to such a question may be strongly conditioned by the nature of the numerical integration process which is used. For this reason, a treatment of the case where the integrations are approximate is not attempted. The more modest goal of investigating convergence for exact integrations probably can be accomplished by some procedure analogous to the ordinary Picard-Lindelöf existence proof. However, this is left for treatment elsewhere.

Application to System With Two Degrees of Freedom

Consider a nonlinear dynamic vibration absorber with cubic spring coupling, which can be described[5] by the equations

$$\left.\begin{aligned} \Omega^2 y_1(\tau) &= \cos\tau + (\Lambda^2 y_2 + \nu y_2^3) - y_1 \\ -\Omega^2 y_2(\tau) &= \cos\tau + M(\Lambda^2 y_2 + \nu y_2^3) - y_1 \end{aligned}\right\} \quad \ldots\ldots [7]$$

Here, $y_1(\tau)$ and $y_2(\tau)$ are, respectively, the dimensionless displacement of the main mass and relative displacement of main mass and absorber. Dimensionless time is denoted by τ, and ν is the coefficient of cubic nonliniarity in the absorber spring. These can be written in normal form with $x_1 = y_1$, $x_2 = \dot{y}_1$, $x_3 = y_2$, $x_4 = \dot{y}_2$ as

$$\left.\begin{aligned} \dot{x}_1(\tau) &= x_2(\tau) \\ \dot{x}_2(\tau) &= \frac{1}{\Omega^2}\,[\cos\tau + (\Lambda^2 x_3 + \nu x_3^3) - x_1] \\ \dot{x}_3(\tau) &= x_4(\tau) \\ \dot{x}_4(\tau) &= -\frac{1}{\Omega^2}\,[\cos\tau + M(\Lambda^2 x_3 + \nu x_3^3) - x_1] \end{aligned}\right\} \quad \ldots [8]$$

Consider that $x_1(0) = a$, $x_3(0) = b$, and $x_2(0) = x_4(0) = 0$. Furthermore, if we seek a solution with the period of the exciting force, we have the additional conditions $x_1(\pi/2) = x_3(\pi/2) = 0$. As 0th approximations, we take

$$x_1^{(0)}(\tau) = a\cos\tau,\ x_3^{(0)}(\tau) = b\cos\tau$$

Then

$$x_2^{(1)}\left(\tau; a, b; \frac{\pi}{2}\right) = \frac{1}{\Omega^2}\int_0^\tau [\cos w + (\Lambda^2 b\cos w + \nu b^3\cos^3 w) - a\cos w]\,dw$$

$$x_4^{(1)}\left(\tau; a, b; \frac{\pi}{2}\right) = -\frac{1}{\Omega^2}\int_0^\tau [\cos w + M(\Lambda^2 b\cos w + \nu b^3\cos^3 w) - a\cos w]\,dw$$

and

$$x_1^{(1)}\left(\tau; a, b; \frac{\pi}{2}\right) = -\int_\tau^{\pi/2} x_2^{(1)}\left(v; a, b; \frac{\pi}{2}\right) dv$$

$$x_3^{(1)}\left(\tau; a, b; \frac{\pi}{2}\right) = -\int_\tau^{\pi/2} x_4^{(1)}\left(v; a, b; \frac{\pi}{2}\right) dv$$

The latter are analogs of Equations [5], with the unknown parameters a and b rather than a and T.

Evaluating these integrals, we find

$$\left.\begin{aligned} -\Omega^2 x_1^{(1)}\left(\tau; a, b; \frac{\pi}{2}\right) &= [1 - a + (\Lambda^2 b + 3\nu b^3/4)]\cos\tau + \nu b^3/36\cos 3\tau \\ \Omega^2 x_3^{(1)}\left(\tau; a, b; \frac{\pi}{2}\right) &= [1 - a + M(\Lambda^2 b + 3\nu b^3/4)]\cos\tau + M\,\nu b^3/36\cos 3\tau \end{aligned}\right\} \quad \ldots [9]$$

Re-using the initial condition on x_1 and x_3, we obtain

$$\left.\begin{aligned} -\Omega^2 a &= 1 - a + (\Lambda^2 b + 7\nu b^3/9) \\ \Omega^2 b &= 1 - a + M(\Lambda^2 b + 7\nu b^3/9) \end{aligned}\right\} \quad \ldots\ldots [10]$$

These equations determine (to a first approximation) the values of a and b which are compatible with the requirement that the solutions vanish at $\tau = \pi/2$, as functions of a dimensionless "excitation frequency" Ω.

At this point, one has three options in proceeding. For many purposes, he may consider the amplitude relationships implicit in Equations [10] as his final answer. They suffice to give approximate response curves as functions of the problem parameters and to give them fairly closely for small values of the nonlinearity parameter ν. However, if a higher-order approximation to the answer is desired, there is still the choice of proceeding analytically or numerically. If numerical values of the problem parameters are known, then one may expect that the numerical procedure of Brock would converge rapidly, using Equations [10] to write the first approximation

$$\left.\begin{aligned} x_1^{(1)}\left(\tau; a, b; \frac{\pi}{2}\right) &= (a + \nu b^3/36\Omega^2)\cos\tau - (\nu b^3/36\Omega^2)\cos 3\tau \\ x_3^{(1)}\left(\tau; a, b; \frac{\pi}{2}\right) &= (b - \nu b^3 M/36\Omega^2)\cos\tau + (\nu b^3 M/36\Omega^2)\cos^3\tau \end{aligned}\right\} \quad \ldots [11]$$

and using this as a starting point for the iteration. His method, of course, must be generalized somewhat. It seems most convenient to form a tableau such as that of Table 1, in which the coefficients for epoch 1 are merely denoted by 0.9 for convenience. The values for $\dot{x}_1$ and $\dot{x}_3$ are found in terms of a and b

[5] "Synthesis of a Nonlinear Dynamic Vibration Absorber," by R. E. Roberson, *Journal of The Franklin Institute*, vol. 253, September, 1952.

TABLE 1 BROCK'S METHOD FOR A SYSTEM WITH TWO DEGREES OF FREEDOM

	Epoch	0	1	...	N
Stage 1	$x_1^{(1)}$	a	$0.9a$	...	0
	$x_2^{(1)}$	b	$0.9b$	...	0
	$\dot{x}_1$				
	$\dot{x}_2$				
	$x_1^{(2)}$	(next approximation)			
	$\dot{x}_2$				
	$x_2^{(2)}$	(next approximation)			

according to Equations [7], and the Stodola process used to integrate these second derivatives. No difficulty is encountered with the explicit appearance of the parameters a and b, the integrations merely being performed on their coefficients separately. On the other hand, the first approximations of Equations [11] may be used in exactly the same way as $x_1^{(0)}$ and $x_2^{(0)}$ in the analytical approach. After integrating and re-using the initial condition, the analogs of Equations [10] become

$$\left.\begin{aligned} -\Omega^2 a &= 1 - a + (\Lambda^2 b + 7\nu b^3/9) + \Phi \\ \Omega^2 b &= 1 - a + M(\Lambda^2 b + 7\nu b^3/9) + M\Phi \end{aligned}\right\} \quad \ldots [12]$$

where

$$\Phi = (1 - \Lambda^2 M)\nu b^3/324\Omega^2 + \left(\frac{9b - 425}{300}\right) M\,\nu^2 b^5/36\Omega^2 + \left(\frac{16{,}025 - 441b}{7350}\right) M^2\nu^3 b^7/1296\Omega^4 + \left(\frac{1498b - 57{,}025}{44{,}100}\right) M^2\nu^4 b^9/44{,}656\Omega^6 \ldots [13]$$

It is apparent that the analytical approach is becoming unwieldy at this point, but it is still possible to obtain useful results from this second approximation.

One further comment on this example is appropriate. The Duffing method for finding an approximate amplitude relationship is superficially somewhat different from the method just presented. If it is applied to the same example, one obtains

$$-\Omega^2 a = 1 - a + (\Lambda^2 b + 3\nu b^3/4)$$
$$\Omega^2 b = 1 - a + M(\Lambda^2 b + 3\nu b^3/4)$$

which are very close to the relations of Equations [10]. The difference comes only from the fact that in the present method, the $\cos 3\tau$-term is included in setting the amplitude of the approximation equal to the initial condition. Thus the relationship between the present method and that of Duffing is very close and bears further investigation in the general case.

Application to a Dissipative System

Consider the system with one degree of freedom described by

$$\ddot{x} = -c\dot{x} - \lambda^2 x - \nu x^3 + \cos t \quad \ldots [14]$$

We seek a solution with the period of the driving term. However, the presence of damping means that the response will be out of phase with the excitation. One can choose an approximate solution of the form

$$x^{(0)}(t) = a\cos t + b\sin t$$

with the two undetermined constants a and b, or one can suppose that the solution is simply

$$x^{(0)}(t) = a\cos t$$

and that the driving force has the phase angle φ relative to the origin of time determined by this assumption. Let $x = x_1$, $\dot{x} = x_2$ and adopt the latter course, so that

$$\dot{x}_1 = x_2 \quad \ldots [15]$$
$$\dot{x}_2 = -[cx_2 + \lambda^2 x_1 + \nu x_1^3 - \cos(t + \varphi)]$$

Assume

$$\left.\begin{aligned} x_1^{(0)}\left(t;\, a,\, \varphi;\, \frac{\pi}{2}\right) &= a\cos t \\ x_2^{(0)}\left(t;\, a,\, \varphi;\, \frac{\pi}{2}\right) &= -a\sin t \end{aligned}\right\} \quad \ldots [16]$$

Then

$$x_2^{(1)}\left(t;\, a,\, \varphi;\, \frac{\pi}{2}\right) = -\int_0^t \left[-ca\sin\tau + \lambda^2 a\cos\tau + \frac{3\nu a^3}{4}\cos\tau + \frac{\nu a^3}{4}\cos 3\tau - \cos(\tau + \varphi)\right] d\tau$$
$$= -ca\cos t - \lambda^2 a\sin t - \frac{3\nu a^3}{4}\sin t - \frac{\nu a^3}{12}\sin 3t + \sin(t + \varphi) + ca - \sin\varphi$$

and by Equations [5]

$$x_1^{(1)}\left(t;\, a,\, \varphi;\, \frac{\pi}{2}\right) = -ca(1 - \sin t) + \lambda^2 a\cos t + \frac{3\nu a^3}{4}\cos t + \frac{\nu a^3}{36}\cos 3t + \cos\left(\frac{\pi}{2} + \varphi\right) - \cos(t + \varphi) - [ca + \sin\varphi]\left(\frac{\pi}{2} - t\right)$$

The periodicity requirement on x_1 leads to the choice of φ: $\sin\varphi = ca$. Then

$$x_1^{(1)}\left(t;\, a,\, \varphi;\, \frac{\pi}{2}\right) = \left(\lambda^2 a + \frac{3\nu a^3}{4} - \sqrt{1 - a^2c^2}\right)\cos t + \frac{\nu a^3}{36}\cos 3t \ldots [17]$$

Enforcing the initial condition $x_1(0) = a$, one has the amplitude equation

$$(\lambda^2 - 1)a + \frac{7\nu a^3}{9} = \sqrt{1 - a^2c^2} \quad \ldots [18]$$

If a numerical approach similar to Brock's were desired instead, it would be necessary only to use some such scheme as Table 2. (Typical rather than calculated coefficient values are shown, and iteration starts with first approximation. For $\dot{x}_2$, coefficients appropriate to the ith epoch, found from Equations [15], are denoted by α_i, β_i, γ_i.) One condition may be put on a and φ at once, by equating the value of $x_1^{(2)}$ at epoch 0 to a. However, a second condition on the two quantities (corresponding to the periodicity requirement used analytically) is not so obvious.

TABLE 2 BROCK'S METHOD FOR A DISSIPATIVE SYSTEM

Epoch	0	1	...	N
$x_1^{(1)}$	a	$.9a$	...	$-a$
$x_2^{(1)}$	0	$.1a$	...	0
$\dot{x}_2$	$\alpha_0 + \beta_0\cos\varphi + \gamma_0\sin\varphi$	$\alpha_1 + \beta_1\cos\varphi + \gamma_1\sin\varphi$	...	$\alpha_N + \beta_N\cos\varphi + \gamma_N\sin\varphi$
$x_1^{(2)}$	(obtained from $\dot{x}_2$ by numerical integration)			
$x_1^{(2)}$	(obtained from $x_1^{(2)}$ by numerical integration)			

It seems necessary, in this case, to fix the Nth epoch at $t = \pi$ rather than making the customary choice $t = \pi/2$. The conditions used in integration are then that $x_2 = 0$ at epoch 0 and $x_2 = 0$, $x_1 = -a$ at epoch N. The value of $x_2^{(2)}(N)$ obtained by integrating $\dot{x}_2$ will not be zero in the table but will involve the parameters a and φ. Setting this table value equal to zero at the end of the approximation stage then establishes a second condition on a and φ. The two conditions suffice to determine both parameter values. This example might have been made to include a parameter Ω, a dimensionless forcing frequency, as well. Then the a and φ would be given as functions of Ω by these conditions.

Natural Frequencies of Twisted Cantilever Beams

By D. D. ROSARD,[1] LESTER, PA.

When a cantilever beam, an aircraft propeller, a turbine or compressor blade, is twisted, the natural frequencies of vibration may be changed appreciably. The effect of twist depends on the width-to-thickness ratio. An experimental and analytical investigation was made of the effect of twist for various width-to-thickness ratios.

Introduction

THE determination of natural frequencies of twisted cantilever beams has received increasing interest in the past few years due to the direct application to turbine and compressor blades, as well as aircraft propellers.

Several papers have been published recently concerning the effect of twist on the natural frequencies of cantilever beams,[2,3] but they fail to point out that this effect is only a special case of coupled vibration and follows the same simple law as other forms of coupled vibration. This law may be stated as follows:

If two vibrating systems having nearly equal natural frequencies are coupled together, the resulting system has one natural frequency below the lower uncoupled frequency and one natural frequency above the higher uncoupled frequency.

In this beam-vibration problem, the two vibrating systems involved are the second-mode beam vibration in the flexible direction and the first-mode beam vibration in the stiff direction. In a uniform beam, these two uncoupled frequencies are equal for a width-to-thickness ratio of 6.36. The coupling is introduced by the twist of the beam.

The simple case of uniform beams having ratios of width to thickness varying from 1 to 12 is treated to demonstrate the vibration characteristics. Results were obtained both experimentally and analytically (with an analog computer).

Natural Frequencies of Untwisted Uniform Cantilever Beams

The fundamental frequency of a uniform cantilever beam is

$$f_1 = \frac{3.52}{2\pi l^2}\sqrt{\frac{EI}{\rho A}} = \frac{3.52h}{2\pi l^2}\sqrt{\frac{E}{12\rho}}$$

where

E = modulus of elasticity

I = moment of inertia of beam cross section = $\frac{1}{12}bh^3$

ρ = mass density

A = cross-section area = bh

b = width

h = thickness

l = length of beam

We will make our results dimensionless by expressing all frequencies in terms of the fundamental, f_1. The second-mode frequency is $f_2 = 6.36\ f_1$. The third-mode frequency is $f_3 = 17.53\ f_1$. The beam can also vibrate in the "stiff" direction, in which the fundamental frequency will be

$$F_1 = \frac{b}{h} f_1$$

It will be noted that for a square beam ($b/h = 1$), F_1 is equal to f_1. As the width of the beam is increased, F_1 increases until it becomes equal to f_2 for $b/h = 6.36$. As the width is increased further, F_1 becomes larger than f_2 and becomes equal to f_3 for $b/h = 17.53$.

Natural Frequencies of Twisted Uniform Cantilever Beams

When the beam is twisted, vibrations in the flexible and stiff direction no longer take place independently. They become coupled together and give rise to complex modes which are best identified by their order in increasing frequency. The first mode has the lowest frequency, the second mode is the next highest, and so on. The effect of twist on the first mode is very small.

Of special interest is the effect of twist on the second and third modes. Usually, we think of second and third-mode vibrations as taking place in the same plane as the first mode but with one and two nodal points, respectively. In Fig. 1 the second mode would be f_2 and the third mode would be f_3. For thin beams, where the width-to-thickness ratio is 20 or more, this conception brings no difficulties, because the second and third modes as we have just defined them are also second and third in order of increasing frequency. In such wide beams, the effect of twist on the second and third modes is relatively small.

However, as the width-to-thickness ratio decreases, Fig. 1 shows that an extra mode of vibration appears and obscures the identity of the second and third modes. In Fig. 2 the deflec-

TABLE 1 RATIO OF NATURAL FREQUENCIES TO UNTWISTED FUNDAMENTAL MODE (TEST DATA)

Total twist =		0°	10°	20°	30°	40°
$b/h = 4$		1.0	1.0	1.0	1.0	1.0
		3.99	3.99	3.81	3.64	3.44
		6.30	6.32	6.5	6.85	7.3
1/4 × 1 × 11 beam		17.5	17.5	17.2	16.7	16.2
$b/h = 6$		1.0	1.0	1.0	1.0	1.0
		5.85	5.32	4.8	4.5	4.1
		6.34	6.9	7.5	8.3	9.1
1/4 × 1½ × 11 beam		17.65	17.5	17.1	16.6	16.1
$b/h = 8$		1.0	1.0	1.0	1.0	1.0
		6.3	5.9	5.3	4.7	4.2
		7.45	7.9	8.8	9.8	10.8
1/4 × 2 × 11 beam		17.5	17.4	17.1	16.5	16.0
$b/h = 12$		1.0	1.0	1.0	1.0	1.0
		6.28	6.0	5.6	4.8	4.5
		11.0	11.2	12.2	13.3	14.1
1/4 × 3 × 11 beam		17.5	17.5	17.1	17.4	16.6

[1] Turbine Engineering Department, Westinghouse Electric Corporation. Jun. ASME.

[2] "Influence of Twist in Turbine Blades on Natural Frequencies and Directions of Vibration," by J. Geiger, *Engineers' Digest*, vol. 11, April, 1950, pp. 115–118.

[3] "Analytical and Experimental Investigation of Effect of Twist on Vibrations of Cantilever Beams," by Alexander Mendelson and Selwyn Gendler, NACA TN-2300, 1951.

Contributed by the Applied Mechanics Division and presented at the Annual Meeting, New York, N. Y., November 30–December 5, 1952, of The American Society of Mechanical Engineers.

Discussion of this paper should be addressed to the Secretary, ASME, 29 West 39th Street, New York, N. Y., and will be accepted until July 10, 1953, for publication at a later date. Discussion received after the closing date will be returned.

Note: Statements and opinions advanced in papers are to be understood as individual expressions of their authors and not those of the Society. Manuscript received by ASME Applied Mechanics Division, June 2, 1952. Paper No. 52—A-15.

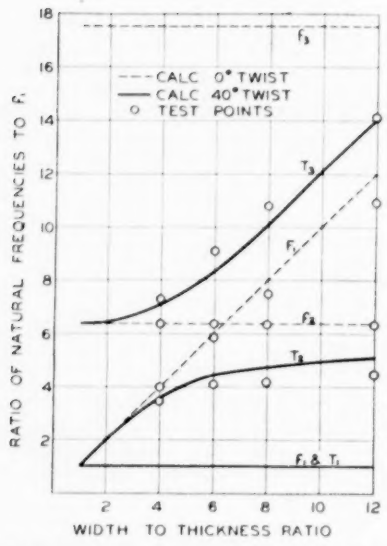

FIG. 1 VARIATION OF NATURAL FREQUENCIES OF A UNIFORM RECTANGULAR CANTILEVER BEAM AS A FUNCTION OF THE WIDTH-TO-THICKNESS RATIO b/h

(f_1, f_2, and f_3 are the first, second, and third modes in the flexible direction for the untwisted beam; F_1 is the first mode in the stiff direction for the untwisted beam; T_1, T_2, and T_3 are the first three modes of the beam with 40-deg total twist.)

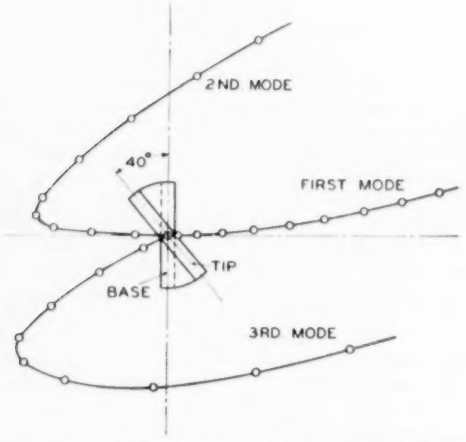

FIG. 2 CALCULATED MODE SHAPES FOR $b/h = 8$: TOTAL TWIST = 40 DEG

tion in these two modes of vibration is plotted. This plot shows the x, y-locations of the centers of ten equal length sections as shown in Fig. 3. Note that the three modes of vibration have no connection with each other and only the relative deflections at one instant are shown for each mode. During vibration, each point moves along a line passing through the vertical axis.

When looking from the direction of the 40-deg tip angle, both the second and third modes seem to have one nodal point, and could be thought to be characteristic second-mode vibrations. The difference lies in the manner in which the vibration in the stiff axis couples to the characteristic second mode. The effect of this coupling on the frequencies is appreciable in the range of width-to-thickness ratios between 4 and 12. For width-to-thickness ratios below 4, the second mode becomes well defined

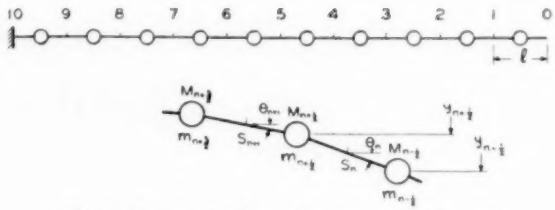

FIG. 3 CANTILEVER BEAM DIVIDED IN TEN SECTIONS

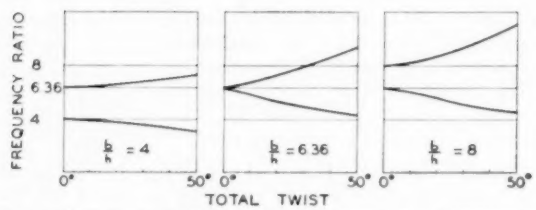

FIG. 4 VARIATION OF NATURAL FREQUENCIES AS A FUNCTION OF TOTAL TWIST

(When the beam is twisted, the lower frequency is decreased and the higher frequency is increased.)

again, but is third in order of increasing frequency, while the fundamental in the stiff direction is second in order of increasing frequencies.

In Fig. 4, for example, the lower frequency line, which is second in order of increasing frequencies, is recognized as the fundamental in the stiff direction for $b/h = 4$, and as the characteristic second mode for $b/h = 8$. For $b/h = 6.36$, where the untwisted fundamental frequency in the stiff direction and second-mode frequency in the flexible direction are equal, the lower and upper lines can only be differentiated by their frequencies.

EXPERIMENTAL PROCEDURE

Beams of various lengths and width-to-thickness ratios were welded to a heavy bedplate. Vibrations were excited by hitting the beams with a hammer. A microphone was used in conjunction with a "Stroboconn" to measure the frequencies of vibration, Figs. 5 and 6.

To excite the various modes of vibration, the hammer must be used with some finesse; the beam must be hit at the proper location, and in the proper direction. For the lower frequencies, a soft hammer is used, while for the higher frequencies a hard hammer is used. To obtain a good signal, the microphone also is held close to the position of maximum amplitude. All this becomes instinctive after a little practice.

To check whether the support flexibility had any appreciable effect on our results, one beam was tested again on a 7-ton block. No difference in frequencies was noted.

A tapered model also was tested on this block to check frequency calculations of a tapered twisted blade. Test results agreed with the calculations.

CALCULATION METHOD

The natural frequencies of a twisted beam, whether uniform or tapered can be calculated as shown in the Appendix.

These equations are not as refined as the ones used by Myklestad,[4] but were found to be accurate within 1 or 2 per cent for reasonable tapers usually encountered in turbine or compressor blades.

These equations can be solved readily by setting up an equiva-

[4] "Vibration Analysis," by N. O. Myklestad, McGraw-Hill Book Company, Inc., New York, N. Y., 1944.

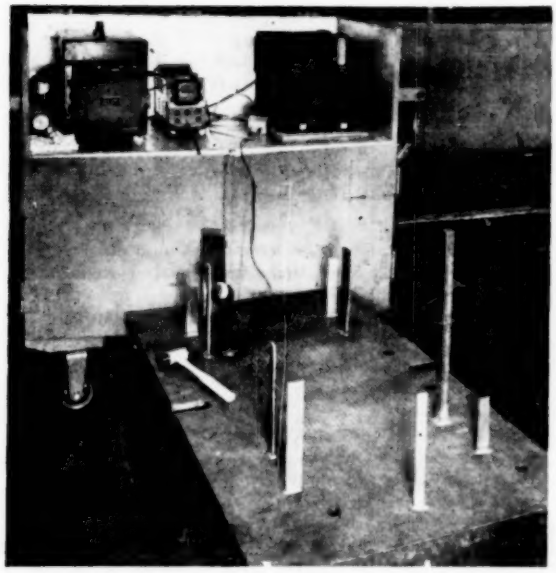

Fig. 5 Test Setup

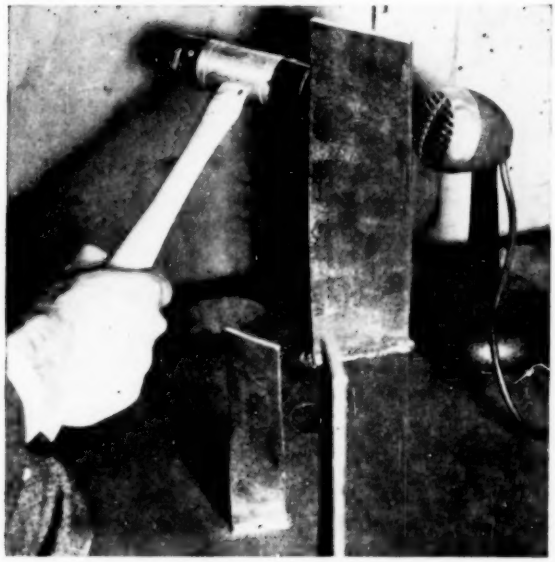

Fig. 6 Location and Direction of Hammer Blows Must Be Varied to Excite Various Modes of Vibration

lent electrical network, or when better accuracy is desired, by means of punched-card machines.

Differences Between Calculations and Experiments

The differences between calculations and experiments can be attributed to two sources of error, as follows:

1 Because the purpose of this investigation was not to determine the degree of accuracy of the calculations, but only to establish a general pattern, the experimental methods were kept as simple as possible. Although the total twist produced in the beams was measured with reasonable accuracy, the twisting method used could not produce a uniform twist, but on the contrary, caused very little twist at the base and tip, and a correspondingly larger fraction of the twist in the center portion of the beam.

2 The calculations assume a long beam following the classical beam formulas, whereas, especially in the wider beams, the decreasing length-to-width ratio changes the nature of the problem to a cantilever-plate vibration.

Acknowledgments

The author wishes to express his appreciation to his associates in the Westinghouse Electric Corporation for their co-operation and to Prof. J. P. Den Hartog for suggesting this study. The calculations were made at the Westinghouse Analog Computer Laboratory.

Appendix

Calculation of Natural Modes of Bending Vibration of a Twisted Cantilever Beam

Divide the beam in 10 sections of equal length, Fig. 3. The mass of each section is concentrated at its mid-point. The flexibility of each section is also concentrated at its mid-point and considered constant within the section. Shears and slopes are measured at the ends of each section. Moments and deflections are measured at the centers of each section.

The following relations can be written

Deflection

$$y_{n+1/2} = y_{n-1/2} - \theta_n{}^y\, l \qquad [1]$$

Shear

$$S_{n+1}{}^y = S_n{}^y + m_{n+1/2}\,\omega^2\, y_{n+1/2} \qquad [2]$$

Moment

$$M_{n+1/2}{}^y = M_{n-1/2}{}^y + S_n{}^y\, l \qquad [3]$$

Slope

$$\theta_{n+1}{}^y = \theta_n{}^y - M_{n+1/2}{}^y f_{n+1/2}{}^y\, l - M_{n+1/2}{}^x f_{n+1/2} l \qquad [4]$$

where f^y, f, are the flexibility coefficients

In dimensionless form, these relations become

$$\bar{y}_{n+1/2} = \bar{y}_{n-1/2} - \bar{\theta}_n{}^y \qquad [5]$$

$$\bar{S}_{n+1}{}^y = \bar{S}_n{}^y + K\bar{m}_{n+1/2}\,\bar{y}_{n+1/2} \qquad [6]$$

$$\bar{M}_{n+1/2}{}^y = \bar{M}_{n-1/2}{}^y + \bar{S}_n{}^y \qquad [7]$$

$$\bar{\theta}_{n+1}{}^y = \bar{\theta}_n{}^y - \bar{M}_{n+1/2}{}^y F_{n+1/2}{}^y - \bar{M}_{n+1/2}{}^x F_{n+1/2} \qquad [8]$$

(Similar relations are also written in the x-direction)

where

$$K = \frac{1}{EI_0}\,\rho A_0\, l^4\,\omega^2$$

$$\bar{m} = \frac{m}{m_0}$$

$$F_x = \frac{I_0}{I_{\min}}\sin^2\alpha + \frac{I_0}{I_{\max}}\cos^2\alpha$$

$$F_y = \frac{I_0}{I_{\min}}\cos^2\alpha + \frac{I_0}{I_{\max}}\sin^2\alpha$$

$$F = \left(\frac{I_0}{I_{\min}} - \frac{I_0}{I_{\max}}\right)\sin\alpha\cos\alpha$$

Starting at the free end, let the following four quantities be given

$$\bar{\theta}_1^{\,y} \qquad \bar{\theta}_1^{\,z} \qquad \bar{y}_{1/2} \qquad \bar{z}_{1/2}$$

The following four quantities can be computed immediately

$$\bar{S}_1^{\,y} = K\bar{m}_{1/2}\,\bar{y}_{1/2} \qquad \bar{S}_1^{\,z} = K\bar{m}_{1/2}\,\bar{z}_{1/2}$$

$$\bar{M}_{1^1/_2}{}^{y} = \bar{S}_1^{\,y} \qquad \bar{M}_{1^1/_2}{}^{z} = \bar{S}_1^{\,z}$$

From these eight starting quantities at the free end and the iteration Equations [5] through [8] with their z-counterparts, every other shear, moment, and slope and deflection in the blade can be computed as functions of $\bar{\theta}_1^{\,y}$, $\bar{\theta}_1^{\,z}$, $\bar{y}_{1/2}$, and $\bar{z}_{1/2}$.

In particular, we can solve for

$$\bar{\theta}_{10}{}^{y} = A_{11}\,\bar{\theta}_1^{\,y} + A_{12}\,\bar{y}_{1/2} + A_{13}\,\bar{\theta}_1^{\,z} + A_{14}\,\bar{z}_{1/2} = 0$$
$$\bar{y}_{9^1/_2} = A_{21}\,\bar{\theta}_1^{\,y} + A_{22}\,\bar{y}_{1/2} + A_{23}\,\bar{\theta}_1^{\,z} + A_{24}\,\bar{z}_{1/2} = 0$$
$$\bar{\theta}_{10}{}^{z} = A_{31}\,\bar{\theta}_1^{\,y} + A_{32}\,\bar{y}_{1/2} + A_{33}\,\bar{\theta}_1^{\,z} + A_{34}\,\bar{z}_{1/2} = 0$$
$$\bar{z}_{9^1/_2} = A_{41}\,\bar{\theta}_1^{\,y} + A_{42}\,\bar{y}_{1/2} + A_{43}\,\bar{\theta}_1^{\,z} + A_{44}\,\bar{z}_{1/2} = 0$$

The following determinant should then be equal to 0

$$\begin{vmatrix} A_{11} & A_{12} & A_{13} & A_{14} \\ A_{21} & A_{22} & A_{23} & A_{24} \\ A_{31} & A_{32} & A_{33} & A_{34} \\ A_{41} & A_{42} & A_{43} & A_{44} \end{vmatrix} = 0$$

By plotting the value of the determinant for a number of frequencies (by varying K) in the neighborhood of a natural frequency, a curve is obtained which passes through zero at the natural frequency.

An Analytical Theory of the Creep Deformation of Materials

By YOH-HAN PAO[1] and JOSEPH MARIN,[2] STATE COLLEGE, PA.

This paper reports on the formulation of an analytical theory of creep. This theory is proposed for an idealized material and may be applied to those materials whose behavior conforms to that of this ideal material. The theory takes into account the initial elastic strain, the transient creep strain, and the minimum rate creep strain. Unlike previous theories, this theory is capable of representing the simultaneous action of creep and creep recovery and may be used for conditions of varying as well as constant stresses. In this respect the theory is more general than those presented in the past. The new theory is of particular importance in the design of many new military and domestic applications where high temperatures over short periods of time make the initial short-time creep strains of importance.

Introduction

THERE are many materials which behave like elastic materials when loaded and unloaded rapidly, but behave like non-Newtonian fluids when subjected to a constant stress. Both aspects of material behavior are present when the material is subjected for any finite length of time to constant or varying stresses. This flow phenomenon is also called creep deformation. Metals at moderate and high temperatures and plastics at room temperatures behave in the foregoing manner.

Such materials are sometimes used at these temperatures in structures and machines. The redistribution of stress or the excessive deformations that might occur due to creep become important practical design considerations.

The analysis of the behavior of such structures can be achieved only if knowledge of the actual behavior of materials is combined with the mathematical techniques of analytical mechanics.

It is rather unfortunate therefore that those who are familiar with the phenomenon of creep deformation of materials are usually too engrossed with the materials aspect of the problem to give much thought to the application of their knowledge to the solution of engineering design problems. On the other hand, those interested in theoretical mechanics are sometimes not sufficiently familiar with the complexities of the phenomenon of the creep deformation of materials. The simplifying assumptions used in their theoretical solutions are often in direct contradiction with actual material behavior. On other occasions the theoretical expressions used are not capable of representing all the different aspects of the phenomenon and the solutions obtained are applicable only to special cases.

The theory proposed in this paper is based on existing experimental evidence. The analytical expressions are derived theoretically and are capable of representing the creep behavior of materials under varying as well as constant stresses. Furthermore, the mathematical simplicity of these expressions permits them to be used in the solution of engineering problems.

Before the proposed theory is explained, a brief review will be made of the phenomenological nature of the creep deformation of materials and of the previous work done in this field.

Phenomenological Nature of Creep Deformation

Experimental observations of the creep deformation of materials show that many materials which have widely differing molecular structures follow a surprisingly common general pattern in so far as their macroscopic behavior during creep deformation is concerned.

Some idea of the creep deformation of a material may be obtained from constant-load and constant-temperature creep tests of this material.

Fig. 1 shows a family of creep curves for specimens subjected to different constant static loads, all specimens being maintained at the same temperature. The creep strain is plotted as a function of time.

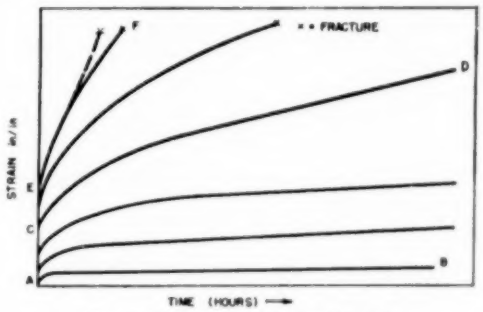

Fig. 1 A Family of Creep Curves

To a different scale, the curves also could represent a family of creep curves for specimens tested at different temperatures, all specimens being subjected to the same constant static load.

The curves shown in Fig. 1 are typical of the results obtained from tests of many different kinds of materials including ferrous and nonferrous alloys, rigid homogeneous high polymers, and laminated plastics.

Furthermore the creep curves themselves are very nearly similar geometrically. A creep curve typical of the curves indicated in Fig. 1 is shown in Fig. 2. This curve consists of three characteristic parts:

(*a*) The initial part where the deformation is not a creep deformation and occurs immediately on loading. It may be an elastic or a plastic deformation.

(*b*) The transient part where the deformation is characterized by a decreasing rate of deformation. The low-temperature

---

[1] Assistant Professor of Engineering Mechanics, Pennsylvania State College. Jun. ASME.

[2] Professor of Engineering Mechanics and Research Professor of Engineering Materials, Pennsylvania State College. Mem. ASME.

Presented at the National Conference of the Applied Mechanics Division, Minneapolis, Minn., June 18–20, 1953, of The American Society of Mechanical Engineers.

Discussion of this paper should be addressed to the Secretary, ASME, 29 West 39th Street, New York, N. Y., and will be accepted until July 10, 1953, for publication at a later date. Discussion received after the closing date will be returned.

Note: Statements and opinions advanced in papers are to be understood as individual expressions of their authors and not those of the Society. Manuscript received by ASME Applied Mechanics Division, August 4, 1952. Paper No. 53—APM-3.

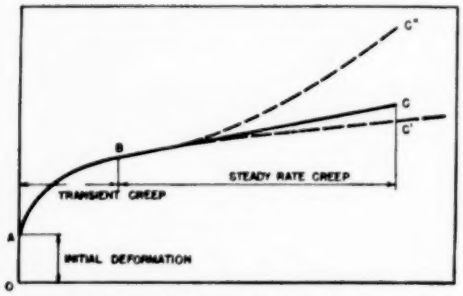

FIG. 2 A TYPICAL CREEP CURVE

curves tend asymptotically toward a zero creep rate, while the high-temperature curves tend toward a constant creep rate.

(*c*) The minimum rate part which is present in cases where the creep rate of the transient part does not vanish. The final part of the creep curve may take the form of *B-C*, *B-C'*, or *B-C"*.

In general, the creep curve is of the form *B-C'*. Occasionally it may take the form of a straight line *B-C* or it often may be approximated by a straight line. The slope of the straight line is called the minimum creep rate.

Sometimes the final part of the creep curve is of the form *B-C"*. It has been shown (1)[3] that for some cases the point of inflection and the stage of accelerating creep rates can be eliminated by maintaining the stress rather than the load constant.

After a certain period of time, the exact length of which would vary with the kind of material being tested and the magnitude of the load applied, the specimen fails by creep rupture. The final form of the creep curve determines whether this failure by fracture occurs at *C*, *C'*, or *C"*.

If the specimen is not allowed to progress to failure but is unloaded, some of the deformation is recovered. A typical creep curve and recovery curve are shown in Fig. 3.

There is a lack of agreement among investigators about the extent of creep recovery in materials, especially for the case of metals. Fortunately, some experimental studies have been made on this subject by Tapsell and Prosser (2), Chevenard (3), Bailey (4), and Johnson (5). These studies show that for the metals and stress levels investigated most of the transient creep is recoverable.

In engineering service, the load or stress may vary in magnitude from time to time. Under such conditions, creep and creep recovery may occur simultaneously. The situation is more complicated if the material is subjected to combined stresses and if these combined stresses also vary in magnitude.

SURVEY OF PREVIOUS ANALYTICAL THEORIES OF CREEP

In the early work, the initial deformation and the transient creep were considered to be negligible in comparison with the minimum rate creep and this method is still perhaps adequate where the stresses are of nearly constant magnitude and where the length of time is long. Soderberg (6), Odquist (7), and Marin (8) proposed essentially identical forms of theories for representing the principal minimum creep rates in terms of the principal stresses. These theories are based on the following assumptions:

(*a*) The volume of the material remains unchanged during creep deformation and that this condition can be expressed approximately as

$$\epsilon_{p1} + \epsilon_{p2} + \epsilon_{p3} = 0 \qquad [1]$$

(*b*) The directions of the principal shear strains coincide with those of the principal shear stresses.

(*c*) The distortion strain energy or the octahedral shear stress is the determining factor affecting the creep of the material.

The material was assumed to be homogeneous and to behave the same in tension as in compression.

In the case of simple stress the minimum creep rate was expressed as

$$C = B\sigma^n \qquad [2]$$

where C = the minimum creep rate, σ = the stress, and B and n are material constants.

Using the foregoing assumptions, the principal creep rates in the case of combined stresses are shown to be

[3] Numbers in parentheses refer to the Bibliography at the end of the paper.

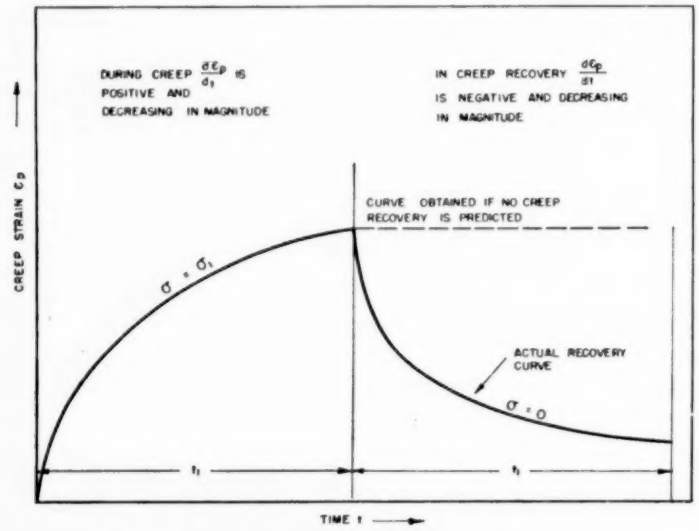
DURING CREEP $\frac{d\epsilon_p}{dt}$ IS POSITIVE AND DECREASING IN MAGNITUDE
IN CREEP RECOVERY $\frac{d\epsilon_p}{dt}$ IS NEGATIVE AND DECREASING IN MAGNITUDE
CREEP STRAIN ϵ_p
CURVE OBTAINED IF NO CREEP RECOVERY IS PREDICTED
$\sigma = \sigma_1$
ACTUAL RECOVERY CURVE
$\sigma = 0$
t_1
t_2
TIME t

FIG. 3 CREEP AND CREEP RECOVERY

$$C_1 = \frac{B}{2^{\frac{n+1}{2}}}\left[(\sigma_1-\sigma_2)^2+(\sigma_2-\sigma_3)^2+(\sigma_2-\sigma_1^2)\right]^{\frac{n-1}{2}}\left[(\sigma_1-\sigma_2)-(\sigma_3-\sigma_1)\right]$$

$$C_2 = \frac{B}{2^{\frac{n+1}{2}}}\left[(\sigma_1-\sigma_2)^2+(\sigma_2-\sigma_3)^2+(\sigma_3-\sigma_1)^2\right]^{\frac{n-1}{2}}\left[(\sigma_2-\sigma_3)-(\sigma_1-\sigma_2)\right] \quad \ldots [3]$$

$$C_3 = \frac{B}{2^{\frac{n+1}{2}}}\left[(\sigma_1-\sigma_2)^2+(\sigma_2-\sigma_3)^2+(\sigma_3-\sigma_1)^2\right]^{\frac{n-1}{2}}\left[(\sigma_3-\sigma_1)-(\sigma_2-\sigma_3)\right]$$

where σ_1, σ_2, and σ_3 are the principal stresses, and C_1, C_2, C_3 are the principal minimum creep rates.

Bailey (4) carried out experiments on the creep of thin-walled tubes subjected to tension and torsion. By the procedure of curve fitting, he found that the principal creep rates could be expressed as

$$C_1 = \frac{B}{2^{m+1}}\left[(\sigma_1-\sigma_2)^2+(\sigma_2-\sigma_3)^2+(\sigma_3-\sigma_1)^2\right]^m\left[(\sigma_1-\sigma_2)^{n-2m}-(\sigma_3-\sigma_1)^{n-2m}\right]$$

$$C_2 = \frac{B}{2^{m+1}}\left[(\sigma_1-\sigma_2)^2+(\sigma_2-\sigma_3)^2+(\sigma_3-\sigma_1)^2\right]^m\left[(\sigma_2-\sigma_3)^{n-2m}-(\sigma_1-\sigma_2)^{n-2m}\right] \quad \ldots [4]$$

$$C_3 = \frac{B}{2^{m+1}}\left[(\sigma_1-\sigma_2)^2+(\sigma_2-\sigma_3)^2+(\sigma_3-\sigma_1)^2\right]^m\left[(\sigma_3-\sigma_1)^{n-2m}-(\sigma_2-\sigma_3)^{n-2m}\right]$$

In Bailey's theory the three experimental constants B, m, n need to be determined in place of the two constants required by the Soderberg-Marin theory. Marin (8) compared the results obtained by the application of the two theories to test data obtained from creep tests of lead tubes subjected to torsion and showed that the results from each theory agreed equally well with test results.

Marin and Pao (9) have since extended Marin's theory to take into account the initial deformation also. In this later extension all of the creep strain and elastic strain are represented by an intercept strain. Although this represented one more step in the development of the theory, the theory was still not adequate for short periods of time and for varying stresses.

Bailey (10) has since also extended the expression

$$\epsilon_p = R\sigma^n t^m \quad \ldots [5]$$

to the case of combined stresses following the same procedure used by Soderberg, Marin, and Odquist. The resulting expressions then take into account transient creep as well as minimum rate creep. The theory is of such a form, however, that it is not capable of representing the simultaneous action of creep recovery and creep, and is therefore inadequate for conditions of varying stresses.

Proposed Theory of Creep

Basic Postulates. The theory proposed in the following is for an idealized material. Some experimental evidence exists to show that this idealized material is representative of many actual materials and the results derived are, therefore, of more than mere theoretical interest.

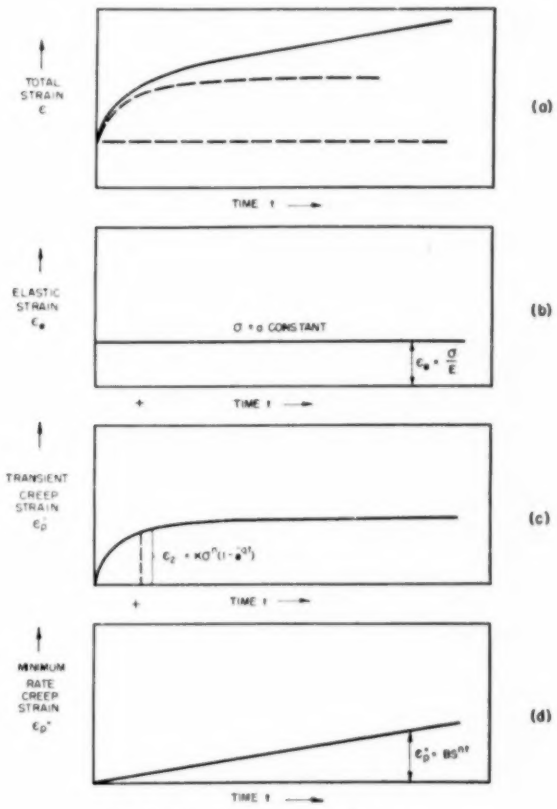

Fig. 4 Components of Strain

The postulates of the proposed theory are as follows:

(*a*) The total strain of this material at any constant temperature and at any time is composed of three independent component parts, i.e., the elastic strain, the transient strain, and the minimum creep strain, as shown in Fig. 4, for the case of a constant stress σ.

(*b*) The magnitude of the elastic strain is proportional to the stress, or by Hooke's law

$$\epsilon_e = \frac{\sigma}{E} \quad \ldots [6]$$

(*c*) The transient creep strain is related to the stress by the condition that the transient creep rate is a function of the stress and the transient creep strain, or

$$\frac{d\epsilon_p'}{dt} = f_1(\epsilon_p', \sigma) \quad \ldots [7]$$

where

$\frac{d\epsilon_p'}{dt}$ = transient creep rate

ϵ_p' = transient creep strain

σ = applied stress

Furthermore, it is assumed that the transient creep strain is fully recoverable.

(*d*) The minimum rate creep strain is related to the stresses by

the relation that the minimum creep rate is a function of the stress alone, or

$$\frac{d\epsilon_p''}{dt} = f_2(\sigma) \quad [8]$$

where

ϵ_p'' = minimum rate creep strain

$\frac{d\epsilon_p''}{dt}$ = minimum creep rate

$f_2(\sigma)$ = some function of applied stress

It also is assumed that the minimum rate creep strain is of a permanent nature. The main features of the proposed theory are contained in the postulates (*a*), (*b*), (*c*), and (*d*). The exact relationships for expressions f_1 and f_2 remain to be formulated.

Theoretical Determination of f_1 and f_2. The functions f_1 and f_2 may be determined from the existing knowledge of the phenomenological nature of creep and from the postulates of the proposed theory.

Term f_2 expresses the relation between the stress and the minimum creep rate. If the material were a Newtonian fluid, f_2 would be of the form

$$\frac{d\epsilon_p''}{dt} = B\sigma \quad [9]$$

However, experimental data show that materials in creep behave more like non-Newtonian fluids and the simplest assumption that can be made would be that the minimum creep rate is not proportional to the stress but rather to some power of the stress, namely

$$\frac{d\epsilon_p''}{dt} = B\sigma^n \quad [10]$$

It is seen that Equation [9] is but a special case of Equation [10].

Term f_1 expresses the relation between the transient creep rate, the transient creep strain, and the stress. Experimental data show that the transient creep rate is not proportional to the stress but rather to some power of the stress and that the transient creep rate decreases with increase of transient creep strain and vanishes when the latter reaches a maximum value. All these facts can be incorporated in the expression

$$\frac{d\epsilon_p'}{dt} = K'\sigma^n - q\epsilon_p' = q(K\sigma^n - \epsilon_p') \quad [11]$$

The exponent n used here is the same as that used in Equation [10]. The thought is that although the two components of creep strain are assumed to be independent, nevertheless they occur in the same material and the influences of stress on the creep rates are probably of the same nature. The fact that the transient creep rate decreases with increase in transient creep strain and that the transient creep rate vanishes for a maximum value of the transient creep strain is expressed most simply by the linear relationship shown in Equation [11].

Creep and Creep Recovery. In the case of varying stress, the total strain after some length of time may be written as

$$\epsilon = \epsilon_e + \epsilon_p' + \epsilon_p'' = \frac{\sigma}{E} + \int_0^t \frac{d\epsilon_p'}{dt}\,dt + \int_0^t \frac{d\epsilon_p''}{dt}\,dt \quad [12]$$

or

$$\epsilon = \frac{\sigma}{E} + \int_0^t q(K\sigma^n - \epsilon_p')dt + \int_0^t B\sigma^n\,dt \quad [13]$$

where σ is some function of time.

If the stress σ is constant, the total strain at some time is by integration of Equation [13]

$$\epsilon = \frac{\sigma}{E} + K\sigma^n(1 - e^{-qt}) + B\sigma^n t \quad [14]$$

The components expressed in Equation [14] are shown in Fig. 4.

If the material has been subjected to a constant stress σ_s for a length of time t_1, the total strain is then

$$\epsilon = \frac{\sigma_s}{E} + K\sigma_s^n(1 - e^{-qt_1}) + B\sigma_s^n t = \epsilon_{e_s} + \epsilon_{ps}' + \epsilon_{ps}'' \quad [15]$$

When the stress is then completely removed, the elastic strain is recovered instantly. The transient creep strain is recovered with time. The transient creep rate right after unloading is given by Equation [11], or

$$\frac{d\epsilon_p'}{dt} = -q\epsilon_{ps}' \quad [16]$$

Integrating this differential equation and substituting the boundary condition $\epsilon_p' = \epsilon_{ps}'$ at $t = t_1$, the recovery relation of the transient component becomes the reversed image of the transient creep curve or

$$\epsilon_p' = \epsilon_{ps}'\, e^{-q(t-t_1)} \quad [17]$$

In accordance with postulate (*d*) of the theory, however, the minimum creep strain ϵ_p'' is not recovered.

In cases where the stress is decreased but not removed completely, creep recovery may or may not occur. Thus if a specimen has been subjected to a stress σ_s for a period of time such that a transient creep strain ϵ_{ps}' has been developed, and if the stress is then decreased to a value σ_f, the transient creep rate immediately after the decrease in stress is given by Equation [11] as

$$\frac{d\epsilon_p'}{dt} = q(K\sigma_f^n - \epsilon_{ps}') \quad [18]$$

In expression if $|K\sigma_f^n| < |\epsilon_{ps}'|$ recovery of transient strain takes place. However, if $|K\sigma_f^n| > |\epsilon_{ps}'|$, there is no recovery and the transient creep strain continues to increase until a maximum value of $K\sigma_f^n$ is reached.

Incidentally, this explains why in short-time creep experiments of metals at high temperatures, many investigators found that there was no creep recovery with decrease of load. On the other hand, references (2, 3, 4, 5) show quite conclusively that most of the transient creep strain is recovered upon complete removal of stress.

Extension of Theory to Case of Combined Stresses. The theory has so far been derived only for the case of uniaxial stresses. However, in the following it is extended to the case of combined stresses. The theory to be developed takes into account the transient and minimum rate creep components and is proposed for both constant as well as varying stresses. Because the material is assumed to be homogeneous, and isotropic, the theory can be discussed in terms of the principal stresses and strains.

In accordance with postulate (*a*) of the theory, each of the principal strains is considered to be composed of three independent components. This may be written as

$$\left.\begin{aligned}\epsilon_1 &= \epsilon_{e1} + \epsilon_{p1}' + \epsilon_{p1}''\\ \epsilon_2 &= \epsilon_{e2} + \epsilon_{p2}' + \epsilon_{p2}''\\ \epsilon_3 &= \epsilon_{e3} + \epsilon_{p3}' + \epsilon_{p3}''\end{aligned}\right\} \quad [19]$$

where

ϵ = total strain
ϵ_e = elastic strain
ϵ_p' = transient creep strain
ϵ_p'' = minimum rate creep strain

and the subscripts 1, 2, and 3 denote the three principal axes.

In the following the independent components are considered separately as follows:

(*a*) *Elastic strains:* By Hooke's law, the principal elastic strains in terms of the principal stresses are

$$\left.\begin{aligned} \epsilon_{e1} &= \frac{1}{E}\,[\sigma_1 - \nu(\sigma_2 + \sigma_3)] \\ \epsilon_{e2} &= \frac{1}{E}\,[\sigma_2 - \nu(\sigma_1 + \sigma_3)] \\ \epsilon_{e3} &= \frac{1}{E}\,[\sigma_3 - \nu(\sigma_1 + \sigma_2)] \end{aligned}\right\} \quad [20]$$

where

E = Young's modulus of material
ν = Poisson's ratio of material

Equations [20] are an extension of postulate (*b*) of the theory to the case of combined stresses.

Before the transient creep strains and the minimum rate creep strains are discussed, it will be assumed that hydrostatic stresses do not cause creep strains. In so far as creep is concerned, it is then possible to represent any three-dimensional stress system by a two-dimensional stress system with equivalent shear stresses; that is, in Fig. 5 the stress system shown in Fig. 5 (*a*) may be replaced by the sum of the stresses shown in Fig. 5 (*b*) and Fig. 5 (*c*). The principal stresses σ_1, σ_2, and σ_3 are then replaced by a system of hydrostatic stresses σ_3, σ_3, and σ_3 which do not cause creep strains, and a two-dimensional system of stresses S_1 and S_2 which have shear stresses equivalent to those of the original system of stresses shown in Fig. 5 (*a*).

In so far as creep strains are concerned, the stresses σ_1, σ_2, and σ_3 can then be replaced by the stresses shown in Fig. 5 (*c*) or

$$\left.\begin{aligned} S_1 &= \sigma_1 - \sigma_3 \\ S_2 &= \sigma_2 - \sigma_3 \\ S_3 &= \sigma_3 - \sigma_3 = 0 \end{aligned}\right\} \quad [21]$$

The stress system described by Equations [21] is then used in the following development of the theory:

(*b*) *Transient creep strains:* The following assumptions are made in order to determine expressions for transient creep strains:

1 Transient creep strains do not cause change of volume, or

$$\epsilon_{p1}' + \epsilon_{p2}' + \epsilon_{p3}' = 0 \quad [22]$$

2 The principal transient shear creep rates are proportional to the principal shear stresses, or

$$\frac{\dfrac{d\epsilon_{p1}'}{dt} - \dfrac{d\epsilon_{p2}'}{dt}}{S_1 - S_2} = \frac{\dfrac{d\epsilon_{p1}'}{dt} - \dfrac{d\epsilon_{p3}'}{dt}}{S_2} = \frac{\dfrac{d\epsilon_{p2}'}{dt} - \dfrac{d\epsilon_{p1}'}{dt}}{-S_1} = G \quad [23]$$

From Equations [22] and [23] solving simultaneously for $(d\epsilon_{p1}')/(dt)$ and $(d\epsilon_{p2}')/(dt)$

$$\frac{d\epsilon_{p1}'}{dt} = \frac{(2S_1 - S_2)}{3}\,G \quad [24]$$

and

$$\frac{d\epsilon_{p2}'}{dt} = \frac{(2S_2 - S_1)}{3}\,G \quad [25]$$

For the case of constant stresses, the two Equations [24] and [25] can be integrated or

$$\frac{\epsilon_{p1}'}{\epsilon_{p2}'} = \frac{2S_1 - S_2}{2S_2 - S_1} \quad [26]$$

In the uniaxial case, the relation between transient creep rate and stress was given in Equation [11] by

$$\frac{d\epsilon_p'}{dt} = q(K\sigma^n - \epsilon_p') \quad [27]$$

Multiplying each term of Equation [27] by the stress σ

$$\sigma\,\frac{d\epsilon_p'}{dt} = q(K\sigma^{n+1} - \sigma\epsilon_p') \quad [28]$$

which also may be written as

$$\frac{dV'}{dt} = q\left[K(\sigma^2)^{\frac{n+1}{2}} - V'\right] \quad [29]$$

where $V' = \sigma\epsilon_p'$ = work done on the material by the constant stress σ and

$$\frac{dV'}{dt} = \sigma\,\frac{d\epsilon_p'}{dt} = \text{rate of work being done on material}$$

In order that Equation [29] may be applied to cases of combined stresses, it should be written in a more general form as

$$\frac{dV'}{dt} = q\left[K(S^2)^{\frac{n+1}{2}} - V'\right] \quad [30]$$

where

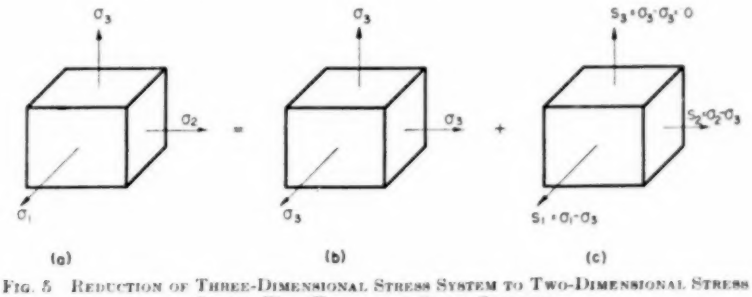

FIG. 5 REDUCTION OF THREE-DIMENSIONAL STRESS SYSTEM TO TWO-DIMENSIONAL STRESS SYSTEM WITH EQUIVALENT SHEAR STRESSES

S^2 = some function of principal stresses

$$V' = S_1 \epsilon_{p1}' + S_2 \epsilon_{p2}' \quad [31]$$

and

$$\frac{dV'}{dt} = S_1 \frac{d\epsilon_{p1}'}{dt} + S_2 \frac{d\epsilon_{p2}'}{dt} \quad [32]$$

If Equation [30] is to represent a physical law, S^2 will have to be a stress invariant or a function of several stress invariants. Furthermore, the assumption that only shear stresses cause creep strains suggests that S^2 may be written, in general, as

$$S^2 = [(\sigma_1 - \sigma_2)^2 + (\sigma_2 - \sigma_3)^2 + (\sigma_3 - \sigma_1)^2] \quad [33]$$

since the right-hand side of Equation [33] is proportional to the octahedral shear stress as well as the second stress invariant. For the case of uniaxial stress, Equation [33] reduces to

$$S^2 = \sigma^2 \quad [34]$$

For the stress system shown in Fig. 5(*c*), Equation [33] reduces to

$$S^2 = S_1^2 + S_2^2 - S_1 S_2 \quad [35]$$

Substitution of Equations [31], [32], and [35] into Equation [30] gives

$$S_1 \frac{d\epsilon_{p1}'}{dt} + S_2 \frac{d\epsilon_{p2}'}{dt} = q \left[K(S_1^2 + S_2^2 - S_1 S_2)^{\frac{n+1}{2}} - (S_1 \epsilon_{p1}' + S_2 \epsilon_{p2}') \right] \quad [36]$$

Placing value of creep rates from Equations [24] and [25] in [36]

$$\frac{S_1(2S_1 - S_2)}{3} G + \frac{S_2(2S_2 - S_1)}{3} G = q \left[K(S_1^2 + S_2^2 - S_1 S_2)^{\frac{n+1}{2}} - (S_1 \epsilon_{p1}' + S_2 \epsilon_{p2}') \right] \quad [37]$$

or

$$G = \frac{3}{2} qK(S_1^2 + S_2^2 - S_1 S_2)^{\frac{n-1}{2}} - \frac{3}{2} q \frac{(S_1 \epsilon_{p1}' + S_2 \epsilon_{p2}')}{(S_1^2 + S_2^2 - S_1 S_2)} \quad [38]$$

Substituting ϵ_{p2}' in terms of ϵ_{p1}' from Equation [26] in Equation [38]

$$G = \frac{3}{2} qK (S_1^2 + S_2^2 - S_1 S_2)^{\frac{n-1}{2}} - \frac{3}{2} q \left[S_1 \epsilon_{p1}' + \frac{S_2 \epsilon_{p1}'(2S_2 - S_1)}{(2S_1 - S_2)} \right] \frac{1}{(S_1^2 + S_2^2 - S_1 S_2)} \quad [39]$$

Placing G from Equation [39] into Equation [24] gives

$$\frac{d\epsilon_{p1}'}{dt} = \frac{Kq}{2} (S_1^2 + S_2^2 - S_1 S_2)^{\frac{n-1}{2}} (2S_1 - S_2) - q\epsilon_{p1}' \quad [40]$$

Similarly, by use of Equations [25], [26], and [39] it may be shown that

$$\frac{d\epsilon_{p2}'}{dt} = \frac{Kq}{2} (S_1^2 + S_2^2 - S_1 S_2)^{\frac{n-1}{2}} (2S_2 - S_1) - q\epsilon_{p2}' \quad [41]$$

By using the assumption of constancy of volume as given by Equation [22] together with Equations [40] and [41]

$$\frac{d\epsilon_{p3}'}{dt} = \frac{Kq}{2} (S_1^2 + S_2^2 - S_1 S_2)^{\frac{n-1}{2}} (-S_1 - S_2) - q\epsilon_{p3}' \quad [42]$$

Equations [40], [41], and [42] reduce to Equation [27] for the case of uniaxial stress, thereby affording a check to this analysis. These equations also are capable of representing negative creep rates required by the creep-recovery relations as shown in Fig. 3: that is, in Equation [40], if the stresses were removed, the negative creep rate of recovery is given by

$$\frac{d\epsilon_{p1}'}{dt} = -q\epsilon_{p1}' \quad [43]$$

Although the process of the extension of the theory to the case of combined stresses was done for the case of constant stresses, it has been shown that the expressions are capable of representing creep recovery as well as creep under loading conditions. For this reason the expressions given by Equations [40], [41], and [42] are assumed to be valid for varying stresses as well.

(*c*) *Minimum rate creep strains:* In the case of minimum rate creep strains, Equation [10] also may be extended to combined stresses.

Multiplication of each term of Equation [10] by σ gives

$$\sigma \frac{d\epsilon_p''}{dt} = B\sigma^{n+1} \quad [44]$$

or

$$\frac{d\sigma\epsilon_p''}{dt} = B\sigma^{n+1} \quad [45]$$

Equation [45] also may be written as

$$\frac{dV''}{dt} = B(\sigma^2)^{\frac{n+1}{2}} \quad [46]$$

where

$\sigma\epsilon_p'' = V''$ = work done on material

$\frac{dV''}{dt}$ = rate of work being done on material

In order that Equation [46] may be applied to cases of combined stresses, it should be written in a more general form or

$$\frac{dV''}{dt} = B(\overline{S^2})^{\frac{n+1}{2}} \quad [47]$$

where

$\overline{S^2}$ = some function of principal stresses

$$V'' = S_1 \epsilon_{p1}'' + S_2 \epsilon_{p2}'' \quad [48]$$

$$\frac{dV''}{dt} = S_1 \frac{d\epsilon_{p1}''}{dt} + S_2 \frac{d\epsilon_{p2}''}{dt} \quad [49]$$

Following the same reasoning described previously in the section dealing with transient creep strains, it is assumed that S^2 may be written as

$$\overline{S^2} = S_1^2 + S_2^2 - S_1 S_2 \quad [50]$$

Substitution of $(dV'')/(dt)$ and $\overline{S^2}$ from Equations [49] and [50] in Equation [47] gives

$$S_1 \frac{d\epsilon_{p1}''}{dt} + S_2 \frac{d\epsilon_{p2}''}{dt} = B(S_1^2 + S_2^2 - S_1 S_2)^{\frac{n+1}{2}} \quad [51]$$

It also will be assumed:

1 The minimum rate creep strains produced no change in volume of the material or

$$\epsilon_{p1}'' + \epsilon_{p2}'' + \epsilon_{p3}'' = 0 \quad \ldots\ldots\ldots\ldots\ldots\ldots [52]$$

2 The principal minimum rate shear creep rates are proportional to the principal stresses or

$$\frac{\frac{d\epsilon_{p1}''}{dt} - \frac{d\epsilon_{p2}''}{dt}}{S_1 - S_2} = \frac{\frac{d\epsilon_{p2}''}{dt} - \frac{d\epsilon_{p3}''}{dt}}{S_2} = \frac{\frac{d\epsilon_{p3}''}{dt} - \frac{d\epsilon_{p1}''}{dt}}{-S_1} = F \quad [53]$$

From Equations [51], [52], and [53] and following the same procedure used in the case of the transient creep strains, it can be shown that

$$\left.\begin{aligned} \frac{d\epsilon_{p1}''}{dt} &= \frac{B}{2}(S_1^2 + S_2^2 - S_1S_2)^{\frac{n-1}{2}}(2S_1 - S_2) \\ \frac{d\epsilon_{p2}''}{dt} &= \frac{B}{2}(S_1^2 + S_2^2 - S_1S_2)^{\frac{n-1}{2}}(2S_2 - S_1) \\ \frac{d\epsilon_{p3}''}{dt} &= -\frac{B}{2}(S_1^2 + S_2^2 - S_1S_2)^{\frac{n-1}{2}}(S_1 + S_2) \end{aligned}\right\} \quad [54]$$

For any system of stresses σ_1, σ_2, and σ_3, the three principal strains at any time t, are by Equations [20], [40], [41], [42], [54]

$$\left.\begin{aligned} \epsilon_1 &= \epsilon_{e1} + \epsilon_{p1}' + \epsilon_{p1}'' = \frac{1}{E}[\sigma_1 - \nu(\sigma_2 + \sigma_3)] + \int_0^t \frac{d\epsilon_{p1}'}{dt}dt + \int_0^t \frac{d\epsilon_{p1}''}{dt}dt \\ \epsilon_2 &= \epsilon_{e2} + \epsilon_{p2}' + \epsilon_{p2}'' = \frac{1}{E}[\sigma_2 - \nu(\sigma_1 + \sigma_3)] + \int_0^t \frac{d\epsilon_{p2}'}{dt}dt + \int_0^t \frac{d\epsilon_{p2}''}{dt}dt \\ \epsilon_3 &= \epsilon_{e3} + \epsilon_{p3}' + \epsilon_{p3}'' = \frac{1}{E}[\sigma_3 - \nu(\sigma_1 + \sigma_2)] + \int_0^t \frac{d\epsilon_{p3}'}{dt}dt + \int_0^t \frac{d\epsilon_{p3}''}{dt}dt \end{aligned}\right\} \quad [55]$$

For the case of constant stresses, Equations [55] may be integrated to give

$$\left.\begin{aligned} \epsilon_1 &= \frac{1}{E}[\sigma_1 - \nu(\sigma_2 + \sigma_3)] + \frac{K}{2}\left[\frac{(\sigma_1 - \sigma_2)^2 + (\sigma_2 - \sigma_3)^2 + (\sigma_3 - \sigma_1)^2}{2}\right]^{\frac{n-1}{2}}[2\sigma_1 - \sigma_2 - \sigma_3] \\ &\quad [1 - e_n^{-qt}] + \frac{B}{2}\left[\frac{(\sigma_1 - \sigma_2)^2 + (\sigma_2 - \sigma_3)^2 + (\sigma_3 - \sigma_1)^2}{2}\right]^{\frac{n-1}{2}}[2\sigma_1 - \sigma_2 - \sigma_3]t \\ \epsilon_2 &= \frac{1}{E}[\sigma_2 - \nu(\sigma_1 + \sigma_3)] + \frac{K}{2}\left[\frac{(\sigma_1 - \sigma_2)^2 + (\sigma_2 - \sigma_3)^2 + (\sigma_3 - \sigma_1)^2}{2}\right]^{\frac{n-1}{2}}[2\sigma_2 - \sigma_1 - \sigma_3] \\ &\quad [1 - e_n^{-qt}] + \frac{B}{2}\left[\frac{(\sigma_1 - \sigma_2)^2 + (\sigma_2 - \sigma_3)^2 + (\sigma_3 - \sigma_1)^2}{2}\right]^{\frac{n-1}{2}}[2\sigma_2 - \sigma_1 - \sigma_3]t \\ \epsilon_3 &= \frac{1}{E}[\sigma_3 - \nu(\sigma_1 + \sigma_2)] + \frac{K}{2}\left[\frac{(\sigma_1 - \sigma_2)^2 + (\sigma_2 - \sigma_3)^2 + (\sigma_3 - \sigma_1)^2}{2}\right]^{\frac{n-1}{2}}[2\sigma_3 - \sigma_1 - \sigma_2] \\ &\quad [1 - e_n^{-qt}] + \frac{B}{2}\left[\frac{(\sigma_1 - \sigma_2)^2 + (\sigma_2 - \sigma_3)^2 + (\sigma_3 - \sigma_1)^2}{2}\right]^{\frac{n-1}{2}}[2\sigma_3 - \sigma_1 - \sigma_2]t \end{aligned}\right\} \quad [56]$$

By Equations [56] the strains ϵ_1, ϵ_2, and ϵ_3 at a time t are now completely defined in terms of the stresses σ_1, σ_2, and σ_3 and the material constants E, ν, K, B, n, and q.

Effect of Temperature

The theory in its present form is limited to the case of constant temperature. The limitation is not drastic as it might seem because all parts of a structural member often may be at a uniform temperature.

Furthermore, both theory and experiments have shown that the effect of temperature is to cause creep strains to increase by a factor of $e^{-a/kT}$ where a is a constant and T is the absolute temperature. In the expression

$$\frac{d\epsilon_p''}{dt} = B\sigma^n$$

the quantity $B\sigma^n$ would increase with temperature by the factor of $e^{-a/kT}$. However, experiments also show that the exponent n decreases with temperature and the variation of B is influenced by this fact.

In due time, the authors will attempt to incorporate the effect of temperature into the analytical expressions given by the present theory in the simplest manner possible.

Determination of Experimental Constants

This theory is assumed to be applicable to any material whose tension-creep behavior conforms to that of the idealized material.

The material constants can be obtained from a simple tension-creep test in the following manner:

By taking the longitudinal and lateral deformation readings immediately after application of the load, the constants E and ν can be obtained.

If the specimen is then maintained at a constant stress for sufficient length of time t_1 so that the slope of the creep curve becomes approximately constant, the minimum creep rate is then given approximately by that constant slope. This procedure should be applied to several specimens tested simultaneously at different stress levels. A plot of stress and the minimum creep rate C on a log-log plot can then be used to obtain B and n constants in the relation $C = B\sigma^n$.

The transient creep strains can be obtained by subtracting the elastic strains and the minimum rate creep strains from the total strains. The variation of the maximum transient creep strains with stress usually can be expressed in the form of $K\sigma^n$, and the

constants K and n can then be determined. The constant q is obtained by fitting the expression $K\sigma^n(1 - e_s^{-qt})$ to the transient creep-strain component. The value q selected is the one giving the best agreement at the time intervals considered to be of maximum importance for the particular problem.

The stresses are then removed and the specimens are allowed to recover for an additional period of time t_1. The strains recovered immediately after unloading are the elastic strains. After the end of the additional period of time t_1, the creep strain recovered may be considered to be the maximum transient creep strains. The remaining permanent deformation when divided by the original period of time t_1 should give values for the minimum creep rates that agree fairly well with those values given by the slopes of the creep curves. Thus the values of K, B, and n obtained from the creep curve may be checked by data obtained from the recovery curve.

If the exponent n is not an integer, it will not be possible to apply the expressions so obtained to the analytical solution of engineering problems. It is suggested therefore that where n in the expressions $K\sigma^n$ and $B\sigma^n$ is not an integer, that n be replaced by the integer nearest to it. If the values of the constants K and B are adjusted accordingly, the errors caused by this approximation are often surprisingly small. Furthermore, it is suggested that whenever possible n should be adjusted to be an odd integer as the signs for compressive stresses and strains are then automatically taken care of.

Another possibility would be to take the two odd integers bracketing the actual value of n as determined from tension-creep data and solve the problem for these two values of n. The final result then may be determined by interpolating proportionately between the results obtained for the odd integral values of n.

Summary and Conclusions

A theory has been developed in this paper for the creep deformation of materials. The theory takes into account the initial elastic deformation, the transient creep, and the minimum rate creep. The basic postulates of the theory are simple and agree with the phenomenological nature of the creep deformation of materials. The actual analytical relations used are obtained from simple mathematical assumptions and are capable of representing creep recovery as well as creep.

The theory is proposed for simple and combined stress system and for constant and varying stresses.

Acknowledgments

The authors acknowledge their appreciation to the Research Corporation for their sponsorship and financial assistance that made this work possible.

BIBLIOGRAPHY

1 "On the Viscous Flow in Metals and Allied Phenomena," by E. N. da C. Andrade, Proceedings of the Royal Society of London, series A, vol. 84, 1910, p. 1.

"The Flow in Metals Under Large Constant Stresses," by E. N. da C. Andrade, Proceedings of the Royal Society, vol. 90, 1914, p. 329.

2 "High Sensitivity Creep Testing Equipment at the National Physical Laboratory," by H. J. Tapsell and L. E. Prosser, *Engineering*, vol. 137, 1934, p. 212.

3 "Étude Experimentalle de la Déformation Visquese des Fils de Fer et de Neckel," by P. Chevenard, Review Me't, 1934 p. 473.

4 "The Utilization of Creep Test Data in Engineering Design," by R. W. Bailey, *Engineering*, vol. 140, 1935, p. 595.

5 "The Creep Recovery of a 0.17 Per Cent Carbon Steel," by A. Johnson, Proceedings of The Institution of Mechanical Engineers, London, England, 1941, p. 187.

6 "The Interpretation of Creep Tests for Machine Design," by C. R. Soderberg, Trans. ASME, vol. 58, 1936, p. 733.

7 "Theory of Creep Under the Action of Combined Stresses With Applications to High-Temperature Machinery," by F. Odquist, Proceedings of the Royal Swedish Institute for Engineering Research, No. 141, 1936; see also Proceedings of the Fourth International Congress of Applied Mechanics, 1934, p. 238.

8 "Design of Members Subjected to Creep at High Temperatures," by J. Marin, Journal of Applied Mechanics, Trans. ASME, vol. 59, 1937, pp. A-21–A-24.

9 "A Theory for Combined Creep Stress-Strain Relations for Materials With Different Properties in Tension and Compression," by J. Marin and Yoh-Han Pao, presented at the first U. S. Congress for Applied Mechanics, Chicago, Ill., 1951, and to be published in the Proceedings of the Congress.

10 "Creep Relationships and Their Applications to Pipes, Tubes and Cylindrical Parts Under Internal Pressure," by R. W. Bailey, Proceedings of The Institution of Mechanical Engineers, London, England, vol. 164, 1951, pp. 425–431.

Influence of Viscous Effects on Impact Tubes[1]

By C. W. HURD,[2] K. P. CHESKY,[3] and A. H. SHAPIRO[4]

Experiments were conducted to determine the effect of viscosity on the pressure rise recorded by a blunt-nosed impact tube in incompressible flow. The results are presented in terms of the pressure coefficient ($C_p \equiv 2\Delta p/\rho V_\infty^2$) as a function of Reynolds number (Rey $\equiv V_\infty a/\nu$), where Δp is the excess of stagnation-point pressure over free-stream static pressure, V_∞ is the free-stream velocity, a is the radius of the impact tube, ρ is the fluid density, and ν is the kinematic viscosity of the fluid. Above Reynolds numbers of 1000, there is no effect of viscosity, and C_p is equal to unity. Between Rey $\leqq 50$ and Rey $\leqq 1000$, C_p is slightly less than unity, but has a minimum value of 0.99. For values of Rey less than 50, C_p is always greater than unity. When the Reynolds number is below unity, the pressure rise is independent of the fluid density, and the data may be represented approximately by the formula $C_p \leqq 5.6/\text{Rey}$. The results are compared with the experimental investigations of Barker and of Homann, and with the theoretical studies of Stokes and of Homann.

Introduction

In the usual interpretation of impact-tube readings, it is assumed that the fluid on the stagnation streamline is brought to rest without viscous forces and that the opening in the tube measures the static pressure at the stagnation point. This interpretation is subject to two sources of error:

1 If the hole in the tube is not minute compared with the diameter of the tube, there will be a complex flow pattern near and within the hole, and the average pressure registered within the tube will to some degree differ from the stagnation-point pressure. A similar deviation will occur if the impact tube is not perfectly aligned with the flow.

2 If the Reynolds number of the flow, referred to the impact-tube radius as a characteristic length, is not very large compared with unity, the viscous forces acting in the fluid may be of sufficient size compared with the inertia forces as to make the Bernoulli formula inapplicable.

The investigation reported here is concerned with the second of these problems, i.e., the effects of Reynolds number on the pressure rise recorded by an impact tube. As described in more detail later, experiments were made with a small pitot tube which was towed at various speeds in a circular towing tank containing liquids of various viscosities.

Fields of Application. Some types of experimental investigations in which viscous effects may significantly influence impact-tube readings include the following:

1 Wake surveys behind compressor and turbine cascades, using very small impact tubes.

2 Velocity traverses in boundary layers, using extremely minute impact tubes.

3 Measurement of impact pressures in very viscous liquids.

4 Measurement of impact pressures in air flow at hypersonic speeds, where the air density (and hence the Reynolds number) is likely to be very small.

Dimensionless Coefficients. The experimental results are expressed in dimensionless terms by means of a pressure coefficient C_p, and a Reynolds number, Rey, defined, respectively, by

$$C_p \equiv (p_i - p_\infty) \Big/ \frac{1}{2}\rho V_\infty^2 \qquad [1]$$

$$\text{Rey} \equiv \rho V_\infty a/\mu = V_\infty a/\nu \qquad [2]$$

where p_i denotes the pressure registered in the impact tube, p_∞ denotes the free-stream pressure far upstream of the impact tube and at the same elevation, V_∞ denotes the velocity of the impact tube relative to the undisturbed fluid, a denotes the radius of the cylindrical portion of the impact tube, and ρ, μ, and ν denote, respectively, the density, coefficient of viscosity, and kinematic viscosity of the fluid.

It may be shown from similarity considerations that for an impact tube of given geometry moving steadily in an incompressible fluid the pressure coefficient C_p is a function only of the Reynolds number, Rey. Bernoulli's formula, it may be noted, yields $C_p = 1$, a result which is presumably correct for very high Reynolds numbers.

Previous Work. The earliest experimental investigation of the influence of viscosity was that of Miss Barker (2) in the range of Reynolds numbers from 3.5 to 50, who concluded that for Reynolds numbers less than 30 the measured value of C_p exceeds unity by an amount which is no longer negligible. Homann (3) made measurements over the range of Reynolds numbers from 0.1 to 60 and found similar but not identical results, the deviation of C_p from unity at Rey = 60 being about 5 per cent.

No exact theoretical solutions for the effect of viscosity on impact-tube readings exist. In the range of very low Reynolds numbers (creeping flow), the famous solution of Stokes (4) yields, for the normal stress at the nose of a sphere, the formula $C_p = 3/\text{Rey}$ a result which may be taken as indicative of the order of magnitude to be expected for actual impact tubes for Reynolds numbers less than about unity. More recently, Homann (5) and Chambré (6) used thin boundary-layer theory to calculate the pressure at the nose of a sphere. Their result, which may be expressed as

$$C_p = 1 + \frac{6}{\text{Rey} + 0.457\sqrt{\text{Rey}}} \qquad [3]$$

presumably should apply only when the boundary-layer thickness at the stagnation point is small compared with the radius, that is, only when the Reynolds number is greater than about 10.

---

[1] Based on a thesis by Hurd and Chesky while attached to the U. S. Naval Post Graduate School at the Massachusetts Institute of Technology, Cambridge, Mass. (1)[5]

[2] Commander, USN, % Supervisor of Shipbuilding and Naval Inspector of Ordnance, Electric Boat Company, Groton, Conn.

[3] Lieutenant Commander, USN, % Boston Naval Shipyard, Boston, Mass.

[4] Professor of Mechanical Engineering, Massachusetts Institute of Technology. Mem. ASME.

[5] Numbers in parentheses refer to the Bibliography at the end of the paper.

Presented at the National Conference of the Applied Mechanics Division, Minneapolis, Minn., June 18–20, 1953, of The American Society of Mechanical Engineers.

Discussion of this paper should be addressed to the Secretary, ASME, 29 West 39th Street, New York, N. Y., and will be accepted until July 10, 1953, for publication at a later date. Discussion received after the closing date will be returned.

Note: Statements and opinions advanced in papers are to be understood as individual expressions of their authors and not those of the Society. Manuscript received by ASME Applied Mechanics Division, August 4, 1952. Paper No. 53—APM-10.

Experimental Apparatus and Procedure

Towing Tank. The general arrangement of the apparatus is shown schematically in Fig. 1. The circular towing tank had a mean diameter of 10 ft and a rectangular cross section 8 in. wide × 10 in. high with the liquid level maintained about 8 in. from the bottom. Thirty-two fly-screen damping baffles were inserted at uniform intervals to minimize circulatory flows induced by the drag of the pitot tube on the fluid. The openings in the damping screens through which the pitot tube passed were very large compared with the diameter of the pitot tube, thus minimizing interference effects between the screens and impact tube.

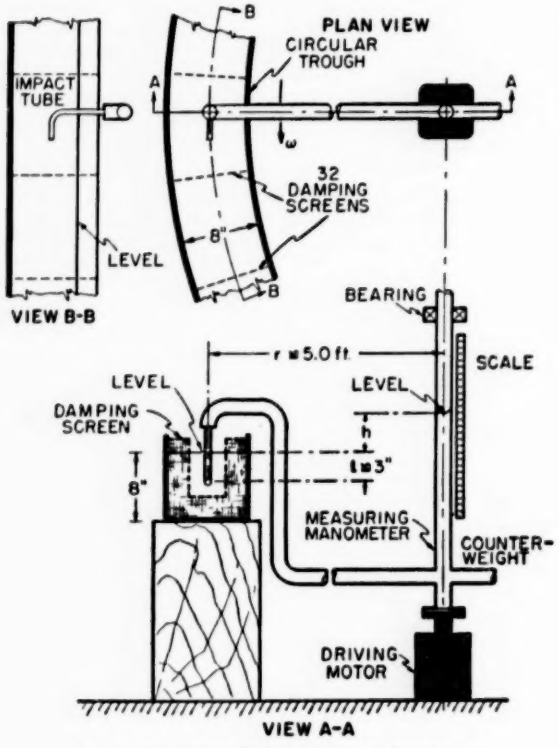

Fig. 1 Schematic Arrangement of Apparatus

The impact tube was carried on a rigid, counterbalanced arm driven by a variable-speed (1 to 60 rpm) motor placed on the center line of the tank.

The impact pressure at the mouth of the pitot tube was allowed to communicate with fluid in the rotating arm and thence to a column of fluid in a large-diameter glass tube on the axis of rotation. Impact pressures were inferred from the level of the fluid in this manometric tube.

Complete details of the apparatus, together with descriptions of the procedures employed for leveling, alignment, calibration, and methods of correcting for many minor errors, are given in reference (1).

Impact Tube. Details of the impact tube are shown in Fig. 2. The tube was made of 0.072-in-OD hyperdermic tubing, with a 0.010-in. wall, and the end of the tube was cut off square, as shown in the enlarged portion of Fig. 2. The shank of the tube was streamlined in order to reduce the drag exerted by the moving tube on the liquid.

Measurements. By determining the angular velocity of the rotating arm (through counting revolutions in a given time), and by measuring the diameter of the circle traced out by the tip of the impact tube, the linear speed V_∞ of the tip of the probe was found with great accuracy.

The kinematic viscosity of each liquid used was determined by a Saybolt viscosimeter over the appropriate range of temperatures. The liquid temperature in each run was substantially equal to that of the room, and it was measured by a mercury-glass thermometer.

The height h of the fluid in the central manometer tube above the level in the towing tank was observed with a transit. Taking account of the centrifugal pressure gradients produced by the arm rotating with the angular speed ω, the impact pressure p_i just behind the mouth of the probe may be written as

$$p_i = p_a + \rho g(h + l) + \frac{\rho}{2}\omega^2 r^2$$

where p_a is the atmospheric pressure and r is the radius arm to the

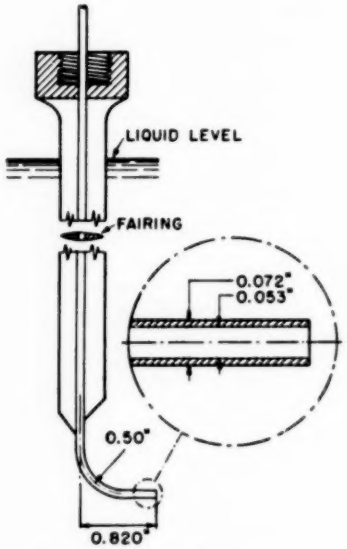

Fig. 2 Detail of Impact Tube

tip of the probe. The free-stream pressure at the elevation of the probe mouth may be expressed as

$$p_\infty = p_a + \rho g l$$

Subtracting the second of these equations from the first, and noting that $\omega r = V_\infty$, we get

$$p_i - p_\infty = \rho g h + \frac{\rho}{2} V_\infty^2$$

or

$$C_p \equiv \frac{p_i - p_\infty}{\frac{1}{2}\rho V_\infty^2} = 1 + \frac{2gh}{V_\infty^2} \quad \ldots\ldots\ldots\ldots [4]$$

If the fluid were without viscosity, the dynamic pressure rise at the tube mouth would be exactly canceled by the centrifugal pressure drop in the rotating arm, the displacement h would be zero, and C_p would be equal to unity. Hence the displacement of the liquid level in the central tube from its position when the arm is

stationary is a direct measure of the influence of viscosity, inasmuch as this displacement is zero for an inviscid fluid.

Induced Circulation of Liquid in Tank. The drag exerted by the moving pitot tube tends to set the liquid in motion in the direction of rotation. However, friction at the walls of the towing tank tends to resist this circulatory motion of the liquid, and a steady-state value of mean liquid velocity is reached when the propelling drag of the pitot tube is just balanced by the resisting drag of the tank. With no damping screens present the induced fluid velocity was large enough to cause troublesome errors. The presence of the 32 damping screens apparently reduced the induced velocity to at most a few tenths of 1 per cent of the probe velocity.

Range of Variables. The liquids used ranged from water with a kinematic viscosity of 1 centistoke to a heavy oil with a kinematic viscosity of 150 centistokes. Probe speeds varied from a minimum of 0.5 fps to a maximum of 16 fps. The various combinations of V_∞ and ν were such that there were overlappings in the Reynolds-number ranges which could be covered with the several liquids. By thus operating at the same Reynolds number with different velocities it was possible to ascertain that there were no free-surface (Froude-number) effects.

Results

All the experimental data of the present investigation are plotted in Fig. 3. In Fig. 4 the data in the range of higher Reynolds numbers are plotted on an enlarged vertical scale, and for comparison, there are also plotted the results of Miss Barker reduced to the dimensionless form employed here.

slight indication to this effect in an early investigation by Fry and Tyndall (7). In this connection it should be noted that neither Miss Barker (2) nor Homann (3) made tests at sufficiently large Reynolds numbers for this lowering of C_p below unity to be clearly observable.

For Reynolds numbers below 50, Figs. 3 and 4 show that the influence of viscous forces is to increase the pressure rise on the stagnation streamline, thus leading to values of C_p greater than unity.

Range of Very Low Reynolds Numbers. For vanishingly small Reynolds numbers, the inertia forces acting in the fluid become negligibly small compared with the viscous forces. There ensues the well-known "creeping flow" of Stokes. Since inertial effects are of no consequence, it follows that the pressure rise on the stagnation streamline is independent of the fluid density. This condition can be met only when the relation between pressure coefficient and Reynolds number is of the form

$$C_p = \text{const}/\text{Rey} \quad [5]$$

Hence dimensional reasoning indicates that at very low Reynolds numbers the curve of C_p versus Rey on log-log paper should approach a straight line with a slope of —1.

The experimental data, Fig. 3, are in accord with the rule stated in the foregoing. For values of Rey less than about unity it appears that the data of the tests may be represented with good accuracy by the formula

$$C_p \cong 5.6/\text{Rey} \quad [6]$$

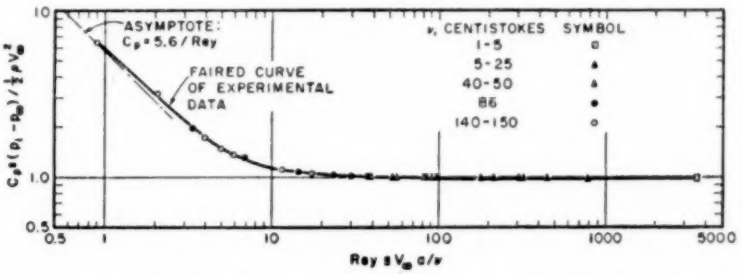

Fig. 3 Experimental Data Over Entire Range of Reynolds Numbers

Range of High Reynolds Numbers. As the Reynolds number increases without end the viscous forces acting in the fluid become vanishingly small compared with the inertia forces, and the pressure coefficient C_p (according to Bernoulli's equation) should approach unity. The data in Fig. 4 confirm this hypothesis. Here it should be noted that the value of V_∞ was taken to be the linear speed of the probe tip. Owing to the small steady-state motion of the liquid in the tank, the actual relative speed between liquid and probe was slightly less than the probe speed, and, therefore, the values of C_p shown in Figs. 3 and 4 are slightly less than the correct values. However, the data at the highest Reynolds numbers in Fig. 4 suggest that this error is of the order of 0.3 per cent, and that the departure of C_p from unity is not discernible at Reynolds numbers greater than about 1000. The error introduced by the steady-state induced motion in the tank may, for Reynolds numbers greater than 1000, be approximately canceled by increasing the ordinates in Fig. 4 by 0.003.

In the range of high Reynolds numbers the flow is essentially a potential flow modified by small viscous effects confined to thin boundary layers. For Reynolds numbers greater than 50, Fig. 4 shows that the effect of viscosity is to decrease the value of C_p below the asymptotic value of unity. This is a somewhat surprising result which hitherto has not been observed, except for a

Comparison With Other Experiments

Experiments of Miss Barker (2). Fig. 4 shows a general accord

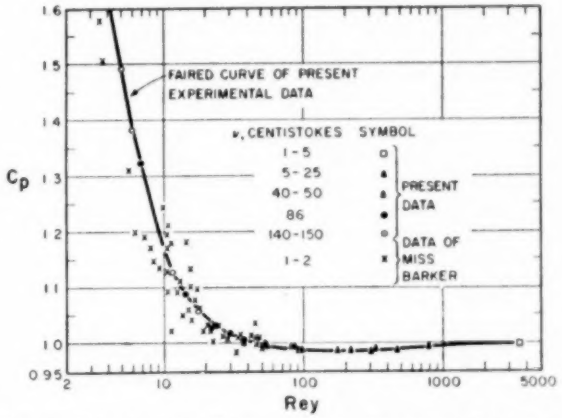

Fig. 4 Experimental Data in Upper Range of Reynolds Numbers, and Comparison With Data of Miss Barker (2)

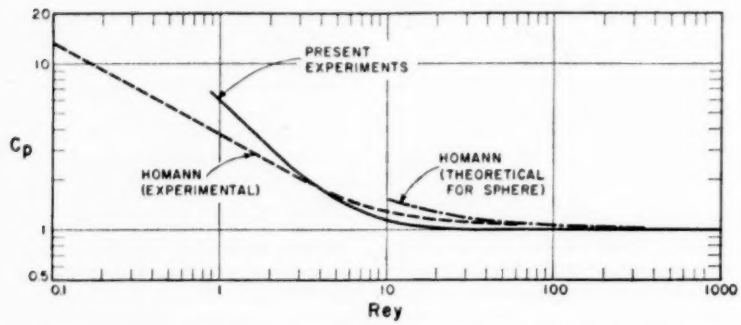

FIG. 5 COMPARISON OF RESULTS OF PRESENT EXPERIMENTS WITH EXPERIMENTAL RESULTS OF HOMANN FOR IMPACT TUBES, AND WITH THEORETICAL RESULTS OF HOMANN FOR PRESSURE AT NOSE OF A SPHERE

between the present data and the data of Miss Barker, although the large scatter in Miss Barker's results makes an exact comparison difficult. In any case it is felt that Miss Barker's experimental method was not entirely reliable at low Reynolds numbers. The method involved the use of a pitot tube of 0.1 cm diam placed at the center of a pipe of 1.1 cm diam in which there existed a Poiseuille flow. The difficulty here is that at low Reynolds numbers the effects of viscosity propagate to considerable distances from the pitot tube, and so unknown errors are introduced as a result of nonuniformity in the flow and of interference effects produced by the wall of the pipe. Indeed, the experiments reported in the present paper were preceded by an experimental investigation (8) similar to Miss Barker's, except for a very much more favorable geometry, namely, an impact tube of 0.072 in. diam at the center of a pipe of 3.26 in. diam; nevertheless the results were not considered reliable.

Experiments of Homann (3) The mean curve expressing the experimental results of Homann are compared in Fig. 5 with the mean curve in Fig. 3 for the data reported here. No reason has been found for the serious discrepancies between Homann's results and the present data except possibly that the shapes of the impact tubes may have been different. Unfortunately, there is no description of the impact-tube geometry in Homann's paper. Although the experimental procedure employed by Homann seems quite sound, and his results show very little scatter, it is noteworthy that at low Reynolds numbers his results obey the law $C_p = \text{const}/\text{Rey}^{0.567}$. There is no tendency to deviate from this relation even for values of Rey as low as 0.1. This is indeed surprising, for there is no way of escaping the requirement that the relation between C_p and Rey must asymptotically approach Equation [5] as the Reynolds number becomes very small. Thus the nature of his results throws doubt on the validity of Homann's data at low Reynolds numbers.

COMPARISON WITH THEORY

Stokes' Law. Considering the difference in geometry between a sphere with an infinitesimal hole at its nose and the impact tube used for the present tests, the agreement between Equation [6] (for low Reynolds numbers) and the Stokes' solution for the normal stress at the nose of a sphere in creeping flow ($C_p = 3/\text{Rey}$) is considered to be quite satisfactory. It also is significant that the experimental data begin to deviate appreciably from Equation [6] at about Rey $\cong$ 1, for it is well known (9) that a similar deviation from Stokes' law of drag for spheres occurs at about Rey $\cong$ 1.

The difference between the factors 3 and 5.6 for the sphere and blunt impact tube is a measure of the influence of probe shape and suggests that at very low Reynolds numbers the calibration of the probe is quite sensitive to its shape.

Homann's Theory (5). The theory of Homann for the pressure at the nose of a sphere for comparatively high Reynolds numbers, Equation [3], is compared with the experimental results in Fig. 5. Of course a direct comparison is impossible because of the difference in geometries. For Rey > 10, where the Homann theory is presumably applicable, the viscosity correction of the Homann formula is several times the measured correction. The observed decrease of C_p below unity for Rey > 50 is not at all accounted for by the theory. Whether these deviations are entirely the result of differences in geometry or whether they reflect inadequacies of the theory is not clear.

Homann made experiments (5) with spheres to check directly his theory for the pressure at the nose of a sphere. His tests, which were made over a range of Reynolds numbers from 2 to 80, were in generally good agreement with Equation [3] and the curve marked "Homann (theoretical)" in Fig. 5. The discrepancy between this curve and the curve representing the data reported here is a further indication of the importance of probe shape when viscous effects are significant.

BIBLIOGRAPHY

1 "Experimental Investigation of the Effects of Viscous Forces Upon Pitot Tube Readings," by C. W. Hurd and K. P. Chesky, thesis for Degree of Naval Engineer, M.I.T., 1951.

2 "On the Use of Very Small Pitot-Tubes for Measuring Wind Velocity," by M. Barker, Proceedings of the Royal Society, series A, vol. 101, 1922, pp. 435–445.

3 "Einfluss grosser Zahigkeit bei Stromung um Zylinder," by F. Homann, *Forschung auf dem Gebiete des Ingenieurwesens*, vol. 7, 1936, pp. 1–10.

4 "The Mechanics of Viscous Fluids," by L. Prandtl, *Aerodynamic Theory*, edited by W. F. Durand, Durand Reprinting Committee, Pasadena, Calif., vol. 3, 1943, pp. 69–74.

5 "The Effect of High Viscosity on the Flow Around a Cylinder and Around a Sphere," by F. Homann, NACA Technical Memo No. 1334, 1952.

6 "The Theory of the Impact Tube in a Viscous Compressible Gas," by P. L. Chambré, Report No. HE-150-50, Department of Engineering, University of California, Berkeley, Calif., 1948.

7 "On the Value of the Pitot Constant," by J. D. Fry and A. M. Tyndall, *Philosophical Magazine*, vol. 21, 1911, pp. 348–366.

8 "The Effect of Reynolds Number on Impact Tube Calibration," by H. A. Gerdes, D. M. Brooks, and J. F. Kalina, thesis for Degree of Naval Engineer, M.I.T., 1950.

9 "Applied Hydro- and Aeromechanics," by L. Prandtl and O. G. Tietjens, first edition, McGraw-Hill Book Company, Inc., New York, N. Y., 1934, p. 54.

Axisymmetric Flexural Temperature Stresses in Circular Plates

By J. E. GOLDBERG,[1] LAFAYETTE, IND.

The problem to be considered is that of determining the flexural stresses which result from temperature differences T between corresponding points on the upper and lower faces of circular plates (T = temperature at lower face minus temperature at upper face), when T is assumed to vary only with the distance from the center of the plate. This problem arises, for example, in the design of heated or cooled cylindrical processing tanks or vessels. In such cases, heat may be applied to the circular bottom of the vessel by a single concentric burner or heating element or by a ring of burners or elements, and the resulting temperature distribution will be approximately axisymmetric.

THIS analysis applies specifically to the special case of a circular plate in which the temperatures (a) vary linearly between corresponding points on the upper and lower surfaces, (b) are zero at any instant over the entire median surface, and (c) vary only slowly with time. Condition (b) may be replaced by a more general statement since a theorem stated by Biot[2] leads to the conclusion that a two-dimensional temperature distribution in simply connected uniform plates results in a condition of constant membrane stresses, provided this result is compatible with the boundary conditions.

At any rate, under certain conditions the well-known two-dimensional elasticity solution for radial temperature gradients may be superimposed upon the present flexural solution to take care of variations in the median plane. Clearly, the solution for normal pressures upon the plate also may be superimposed under essentially similar conditions.

In the derivation of formulas for flexure due to an arbitrary axisymmetric temperature-difference curve, we first determine the effects throughout the plate of a small tractable temperature difference ΔT, over a concentric area of radius b lying within the plate. Formulas for the total effects due to the actual temperature-difference curve are obtained by integrating the foregoing results with respect to T.

We begin with the concept of an infinite plate at uniform temperature. Imagine that a circular disk of radius b is cut from the plate, Fig. 1, and its temperature distribution is changed so that a uniform temperature difference ΔT exists between its upper and lower surfaces with a constant gradient in the direction of the thickness. The disk would curl to a spherical surface with a curvature proportional to ΔT. Restoration of the connection between the disk and the remainder of the plate requires that equal and opposite moments be applied at the edge of the disk and at the edge of the hole in the infinite plate so that the adjacent slopes of the disk and the plate are made equal. After determining the magnitude of these edge moments, the moments and slopes throughout the entire plate may be calculated. These are due, it is recalled, only to a uniform temperature difference ΔT existing over a circular area of radius b. However, by direct superposition, these moments and slopes may be combined with those due to other incremental temperature differences which exist over their corresponding concentric area. Thus the total moment or slope at a point is determined by superposition or integration of certain functions of the area under the temperature-difference curve.

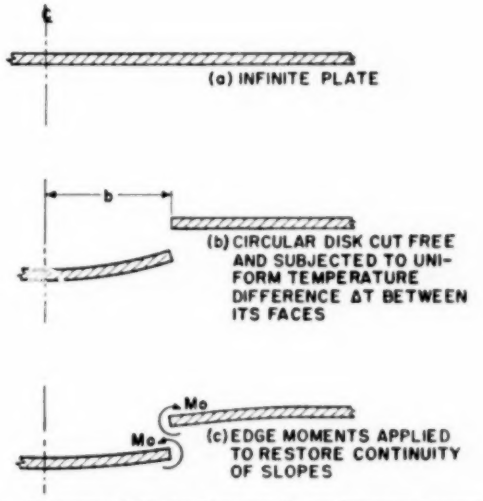
t
(a) INFINITE PLATE
b
(b) CIRCULAR DISK CUT FREE AND SUBJECTED TO UNIFORM TEMPERATURE DIFFERENCE ΔT BETWEEN ITS FACES
Mo
Mo
(c) EDGE MOMENTS APPLIED TO RESTORE CONTINUITY OF SLOPES

FIG. 1 DIAMETRAL SECTION THROUGH PLATE SHOWING SUCCESSIVE STAGES IN DERIVATION

A solution to this problem may also be obtained by direct integration of the nonhomogeneous form of Poisson's equilibrium equation.

DERIVATION

If a free circular plate is heated or cooled so that a uniform temperature gradient exists between the top and bottom surfaces, the plate curls to a spherical surface with radial slopes

$$\phi = \frac{\alpha r}{h}(\Delta T)$$

where

α = thermal coefficient of linear expansion
r = radial co-ordinate
h = uniform thickness of plate
ΔT = uniform temperature difference between top and bottom surfaces, a greater temperature on bottom corresponding to a positive ΔT (ΔT is, ultimately, a portion or "slice" of area under actual temperature-difference curve, Fig. 2)

[1] Associate Professor, School of Civil Engineering and Engineering Mechanics, Purdue University.

[2] "A General Property of Two-Dimensional Thermal Stress Distribution," by M. A. Biot, *Philosophical Magazine*, vol. 19, March, 1935, p. 540.

Presented at the National Conference of the Applied Mechanics Division, Minneapolis, Minn., June 18–20, 1953, of THE AMERICAN SOCIETY OF MECHANICAL ENGINEERS.

Discussion of this paper should be addressed to the Secretary, ASME, 29 West 39th Street, New York, N. Y., and will be accepted until July 10, 1953, for publication at a later date. Discussion received after the closing date will be returned.

NOTE: Statements and opinions advanced in papers are to be understood as individual expressions of their authors and not those of the Society. Manuscript received by ASME Applied Mechanics Division, December 21, 1951. Paper No. 53—APM-5.

If the disk is also acted upon by a uniform edge moment M_0, then

$$\phi = \frac{M_0 r}{D(1+\mu)} + \frac{\alpha r}{h}(\Delta T) \quad \ldots\ldots [1]$$

In order to attach this partially heated or cooled disk to the unheated infinite plate from which we may assume it had been cut requires that the slopes at the edges of the disk and the hole be equal. In terms of the stiffness of the disk and of the plate (see Appendix) this requirement becomes

$$\frac{-M_0 b}{D(1-\mu)} = \frac{M_0 b}{D(1+\mu)} + \frac{\alpha b}{h}(\Delta T)$$

or

$$M_0 = -\frac{\alpha D(1-\mu^2)}{2h}\Delta T \quad \ldots\ldots [2]$$

Conditions throughout the disk are uniform, and for all points $r < b$

$$\left.\begin{aligned} M_1 &= M_2 = -\frac{k_m}{2}(\Delta T) \\ \phi &= \frac{k_s r}{2}(\Delta T) \end{aligned}\right\} \quad \ldots\ldots [3]$$

where

$$\left.\begin{aligned} k_m &= \frac{\alpha D(1-\mu^2)}{h} = \frac{\alpha E h^2}{12} \\ k_s &= \frac{\alpha(1+\mu)}{h} \end{aligned}\right\} \quad \ldots\ldots [4]$$

For $r > b$, by Equations [18] and [19] of the Appendix

$$\left.\begin{aligned} M_1 &= -M_2 = -\frac{k_m}{r^2}\left(\frac{b^2}{2}\Delta T\right) \\ \phi &= \frac{k_s}{r}\left(\frac{b^2}{2}\Delta T\right) \end{aligned}\right\} \quad \ldots\ldots [5]$$

The term $b^2\Delta T/2$ is equal to the statical moment, about the origin, of a strip of the temperature-difference chart which has a height ΔT and a length b (measured from the origin of the plate).

Comparison of the expressions for the moments as given by Equations [3] and [5] discloses that while M_1 is single-valued at $r = b$, M_2 will be discontinuous if ΔT is finite.

In analyzing the total stresses and total slope at an interior point, $r = \rho$, it is convenient to refer to the differential-temperature curve, Fig. 2, and to retain the assumption for the time being, that the actual plate is a region in an infinite plate.

We observe that for all increments dT, for which $b \leq \rho$, the contribution to moments and slopes is given by Equations [5]; and their total effect is calculated by integrating these expressions. The result is equivalent to taking the statical moment of area A_1, Fig. 2, and multiplying this quantity by certain physical constants of the plate to obtain the moment and slope contributions

$$\left.\begin{aligned} M_1' &= -M_2' = -\frac{k_m}{\rho^2}(A_1)(\bar{b}_1) \\ \phi' &= \frac{k_s}{\rho}(A_1)(\bar{b}_1) \end{aligned}\right\} \quad \ldots\ldots [6]$$

We observe also that for all increments dT, for which $b > \rho$, the contribution to moments and slopes is given by Equations [3]; and the total effect is obtained by integrating these expressions. The result is equivalent to

$$\left.\begin{aligned} M_1'' &= M_2'' = -\frac{k_m}{2}T_\rho \\ \phi'' &= \frac{k_s}{2}\rho T_\rho \end{aligned}\right\} \quad \ldots\ldots [7]$$

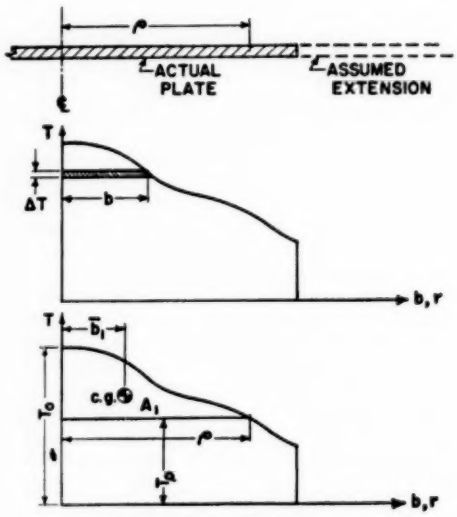

FIG. 2 GENERAL TEMPERATURE-DIFFERENCE CHART

Thus, for a point $r = \rho$ in an infinite plate, the bending moments and slope are obtained merely by adding Equations [6] and [7], which give, in terms of the quantities shown in Fig. 2

$$\left.\begin{aligned} M_1 &= -\frac{k_m}{\rho^2}(A_1)(\bar{b}_1) - \frac{k_m}{2}T_\rho \\ M_2 &= \frac{k_m}{\rho^2}(A_1)(\bar{b}_1) - \frac{k_m}{2}T_\rho \\ \phi &= \frac{k_s}{\rho}(A_1)(\bar{b}_1) + \frac{k_s}{2}\rho T_\rho \end{aligned}\right\} \quad \ldots\ldots [8]$$

Since the foregoing expressions give the moments and slopes on the assumption of an infinite plate, upon these must be superimposed the moments and slopes which are required at the edge of the plate to adjust the results obtained at $r = c$ for an infinite plate to the moment and slope prescribed at that location.

It is worthy of note that the last term in each of Equations [8] implies the easily proved fact that if a temperature difference is applied to an annular region of an infinite plate, the circular region within the inner boundary of the annulus is stress-free. Thus the effect, in an infinite plate, of a rising (or falling) portion of the T-curve in the region $r > \rho$ would be offset by a corresponding falling (or rising) portion of the curve in the same region; and thus such humps and valleys may be neglected. Their effect, however, must be included in computing moments and slopes at points beyond such hump or valley and, of course, they must be considered in establishing the actual conditions at the edge of a finite plate. That is to say, such hump or valley at $r < \rho$ must be included in A_1 and, of course, will be considered in computing $\bar{b}_1$.

ADJUSTMENT OF EDGE CONDITIONS

We turn now to consideration of the moments and slope at the edge of a circular plate of radius c such as might form the bottom of a cylindrical tank. Were this plate to be a portion of an infinite plate, the moments and slope would be calculated by integrating Equations [5] for $r = c$ and $b = b(T)$

$$\left.\begin{aligned} M_1 &= -M_2 = -\frac{k_m}{c^2}\int_0^{T(0)} \frac{b^2}{2}\,dT \\ \phi &= \frac{k_s}{c}\int_0^{T(0)} \frac{b^2}{2}\,dT \end{aligned}\right\} \quad \ldots\ldots [9]$$

The integrals cover the area under the curve of b (T) versus T, Fig. 3, and have the simple physical interpretation of the statical moment, about the center of the plate, of the area under the curve, i.e., A_2 times b_2.

Generally, the moments and slope as given by Equations [9] do not satisfy the actual edge conditions. This situation, however, is rectified merely by applying an additional edge moment at $r = c$

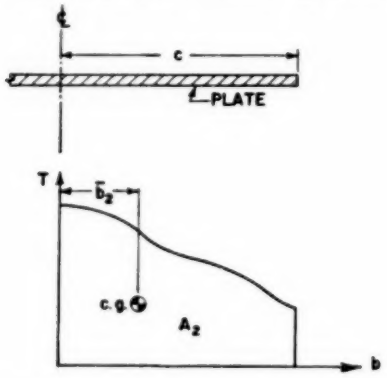

FIG. 3 TEMPERATURE-CURVE PROPERTIES REQUIRED FOR STRESS AND SLOPE CALCULATIONS AT EDGE OF PLATE

which, in combination with Equations [9], will give the desired slope or moment. Since the region $r \leq c$ constitutes a uniform disk, the additional moments are constant throughout the plate and the relation between the additional slope and additional moment is given by Equations [16] of the Appendix

$$\Delta\phi = \frac{\Delta M_c r}{D(1+\mu)} \quad \ldots\ldots\ldots\ldots\ldots\ldots [10]$$

If, for example, the edge of the plate is hinged, the total moment at $r = c$ must be zero and, by Equations [9]

$$\Delta M_c = \frac{k_m}{c^2} \int_0^{T_{(0)}} \frac{b^2}{2}\, dT \quad \ldots\ldots\ldots\ldots\ldots [11]$$

and this additional moment must be added to M_1 and M_2 as given by Equations [7] and [8].

If, on the other hand, the plate is built in, an edge moment must be added which reduces the edge slope as given by Equations [9] to zero. The magnitude of this additional moment is

$$\Delta M_c = -\frac{k_s D(1+\mu)}{c^2} \int_0^{T_{(0)}} \frac{b^2}{2}\, dT \quad \ldots\ldots\ldots [12]$$

and this amount is to be added to M_1 and M_2 throughout the plate.

EXAMPLES

Example 1. Built-in 0.25-in. steel plate, radius = 20 in., temperature difference T between lower and upper surfaces as shown in Fig. 4. Required: Moments and slopes at $\rho = 0$, 10, 20

$$E = 30 \times 10^6 \text{ psi}$$
$$\alpha = 6.5 \times 10^{-6} \text{ in/in per deg F}$$
$$\mu = 0.3$$
$$D = \frac{30 \times 10^6 (0.25)^3}{12(1 - 0.09)} = 42.93 \times 10^3$$

$$k_m = \frac{\alpha E h^3}{12} = \frac{6.5 \times 10^{-6} \times 30 \times 10^6 (0.25)^3}{12} = 1.0156$$

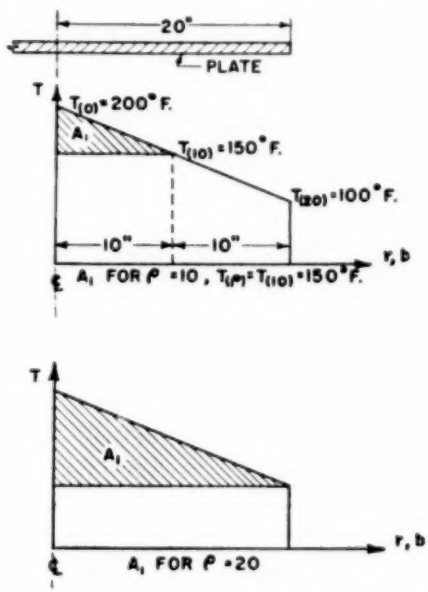

FIG. 4 TEMPERATURE-DIFFERENCE CURVE FOR EXAMPLE 1

$$k_s = \frac{\alpha(1+\mu)}{h} = \frac{6.5 \times 10^{-6}(1 + 0.3)}{0.25} = 33.80 \times 10^{-6}$$

$$k_s \left[\frac{D(1+\mu)}{c^2}\right] = \frac{33.8 \times 10^{-6} \times 42.93 \times 10^3 (1 + 0.3)}{(20)^2} = 4.7154 \times 10^{-3}$$

By Equations [8]

At $\rho = 0$

$$M_1 = 0 - \frac{1.0156}{2}(200) = -101.56$$

$$M_2 = 0 - \frac{1.0156}{2}(200) = -101.56$$

$$\phi = 0$$

At $\rho = 10$

$$A_1 = 50 \times {}^1/_2 \times 10 = 250$$
$$\bar{b} = {}^1/_3 \times 10$$

$$M_1 = \frac{-1.0156}{(10)^2}(250)\left(\frac{10}{3}\right) - \frac{1.0156}{2}(150) = -84.67 \text{ lb in/in}$$

$$M_2 = \frac{1.0156}{(10)^2}(250)\left(\frac{10}{3}\right) - \frac{1.0156}{2}(150) = -67.67 \text{ lb in/in}$$

$$\phi = \frac{33.8 \times 10^{-6}}{10}(250)\left(\frac{10}{3}\right) + \frac{33.8 \times 10^{-6}}{2}(10)(150) = 28.167 \times 10^{-3} \text{ radians}$$

At $\rho = 20$

$$A_1 = 100 \times {}^1/_2 \times 20 = 1000$$
$$\bar{b} = {}^1/_3 \times 20$$

$$M_1 = \frac{-1.0156}{(20)^2}(1000)\left(\frac{20}{3}\right) - \frac{1.0156}{2}(100) = -67.71 \text{ lb in/in}$$

$$M_2 = \frac{1.0156}{(20)^2}(1000)\left(\frac{20}{3}\right) - \frac{1.0156}{2}(100) = 33.85 \text{ lb in/in}$$

$$\phi = \frac{33.8 \times 10^{-6}}{20}(1000)\left(\frac{20}{3}\right) + \frac{33.8 \times 10^{-6}}{2}(20)(100)$$

$$= 45.07 \times 10^{-3} \text{ radians}$$

To reduce ϕ at the edge to zero requires additional moments ΔM_1 and ΔM_2 throughout the plate which are calculated by Equation [12] or, since ϕ is already known for the infinite plate, calculated merely by inverting Equations [16] of the Appendix

$$\Delta M_1 = \Delta M_2 = \frac{-D(1+\mu)\phi}{r}$$

$$= \frac{-42.93 \times 10^3 (1.3)(45.07 \times 10^{-3})}{20} = -125.77 \text{ lb in/in}$$

The correction to the slopes is merely

$$\Delta\phi = -45.07 \times 10^{-3}\left(\frac{r}{20}\right)$$

Final moments, slopes, and bending stresses ($\sigma = 6M/h^2$) are given in Table 1.

TABLE 1 FINAL MOMENTS, SLOPES, AND BENDING STRESSES, EXAMPLE 1

	ρ = 0	ρ = 10	ρ = 20
M_1 lb in/in	−227.33	−210.44	−193.48
M_2 lb in/in	−227.33	−193.44	−159.62
ϕ radians	0	5.63×10^{-3}	0
σ_1 psi (±)	21824	20202	18574
σ_2 psi (±)	21824	18570	15324

Example 2. Plate of Example 1, but hinged at edge. Calculation of moments and slopes for infinite plate same as in Example 1. Correction to M_1 and M_2 throughout plate is such as to reduce M_1 at $\rho = 20$ to zero

$$\Delta M_1 = 67.71$$

By Equation [10]

$$\Delta\phi = \frac{67.71\, r}{42.93 \times 10^3 (1.3)} = 1.2051 \times 10^{-3} r$$

Final moments, slopes, and bending stresses are given in Table 2.

TABLE 2 FINAL MOMENTS, SLOPES, AND BENDING STRESSES, EXAMPLE 2

	ρ = 0	ρ = 10	ρ = 20
M_1	−33.85	−16.96	0
M_2	−33.85	+ 0.04	+33.86
ϕ	0	40.22×10^{-3}	69.17×10^{-3}
σ_1 (±)	3250	1628	0
σ_2 (±)	3250	.....	3250

Example 3. Plate of Example 1 but with elastic edge conditions (such as might be provided by cylindrical wall of tank) $M_e = 15 \times 10^3 \phi_e$.

From Example 1, the moment at the edge of the plate on the assumption of a clamped condition is $M_1 = -193.48$ lb in/in.

By Equations [16] of the Appendix the stiffness of the plate is

$$\frac{\Delta M_1}{\phi_e} = \frac{D(1+\mu)}{20} = \frac{42.93 \times 10^3 (1.3)}{20} = 2.790 \times 10^3$$

The equilibrium condition between the edge of the plate and the elastic restraint is

$$-193.48 + 2.790 \times 10^3 \phi_e + 15 \times 10^3 \phi_e = 0$$

or

$$\phi_e = 10.876 \times 10^{-3} \text{ radians}$$

Moments to be added to the moments of Example 1 are

$$\Delta M_1 = \Delta M_2 = 2.790 \times 10^3 (10.876 \times 10^{-3}) = 30.34 \text{ lb in/in.}$$

Appendix

Axisymmetric bending of thin circular plates and circular rings by edge moments satisfies the following differential equation,[3] due to Poisson

$$\frac{d^2\phi}{dr^2} + \frac{1}{r}\frac{d\phi}{dr} - \frac{\phi}{r^2} = 0 \qquad [13]$$

where ϕ is the local slope of the plate measured along the radius, r

The general solution of this equation is

$$\phi = Ar + \frac{B}{r} \qquad [14]$$

where A and B are arbitrary constants.

The bending moments per unit width acting upon a circumferential arc and upon a radial line are, respectively,

$$\left.\begin{aligned} M_1 &= D\left(\frac{d\phi}{dr} + \mu\frac{\phi}{r}\right) \\ M_2 &= D\left(\frac{\phi}{r} + \mu\frac{d\phi}{dr}\right) \end{aligned}\right\} \qquad [15]$$

where

D = flexural rigidity of plate = $\dfrac{Eh^3}{12(1-\mu^2)}$

E = modulus of elasticity

h = thickness of plate

μ = Poisson's ratio

Consider a circular disk of radius b, subjected to a uniform moment M_0 around its periphery. By symmetry $\phi = 0$ at $r = 0$. Thus B in Equation [14] is zero. At $r = b$, $M_1 = M_0$ and it follows from Equations [15] and [14] that

$$\left.\begin{aligned} A &= \frac{M_0}{D(1+\mu)} \\ \phi &= \frac{M_0 r}{D(1+\mu)} \end{aligned}\right\} \qquad [16]$$

and throughout the disk

$$M_1 = M_2 = M_0 \qquad [17]$$

Consider now an infinite plate from which a disk of radius b has been removed, and assume that a uniform moment M_0 is applied at the edge of the hole. Since the moments must approach zero as r increases indefinitely, it follows from Equations [14] and [15] that $A = 0$ and

$$B = \frac{-M_0 b^2}{D(1-\mu)}$$

The slope and moments for $r \geq b$ are

$$\phi = \frac{-M_0 b^2}{rD(1-\mu)} \qquad [18]$$

$$M_1 = -M_2 = \frac{M_0 b^2}{r^2} \qquad [19]$$

[3] "Strength of Materials," by S. Timoshenko, part 2, second edition, D. Van Nostrand Company, Inc., New York, N. Y., 1941, pp. 135–137; see also "Theory of Plates and Shells," by S. Timoshenko, first edition, McGraw-Hill Book Company, Inc., New York, N. Y., 1940, pp. 55–58.

Transient Thermal Stresses in Slabs and Circular Pressure Vessels[1]

By M. P. HEISLER,[2] DOWNEY, CALIF.

This paper presents the results of computations for determining transient thermal stresses in slabs and circular pressure vessels. The process of solution adopted is to substitute transient-temperature formulas into the already available stress expressions. The expressions for thermal shock are transformed by means of a simple integral theorem into a form appropriate for analyzing the thermal processes commonly used to relieve thermal shock. A new dimensionless stress parameter is defined and applied to the determination of optimum heating or cooling times of massive pressure vessels.

Nomenclature

The following nomenclature is used in the paper:

a = inner radius of hollow cylinder, ft

b = outer radius of hollow cylinder, ft

$\sigma_y(x, t)$ = thermal stresses induced in directions parallel to the mid-plane of plate, psf

x = distance measured from mid-plane of plate, ft

E = Young's modulus of elasticity, psf

α = coefficient of linear expansion, ft/ft, deg F

μ = Poisson's ratio, dimensionless

L = half-thickness of plate, ft

$t = t(n, N)$ = temperature at n and N, deg F

t_a = ambient temperature, deg F

τ = time, hours

q = volumetric rate of heat generation, Btu/ft^3, hr

k = thermal conductivity, Btu/ft, hr, deg F

h = surface heat transfer coefficient, Btu/ft^2, hr, deg F

c = rate of increase of ambient temperature, deg F/hr

d = thermal diffusivity = (conductivity)/(volumetric specific heat), ft^2/hr

$n = x/L$, dimensionless

N = Fourier modulus $= d\tau/L^2$ or $d\tau/a^2$, dimensionless

m = inverse Nusselt number $= k/hL$, dimensionless

$X_1(n, N)$ = dimensionless stress parameter, $\dfrac{\sigma(1-\mu)}{\alpha E t_a}$

$X_2(n, N)$ = dimensionless stress parameter, $\dfrac{\sigma(1-\mu)d}{\alpha E(cL^2)}$ or $\dfrac{\sigma(1-\mu)d}{\alpha E(ca^2)}$

$X_3(n, N)$ = dimensionless stress parameter, $\dfrac{\sigma(1-\mu)k}{\alpha E(qL^2)}$ or $\dfrac{\sigma(1-\mu)k}{\alpha E(qa^2)}$

$T_1(n, N)$ = dimensionless temperature parameter $= t/t_a$

$T_2(n, N)$ = dimensionless temperature parameter, $\dfrac{t}{(cL^2/d)}$ or $\dfrac{t}{(ca^2/d)}$

$T_3(n, N)$ = dimensionless temperature parameter, $\dfrac{t}{(qL^2/k)}$ or $\dfrac{t}{(qa^2/k)}$

$\exp(x) = e^x$, where e is base of Naperian logarithms

erfc = complementary error function

$M = m/\sqrt{N}$

Introduction

Current interest in the high-temperature operation of large pressure vessels—for example, those proposed for nuclear power reactors—necessitates a closer evaluation of thermal stress as a possible source of pressure-vessel failure. As a specific example we may cite the emergency cooling of a pressurized reactor. Here, because of certain nuclear phenomena associated with the process of fissioning, it is a matter of considerable importance to keep the cooling time of the pressurized shell down to a bare minimum. A rational estimation of the down time is predicated largely upon the ability to analyze the magnitude of the thermal stress induced by the cooling process.

As another illustration we cite the interest in high-temperature designs using ceramic and ceramal materials, which are relatively weak in thermal shock. The problem is somewhat different from that of the pressure vessel. Where for pressure vessels we seek a cooling process such that the maximum induced thermal stress will not exceed the design working stress of the material, for ceramics and ceramals we seek materials having physical and thermal properties able to withstand the mutations of an abnormal temperature process. In the former we fit the process to the material, in the latter the material to the process. The ultimate feasibility of liquid-metal cooling in the production of power, either directly or as a by-product of the manufacture of fissionable material, rests largely upon the development of materials having adequate resistance to spalling, corrosion, and thermal shock. Hence it is of some importance to have a consistent theory of resistance to thermal shock and the mechanisms used to alleviate it.

Although there is an abundant literature on the subject of thermal stresses,[3] very few of these works give numerical results which are adequate for practical applications. Of these Jaeger (1)[3] gives fairly complete results for the numerical evaluation of stresses in a solid cylinder which is initially at a uniform temperature and which loses heat through a boundary layer to an

---

[1] This paper is based upon work conducted for the Atomic Energy Commission under Contract AT 11-1-GEN-8.

[2] Research Engineer, Atomic Energy Research Department, North American Aviation, Inc.

Presented at the National Conference of the Applied Mechanics Division, Minneapolis, Minn., June 18–20, 1953, of The American Society of Mechanical Engineers.

Discussion of this paper should be addressed to the Secretary, ASME, 29 West 39th Street, New York, N. Y., and will be accepted until July 10, 1953, for publication at a later date. Discussion received after the closing date will be returned.

Note: Statements and opinions advanced in papers are to be understood as individual expressions of their authors and not those of the Society. Manuscript received by ASME Applied Mechanics Division, August 22, 1952. Paper No. 53—APM-8.

[3] An extensive Bibliography is given by Gatewood in the *Philosophical Magazine*, vol. 32, 1941, p. 282. Additional references (numbers in parentheses) are given in the Bibliography at the end of the paper.

ambient at zero temperature. He also gives a general solution for the hollow cylinder, but the formulas are rather complicated and require considerable formal manipulation in order to make them tractable for specific applications. The numerical results obtained by Kent (2), Dahl (3), Murray (4) et al, hold only for constant or linearly varying surface temperatures, and hence the scope of their application is limited.

The primary purpose of this paper is to give numerical results which can predict: (*a*) In the case of unavoidable thermal shock whether or not there exists the possibility of structural hazards; (*b*) in the heating or cooling of massive pressure vessels, the maximum permissible speed of the thermal process consistent with the stress limitations imposed in order to avoid possible vessel failure. Under the heading of thermal shock we include both instantaneous changes in ambient temperatures (such as occur in quenching) and surface heating by high-frequency induction, since, as shown in reference (5), these two physically dissimilar types of heating are mathematically identical. In a similar fashion we include under the generic term "alleviation of thermal shock" the case of internal heat generation because here too there exists an identity in mathematical form. It is not intended, however, to convey the impression that heating by internal sources is a method customarily used to forestall excessive thermal stress.

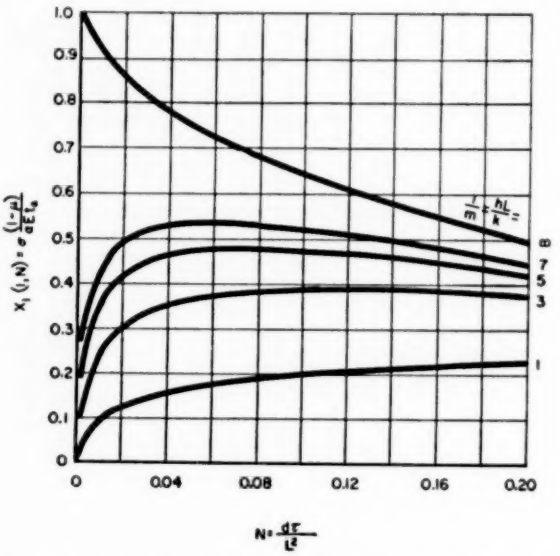

FIG. 1 SURFACE THERMAL STRESSES FOR SUDDEN INCREASE IN AMBIENT TEMPERATURE

THERMAL SHOCK AND ITS ALLEVIATION

All previous expressions for thermal shock have been derived for the case of sudden change in surface temperature. In this paper we consider the more general case of surface heat-transfer resistance. The implications of an ill-advised neglect of surface resistance is portrayed graphically in Fig. 1. We see that the assumption of an infinite modified Nusselt number ($1/m$) (which corresponds to a constant surface temperature) may lead to excessive conservatism in design. For example, a process characterized by a Nusselt number equal to 7—an order of magnitude common to many quenching operations—would cause a maximum thermal stress only 53 per cent as large as that calculated on the assumption of constant surface temperature. A Nusselt number of 3 yields a stress which is approximately 38 per cent that of constant surface temperature. The latter case corresponds roughly to conditions occurring in the heating-up of steel billets in a continuous furnace.

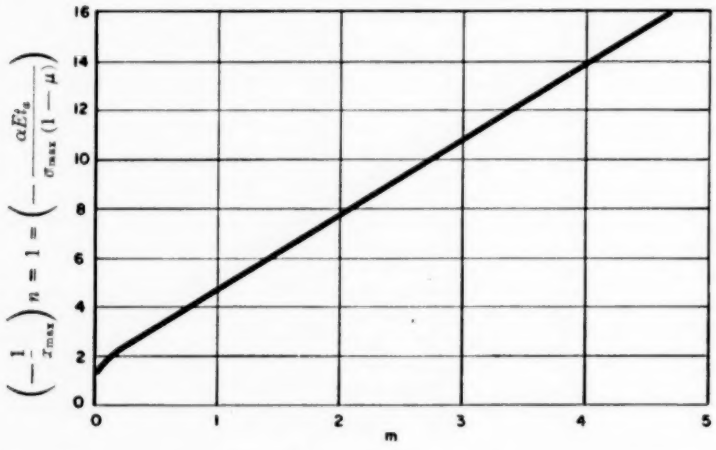

FIG. 2 VARIATION OF MAXIMUM SURFACE STRESS WITH RELATIVE BOUNDARY RESISTANCE
(Slab subjected to sudden increase in ambient temperature.)

Fig. 1 also reveals that the point of maximum thermal stress is a delayed function of time, the delay becoming increasingly pronounced as the boundary resistance is increased. The time variation of the maximum stress is plotted in Fig. 3, versus the rela-

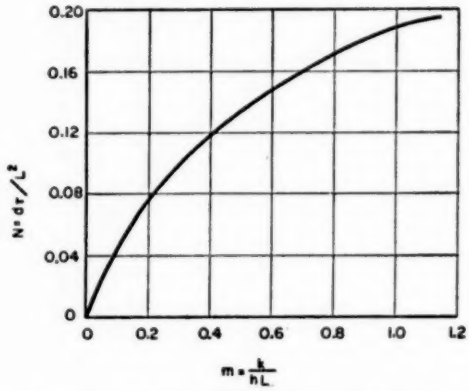

FIG. 3 PLOT SHOWING TIME AT WHICH MAXIMUM SURFACE STRESS OCCURS AS FUNCTION OF RELATIVE BOUNDARY RESISTANCE

tive boundary resistance; the variation of the maximum with resistance is plotted in Fig. 2. The values were obtained by differentiating the stress function with respect to time and setting the resultant equal to zero. (The derivation is given later in the text.)

The results shown in Figs. 1, 2, and 3 have been derived on the assumption of infinite slab geometry, assuming one face insulated and the other exposed to a suddenly changed ambient. However, they also can be applied with reasonable accuracy to curved surfaces providing that the radius of curvature is everywhere large compared with the thickness of the slab. In general, large pressure vessels satisfy this condition. Cases involving thick-walled vessels require special formulation. Jaeger has derived solutions for hollow cylinders under rather general boundary conditions. A slightly modified form of his results are included in section (*B*). Unfortunately, the formulas are complicated enough to preclude a generalized graphical presentation, and hence a painstaking evaluation must be performed for each particular case as it arises.

The thermal shock discussed in the preceding paragraphs can be avoided by raising or lowering the temperature of the material gradually; in customary practice this is accomplished by means of an almost linearly varying ambient. It then becomes a question of considerable importance—particularly in the warmup or shutdown of massive pressure vessels—to determine the maximum rate at which heating or cooling can progress, because heating at lower than the maximum rate may result in a longer heating period than comfortably can be tolerated, and

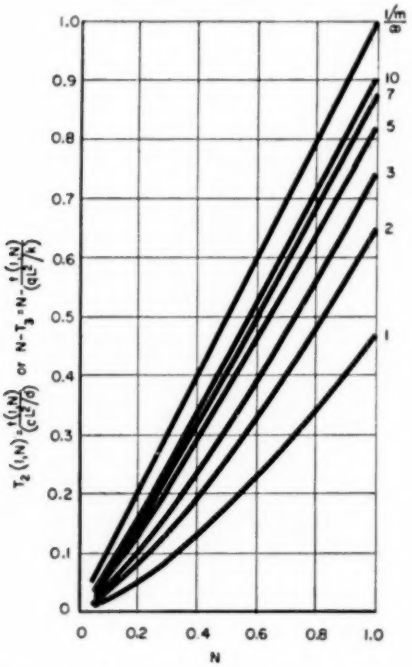

FIG. 4 TRANSIENT SURFACE TEMPERATURES FOR UNIFORMLY INCREASING AMBIENT TEMPERATURE OR UNIFORM INTERNAL HEAT GENERATION

heating at higher than the maximum rate may cause the material to fail.

The temperature-time variation for infinite slabs having uniform heat generation or linearly varying ambient temperature is shown in Figs. 4 and 5. Along the ordinate we have plotted T_2, the dimensionless temperature ratio for internal heat sources, and $N - T_3$, where T_3 is the dimensionless temperature ratio for a linearly varying ambient temperature. Because of the mathematical similarity of the temperature functions it is possible to express the dimensionless stress ratio for these two types of heating by a single set of graphs, Figs. 6 and 7. The figures hold for Nusselt numbers ranging between 1 and ∞ and values of Fourier modulus up to 5. It was found convenient to use $X_2 + {}^1/_3$ and $X_3 + {}^1/_3$ as ordinates. It can be seen that the maximum stress occurs at steady state and is given by $X_2 = -X_3 = -{}^1/_3$.

For purposes of evaluation our primary interest is to determine an optimum heating or cooling rate. Figs. 4, 5, 6, and 7 will yield this only through a tedious trial-and-error procedure. We can avoid the trial-and-error process by defining a new parametric ratio as follows

$$\frac{X_2(1,N)}{T_2(1,N)} = \frac{(1-\mu)d\sigma(1,N)}{\alpha EcL^2} \Big/ \frac{t(1,N)d}{(cL^2)} = \frac{(1-\mu)\sigma(1,N)}{{}^1\alpha Et(1,N)}$$

The ratio is plotted in Fig. 8 for values of $1/m$ between 1 and ∞ and N up to 25. The significance of the ratio will become clear by considering the cooling of a large circular pressure vessel such as might serve as a container for a high-temperature power-production reactor. The vessel is assumed to have the material properties given in Table 1.

TABLE 1 PROPERTIES OF POWER-PRODUCTION REACTOR

Conductivity	26 Btu/ft, hr, deg F	(k)
Diffusivity	0.577 sq ft/hr	(d)
Wall thickness	0.5 ft	(L)
Coefficient of thermal expansion	6.7×10^{-6} in/in, deg F	(α)
Modulus of elasticity	30×10^6 psi	(E)
Poisson's ratio	0.3	(μ)

Water at 500 F is flowing through the vessel, and the average heat-transfer coefficient between water and vessel is calculated to

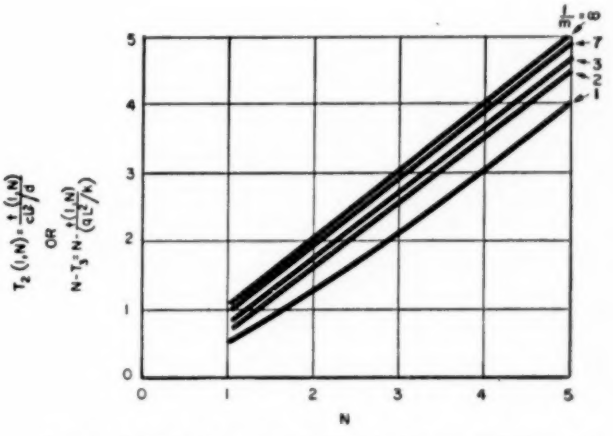

FIG. 5 TRANSIENT SURFACE TEMPERATURES FOR UNIFORMLY INCREASING AMBIENT TEMPERATURE OR UNIFORM INTERNAL HEAT GENERATION

be 360 Btu/sq ft, hr, deg F. The maximum permissible working stress is set at 18,000 psi. We wish to know the maximum linear rate at which the water can be cooled by an external heat exchanger in order to lower the surface temperature of the vessel

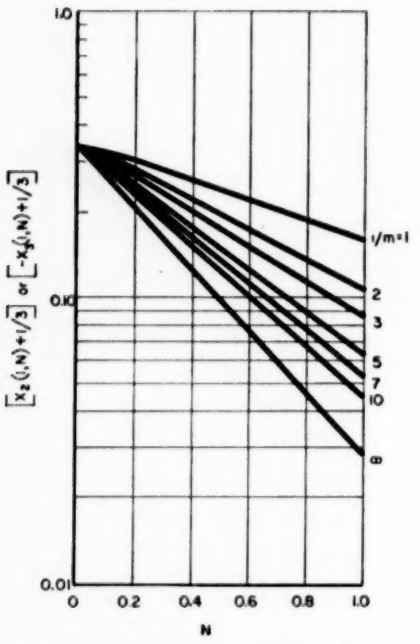

FIG. 6 VARIATION OF SURFACE STRESS WITH TIME IN SLAB SUBJECTED TO UNIFORMLY INCREASING AMBIENT TEMPERATURE OR UNIFORM INTERNAL HEAT GENERATION

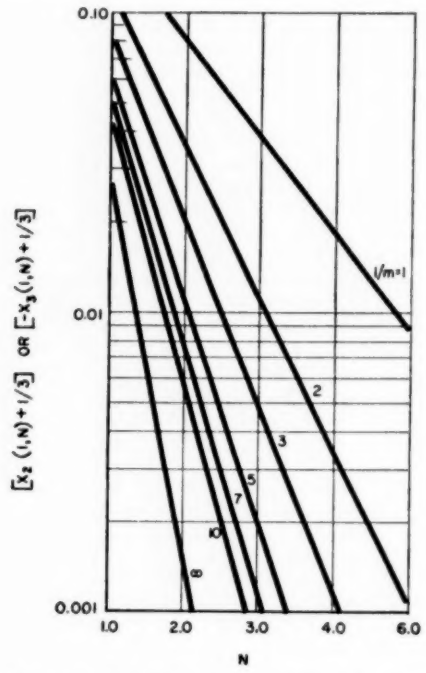

FIG. 7 VARIATION OF SURFACE STRESS WITH TIME IN SLAB SUBJECTED TO UNIFORMLY INCREASING AMBIENT TEMPERATURE OR UNIFORM INTERNAL HEAT GENERATION

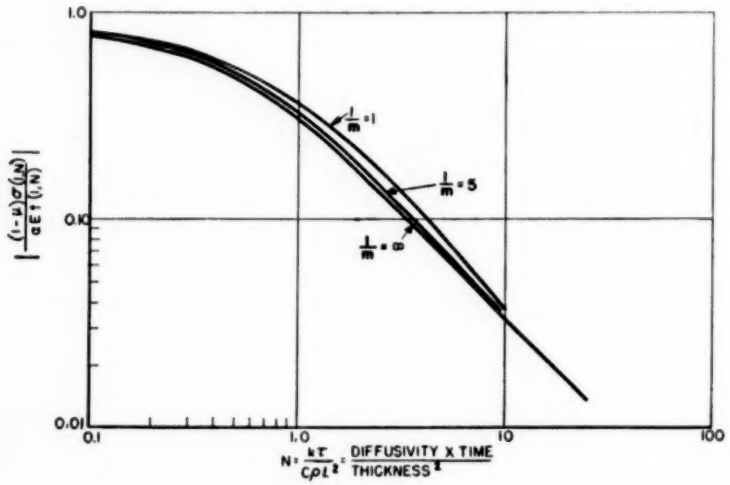

FIG. 8 CHART FOR DETERMINING MAXIMUM HEATING OR COOLING RATES IN SLABS SUBJECTED TO UNIFORMLY INCREASING AMBIENT TEMPERATURE OR UNIFORM INTERNAL HEAT GENERATION

from 500 F to 100 F and at the same time not exceed the maximum working stress. Assuming slab geometry applies and that the outer surface is well insulated, we can say:

(*a*) The maximum stress tending to rupture the vessel will be tensile and will occur at the inner surface of the vessel.

(*b*) The most rapid cooling rate will be such that the surface stress will equal the prescribed maximum stress at the moment the surface temperature reaches 100 F.

The total surface stress consists of two parts, a tensile stress caused by cooling and a tensile stress caused by the static pressure of the water in the vessel. As the water temperature is lowered, the stress resulting from pressure rapidly decreases and virtually vanishes at a water temperature of approximately 200 F. The thermal tensile stress, however, increases as cooling progresses, reaching its maximum value when a steady rate of temperature change prevails throughout the shell. Hence it is reasonable to assume that the pressure stress will disappear before the thermal stress reaches its peak and that the total stress at the end of cooling virtually will be of thermal origin. Under these assumptions

$$\sigma(1,N) = 18{,}000 \text{ psi}$$

$$t(1,N) = 500 - 100 = 400 \text{ F}$$

Then

$$\frac{(1-\mu)\sigma(1,N)}{\alpha E t(1,N)} = \frac{(1-0.3)\,18000}{6.7 \times 10^{-6} \times 30 \times 10^{6} \times 400} = 0.188$$

and

$$\frac{1}{m} = \frac{h\,L}{k} = \frac{360 \times 0.5}{26} = 6.93$$

Entering Fig. 8 with these values we find

$$N = 1.9$$

With $1/m = 6.93$ and $N = 1.9$, we now go to Fig. 5 and obtain

$$\frac{t(1,N)}{cL^2/d} = 1.85$$

From this we can calculate c, the linear rate of cooling, as follows

$$c = \frac{1.85\,t\,(1,N)}{L^2/d} = \frac{1.85 \times 400}{(0.5)^2/0.577} = 500 \text{ deg F/hr}$$

The time required to cool the surface to 100 F is found from the definition of the Fourier modulus

$$N = \frac{d\tau}{L^2} = 1.9$$

Therefore

$$\tau = 1.9\,\frac{L^2}{d} = 1.9\,\frac{(0.5)^2}{0.577} = 0.82 \text{ hr}$$

The time variation of surface stress is shown in Fig. 9. The broken line is the pressure-stress variation, based upon the satu-

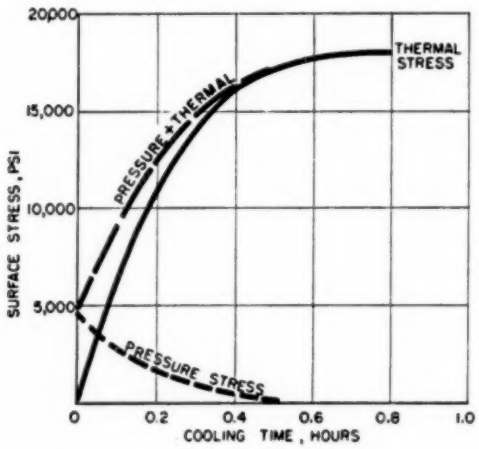

FIG. 9 TIME VARIATION OF SURFACE STRESS

ration pressure of the water. The solid line is the thermal-stress variation based upon a linear cooling rate of 500 deg F/hr. The dash-dot line is the total stress, that is, the sum of pressure and thermal stress. It can be seen that, as assumed, the pressure stress is relieved completely before the thermal stress reaches the prescribed maximum value of 18,000 psi. At no point does the sum of pressure plus thermal stress exceed 18,000 psi.

The figure also illustrates how rapidly the thermal stress builds up with time; evidently very little cooling time can be saved by using a more elaborate cooling system, for example, one which has a gradually decreasing cooling rate designed to keep the thermal stress at or near 18,000 psi throughout the cooling period.

SOLUTIONS

The process of solution adopted here is to substitute transient-temperature formulas into the already available stress expressions. These expressions are well known for thermal processes characterized by a sudden change in ambient temperature. The temperature expressions for thermal processes involving a linearly varying ambient are obtained by taking the time integral of the known solutions for a sudden change in ambient temperature. The validity of this procedure is demonstrated in the Appendix.

In the first of the following sections we derive the transient stress equations for plates, using the known temperature expressions. We then integrate these expressions with respect to time, thereby obtaining the transient stress formulas for internal source and linearly varying ambient-temperature heating. In the second section we repeat the procedure for cylinders, integrating the stress and temperature equations derived by Jaeger for step heating.

(*A*) *Temperature and Stress Equations for Plates.* Let us consider an isotropic solid. If E is Young's modulus; μ, Poisson's ratio; α, the coefficient of linear thermal expansion of the material; and $t(x, \tau)$ the temperature at any point x and time τ, the thermal stress equation is given by the following formula (6)

$$\sigma_y(x,\tau) = \sigma_z(x,\tau) = \frac{E\alpha}{1-\mu}\left[\frac{1}{2L}\int_{-L}^{L} t(x,\tau)dx + \frac{3x}{2L^3}\int_{-L}^{L} x\,t(x,\tau)dx - t(x,\tau)\right] \quad [1]$$

where L is the half-thickness of the plate and σ_z and σ_y are the normal components of the stress tensor in the direction parallel to the mid-plane of the plate.

If the temperature field is symmetrically distributed about the mid-plane, the second integral is zero, and Equation [1] reduces to

$$\sigma_y(x,\tau) = \sigma_z(x,\tau) = \frac{E\alpha}{1-\mu}\left[\frac{1}{L}\int_{0}^{L} t(x,\tau)\,dx - t(x,\tau)\right] \quad [2]$$

Equation [2] can be reduced to convenient dimensionless form for instantaneous increase in ambient temperature, linearly increasing ambient temperature, and internal heat sources by the following substitutions

$$T_1(n,N) = \frac{t(n,N)}{t_a} \quad [3]$$

$$T_2(n,N) = \frac{t(n,N)}{(cL^2/d)} \quad [4]$$

$$T_3(n,N) = \frac{t(n,N)}{(qL^2/k)} \quad [5]$$

where $n = x/L$, $N = d\tau/L^2$, and t_a is the instantaneous increase of the ambient temperature, c is a constant which expresses the rate of increase of ambient temperature, and q defines the uniform volumetric rate of heat generation.

By substituting Equations [3], [4] and [5] into Equation [2], noting that X_2 can be expressed as the time integral of X_1 (see first section of Appendix) and that the absolute magnitudes of X_2 and X_3 are equal (see second section of Appendix) we can derive the following relations

$$X_1 = \frac{\sigma(1-\mu)}{\alpha E t_a} = \int_0^1 T_1 dn - T_1 \quad [6]$$

$$X_2 = \frac{\sigma(1-\mu)d}{\alpha E(cL^2)} = \int_0^N X_1 dN \quad [7]$$

$$X_3 = \frac{\sigma(1-\mu)k}{\alpha E(qL^2)} = -X_2 \quad [8]$$

In Equation [8] X_3 is the stress arising from an increasing ambient temperature. If the ambient temperature is decreasing, X_3 and X_2 have the same sign such that in both cases regions near the uninsulated surface are in tension and regions near the insulated surface are in compression.

The known temperature solution of Case 1 is (5, 7, 8, 9)

$$T_1 = 1 - 2\sum_{j=1}^{\infty} \frac{\sin w_j \cos(w_j n)}{w_j + \sin w_j \cos w_j} \exp(-w_j^2 N) \quad [9]$$

where

$$mw_j = \cot w_j \quad [10]$$

The temperature distributions for Cases 2 and 3 can be derived from Case 1 (see first section of Appendix). They are

$$T_2 = N - \frac{1 - n^2 + 2m}{2} + 2\sum_{j=1}^{\infty} \frac{\sin w_j \cos(w_j n) \exp(-w_j^2 N)}{w_j^2(w_j + \sin w_j \cos w_j)} \quad [11]$$

$$T_3 = N - T_2 \quad [12]$$

The transient thermal-stress distributions are obtained by applying to Equations [9], [11], and [12] the operations defined by Equations [6], [7], and [8]. This yields

$$X_1 = 2\sum_{j=1}^{\infty} \frac{\sin w_j \cos(w_j n)}{w_j + \sin w_j \cos w_j} \left(1 - \frac{\sin w_j}{w_j \cos(w_j n)}\right) \times \exp(-w_j^2 N) \quad [13]$$

$$X_2 = -X_3 = \frac{1}{6} - \frac{n^2}{2} - 2\sum_{j=1}^{\infty} \frac{\sin w_j \cos(w_j n)}{w_j^2(w_j + \sin w_j \cos w_j)} \times \left(1 - \frac{\sin w_j}{w_j \cos(w_j n)}\right) \exp(-w_j^2 N) \quad [14]$$

It should be noted that since X_1, X_2, and X_3 are monotonic and symmetric about the insulated surface of the plate, the maximum stress must occur at $n = 1$. In the case of heating, i.e., T_1, T_2, $T_3 > 0$, X_1, and X_2 at $n = 1$ will be compressive and X_3 will be tensile. The converse is true during cooling. Consequently, the numerical evaluation of the stress equations has been carried out only for the surface, $n = 1$.

1 *Solutions Suitable for Small Values of Time.* The convergence of Equations [9], [11], [13], and [14] is slow if N is small. For $N \geq 0.2$, retaining only the first term in the series results in an accuracy of about 2 per cent, which, in view of the uncertainty in the values of the physical properties introduced, is sufficient for most engineering calculations. If $N \geq 0.1$, the same order of accuracy can be obtained by retaining only two terms. For many cases of thermal shock, involving relatively small boundary resistances, N of the order of 0.01 occurs, and it is important to have approximate formulas which are valid for this region. Rigorous formulas can be obtained by using the method developed by Goldstein (10). The relationships derived previously still hold, but error functions are now involved, and in the following it will be convenient to use the method of the Laplace transform. Let us define

$$t_j = \int_0^{\infty} T_j e^{-sN} dN, \ (j = 1, 2, 3) \quad [15]$$

and

$$x_j = \int_0^{\infty} X_j e^{-sN} dN$$

Then

$$t_1 = \frac{\cosh(\sqrt{s}n)}{s(\cosh\sqrt{s} + m\sqrt{s}\sinh\sqrt{s})} \quad [16]$$

$$t_2 = \frac{\cosh(\sqrt{s}n)}{s^2(\cosh\sqrt{s} + m\sqrt{s}\sinh\sqrt{s})} \quad [17]$$

In view of the invariance properties of the Laplace transform with respect to the second variable, it follows that

$$x_j = \int_0^1 t_j dn - t_j \quad [18]$$

hence

$$x_1 = \frac{\sinh\sqrt{s} - \sqrt{s}\cosh(\sqrt{s}n)}{s^{3/2}(\cosh\sqrt{s} + m\sqrt{s}\sinh\sqrt{s})} \quad [19]$$

$$x_2 = \frac{\sinh\sqrt{s} - \sqrt{s}\cosh(\sqrt{s}n)}{s^{5/2}(\cosh\sqrt{s} + m\sqrt{s}\sinh\sqrt{s})} \quad [20]$$

Since, for large x

$$\sinh x \cong \cosh x \cong \frac{e^x}{2} \quad [21]$$

we find at the surface ($n = 1$)

$$t_1(1,s) \cong \frac{1}{s(1 + m\sqrt{s})} \quad [22]$$

$$t_2(1,s) \cong \frac{1}{s^2(1 + m\sqrt{s})} \quad [23]$$

$$x_1(1,s) \cong \frac{1 - \sqrt{s}}{s^{3/2}(1 + m\sqrt{s})} \quad [24]$$

$$x_2(1,s) \cong \frac{1 - \sqrt{s}}{s^{5/2}(1 + m\sqrt{s})} \quad [25]$$

The inverse transforms give

$$T_1(1,N) = 1 - \exp\left(\frac{1}{M^2}\right)\operatorname{erfc}\left(\frac{1}{M}\right) \quad [26]$$

$$T_2(1,N) = N\left[M^2 + 1 - \frac{2M}{\sqrt{\pi}} - M^2\exp\left(\frac{1}{M^2}\right)\operatorname{erfc}\left(\frac{1}{M}\right)\right] \quad [27]$$

$$T_3(1,N) = N - T_2(1,N) \quad [28]$$

$$X_1(1,N) = 2\sqrt{\frac{N}{\pi}} - (m+1)\left[1 - \exp\left(\frac{1}{M^2}\right)\operatorname{erfc}\left(\frac{1}{M}\right)\right] \quad [29]$$

$$X_2(1,N) = -X_3(1,N) = N\left[\sqrt{\frac{N}{\pi}}\left(\frac{4}{3} + 2M^2\right) + \frac{2M}{\sqrt{\pi}} - (M\sqrt{N} + 1)(1 + M^2 - M^2\exp\left(\frac{1}{M^2}\right)\operatorname{erfc}\left(\frac{1}{M}\right)\right] \quad [30]$$

2 *Maximum Stress.* The maximum stress will of course occur at $\partial X/\partial N = 0$ and is given by

$$X(1,N)_{max} = 2\sqrt{\frac{N}{\pi}} - \frac{M}{\sqrt{\pi}} \exp\left(\frac{1}{M^2}\right) \operatorname{erfc}\left(\frac{1}{M}\right) - 1 \quad [31]$$

in which N is determined from

$$\frac{1}{1+m} = \frac{\sqrt{\pi N}}{m} \exp\left(\frac{N}{m^2}\right) \operatorname{erfc} \frac{\sqrt{N}}{m} \quad [32]$$

Equations [31] and [32] are valid for $N \leq 0.2$. For $N \geq 0.2$, Equation [13] applies. Since only one term in the series is necessary for values of $N > 0.2$, it follows that the stress for the cases not covered by Equations [31] and [32] decreases monotonically from a maximum which occurs in the neighborhood of 0.2. The truth of this is also apparent from Fig. 1 which shows that maximum stresses for $m \geq 1$ occur for some value of N in the neighborhood of 0.2. Hence the maximum stress is given by

$$X_{1\,max} = 2\,\frac{\sin w_1}{w_1 + \sin w_1 \cos w_1}\left(1 - \frac{\sin w_1}{w_1 \cos w_1}\right)\exp(0.2\,w_1^2) \quad [33]$$

When m is large, Equation [33] can be simplified still further; in order to do this, we note that for large m, the first root of $mw = \cot w$ is approximately zero. Using the form

$$\frac{1}{m} = w \tan w \quad [34]$$

expanding tan w into a trigonometric series and retaining only the first term leads to $1/m = w^2$. Also, for small values of w

$$\frac{2 \sin w}{w + \sin w \cos w} \approx 1 \quad [35]$$

Consequently, with the foregoing approximation, Equation [33] reduces to

$$X_{1\,max} = -\exp(-0.2/m)\left(\frac{\sin w}{w} - \cos w\right) \quad [36]$$

Expanding sin w and cos w and noting that $\exp(-0.2/m) \approx 1 - 0.2/m$ for large m, we finally obtain

$$X_{1\,max} = -\left(1 - \frac{0.2}{m}\right)\left(\frac{1}{3m} - \frac{1}{6m^2}\right) \quad [37]$$

This is correct to within about 3 per cent for $m = 5.0$. When m is greater than 10, we can use

$$X_{1\,max} = -\frac{1}{3m} \quad [38]$$

which will yield answers correct to two significant figures.

(*B*) *Temperature and Stress Equations for Hollow Cylinders.* 1 *Stresses for Sudden Increase in Ambient Temperature—Case 1:* Jaeger (1) has derived a general solution for the hollow cylinder $a < r < b$, with zero initial temperature and with the boundary conditions

$$\left.\begin{aligned} k\frac{\partial t}{\partial r} - h_1(t - t_1) &= 0, \qquad r = a \\ k\frac{\partial t}{\partial r} + h_2(t - t_2) &= 0, \qquad r = b \end{aligned}\right\} \quad [39]$$

where h_1 and h_2 are the heat-transfer coefficients of surfaces a and b, respectively, and t_1 and t_2 are the temperatures of the ambients facing these surfaces. He gives the tangential stress in the form

$$\frac{\sigma(1-\mu)}{E\alpha} = \frac{abh_1h_2(t_2 - t_1)}{2\,bh_2k + 2\,ah_1k + 2\,abh_1h_2}\log\frac{b}{a}\left[\frac{b^2(r^2+a^2)}{r^2(b^2-a^2)} - 1 - \log\frac{r}{a}\right] - \sum_{s=1}^{\infty} e^{-\beta_s^2 d\tau} F(\beta_s)\left[\frac{b(r^2+a^2)\,C_1(b\beta_s)}{r^2(b^2-a^2)\beta_s} + \frac{C_1(r\beta_s)}{r\beta_s} - C_0(r\beta_s) - \frac{2h_1(b^2+r^2)}{\pi r^2(b^2-a^2)\beta_s^2}\right] \quad [40]$$

where

$$C_0(x) = J_0(x)\,[k\beta_s Y_1(a\beta_s) + h_1 Y_0(a\beta_s)] - Y_0(x)\,[k\beta_s J_1(a\beta_s) + h_1 J_0(a\beta_s)] \quad [41]$$

$$C_1(x) = J_1(x)\,[k\beta_s Y_1(a\beta_s) + h_1 Y_0(a\beta_s)] - Y_1(x)\,[k\beta_s J_1(a\beta_s) + h_1 J_0(a\beta_s)] \quad [42]$$

$$F(\beta_s) = \frac{\pi^2[k\beta_s J_1(b\beta_s) - h_2 J_0(b\beta_s)]^2\{h_1t_1[k\beta_s J_1(b\beta_s) - h_2 J_0(b\beta_s)] + h_2t_2[k\beta_s J_1(a\beta_s) + h_1 J_0(a\beta_s)]\}}{(h_1^2 + k^2\beta_s^2)\,[k\beta_s J_1(b\beta_s) - h_2 J_0(b\beta_s)]^2 - (h_2^2 + k^2\beta_s^2)\,[k\beta_s J_1(a\beta_s) + h_1 J_0(a\beta_s)]^2} \quad [43]$$

where $\pm\beta_s$, $s = 1, 2, \ldots$, are the roots (all real and simple) of

$$[k\beta J_1(a\beta) + h_1 J_0(ab)]\,[k\beta Y_1(b\beta) - h_2 Y_0(b\beta)] - [k\beta J_1(b\beta) - h_2 J_0(b\beta)]\,[k\beta Y_1(a\beta) + h_1 Y_0(a\beta)] = 0 \quad [44]$$

For a hollow cylinder whose outer surface is insulated and whose inner surface faces an ambient at temperature t_1, we have $h_2 = 0$. Hence Equations [40], [41], [42], [43] and [44] reduce to

$$X_1 = \frac{\sigma(1-\mu)}{E\alpha t_1} = -\sum_{s=1}^{\infty} e^{-\beta_s^2 d\tau} f(\beta_s)\left[\frac{b(r^2+a^2)\,C_1(b\beta_s)}{r^2(b^2-a^2)\beta_s} + \frac{C_1(r\beta_s)}{r\beta_s} - C_0(r\beta_s) - \frac{2h_1(b^2+r^2)}{\pi r^2(b^2-a^2)\beta_s^2}\right] \quad [45]$$

$C_0(x)$ and $C_1(x)$ are unchanged and

$$f(\beta_s) = \frac{\pi^2[k\beta_s J_1(b\beta_s)]^2\{h_1[k\beta_s J_1(b\beta_s)]\}}{(h_1^2 + k^2\beta_s^2)\,[k\beta_s J_1(b\beta_s)]^2 - (k\beta_s)^2\,[k\beta_s J_1(a\beta_s) + h_1 J_0(a\beta_s)]^2} \quad [46]$$

2 *Stress Equations for Uniformly Changing Ambient Temperature and Uniform Heat Generation.* It can be shown that the stress relations connecting X_1, X_2, and X_3, which were derived in section (*A*) are also valid for hollow cylinders whose outer surface is insulated.

Hence we have

$$\left.\begin{aligned} X_2 &= \int_0^N X_1 dN \\ X_3 &= -X_2 \end{aligned}\right\} \quad \ldots\ldots\ldots\ldots [47]$$

where N is now defined as $d\tau/a^2$. Applying these to the preceding stress equations we get

$$X_2 = \frac{\sigma(1-\mu)d}{\alpha E(ca^2)} = \frac{-1}{16\,a^2r^2}\left(3r^4 - a^2r^2 - a^2b^2 - 5b^2r^2 - 4r^2b^2\ln\frac{r}{a} + \frac{4b^4(r^2+a^2)}{b^2-a^2}\ln\frac{b}{a}\right)$$

$$+\sum_{s=1}^{\infty} e^{-\beta_s^2 d\tau}\frac{f(\beta_s)}{(a\beta_s)^2}\left[\frac{b(r^2+a^2)C_1(b\beta_s)}{r^2(b^2-a^2)\beta_s} + \frac{C_1(r\beta_s)}{r\beta_s} - C_0(r\beta_s) - \frac{2b_1(b^2+r^2)}{\pi\, r^2(b^2-a^2)\beta_s^2}\right] \quad [48]$$

and

$$-X_2 = X_3 = \frac{\sigma(1-\mu)k}{\alpha E(qa^2)} \quad \ldots\ldots\ldots\ldots [49]$$

3 *Temperature Expressions for Sudden Increase in Ambient Temperature.* Jaeger (1) also gives a general equation for temperature distributions in shells having zero initial temperature and subject to the boundary conditions Equations [39] in the form

$$t = \frac{ah_1t_1\left(k + bh_2\log\frac{b}{r}\right) + bh_2t_2\left(k + ah_1\log\frac{r}{a}\right)}{bh_2k + ah_1k + abh_1h_2\log\frac{b}{a}}$$

$$-\sum_{s=1}^{\infty} e^{-\beta_s^2 d\tau} F(\beta_s)C_0(r\beta_s) \quad \ldots\ldots\ldots\ldots [50]$$

where the β_s are found from Equation [46].

As in item (1), we find the temperature for an insulated shell by setting $h_2 = 0$. Then Equation [50] reduces to

$$\frac{t}{t_1} = T_1' = 1 - \sum_{s=1}^{\infty} e^{-\beta_s^2 d\tau} f(\beta_s)C_0(r\beta_s) \quad \ldots\ldots [51]$$

4 *Temperature Equations for Uniformly Varying Ambient Temperature and Uniform Heat Generation.* We can use Equation [51] to obtain temperature equations for uniformly varying ambient and uniform power generation by using as before the relation

$$T_2' = \int_0^N T_1'\, dN$$

This yields

$$T_2' = \frac{t}{ca^2/d} = N - \left[\frac{\left(\frac{b^2}{a^2} - 1\right)k}{2ah_1} + \frac{1}{4}\left(1 - \frac{r^2}{a^2} + \frac{2b^2}{a^2}\ln\frac{r}{a}\right)\right]$$

$$+\sum_{s=1}^{\infty} e^{-\beta_s^2 d\tau}\frac{f(\beta_s)C_0(r\beta_s)}{(a\beta_s)^2} \quad \ldots [52]$$

$$T_3' = \frac{t}{qa^2/k} = N - T_2'$$

Clearly the stress and temperature formulas for hollow cylinders pose difficult problems in evaluation. The roots of Equation [44] have not yet been evaluated. Also, an additional parameter, b/a, is involved, and a general graphical presentation such as can be made for the case of plates is difficult because of the large number of graphs which would now be required. While no general graphical presentation will be attempted here, the formulas quoted allow evaluation for particular cases as they occur.

BIBLIOGRAPHY

1 "On Thermal Stresses in Circular Cylinders," by J. C. Jaeger, *Philosphical Magazine*, vol. 36, 1945, pp. 414–428.

2 "Thermal Stresses in Spheres and Cylinders," by C. H. Kent, Trans. ASME, vol. 54, 1932, pp. 185–196.

3 "Temperature and Stress Distributions in Hollow Cylinders," by O. G. C. Dahl, Trans. ASME, vol. 46, 1924, pp. 161–208.

4 "Thermal Stresses and Strains in a Finite Cylinder With No Surface Forces," by F. H. Murray, AECD-2966, January, 1945.

5 "Temperature Charts for Induction and Constant-Temperature Heating," by M. P. Heisler, Trans. ASME, vol. 69, 1947, pp. 227–236.

6 "Theory of Elasticity," by S. Timoshenko, McGraw-Hill Book Company, Inc., New York, N. Y., 1934, section 65.

7 "Tafeln uber Abkuhlungsvorgange Einfachen Korper," by Hans Bachmann, Julius Springer, Berlin, Germany, 1938.

8 "Einfuhrung in die Lehre von der Warmeubertragung," by H. Groeber, Julius Springer, Berlin, Germany, 1926.

9 "Heat Conduction in Solids," by H. S. Carslaw and J. C. Jaeger, Oxford University Press, London, England, 1947.

10 "Two Dimensional Diffusion Problems," by S. Goldstein, Proceedings of the London Mathematical Society, vol. 34, 1932, p. 51. "Application of Heaviside's Operational Method to Problems in Heat Conduction," Zeitschrift für Angewandte Mathematik und Mechanik, vol. 12, 1932, p. 234.

11 "A Mathematical Analysis of a Number of Dielectric Heating Problems," by M. P. Heisler, Advance paper 48—S-9, presented at the ASME Spring Meeting, March, 1948.

12 "Temperature Charts for Heating With Internal Heat Sources," by V. Paschkis and M. P. Heisler, Paper No. 49—F-26, presented at the ASME Fall Meeting, September, 1949.

13 "Temperature of and Stresses in Cylindrical Fuel Elements During Pile Flashes," by M. Clark, BNL-86, October, 1950.

14 "On Thermal Stresses, Strains, and Warping," by F. H. Murray and G. Young, AECD-2960, May, 1944.

15 "Thermal Stresses in Hollow Cylinders," by R. Williamson and G. Young, CP-249, September, 1942.

16 "Thermal Stresses and Strains in a Finite Cylinder With No Surface Forces," by F. H. Murray, AECD-2966, January, 1945.

17 "Temperature and Thermal Stresses in Pile Fuel Rods," by C. A. Hutchinson, CP-3493.

18 "Stresses in Long, Thin-Walled Cylinders Due to an Axial Temperature Gradient," by G. Horvay and W. P. Manger, KAPL-390, August, 1950.

19 "Numerical Method for Stress Analysis of Stiffened Shell Structures Under Non-Uniform Temperature Distributions," by R. Heldenfels, NACA-TN-2241, November, 1950.

20 "The Effect of Non-Uniform Temperature Distributions on the Stresses and Distortions of Stiffened-Shell Structures," by R. Heldenfels, NACA-TN-2240, November, 1950.

21 "Preliminary Research Report; an Experimental Investigation of Thermal Stresses in Reactor Materials," by S. Miller, J. Draghic, and W. J. Koshuba, NEPA-1653, October, 1950.

22 "Thermal Stresses in Plates," by J. L. Maulbetsch, JOURNAL OF APPLIED MECHANICS, Trans. ASME, vol. 57, 1935, pp. A-141–146.

23 "Thermal Stress in Power Producing Elements," by A. S. Thompson, NAA-SR-17.

Appendix

PROOF THAT $X_2 = \int_0^N X_1 dN$

The demonstration follows from the fact that

$$T_2 = \int_0^N T_1 dN \quad \text{[53]}$$

To prove Equation [53] we go back to the partial differential equations for one-dimensional heat flow in a slab facing a constant-temperature ambient. The equations are

$$\left.\begin{aligned} \frac{\partial^2 T_1}{\partial x^2} &= \frac{\partial T_1}{\partial N} \\ \frac{\partial T_1}{\partial n} &= 0, \quad (n = 0) \\ \frac{\partial T_1}{\partial n} &= \frac{1 - T_1}{m}, \quad (n = 1) \\ T_1(n, 0) &= 0 \end{aligned}\right\} \quad \text{[54]}$$

Integrate Equations [54] between zero and N. Since, in this case, interchanging order of differentiation and integration is permissible, we get

$$\left.\begin{aligned} \frac{\partial^2}{\partial x^2}\int_0^N T_1\, dN &= \int_0^N \frac{\partial T_1}{\partial N}\, dN = T_1(n,N) - T_1(n,0) \\ \frac{\partial}{\partial n}\int_0^N T_1\, dN &= 0, (n = 0) \\ \frac{\partial}{\partial n}\int_0^N T_1\, dN &= \frac{N - \int_0^N T_1\, dN}{m}, \quad (n = 1) \end{aligned}\right\} \quad \text{[55]}$$

which by virtue of Equations [53] and [54] is equivalent to

$$\left.\begin{aligned} \frac{\partial^2 T_2}{\partial x^2} &= \frac{\partial T_2}{\partial N} \\ \frac{\partial T_2}{\partial n} &= 0, \quad (n = 0) \\ \frac{\partial T_2}{\partial n} &= \frac{N - T_2}{m}, \quad (n = 1) \end{aligned}\right\} \quad \text{[56]}$$

Note that $T_1(n, 0) = 0$ by definition and Equation [53] is equivalent to

$$\frac{\partial T_2}{\partial N} = T_1(n, N)$$

But Equations [56] constitute the set of partial differential equations which characterizes heat flow in a slab facing an ambient varying uniformly with time. Hence T_2 is the dimensionless temperature ratio corresponding to a uniformly varying ambient.

To establish that

$$X_2 = \int_0^N X_1 dN \quad \text{[57]}$$

we merely integrate

$$X_1 = \int_0^1 T_1 dn - T_1$$

between 0 and N, interchange the order of integration—this is permissible because of continuity of the functions involved—and obtain

$$\int_0^N X_1 dN = \int^1 \left(\int_0^N T_1\, dN\right) dn - \int^N T_1\, dN \quad \text{[58]}$$

which, by Equation [53] can be written

$$\int_0^N X_1\, dN = \int_0^1 T_2\, dn - T_2 = X_2 \quad \text{[59]}$$

PROOF THAT $X_2 = -X_3$

It is obvious that once we establish Equation [12] the proof will follow from the temperature-stress Equation [2], since N no longer appears in the stress equation.

To establish Equation [12] substitute

$$T_2 = N - T_3 \quad \text{[60]}$$

into Equations [56]. By performing the indicated differentiations, we obtain

$$\left.\begin{aligned} \frac{\partial^2 T_3}{\partial n^2} + 1 &= \frac{\partial T_3}{\partial N} \\ \frac{\partial T_3}{\partial n} &= 0, \text{ for } n = 0 \\ -\frac{\partial T_3}{\partial n} &= \frac{T_3}{m}, \text{ for } n = 1 \end{aligned}\right\} \quad \text{[61]}$$

Equations [61] are obviously the set of PDE's which characterizes a slab having internal heat generation and losing heat to an ambient at zero temperature. Hence, inserting Equation [60] into Equation [2] we obtain

$$X_3 = -\int_0^1 T_3 dn + T_3 = -X_4$$

The Shearing of a Rectangular Block Between Rough Plates

By J. W. CRAGGS,[1] DUNDEE, SCOTLAND

In a recently published paper, W. T. Read[2] gives an approximate solution of a problem in elasticity which occurs in the testing of materials. This is the problem of determining the stresses in a rectangular block when a pair of opposite faces are mutually displaced in the direction of an edge. The conditions are not those of uniform shear, for that would imply shear stresses on the free faces of the block. In the present paper an analytical solution of the same problem is obtained and the results are compared for a particular case. The method used is a particular case of the general method described by G. Pickett.[3]

Statement of Problem

CONSIDER an infinitely long bar of material, of rectangular cross section, the faces being the planes $x = \pm a$, $y = \pm b$. Let the faces $y = b$, $y = -b$ be displaced relatively to each other in the x-direction by an amount corresponding to a state of uniform shear of unit magnitude. Such a state of shear would imply unit shear stress on the faces $x = \pm a$, but under the conditions of the problem these faces are to be free from stress. The final stress distribution is therefore the sum of a uniform unit shear and a correction state, determined by the boundary conditions of zero displacement at $y = \pm b$ with zero normal stress, and applied shear minus 1 at $x = \pm a$. It is required, then to find the plane strain-stress distribution in the region $-a < x < a$, $-b < y < b$, subject to these boundary conditions.

The Analytical Solution

Define an Airy stress function χ, in the usual way, then the equation for χ is

$$\nabla^4\chi = 0 \quad \ldots\ldots [1]$$

where ∇^2 is Laplace's operator in two dimensions, and the boundary conditions on $x = \pm a$ are

$$\chi_{yy} = 0, \quad \chi_{xy} = -1, \quad -b < y < b \quad \ldots\ldots [2]$$

Write

$$\chi = \sum_{n=0}^{\infty} \sin\frac{(2n+1)\pi y}{2b}\left[A_n \sinh\frac{(2n+1)\pi x}{2b} + \frac{(2n+1)\pi x}{2b} B_n \cosh\frac{(2n+1)\pi x}{2b}\right] + \sum_{m=0}^{\infty} \sin\frac{m\pi x}{a}\left(C_m \sinh\frac{m\pi y}{a} + \frac{m\pi y}{a} D_m \cosh\frac{m\pi y}{a}\right) \quad \ldots\ldots [3]$$

then

$$\nabla^2\chi = 2\sum_{n=0}^{\infty} N^2 B_n \sin Ny \sinh Nx + 2\sum_{m=0}^{\infty} M^2 D_m \sin Mx \sinh My \quad \ldots\ldots [4]$$

where $N = (2n+1)\pi/(2b)$, $M = m\pi/a$

Now choose

$$\frac{\partial\xi}{\partial x} = \frac{\partial\eta}{\partial y} = (1-\nu)\nabla^2\chi$$

where ν is Poisson's ratio. Then

$$\xi = 2(1-\nu)\sum_n NB_n \sin Ny \cosh Nx - 2(1-\nu)\sum_m MD_m \cos Mx \sinh My$$

$$\eta = -2(1-\nu)\sum_n NB_n \cos Ny \sinh Nx + 2(1-\nu)\sum_m MD_m \sin Mx \cosh My$$

But[4]

$$\frac{Eu}{1+\nu} = \xi - \frac{\partial\chi}{\partial x}, \quad \frac{Ev}{1+\nu} = \eta - \frac{\partial\chi}{\partial y}$$

so

$$\frac{Eu}{1+\nu} = \sum_n \{[(1-2\nu)B_n - A_n]\cosh Nx - NxB_n \sinh Nx\} N \sin Ny - \sum_m \{[2(1-\nu)D_m + C_m]\sinh My + MyD_m \cosh My\} M \cos Mx \quad \ldots\ldots [5]$$

and

$$\frac{Ev}{1+\nu} = -\sum_n \{[2(1-\nu)B_n + A_n]\sinh Nx + NxB_n \cosh Nx\} N \cos Ny + \sum_m \{[(1-2\nu)D_m - C_m]\cosh My - MyD_m \sinh My\} M \sin Mx \quad \ldots\ldots [6]$$

The first Equation [2] gives

---

[1] Mathematics Department, University College.

[2] "Effect of Stress-Free Edges in Plane Shear of a Flat Body," by W. T. Read, JOURNAL OF APPLIED MECHANICS, Trans. ASME, vol. 72, 1950, pp. 349–352.

[3] "Application of the Pourifer Method to the Solution of Certain Boundary Problems in the Theory of Elasticity," by G. Pickett, JOURNAL OF APPLIED MECHANICS, Trans. ASME, vol. 66, 1944, p. A-176.

Presented at the National Conference of the Applied Mechanical Division, Minneapolis, Minn., June 18–20, 1953, of THE AMERICAN SOCIETY OF MECHANICAL ENGINEERS.

Discussion of this paper should be addressed to the Secretary, ASME, 29 West 39th Street, New York, N. Y., and will be accepted until July 10, 1953, for publication at a later date. Discussion received after the closing date will be returned.

NOTE: Statements and opinions advanced in papers are to be understood as individual expressions of their authors and not those of the Society. Manuscript received by ASME Applied Mechanics Division, November 19, 1951. Paper No. 53—APM-1.

[4] "Treatise on the Mathematical Theory of Elasticity," by A. E. H. Love, fourth edition, Cambridge University Press, Cambridge, England, 1927, p. 205.

$$-\sum_{n=0}^{\infty} N^2 \sin Ny(A_n \sinh Na + NaB_n \cosh Na) = 0$$

which is satisfied by

$$A_n = -Na \coth NaB_n \quad \ldots\ldots\ldots\ldots\ldots [7]$$

The condition $v = 0$, at $y = \pm b$ implies similarly that

$$C_m = (1-2\nu)D_m - MbD_m \tanh Mb \quad \ldots\ldots\ldots [8]$$

On $y = \pm b$, u also vanishes identically, so

$$\sum_{n=0}^{\infty} N(-)^n \{[(1-2\nu)B_n - A_n] \cosh Nx - NxB_n \sinh Nx\}$$
$$= \sum_{m=0}^{\infty} M \cos Mx \{[2(1-\nu)D_m + C_m]\sinh Mb + MbD_m \cosh Mb\} \ldots [9]$$

Inversion of the Fourier series, and substitution from Equations [7] and [8] leads to

$$a(-)^m MD_m[(3-4\nu)\sinh Mb + Mb \operatorname{sech} Mb]$$
$$= 4\sum_{n=0}^{\infty} (-)^n N^2 P_{n,m} B_n \sinh Na, \; m \neq 0 \ldots [10]$$

and

$$\lim_{m\to 0} aMD_m [(3-4\nu)\sinh Mb + Mb \operatorname{sech} Mb]$$
$$= 2\sum_{n=0}^{\infty} (-)^n N^2 P_{n,0} B_n \sinh Na \quad \ldots\ldots\ldots\ldots [10a]$$

where

$$P_{n,m} = \frac{(1-\nu)N^2 - \nu M^2}{(M^2+N^2)^2}$$

Finally the second Equation [2] implies

$$1 = \sum_{n=0}^{\infty} N^2 \cos Ny[(A_n + B_n)\cosh Na + Na \sinh Na]$$
$$+ \sum_{m=0}^{\infty} M^2(-)^m [(C_m + D_m)\cosh My + MyD_m \sinh My]$$

which leads to

$$(-)^n N^2 B_n(\cosh Na - Na \operatorname{cosech} Na)$$
$$= 2/Nb - 4/b \sum_{m=0}^{\infty} (-)^m M^2 N D_m P_{n,m} \cosh Mb \ldots [11]$$

Now write

$$\beta_n = (-)^n NB_n(\cosh Na - Na \operatorname{cosech} Na)$$
$$\delta_m = (-)^m MD_m[(3-4\nu)\sinh Mb + Mb \operatorname{sech} Mb]$$

then

$$\beta_n = \frac{2}{bN^2} - \frac{4}{b^2}\sum_{m=0}^{\infty} P_{n,m} \frac{Mb \cosh Mb}{(3-4\nu)\sinh Mb + Mb \operatorname{sech} Mb}\delta_m \ldots [12]$$

and

$$\delta_m = \frac{4}{a^2}\sum_{n=0}^{\infty} P_{n,m} \frac{Na \sinh Na}{\cosh Na - Na \operatorname{cosech} Na}\beta_n, \; m \neq 0 \quad \ldots [13]$$

with

$$\delta_0 = \frac{2}{a^2}\sum_{n=0}^{\infty} P_{n,0} \frac{Na \sinh Na}{\cosh Na - Na \operatorname{cosech} Na}\beta_n \ldots [13a]$$

It is easy to show that the two infinite sets of equations have a solution with $\beta_n = 0(1/N^2)$ and $\delta_m = 0(1/M^2)$ as n and m, respectively, tend to infinity, and that the series in the equations are then all convergent.

Next consider the convergence of the solution

$$\chi = \sum_{n=0}^{\infty} \frac{\sin Ny(x\cosh Nx - a \coth Na \sinh Nx)(-)^n}{\cosh Na - Na \operatorname{cosech} Na}\beta_n + \sum_{m=0}^{\infty} \frac{\sin Mx\{[(1-2\nu) - Mb\tanh Mb]\sinh My + My\cosh My\}(-)^m}{M(3-4\nu)\sinh Mb + Mb \operatorname{sech} Mb}\delta_m$$

Both series, and all their first and second partial derivatives with respect to x and y, are convergent except at $x = \pm a$, $y = \pm b$.

Therefore the stress components may be computed everywhere except at the corners, where there are singularities. A discussion of this type of singularity has been given by M. Knein.[5]

For the purpose of computation, it is sufficient to keep a small number of terms in the series of Equation [3]. A measure of the accuracy of the results is then given by the closeness of the approximation to the boundary conditions, when the finite series is used.

Numerical Results

The solution has been computed for $a = 2b$, with $\nu = 1/3$. Five terms were retained in each of the infinite series, and the values of the coefficients were then

$\beta_0 = 0.671$, $\beta_1 = 0.0689$, $\beta_2 = 0.0351$, $\beta_3 = 0.0206$, $\beta_4 = 0.0137$

$\delta_0 = 0.307$, $\delta_1 = 0.0970$, $\delta_2 = -0.0089$, $\delta_3 = -0.0128$, $\delta_4 = -0.0107$

The resulting stress distribution is given in Table 1, which gives σ_{yy}, σ_{xy}, σ_{xx}, respectively, reading downward.

The entries in the penultimate line (shear stress at $x = 2b$) would be all equal to -1 for a correct solution. The accuracy of the solution is, however, rather better than this line indicates, as the series converges more rapidly at points away from the boundaries.

The integral of the shear stress over the boundary $y = b$ is found to be $-4b(0.0153)$, and the accuracy of this figure is about

TABLE 1 STRESS DISTRIBUTION

x/b		$b/4$	$b/2$	$3b/4$	b
0	0.000	0.000	0.000	0.000	0.000
	0.041	0.031	0.007	−0.023	−0.011
	0.000	0.000	0.000	0.000	0.000
$b/2$	0.000	−0.002	−0.010	−0.015	−0.033
	0.044	0.033	0.002	−0.037	−0.133
	0.000	−0.038	−0.063	−0.059	−0.016
	0.000	−0.050	−0.091	−0.112	−0.167
	0.005	−0.003	−0.030	−0.077	−0.140
	0.000	−0.080	−0.146	−0.166	−0.062
$3b/2$	0.000	−0.259	−0.431	−0.574	−0.619
	−0.239	−0.232	−0.217	−0.213	−0.174
	0.000	−0.088	−0.189	−0.263	−0.279
$2b$	0.000	−0.343	−1.270	−1.252	−4.197
	−1.127	−0.965	−0.934	−1.110	−0.176
	0.000	0.000	0.000	0.000	0.000

[5] "Zur Theorie des Druckversuchs," by M. Knein, Abhandlungen an den Aerodynamischen Institut der Technischen Hochschule Aachen, No. 7, 1927, pp. 43–62.

1 per cent. Thus for a block of width-thickness ratio 2, the shear stress required to give a given relative displacement of the surfaces is about 15 per cent less than that calculated on the assumption of uniform shear. This result is almost exactly half way between the limits plotted in Read's paper.[3] Note that the result is correct only for plane strain. For a finite block a correction is needed owing to the fact that the rough plates constrain the lengthwise movement of the specimen. However, the integrated stress over a cross section of constant z is zero in the present solution, so this effect cannot be very large.

The Torsion of Spiral Rods

By H. ŌKUBO,[1] SENDAI, JAPAN

The equations of equilibrium with those of compatibility are derived in two-dimensional forms for the present problem. They are simplified in two extreme cases where (1) The angle between the helix and the axis of helix is small, and (2) The angle between the helix and the plane perpendicular to the axis of helix is small. Using them, expressions for stresses are derived in the forms, which contain two arbitrary functions satisfying the Laplace or a similar equation, and the Airy equation, respectively. As an illustration of the procedure, a detailed solution for a coiled helical spring with a circular section is obtained by means of successive approximations.

THE torsion and stretching problems of spiral rods were treated in our earlier papers.[2] The present paper is a continuation of the previous studies. In the previous calculations, the equations of equilibrium expressed in terms of displacements were used, but in this paper the equations of equilibrium expressed in terms of stresses with those of compatibility are used, since they are more convenient for analysis in the case where the angle between the helix and the plane perpendicular to the axis of helix is small.

Equations of Equilibrium

If there are no body forces, the equations of equilibrium can be presented in the forms

$$\left.\begin{aligned} \frac{\partial \sigma_x}{\partial x} + \frac{\partial \tau_{xy}}{\partial y} + \frac{\partial \tau_{zx}}{\partial z} &= 0 \\ \frac{\partial \sigma_y}{\partial y} + \frac{\partial \tau_{yz}}{\partial z} + \frac{\partial \tau_{xy}}{\partial x} &= 0 \\ \frac{\partial \sigma_z}{\partial z} + \frac{\partial \tau_{zx}}{\partial x} + \frac{\partial \tau_{yz}}{\partial y} &= 0 \end{aligned}\right\} \quad \ldots\ldots\ldots\ldots [1]$$

and the six conditions of compatibility are

$$\left.\begin{aligned} (1+\nu)\nabla^2\sigma_x + \frac{\partial^2 \Theta}{\partial x^2} = 0, \quad (1+\nu)\nabla^2\tau_{yz} + \frac{\partial^2 \Theta}{\partial y \partial z} &= 0 \\ (1+\nu)\nabla^2\sigma_y + \frac{\partial^2 \Theta}{\partial y^2} = 0, \quad (1+\nu)\nabla^2\tau_{zx} + \frac{\partial^2 \Theta}{\partial x \partial z} &= 0 \\ (1+\nu)\nabla^2\sigma_z + \frac{\partial^2 \Theta}{\partial z^2} = 0, \quad (1+\nu)\nabla^2\tau_{xy} + \frac{\partial^2 \Theta}{\partial x \partial y} &= 0 \end{aligned}\right\} \quad \ldots [2]$$

where ν is the Poisson ratio, and

$$\nabla^2 = \frac{\partial^2}{\partial x^2} + \frac{\partial^2}{\partial y^2} + \frac{\partial^2}{\partial z^2}, \quad \Theta = \sigma_x + \sigma_y + \sigma_z$$

We shall take the axis of helix as the axis of z, and make the following transformation

$$x + iy = e^{ikz}(x' + iy') \quad \ldots\ldots\ldots\ldots [3]$$

where k is a constant which specifies the inclination of the helix. Assuming that all stresses, referred to the new co-ordinates, are independent of z, we have the equations of equilibrium and the conditions of compatibility in the forms

$$\left.\begin{aligned} \frac{\partial \sigma_x'}{\partial x'} + \frac{\partial \tau_{x'y'}}{\partial y'} + kD(\tau_{x'z}) - k\tau_{y'z} &= 0 \\ \frac{\partial \sigma_{y'}}{\partial y'} + \frac{\partial \tau_{x'y'}}{\partial x'} + kD(\tau_{y'z}) + k\tau_{x'z} &= 0 \\ \frac{\partial \tau_{x'z}}{\partial x'} + \frac{\partial \tau_{y'z}}{\partial y'} + kD(\sigma_z) &= 0 \end{aligned}\right\} \quad \ldots\ldots [4]$$

$$\left.\begin{aligned} &\nabla_1^2\sigma_{x'} + k^2D^2(\sigma_{x'}) - 4k^2D(\tau_{x'y'}) - 2k^2\sigma_{x'} + 2k^2\sigma_{y'} \\ &\qquad + \frac{1}{1+\nu}\frac{\partial^2\Theta}{\partial x'^2} = 0 \\ &\nabla_1^2\sigma_{y'} + k^2D^2(\sigma_{y'}) + 4k^2D(\tau_{x'y'}) + 2k^2\sigma_{x'} \\ &\qquad - 2k^2\sigma_{y'} + \frac{1}{1+\nu}\frac{\partial^2\Theta}{\partial y'^2} = 0 \\ &\nabla_1^2\tau_{x'y'} + k^2D^2(\tau_{x'y'}) + 2k^2D(\sigma_{x'}) - 2k^2D(\sigma_{y'}) \\ &\qquad - 4k^2\tau_{x'y'} + \frac{1}{1+\nu}\frac{\partial^2\Theta}{\partial x'\partial y'} = 0 \\ &\nabla_1^2\sigma_z + k^2D^2(\sigma_z) + \frac{k^2}{1+\nu}D^2(\Theta) = 0 \\ &\nabla_1^2\tau_{y'z} + k^2D^2(\tau_{y'z}) + 2k^2D(\tau_{x'z}) - k^2\tau_{y'z} \\ &\qquad + \frac{k}{1+\nu}\left[D\left(\frac{\partial\Theta}{\partial y'}\right) + \frac{\partial\Theta}{\partial x'}\right] = 0 \\ &\nabla_1^2\tau_{x'z} + k^2D^2(\tau_{x'z}) - 2k^2D(\tau_{y'z}) - k^2\tau_{x'z} \\ &\qquad + \frac{k}{1+\nu}\left[D\left(\frac{\partial\Theta}{\partial x'}\right) - \frac{\partial\Theta}{\partial y'}\right] = 0 \end{aligned}\right\} \quad \ldots [5]$$

where

$$\nabla_1^2 = \frac{\partial^2}{\partial x'^2} + \frac{\partial^2}{\partial y'^2}, \quad D = y'\frac{\partial}{\partial x'} - x'\frac{\partial}{\partial y'}$$

$$D^2 = \left(y'\frac{\partial}{\partial x'} - x'\frac{\partial}{\partial y'}\right)\left(y'\frac{\partial}{\partial x'} - x'\frac{\partial}{\partial y'}\right)$$

The stresses which satisfy the differential Equations [4] and [5] are the functions of x' and y'. Hence, if the boundary conditions be given in forms independent of z, we can reduce the problem to a two-dimensional one.

When the angle between the helix and the axis of z is small, k becomes small, and for torsion all stresses except $\tau_{x'z}$, $\tau_{y'z}$ become small, since these stresses vanish for a straight rod. Hence,

---

[1] Tōhoku University.

[2] "The Torsion and Stretching of Spiral Rods (1)," by H. Ōkubo, *Quarterly of Applied Mathematics*, vol. 9, 1951, p. 263; the second report under the same title is still in press.

Presented at the National Conference of the Applied Mechanics Division, Minneapolis, Minn., June 18–20, 1953, of The American Society of Mechanical Engineers.

Discussion of this paper should be addressed to the Secretary, ASME, 29 West 39th Street, New York, N. Y., and will be accepted until July 10, 1953, for publication at a later date. Discussion received after the closing date will be returned.

Note: Statements and opinions advanced in papers are to be understood as individual expressions of their authors and not those of the Society. Manuscript received by ASME Applied Mechanics Division, July 29, 1952. Paper No. 53—APM-2.

if we neglect small quantities of the second order, Equations [4] and [5] reduce to

$$\left.\begin{aligned} \frac{\partial \sigma_{x'}}{\partial x'} + \frac{\partial \tau_{x'y'}}{\partial y'} + kD(\tau_{x'z}) - k\tau_{y'z} &= 0 \\ \frac{\partial \sigma_{y'}}{\partial y'} + \frac{\partial \tau_{x'y'}}{\partial x'} + kD(\tau_{y'z}) + k\tau_{x'z} &= 0 \\ \frac{\partial \tau_{x'z}}{\partial x'} + \frac{\partial \tau_{y'z}}{\partial y'} &= 0 \end{aligned}\right\} \quad \cdots\cdots [6]$$

$$\left.\begin{aligned} \nabla_1^2\sigma_{x'} + \frac{1}{1+\nu}\frac{\partial^2\Theta}{\partial x'^2} &= 0 \\ \nabla_1^2\sigma_{y'} + \frac{1}{1+\nu}\frac{\partial^2\Theta}{\partial y'^2} &= 0 \\ \nabla_1^2\tau_{x'y'} + \frac{1}{1+\nu}\frac{\partial^2\Theta}{\partial x'\partial y'} &= 0 \\ \nabla_1^2\sigma_z &= 0 \\ \nabla_1^2\tau_{y'z} = \nabla_1^2\tau_{x'z} &= 0 \end{aligned}\right\} \quad \cdots\cdots [7]$$

The third Equation [6] with the last Equation [7] are the ones for the torsion problem of a straight rod. The remaining equations are the ones for a plane problem. Hence the stresses which satisfy Equations [6] and [7] can be represented in the forms

$$\left.\begin{aligned} \sigma_{x'} &= \frac{\partial^2\phi}{\partial y'^2} - 2Gk(\zeta f + \bar{\zeta}\bar{f}) \\ \sigma_{y'} &= \frac{\partial^2\phi}{\partial x'^2} \\ \sigma_z &= \nu\nabla_1^2\phi + 2Gk(\zeta f + \bar{\zeta}\bar{f}) + C \\ \tau_{x'y'} &= -\frac{\partial^2\phi}{\partial x'\partial y'} - iGk(\zeta f - \bar{\zeta}\bar{f}) \\ \tau_{x'z} &= G[i(f - \bar{f}) - \alpha y'] \\ \tau_{y'z} &= -G[f + \bar{f} - \alpha x'] \end{aligned}\right\} \quad \cdots\cdots [8]$$

where G is the modulus of rigidity, C, α are constants, and

$$\nabla_1^4\phi = 0, f = f(\zeta), \bar{f} = \bar{f}(\bar{\zeta}), \zeta = x' + iy', \bar{\zeta} = x' - iy'$$

The arbitrary functions ϕ, f, and the unknown constants C, α contained in the expressions of the stresses are determined from

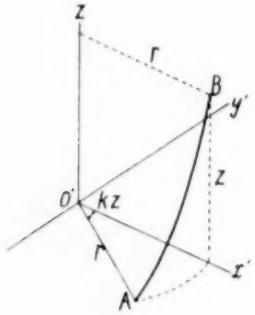

FIG. 1

the boundary conditions by a usual way, if the shape of the section be specified, but as the further analysis is quite similar to that already shown in our previous papers, it will be omitted here.

It is seen from the character of the problem that the stresses at every point on the spiral A-B, Fig. 1, are the same. Hence the expressions for stresses at the points A and B, referred to the cylindrical polar co-ordinates, are the same. Remembering the relation that $\theta = -kz$, let us make the transformation of co-ordinates; then Equations [4] and [5] reduce to

$$\left.\begin{aligned} \frac{\partial \tau_{r\theta}}{\partial r} + \frac{\partial \tau_{\theta z}}{\partial z} + \frac{2}{r}\tau_{r\theta} - \frac{1}{kr}\frac{\partial \sigma_\theta}{\partial z} &= 0 \\ \frac{\partial \sigma_r}{\partial r} + \frac{\partial \tau_{rz}}{\partial z} + \frac{\sigma_r - \sigma_\theta}{r} - \frac{1}{kr}\frac{\partial \tau_{r\theta}}{\partial z} &= 0 \\ \frac{\partial \tau_{rz}}{\partial r} + \frac{\partial \sigma_z}{\partial r} + \frac{\tau_{rz}}{r} - \frac{1}{kr}\frac{\partial \tau_{\theta z}}{\partial z} &= 0 \end{aligned}\right\} \quad \cdots\cdots [9]$$

$$\left.\begin{aligned} &\nabla_1^2\sigma_r + \frac{1}{k^2r^2}\frac{\partial^2\sigma_r}{\partial z^2} - \frac{2}{r^2}(\sigma_r - \sigma_\theta) \\ &\qquad + \frac{4}{kr^2}\frac{\partial \tau_{r\theta}}{\partial z} + \frac{1}{1+\nu}\frac{\partial^2\Theta}{\partial r^2} = 0 \\ &\nabla_1^2\sigma_\theta + \frac{1}{k^2r^2}\frac{\partial^2\sigma_\theta}{\partial z^2} + \frac{2}{r^2}(\sigma_r - \sigma_\theta) - \frac{4}{kr^2}\frac{\partial \tau_{r\theta}}{\partial z} \\ &\qquad + \frac{1}{1+\nu}\left(\frac{1}{k^2r^2}\frac{\partial^2\Theta}{\partial z^2} + \frac{1}{r}\frac{\partial\Theta}{\partial r}\right) = 0 \\ &\nabla_1^2\tau_{r\theta} + \frac{1}{k^2r^2}\frac{\partial^2\tau_{r\theta}}{\partial z^2} - \frac{4}{r^2}\tau_{r\theta} - \frac{2}{kr^2}\left(\frac{\partial \sigma_r}{\partial z} - \frac{\partial \sigma_\theta}{\partial z}\right) \\ &\qquad - \frac{1}{(1+\nu)kr}\left(\frac{\partial^2\Theta}{\partial r\partial z} - \frac{1}{r}\frac{\partial\Theta}{\partial z}\right) = 0 \\ &\nabla_1^2\sigma_z + \frac{1}{k^2r^2}\frac{\partial^2\sigma_z}{\partial z^2} + \frac{1}{1+\nu}\frac{\partial^2\Theta}{\partial z^2} = 0 \\ &\nabla_1^2\tau_{\theta z} + \frac{1}{k^2r}\frac{\partial^2\tau_{\theta z}}{\partial z^2} - \frac{2}{kr^2}\frac{\partial \tau_{rz}}{\partial z} - \frac{1}{r^2}\tau_{\theta z} \\ &\qquad - \frac{1}{(1+\nu)kr}\frac{\partial^2\Theta}{\partial z^2} = 0 \\ &\nabla_1^2\tau_{rz} + \frac{1}{k^2r}\frac{\partial^2\tau_{rz}}{\partial z^2} + \frac{2}{kr^2}\frac{\partial \tau_{\theta z}}{\partial z} - \frac{1}{r^2}\tau_{rz} \\ &\qquad + \frac{1}{(1+\nu)}\frac{\partial^2\Theta}{\partial r\partial z} = 0 \end{aligned}\right\} \quad \cdots [10]$$

where

$$\Theta = \sigma_r + \sigma_\theta + \sigma_z, \quad \nabla_1^2 = \frac{\partial^2}{\partial r^2} + \frac{1}{r}\frac{\partial}{\partial r} + \frac{\partial^2}{\partial z^2}$$

Equations [9] and [10] are two-dimensional ones referred to r and z. When k is small, it is convenient for calculations to specify the shape of the rod by a section perpendicular to the axis of the spiral, but when k is large it becomes favorable to specify the shape of a section cut by an axial plane. Equations [4], [5] become inconvenient in the latter case and Equations [9], [10] are more useful.

When the angle between the helix and the plane perpendicular to the z-axis is small, k is large and all stresses except $\tau_{r\theta}$, $\tau_{\theta z}$ become small, since these stresses vanish in the extreme case where k is infinity.

Neglecting small quantities of the higher order, we have

$$\left.\begin{aligned}
&\frac{\partial \tau_{r\theta}}{\partial r} + \frac{\partial \tau_{\theta z}}{\partial z} + \frac{2}{r}\tau_{r\theta} = 0 \\
&\frac{\partial \sigma_r}{\partial r} + \frac{\partial \tau_{rz}}{\partial z} + \frac{\sigma_r - \sigma_\theta}{r} = \frac{1}{kr}\frac{\partial \tau_{r\theta}}{\partial z} \\
&\frac{\partial \tau_{rz}}{\partial r} + \frac{\partial \sigma_z}{\partial z} + \frac{1}{r}\tau_{rz} = \frac{1}{kr}\frac{\partial \tau_{\theta z}}{\partial z}
\end{aligned}\right\} \quad \ldots\ldots\ldots [11]$$

$$\left.\begin{aligned}
&\nabla_1^2 \tau_{r\theta} - \frac{4}{r^2}\tau_{r\theta} = 0 \\
&\nabla_1^2 \tau_{\theta z} - \frac{1}{r^2}\tau_{\theta z} = 0 \\
&\nabla_1^2 \sigma_r - \frac{2}{r^2}(\sigma_r - \sigma_\theta) + \frac{1}{1+\nu}\frac{\partial^2 \Theta}{\partial r^2} + \frac{4}{kr^2}\frac{\partial \tau_{r\theta}}{\partial z} = 0 \\
&\nabla_1^2 \sigma_\theta + \frac{2}{r^2}(\sigma_r - \sigma_\theta) + \frac{1}{1+\nu}\frac{1}{r}\frac{\partial \Theta}{\partial r} - \frac{4}{kr^2}\frac{\partial \tau_{r\theta}}{\partial z} = 0 \\
&\nabla_1^2 \sigma_z + \frac{1}{1+\nu}\frac{\partial^2 \Theta}{\partial z^2} = 0 \\
&\nabla_1^2 \tau_{rz} - \frac{1}{r^2}\tau_{rz} + \frac{1}{1+\nu}\frac{\partial^2 \Theta}{\partial r \partial z} + \frac{2}{kr^2}\frac{\partial \tau_{\theta z}}{\partial z} = 0
\end{aligned}\right\} \quad \ldots [12]$$

Let us take for the shearing stresses $\tau_{r\theta}, \tau_{\theta z}$ the expressions

$$\tau_{r\theta} = -\frac{1}{r^2}\frac{\partial \phi_1}{\partial z}, \quad \tau_{\theta z} = \frac{1}{r^2}\frac{\partial \phi_1}{\partial r} \quad \ldots\ldots [13]$$

Then, the first Equation [11] and the first and second Equations [12] are satisfied, if ϕ_1 satisfies the equation

$$\frac{\partial^2 \phi_1}{\partial r^2} - \frac{3}{r}\frac{\partial \phi_1}{\partial r} + \frac{\partial^2 \phi_1}{\partial z^2} = C \quad \ldots\ldots [14]$$

in which C is a constant.

Substituting the expressions for the shearing stresses Equations [13], into the remaining Equations [11] and [12], we have six equations for the other stresses. Consider now a stress system

$$\left.\begin{aligned}
\sigma_r^{(0)} &= \frac{1}{kr}\frac{\partial}{\partial r}\left(\frac{1}{r}\frac{\partial \phi_1}{\partial r} + \frac{1}{1-2\nu}\frac{\partial^2 \phi_1}{\partial z^2}\right) \\
&\quad + \frac{2}{kr^2}\frac{\partial}{\partial r}\left(\frac{1}{r}\int\int \frac{\partial \phi_1}{\partial r}\,dz\,dz\right) - \frac{C}{kr^2}\log r \\
\sigma_\theta^{(0)} &= -\frac{1}{kr}\frac{\partial}{\partial r}\left(\frac{1}{r}\frac{\partial \phi_1}{\partial r}\right) \\
&\quad - \frac{2}{kr^2}\frac{\partial}{\partial r}\left(\frac{1}{r}\int\int \frac{\partial \phi_1}{\partial r}\,dz dz\right) + \frac{C}{kr^2}\log r \\
\sigma_z^{(0)} &= \frac{1}{(1-2\nu)kr}\frac{\partial}{\partial r}\left\{\frac{2(1+\nu)}{r}\frac{\partial \phi_1}{\partial r} - \frac{\partial^2 \phi_1}{\partial z^2}\right\} \\
\tau_{rz}^{(0)} &= \frac{1}{(1-2\nu)kr}\frac{\partial^3 \phi_1}{\partial z^3} - \frac{1}{kr^2}\frac{\partial}{\partial r}\left[\frac{2(1+\nu)}{1-2\nu}\frac{\partial \phi_1}{\partial z}\right. \\
&\quad \left. + \frac{1}{r}\int \frac{\partial \phi_1}{\partial r}\,dz\right]
\end{aligned}\right\} \quad \ldots [15]$$

We may show that the stresses, Equations [15], satisfy the remaining six equations. Remembering the relation, Equation [14], we have

$$\frac{\partial \sigma_r^{(0)}}{\partial r} + \frac{\sigma_r^{(0)} - \sigma_\theta^{(0)}}{r} = \frac{1}{(1-2\nu)kr}\frac{\partial^3 \phi_1}{\partial r^2 \partial z^2} + \frac{1}{kr^2}\frac{\partial}{\partial r}\left(\frac{1}{r}\frac{\partial \phi_1}{\partial r}\right) - \frac{1}{kr^2}\frac{\partial^3 \phi_1}{\partial r \partial z^2} - \frac{1}{kr^2}\frac{\partial^2 \phi_1}{\partial z^2}$$

$$\frac{\partial \tau_{rz}^{(0)}}{\partial z} = \frac{1}{(1-2\nu)kr}\frac{\partial^2}{\partial z^2}\left(\frac{\partial^2 \phi_1}{\partial z^2} - \frac{3}{r}\frac{\partial \phi_1}{\partial r}\right) - \frac{1}{kr^2}\frac{\partial}{\partial r}\left(\frac{1}{r}\frac{\partial \phi_1}{\partial r}\right) + \frac{1}{kr^2}\frac{\partial^3 \phi_1}{\partial r \partial z^2}$$

Hence it becomes

$$\frac{\partial \sigma_r^{(0)}}{\partial r} + \frac{\partial \tau_{rz}^{(0)}}{\partial z} + \frac{\sigma_r^{(0)} - \sigma_\theta^{(0)}}{r} = \frac{1}{(1-2\nu)kr}\frac{\partial^2}{\partial z^2}\left(\frac{\partial^2 \phi_1}{\partial r^2} - \frac{3}{r}\frac{\partial \phi_1}{\partial r} + \frac{\partial^2 \phi_1}{\partial z^2}\right) - \frac{1}{kr^2}\frac{\partial^2 \phi_1}{\partial z^2} = -\frac{1}{kr^2}\frac{\partial^3 \phi_1}{\partial z^3} = \frac{1}{kr}\frac{\partial \tau_{rz}}{\partial z}$$

We have thus proved that the stress system satisfies the second Equation [11], and in a similar way we may show that the stress system satisfies the other five equations. Accordingly, we can take for the remaining stresses the expressions

$$\left.\begin{aligned}
\sigma_r &= \sigma_r^{(0)} + \frac{\partial}{\partial z}\left(\nu\nabla_1^2 \phi_2 - \frac{\partial^2 \phi_2}{\partial r^2}\right) \\
\sigma_\theta &= \sigma_\theta^{(0)} + \frac{\partial}{\partial z}\left(\nu\nabla_1^2 \phi_2 - \frac{1}{r}\frac{\partial \phi_2}{\partial r}\right) \\
\sigma_z &= \sigma_z^{(0)} + \frac{\partial}{\partial z}\left\{(2-\nu)\nabla_1^2 \phi_2 - \frac{\partial^2 \phi_2}{\partial z^2}\right\} \\
\tau_{rz} &= \tau_{rz}^{(0)} + \frac{\partial}{\partial r}\left\{(1-\nu)\nabla_1^2 \phi_2 - \frac{\partial^2 \phi_2}{\partial z^2}\right\}
\end{aligned}\right\} \quad \ldots\ldots [16]$$

provided that

$$\nabla_1^2 \nabla_1^2 \phi_2 = 0 \quad \ldots\ldots [17]$$

The expression of the stresses, Equations [13] and [16], is the counterpart of Equations [8] for the extreme case of large k.

If the equation

$$F(r, z) = 0 \quad \ldots\ldots [18]$$

represents the bounding curve of the axial section of the rod, the condition that the surface of the rod is free from traction is

$$\left.\begin{aligned}
&\tau_{r\theta}\frac{\partial F}{\partial r} + \tau_{\theta z}\frac{\partial F}{\partial z} = 0 \\
&\sigma_r \frac{\partial F}{\partial r} + \tau_{rz}\frac{\partial F}{\partial z} - \frac{1}{kr}\tau_{r\theta}\frac{\partial F}{\partial z} = 0 \\
&\tau_{rz}\frac{\partial F}{\partial r} + \sigma_z \frac{\partial F}{\partial z} - \frac{1}{kr}\tau_{\theta z}\frac{\partial F}{\partial z} = 0
\end{aligned}\right\} \quad \ldots\ldots [19]$$

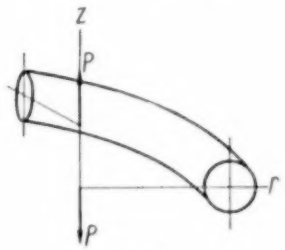

Fig. 2

Consider a spiral rod submitted to a pair of axial forces P, as shown in Fig. 2. Then, the further condition is that the result-

ants of $\tau_{r\theta}$ and σ_θ taken over the section and also the bending moment due to σ_θ vanish, and

$$\int\int \tau_{\theta z} dr dz = P \quad \ldots\ldots\ldots\ldots\ldots\ldots [20]$$

It may be seen from Equations [11], [12], [19], and [20], the shearing stresses $\tau_{r\theta}$, $\tau_{\theta z}$ can be determined quite independently from other stresses, and these shearing stresses are the ones for a ring sector submitted to a pair of axial forces. If these stresses be obtained, substituting them into the remaining Equations [11], [12], and [19], we can reduce the problem to the one for an axially symmetrical stress distribution. The procedure for this case is similar to that for the case of small k, already shown.

Application of Procedure

As an illustration of the procedure, we consider a heavy helical spring with a circular section, taking the helical angle into consideration. We denote the radius and the pitch of the coils by R and s, respectively, and the radius of the wire by a, as is shown in Fig. 3. A case like this has been treated by several previous

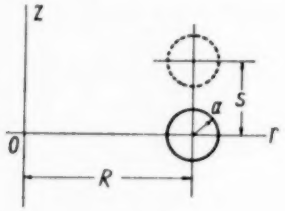

Fig. 3

authors, though they neglected the effect of the helical angle. Those results, however, immediately can be applicable to our calculations. We shall take the approximate solution, worked out by Göhner,[2] and proceed with our further calculations by means of successive approximations similar to his method of approach. The third approximation for the stresses in a ring sector, obtained by him, is

$$\left.\begin{aligned} \tau_{r\theta} &= \frac{2PR}{\pi a^4}\left[\zeta - \frac{5}{4}\frac{\xi\zeta}{R} + \frac{\zeta}{16R^2}(27\xi^2 + 5\zeta^2 - 10a^2)\right] \\ \tau_{\theta z} &= \frac{2PR}{\pi a^4}\left[-\xi + \frac{7\xi^2}{8R} - \frac{3}{8R}(\zeta^2 - a^2)\right. \\ &\qquad \left. - \frac{13}{16}\frac{\xi^3}{R^2} + \frac{9}{16}\frac{\xi\zeta^2}{R^2} - \frac{1}{4}\frac{a^2\xi}{R^2}\right] \end{aligned}\right\} \ldots [21]$$

where $r = R + \xi$, $z = \zeta$.

Substituting the stresses, Equations [21], into Equations [11], [12], and [19], and assuming ξ/R as a small quantity compared to unity, and using the expansions

$$\left.\begin{aligned} \frac{1}{r} &= \frac{1}{R}\left(1 - \frac{\xi}{R} + \frac{\xi^2}{R^2} - \ldots\ldots\right) \\ \frac{1}{r^2} &= \frac{1}{R^2}\left(1 - \frac{2\xi}{R} + \frac{3\xi^2}{R^2} - \ldots\ldots\right) \end{aligned}\right\} \ldots\ldots [22]$$

we shall solve the differential equations by means of successive approximations.

[2] "Schubspannungsverteilung im Querschnitt einer Schraubenfeder," by O. Göhner, *Ingenieur Archiv*, vol. 1, 1930, p. 619.

As a first approximation, we take the equations of equilibrium and the conditions of compatibility in the forms

$$\left.\begin{aligned} &\frac{\partial \sigma_r^{(1)}}{\partial \xi} + \frac{\partial \tau_{rz}^{(1)}}{\partial \zeta} = \frac{2P}{\pi k a^4}, \quad \frac{\partial \tau_{rz}^{(1)}}{\partial \xi} + \frac{\partial \sigma_z^{(1)}}{\partial \zeta} = 0 \\ &\nabla_1^2 \sigma_r^{(1)} + \frac{1}{1+\nu}\frac{\partial^2 \Theta^{(1)}}{\partial \xi^2} = 0, \quad \nabla_1^2 \sigma_\theta^{(1)} = 0 \\ &\nabla_1^2 \sigma_z^{(1)} + \frac{1}{1+\nu}\frac{\partial^2 \Theta^{(1)}}{\partial \zeta^2} = 0, \quad \nabla_1^2 \tau_{rz}^{(1)} \\ &\qquad + \frac{1}{1+\nu}\frac{\partial^2 \Theta^{(1)}}{\partial \xi \partial \zeta} = 0 \end{aligned}\right\} \ldots [23]$$

with the condition that

$$\xi \sigma_r^{(1)} + \zeta \tau_{rz}^{(1)} - \frac{2P}{\pi k a^4}\zeta^2 = 0,$$

$$\xi \tau_{rz}^{(1)} + \zeta \sigma_z^{(1)} + \frac{2P}{\pi k a^4}\xi\zeta = 0 \ldots [24]$$

on the bounding circle $\xi^2 + \zeta^2 = a^2$, in which

$$\nabla_1^2 = \frac{\partial^2}{\partial \xi^2} + \frac{\partial^2}{\partial \zeta^2}, \quad \Theta^{(n)} = \sigma_r^{(n)} + \sigma_\theta^{(n)} + \sigma_z^{(n)}, \quad n = 1, 2, \ldots .$$

As a first approximation, we take the stresses

$$\sigma_r^{(1)} = \sigma_\theta^{(1)} = 0, \quad \tau_{rz}^{(1)} = \frac{2P}{\pi k a^4}\zeta, \quad \sigma_z^{(1)} = -\frac{4P}{\pi k a^4}\xi \ldots [25]$$

which satisfy Equations [23] with the boundary condition, Equations [24].

To get the second approximation, we shall find a stress system which satisfies the equations

$$\left.\begin{aligned} &\frac{\partial \sigma_r^{(2)}}{\partial \xi} + \frac{\partial \tau_{rz}^{(2)}}{\partial \zeta} + \frac{1}{R}(\sigma_r^{(1)} - \sigma_\theta^{(1)}) + \frac{9P\xi}{2\pi k a^4 R} = 0 \\ &\frac{\partial \tau_{rz}^{(2)}}{\partial \xi} + \frac{\partial \sigma_z^{(2)}}{\partial \zeta} + \frac{1}{R}\tau_{rz}^{(1)} + \frac{3P\zeta}{2\pi k a^4 R} = 0 \\ &\nabla_1^2 \sigma_r^{(2)} + \frac{1}{1+\nu}\frac{\partial^2 \Theta^{(2)}}{\partial \xi^2} + \frac{1}{R}\frac{\partial \sigma_r^{(1)}}{\partial \xi} + \frac{8P}{\pi k a^4 R} = 0 \\ &\nabla_1^2 \sigma_\theta^{(2)} + \frac{1}{R}\frac{\partial \sigma_\theta^{(1)}}{\partial \xi} + \frac{1}{(1+\nu)R}\frac{\partial \Theta^{(1)}}{\partial \xi} - \frac{8P}{\pi k a^4 R} = 0 \\ &\nabla_1^2 \sigma_z^{(2)} + \frac{1}{1+\nu}\frac{\partial^2 \Theta^{(2)}}{\partial \zeta^2} + \frac{1}{R}\frac{\partial \sigma_z^{(1)}}{\partial \xi} = 0 \\ &\nabla_1^2 \tau_{rz}^{(2)} + \frac{1}{1+\nu}\frac{\partial^2 \Theta^{(2)}}{\partial \xi \partial \zeta} + \frac{1}{R}\frac{\partial \tau_{rz}^{(1)}}{\partial \xi} = 0 \end{aligned}\right\} \ldots [26]$$

and also the boundary condition

$$\left.\begin{aligned} &\xi \sigma_r^{(2)} + \zeta \tau_{rz}^{(2)} + \frac{9P\xi\zeta^2}{2\pi k a^4 R} = 0 \\ &\xi \tau_{rz}^{(2)} + \zeta \sigma_z^{(2)} - \frac{P\zeta}{4\pi k a^4 R}(15\xi^2 - 3\zeta^2 + 3a^2) = 0 \end{aligned}\right\} \ldots [27]$$

Substituting the stresses for the first approximation into Equations [26], and remembering the condition that the resultant of σ_θ taken over the section vanishes, we have a stress system satisfying the differential Equations [26] with the boundary condition Equations [27], as

$$\left.\begin{aligned}
\sigma_r^{(2)} &= -\frac{P}{4\pi ka^4R(1+\nu)}\left[(7+6\nu)\xi^2\right.\\
&\qquad\left.+(21+18\nu)\zeta^2-(7+6\nu)a^2\right]\\
\sigma_\theta^{(2)} &= \frac{P}{2\pi ka^4R(1+\nu)}\left[(1+3\nu+4\nu^2)\xi^2\right.\\
&\qquad\left.+(11+5\nu-4\nu^2)\zeta^2-(3+2\nu)a^2\right]\\
\sigma_z^{(2)} &= \frac{P}{4\pi ka^4R(1+\nu)}\left[(17+20\nu)\xi^2-(5+4\nu)\zeta^2\right.\\
&\qquad\left.+(5+4\nu)a^2\right]\\
\tau_{rz}^{(2)} &= -\frac{P(2+3\nu)}{2\pi ka^4R(1+\nu)}\xi\zeta
\end{aligned}\right\}\quad\ldots[28]$$

For the third approximation, we consider a stress system satisfying the differential equations

$$\left.\begin{aligned}
&\frac{\partial\sigma_r^{(3)}}{\partial\xi}+\frac{\partial\tau_{rz}^{(3)}}{\partial\zeta}+\frac{1}{R}(\sigma_r^{(2)}-\sigma_\theta^{(2)})\\
&\quad-\frac{\xi}{R^2}(\sigma_r^{(1)}-\sigma_\theta^{(1)})=\frac{P}{8\pi ka^4R^2}(63\xi^2+15\zeta^2-10a^2)\\
&\frac{\partial\tau_{rz}^{(3)}}{\partial\xi}+\frac{\partial\sigma_z^{(3)}}{\partial\zeta}+\frac{1}{R}\tau_{rz}^{(2)}-\frac{\xi}{R^2}\tau_{rz}^{(1)}=\frac{15P}{4\pi ka^4R^2}\xi\zeta\\
&\nabla_1^2\sigma_r^{(3)}+\frac{1}{1+\nu}\frac{\partial^2\Theta^{(3)}}{\partial\xi^2}+\frac{1}{R}\frac{\partial\sigma_r^{(2)}}{\partial\xi}-\frac{\xi}{R^2}\frac{\partial\sigma_r^{(1)}}{\partial\xi}\\
&\qquad-\frac{2}{R^2}(\sigma_r^{(1)}-\sigma_\theta^{(1)})-\frac{26P}{\pi ka^4R^2}\xi=0\\
&\nabla_1^2\sigma_\theta^{(3)}+\frac{1}{R}\frac{\partial\sigma_\theta^{(2)}}{\partial\xi}+\frac{1}{(1+\nu)R}\frac{\partial\Theta^{(3)}}{\partial\xi}\\
&\qquad+\frac{2}{R^2}(\sigma_r^{(1)}-\sigma_\theta^{(1)})-\frac{\xi}{R^2}\frac{\partial\sigma_\theta^{(1)}}{\partial\xi}\\
&\qquad-\frac{\xi}{(1+\nu)R^2}\frac{\partial\Theta^{(1)}}{\partial\xi}+\frac{26P}{\pi ka^4R^2}\xi=0\\
&\nabla_1^2\sigma_z^{(3)}+\frac{1}{1+\nu}\frac{\partial^2\Theta^{(3)}}{\partial\zeta^2}+\frac{1}{R}\frac{\partial\sigma_z^{(2)}}{\partial\xi}-\frac{\xi}{R^2}\frac{\partial\sigma_z^{(1)}}{\partial\xi}=0\\
&\nabla_1^2\tau_{rz}^{(3)}+\frac{1}{1+\nu}\frac{\partial^2\Theta^{(3)}}{\partial\xi\partial\zeta}+\frac{1}{R}\frac{\partial\tau_{rz}^{(2)}}{\partial\xi}\\
&\qquad-\frac{\xi}{R^2}\frac{\partial\tau_{rz}^{(1)}}{\partial\xi}-\frac{1}{R^2}\tau_{rz}^{(1)}-\frac{3P}{\pi ka^4R^2}\zeta=0
\end{aligned}\right\}\quad\ldots[29]$$

and the boundary condition

$$\left.\begin{aligned}
&\xi\sigma_r^{(3)}+\zeta\tau_{rz}^{(3)}-\frac{P\zeta^2}{8\pi ka^4R^2}(63\xi^2+5\zeta^2-10a^2)=0\\
&\xi\tau_{rz}^{(3)}+\zeta\sigma_z^{(3)}+\frac{P\xi\zeta}{8\pi ka^4R^2}(43\xi^2-15\zeta^2+10a^2)=0
\end{aligned}\right\}\quad\ldots[30]$$

Substituting the stresses, Equations [25] and [28] into [29], and integrating the differential equations, we have a third stress system. The stress system, satisfying the boundary condition, Equations [30], with the condition that the bending moment due to σ_θ vanishes, becomes

$$\left.\begin{aligned}
\sigma_r^{(3)} &= \frac{P\xi}{6\pi ka^4R^2(1+\nu)}\left[(20+21\nu+4\nu^2)(\xi^2-a^2)\right.\\
&\qquad\left.+6(11+10\nu)\zeta^2\right]\\
\sigma_\theta^{(3)} &= -\frac{P\xi}{6\pi ka^4R^2(1+\nu)}\left[(11+17\nu+16\nu^2\right.\\
&\qquad+4\nu^3)\xi^2+6(13+8\nu-6\nu^2-2\nu^3)\zeta^2\\
&\qquad\left.-\frac{a^2}{2}(37+33\nu+4\nu^2)\right]\\
\sigma_z^{(3)} &= -\frac{P\xi}{12\pi ka^4R^2(1+\nu)}\left[(43+57\nu+8\nu^2)\xi^2\right.\\
&\qquad\left.-39(1+\nu)\zeta^2+24(1+\nu)a^2\right]\\
\tau_{rz}^{(3)} &= \frac{P\zeta}{24\pi ka^4R^2(1+\nu)}\left[3(1+3\nu)\xi^2\right.\\
&\qquad\left.+(13-9\nu-16\nu^2)\zeta^2-2(14+3\nu-8\nu^2)a^2\right]
\end{aligned}\right\}\quad\ldots[31]$$

By using the stress systems in Equations [25], [28], and [31], we can find the stresses for the third approximation, from the relation that

$$\left.\begin{aligned}
&\sigma_r=\sigma_r^{(1)}+\sigma_r^{(2)}+\sigma_r^{(3)},\quad \sigma_\theta=\sigma_\theta^{(1)}+\sigma_\theta^{(2)}+\sigma_\theta^{(3)}\\
&\sigma_z=\sigma_r^{(1)}+\sigma_z^{(2)}+\sigma_z^{(3)},\quad \tau_{rz}=\tau_{rz}^{(1)}+\tau_{rz}^{(2)}+\tau_{rz}^{(3)}
\end{aligned}\right\}\quad\ldots[32]$$

Among the stresses, Equations [32], σ_z and τ_{rz} are predominating, and they are

$$\left.\begin{aligned}
\sigma_z &= -\frac{2P}{\pi ka^4}\left[\left(2+\frac{a^2}{R^2}\right)\xi-\frac{17+20\nu}{8(1+\nu)}\frac{\xi^2}{R}\right.\\
&\qquad-\frac{5+4\nu}{8(1+\nu)}\frac{a^2-\zeta^2}{R}+\frac{43+57\nu+8\nu^2}{24(1+\nu)}\frac{\xi^3}{R^2}\\
&\qquad\left.-\frac{13}{8}\frac{\xi\zeta^2}{R^3}\right]\\
\tau_{rz} &= \frac{2P}{\pi ka^4}\left[\left(1-\frac{(14+3\nu-8\nu^2)a^2}{24(1+\nu)R^2}\right)\zeta\right.\\
&\qquad-\frac{2+3\nu}{4(1+\nu)}\frac{\xi\zeta}{R}+\frac{1+3\nu}{16(1+\nu)}\frac{\xi^2\zeta}{R^2}\\
&\qquad\left.+\frac{13-9\nu-16\nu^2}{48(1+\nu)}\frac{\zeta^3}{R^3}\right]
\end{aligned}\right\}\quad\ldots[33]$$

For $R=5a$, the stresses σ_z and τ_{rz} on the axes of ξ and ζ are calculated from Equations [33], and are shown in Figs. 4 and 5, ν being assumed as 0.3. The normal stress σ_z attains its maximum at the inner end of the horizontal diameter ($\xi=-a$, $\zeta=0$), the amount of which is

$$(\sigma_z)_{\max}=\frac{Ps}{\pi^2a^2}\left\{2+\frac{11+12\nu}{4(1+\nu)}\frac{a}{R}+\frac{67+81\nu+8\nu^2}{24(1+\nu)}\frac{a^2}{R^2}\right\}\quad\ldots[34]$$

The shearing stress τ_{rz} attains its maximum amount of

$$(\tau_{rz})_{\max}=\frac{Ps}{\pi^2a^2}\left(1-\frac{5}{16}\frac{a^2}{R^2}\right)\quad\ldots[35]$$

at both ends of the vertical diameter ($\xi=0$, $\zeta=\pm a$).

The greatest stress occurring in the rod is the shearing stress $\tau_{\theta z}$ at the inner end of the horizontal diameter where σ_z becomes maximum. From Equation [21] it becomes

$$(\tau_{\theta z})_{\max}=\frac{2PR}{\pi a^2}\left(1+\frac{5}{4}\frac{a}{R}+\frac{17}{16}\frac{a^2}{R^2}\right)\quad\ldots[36]$$

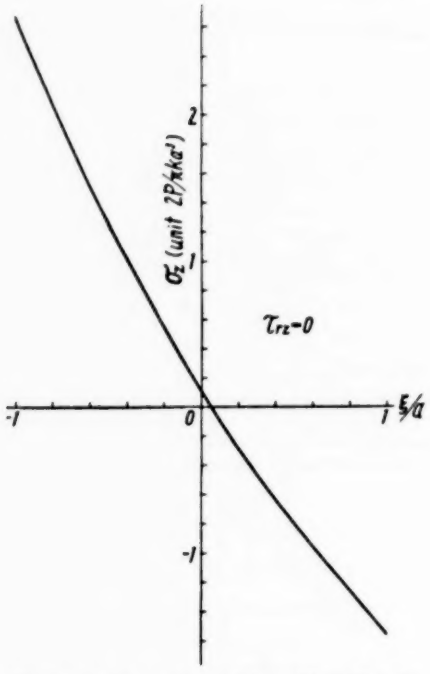

FIG. 4 σ_z AND τ_{rz} ON THE ξ-AXIS, WHEN $R = 5a$

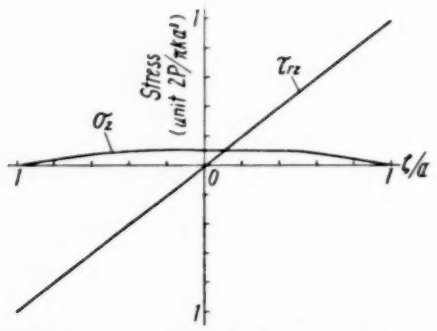

FIG. 5 σ_z AND τ_{rz} ON THE ζ-AXIS, WHEN $R = 5a$

The maximum values of σ_z and τ_{rz}, calculated from Equations [34] and [35], for several values of a/R, are shown in Table 1, s being assumed as $3a$. For convenience of comparison, the corresponding values of the greatest stress are also given in the same table (unit $2P/\pi a^2$)

TABLE 1 MAXIMUM VALUES OF σ_z, τ_{rz}, AND $\tau_{\theta\theta}$

R/a	4	5	6	8
$(\sigma_z)_{max}$	1.38	1.28	1.22	1.14
$(\tau_{rz})_{max}$	0.47	0.47	0.47	0.48
$(\tau_{\theta\theta})_{max}$	5.52	6.46	7.43	9.38

ACKNOWLEDGMENT

A grant for science research has been given for this study by the Education Ministry of Japan.

Reinforced Circular Holes in Bending With Shear[1]

By S. R. HELLER, JR.,[2] WASHINGTON, D. C.

The object of this paper is the determination of the effect of the reinforcement of circular holes on the stress distribution in the webs of beams subjected to bending with shear. A theoretical solution for a bead-type reinforcement, i.e., small radial thickness, is developed. The stress distribution in the web for arbitrary shape reinforcement is based on the work of Reissner and Morduchow (1).[3] The theory developed is valid provided the diameter of the hole does not exceed one fourth of the depth of the beam.

Nomenclature

The following nomenclature is used in the paper:

- A_r = cross-sectional area of reinforcement ring plus adjacent web area
- A = area: with subscript f and w, area of flange (gross) and web, respectively
- C_{mn} = arbitrary constants in stress function φ
- E = modulus of elasticity; with subscripts r and w, of reinforcement and web, respectively
- h = half-height of web
- I = moment of inertia; with subscript r, of the reinforcement about its centroid
- k_{mn} = abbreviations for products of C_{mn} and powers of r_1
- L = distance
- M = bending moment
- m, n = subscripts for orders of terms of stress function
- P = load
- $P_n(r)$, $Q_n(r)$ = coefficients in stress function
- r = radial polar co-ordinate; measured from center of cutout
- r_0 = radial distance from center of cutout to center line of reinforcement
- r_1 = radial distance from center of cutout to outer edge of reinforcement (junction with web)
- r_2 = radial distance from center of cutout to inner edge of reinforcement (edge of hole)
- t = thickness; with subscripts f, r, and w, of flange, reinforcement, and web, respectively.
- x, y = Cartesian co-ordinates with origin at center of cutout, x-axis parallel with flanges
- α = dimensionless parameter of area of reinforcement, $\left(\frac{E_r}{E_w}\right)\left(\frac{A_r}{r_0 t_w}\right) 2(1+\nu)$
- β = dimensionless parameter of moment of inertia of reinforcement: $\left(\frac{E_r}{E_w}\right)\left(\frac{I_r}{r_0^3 t_w}\right) 24(1+\nu)$
- δ = dimensionless parameter of thickness of reinforcement, $\frac{t_r}{2r_0}$
- θ = angular polar co-ordinate; measured from y-axis clockwise
- λ = dimensionless parameter of flange thickness, t_f/h
- ν = Poisson's ratio
- ρ = dimensionless parameter of shear: $\frac{3}{2(1-\lambda)} - \left(\frac{A_w h^2}{2I}\right)\left(\frac{\omega}{1-\omega}\right)$
- Σ = summation
- σ_L = nominal bending stress at extreme fiber
- σ_x, σ_y = normal stresses in x- and y-directions, respectively
- σ_r, σ_θ = radial and tangential stresses, respectively
- τ = average shear stress, P/A_w
- τ_{xy} = shear stress for Cartesian co-ordinates
- $\tau_{r\theta}$ = shear stress for polar co-ordinates
- φ = stress function for web
- ω = dimensionless parameter of flange area (gross) A_f/A

Introduction

The solution is based on the usual assumptions of plane elasticity; homogeneous, isotropic material within the elastic limit; "small" displacements: and uniform stress across the thickness of the plates with no stress normal to the plane of the plates. A stress function which satisfies the biharmonic equation must also satisfy the boundary conditions:

1 At great distances from the hole, $r \gg r_2$, the stress distribution tends to conform to that of the uncut web.

2 At the inner boundary of the hole, $r = r_2$, there are no external forces.

3 At the junction of the ring and the web, $r = r_1$, the radial and tangential displacements of the ring are equal to those of the web.

4 At the junction of the ring and the web, $r = r_1$, the forces acting at the outer edge of the ring are equal and opposite to those acting at the inner edge of the web.

For arbitrary shape reinforcement, the bending theory for curved bars may be used to determine the stresses in the reinforcement. The solution is predicated on the center of the hole coinciding with the neutral axis of the beam.

Throughout this discussion the orientation of co-ordinates and stresses is as shown in Fig. 1. The geometry and notation for bending with shear are shown in Fig. 2. The two elements of bending with shear on which the analysis is based are shown in Fig. 3. In addition to the usual parameters of stress analysis, a measure of the influence of shear is introduced (2), τ/σ_L, the ratio of nominal shear to nominal bending stresses.

---

[1] Abstracted from the author's Doctoral dissertation submitted to the Department of Naval Architecture and Marine Engineering, Massachusetts Institute of Technology, 1951. Presented at the Eighth International Congress on Theoretical and Applied Mechanics, Istanbul, Turkey, August, 1952.

[2] Lieutenant Commander, U. S. Navy: Hull Design Branch, Bureau of Ships, Navy Department.

[3] Numbers in parentheses refer to the Bibliography at the end of the paper.

Presented at the National Conference of the Applied Mechanics Division, Minneapolis, Minn., June 18–20, 1953, of The American Society of Mechanical Engineers.

Discussion of this paper should be addressed to the Secretary, ASME, 29 West 39th Street, New York, N. Y., and will be accepted until July 10, 1953, for publication at a later date. Discussion received after the closing date will be returned.

Note: Statements and opinions advanced in papers are to be understood as individual expressions of their authors and not those of the Society. Manuscript received by ASME Applied Mechanics Division, September 25, 1953. Paper No. 53—APM-9.

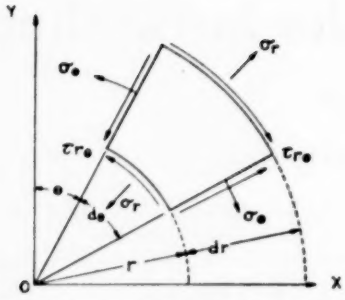

FIG. 1(a) POSITIVE ORIENTATION OF CO-ORDINATES AND STRESSES

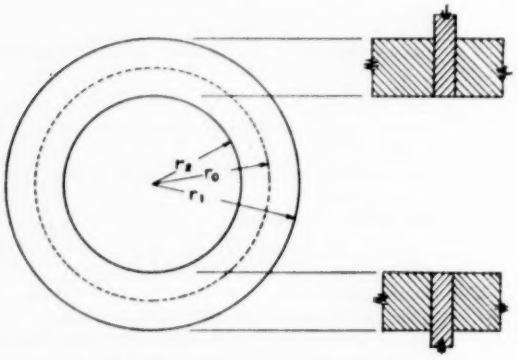

FIG. 1(b) GEOMETRY AND NOTATION OF REINFORCEMENT

From Fig. 2, for the uncut beam at the location of the hole, the usual beam formulas give

$$\text{Nominal shear} = \frac{P}{2ht_w}$$

$$\text{Nominal bending} = \frac{PLh}{I}$$

from which the ratio of nominal shear to nominal bending stresses becomes

$$\frac{\tau}{\sigma_L} = \frac{I}{2h^2Lt_w} \quad \ldots\ldots\ldots\ldots\ldots\ldots\ldots\ldots [1]$$

GENERAL EQUATIONS FOR WEB

Reissner and Morduchow have developed expressions for the cross-sectional properties of the reinforcement in terms of the stress function in the web which are valid for any shape of reinforcement[4]

$$A_r = \left(\frac{r_0 t_w}{S}\right)\left(\frac{E_w}{E_r}\right)\left[\left(\sum_0 P_n' \cos n\theta + \sum_1 Q_n' \sin n\theta\right)_{r=r_1}^{n\neq 1} + \frac{C_2}{t_w}\sin\theta + \frac{C_3}{t_w}\cos\theta\right] \quad [2a]$$

where $S = \sum_0 \cos n\theta \{n^2\nu r_1^{-1}P_n - \nu P_n' + P_n'' r_1 + n^2\delta[\nu P_n' - r_1^{-1}P_n + (n^2-1)\int P_n r^{-2}dr]\}\ r = r_1 + \sum_1 \sin n\theta \{n^2\nu r_1^{-1}Q_n - \nu Q_n' + Q_n'' r_1 + n^2\delta[\nu Q_n' - r_1^{-1}Q_n + (n^2-1)\int Q_n r^{-2}dr]\}\ r = r_1$

[4] Reference (1) equations [7a] and [7b], p. 8.

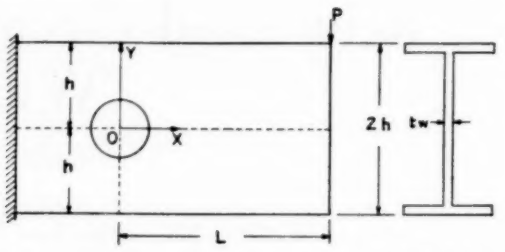

FIG. 2 GEOMETRY AND NOTATION FOR BENDING WITH SHEAR

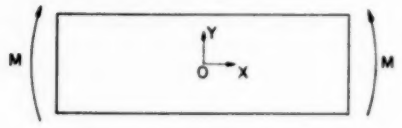

FIG. 3(a) BEAM IN PURE BENDING

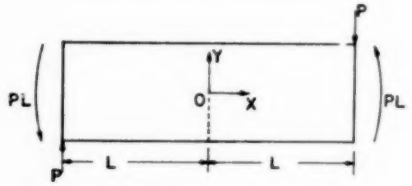

FIG. 3(b) BEAM WITH PURE SHEAR AT Y-AXIS

and

$$I_r = \left(\frac{r_0^3 t_w}{T}\right)\left(\frac{E_w}{E_r}\right)\left\{\left[\sum_0 r_0^{-1}\cos n\theta(r_1 P_n' - [r_0 P_n']_{n\neq 1} - P_n) + \sum_1 r_0^{-1}\sin n\theta(r_1 Q_n' - [r_0 Q_n']_{n\neq 1} - Q_n)\right] r = r_1 + \frac{C_1}{r_0 t_w} - \frac{C_2}{t_w}\sin\theta - \frac{C_3}{t_w}\cos\theta\right\} \quad [2b]$$

where

$T = \sum_0 (n^2-1)\cos n\theta [r_1^{-1}P_n - \nu P_n' - (n^2-1)\int P_n r^{-2}dr]\ r = r_1 + \sum_1 (n^2-1)\sin n\theta\ [r_1^{-1}Q_n - \nu Q_n' - (n^2-1)\int Q_n r^{-2}dr]\ r = r_1$

where prime (′) indicates differentiation with respect to r. These equations satisfy boundary conditions 2, 3, and 4, given previously. Boundary condition 1, of course, must be satisfied by the stress function itself.

Equations [2a] and [2b] are extremely important. Equivalent reinforcement means that the reinforcement prevents any change in the stress distribution in the web from that existing in the uncut beam. Therefore, for any type loading and equivalent reinforcement, P_n and Q_n are given. Thus the substitution of the given P_n and Q_n into Equations [2a] and [2b] gives the distribution of cross-sectional area and moment of inertia of the reinforcement ring required to replace with elastic equivalence that portion of the web that has been cut out. Such a reinforcement is not always of practical dimensions.

Pure Bending

It has been shown[5] that it is practically impossible to design a reinforcement that is the elastic equivalent of the cutout for the case of pure bending, Fig. 3(*a*). Reissner and Morduchow also[6] obtained the solution for pure bending with any reinforcement

$$\left.\begin{aligned}
\sigma_r &= -\frac{Mr}{4I}(\cos\theta - \cos 3\theta) - 2k_{31}\left(\frac{r_1}{r}\right)^3\cos\theta \\
&\quad -\left[12k_{23}\left(\frac{r_1}{r}\right)^5 + 10k_{43}\left(\frac{r_1}{r}\right)^3\right]\cos 3\theta \\
\sigma_\theta &= -\frac{Mr}{4I}(3\cos\theta + \cos 3\theta) + 2k_{31}\left(\frac{r_1}{r}\right)^3\cos\theta \\
&\quad +\left[12k_{23}\left(\frac{r_1}{r}\right)^5 + 2k_{43}\left(\frac{r_1}{r}\right)^3\right]\cos 3\theta \\
\tau_{r\theta} &= -\frac{Mr}{4I}(\sin\theta + \sin 3\theta) - 2k_{31}\left(\frac{r_1}{r}\right)^3\sin\theta \\
&\quad -\left[12k_{23}\left(\frac{r_1}{r}\right)^5 + 6k_{43}\left(\frac{r_1}{r}\right)^3\right]\sin 3\theta
\end{aligned}\right\} \quad \ldots [3]$$

where

$$\left.\begin{aligned}
\frac{k_{31}}{K} &= -3\,\frac{2(1+\delta) - \alpha\left[\frac{3-\nu}{1+\nu} - \frac{1-3\nu}{2(1+\nu)}\,\delta\right]}{\alpha\left(1-\frac{\delta}{2}\right) + 2(1+\delta)} \\
\frac{k_{23}}{K} &= -\frac{1}{D}\left\{\left[1-\alpha\left(1+\frac{9}{2}\delta\right)\right]\left[1+\beta\,\frac{5+\nu}{3(1+\nu)}+2\delta\right]\right. \\
&\quad \left. +(1-\beta-2\delta)\left[\frac{1}{3}+\alpha\,\frac{2+10\nu-9\delta(5+\nu)}{6(1+\nu)}\right]\right\} \\
\frac{k_{43}}{K} &= -\frac{1}{D}\left\{\left[1-\alpha\left(1+\frac{9}{2}\delta\right)\right](1+\beta+4\delta)\right. \\
&\quad \left. +(1-\beta-2\delta)\left[1+\alpha\left(2-\frac{9}{2}\delta\right)\right]\right\} \\
D &= \left[1+\alpha\left(2-\frac{9}{2}\delta\right)\right]\left[1+\beta\,\frac{5+\nu}{3(1+\nu)}+2\delta\right] \\
&\quad -(1+\beta+4\delta)\left[\frac{1}{3}+\alpha\,\frac{2+10\nu-9\delta(5+\nu)}{6(1+\nu)}\right]
\end{aligned}\right\} \quad \ldots [4]$$

$$K = \frac{Mr_1}{24I}$$

In many cases in practice the reinforcing rings are quite narrow; i.e., β and δ are quite small. The constraint stresses then are, with negligible error, functions of the cross-sectional area of the reinforcement alone. Equations [4] for $\nu = 0.3$, become

$$\left.\begin{aligned}
\frac{2k_{31}}{K} &= -6\,\frac{2-2.077\alpha}{2+\alpha}, \qquad \frac{k_{23}}{K} = -\frac{1.333-0.359\alpha}{0.667+1.359\alpha}, \\
\frac{k_{43}}{K} &= \frac{2+\alpha}{0.667+1.359\alpha}
\end{aligned}\right\} \quad \ldots [5]$$

[5] Reference (1), appendix E, pp. 42–43.
[6] Ibid., equations [29], p. 25.

For $\alpha = 0$, i.e., no reinforcement; hole of radius r_1. At $r = r_1$, Equations [3] become

$$\left.\begin{aligned}
(\sigma_r) &= 0 \\
(\sigma_\theta) &= \frac{Mr_1}{I}(\cos\theta + \cos 3\theta) \\
(\tau_{r\theta}) &= 0
\end{aligned}\right\} \quad \ldots [3a]$$

which agrees with the solution given in reference (3).

Bending With Shear

If an I-beam is subjected to bending with shear about an axis perpendicular to the plane of the web, see Fig. 3, the stress distribution can be approximated to a satisfactory degree[7] by

$$\left.\begin{aligned}
\sigma_x &= \frac{P}{I}(L-x)y \\
\sigma_y &= 0 \\
\tau_{xy} &= -\tau\left\{\frac{3}{2(1-\lambda)} - \frac{A_w h^2}{2I}\left[\left(\frac{y}{h}\right)^2 + \frac{\omega}{1-\omega}\right]\right\}_{|y|\le h-t_f} \\
\tau_{xy} &= -\tau\,\frac{A_w h^2}{2I}\left[1-\left(\frac{y}{h}\right)^2\right]_{|y|\ge h-t_f}
\end{aligned}\right\} \quad \ldots [6]$$

for the uncut beam. The stress function corresponding to Equations [6] for the web alone is

$$\varphi = -\frac{P}{6I}xy^3 + \frac{PL}{6I}y^3 + \tau\rho xy \quad \ldots [6a]$$

This is equivalent to the sum of two stress functions

$$\varphi_1 = \frac{PLy^3}{6I}$$

corresponding to pure bending with $M = -PL$ and

$$\varphi_2 = -\frac{P}{6I}xy^3 + \tau\rho xy$$

corresponding to the loading of Fig. 3(*b*). By transformation of φ into polar co-ordinates and substitution into Equations [2*a*] and [2*b*], it is found that it is impossible to provide reinforcement that is the elastic equivalent of the cutout.

To determine the approximate additional stresses, there must be added to the stress function terms from equations [3*b*] of reference (1) with due consideration of boundary condition 1.

Thus for the stresses in the web under bending with shear with a reinforced cutout

$$\left.\begin{aligned}
\varphi_2 &= Q_2\sin 2\theta + Q_4\sin 4\theta \\
Q_2 &= C_{22}r^4 + C_{12}r^2 + C_{22}r^{-2} + C_{42} \\
Q_4 &= C_{14}r^4 + C_{24}r^{-4} + C_{44}r^{-2}
\end{aligned}\right\} \quad \ldots [7]$$

The substitution of Equations [7] into Equations [2*a*] and [2*b*] with subsequent clearing of fractions and equating of coefficients of like trigonometric terms yields the constraint coefficients in terms of which the stresses become

[7] This is based on approximate theory that the web of an I-beam takes most of the shearing force and that the shearing stresses are constant across the web thickness; reference (4), p. 305.

$$\left.\begin{aligned}
\sigma_r &= -\tau\rho \sin 2\theta + \frac{Pr^2}{4I} \sin 4\theta - \left[6k_{22}\left(\frac{r_1}{r}\right)^4 + 4k_{42}\left(\frac{r_1}{r}\right)^2\right] \sin 2\theta - \left[20k_{24}\left(\frac{r_1}{r}\right)^6 + 18k_{44}\left(\frac{r_1}{r}\right)^4\right] \sin 4\theta \\
\sigma_\theta &= -\left(\frac{Pr^2}{2I} - \tau\rho\right) \sin 2\theta - \frac{Pr^2}{4I} \sin 4\theta + 6k_{22}\left(\frac{r_1}{r}\right)^4 \sin 2\theta + \left[20k_{24}\left(\frac{r_1}{r}\right)^6 + 6k_{44}\left(\frac{r_1}{r}\right)^4\right] \sin 4\theta \\
\tau_{r\theta} &= \left(\frac{Pr^2}{4I} - \tau\rho\right) \cos 2\theta + \frac{Pr^2}{4I} \cos 4\theta + \left[6k_{22}\left(\frac{r_1}{r}\right)^4 + 2k_{42}\left(\frac{r_1}{r}\right)^2\right] \cos 2\theta + \left[20k_{24}\left(\frac{r_1}{r}\right)^6 + 12k_{44}\left(\frac{r_1}{r}\right)^4\right] \cos 4\theta
\end{aligned}\right\} \quad \ldots [8]$$

$$\left.\begin{aligned}
\frac{k_{22}}{K} &= \frac{1}{M}\left[\left\{\frac{r_1}{L}\left[4 - 2\alpha\left(\frac{3 + 4\nu\delta}{1 + \nu}\right)\right] + \frac{\tau\rho}{2K}\left[2 - \alpha(1 + 4\delta)\right]\right\}\left[1 + \delta + \frac{\beta}{2(1 + \nu)}\right] + \left\{\frac{r_1}{L}\left[1 - 3\delta - \frac{\beta\nu}{2(1 + \nu)}\right] + \frac{\tau\rho}{2K}\left(1 - \delta - \frac{\beta}{4}\right)\right\}\frac{2\alpha(\nu - 4\delta)}{1 + \nu}\right] \\
\frac{k_{42}}{K} &= -\frac{1}{M}\left[\left\{\frac{r_1}{L}\left[4 - 2\alpha\left(\frac{3 + 4\nu\delta}{1 + \nu}\right)\right] + \frac{\tau\rho}{2K}\left[2 - \alpha(1 + 4\delta)\right]\right\}\left(1 + 3\delta + \frac{\beta}{4}\right) + \left\{\frac{r_1}{L}\left[1 - 3\delta - \frac{\beta\nu}{2(1 + \nu)}\right] + \frac{\tau\rho}{2K}\left(1 - \delta - \frac{\beta}{4}\right)\right\}\left[2 + \alpha(3 - 4\delta)\right]\right] \\
M &= \left[2 + \alpha(3 - 4\delta)\right]\left[1 + \delta + \frac{\beta}{2(1 + \nu)}\right] - \left(1 + 3\delta + \frac{\beta}{4}\right)\left[\frac{2\alpha(\nu - 4\delta)}{1 + \nu}\right] \\
\frac{k_{24}}{K} &= \frac{r_1}{2LN}\left\{\left[4 - 2\alpha(3 + 16\delta)\right]\left[1 + 3\delta + \beta\frac{5(3 + \nu)}{4(1 + \nu)}\right] + \left(1 - 3\delta - \frac{5\beta}{2}\right) \times \left[2 + \alpha\frac{3 + 9\nu - 16\delta\,(3 - \nu)}{1 + \nu}\right]\right\}
\end{aligned}\right\} \quad \ldots [9]$$

$$\left.\begin{aligned}
\frac{k_{44}}{K} &= -\frac{r_1}{2LN}\left\{\left[4 - 2\alpha(3 + 16\delta)\right]\left(1 + 5\delta + \frac{5}{2}\beta\right) + \left(1 - 3\delta - \frac{5}{2}\beta\right)\left[4 + 2\alpha\left(\frac{3 + 5\nu}{1 + \nu} - 16\delta\right)\right]\right\} \\
N &= \left[4 + 2\alpha\left(\frac{3 + 5\nu}{1 + \nu} - 16\delta\right)\right]\left[1 + 3\delta + \beta\frac{5(3 + \nu)}{4(1 + \nu)}\right] - \left(1 + 5\delta + \frac{5}{2}\beta\right)\left[2 + \alpha\frac{3 + 9\nu - 16\delta\,(3 - \nu)}{1 + \nu}\right] \\
K &= -\frac{PLr_1}{24I}
\end{aligned}\right\} \quad \ldots [9] \textit{ (cont.)}$$

When β and δ are negligibly small (see section Pure Bending), the constraint stresses are functions of α alone. Equations [9], for $\nu = 0.3$, become

$$\left.\begin{aligned}
\frac{k_{22}}{K} &= \frac{\frac{r_1}{L}(4 - 4.153\alpha) + \frac{\tau\rho}{K}(1 - 0.269\alpha)}{2 + 2.538\alpha} \\
\frac{k_{42}}{K} &= -\frac{\frac{r_1}{L}(6 - 1.615\alpha) + \frac{\tau\rho}{K}(2 + \alpha)}{2 + 2.538\alpha} \\
\frac{k_{24}}{K} &= \frac{r_1}{2L}\left(\frac{6 - 1.615\alpha}{2 + 2.538\alpha}\right) \\
\frac{k_{44}}{K} &= -\frac{r_1}{2L}\left(\frac{8 - 0.923\alpha}{2 + 2.538\alpha}\right)
\end{aligned}\right\} \quad \ldots [10]$$

For $\alpha = 0$, i.e., no reinforcement; hole of radius r_1. At $r = r_1$, Equations [8] become

$$\left.\begin{aligned}
(\sigma_r) &= 0 \\
(\sigma_\theta) &= \left(4\tau\rho - \frac{Pr_1^2}{I}\right) \sin 2\theta - \frac{Pr_1^2}{I} \sin 4\theta \\
(\tau_{r\theta}) &= 0
\end{aligned}\right\} \quad \ldots [8a]$$

which agrees with the solution given in reference (2).

Furthermore, for $\lambda = \omega = 0$, i.e., a rectangular plate (no flanges), $\rho = 3/2$, Equations [8a] become

$$\left.\begin{aligned}
(\sigma_r) &= 0 \\
(\sigma_\theta) &= \left(6\tau - \frac{Pr_1^2}{I}\right) \sin 2\theta - \frac{Pr_1^2}{I} \sin 4\theta \\
(\tau_{r\theta}) &= 0
\end{aligned}\right\} \quad \ldots [8b]$$

which agrees with the solution given in reference (5).

For the complete stress distribution in the web for bending with shear, corresponding to Fig. 2, Equations [3] and [8] are added

$$\left.\begin{aligned}
\sigma_r &= \frac{PLr}{4I}(\cos\theta - \cos 3\theta) - \tau\rho \sin 2\theta + \frac{Pr^2}{4I}\sin 4\theta \\
&\quad - K\left\{2\frac{k_{31}}{K}\left(\frac{r_1}{r}\right)^3\cos\theta \right. \\
&\qquad + \left[12\frac{k_{23}}{K}\left(\frac{r_1}{r}\right)^5 + 10\frac{k_{42}}{K}\left(\frac{r_1}{r}\right)^3\right]\cos 3\theta \\
&\quad + \left[6\frac{k_{22}}{K}\left(\frac{r_1}{r}\right)^4 + 4\frac{k_{42}}{K}\left(\frac{r_1}{r}\right)^2\right]\sin 2\theta \\
&\quad \left. + \left[20\frac{k_{24}}{K}\left(\frac{r_1}{r}\right)^6 + 18\frac{k_{44}}{K}\left(\frac{r_1}{r}\right)^4\right]\sin 4\theta\right\} \\
\sigma_\theta &= \frac{PLr}{4I}(3\cos\theta + \cos 3\theta) - \left(\frac{Pr^2}{2I} - \tau\rho\right)\sin 2\theta \\
&\quad - \frac{Pr^2}{4I}\sin 4\theta \\
&\quad + K\left\{2\frac{k_{31}}{K}\left(\frac{r_1}{r}\right)^3\cos\theta + \left[12\frac{k_{23}}{K}\left(\frac{r_1}{r}\right)^5\right.\right. \\
&\qquad \left. + 2\frac{k_{42}}{K}\left(\frac{r_1}{r}\right)^3\right]\cos 3\theta \\
&\quad + 6\frac{k_{22}}{K}\left(\frac{r_1}{r}\right)^4\sin 2\theta + \left[20\frac{k_{24}}{K}\left(\frac{r_1}{r}\right)^6\right. \\
&\qquad \left.\left. + 6\frac{k_{44}}{K}\left(\frac{r_1}{r}\right)^4\right]\sin 4\theta\right\} \\
\tau_{r\theta} &= \frac{PLr}{4I}(\sin\theta + \sin 3\theta) + \left(\frac{Pr^2}{4I} - \tau\rho\right)\cos 2\theta \\
&\quad + \frac{Pr^2}{4I}\cos 4\theta \\
&\quad - K\left\{2\frac{k_{31}}{K}\left(\frac{r_1}{r}\right)^3\sin\theta + \left[12\frac{k_{23}}{K}\left(\frac{r_1}{r}\right)^5\right.\right. \\
&\qquad \left. + 6\frac{k_{42}}{K}\left(\frac{r_1}{r}\right)^3\right]\sin 3\theta \\
&\quad - \left[6\frac{k_{22}}{K}\left(\frac{r_1}{r}\right)^4 + 2\frac{k_{42}}{K}\left(\frac{r_1}{r}\right)^2\right]\cos 2\theta \\
&\quad \left. - \left[20\frac{k_{24}}{K}\left(\frac{r_1}{r}\right)^6 + 12\frac{k_{44}}{K}\left(\frac{r_1}{r}\right)^4\right]\cos 4\theta\right\}
\end{aligned}\right\} \quad \ldots [11]$$

where the constraint coefficients are evaluated from Equations [4] and [9] with

$$K = -\frac{PLr_1}{24I}$$

With the introduction of the nominal bending stress at the extreme fiber directly over the hole, $\sigma_L = PLh/I$, Equations [11] become nondimensional

$$\left.\begin{aligned}
\frac{\sigma_r}{\sigma_L} &= \frac{r}{4h}(\cos\theta - \cos 3\theta) - \frac{\tau}{\sigma_L}\rho\sin 2\theta \\
&\quad + \frac{r^2}{4hL}\sin 4\theta \\
&\quad + \frac{r_1}{24h}\left\{2\frac{k_{31}}{K}\left(\frac{r_1}{r}\right)^3\cos\theta + \left[12\frac{k_{23}}{K}\left(\frac{r_1}{r}\right)^5\right.\right. \\
&\qquad \left. + 10\frac{k_{42}}{K}\left(\frac{r_1}{r}\right)^3\right]\cos 3\theta \\
&\quad + \left[6\frac{k_{22}}{K}\left(\frac{r_1}{r}\right)^4 + 4\frac{k_{42}}{K}\left(\frac{r_1}{r}\right)^2\right]\sin 2\theta \\
&\quad \left. + \left[20\frac{k_{24}}{K}\left(\frac{r_1}{r}\right)^6 + 18\frac{k_{44}}{K}\left(\frac{r_1}{r}\right)^4\right]\sin 4\theta\right\} \\
\frac{\sigma_\theta}{\sigma_L} &= \frac{r}{4h}(3\cos\theta + \cos 3\theta) - \left(\frac{r^2}{2hL} - \frac{\tau}{\sigma_L}\rho\right)\sin 2\theta \\
&\quad - \frac{r^2}{4hL}\sin 4\theta - \frac{r_1}{24h}\left\{2\frac{k_{31}}{K}\left(\frac{r_1}{r}\right)^3\cos\theta\right. \\
&\quad + \left[12\frac{k_{23}}{K}\left(\frac{r_1}{r}\right)^5 + 2\frac{k_{42}}{K}\left(\frac{r_1}{r}\right)^3\right]\cos 3\theta \\
&\quad + 6\frac{k_{22}}{K}\left(\frac{r_1}{r}\right)^4\sin 2\theta + \left[20\frac{k_{24}}{K}\left(\frac{r_1}{r}\right)^6\right. \\
&\qquad \left.\left. + 6\frac{k_{44}}{K}\left(\frac{r_1}{r}\right)^4\right]\sin 4\theta\right\} \\
\frac{\tau_{r\theta}}{\sigma_L} &= \frac{r}{4h}(\sin\theta + \sin 3\theta) + \left(\frac{r^2}{4hL} - \frac{\tau}{\sigma_L}\rho\right)\cos 2\theta \\
&\quad + \frac{r^2}{4hL}\cos 4\theta \\
&\quad + \frac{r_1}{24h}\left\{2\frac{k_{31}}{K}\left(\frac{r_1}{r}\right)^3\sin\theta + \left[12\frac{k_{23}}{K}\left(\frac{r_1}{r}\right)^5\right.\right. \\
&\qquad \left. + 6\frac{k_{42}}{K}\left(\frac{r_1}{r}\right)^3\right]\sin 3\theta \\
&\quad - \left[6\frac{k_{22}}{K}\left(\frac{r_1}{r}\right)^4 + 2\frac{k_{42}}{K}\left(\frac{r_1}{r}\right)^2\right]\cos 2\theta \\
&\quad \left. - \left[20\frac{k_{24}}{K}\left(\frac{r_1}{r}\right)^6 + 12\frac{k_{44}}{K}\left(\frac{r_1}{r}\right)^4\right]\cos 4\theta\right\}
\end{aligned}\right\} \quad . [11a]$$

Since special interest is attached to the stresses at the junction of the reinforcement and the web, the special case of Equations [11a] with $r = r_1$ will now be evaluated. As is customary, the hole is assumed to be "small" compared with the web. It has been found[5] that such an analysis is accurate if the diameter of the hole does not exceed one fourth the depth of the web. In keeping with the usual bending theory, the depth of the beam is considered small compared with the length. Hence $r_1/L \approx 0$, while r_1/h is small, but finite. Therefore the constraint coefficients of Equations [9] become

[5] Reference (6), p. 3, and reference (5), p. 217.

$$
\left.\begin{aligned}
2\frac{k_{22}}{K} &\approx \frac{\tau\rho}{KD}\left\{[2-\alpha(1+4\delta)]\left[1+\delta+\frac{\beta}{2(1+\nu)}\right]\right. \\
&\quad \left.+\left(1-\delta-\frac{\beta}{4}\right)\left[\frac{2\alpha(\nu-4\delta)}{1+\nu}\right]\right\} \\
2\frac{k_{42}}{K} &\approx -\frac{\tau\rho}{KD}\left\{[2-\alpha(1+4\delta)]\left(1+3\delta+\frac{\beta}{4}\right)\right. \\
&\quad \left.+\left(1-\delta-\frac{\beta}{4}\right)[2+\alpha(3-4\delta)]\right\} \\
\frac{k_{24}}{K} &\approx 0;\quad \frac{k_{44}}{K} \approx 0 \\
D &= [2+\alpha(3-4\delta)]\left[1+\delta+\frac{\beta}{2(1+\nu)}\right] \\
&\quad -\left(1+3\delta+\frac{\beta}{4}\right)\left[\frac{2\alpha(\nu-4\delta)}{1+\nu}\right]
\end{aligned}\right\} \quad \ldots [9a]
$$

Equations [9a] become slightly more useful when the σ_L notation is used

$$
\left.\begin{aligned}
\frac{2k_{22}}{K} &\approx -\frac{\tau}{\sigma_L}\rho\frac{24h}{r_1}\frac{k'_{22}}{K} \\
\frac{2k_{42}}{K} &\approx -\frac{\tau}{\sigma_L}\rho\frac{24h}{r_1}\frac{k'_{42}}{K}
\end{aligned}\right\} \quad \ldots\ldots\ldots [9b]
$$

where

$$
\frac{k'_{22}}{K} = \frac{1}{M}\left\{[2-\alpha(1+4\delta)]\left[1+\delta+\frac{\beta}{2(1+\nu)}\right]+\left(1-\delta-\frac{\beta}{4}\right)\left[\frac{2\alpha\,(\nu-4\delta)}{1+\nu}\right]\right\}
$$

$$
\left.\begin{aligned}
\frac{k'_{42}}{K} &= -\frac{1}{M}\left\{[2-\alpha(1+4\delta)]\left(1+3\delta+\frac{\beta}{4}\right)\right. \\
&\quad \left.+\left(1-\delta-\frac{\beta}{4}\right)[2+\alpha(3-4\delta)]\right\} \\
M &= [2+\alpha(3-4\delta)]\left[1+\delta+\frac{\beta}{2(1+\nu)}\right] \\
&\quad -\left(1+3\delta+\frac{\beta}{4}\right)\left[\frac{2\alpha(\nu-4\delta)}{1+\nu}\right]
\end{aligned}\right\} \quad \ldots [9c]
$$

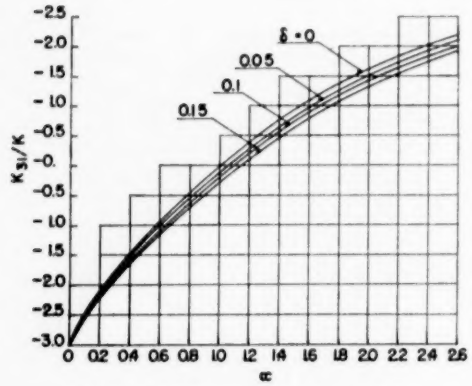

FIG. 4 k_{31}/K VERSUS α, CONTOURS OF δ

For the junction of the reinforcement with the web, $r = r_1$, Equations [11a] become

$$
\left.\begin{aligned}
\left(\frac{\sigma_r}{\sigma_L}\right) &= \frac{r_1}{4h}(\cos\theta-\cos 3\theta)-\frac{\tau}{\sigma_L}\rho\sin 2\theta \\
&\quad +\frac{r_1}{24h}\left[2\frac{k_{21}}{K}\cos\theta+\left(12\frac{k_{23}}{K}+10\frac{k_{43}}{K}\right)\cos 3\theta\right] \\
&\quad -\frac{\tau}{\sigma_L}\rho\left(3\frac{k'_{22}}{K}+2\frac{k'_{42}}{K}\right)\sin 2\theta \\
\left(\frac{\sigma_\theta}{\sigma_L}\right) &= \frac{r_1}{4h}(3\cos\theta+\cos 3\theta)+\frac{\tau}{\sigma_L}\rho\sin 2\theta \\
&\quad -\frac{r_1}{24h}\left[2\frac{k_{21}}{K}\cos\theta+\left(12\frac{k_{23}}{K}+2\frac{k_{43}}{K}\right)\cos 3\theta\right] \\
&\quad +3\frac{\tau}{\sigma_L}\rho\frac{k'_{22}}{K}\sin 2\theta \\
\left(\frac{\tau_{r\theta}}{\sigma_L}\right) &= \frac{r_1}{4h}(\sin\theta+\sin 3\theta)-\frac{\tau}{\sigma_L}\rho\cos 2\theta \\
&\quad +\frac{r_1}{24h}\left[2\frac{k_{21}}{K}\sin\theta+\left(12\frac{k_{23}}{K}+6\frac{k_{43}}{K}\right)\sin 3\theta\right] \\
&\quad +\frac{\tau}{\sigma_L}\rho\left(3\frac{k'_{22}}{K}+\frac{k'_{42}}{K}\right)\cos 2\theta
\end{aligned}\right\} \quad \ldots [11b]
$$

For the usual type reinforcement, $\delta < 0.2$, the reinforcing ring may be treated as a straight beam[9] and hence the tangential stress at the inner edge of the reinforcement will be substantially the same as the tangential stress at the junction of the reinforcement with the web. For convenience, the results of cross-fairing of the calculated values of constraint coefficients, based on rectangular-type reinforcement (standard pipe) used by the author in an experimental investigation,[10] are plotted in Figs. 4 to 8. These curves include a typical allowance of β for that type of reinforcement.

CONCLUSIONS

1 The theoretical stress distribution for a beam subjected to bending with shear and with a circular cutout reinforced with a bead is given in Equations [11] with the constraint coefficients

[9] Reference (1), appendix A, p. 33.

[10] Reported in the author's Doctoral Dissertation, "Reinforced Circular Holes in Bending With Shear," footnote 1.

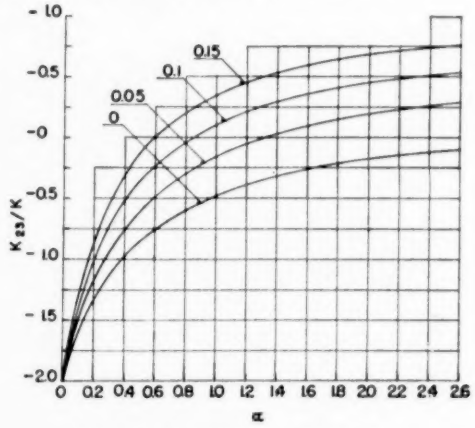

FIG. 5 k_{23}/K VERSUS α, CONTOURS OF δ

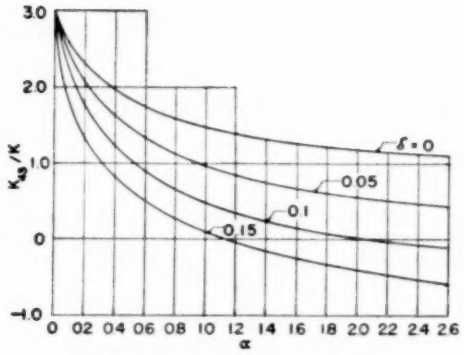

FIG. 6 k_{22}/K VERSUS α, CONTOURS OF δ

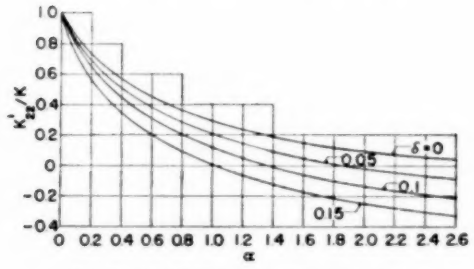

FIG. 7 k'_{22}/K VERSUS α, CONTOURS OF δ

evaluated according to Equations [4] and [9]. As might be expected, the maximum effect of the cutout is at the hole with little, if any, difference between the stresses at the inner edge of the hole and at the junction of the reinforcement and the web. The solution is satisfactory for engineering purposes provided the ratio of the diameter of the hole to the depth of web does not exceed 0.25.

2 It is impossible to design a reinforcement for a circular cut-

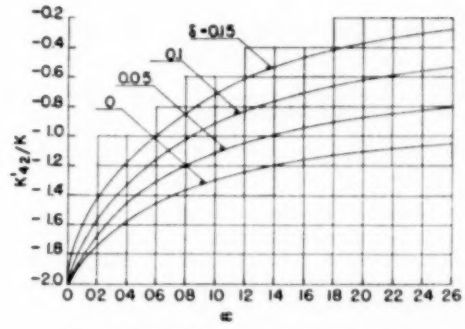

FIG. 8 k'_{42}/K VERSUS α, CONTOURS OF δ

out subjected to bending with shear which will restore the stress distribution existing prior to the cut.

3 For the usual type of reinforcement—a bead in contrast to a doubler plate—the shape is immaterial; the area supplied is paramount. In short, the reinforcement does its work in tension or compression, not in bending.

BIBLIOGRAPHY

1 "Reinforced Circular Cutouts in Plane Sheets," by H. Reissner and M. Morduchow, National Advisory Committee for Aeronautics, Technical Note No. 1852, Washington, D. C., April, 1949.

2 "The Stresses Around a Small Opening in a Beam Subjected to Bending With Shear," by S. R. Heller, Jr., Proceedings of the First U. S. National Congress for Applied Mechanics (being printed), Chicago, Ill.

3 "Effect of a Circular Hole on the Stress Distribution Under Uniform Bending Moment," by Z. Tuzi, Scientific Papers of the Tokyo Research, vol. 9, August 20, 1928.

4 "Theory of Elasticity," by S. Timoshenko, McGraw-Hill Book Company, Inc., New York, N. Y., first edition, 1934.

5 "Biharmonic Analysis in a Perforated Strip," by R. C. J. Howland and A. C. Stevenson, Philosophic Transactions of the Royal Society of London, series A, vol. 232, 1933, pp. 155–222.

6 "An Analysis of the Stresses in a Flat Plate With a Reinforced Circular Hole Under Edge Forces," by C. Gurney, Aeronautical Research Committee, R. and M. No. 1834, London, England, 1938

Some New Types of Orthotropic Plates Laminated of Orthotropic Material[1]

By C. BASSEL SMITH,[2] GAINESVILLE, FLA.

Plywood plates are usually constructed so that the grain of adjacent plies is perpendicular. Such laminated plates possess two perpendicular axes of elastic symmetry. In this discussion plywood plates having other than 90 degree angles between the grain of adjacent plies are considered. First, a two-ply plate with the grain of one ply making any arbitrary angle with the grain of the other ply is discussed. It is shown that this plate, when in a state of plane stress or when subjected to small deflections, possesses the same two perpendicular axes of elastic symmetry. By making use of the formulas obtained for the two-ply plate, it is shown how to construct a plate of any number of plies (the adjacent plies not necessarily having their grain perpendicular) possessing the same type of elastic symmetry as the two-ply plate.

Introduction

EACH ply of a plywood plate can be considered to be an orthotropic plate. This implies that the material of the individual plies is accurately flat-grain; that is, the directions of the grain and of the annual rings are parallel to the faces of the plies, and the variations of the elastic constants from springwood to summerwood are disregarded. Materials other than wood can be considered to be orthotropic. Hence, though we shall speak of the grain direction in the orthotropic plates discussed, the analysis applies equally well to any orthotropic plate.

In this discussion we will consider composite plates laminated of thin orthotropic plates or plies. In addition, the composite plate will be taken to be thin. Also, each ply will be assumed to be identical in thickness and elastic properties. If, as is usually done, we take the grain of adjacent plies to be perpendicular, the laminated plate will behave elastically as an orthotropic plate. When the plies are put together so that the direction of the grain of adjacent plies makes any arbitrary angle with each other, the laminated plate, in general, will not behave as an orthotropic plate. However, we shall show that it is possible to use other than a right angle between the grain directions of adjacent plies and still have the composite plate behave as an orthotropic plate. For wood, such a construction would possess a much greater resistance to shearing stress than the usual type.

Stress-Strain Relations in Orthotropic Media

Before we proceed to a discussion of laminated plates, it will be necessary to derive some rather general relations connecting stresses and strains in orthotropic material.

Let us consider an orthotropic material, the points of which are referred to a given orthogonal, Cartesian co-ordinate system $\bar{x}^i$. If the co-ordinate planes are the planes of elastic symmetry, Hooke's law can be written in the form[3]

$$\bar{e}_{mn} = \delta_{mn} a_{mj} \bar{\tau}_{jj} + (1 - \delta_{mn}) b_{mn} \bar{\tau}_{mn} \quad [1]$$

($m, n, j = 1, 2, 3$, and we sum on j only)

where δ_{mn} is the Kronecker delta, and a_{mj} and b_{mn} (both symmetric systems) are the elastic constants.

Let a new system of orthogonal, Cartesian co-ordinates x^i be specified relative to the old system $\bar{x}^i$ by the table of direction

TABLE 1 DIRECTION COSINES

	$\bar{x}^1$	$\bar{x}^2$	$\bar{x}^3$
x^1	d_{11}	d_{12}	d_{13}
x^2	d_{21}	d_{22}	d_{23}
x^3	d_{31}	d_{32}	d_{33}

cosines (Table 1). In this system d_{ij} is the cosine of the angle between the x^i- and the $\bar{x}^j$-axes. We shall take

$$\left.\begin{aligned} d_{11} = \cos\theta,\ d_{12} = -\sin\theta,\ d_{21} = \sin\theta,\ d_{22} = \cos\theta \\ d_{33} = 1,\ d_{13} = d_{23} = d_{31} = d_{32} = 0 \end{aligned}\right\} \quad [2]$$

It is evident that the new system is obtained from the old by rotating the latter through an angle $-\theta$ about the $\bar{x}^3$-axis. The components of the stress tensor transform according to the law

$$\bar{\tau}_{mn} = d_{rm} d_{sn} \tau_{rs} \quad [3]$$

and for the strain tensor, the transformation we will use is

$$e_{pq} = d_{pm} d_{qn} \bar{e}_{mn} \quad [4]$$

Inserting Equation [3] into Equation [1] and substituting the resulting equation into Equation [4] gives

$$e_{pq} = d_{pm} d_{qn} [\delta_{mn} a_{mj} d_{rj} d_{sj} \tau_{rs} + (1 - \delta_{mn}) b_{mn} d_{rm} d_{sn} \tau_{rs}] \quad [5]$$

If we use the notation[4]

$$e_{11} = e_1,\ e_{22} = e_2,\ e_{33} = e_3,\ 2e_{23} = e_4,\ 2e_{13} = e_5,\ 2e_{12} = e_6$$

$$\tau_{11} = \tau_1,\ \tau_{22} = \tau_2,\ \tau_{33} = \tau_3,\ \tau_{23} = \tau_4,\ \tau_{13} = \tau_5,\ \tau_{12} = \tau_6$$

and the equations given in Equations [2], Equation [5] can be written in the form

$$e_i = c_{ij} \tau_j \quad [6]$$

with the constants c_{ij} (where c_{ij} is a symmetric system) given by the equations

$$\begin{aligned}
c_{11} &= a_{11}\cos^4\theta + 2(a_{12} + b_{12})\sin^2\theta\cos^2\theta + a_{22}\sin^4\theta \\
c_{12} &= (a_{11} + a_{22} - 2b_{12})\sin^2\theta\cos^2\theta + a_{12}(\sin^4\theta + \cos^4\theta) \\
c_{13} &= a_{11}\cos^2\theta + a_{23}\sin^2\theta \\
c_{16} &= 2(a_{11} - a_{12} - b_{12})\sin\theta\cos^3\theta + 2(a_{12} - a_{22} + b_{12})\sin^3\theta\cos\theta \\
c_{22} &= a_{11}\sin^4\theta + 2(a_{12} + b_{12})\sin^2\theta\cos^2\theta + a_{22}\cos^4\theta \\
c_{23} &= a_{13}\sin^2\theta + a_{23}\cos^2\theta \\
c_{26} &= 2(a_{11} - a_{12} - b_{12})\sin^2\theta\cos\theta \\
&\quad + 2(a_{12} - a_{22} + b_{12})\sin\theta\cos^3\theta \\
c_{33} &= a_{33}
\end{aligned} \quad [7]$$

[1] This research was prepared under an Office of Naval Research contract.

[2] Professor of Mathematics, University of Florida.

Presented at the National Conference of the Applied Mechanics Division, Minneapolis, Minn., June 18–20, 1953, of The American Society of Mechanical Engineers.

Discussion of this paper should be addressed to the Secretary, ASME, 29 West 39th Street, New York, N. Y., and will be accepted until July 10, 1953, for publication at a later date. Discussion received after the closing date will be returned.

Note: Statements and opinions advanced in papers are to be understood as individual expressions of their authors and not those of the Society. Manuscript received by ASME Applied Mechanics Division August 18 1952. Paper No. 53—APM-6.

[3] Sokolnikoff's notations for the stress and strain components are used (I. S. Sokolnikoff, "Mathematical Theory of Elasticity," McGraw Hill Book Company, New York, N. Y., 1946). Equation [1] is equivalent to the Hooke's law for orthotropic media given by Sokolnikoff, p. 63.

[4] Ibid., p. 60.

$$c_{36} = 2(a_{12} - a_{23}) \sin\theta\cos\theta$$
$$c_{44} = 2(b_{13}\sin^2\theta + b_{23}\cos^2\theta)$$
$$c_{45} = 2(b_{13} - b_{23}) \sin\theta\cos\theta$$
$$c_{55} = 2(b_{13}\cos^2\theta + b_{23}\sin^2\theta)$$
$$c_{66} = 4(a_{11} - 2a_{12} + a_{22} - b_{12})\sin^2\theta\cos^2\theta + 2b_{12}(\sin^4\theta + \cos^4\theta)$$

$$c_{14} = c_{15} = c_{24} = c_{25} = c_{34} = c_{35} = c_{46} = c_{56} = 0$$

It is important to note that the constants c_{16}, c_{26}, c_{36}, and c_{45} (and of course c_{61}, c_{62}, c_{63}, and c_{54}) all change sign with θ, but the remaining c_{ij} do not.

The General Two-Ply Plate

Now that the general equations connecting stresses and strains have been obtained, it will be more satisfactory to denote the variables x^1, x^2, and x^3 by x, y, and z, respectively. We shall also introduce the following notations

$$e_{xx} = e_1,\ e_{yy} = e_2,\ e_{zz} = e_3,\ e_{yz} = e_4,\ e_{zx} = e_5,\ e_{xy} = e_6$$

$$X_x = \tau_1,\ Y_y = \tau_2,\ Z_z = \tau_3,\ Y_z = \tau_4,\ Z_x = \tau_5,\ X_y = \tau_6$$

Let us take a two-ply plate made of two thin orthotropic plates with the xy-plane being the plane separating the two plies. Let the thickness of each ply be $h/2$, and take the ply lying between the planes $z = -h/2$ and $z = 0$ as the first ply. Let the direction of the grain in the first ply make an angle of $+\theta$ with the positive x-axis, and let the direction of the grain in the second ply make an angle of $-\theta$ with the positive x-axis. For simplicity we shall suppose θ to have any value from zero to 90 deg.

We shall show that this general type of two-ply plate when in a state of plane stress will possess two mutually perpendicular axes of elastic symmetry. Similarly, we will show that for small deflections the bent plate will have the same two mutually perpendicular axes of elastic symmetry.

General Two-Ply Plate in a State of Plane Stress

If a state of plane stress exists in planes parallel to the xy-plane, the stress components Z_z, Y_z, and Z_x are assumed to vanish and from Equation [6] it can be shown that at a point in the first ply we can write[5]

$$\left.\begin{aligned} X_x &= s_{11}e_{xx} + s_{12}e_{yy} + s_{13}e_{xy} \\ Y_y &= s_{21}e_{xx} + s_{22}e_{yy} + s_{23}e_{xy} \\ X_y &= s_{31}e_{xx} + s_{32}e_{yy} + s_{33}e_{xy} \end{aligned}\right\} \quad \ldots\ldots\ldots\ldots [8]$$

where the constants s_{ij} (where s_{ij} is a symmetric system) are given as follows

$$\left.\begin{aligned} s_{11} &= (c_{22}c_{66} - c_{26}^2)/D,\ s_{12} = (c_{16}c_{26} - c_{12}c_{66})/D \\ s_{13} &= (c_{12}c_{26} - c_{22}c_{16})/D,\ s_{22} = (c_{11}c_{66} - c_{16}^2)/D \\ s_{23} &= (c_{12}c_{16} - c_{11}c_{26})/D,\ s_{33} = (c_{11}c_{22} - c_{12}^2)/D \end{aligned}\right\} \quad \ldots\ldots [9]$$

and where

$$D = \begin{vmatrix} c_{11} & c_{12} & c_{16} \\ c_{21} & c_{22} & c_{26} \\ c_{16} & c_{26} & c_{66} \end{vmatrix} \quad \ldots\ldots\ldots\ldots\ldots [10]$$

From the expressions for the c_{ij} given in Equations [7], it follows that the constants s_{13}, s_{23}, s_{31}, and s_{32} change sign with θ while the remaining s_{ij} do not. Thus Equations [8] hold also in the second layer provided we change the sign in front of the coefficients s_{13}, s_{23}, s_{31}, and s_{32}. For a state of plane stress it is plausible to assume that at a given point (x, y) the components of strain e_{xx}, e_{yy}, and e_{xy} are the same in both plies, and if we denote the mean stress components[6] by X_x^*, Y_y^*, and X_y^*, then we can write

$$\left.\begin{aligned} X_x^* &= s_{11}e_{xx} + s_{12}e_{yy} \\ Y_y^* &= s_{21}e_{xx} + s_{22}e_{yy} \\ X_y^* &= s_{33}e_{xy} \end{aligned}\right\} \quad \ldots\ldots\ldots\ldots\ldots [11]$$

Equations [11] show that in a state of plane stress the composite plate will possess two mutually perpendicular axes of elastic symmetry, and the plate can be said to be an orthotropic plate as long as it is in a state of plane stress.

General Two-Ply Plate Bent by a Load Normal to Its Faces

Suppose the general two-ply plate with finite dimensions is supported along its edges, and is subjected to a distribution of load normal to its faces. For small deflections, the strain components have the values[7]

$$e_{xx} = -z\frac{\partial^2 w}{\partial x^2},\ e_{yy} = -z\frac{\partial^2 w}{\partial y^2},\ e_{xy} = -2z\frac{\partial^2 w}{\partial x\partial y} \quad \ldots [12]$$

where w denotes the deflection of a point in the middle surface of the plate. The stress component Z_z is assumed to vanish. Then from Equation [6] it follows again that at a point in the first ply the relations connecting e_{xx}, e_{yy}, and e_{xy}, and the stress components X_x, Y_y, and X_y are the same as Equations [8]. Similarly, at a point in the second ply Equations [8] hold also provided we change the sign in front of the coefficients s_{13}, s_{23}, s_{31}, and s_{32}.

The differential equation for the deflection w is readily obtained from the conditions for the equilibrium of an element of the plate.[8]

The bending and twisting moments are obtained by integrating the products of z and the various stress components over the thickness of the plate.

Thus

$$\left.\begin{aligned} M_x &= \int_{-h/2}^{h/2} X_x\, z\, dz, \quad M_y = \int_{-h/2}^{h/2} Y_y\, z\, dz \\ M_{xy} &= \int_{-h/2}^{h/2} X_y\, z\, dz \end{aligned}\right\} \quad \ldots\ldots [13]$$

From Equations [8], [12], and [13], we have

$$\left.\begin{aligned} M_x &= -\left(s_{11}\frac{\partial^2 w}{\partial x^2} + s_{12}\frac{\partial^2 w}{\partial y^2}\right)h^3/12 \\ M_y &= -\left(s_{12}\frac{\partial^2 w}{\partial x^2} + s_{22}\frac{\partial^2 w}{\partial y^2}\right)h^3/12 \\ M_{xy} &= -2s_{33}\frac{\partial^2 w}{\partial x\partial y}h^3/12 \end{aligned}\right\} \quad \ldots\ldots [14]$$

The components of the vertical shear are given by the equations

$$P_x = \frac{\partial M_x}{\partial x} + \frac{\partial M_{xy}}{\partial y},\quad P_y = \frac{\partial M_{xy}}{\partial x} + \frac{\partial M_y}{\partial y} \quad \ldots\ldots [15]$$

and the condition for equilibrium of forces normal to the plate leads to the equation

$$\frac{\partial P_x}{\partial x} + \frac{\partial P_y}{\partial y} = -p \quad \ldots\ldots\ldots\ldots [16]$$

[5] To obtain Equations [8] from Equation [6], we ignore the equation $e_{zz} = c_{31}X_x + c_{32}Y_y + c_{33}X_y$.

[6] The arithmetic mean of X_x in the first ply and X_x in the second ply is called X_x^*, etc.

[7] See, for example, A. Nadai, Elastische Platten (Berlin, 1925), p. 19.

[8] Ibid., p. 20.

where p is the normal load per unit area.

Inserting Equations [14] into Equations [15], and substituting the resulting equations into Equation [16] gives

$$s_{11}\frac{\partial^4 w}{\partial x^4} + 2(s_{12} + 2s_{33})\frac{\partial^4 w}{\partial x^2 \partial y^2} + s_{22}\frac{\partial^4 w}{\partial y^4} = 12p/h^3 \quad [17]$$

The form of Equation [17] is well known and shows that the plate will behave as an orthotropic plate when subjected to small deflections. The axes of elastic symmetry are the x- and y-axes.

Laminated Orthotropic Plates With More Than Two Plies

It is now possible, by making use of the ideas developed for the general two-ply plate, to construct a quite general plate of several plies that will possess the same type of elastic symmetry. First, we will show how to construct such a plate with four plies where each ply will be taken to be of thickness $h/4$. To describe the construction, let us take the xy-plane as the middle plane of the plate, and number the plies, in order, from one to four as we proceed upward from the bottom ply (the ply lying between the planes $z = -h/2$ and $z = -h/4$). The angle between the direction of the grain in each ply and the positive x-axis will be taken as follows:

In the first ply take the angle to be $+\theta_1$.
In the second ply take the angle to be $+\theta_2$.
In the third ply take the angle to be $-\theta_2$.
In the fourth ply take the angle to be $-\theta_1$.

In these θ_i ($i = 1, 2$) can have any value from -90 deg to $+90$ deg. If now the plate is in a state of plane stress or subjected to small deflections, it follows readily, by a simple extension of the mathematical analyses given for the general two-ply plate, that the x- and y-axes are axes of elastic symmetry of the plate. It is now easy to construct a plate of any even number of plies possessing the elastic symmetry described. To do this, we must orient the plies so that any two plies situated symmetrically with respect to the middle plane (the xy-plane) have the x-axis as the bisector of the angle formed by their two grain directions. This angle if we desire can be taken to be either 0 or 90 deg. Other possibilities readily present themselves.

Effective Shearing Modulus of General Two-Ply Plate

From the last of Equations [11] we see that the coefficient s_{33} can be interpreted as the effective shearing modulus of the laminated plate where this modulus is associated with the directions of x and y. In the usual laminated orthotropic plate the effective shearing modulus is generally associated with the directions parallel and perpendicular to the grain of a face ply. In this case, assuming all plies are identical, the effective modulus is the same as the shearing modulus associated with similar directions of any single ply. However, for the general two-ply plate this will not necessarily be true. Hence it will be of interest to see if it is possible to construct a general two-ply plate with an effective shearing modulus appreciably larger than the corresponding modulus of a single ply. This would be of particular interest in the case of plywood where the shearing modulus of a single ply is relatively small, usually being about 6 or 7 per cent of the Young's modulus in the direction of the grain.

As an illustration, values of modulus s_{33} as given by Equations [7], [9], and [10] were computed for several two-ply plywood plates of Sitka spruce. The plies of all the plates were taken to be identical and to be rotary cut. However, the angle θ, where 2θ is the angle formed by the grain directions of the two plies of each plate, was taken to be different for different plates. The values of the elastic constants of Sitka spruce were taken to be

$$E_L = 1.679 \times 10^6 \text{ psi}, \quad \mu_{LT} = 0.112 \times 10^6 \text{ psi}$$
$$E_T = 0.076 \times 10^6 \text{ psi}, \quad \sigma_{LT} = 0.464$$

where E_L and E_T are Young's moduli, the letters L and T denoting longitudinal and tangential directions, respectively; μ_{LT} is the shearing modulus associated with the same two directions; and σ_{LT} is the Poisson's ratio associated with tension parallel to the direction L and contraction parallel to the direction T. From Equation [1] it follows that

$$a_{11} = 1/E_L, \quad a_{12} = -\sigma_{LT}/E_L$$
$$a_{22} = 1/E_T, \quad b_{12} = 1/2\mu_{LT}$$

The results of the calculations for several values of θ are given in Table 2.

TABLE 2 VALUES OF THE SHEARING MODULUS s_{33}

θ, deg	$s_{33} \times 10^{-6}$, psi
0	0.112
5	0.121
15	0.190
25	0.296
35	0.389
45	0.425

These values of the modulus s_{33} increase rather rapidly as θ changes from 0 up to 45 deg as we might expect, and show a substantial increase in the value of the effective modulus over the value of μ_{LT}, the shearing modulus of a single ply, for values of θ as small as 15 deg.

High-Temperature Compression Testing of Graphite[1]

By LEON GREEN, JR.,[2] AZUSA, CALIF.

Experiments on the compression of graphite cylinders at elevated temperatures are described. It is found that the short-time compressive strength increases with temperature in the range from room temperature to 2000 C, a variation which is consistent with the previously reported behavior of the tensile strength. Photographs of typical modes of deformation and their corresponding stress-strain curves are presented, but a limited degree of temperature control renders the curves semiquantitative in nature. The large, mutually opposing influences of temperature and strain rate are illustrated by photographs of typical failures, and stress-relaxation curves manifest the plasticity of graphite at high temperatures.

Introduction

THE unusual plastic and elastic properties exhibited by graphite under tension, torsion, and flexure at elevated temperatures (1, 2, 3)[3] aroused interest in its high-temperature behavior under compression. It was desired, for instance, to check the temperature dependence of the short-time breaking strength, since the tensile strength of graphite had been found to increase markedly with temperature up to about 2500 C. At such temperatures the effect of strain rate was known to be large, and it was desired to illustrate this effect at least qualitatively. Since graphite is finding an increasing number of high-temperature structural applications, knowledge of its compressive properties was also desirable for design purposes.

Equipment

The specimens used in the compression tests were right circular cylinders (0.5 in. diam, 1 in. height) of grade AUF[4] graphite. In order to obtain material of maximum uniformity, the specimens were cut from the central 4-in-diam core of the 15-in-diam extruded graphite rod, with their axes parallel to the direction of extrusion.

The furnace used in the high-temperature testing is diagrammed in Fig. 1 which shows that the graphite specimen was compressed between two water-cooled copper electrodes. The image of the specimen (heated to incandescence by the passage of a direct current from a 25-kw motor-generator set) was focused on a ground-glass screen by means of an achromatic lens in one of the furnace windows. End blocks of ungraphitized carbon hindered heat flow away from the specimen and provided interfaces of high heat-generation rate, thus holding the maximum longitudinal surface-temperature difference along the specimen to about 2 per cent of the total temperature. A measurable radial temperature gradient must have existed within the specimen, but for purpose of the present preliminary study, the average surface temperature (as measured by an optical pyrometer viewing through a quartz window) was taken as the specimen temperature. The tests were conducted in a vacuum of about 30 microns.

The equipment used for compressing the graphite was a laboratory-made testing machine in which the stress was applied by a hydraulic cylinder. A loading mechanism consisting essentially of a Vickers pump, two Adel flow-control valves, and a four-way valve, as shown in Fig. 2, was constructed for this machine in order to permit operation at a variety of loading rates. The net force on the specimen was established (with precision sufficient for the present exploratory study) by subtracting from the total cylinder pressure that pressure which was required to support the furnace and the moving bed of the testing machine. The cylinder pressure was indicated by two Bourdon gages, one on the control board, and one on the panel containing the ground-glass projection screen. Viewing this panel, on which an electric timer also was mounted, by means of a Bell and Howell 35-mm type A-4-A bomb-spotting camera provided a photographic record of the specimen deformation as a function of stress and time. Strain was determined by projecting the film with a microfilm viewer and measuring the length of the specimen image with a vernier caliper. A 6-in. steel rule cemented to the ground-glass panel served as a reference length for correction of the strain measurements.

Results and Discussion

Breaking Strength. In measurements of breaking strength, it is desirable to control the testing by carrying out all the measurements at a constant rate of strain or rate of stress increase. No such control was possible in the present work, however, since the simple hydraulic loading system used here permitted only the velocity of the machine bed, or head rate, to be fixed.

The short-time compressive strength of AUF graphite is presented as a function of testing temperature in Fig. 3. The scatter seen there is attributed to density variations in the specimens, and to differences in specimen alignment in the testing machine. It is well known (4) that the results of axial compression tests are highly sensitive to the alignment of the specimen between the two bearing surfaces; special precautions are usually necessary to assure that the lateral extension of all cross sections is the same. In the present high-temperature tests, however, no lubrication of the bearing surfaces was attempted; the nonuniformity of stress at the ends of the specimen resulting from friction between the specimen and the carbon end blocks was accepted as an inherent error. Despite the scatter shown by the points in Fig. 3, it is apparent that the short-time compressive strength of AUF graphite increases with temperature in a fashion closely paralleling its short-time tensile strength, a curve of which is included for comparison. The tensile strengths of

---

[1] This paper is based upon studies conducted at North American Aviation, Inc., for the Atomic Energy Commission under Contract AT-11-1-GEN-8.

[2] Solid Engine and Chemical Division, Aerojet Engineering Corporation. Jun. ASME.

[3] Numbers in parentheses refer to the Bibliography at the end of the paper.

[4] National Carbon Company.

Presented at the National Conference of the Applied Mechanics Division, Minneapolis, Minn., June 18–20, 1953, of The American Society of Mechanical Engineers.

Discussion of this paper should be addressed to the Secretary, ASME, 29 West 39th Street, New York, N. Y., and will be accepted until July 10, 1953, for publication at a later date. Discussion received after the closing date will be returned.

Note: Statements and opinions advanced in papers are to be understood as individual expressions of their authors and not those of the Society. Manuscript received by ASME Applied Mechanics Division, August 4, 1952. Paper No. 53—APM-4.

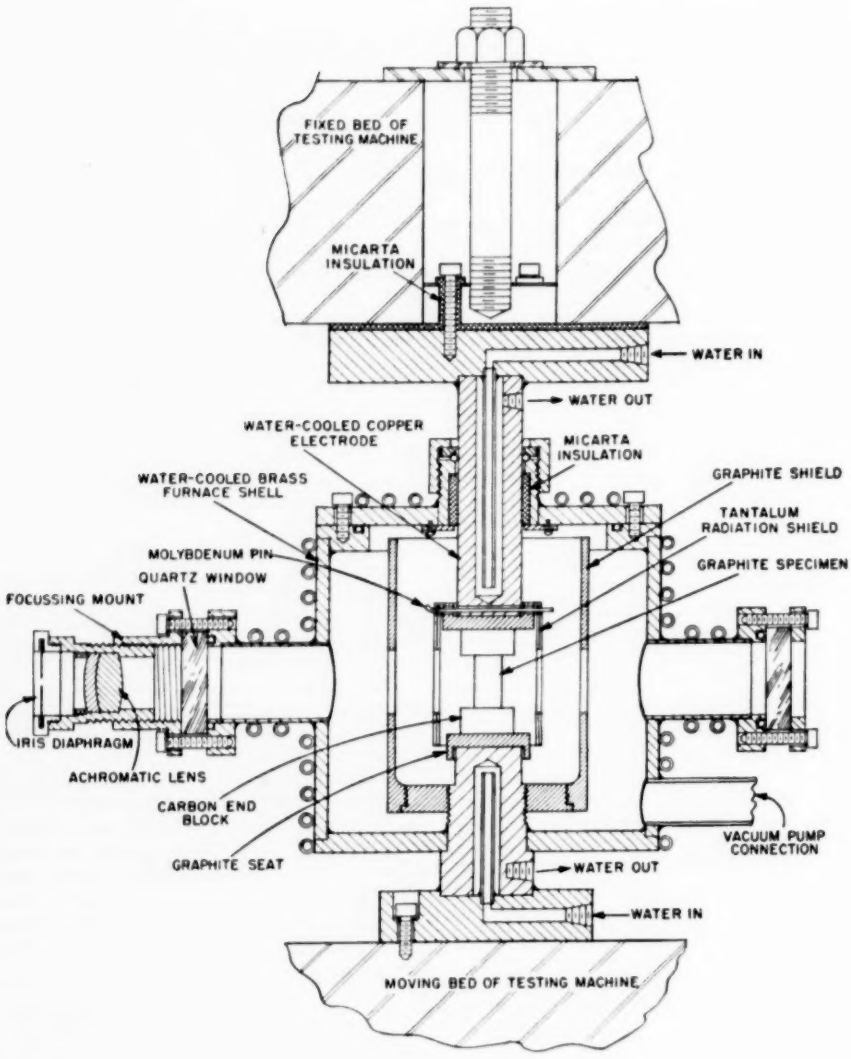

FIG. 1 SCHEMATIC CROSS SECTION OF FURNACE USED IN HIGH-TEMPERATURE COMPRESSION TESTS

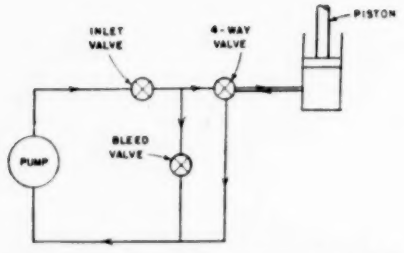

FIG. 2 SCHEMATIC DIAGRAM OF HYDRAULIC LOADING SYSTEM

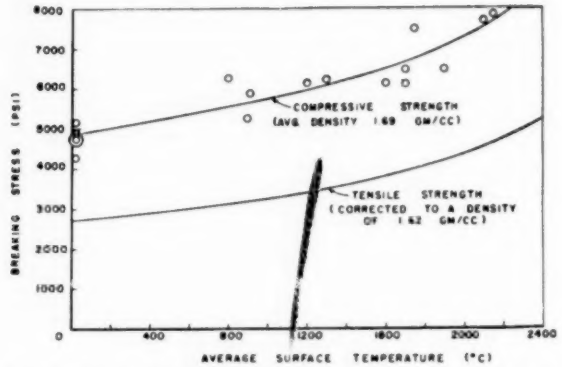

FIG. 3 SHORT-TIME COMPRESSIVE AND TENSILE STRENGTHS OF AUF GRAPHITE VERSUS TEMPERATURE

various grades of graphite show maxima at about 2500 C, as may be seen in Fig. 4, which is taken from reference (1).

The increase of the short-time strength of graphite with increasing temperature is at present a subject of considerable speculation. The usual hypothesis for this unusual dependence is typified by that of Duckworth (5), who suggests that since a similar maximum in strength-temperature behavior is observed in some ceramics, "the explanation might lie in common structural characteristics. All of these materials consist of inclusions, a bonding phase, and pores. Internal stresses in the inclusions and in the bonding phase would decrease with increases in temperature, until the temperature at which the stresses had been 'frozen in' is reached. The size of the pores also would be temperature-dependent, and the stress-concentrating action of a pore varies with its size. Hence the magnitude of stress peaks in minute volumes of the graphite is a function of temperature. With fracture occurring when a stress peak reaches a critical magnitude, it seems logical that increases in temperature cause such a decrease in dangerous stress peaks as to require an increased external stress for fracture."

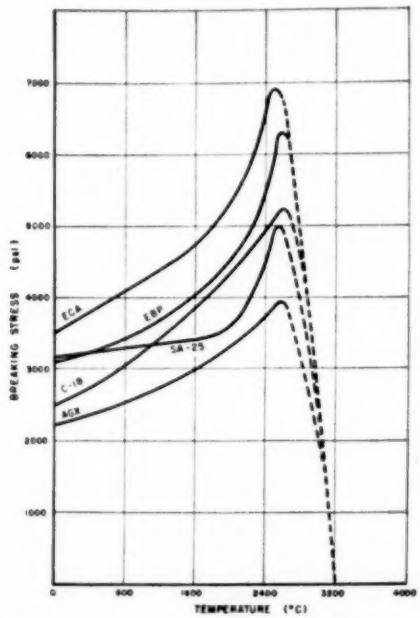

FIG. 4 SHORT-TIME TENSILE STRENGTH OF VARIOUS GRADES OF NATIONAL CARBON COMPANY GRAPHITE VERSUS TEMPERATURE

It is believed that the foregoing explanation cannot be accepted without reservation, since the structure of pure, unimpregnated, polycrystalline graphite is not similar to that of ceramic ware; in completely graphitized carbon, no bonding phase would be expected to exist. This belief is supported by Fig. 5 which presents an electron photomicrograph[5] of an 0.1-micron slice of AUF graphite. No bonding phase is visible; the particles appear to have been joined by a sintering process. The increase in the strength of this material with temperature cannot be attributed to the relief of residual stresses, for then the room-temperature strength of the stress-relieved material should be improved. This was not found to be the case. The stress concentrations at the points of union between the individual particles must be great indeed, but again it is not clear why the smoothing of such local stress peaks by plastic flow at high temperature would not then effect a significant change in the low-temperature strength of the material.

[5] This photomicrograph was taken by D. C. Pease and R. F. Baker of the School of Medicine, University of Southern California.

It is believed that the apparent maximum in the strength-temperature curve may be attributed to the influence of creep. At temperatures higher than roughly 2400 C, the rate of creep becomes predominant, the dependence of the apparent strength upon the strain rate becomes pronounced, and the "short-time" test becomes meaningless. The location of the maximum point in Fig. 4 at about 2500 C is therefore not significant, since a decrease in the rate of loading would shift it to a lower temperature.

Stress-Strain Curves. Experimentation revealed that electrical heating of the specimen would not permit the study of stress-strain curves at constant temperature. As the stress increased, the contact between the carbon and graphite surfaces, Fig. 1, became more intimate, the current through the specimen increased, and the temperature rose accordingly. This difficulty had been avoided in the breaking-strength tests by seating the elements firmly at a stress well below the breaking point, bringing the specimen to the desired temperature, and loading rapidly to failure. In tests starting at low stress levels, however, the effect could not be minimized without destroying the uniformity of the temperature distribution along the specimen. Manual adjustments of the rheostat controlling the generator current could not be made rapidly enough to compensate for the resistance change in the specimen circuit, and so stress-strain curves obtained with increasing temperature were accepted for purpose of qualitative comparison. Two such curves obtained at a constant head rate, but at two different initial temperatures, are presented in Fig. 6.

Photographs of the two specimens in Fig. 6, at various periods in their lives, are shown in Figs. 7 and 8. In the higher tempera-

FIG. 5 ELECTRON PHOTOMICROGRAPH OF SLICE OF AUF GRAPHITE
(Scale is indicated by a 1-micron reference length shown in lower right-hand corner. Light areas correspond to voids, and small particles indicate plane of focus.)

ture test, where the effects of creep are large, failure occurs slowly, apparently aided by creep-buckling induced by local softening of the carbon end blocks. The film record revealed that the appearance of the buckling tendency coincided with a drop in the stress-strain curve. At the lower temperature, by contrast, failure occurred suddenly in the form of brittle fracture, thus producing the flash shown in the photograph.

Types of Failure. The large influence of strain rate on the mechanical properties of graphite is indicated qualitatively by the foregoing results; the apparent strength increases with temperature as long as the rate of strain (with increasing stress) to which the specimen is subjected is large compared to the creep

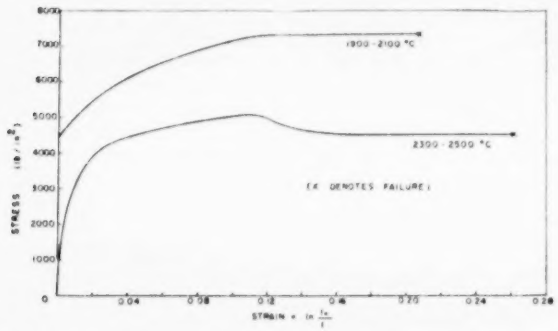

FIG. 6 STRESS-STRAIN CURVES OBTAINED AT DIFFERENT TEMPERATURE LEVELS

FIG. 9 EXAMPLES OF "BRITTLE" FRACTURES OBTAINED IN TEMPERATURE RANGE 20–2000 C

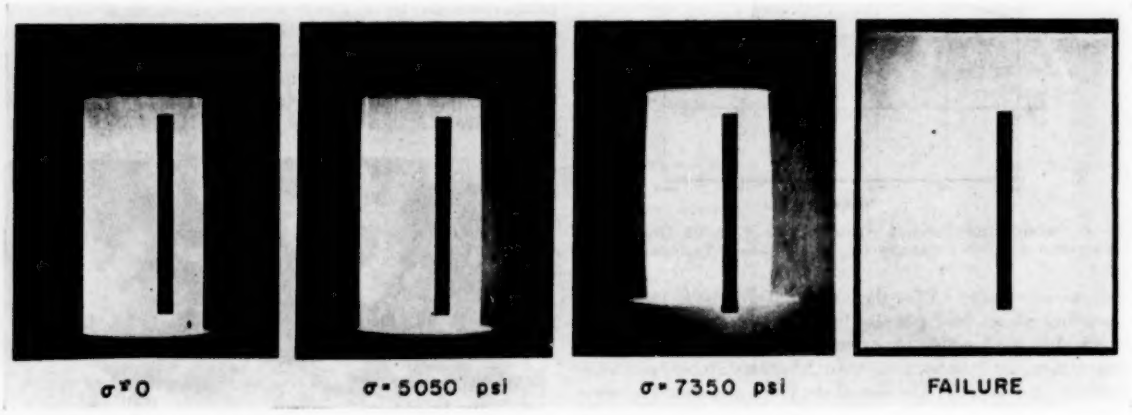

FIG. 7 STAGES IN FRACTURE OF GRAPHITE SPECIMEN IN RANGE 1900–2100 C

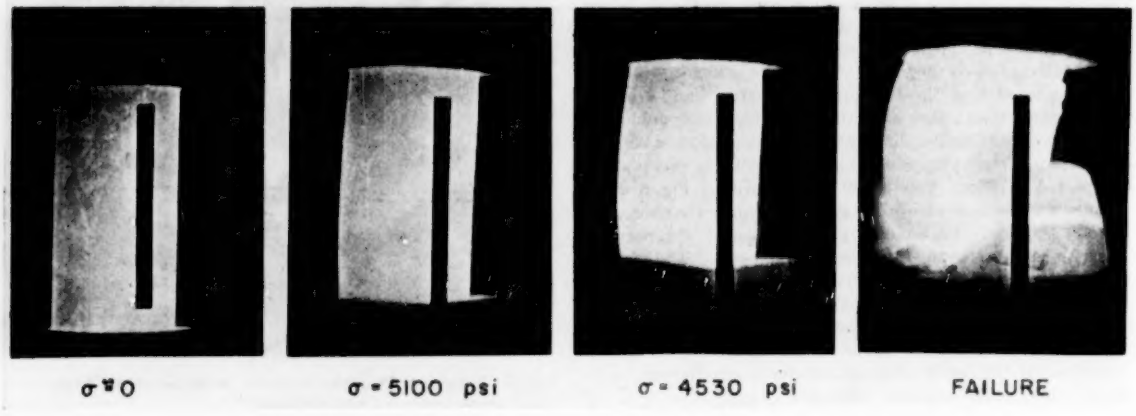

FIG. 8 STAGES IN FRACTURE OF GRAPHITE SPECIMEN IN RANGE 2300–2500 C

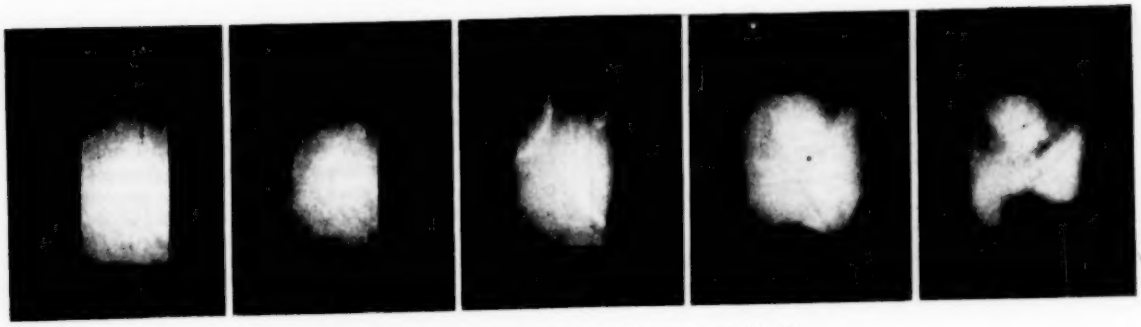

FIG. 10 FRACTURE OF GRAPHITE SPECIMEN AT 2000 C
(Consecutive frames at about 1200 frames per sec.)

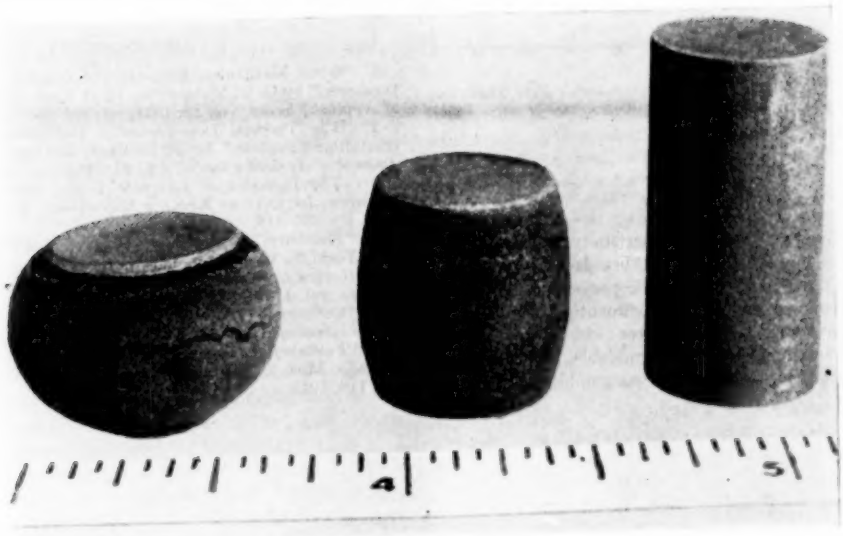

FIG. 11 EXAMPLES OF SPECIMENS COMPRESSED AT HIGH TEMPERATURES
(From right to left, specimens shown were *a* untested, *b* tested at about 2400 C, *c* tested at about 2600 C.)

rate, or rate of strain increase under constant stress. Under such conditions, failure occurs by a fracture of the "brittle" type, examples of which are shown in Fig. 9. These fractures are typical of the failures which were obtained at temperatures from 20 C to about 2000 C, a range in which creep did not materially influence the results. In an attempt to study the brittle failure of graphite more closely, the image of a specimen fractured at 2000 C was photographed at about 1200 frames per sec by a Western Electric "Fastax" 16-mm camera. Five consecutive frames from the film are shown in Fig. 10, and it may be seen from the sudden appearance of the fracture lines in the third frame that, despite the elevated temperature, complete failure occurred in less than 1 millisec.

At high temperatures and low rates of strain, as mentioned earlier, the specimens deform plastically by creep, which, in the case of graphite, is best regarded as a diffusion process (6).[6]

[6] In the various experiments referred to in the foregoing discussion, the graphite specimens showed no indication of a permanent plastic deformation (short of fracture) attributable to a slip mechanism. In an effort to detect evidences of work-hardening as a result of short-time plastic deformation, filings of AUF graphite were pulverized in a mortar and pestle and classified by Tyler screens. The $-250 + 300$ fraction was retained, and half of it was annealed in vacuo at 1500 C for 2 hr. The annealed and unannealed portions were then subjected to x-ray analysis. Examination by means of a North American Phillips automatic recording goniometer revealed no apparent change in the amplitude and shape of the lines of the diffraction pattern as a result of the attempted cold-working.

Examples of specimens compressed at high temperatures are shown in Fig. 11. The shiny crust visible on the specimen which was compressed at the highest temperature seems to have been formed as a result of an impurity in the carbon end blocks. The apparent density of the two specimens shown was found to have been increased as a result of the compression.

Stress-Relaxation Curves. Measurements of creep under constant stress could not be made with the available equipment, so the rate of stress relaxation at constant strain was substituted as a measure of the high-temperature plasticity of the material. Stress-relaxation curves obtained at 2300, 2500, and 2600 C are presented in Fig. 12. The specimen temperature was substantially constant during the course of these tests. However, since the softening of the end blocks contributed in an unknown (although presumably small) degree to the total observed rate of relaxation, the curves are again only semiquantitative in nature. Nevertheless, the rapid rate of stress decay shown by these curves emphasizes the considerable plasticity of graphite at the extreme temperatures involved.

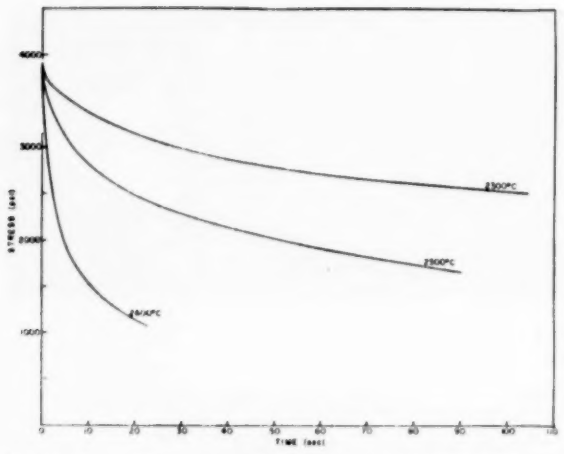

FIG. 12 STRESS-RELAXATION CURVES OBTAINED AT 2300, 2500, AND 2600 C

CONCLUSION

From the results of the exploratory experiments described, it is concluded that the mechanical properties of graphite and their thermal dependence deserve further study with equipment of increased precision and flexibility. It is suggested that experiments conducted under large hydrostatic pressures might prove highly informative, although the experimental difficulties involved by such tests at high temperatures (which would require the use of an inert gas) might prove formidable. There is good reason to expect that in such experiments graphite may exhibit increasingly ductile behavior as the pressure level is raised, in a fashion possibly analogous to the behavior exhibited by marble in the classical experiments by von Kármán (7). Finally, the possibility of increasing the density of unavoidably porous commercial graphite by compressing it at a temperature high enough and at a rate slow enough to insure that all the deformation occurs by a diffusion mechanism without any local fracturing appears especially attractive, since completely bonded graphite of maximum theoretical density (2.25 grams per cu cm) almost certainly would exhibit greatly improved strength properties.

ACKNOWLEDGMENTS

The author gratefully acknowledges the contributions of many individuals, notably J. McGee, who performed and interpreted the x-ray work; S. Becker, who machined the graphite elements; and D. Whitlock, who assembled a large part of the equipment.

BIBLIOGRAPHY

1 "Some Mechanical Properties of Graphite at Elevated Temperatures," by C. R. Malmstrom, R. D. Keen, and L. Green, *Journal of Applied Physics*, vol. 22, 1951, pp. 593–600.

2 "The Thermal Dependence of the Elastic Moduli of Polycrystalline Graphite," by F. E. Faris, L. Green, and C. A. Smith, *Journal of Applied Physics*, vol. 23, 1952, pp. 89–95.

3 "The Behavior of Graphite Under Alternating Stress," by L. Green, JOURNAL OF APPLIED MECHANICS, Trans. ASME, vol. 73, 1951, pp. 345–348.

4 "Plasticity," by A. Nadai, McGraw-Hill Book Company, Inc., New York, N. Y., 1931, p. 108.

5 Review of reference (1), by W. Duckworth, *Applied Mechanics Reviews*, vol. 4, 1951, pp. 563–564.

6 "Diffusional Viscosity of a Polycrystalline Solid," by C. Herring, *Journal of Applied Physics*, vol. 21, 1950, pp. 437–445.

7 "Festigkeitsversuche unter allseitigem Druck," by T. von Kármán, Mitt. ü. Forschungsarb. d. Vereines deutscher Ingenieure, No. 118, 1913.

Discussion

A Matrix Method for Flexibility Analysis of Piping Systems[1]

E. G. Baker.[2] The method proposed by the author for calculating piping flexibility has been tested on a two-anchor high-temperature steam line in a marine installation. Tentative comments and conclusions resulting from this trial run are as follows:

In general, the author's method is found to be very convenient and concise. Calculations for a given pipe element are carried out in all three co-ordinate planes at one time, and on one calculation sheet, instead of being scattered among various tabulation and graph sheets as in the case of the method previously in use in our office.

An advantage not mentioned by the author is that the contribution of each pipe element to the flexibility of the line as a whole is clearly evident at all times, and is not merged with the flexibility of other adjacent elements. This implies, for instance, that errors made in the calculation of any particular element will not affect the calculations for other elements, and will affect the line as a whole only in proportion to the contribution of that element to the flexibility of the whole line. The value of this feature is apparent. It will be seen that correction of an error occurring at any step does not require the recalculation of all subsequent steps. Furthermore, changes made to one or two elements in the pipe line will affect the flexibility calculations only for the altered pipe elements, and all flexibility calculations for unaltered elements remain valid. This is a weighty consideration to the designer of marine piping, because changes to the piping during design and construction of the vessel are frequent.

The author's formulas for the B-transformation, in Tables 1 and 3, are considered to be an important step forward in the application of matrix methods to practical calculations. Together with the orientation tables, they obviate the necessity for matrix multiplication in calculating two-anchor lines, except for pipe bends in an oblique plane. On the other hand, matrix multiplication remains available for checking purposes where desired. This is an excellent feature and one especially useful for detecting errors in sign, which are a particular plague of piping-flexibility calculations.

The treatment of straight runs of pipe not parallel to a co-ordinate axis can be substantially simplified, as follows: If the base point be taken at the mid-length of the pipe, the influence coefficients for any straight run, however oriented, are given by Table 1 of this discussion (the common factor $1/EI$ has been omitted). In this table, a_1, a_2, a_3 are direction cosines of the pipe. (In the author's illustrative example, the direction cosines are $^3/_{13}$, $^{12}/_{13}$, and $-^4/_{13}$, respectively.) For straight runs oriented parallel to a co-ordinate plane, one of the direction cosines will vanish. (This leads to formulas equivalent to the author's Table 9). For straight runs oriented parallel to a co-ordinate axis, two of the direction cosines vanish. It is evidently unnecessary to resort to orientation tables or matrix multiplication for straight runs, and the influence coefficients can be written down immediately in every case.

The author's method has not yet been tried against an actual three-anchor problem. However, an exploratory effort was made to ascertain the step-by-step formulation of such a problem, which may prove of interest to others, as the author's treatment of multiple-anchor lines, although admirably complete, is rather difficult to follow for the non-mathematician.

TABLE 1 INFLUENCE COEFFICIENTS FOR STRAIGHT RUNS

$$\begin{bmatrix} \frac{(1-a_1^2)L^3}{12} & -\frac{a_1a_2L^3}{12} & -\frac{a_1a_3L^3}{12} & & & \\ & \frac{(1-a_2^2)L^3}{12} & -\frac{a_2a_3L^3}{12} & & & \\ & & \frac{(1-a_3^2)L^3}{12} & & & \\ & & & (1+a_1^2\mu)L & a_1a_2\mu L & a_1a_3\mu L \\ & & & & (1+a_2^2\mu)L & a_2a_3\mu L \\ & & & & & (1+a_3^2\mu)L \end{bmatrix}$$

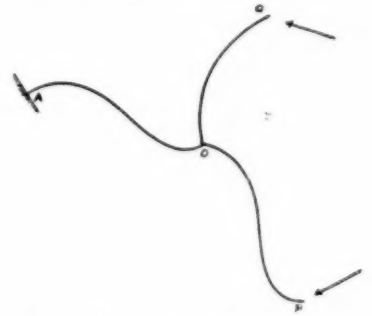

Fig. 1 Three-Anchor Piping System

1 Referring to Fig. 1 of this discussion, compute the influence coefficients which represent the deflections and rotations of

AO at O due to forces and moments at O
OP at P due to forces and moments at P
OQ at Q due to forces and moments at Q

2 Apply a set of arbitrary (unknown) forces and moments at P.

3 Compute the corresponding deflections and rotations at point Q due to flexibility in line AO by the matrix formula $\bar{B}_{QO}\,C_{AO}\,B_{PO}$ where B_{PO} is a matrix whose elements, other than 0 and 1, are components of a line vector running from point P to point O (see Table 2 of this discussion). $\bar{B}_{QO}$ is the transpose of a similar matrix formed from the vector running from Q to O; and C_{AO} is the matrix of the first set of influence coefficients found in step 1.

TABLE 2 MATRIX FOR B-TRANSFORMATION

$$\begin{bmatrix} 1 & 0 & 0 & 0 & 0 & 0 \\ 0 & 1 & 0 & 0 & 0 & 0 \\ 0 & 0 & 1 & 0 & 0 & 0 \\ 0 & z & -y & 1 & 0 & 0 \\ -z & 0 & x & 0 & 1 & 0 \\ y & -x & 0 & 0 & 0 & 1 \end{bmatrix}$$

4 Compute the deflections and rotations at point P, due to the flexibility of line AO, by the formula $\bar{B}_{PO}\,C_{AO}\,B_{PO}$ which is the author's Equation [9].

[1] By J. E. Brock, published in the December, 1952, issue of the Journal of Applied Mechanics, Trans. ASME, vol. 74, pp. 501–516.

[2] Engineering Technical Staff, American Bureau of Shipping. Mem. ASME.

5 Add the deflections and rotations at P due to flexibility in line OP, as found in step 1, to those computed in step 4.

6 Repeat steps 2 to 5 for arbitrary forces and moments applied at point Q, noting that $\bar{B}_{PO}\, C_{AO}\, \bar{B}_{QO}$ is the transpose of $\bar{B}_{QO}\, C_{AO}\, B_{PO}$.

7 Apply the boundary conditions for prescribed deflections at P and Q. This yields 12 equations in the arbitrary forces and moments.

8 Solve these equations for the actual forces and moments at P and Q.

It is to be remarked that if, in Fig. 1, herewith, the line OQ is imagined to be very short and stiff, the foregoing formulation evidently reduces to a solution of the two-anchor problem with a constraint at O.

P. T. Hoath.[3] The writer, while engaged on steam pipe-work design over a long period, personally stressed out about 75 pipes. Of these about 40 were single-plane two-anchor, 25 three-dimensional two-anchor, 5 three-dimensional three-anchor, and the rest mixed two-dimensional three-anchor, one two-dimensional four-anchor, a case where a rotation was applied to a pipe end and some special problems with various odd constraints. The point of this list is that the vast majority of calculations in practice are two-anchor problems. Next, all methods of calculation must essentially comprise the following stages:

1 Calculating the elastic properties of the pipes forming the various branches.

2 Setting up the simultaneous equations.

3 Solving the simultaneous equations.

4 (A by no means negligible step) Finding out the point at which maximum stress (or bending moment) occurs and working out the stress there.

In the case of two-anchor problems, however, the special condition that there is no rotation of the free end of the pipe leads to a reduction in the unknowns in the two-dimensional case from three to two and in the three-dimensional case from six to three. (It is appreciated that this latter involves the neglect of certain secondary rotations but from a practical point of view it can be confirmed readily that this does not matter.) The author, from his introductory remarks, evidently fully appreciates all this and it is assumed that he would not in fact use the method he presents to solve the example he uses as an illustration.

When one comes to the three-anchor problem, considering for the moment in particular the three-dimensional case, there is no short cut for stage 1, and all the components of the six $\times$ six matrix for each branch must be worked out. It is in stage 2, i.e., setting up the equations, that the matrix formulation of the flexibility coefficients becomes worth while. To illustrate this point it is suggested that the worked example of a three-dimensional three-anchor problem given in the writer's 1947 paper (author's reference 5) be compared with the example given by Vinieratos and Zeno,[4] in which, in fact, the flexibility coefficients for one branch were worked out twice and the superiority of the matrix formulation will be apparent. Stage 3 and stage 4 are the same whatever method is adopted. There is no escape from the solution of 12 simultaneous equations.

The main question is does the matrix method advocated by the author of forming the flexibility matrices in stage 1 above offer any advantage over alternative methods, in particular, say, the graphoanalytical method? The writer's view is that the graphoanalytical method has two advantages to offer: (*a*) The non-diagonal elements of the matrix are worked out by completely independent calculations for pairs of elements symmetrical about the diagonal so that there is a very powerful check by Maxwell's reciprocal theorem; (*b*) in the writer's view the "motivation" is much stronger. As an engineer, he finds it much easier to visualize a pipe with a unit force or moment acting on the free end of it and consider what happens than to handle arithmetical calculations which do not seem to have obvious physical significance.

Thus summing these views from the purely practical point of view, the matrix formulation of pipe-work problems has little to offer for the ordinary two-anchor problem which comprises the vast majority of actual calculations. For three-anchor problems or problems with constraints it possesses considerable advantage in setting up the simultaneous equations (and in fact it was for just this purpose that the matrix method was developed and included in the writer's 1947 paper, author's reference 5) but there is no necessity to use matrix methods to obtain the matrices, and the use of the graphoanalytical method has the advantage of using methods with which one can have become familiar in dealing with two-anchor problems. In mentioning the matrix presentation in 1947, no originality was claimed as it is implicit in, for example, the M. W. Kellogg Company's publication "Design of Piping Systems" (author's reference 2). The only thing lacking is the word matrix, and, of course, an explicit statement of the matrix transformations produced by the author in matrix form.

These comments may appear rather critical of the author's paper but they are not meant to be, and in the writer's view the paper serves a useful purpose in presenting the concept of a flexibility matrix for a pipe and in particular, in giving in matrix form the transformations for shift of origin and rotation of axes.

Author's Closure

The author wishes to thank Dr. Baker and Commander Hoath for their interesting discussions.

Dr. Baker has made a welcome addition to the paper by his treatment of straight runs which do not lie in a plane parallel to one of the co-ordinate planes. The degree of arbitrariness which was involved in the author's treatment of a typical case (Fig. 7 of the paper) was evidence that a better treatment might be expected. That it would be as simple and as elegant as the form given in Table 1 of Dr. Baker's discussion was not expected. It should be clear but possibly is worth pointing out specifically that the matrix given in Table 1 of the discussion is a symmetrical matrix (the nonzero symmetrical elements are not displayed) in which the third-order null matrix occupies the upper right and lower left positions.

The author is grateful to Dr. Baker for private correspondence which points out that the expression $(\sin\theta_2 - \sin\theta_1)$ appearing in items A and D of Table 5 of the paper *should* read $(\sin 2\theta_2 - \sin 2\theta_1)$.

Dr. Baker's approach to a three-anchor problem may be abbreviated substantially, a directly motivated derivation being as follows (for convenience, reletter the points A, P, Q of Dr. Baker's Fig. 1 to read P_1, P_2, P_3 in any order): Let $\mathbf{\Delta}_i$ = compliance matrix at point O for branch OP_i presumed fixed at P_i and free at O, $(i = 1, 2, 3)$. These $\mathbf{\Delta}_i$ are 6×6 symmetrical matrices of deflections observed at O due to unit forces applied at O. Similarly, let the 6×1 column matrix $\mathbf{D}_i = -\mathbf{N}_{OP_i} - \mathbf{M}_{P_i} =$ (negatives of) free expansions of branch OP_i observed at O and including motions of anchor point P_i if any. Also, let the 6×1 column matrix $\mathbf{F}_i$ = actual forces applied at O to branch OP_i; these are the unknowns we wish to determine. Finally, let the 6×1 column matrix $\mathbf{D}$ denote the final displacements of point O.

Then, because no external force is applied to the system at O, we have

[3] Commander (E) Royal Navy, Naval Marine Wing, National Gas Turbine Establishment, Pyestock, Nr. Farnborough, Hants, England.

[4] "Piping Flexibility and Stresses," by D. S. Vinieratos and D. R. Zeno, Cornell Maritime Press, New York, N. Y., 1941.

$$\mathbf{F}_1 + \mathbf{F}_2 + \mathbf{F}_3 = \mathbf{O} \quad [1]$$

Also, in the final configuration, the "O-ends" of all three branches will have moved by the amounts $\mathbf{D}$; thus

$$\mathbf{\Delta}_i\mathbf{F}_i = \mathbf{D}_i + \mathbf{D}, (i = 1, 2, 3) \quad [2]$$

Accordingly, we have

$$\mathbf{\Delta}_1\mathbf{F}_1 - \mathbf{D}_1 = \mathbf{\Delta}_2\mathbf{F}_2 - \mathbf{D}_2 = \mathbf{\Delta}\,\mathbf{F}_3 - \mathbf{D}_3 = -\mathbf{\Delta}_3(\mathbf{F}_1 + \mathbf{F}_2) - \mathbf{D}_3 = \mathbf{D} \quad [3]$$

$$\begin{bmatrix} \mathbf{\Delta}_1 + \mathbf{\Delta}_3 & \mathbf{\Delta}_3 \\ \mathbf{\Delta}_3 & \mathbf{\Delta}_2 + \mathbf{\Delta}_3 \end{bmatrix} \begin{bmatrix} \mathbf{F}_1 \\ \mathbf{F}_2 \end{bmatrix} = \begin{bmatrix} \mathbf{D}_1 - \mathbf{D}_3 \\ \mathbf{D}_2 - \mathbf{D}_3 \end{bmatrix} \quad [4]$$

which is a symmetric set of twelve equations in twelve unknowns.

Commander Hoath points out the superiority of this formulation which also is given in his own development. The author emphasizes his agreement with the statement "There is no escape from the solution of twelve simultaneous equations." He feels that except possibly in special cases immediate direct use of the Crout (or similar) direct pivotal method is better than any preliminary reductions or iterative procedures. While these are appealing in conception, the power and speed of modern direct methods are so great that, all things considered, the direct methods are best. It is recognized, of course, that this is a matter of opinion which is not shared universally.

Referring to the final paragraph of Dr. Baker's discussion, the effect of line OQ may always be regarded as that of a more or less complicated constraint in the line AP regarded as a two-anchor problem; conversely, any constraint may be regarded as another branch the elastic properties of which may be given by an appropriate flexibility matrix. The shift in viewpoint may be illuminating in special cases. If line OQ is ideally short and stiff, the corresponding flexibility matrix ($\mathbf{\Delta}_3$, say) becomes null and it is evident from Equation [4] of this closure that the problem breaks up into two separate two-anchor problems.

Commander Hoath's remarks concerning the distribution into categories of the problems with which he has been concerned in marine practice are of considerable interest, especially since they tend generally to agree with such a distribution in stationary practice. That the majority of cases involve two-anchor problems is not unexpected.

The reduction of unknowns from six to three (or from three to two in the two-dimensional case) when there is no end rotation can be done with the matrix method as well as with any of the other methods. The conditions are that coefficients $A_{46} = A_{54}$, $A_{16} = A_{64}$, and $A_{56} = A_{65}$ of the flexibility matrix must vanish (or be negligibly small). Then, partitioning, we may write the equation

$$\mathbf{\Delta F} = \mathbf{D} \quad [5]$$

as

$$\begin{bmatrix} \mathbf{\Delta}_{11} & \mathbf{\Delta}_{12} \\ \mathbf{\Delta}_{21} & \mathbf{\Delta}_{22} \end{bmatrix} \begin{bmatrix} \mathbf{F}_F \\ \mathbf{F}_M \end{bmatrix} = \begin{bmatrix} \delta \\ \mathbf{O} \end{bmatrix} \quad [6]$$

where $\mathbf{\Delta}_{22}$ is now a (third order) *diagonal* matrix the reciprocal of which is simply

$$\mathbf{\Delta}_{22}^{-1} = \begin{bmatrix} (A_{44})^{-1} & 0 & 0 \\ 0 & (A_{55})^{-1} & 0 \\ 0 & 0 & (A_{66})^{-1} \end{bmatrix} \quad [7]$$

Then simple algebra leads to the formulation

$$(\mathbf{\Delta}_{11} - \mathbf{\Delta}_{12}\mathbf{\Delta}_{22}^{-1}\mathbf{\Delta}_{21})\mathbf{F}_F = \delta \quad [8]$$

which amounts to three equations in three unknowns.

In some methods of flexibility analysis, this reduction is inherent in the procedure. That is not to say, however, that the arithmetic operations outlined above have some how been obviated; indeed they have not been, but appear at some earlier stage in such a process.

In the illustrative case in the paper (the Hovgaard bend) small error would be involved in neglecting the coefficients 0.054450, after which the reduction could be accomplished quickly by the transformation mentioned in the foregoing. Commander Hoath is correct in inferring that the author would actually make this simplification in a practical case. However, such a simple reduction is not available in many practical cases where inclined straight lengths are encountered. There the terms $a_i a_j \mu L$ ($i \neq j$) shown in Dr. Baker's Table 1 might be too large to be neglected.

Commander Hoath offers two advantages of the graphoanalytical method, the second of which is a matter of opinion with which the author definitely does not agree. Upon inspection, the first reason appears to lose most of its force. The check afforded by the Maxwell reciprocity law depends upon making two separate calculations for each symmetric pair of nondiagonal elements. Exactly the same sort of check procedure is available with the matrix method: simply do everything twice! As a matter of fact, the Maxwell reciprocity law does not afford a check on the diagonal elements and it is presumed that users of the graphoanalytical method would indeed obtain each diagonal coefficient twice in order to have the same assurance of the correctness of these terms as of the nondiagonal terms.

It might be mentioned that there are numerous simple checks on matrix arithmetic which are not widely known but which are so simple and positive that they should be applied whenever possible. As an example, the multiplication

$$\begin{bmatrix} 3 & -2 & 1 \\ 6 & 4 & -1 \end{bmatrix} \begin{bmatrix} 1 & 3 \\ 2 & 0 \\ -3 & 2 \end{bmatrix} = \begin{bmatrix} -4 & 11 \\ 17 & 16 \end{bmatrix}$$

should be written as

$$\left[\begin{array}{ccc} 3 & -2 & 1 \\ 6 & 4 & -1 \\ \hline 9 & 2 & 0 \end{array}\right] \left[\begin{array}{cc:c} 1 & 3 & 4 \\ 2 & 0 & 2 \\ \hline -3 & 2 & -1 \end{array}\right] = \left[\begin{array}{cc:c} -4 & 11 & 7 \\ 17 & 16 & 33 \\ \hline 13 & 27 & 40 \end{array}\right]$$

the bordering elements in the multiplicands being the column and row sums, respectively, of the actual elements. Then the bordering elements in the product should be the column or row sums of the correct product elements. An error may be located instantly.

The author feels that the contents of the penultimate paragraph of Commander Hoath's discussion are matters of opinion rather than of fact. The extent to which a matrix formulation is implicit in the publication "Design of Piping Systems" appears to the author to be somewhat parallel to that to which flexure theory is implicit in "*Sic tensio ut vis.*" Also, there is a considerable difference between an indication that a certain set of equations may, if desired, be exhibited in matrix form and a complete, unified theory such as is presented in the paper. It may easily be understood that adequate motivation might be lacking from any development which is not unified or complete. While it would be pointless to extend these remarks further, consideration of the development of theory does, however, provide an opportunity to cite some related work of von Mises[8] which recently has come to the author's attention.

[8] "Motorrechnung, ein neues Hilfsmittel der Mechanik," by R. von Mises, *Zeitschrift für angewandte Mathematik und Mechanik*, vol. 4, 1924, pp. 155–181, and "Anwendungen der Motorrechnung," ibid. pp. 193–213. See also "Bermerkung zu dem Aufsatz von Hrn. Ferd. Schleicher über die Formanderung krummer Stabe," ibid., pp. 486–487.

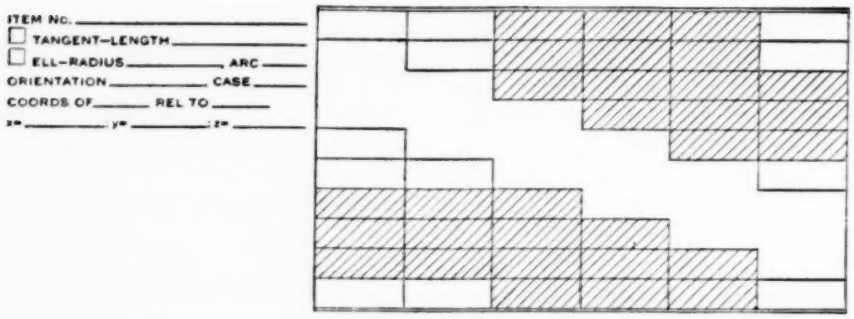

FIG. 2

Finally, the author feels that he himself was premature and mistaken in impugning the usefulness of the matrix method in two-dimensional cases and since writing the paper has actually made considerable use of it in certain two-dimensional cases involving spring hangers. If the reader uses a form (e.g., cf. Sheet 2 of Table 10 of the paper) prepared for use in three-dimensional cases, to avoid confusion it may be well to shade those "boxes" which will not be used; this is indicated in Fig. 2 of this discussion.

Thin Rectangular Plates on Elastic Foundations[1]

D. L. HOLL.[2] In this and previous papers,[3] the senior author and his colleagues have applied the finite Fourier sine transform to the solutions of linear boundary-value problems in thin elastic plates. In all three papers the authors convey the impression that they have enlarged the field of available solutions for these plate problems when the boundary conditions of one pair of opposite edges are arbitrarily assigned deflection and moment conditions and the other pair of opposite edges have general assigned boundary values. All of this extension is supposed to be accomplished by the finite sine transform whose kernel $\sin \alpha x$ ($\alpha = n\pi/a$) vanishes at the edges $x = 0$, $x = a$. They conclude that the final solution is always given by the form (A):

$$w(x, y) = 2/a \sum_{n=1}^{\infty} W_s(\alpha, y) \sin \alpha x, \ \alpha = n\pi/a, \ (n = 1, 2, 3, \ldots)$$

where $W_s(\alpha, y)$ is a properly determined function of y.

The authors have neither proved that solution (A) satisfies the plate equation, nor that it can attain the arbitrarily assigned deflection and moment conditions at the edges $x = 0$, and $x = a$. In all their illustrated examples they have chosen "pinned-edge conditions" at $x = 0$ and $x = a$, and hence obtain the well-known solutions for which the sine transform readily adapts itself and for which the ordinary Fourier-series method applied. No illustrations are provided for nonzero deflection and moment conditions at $x = 0$, $x = a$. In other words, the authors appear to have accomplished the task of obtaining solutions by the finite sine transform which cannot be obtained by the Fourier-series procedure. In this connection Sneddon[4] makes this pertinent statement, "The use of finite Fourier transforms does not solve problems which are incapable of solution by the direct application of the theory of Fourier series but it does facilitate the resolution of boundary-value problems."

In the general theory of linear integral transforms, a particular transformation, if any does exist, depends not only on the range of the independent variable, but also upon the differential forms and boundary conditions if the transform procedure is to reduce the original problem to a simple one. Moreover, the representation of the dependent function as given by the inverse formula as well as its required derivatives should converge to the prescribed values at all points of the closed domain. The writer is not convinced that these requirements are met by the sine transform in the foregoing problem when nonzero conditions of deflection and moment are assigned on the edges $x = 0$ and $x = a$. Consider the authors' Equation [50]: Substitution of this equation into Equation [1] leads to

$$\sum_{n=1}^{\infty} \frac{2}{a} \sin \alpha x \left[\frac{d^4 w_s(\alpha, y)}{dy^4} - \frac{2\alpha^2 d^2 w_s}{dy^2} + (\alpha^4 + k^4) w_s \right] = q(x, y)/D$$

Now if $q(x, y)$ is such that the following integral exists, i.e.

$$\int_0^a q(x, y) \sin \alpha x \, dx = q_s(\alpha, y) \quad \ldots\ldots [1]$$

then Equation [50] satisfies the authors' Equation [1] identically in x and y if

$$\frac{d^4 w_s(\alpha, y)}{dy^4} - 2\alpha^2 \frac{d^2 w_s(d, y)}{dy^2} + (\alpha^4 + k^4) w_s(\alpha, y) \equiv q_s(\alpha, y)/D \quad \ldots\ldots [2]$$

The authors wish to have $w_s(\alpha, y)$ satisfy Equation [2] herewith, with the right member replaced by $Q(\alpha, y)$ where the latter is given by Equation [22] of the paper and contains functions which arise by reason of given assigned deflections and moments.

The writer proposes the following counter example: Consider a rectangular plate occupying the domain $0 \leqq x \leqq a$; $-b \leqq y \leqq b$ with edges $x = 0$ and $y = \pm b$ simply supported (no deflection and no normal moment). The edge $x = a$ has $w(a, y) \equiv 0$ and moment $M_x = M_0 \cos(\pi y/2b) = M_0 \cos \beta y$, $M_0 = \text{const.}$ There is no load $q(x, y)$ and no subgrade reaction, $k = 0$.

The solution is

$$w(x, y) = \frac{M_0}{2D\beta^2 \sinh \beta a} [\beta a \coth \beta a \sinh \beta x - \beta x \cosh \beta x] \cos \beta y \quad \ldots\ldots [3]$$

[1] By H. J. Fletcher and C. J. Thorne, published in the September, 1952, issue of the JOURNAL OF APPLIED MECHANICS, Trans. ASME, vol. 74, pp. 361–368.

[2] Iowa State College, Ames, Iowa.

[3] "Some Thin-Plate Problems by the Sine Transform," by L. I. Deverall and C. J. Thorne, JOURNAL OF APPLIED MECHANICS, Trans. ASME, vol. 73, 1951, pp. 152–156; "Bending of Thin Ring-Sector Plates," by L. I. Deverall and C. J. Thorne, JOURNAL OF APPLIED MECHANICS, Trans. ASME, vol. 73, 1951, pp. 359–363.

[4] "Fourier Transforms," by I. N. Sneddon, McGraw-Hill Book Company, Inc., New York, N. Y., 1951, p. 72.

One observes immediately that $\nabla^4 w = 0$, and $w = 0$ on all edges. An easy check shows the edge moments are $M_x(0, y) = 0$, $M_y(x, \pm b) = 0$, and $M_x(a, y) = M_0 \cos \beta y$ which is the prescribed value.

From the paper we are led to the following equation for this problem

$$\frac{d^4 w_s(\alpha, y)}{dy^4} - 2\alpha^2 \frac{d^2 w_s(\alpha, y)}{dy^2} + \alpha^4 w_s(\alpha, y) = (-1)^{n+1} \frac{aM_0}{D} \cos \beta y \quad [4]$$

with all boundary conditions on the transform $w_s(\alpha, y)$ vanishing at $y = \pm b$. Hence the solution of Equation [4] of this discussion is

$$w_s(\alpha, y) = \frac{(-1)^{n+1} M_0 \cos \beta y}{D(\alpha^2 + \beta^2)^2}$$

and finally one would obtain

$$w(x, y) = \frac{2}{a} \sum_{n=1}^{\infty} \frac{(-1)^{n+1} M_0 \cos \beta y \sin \alpha x}{D(\alpha^2 + \beta^2)^2}$$

as the solution of this example. Does this solution satisfy $\nabla^4 w = 0$ for all x, y values and how does it converge to the boundary value, $M_x = M_0 \cos \beta y$ at $x = a$? Consider what occurs for $\nabla^4 w = 0$, on the line $x = a/2$

$$\nabla^4 w(x, y) = \frac{2}{a} \sum_{n=1}^{\infty} (-1)^{n+1} \frac{M_0}{D} \cos \beta y \sin \alpha x$$

At $(a/2, y)$

$$\nabla^4 w(a/2, y) = \frac{2}{aD} M_0 (1 - 1 + 1 - \ldots\ldots) \cos \beta y$$

and diverges.

Consider another example: Again the unloaded plate occupies the same domain with the edges $x = a$, $y = \pm b$ simply supported. At $x = 0$, there is no normal moment M_x but the deflection is

$w(0, y) = \delta \cos \pi y/2b = \delta \cos \beta y$, where $\delta = \text{const}$, and $\beta = \pi/2b$

The solution

$$w(x, y) = \delta \cos \beta y \left\{ \cosh \beta x - \left[\coth \beta a + \frac{\alpha\beta(1 - \sigma)}{2 \sinh^2 \beta a} \right] \sinh \beta x + \frac{(1 - \sigma)}{2} (\beta x \coth \beta a \cosh \beta x - \beta x \sinh \beta x) \right\}$$

satisfies all the conditions of the problem. The authors' method leads to

$$w_s(\alpha, y) = \frac{\alpha^3 + 2\alpha\beta^2 - \sigma\alpha\beta^2}{(\alpha^2 + \beta^2)^2} \delta \cos \beta y$$

or

$$w(x, y) = \frac{2\delta}{a} \sum_{n=1}^{\infty} \frac{\alpha^3 + 2\alpha\beta^2 - \sigma\alpha\beta^2}{(\alpha^2 + \beta^2)^2} \cos \beta y \sin \alpha x$$

What deflection does this yield at $x = 0$? Consider also the moment sum $M_x + M_y$ at $(a/2, 0)$. This is proportional to $\nabla^2 w$, and at the center of the plate yields

$$\frac{-2\delta}{a} \sum_{n=1}^{\infty} \frac{\alpha^3 + 2\alpha\beta^2 - \sigma\alpha\beta^2}{(\alpha^2 + \beta^2)} \sin \frac{n\pi}{2}$$

This diverges. Similarly, if one computes the shear V_x at $(a, 0)$ it is found to diverge.

Counter examples similar to this are readily devised for rectangular plates on elastic foundation and for curvilinear sector plates bounded by two radii and arcs of two concentric circles.

Authors' Closure

We first call attention to the statement in the paper: "When writing the sine transform (or inverse transform) of any function, we shall assume that the function has properties necessary for that transform (or inverse transform) to exist. Also we assume continuity of all derivatives." (There are similar statements in each paper.) This is intended to state that the solutions given are formal solutions and must be shown to be solutions in any given problem. We will show that the formal solutions given by the methods of our paper to the counter examples proposed by Dr. Holl are the solutions.

We also call attention to example (f) of our paper which is an example of nonzero boundary conditions. It also should be noted that Fourier series converge to the average value at any given point $\frac{1}{2}[f(x_0 +) + f(x_0 -)]$. This requires that boundary conditions at discontinuous points be in the form of limits from the interior rather than values at the boundary.

For Holl's first counter example, our formal solution is

$$w(x, y) = \frac{2M_0 \cos \beta y}{aD} \sum_{n=1}^{\infty} (-1)^{n+1} \frac{\alpha \sin \alpha x}{(\alpha^2 + \beta^2)^2} \quad \ldots\ldots [5]$$

This can be seen to be the solution, Equation [3] of Dr. Holl's discussion, by using the following results from our tables of sine and cosine transforms[5]

$$\frac{2}{a} \sum_{n=1}^{\infty} \frac{\alpha \sin \alpha x}{(\alpha^2 + \beta^2)^2} = \frac{-a \sinh \beta x}{2\beta \sinh^2 \beta a} + \frac{x \cosh \beta(a - x)}{2\beta \sinh \beta a} \quad [6][5]$$

$$\frac{2}{a} \sum_{n=1}^{\infty} f_s(\alpha) (-1)^{n+1} \sin \alpha x = f(a - x) \quad \ldots\ldots [7][6]$$

There results

$$\frac{2}{a} \sum_{n=1}^{\infty} \frac{(-1)^{n+1} \alpha \sin \alpha x}{(\alpha^2 + \beta^2)^2} = \frac{-a \sinh \beta(a - x)}{2\beta \sinh^2 \beta a} + \frac{(a - x) \cosh \beta x}{2\beta \sinh \beta a} \quad \ldots\ldots [8]$$

For his second counter example use in addition to the foregoing formula the following

$$\frac{2}{a} \sum_{n=1}^{\infty} \frac{\alpha^3}{(\alpha^2 + \beta^2)^2} = \frac{\sinh \beta(a - x)}{\sinh \beta a} + \frac{\beta\pi \sinh \beta x}{2 \sinh^2 \beta a} - \frac{\beta x \cosh \beta(a - x)}{2 \sinh \beta a} \quad [9][7]$$

[5] "Sine and Cosine Transforms," by H. J. Fletcher and C. J. Thorne, Studies in Applied Mathematics, University of Utah, Department of Mathematics, no. 8, p. 7, and no. 13, p. 46, 1952.

[6] Ibid., no. 46, p. 13.

[7] Ibid., no. 10, p. 7.

obtaining the solution in Dr. Holl's discussion. This shows that our formal solutions are the Fourier series forms of the solutions.

To show how to differentiate a nonuniformly convergent series without knowing the summed form proceed as noted in our tables[8]

$$w(x) = \frac{1}{\pi}\int_0^\pi w(x)dx + \frac{2}{\pi}\sum_{n=1}^{\infty}\left[\int_0^\pi w(x)\cos nx\,dx\right]\cos nx \quad [10]$$

$$w'(x) = \frac{1}{\pi}\int_0^\pi w'(x)dx + \frac{2}{\pi}\sum_{n=1}^{\infty}\left[\int_0^\pi w'(x)\cos nx\,dx\right]\cos nx \quad [11]$$

We have assumed the derivative to exist in the open interval $(0, \pi)$. Integrating by parts

$$w'(x) = \frac{w(\pi-) - w(0+)}{\pi} + \frac{2}{\pi}\sum_{n=1}^{\infty}\left\{\left[w(x)\cos nx\right]_{0+}^{\pi-} - n\int_0^\pi w\sin nx\,dx\right\}\cos nx \quad [12]$$

Also

$$w(x) = \frac{2}{\pi}\sum_{n=1}^{\infty} w_s(n)\sin nx \quad [13]$$

so

$$w'(x) = \frac{w(\pi-) - w(0+)}{\pi} + \frac{2}{\pi}\sum_{n=1}^{\infty}\left\{\left[w(x)\cos nx\right]_{0+}^{\pi-} + nw_s(n)\right\}\cos nx \quad [14]$$

If $w_s(n)$ is of order $0(1/n^2)$ the series for $w(x)$ is uniformly convergent and hence continuous. Hence $w(0) = w(\pi) = 0$, and also $w(0+) = \lim_{x\to 0+} w(x) = 0$, and $w(\pi-) = \lim_{x\to\pi-} w(x) = 0$.

If the boundary conditions are specified as $w(\pi-) = w(0+) = 0$, then Equation [14] gives $w'(x)$ as the series obtained from $w(x)$ by term-by-term differentiation. Similarly if

$$w(x) = \frac{w_c(0)}{\pi} + \frac{2}{\pi}\sum_{n=1}^{\infty} w_c(n)\cos nx$$

$$w'(x) = \frac{-2}{\pi}\sum_{n=1}^{\infty} nw_c(n)\sin nx$$

if the derivative exists. This is the same as term-by-term differentiation regardless of the boundary conditions.

Applying this to the first example we get

$$w_{xx}(x, y) = \frac{-2M_0}{aD}\cos\beta y\sum_{n=1}^{\infty}\frac{(-1)^{n+1}\alpha^2}{(\alpha^2+\beta^2)^2}\sin\alpha x \quad [15]$$

This is not uniformly convergent; hence we cannot differentiate term by term. Using Equation [14], however, we get

[8] Footnote 5, p. 5.

$$w_{xxx} = \frac{w_{xx}(a-, y) - w_{xx}(0+, y)}{a} + \frac{2}{a}\sum_{n=1}^{\infty}\left[w_{xx}(a-, y)(-1)^n - w_{xx}(0+, y) + \frac{(-1)^{n+1}\alpha^4}{(\alpha^2+\beta^2)^2}\left(-\frac{M_0}{D}\cos\beta y\right)\right]\cos\alpha x \quad [16]$$

or

$$w_{xxx} = \frac{-M_0\cos\beta y}{Da} + \frac{2M_0\cos\beta y}{Da}\sum_{n=1}^{\infty}(-1)^{n+1}\frac{2\alpha^2\beta^2+\beta^4}{(\alpha^2+\beta^2)^2}\cos\alpha x \quad [17]$$

Similarly

$$w_{xxxx} = \frac{-2M_0\cos\beta y}{aD}\sum_{n=1}^{\infty}\frac{2\alpha^3\beta^2+\alpha\beta^4}{(\alpha^2+\beta^2)^2}(-1)^{n+1}\sin\alpha x \quad [18]$$

$$w_{xxyy} = \frac{2M_0\cos\beta y}{aD}\sum_{n=1}^{\infty}\frac{\alpha^2\beta^2}{(\alpha^2+\beta^2)^2}(-1)^{n+1}\sin\alpha x \quad [19]$$

$$w_{yyyy} = \frac{2M_0\cos\beta y}{aD}\sum_{n=1}^{\infty}\frac{\alpha\beta^4}{(\alpha^2+\beta^2)^2}(-1)^{n+1}\sin\alpha x \quad [20]$$

and hence $\nabla^4 w = 0$ in the open region.

In Holl's second example $w(x, y)$ is not uniformly convergent. Applying Equation [14] we get

$$w_x(x, y) = -\frac{\hat{\delta}\cos\beta y}{a} - \frac{2}{a}\hat{\delta}\cos\beta y\sum_{n=1}^{\infty}\frac{(\sigma\beta^2\alpha^2+\beta^4)}{(\alpha^2+\beta^2)^2}\cos\alpha x \quad [21]$$

$$w_{xxx}(x, y) = -\frac{w_{xx}(0+, y)}{a} + \frac{2}{a}\sum_{n=1}^{\infty}\left[-w_{xx}(0+, y) + \frac{\sigma\beta^2\alpha^4+\alpha^2\beta^4}{(\alpha^2+\beta^2)^2}\hat{\delta}\cos\beta y\right]\cos\alpha x \quad [22]$$

Noting that

$$M_x = -D[w_{xx}(0+, y) + \sigma w_{yy}(0+, y)] \quad [23]$$

$$= -D[w_{xx}(0+, y) - \sigma\hat{\delta}\beta^2\cos\beta y] = 0 \quad [24]$$

$$w_{xx}(0+, y) = \hat{\delta}\sigma\beta^2\cos\beta y \quad [25]$$

$$w_{xxx}(x, y) = \frac{-\sigma\hat{\delta}\beta^2\cos\beta y}{a} + \frac{2}{a}\hat{\delta}\cos\beta y\sum_{n=1}^{\infty}\frac{\alpha^2\beta^4(1-2\sigma) - \sigma\beta^6}{(\alpha^2+\beta^2)^2}\cos\alpha x \quad [26]$$

$$w_{xxxx}(x, y) = \frac{2\hat{\delta}\cos\beta y}{a}\sum_{n=1}^{\infty}\frac{\alpha^3\beta^4(-1+2\sigma) + \sigma\beta^6\alpha}{(\alpha^2+\beta^2)^2}\sin\alpha x \quad [27]$$

$$2w_{zzyy}(x, y) = \frac{2\delta \cos \beta y}{a} \sum_{n=1}^{\infty} \frac{-2\sigma\beta^4\alpha^2 - 2\alpha\beta^6}{(\alpha^2 + \beta^2)^2} \sin \alpha x \ldots [28]$$

$$w_{yyyy}(x, y) = \frac{2\delta \cos \beta y}{a} \sum_{n=1}^{\infty} \frac{\alpha^2\beta^4 + 2\alpha\beta^6 - \sigma\alpha\beta^6}{(\alpha^2 + \beta^2)^2} \sin \alpha x \ldots [29]$$

and hence $\nabla^4 w = 0$ in the open region.

A Study of Vanes Singing in Water[1]

G. E. Alves[2] and D. H. Barker.[3] The author found that the Strouhal number (Nb'/V) remained substantially constant if the term b' is taken to be the thickness of the trailing edge b, plus some fraction of the boundary-layer thickness. Previous investigators[4, 5, 6, 7, 8] have found that the Strouhal number was essentially constant if b' is taken as the projected height of the object perpendicular to the direction of flow. Fage and Johansen[6] state that b' is the distance between points of separation of the vortex sheets as they leave the surface of the body. With a flat plate or an airfoil shape at a high angle of attack (greater than 30 deg) this separation is determined by the extreme edges of the object and is the projected height of the plate or airfoil. However, at low angles of attack this relationship does not hold, due perhaps to the movement of the point of separation of the vortex sheets downstream on the object. In the author's investigation, it seems possible that the separation of the vortex sheets did not take place at the maximum breadth but at some point near the trailing edge. Could the author determine from his photographs the points of separation and determine if the projected distance between these points is equal to his value of b'?

It would be interesting to know what the difference was between the plates used in obtaining the data for Tables 1 and 2 of the paper. It also would be interesting to know what effect gradually increasing the maximum thickness of the plate for a constant trailing edge would have on the author's "virtual thickness."

Author's Closure

In answer to the discussers' first question, careful examination of the photographs, which fortunately contain more detail than it was possible to obtain in the reproductions in the paper, does not indicate that the separation occurs ahead of the trailing edge for the vanes in question. The formation of each new vortex can be seen to occur just behind the trailing edge. In answer to the question on the difference between Tables 1 and 2, these plates were as nearly alike as we could make them and the difference is apparently within the experimental errors of measurement.

In regard to the effect of differing maximum plate thicknesses on the value of the "virtual thickness," one plate of twice the maximum thickness, 3/4 in. but otherwise identical with the others was tested and the results shown in Fig. 9 of the paper. If this is compared with Fig. 1 (*b*) for the case of the same trailing edge thickness, 0.125 in., but half the maximum thickness, the frequency speed relationship is seen to be the same; for example, 30 knots gives a frequency of 700 to 750 cps for both. Also, Fig. 9 shows that small angles of attack do not change this relationship. This supports the author's conclusion that on vanes of this type, fare and thin, the trailing edge thickness controls in the Strouhal number.

[1] By C. A. Gongwer, published in the December, 1952, issue of the Journal of Applied Mechanics, Trans. ASME, vol. 74, pp. 432–438.

[2] Chemical Engineer, Engineering Research Laboratory, Engineering Department, E. I. du Pont de Nemours & Company, Wilmington, Del. Mem. ASME.

[3] Chemical Engineer, Engineering Research Laboratory, Engineering Department, E. I. du Pont de Nemours & Company.

[4] "Über Messungen von Wirbelfrequenzen," by H. Blenk, D. Fuchs, and F. Liebers, *Luftfahrtforschung*, 1935, pp. 38–41.

[5] "On the Flow of Air Behind Inclined Flat Plate of Infinite Span," by A. Fage and F. C. Johansen, Proceedings of the Royal Society of London, series A, vol. 116, 1927, pp. 170–197.

[6] "The Structure of Vortex Sheets," by A. Fage and F. C. Johansen, *Philosophical Magazine*, vol. 5, 1928, pp. 417–441.

[7] "Investigation of the Wing-Wake Frequency With Application of the Strouhal Number," by M. Z. Krzywoblocki, *Journal of the Aeronautical Sciences*, vol. 12, 1945, pp. 51–62.

[8] "Vortex Formation Behind Obstacles of Various Section," by E. Tyler, *Philosophical Magazine*, vol. 11, 1931, pp. 849–890.

On a General Method of Solving Second-Order Differential Equations by Phase-Plane Displacements[1]

H. M. Paynter.[2] The graphical technique presented in the paper belongs to the general class of solution procedures often referred to as "curvature methods" of graphical phase-plane integration. These procedures were brought to a high level of refinement by a number of investigators, notable among them Kelvin,[3] Léauté,[4] Meissner,[5] and Braun,[6] in addition to the author's cited references. The present author is to be complimented on his further contributions to this important field.

The delta-method may be considered as a special case of the more general Meissner technique which does not constrain the center of curvature to lie on the displacement axis.[5] However, as the author points out, there are certain inherent advantages in making this restriction even at the expense of accuracy or at the cost of smaller increments to secure the desired accuracy of results.

In the interest of clarifying the procedure from an analytical point of view, and to permit an appraisal of the inherent benefits and weaknesses of this technique, the writer has taken the liberty of presenting still another alternative derivation of the basic working formulas in the following paragraphs.

Beginning with the author's general second-order differential Equation [1]

$$m\ddot{x} + G(x, \dot{x}, t) = 0$$

one may always arbitrarily rearrange this in the form

$$T^2\ddot{x} + x = -\delta(x, \dot{x}, t) \ldots [1]$$

where $T = \sqrt{m/k}$ and $\delta = (G/k) - x$; then, merely by defining the new time variable

$$\tau = t/T \ldots [2]$$

[1] By L. S. Jacobsen, published in the December, 1952, issue of the Journal of Applied Mechanics, Trans. ASME, vol. 74, pp. 543–553.

[2] Assistant Professor of Hydraulic Engineering, Massachusetts Institute of Technology, Cambridge, Mass. Mem. ASME.

[3] "Graphical Solution of Dynamical Problems," by Lord Kelvin, *Philosophical Magazine*, vol. 34, 1892, pp. 443–448.

[4] "Du mouvement trouble des moteurs consecutif a une perturbation brusque. Nouvelle methode graphique pour l'etude complete de ce mouvement," by H. Léauté, *Journal de l'Ecole Polytechnique*, Cahier, 61, 1891, pp. 1–33.

[5] Graphische Analysis vermittelst des Linienbildes einer Function," by E. Meissner, Verlag der Schweiz. Bauzeitung, Zurich, Switzerland, 1932.

[6] "Über die graphische lösung der Differentialgleichung der erzwungenen Schwingunger bei beliebigen Gesets für Dämpfung, Rückstellkraft, und Anreibskraft," by E. Braun, *Ingenieur Archiv*, vol. 8, 1937, pp. 198–202.

the fundamental equations may be expressed by

$$\frac{dv}{d\tau} + x = -\delta(x, v, \tau) \quad [3]$$

$$v = \frac{dx}{d\tau} \quad [4]$$

If this pair is arranged in the form

$$\frac{dv}{d\tau} = -(x + \delta) \quad [3a]$$

$$\frac{dx}{d\tau} = v \quad [4a]$$

and if the second equation is divided by the first, the time increment cancels out and there results the phase equation obtained by the author (Equation [4] of the paper)

$$\frac{dx}{dv} = -\frac{v}{x + \delta}$$

However, for the present it will be more appropriate to return to the normal temporal form as in Equations [3] and [4] of this discussion. The integrals of these equations may be written implicitly beginning from the condition that when

$$\tau = \tau_i, x = x_i, \text{and } v = v_i,$$

namely

$$v = v_i - \int_{\tau_i}^{\tau} x d\tau - \int_{\tau_i}^{\tau} \delta \, d\tau \quad [5]$$

$$x = x_i + \int_{\tau_i}^{\tau} v d\tau \quad [6]$$

For the general case where δ varies arbitrarily with (x, v, τ) no analytic solution exists, since the time integral of δ could not be evaluated. However, for certain special cases of δ-functions solutions may be obtained.

In particular, if δ were identically zero, the phase plot (x, v) would be "circular" having the equation

$$x^2 + v^2 = x_i^2 + v_i^2 = \text{const} \quad [7]$$

and the time plots $x(\tau)$ and $v(\tau)$ would necessarily be sinusoidal and of unit frequency.

Moreover, if $\delta = \delta_i = \text{const}$ over the time interval $\Delta\tau_i = \tau_{i+1} - \tau_i$, then the definite time integral of δ also may be evaluated readily as

$$\int_{\tau_i}^{\tau_{i+1}} \delta d\tau = \delta_i \Delta\tau_i \quad [8]$$

and again the phase plot is circular and is traversed at unit angular velocity, only in this instance the center of the circle is displaced from the origin by the amount δ_i, and the consequent phase equation becomes

$$(x + \delta_i)^2 + v^2 = (x_i + \delta_i)^2 + v_i^2 = \text{const} \quad [9]$$

However, the above relation will be valid only for the time interval from τ_i to τ_{i+1}. Again, these "segments" of the time plots will be sinusoidal.

In effect, Equations [8] and [9] of this discussion may be used in an approximate sense to form the basis of the practical graphical procedure of the author. Viewed in this light, the solution of the "general" second-order equation is reduced to the approximately equivalent forced-vibration problem with a stepwise varying forcing function. Thus Equation [1] of this discussion may be interpreted as a forced undamped vibration equation

$$T^2\ddot{x} + x = -\delta_i(t) \quad [1a]$$

where δ_i varies in stepwise fashion at known or otherwise specified intervals of time. In order for Equation [1a] to represent the solution of Equation [1] of the paper, it is necessary that δ_i be equal to the average value of δ over the time interval $\Delta\tau_i$, that is

$$\delta_i \equiv \overline{[\delta(x, v, \tau)]_i} = \frac{1}{\Delta\tau_i} \int_{\tau_i}^{\tau_{i+1}} \delta \, d\tau \quad [10]$$

Indeed, this solution procedure becomes an analytic piecewise linear approximation to the exact solution, with the goodness of the approximation, at least at the end points of the intervals, depending solely on the ability to determine δ_i. Of course, at the interior points of the interval, which are always represented in this approximation by circular arcs, the accuracy will generally further depend upon the number of steps used. The "ultimate" convergence of the method is assured—except at certain singular points—by the consideration that, at least in the analytic or numerical equivalents of this graphical procedure, the solution must approach the exact solution (even for δ_i taken equal to the initial value $\delta[x_i, v_i, \tau_i]$) as the number of steps becomes infinite with each $\Delta\tau_i$ becoming infinitesimal. Moreover, the analytic solution for each increment may be simply written

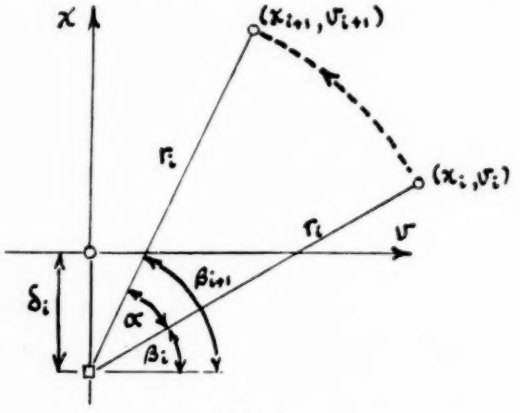

FIG. 1

(for whatever practical value it may have in numerical calculation or in checking the graphical results) as follows, with reference to Fig. 1, herewith

Initial radius, $r_i = \sqrt{(x_i + \delta_i)^2 + v_i^2} = v_i\sqrt{1 + \tan^2\beta_i}$. [11]

Initial angle, $\beta_i = \tan^{-1}\left(\frac{x_i + \delta_i}{v_i}\right)$ [12]

Cyclic increment, $\alpha = \Delta\tau_i$ [13]

Final angle, $\beta_{i+1} = \alpha + \beta_i$ [14]

Final displacement, $x_{i+1} = r_i \sin\beta_{i+1} - \delta_i$ [15]

Final velocity, $v_{i+1} = r_i \cos\beta_{i+1}$ [16]

Thus by judicious use of a table of squares together with trigonometric tables, for many types of δ-functions the numerical equivalent of the δ-method may prove to be as practical as its graphical counterpart.

It should be clear both from the foregoing treatment and from the original paper, that in practical application to nonlinear systems, the δ-method will involve to a certain extent successive approximation interval by interval, to obtain reasonably good values of δ_i. This is particulary true in regions where the "direction" of change in δ (positive or negative) is not evident at the outset of the increment. For a specific example, if $\delta(x, v, \tau) = (x - a)^2 f(t)/(v - b)$, it would be difficult to obtain satisfactory results for x near a and v near b. Certainly, the author's statement "... A subprofessional assistant can ... use the method ..." could not be applied literally to this case. As a matter of fact, the difficulties encountered by all curvature methods under such conditions as this, at branch points and other singularities, constitutes a serious limitation on their general applicability. It is evident by comparing Figs. 3 and 4 of the paper, that precision in the neighborhood of the origin for the case depicted is not practically possible.

Thus if $\delta(x, v, \tau)$ varies in certain critical and sensitive ways with the variables it will be necessary to use great care in the application of this technique. For the general case, unless the oscillatory character of the equation is clearly marked

$$\frac{\partial G}{\partial x} \gg \frac{\partial G}{\partial v}$$

there is no particular reason for preferring the curvature formulation over the more general form

$$\frac{dv}{d\tau} = \gamma(x, v, \tau) \quad [17]$$

for which implicit approximate integrals may also be written as

$$v_{i+1} = v_i + \gamma_i \Delta\tau_i \quad [18]$$

$$\gamma_i = \overline{[\gamma(x, v, \tau)]_i} \quad [19]$$

$$x_{i+1} = x_i + \int_{\tau_i}^{\tau_{i+1}} v d\tau \quad [20]$$

and corresponding to which, graphical procedures exist.

This consideration, in addition to the fact that the phase-plane curvature methods are not practical for nonlinear first-order, as well as third- and higher-order systems, led the writer[7] to the development of a graphical technique, patterned after the Bergeron method for wave-propagation problems,[8] which has come to be called the "slopeline method." This method has been further refined by himself, and collaborators,[9,10] and full details will shortly be available in book form,[11] together with applications to transient and vibration problems of all orders, both linear and nonlinear.

Author's Closure

The opening statement of Professor Paynter's discussion asserts that "curvature" methods of graphical phase-plane integration were brought to a high level of refinement long ago. In reviewing the discusser's references to the work of Lord Kelvin,[5] Léauté,[4] Meissner,[6] and Braun[6] the author finds that only the reference to Braun is relevant to the method of using "curvatures in the phase plane" unless it be maintained for the sake of completeness that many other names including those of Descartes and Euclid also should have been brought in as references.

The phase-plane delta method cannot be considered a special case of the Meissner[6] technique. However, Meissner's method is definitely more general than the phase-plane delta method since it is applicable to differential equations of any order, but this generality is not achieved by phase-plane considerations.

In calling attention to the work of Braun,[6] the discusser has contributed a welcome reference that the author regrets to have missed. Braun deals with the subnormal to the arc ds in Fig. 1(b) of the paper, but does not locate the center of the circular approximation on the x axis.

Professor Paynter's alternative derivation of the phase-plane δ method relationship is instructive as presenting a variant of those given by Professor Klotter and the author. The adjustment of the δ method to numerical calculations as shown in the discusser's Equations [11] to [16] is of interest to people who are numerically inclined, but it is of course not uniquely dependent on his way of deriving the δ relationship.

The author is grateful to the discusser for his attempt to appraise the inherent weaknesses and strengths of the δ method and agrees with him that no curvature procedure will give good accuracy near singular points. This fact, however, does not invalidate the author's statement that a subprofessional assistant can be instructed quickly in how to use the graphical δ method. Of course, the accuracy of a solution will suffer in a singular-point region, but the assistant will become forcefully aware of that by having to draw highly scalloped arcs there; consequently a finer subdivision or simple caution will automatically suggest itself to him.

It is interesting to note that Professor Paynter is planning to give full details of the "slope-line method" in the book[11] he is now preparing.

Errata:

In the author's Equation [4] change v to $-v$, and in connection with the solution of Bessel's equation change $-\delta_0$ to $+\delta_0$.

[7] "Methods and Results From M.I.T. Studies in Unsteady Flow," by H. M. Paynter, *Journal of the BSCE*, vol. 39, April, 1952, pp. 120–165.

[8] "Du coup de belier en hydraulique au coup de foudre en électricité," by L. Bergeron, Dunod, Paris, France, 1950.

[9] "Regulation of Hydroelectric Plants," by A. T. Gifford and H. M. Paynter, M.I.T. 1952 (mimeographed notes).

[10] "Slopeline-Graphical Solutions of Ordinary Nonlinear Differential Equations, With Engineering Applications," by A. C. Hendrickson, M.I.T. SM thesis, 1952 (unpublished).

[11] "Graphical Solution of Engineering Transients," by H. M. Paynter and A. C. Hendrickson (book in preparation).

Bending of a Uniformly Loaded Rectangular Plate With Two Adjacent Edges Clamped and Others Either Simply Supported or Free[1]

A. S. Veletsos.[2] The authors are to be complimented for their valuable paper. It might be of interest to note, however, that the problem of the bending of a uniformly loaded rectangular plate having two adjacent edges clamped and the others simply supported has been treated also by C. P. Siess and N. M. Newmark,[3] who used a modification of the method developed by Timoshenko. Included in this reference are the general solution of the problem and also numerical values for the moments on several sections of a square plate and of a rectangular plate having a ratio of sides equal to 0.5.

[1] By M. K. Huang and H. D. Conway, published in the December, 1952, issue of the Journal of Applied Mechanics, Trans. ASME, vol. 74, pp. 451–460.

[2] Research Associate in Civil Engineering, University of Illinois, Urbana, Ill.

[3] "Moments in Two-Way Concrete Floor Slabs," by Chester P. Siess and Nathan M. Newmark, University of Illinois Engineering Experiment Station Bulletin 385, February, 1950, pp. 90–96.

For the purpose of comparison, the values of the moment on the fixed edge of a square plate which were presented in Table 3 of the paper are listed in the following, together with the corresponding values calculated from the solution obtained by Siess and Newmark:

Location		Clamping moments $\times (1/qa^2)$		
		Huang and		Siess and
x	y	Conway	Stiles	Newmark
$0.2a$	0	−0.0272	−0.0257	−0.0275
$0.4a$	0	−0.0594	−0.0608	−0.0598
$0.6a$	0	−0.0692	−0.0684	−0.0691
$0.8a$	0	−0.0510	−0.0515	−0.0507

Authors' Closure

The authors are grateful to Mr. Veletsos for bringing the work of Siess and Newmark to their attention. The agreement in the values of the clamping moments is most satisfactory.

The Elastic Sphere Under Concentrated Loads[1]

M. M. Frocht.[2] The paper raises several questions regarding the fundamentals in the theory of elasticity. Of particular significance is the conclusion that to the three conditions generally accepted as sufficient for a unique solution a fourth "limit condition" must be added and that failure to include such a fourth condition will, in the case of concentrated loads, lead to pseudosolutions, that is, in essence, to false solutions. This conclusion carries with it the need for a re-examination of the meaning of Saint Venant's principle.

To an experimentalist this paper is significant for an additional reason. It provides another illustration that mathematicians are not infallible and that the ultimate test of a theoretical solution lies in experimental verification.

The agreement between the theoretical results of the authors and the photoelastic results of Frocht and Guernsey are particularly noteworthy because the photoelastic solution is the first complete solution of its kind. The degree of agreement between the two sets of results is indeed remarkable, particularly at the center of the sphere where the difference in the value of (σ_s/σ_0) is about 2 per cent.

On the surface of the sphere, around the equator, where the stresses are relatively small, the agreement is less satisfactory. There the photoelastic value of (σ_z/σ_0) is zero and the theoretical value is 0.30, for $\nu = 0.48$. This aspect of the problem can be investigated by means of a strain-gage test. At the suggestion of the discusser, Messrs. K. P. Milbradt,[3] D. Landsberg,[4] and P. D. Flynn[5] made such a test using an aluminum sphere of 4.87 in. diam for that purpose, Fig. 1, herewith.

Four $^1/_8$-in. SR-4 strain gages were mounted at points A-A, Fig. 2, on the equator. Two gages were set parallel to ϵ_z and the remaining two parallel to ϵ_y. Tests were made at 28,000 lb, 56,000 lb, 84,000 lb, etc., up to 500,000 lb. Typical strain-load curves for several cycles of loading and unloading are shown in Fig. 3.

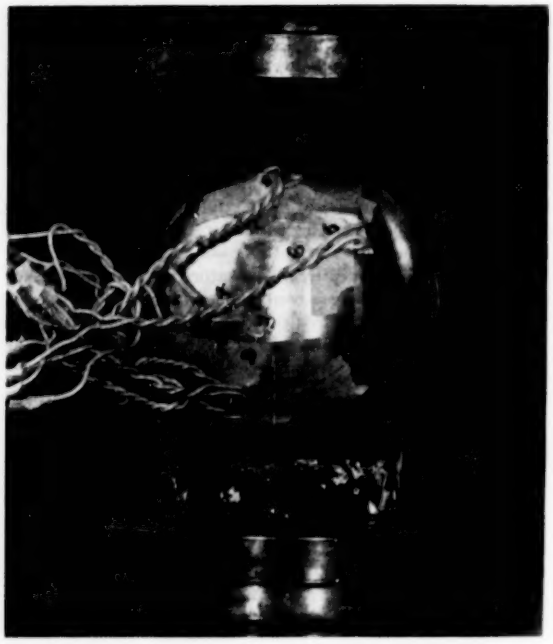

Fig. 1

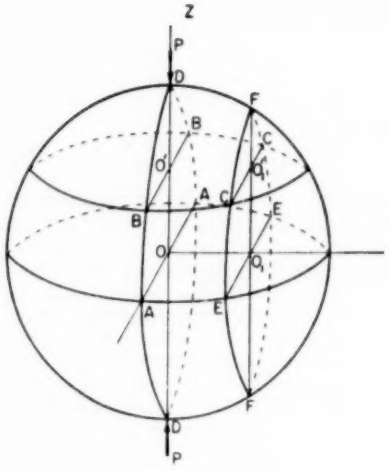

Fig. 2

It will be observed that the stress-strain relation is essentially linear. This linearity extended up to 280,000 lb, and the deviations from linearity at higher loads were small. It also will be noted that recovery was somewhat incomplete in the first stage of each new load. The meaning of this initial set is at present not clear. Perhaps it may be connected with the development of small plastic zones in the region of the applied load.

The stresses were based on the mean recoverable strain. The error resulting from neglecting the initial set is believed to be small.

The final results are summarized in Table 1 of this discussion. The gages thus show that in the equatorial region there exist compressive σ_s stresses of a magnitude of $0.25\sigma_0$ and transverse

[1] By E. Sternberg and F. Rosenthal, published in the December, 1952, issue of the Journal of Applied Mechanics, Trans. ASME, vol. 74, pp. 413–421.

[2] Research Professor of Mechanics, Illinois Institute of Technology, Chicago, Ill. Mem. ASME.

[3] Assistant Professor of Civil Engineering, Illinois Institute of Technology.

[4] Assistant Research Engineer in Experimental Stress Analysis, Illinois Institute of Technology.

[5] Research Corporation Fellow in Experimental Stress Analysis, Illinois Institute of Technology.

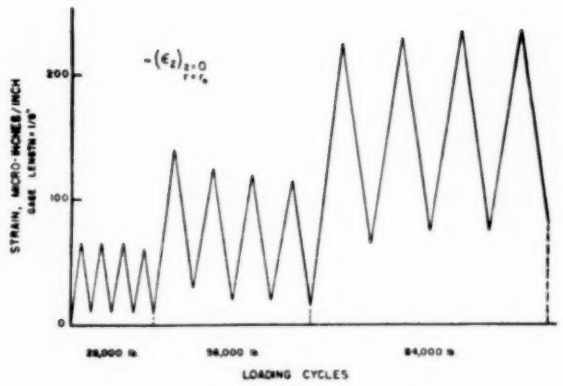

FIG. 3

tensile stresses $0.43\sigma_0$. The corresponding theoretical values for $\nu = 0.32$ are $0.24\sigma_0$ and $0.44\sigma_0$, respectively. The strain-gage tests thus corroborate the analytical conclusions of the authors.

The reason for the small photoelastic error is believed to lie in the thermal stresses developed during the freezing cycle. A discussion of these must be deferred for another occasion.

TABLE 1 RESULTS OF TESTS

	Stresses at $z = 0$, $r = r_0$			
	σ_z/σ_0	σ_r/σ_0	ν	Investigator
Theoretical	−0.24	0.44	0.32	Sternberg and Rosenthal
Strain gage	−0.25	0.43	0.32	Milbradt, Landsberg, and Flynn
Photoelastic	0	0.68	0.48	Frocht and Guernsey

N. J. HOFF.[6] This excellent paper contains a result of much wider significance than the title implies. It shows that the application of a self-equilibrating system of indefinitely large forces to a vanishingly small part of the surface of an elastic body gives rise to strains of not negligible magnitude at finite distances from the part. This seems to contradict Saint Venant's principle. It is the purpose of this discussion to explain the discrepancy by showing that Saint Venant's principle does not necessarily apply in problems involving mathematical singularities.

In so far as the empirical foundation of the principle is concerned there is not much possibility for an argument because no true singularities can arise in nature and no practical concentrated load can cause stresses much in excess of the yield stress of the material. If one re-examines Goodier's[7] strain-energy analysis of the principle, he must conclude that the odd behavior of the stresses discovered by the authors is not really unexpected. Goodier showed that that part of the elastic body, in which the order of magnitude of the stress is the same as the order of magnitude of the applied self-equilibrating tractions, is of the order of magnitude of the linear dimensions of the loaded part of the body. It does not follow from this statement that stresses of a finite magnitude cannot be found at any finite distance from the loaded part if the loading comprises tractions which are indefinitely large, as will now be shown by means of a modification of Goodier's argument.

Let the authors' problem be modified by replacing each concentrated load by statically equivalent distributed loads, acting upon small parts of maximum linear dimensions L_0, of the surface of the sphere. Because of the axial symmetry of the problem, $L_0/2$ may suitably be chosen as the radius of a circle, whose center is the point of attack of the original concentrated load, and which encloses the loaded part. The maximum absolute value of the applied surface tractions in this system S_0 will be denoted by s_0. The system will be so chosen that s_0 is approximately equal to the elastic limit of the material. Let it also be assumed that all the stresses and strains caused in the sphere by the system S_0 are known.

A second system S_1 consists of distributed surface tractions of maximum absolute value s_1 acting upon two small parts, each of maximum linear dimension L_1, of the surface of the sphere. $L_1/2$ will be chosen as the radius of a circle enclosing the loaded part whose center is the point of attack of the original concentrated load. Over each small part the loading is again statically equivalent to the original concentrated load. Obviously, the stresses and strains caused in the sphere by system S_1 can be determined by superposition of the stresses and strains caused by system S_0 and those caused by the combined system $S_2 = S_1 - S_0$. System S_2 contains self-equilibrating surface tractions distributed over two small areas of maximum linear dimension L_0 or L_1, whichever is greater. The maximum absolute value of the surface traction is $s_2 \leq s_0 + s_1$.

It is not unreasonable to consider the stresses and strains caused by system S_0 as the standard solution, and to define that singly connected region of base $(\pi/4)L_0^2$ of the sphere which includes all the points at which the maximum stress is equal to or greater than s_0/n as the region affected by the details of the load distribution. The value of n is to be chosen from considerations of accuracy; $n = 2$ defines a region of large disturbances while outside the disturbed region corresponding to $n = 100$ the effect of the details of the load application is probably always negligible for engineering purposes.

The strains caused by system S_2 in the loaded region are not greater than s_2/G, where G is the shear modulus of the material. If one infinitesimal area of the loaded surface is fixed in space, the relative displacement of any point of the loaded surface with respect to the reference area is not greater than s_2L_0/G if $L_0 > L_1$ provided the effect of the rotations of the elements is neglected. If this effect is taken into account in the authors' problem, the relative displacement cannot be greater than ms_2L_0/G, where m is a positive number of the order of magnitude of unity. As displacement and load may be of the same sign over part of the loaded surface and of opposite sign over the rest, the total work done by the loads during a proportional loading is

$$W < (1/2)(\pi/4)ms_2^2L_0^3/G$$

The singly connected disturbed region just defined will now be approximated by a sphere of diameter D included in the sphere analyzed by the authors and having a common tangent plane with it at the point of attack of the original concentrated load. Inside this sphere the maximum absolute value of the stress is not everywhere greater than or equal to s_0/n, but there are necessarily subregions where this is true. Nevertheless, if n is chosen sufficiently large, s_0/n is much smaller than s_2 and the strain energy stored in the disturbed region

$$U > (\pi/24)(s_0^2/n^2G)D^3$$

[6] Head of Department of Aeronautical Engineering and Applied Mechanics, Polytechnic Institute of Brooklyn, Brooklyn, N. Y. Mem. ASME.

[7] "A General Proof of Saint-Venant's Principle," by J. N. Goodier, *Philosophical Magazine*, Series 7, vol. 23, April, 1937, p. 607; Supplementary Note on "A General Proof of Saint-Venant's Principle," *Philosophical Magazine*, Series 7, vol. 24, August, 1937, p. 325; "An Extension of Saint-Venant's Principle, With Applications," *Journal of Applied Physics*, vol. 13, March, 1942, p. 167. See also "Theory of Elasticity," by S. Timoshenko and J. N. Goodier, second edition, McGraw-Hill Book Company, Inc., New York, N. Y., 1951, p. 150.

It follows then from the principle of the conservation of energy

$$U = W$$

that

$$D < (3\ mn^2)^{1/6}(s_2/s_0)^{2/3}L_0$$

It is of importance that in this equation the reference length L_0 is the diameter of the circle enclosing that loaded region in which the maximum surface traction is approximately equal to the elastic limit of the material. It follows from the equation that the diameter D of the disturbed region is smaller than $(3mn^2)^{1/6}$ times L_0 if $s_2 = s_0$. When the two systems S_0 and S_1 differ little, s_2 is much smaller than s_0 and the disturbed region is small. On the other hand, when S_1 is a concentrated load over each area, $L_1 \to 0$, both s_1 and s_2 are indefinitely large, and the disturbed region may extend over a distance which is the product of L_0 by a very large number. Hence the use of the somewhat artificial, although most useful, mathematical concept of a concentrated load may, in some cases, lead to results in disagreement with experimental evidence.

The argument given implies that no independent nuclei of high stress exist inside the elastic body detached from the high-stress region connected with the loaded surface. Their existence in a homogeneous elastic body would violate the complementary energy principle.

The entire discussion presented referred to a three-dimensional solid body. In a statically determinate framework the forces are uniquely determined by the equilibrium conditions, and self-equilibrating systems of loads applied to a small number of joints may cause large stresses at distances from the loads which are large compared to the maximum distance between any two applied loads. When a large number of redundant bars is contained in the framework, Saint Venant's principle holds reasonably well, as was shown by the writer in an earlier publication.[8]

Finally it should be mentioned that in an investigation dealing with concentrated loads R. von Mises[9] showed that Saint Venant's principle does not, in general, hold for bodies of finite dimensions.

E. H. Lee.[10] The presentation and discussion of this paper emphasized the remarkable differences in the stresses away from the point of concentrated loading given by solutions involving different singularities, in apparent contradiction to the usual interpretation of Saint Venant's principle. It was suggested in the discussion that in the practical application of a problem of this type, such differences could be generated by the details of the contact conditions, such as friction. It would seem that in the case of contact over a small area, such additional surface tractions will always produce negligible changes in stress away from the point of contact, so that the solution presented will apply independently of the details of loading.

The reason for this statement is that such traction systems will be self-equilibrating, for example, in the case of friction a ring of radial shear traction at the surface, and can be considered as force doublets. The force magnitudes will be of the order of the applied normal force and in forming a doublet these will be multiplied by a dimension of the order of the extent of contact. The analysis of the stresses due to such a doublet will involve a smaller order of stress than that corresponding to the resultant applied load. The same also will be true of additional radial forces if the load is applied as pressure in an indentation. In considering the representation of these additional forces as doublets, the limit is taken of the product of force and separation to remain constant, while the force magnitude increases indefinitely, and the separation decreases to zero. However, this product is prescribed by the applied force and the contact dimension, so that the strength of the doublet will be small for small contact area, and the corresponding additional stresses will be negligible compared with those associated with the solution under discussion. The writer wishes to acknowledge help in clarification of these points during conversation with Dr. J. N. Goodier.

Authors' Closure

The authors appreciate the interesting comments of Professors Frocht, Hoff, and Lee. The additional experimental corroboration of the theoretical results is, of course, gratifying. Professor Frocht's remark that the "limit condition" must be *added* to the usual three necessary conditions in order to assure a unique solution to a concentrated-force problem, was evidently prompted by a statement in the paper, the wording of which is apt to be misleading. Actually, the requirement that the solution coincide with the appropriate limit of the solution corresponding to continuous surface tractions which are arbitrarily distributed over regions surrounding the points of application of the prescribed concentrated loads, by itself assures uniqueness and guarantees the satisfaction of the three necessary conditions referred to. The limit condition may thus be regarded as a definition of what is meant by the solution to a problem involving concentrated surface loads, in analogy to Kelvin's definition through a limit process of the concept of an interior concentrated force. The particular choice of these definitions is natural both on theoretical and physical grounds; the usefulness of the idealization of "concentrated forces" so specified ultimately rests on experimental verification. The photoelastic results of Frocht and Guernsey, as well as Professor Lee's observations, are relevant in this connection. It should be mentioned that the present definition of concentrated surface loads is consistent with Kelvin's definition of interior concentrated forces, as is readily confirmed.

A good deal of the discussion appears to center around the result that a solution appropriate to self-equilibrated singularities at the poles of the sphere, and otherwise clearing the surface from tractions, yields finite stresses at the center of the sphere. The authors agree with Professor Hoff that this result does not contradict a rigorous statement of Saint Venant's principle although they would base this statement on a different type of argument.

On this occasion reference should be made to a simultaneous treatment of the problem under discussion by C. Weber.[11] Weber, by different means, obtained the solution to the problem in the series representation designated by S_L in our paper (see Equation [58]). His solution therefore suffers from the convergence deficiencies mentioned in the discussion of S_L. As pointed out in our paper, the singularities inherent in the problem require special and separate attention. Moreover, Weber's paper unfortunately contains two errors which are carried through a major portion of the development and are responsible for the incorrectness of his final stress formulas: the leading term in the denominator of his equation [1;] should read $(n-1)\ (n-2)$ instead of $(n-1)^2$, whereas in his equation [23] the first factor in the numerator of the second fraction should read $(2n+5)$ instead of $(2n+3)$. In conclusion, the authors wish to call attention to a

[8] "The Applicability of Saint-Venant's Principle to Airplane Structures," by N. J. Hoff, *Journal of the Aeronautical Sciences*, vol. 12, October, 1945, p. 455.

[9] "On Saint-Venant's Principle," by R. von Mises, Bulletin of the American Mathematical Society, vol. 51, 1945, p. 555.

[10] Professor of Applied Mathematics, Brown University, Providence, R. I. Mem. ASME.

[11] "Kugel mit Normalgerichteten Einzelkraften," *Zeitschrift für Angewandte Mathematik und Mechanik*, vol. 32, no. 6, 1952, pp. 186–195.

paper by J. L. Synge,[12] in which the closed formulas for the stresses at the center of the sphere were derived directly by altogether different considerations.

On Longitudinal Plane Waves of Elastic-Plastic Strain in Solids[1]

WERNER GOLDSMITH.[2] The author is to be congratulated on a significant contribution in the field of wave propagation in solids, particularly in view of the applicability of the paper to a proper understanding of the mechanism of resistance and failure of metals subjected to contact explosions. Several interesting points have been raised by this presentation.

In the conversion of ordinary tensile and compressive stress-strain curves to those appropriate for longitudinal waves exhibiting no transverse deformation, it is rather surprising to note that the effective yield-point stress—denoted by the symbol 1 in Fig. 2 of the paper—has been increased nearly 100 per cent over the yield point in simple tension for the 24S-T aluminum-alloy specimen. A similar calculation by means of Equation [10] of the paper indicates that materials with a Poisson's ratio $\mu = 0.45$, such as lead, would possess a yield point under the action of plane longitudinal waves equal to 550 per cent of that observed in simple tension tests. These observations lead to the conclusion that the normal elastic range of a material may be extended considerably by imposing external constraints on the motion of the system. The lateral inertia exhibited by a material subjected to high transient loads produces an identical constraining effect and consequent increase in the instantaneous dynamic yield point. This phenomenon is independent of the normal strain-rate sensitive behavior of the material proper, which is also responsible for an apparent increase in the dynamic yield point, as discussed by the author in the last paragraph and further described in reference (4) of the paper.

The conditions of the present analysis involve the most severe type of restriction on any actual particle motion of the system. Thus the yield point for plane longitudinal waves, derived from Equation [10] as

$$\sigma_x = \frac{1-\mu}{1-2\mu}\,\sigma(\epsilon_x^p)$$

presumably represents the upper limit of a specimen subjected to any type of constraint upon its deformation, while the yield point in simple tension may be considered as the lower limit of this parameter. Any system with different constraints should exhibit a yield point intermediate between these two extremes.

In the experiments of references (1) and (7) of the paper, the geometry employed is such that the propagation of strain occurs by means of spherical waves of dilatation rather than by plane longitudinal waves. A comparison of the two systems of propagation shows that in both cases the velocity of elastic waves is given by

$$c_e = \left[\frac{E}{\rho}\,\frac{(1-\mu)}{(1+\mu)(1-2\mu)}\right]^{1/2}$$

Utilizing an idealized tensile stress-strain curve consisting of two straight lines with moduli E and E_1, respectively, and an assumption similar to that represented by Equation [7] of the paper, the writer has shown that the velocity of propagation of spherical plastic waves is given by

$$c_p = \left[\frac{3K(1-2M)}{\rho}\right]^{1/2}$$

where

$$M = \frac{\left(1-\dfrac{E_1}{E}\right)(1-2\mu)+3\mu}{3(1+\mu)}$$

This differs by the correction factor $2M$ from the usual propagation velocity $c_p = [3K/\rho]^{1/2}$ cited by reference (7) of the paper, which was numerically closely substantiated by the author. However, the general treatment required for spherical waves involves considerably greater mathematical complexities than for the case under consideration, particularly in view of the attenuating effect of the divergence of spherical waves. This results in a decrease of the stress amplitudes of both elastic and plastic waves with increasing radius, in addition to the destruction of plastic-wave amplitude due to annihilation by unloading waves. The writer is endeavoring to evaluate some quantitative results along these lines.

J. S. RINEHART.[3] This paper represents a valuable step forward toward our understanding and appreciating the factors which control scabbing of impulsively loaded metal plates. The author mentions (*a*) effect of variable compressibility, (*b*) effect of temperature variations, and (*c*) time and rate effects. Another important factor is the changes which are wrought by energy absorption due to internal friction. In general, this absorption will cause the pulse to be attenuated and to become longer as it moves through the body. It is to be remembered that the momentum of the disturbance must be conserved even though energy is dissipated. A further factor which will contribute to the lengthening of the pulse is the variations of Poisson's ratio and bulk modulus with pressure. These effects have been treated in the case of steel by Kochler and Seitz.[4] The effect of decay is strikingly illustrated by some examples of scabbing of flat plates that were explosively loaded in the manner shown in Fig. 1 of this discussion. The two curves in Fig. 2 show clearly the effect that decay of the wave has on scab thickness.[5,6,7]

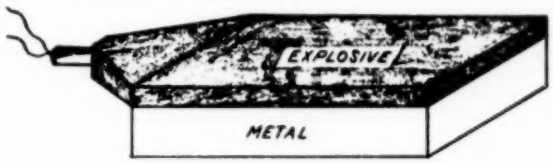

FIG. 1

The author indicates that it may be reasonably assumed that 24S-T aluminum alloy will behave in about the same way as pure

[12] "Upper and Lower Bounds for the Solution of Problems in Elasticity," Proceedings of the Royal Irish Academy, vol. 53, series A, no. 4, 1950, p. 41.

[1] By D. S. Wood, published in the December, 1952, issue of the JOURNAL OF APPLIED MECHANICS, Trans. ASME, vol. 74, pp. 521–525.

[2] Assistant Professor of Engineering Design, University of California, Berkeley, Calif. Jun. ASME.

[3] Research Scientist, Michelson Laboratory, Naval Ordnance Test Station, China Lake, Calif.

[4] "The Stress Waves Produced in a Plate by a Plane Pressure Pulse," by J. S. Koehler and F. Seitz, OSRD Report No. 3230, 1944, (unclassified).

[5] "Investigations of Fracture Produced by Transient Stress Waves," by H. Kolsky and A. C. Shearman, Research 2, 1949, p. 384.

[6] "Behavior of Metals Under High and Rapidly Applied Stresses of Short Duration," by J. S. Rinehart, NavOrd Rept. No. 1138, September 1949.

[7] "Explosive Forces Widen Metallurgical Studies," by J. S. Rinehart, *Steel*, Nov. 20, 1950, p. 98.

aluminum. Our studies with explosive charges indicate the precipitation hardening can affect in a marked way the manner in which an aluminum alloy will react to an impulsive load. Our observations lead us to believe that plastic flow in the case of

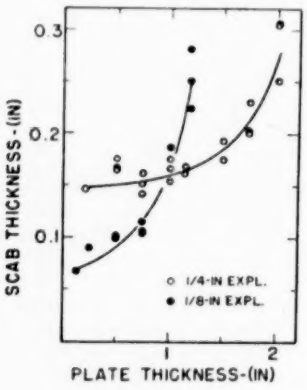

FIG. 2

aluminum alloy in the T-condition is a fairly inhomogeneous process. In the O-condition, aluminum seems to flow in a much more uniform manner. It is likely that a similar marked difference may exist as regards their respective behavior under high hydrostatic pressure. At least, this point should be looked into further.

AUTHOR'S CLOSURE

Dr. Goldsmith points out that for the type of waves considered in this paper, the longitudinal stress, σ_{xx}, required to produce the first yielding of the material may be considerably higher than the yield stress in simple tension or compression. This is, of course, a consequence of the differences in the states of stress in the two cases. If the material exhibited a Poisson's ratio in the elastic range of exactly one half, then the stress accompanying these waves would be equal in all directions, and yielding would never occur, because yielding is only produced by differences between principal stresses.

If the lateral extent of the material in which the waves are propagating is finite, then the lateral stress, σ_y, will be relieved by unloading waves initiated at the free surfaces. The problem then becomes enormously more complex, in general. However, if the time required for an elastic unloading wave of velocity c_0 to travel from the lateral surface to the region of interest is longer than the total time during which the waves are to be considered, then the presence of the lateral surface may be disregarded. Thus the present analysis would apply. The other extreme case occurs in long thin rods when the time required for relaxation of the lateral constraint may be neglected in comparison with the wave travel times of interest. The latter is the case treated by von Kármán, reference 2 of the paper. Experiments in which the geometry is intermediate between the above two extremes may lead to the determination of short-time increases of the dynamic yield point due to the lateral inertia effect, as pointed out by Dr. Goldsmith.

The author appreciates the fact that the mathematical treatment of the propagation of irrotational spherical waves is considerably more complex than in the case of plane waves. It is well that Dr. Goldsmith has pointed out that most of the experiments pertaining to the present discussion involve the propagation of predominantly spherical rather than plane waves. Hence it cannot be expected that an exact correlation be found between the theoretical results of the present paper and the available experimental data. The author has recently become cognizant of a paper by J. L. Lunz[8] on the propagation of spherical elastic-plastic waves which amply illustrates the mathematical difficulties involved.

The author may not be clear as to the nature of the internal friction referred to by Dr. Rinehart as an additional mechanism for energy absorption. However, it seems to the author that the energy absorption due to internal friction of the type usually associated with the decay of elastic vibrations in metals would be negligibly small compared to the energy absorption due to the plastic deformation which is associated with the waves discussed in the paper.

The statement in the paper regarding the similar behaviors of pure aluminum and 24S-T aluminum alloy may be somewhat misleading. The author intended to say only that the hydrostatic compressibility of the two materials as a function of pressure may be expected to be the same. This does not imply that the plastic deformation produced by stress waves of high intensity would be the same in the two materials. The reason for believing that the two materials exhibit the same behavior under hydrostatic compression is that the hydrostatic compressibility is a structure insensitive property. Thus it may be expected that it is not appreciably affected by the relatively small amounts (less than 7 per cent total) of alloying elements present in 24S-T or the precipitation hardening produced by heat-treatment, just as Young's modulus and Poisson's ratio are not affected by heat-treatment or small percentages of alloying elements.

The author wishes to express his appreciation to Drs. Goldsmith and Rinehart for their interesting discussions which have provided valuable clarifications and additions to the paper.

A Simple Method of Determining Plastic Stresses and Strains in Rotating Disks With Nonuniform Metal Properties[1]

T. H. LIN.[2] The author has shown a simple method of solving a very complicated, practical problem. Due to cold-work and temperature gradient, in a turbine disk, the varying of metal properties along the radius has to be considered. From the compatibility and equilibrium conditions, there will be a unique stress and strain variation along the radius. This stress and strain, under a given load at different points along the radius, is the only part of the secant stress-strain curve affecting the distribution of stresses and strains, so long as the deformation theory is valid. Hence a disk, made of nonuniform material under a given load, is equivalent to one of uniform material with stress-strain relationship, the same as existing stress-strain properties of a nonuniform disk under the particular load.

The accuracy of the results depends on the validity of the main assumption: That deformation theory holds; i.e., the ratio of principal stresses remains constant. This is measured by the variation of parameter n at a particular point along the radius with increasing γ_0 up to the value under consideration.

It has been pointed out by the author in her previous papers that the distribution of proportionate strains is essentially inde-

[8] "On the Propagation of Spherical Waves in an Elastic-Plastic Medium," by J. L. Lunz, Prikladnaia Matematika i Mekhanika, vol. 13, 1949, pp. 55–78. Translation No. 13 of Graduate Division of Applied Mathematics, Brown University, Providence, R. I., March, 1951.

[1] By M. H. L. Wu, published in the December, 1952, issue of the JOURNAL OF APPLIED MECHANICS, Trans. ASME, vol. 74, pp. 489–495.

[2] Associate Professor of Aeronautical Engineering, University of Detroit, Detroit, Mich.

pendent of the stress-strain curves of the materials investigated, and the remarkable agreement with experimental data definitely shows that the proposed method would give results with engineering accuracy.

It seems to the writer that it may be worth while (*a*) to find how much deviation in n is permissible for obtaining results of engineering accuracy, and (*b*) to extend this method to include the effect of creep. Assume that the turbine is loaded up instantaneously, the strain distribution without creep is calculated as shown. Then the creep strain for a short interval of time may be found from the properties of the material. Including the creep strain in the plastic strain, a new value of n may be obtained. Calculate the distribution of the principal stresses from the new stress-strain curve. With these principal stresses, the creep for the second interval of time may be calculate[1]. Repeat this step-by-step integration process until the deviation in n exceeds the permissible value. This may give a method to solve the case, including effect of creep to the first approximation.

E. T. Stowell.[2] Few problems in stress distribution have been solved with any exactness in the plastic range of a strain-hardened material. The solutions obtained by the author for axially symmetric problems, of which this paper is one example, have the distinction of falling into this category, as they are exact, or near exact.

The stress distribution in a sheet having a central hole, and loaded in biaxial tension, would not appear to be a difficult problem. Yet even in this apparently simple one-dimensional case, it is not easy to satisfy simultaneously the requirements of compatibility, equilibrium, the stress-strain relations, and the boundary conditions. By a clever choice of parameters, the author has been able to satisfy all these requirements with some exactness. Later, she applied the same method to the problem of the rotating disk with uniform properties, and finally to the present paper, which considers the rotating disk with nonuniform properties.

The nonuniformity in properties is considered to be purely radial in character, of the sort that might arise from a temperature gradient. The author exploited the previously established fact that the strain distribution in such a disk is substantially independent of the material, so that regardless of the nonuniformity in properties, the strain distribution is more or less accurately known. The corresponding stress distribution was then obtained from a knowledge of the stress-strain intensity curves taken at different radii. The rotational speed necessary to achieve any desired maximum strain intensity was computed.

The agreement with experiment is all the more remarkable when it is considered that the comparison is made indirectly on a fracture basis rather than on a stress-distribution basis. The additional assumption involved here is that fracture in the disk will occur when the strain intensity reaches the maximum shown by the simple tension curve. In the writer's opinion, there is some evidence that this assumption is correct, provided the fracture is of the ductile or intergranular type. The check was, however, made on the basis of uniform properties and it is not quite clear how the experimental check confirms the theory of the present paper.

In general, for real materials, results such as those obtained in this series of papers on stress distribution, of which this is the last, could not be carried too far into the plastic range without modification. Most materials, even if elastically isotropic, will begin to exhibit appreciable anisotropy beyond a few per cent strain. The isotropic stress-strain relations used by the author would have to be modified substantially for use at larger strains. It is possible that in certain special situations the anisotropy might not be too important; this may be the case in the present paper.

The great merit of this series of papers, including the present one, lies less in controversial fracture checks than in the following: Problems in stress distribution in the plastic range are going to multiply rapidly as materials are used more and more at elevated temperatures. The chances of solving such problems exactly are quite remote. Approximate methods will have to be developed. Approximate methods, however, require a standard against which they can be assessed. It is the author's unique contribution that she has supplied such a standard in this series of exact solutions.

Author's Closure

The author wishes to thank Professor Lin and Dr. Stowell for their comments on the paper.

Regarding Professor Lin's suggestions, the author's opinion is as follows: (*a*) Detailed consideration of the permissible deviation of n for an actual $\tau(\gamma)$ curve from the value of zero has not been given in the paper. However, the numerical results of two examples given in Table 2 may give some information. The values of n for the two examples are 0.195 and 0.150, which are relatively high values among all the examples calculated in reference (2) of the paper. Even for these high values of n, the errors in $\rho(\omega b)^2$ are only 2.07 per cent and 1.70 per cent. Furthermore, for materials having high n-values another suitable pair of curves, such as curves for n equal to 0.2 or 0.3, given in Figs. 3(*a*) and 3(*b*) of the paper, may be used. This should give very accurate results. (*b*) It is worth while to extend this method to include the effect of creep, because the method is very simple and easy to extend. One may raise the question whether or not all the conditions for the deformation theory, which hold for the materials at room temperature, will also hold for the materials at high temperature with creep. However, it is believed that it can be used to obtain, at least, a first approximate solution.

Dr. Stowell's appreciation of the difficulties involved in solving the problem is greatly appreciated by the author. With regard to the question of the experimental check, the author feels that the conclusion obtained from the check for disks having uniform metal properties can also be applied to the disk having nonuniform metal properties, because no additional approximation is made in the process of extending the method for the uniform case to the nonuniform case. The accuracy of the method, as mentioned in the paper, depends only on the deviation of the value of n for the actual $\tau(\gamma)$ curve from the value of n used (n equal to zero is used in the comparison).

The effect of anisotropy is not too important in the present case as Dr. Stowell expected. It can be seen from Equation [6] that the rotating speed is a function of tangential strain, tangential stress, and radius. Also reference (2) of the paper shows that the distributions of the proportional strains are essentially independent of the stress-strain relations of the material. Therefore the effect of anisotropy on rotating speed is small if the tensile stress-strain relationships of the tangential specimens are used in the computation

[1] Aeronautical Research Scientist, NACA, Langley Field, Va

Free Vibrations of Constrained Beams[1]

H. F. Weinberger.[2] The interesting computational method presented in this paper can be considered as a special case of the following results of the writer (an exception is the case of a continuous elastic foundation, which is not covered by these results):

Let problem A be a beam problem with boundary conditions such that its eigenvalues and eigenfunctions are explicitly known, for example, the authors' "simple beam." Associated with this problem is a "Green's function" or influence function $G(x, y; \Lambda)$. This function is the steady-state solution of the beam under an oscillating unit point force with frequency Λ applied at y. In some cases, for instance for the uniform beam, the function G can be found explicitly from its definition. Otherwise, G can be evaluated from the formula

$$G(x, y; \Lambda) = \Sigma \frac{\phi_r(x)\,\phi_r(y)}{\Lambda^2 - p_r^2} \quad \ldots\ldots [1]$$

which gives the connection of our results with those of the authors.

The problem whose eigenvalues (natural frequencies) are to be found is called problem B. It differs from problem A in that n new conditions

$$J_s[Y] = 0 \quad \ldots\ldots [2]$$

are imposed. At the same time, n other conditions on the solution of problem A are relaxed. For example, if the beam is pinned at the point h_1, the condition $Y(h_1) = 0$ is imposed, while the continuity of the third derivative of Y is no longer required at h_1.

If, now, the condition J_s is imposed on $G(x, y; \Lambda)$ as a function of x, a function of y alone is obtained. We impose condition J_j on this function and write the result as $J_s J_j G(\Lambda)$. This yields an $n \times n$ matrix whose determinant we call $D(\Lambda)$. This is precisely the determinant obtained by the authors. (To obtain their form in Equation [15], the fact that

$$\frac{\partial^3}{\partial x^3} G(x, y; \Lambda)$$

has a discontinuity of magnitude $1/EI(y)$ at $x = y$ must be used.) In terms of this determinant we can find not only the eigenvalues of problem B but also their proper multiplicities, i.e., the number of eigenfunctions associated with them. These are obtained in exactly the same way as the corresponding quantities are obtained from the so-called Weinstein determinant in the Weinstein method for plates; namely, if $M_A(\Lambda)$ and $M_B(\Lambda)$ are the multiplicities of Λ as an eigenvalue of problems A and B, respectively, and if $z(\Lambda)$ is the order of $D(\Lambda)$, i.e., $(\Lambda - \Lambda_0)^{-z(\Lambda_0)} D(\Lambda)$ is regular and nonzero at Λ_0, for any fixed Λ_0; then

$$M_B(\Lambda) = M_A(\Lambda) + z(\Lambda) \quad \ldots\ldots [3]$$

When the zeros of $D(\Lambda)$ are simple and Λ is not an eigenvalue of problem A, this reduces to the results of the paper under discussion.

The occurrence of a Weinstein determinant leads one to inquire as to the relation of this method to the variational method of Weinstein. The latter consists of two parts: a variational idea and a computational method. The variational idea is based on the fact that if one eigenvalue problem is less constrained than another, it has lower eigenvalues. Thus it is possible to obtain a sequence of lower bounds for the eigenvalues of a given problem if another one which is infinitely less constrained has known eigenvalues and eigenfunctions. These lower bounds are the eigenvalues of the known problem with a finite number of added constraints. This variational idea does not concern us here.

However, the fact that makes the Weinstein method of practical interest is that the eigenvalues of a problem obtained by imposing a finite number of constraints on a known eigenvalue problem can be solved explicitly in terms of the Weinstein determinant. It is this part of the Weinstein method that is used in the paper under discussion.

The results given in this discussion hold not only when constraints are imposed, but also when they are removed or substituted, e.g., if the spring constant is changed. This simply means that the computational part of the Weinstein method holds not only for the imposition of constraints but for any finite change of constraints.

Authors' Closure

The authors wish to thank Dr. Weinberger for his succinct and interesting discussion in which he so ably summarizes the existing situation.

The role played by the Green's function had been pointed out by one of us previously, reference (4), so that it was not repeated in the present paper.

The relation between the present method and that of Weinstein is particularly interesting. His procedure for calculating eigenvalues is to relax the outer boundary conditions in such a way as to get a problem which can be solved. Then the solution of the desired problem is approached by letting the boundary conditions approach the desired ones. In our case, however, the outer-boundary conditions remain the same but inner conditions are added which, as Dr. Weinberger points out, introduces discontinuities in the third derivative of the Green's function at the points where the constraints are added. These correspond to introducing reactions at the points of constraint.

Deflection and Stresses in Beams Subjected to Bending and Creep[1]

Folke K. G. Odqvist.[2] The writer appreciates the authors' new method of attack with a close approximation to the total creep over a considerable time. For the initial stages of creep in bending more accurate results will certainly be obtained than with the writer's formulas which correspond to the case $K = 0$ (authors' notation). Nevertheless, attention is drawn to the writer's work Hållfasthetslära, Stockholm, 1948, p. 805 (published in Swedish) where on pp. 737–741 some of authors' cases, including that of Fig. 3, are treated, as well as a few more. There is also to be found an estimation of the influence of shearing stress on deflection.

Authors' Closure

The authors wish to thank Professor Odqvist for his interest in their paper and are glad that attention has been drawn to his fine work in this field. It should be clear, however, that in this particular paper, the authors were more interested in the development of theory rather than in the number of specific cases that could be solved.

[1] By W. F. Z. Lee and Edward Saibel, published in the December, 1952, issue of the Journal of Applied Mechanics, Trans. ASME, vol. 74, pp. 471–477.

[2] University of Maryland, College Park, Md.

[1] By Yoh-Han Pao and Joseph Marin, published in the December, 1952, issue of the Journal of Applied Mechanics, Trans. ASME, vol. 74, pp. 478–484.

[2] Professor, Royal Institute of Technology (Kungl. Tekniska Högskolan), Stockholm, Sweden.

Investigation of Annular Liquid Flow With Concurrent Air Flow in Horizontal Tubes[1]

LUIGI CROCCO.[2] The question of two-phase flow in ducts is still in a rather incomplete state, even in the most specifically defined case where the two phases are distributed concentrically in a round pipe. The author is therefore to be complimented for his investigation on this kind of flow and for the definite contribution he brings on some aspects of the underlying mechanism.

He has concentrated his attention mainly on the transition from laminar to turbulent conditions in an annular liquid film surrounding a gaseous stream. Substantially, what he has done is to determine under various gas-flow conditions and with liquids of different properties the range of critical liquid flow rates at which disturbances were first observed on the film surface, and to compare a nondimensional flow-rate parameter corresponding to these critical rates with the values of the same flow-rate parameter computed for the same liquid and in a single-phase boundary layer in the region where transition from laminar to turbulent conditions takes place. The important result is that the two values coincide reasonably well, with the somewhat unexpected conclusion that the critical flow rate at which film instability begins does not depend on the conditions of the gas stream, and is simply proportional to the diameter of the pipe and to the viscosity of the liquid. It must be observed that these experimentally supported conclusions are in agreement with a suggestion made by Tsien on the limiting film thickness for perfect efficiency of film cooling.[3] It is regrettable that no additional data actually were measured, like film thickness and pressure drop. Both would have provided a check to the correlation between single-phase and two-phase flows.

About the possibility of transferring these results to the case of film cooling in rocket motors, it is necessary to point out that the conditions in rocket motors might be quite different. In the author's tests the liquid was introduced at a point where the gas stream had nearly reached the regime conditions after a long approach section. In a rocket motor both liquid film and gas stream begin simultaneously. Moreover, the combustion produces a comparatively large-scale turbulence, the intensity and distribution of which depend on the injection system. This turbulence might produce on the film local disturbances that cannot find any correspondence in the tests described in the paper. If, nevertheless, the results of the paper are applied to the rocket case, one realizes immediately the importance, already stressed by Tsien,[3] of increasing the viscosity of the liquid, in order to delay the breakaway of liquid droplets and the decrease in cooling effectiveness. Also, by a proper balance between the critical flow rate determined by the author and the total flow rate needed for cooling, the number of successive re-establishments of the film along the cooled wall for optimum effectiveness can be determined.[3]

[1] By A. E. Abramson, published in the September, 1952, issue of the JOURNAL OF APPLIED MECHANICS, Trans. ASME, vol. 74, pp. 267–274.

[2] Robert H. Goddard Professor of Jet Propulsion, Princeton University, Princeton, N. J. Mem. ASME.

[3] "Instruction and Research at the Daniel and Florence Guggenheim Jet Propulsion Center," by H. S. Tsien, *Journal of the American Rocket Society*, No. 81, June, 1950, p. 5.

Book Reviews

Aerodynamics of Propulsion

AERODYNAMICS OF PROPULSION, by Dietrich Küchemann and Johanna Weber. McGraw-Hill Book Company, Inc., New York, N. Y., 1953. Cloth, 6 × 9 in., ix and 340 pp., illus., $9.

REVIEWED BY HUGH L. DRYDEN[1]

THIS interesting book by two former members of the Aerodynamische Versuchsanstalt Gottingen deals essentially with those aerodynamic problems of subsonic jet propulsion which are outside the scope of airfoil theory, i.e., the subsonic aspects of what engineers now call aerothermodynamics. Hence the title is somewhat broader than the actual scope of the book. Compressors, turbines, and propellers are excluded. Only incidental mention is made of transonic and supersonic flow, and rocket engines are not discussed. Within its scope, which is described more fully below, the book provides a treatment of the basic processes and flow phenomena requiring no detailed knowledge of general aerodynamics or of mathematics beyond differential calculus. It will be of interest to those interested in the fundamentals, whether students or aircraft engineers.

After a brief introductory chapter, the authors give a one-dimensional treatment of the basic processes of propulsion, i.e., the conversion of heat into mechanical energy in flow processes, the momentum theorem, and the production of thrust, and the role of these processes in power plants supplying mechanical energy to the flow (propeller), in power plants supplying heat energy to the flow (ramjet and turbojet), and in power plants supplying both heat and mechanical energy to the flow (turbopropeller and ducted fan).

Two-dimensional nonhomogeneous flow problems are then discussed, i.e., problems of flow in which the total energy is not the same in all parts of the flow field. Application is made of potential flow theory of an incompressible nonviscous fluid to such problems by the introduction of singularities including sources, vortexes, and doublets. In two-dimensional problems conformal transformations are helpful.

Chapter 4 treats the subject of air intakes and their design by the method of singularities. Critical Mach numbers and the use of the Prandtl-Glauert rule for compressibility correction are briefly discussed.

Chapter 5 is concerned with fairings of finite length, in particular the flow near the downstream end, leading edge intakes on wings, annular airfoils, and double airfoils. It is stated that optimum fairing shapes can be determined by experiments in water on the shape of cavitation bubbles.

Chapters 6, 7, and 8 deal with the application of the results of the first five chapters to the ducted propeller, the ramjet, and the turbojet engine. Chapter 9, the largest chapter in the book, discusses the losses associated with the installation of jet engines, i.e., inflow and duct losses and external interference drags. Chapter 10 is devoted to the jet and its effect on neighboring surfaces. However, the spreading of a jet into a stream of air of different speed, density, and temperature, a turbulent mixing process, is outside the scope of the discussion. Superposition of flow is assumed to give an approximate computation of the effect of streaming air and of inclination of jet to the flow, starting with the observed spread of a hot jet in still air. Some results of water-tunnel observations of the spreading of a jet in the neighborhood of a wall are included. A short chapter on aerodynamic propulsion in nature seems somewhat foreign to the general content.

The final chapter describes the essentials of the problem of cooling, of chief interest for piston engines, although some consideration was given in Germany to the possible use of heat exchangers in jet engines.

An appendix contains tables of stream functions and velocity components for frequently used singularities—arrangements of three-dimensional sources, doublets, and vortexes along lines, along a ring, over a cylinder, over a disk, and the like.

[1] Director, National Advisory Committee for Aeronautics, Washington, D. C. Fellow ASME.

The Nature of Some of Our Physical Concepts

THE NATURE OF SOME OF OUR PHYSICAL CONCEPTS. By P. W. Bridgman. The Philosophical Library, Inc., New York, N. Y., 1952. Cloth, 6 × 9 in., 64 pp., $2.75

REVIEWED BY JOSEPH H. KEENAN[1]

THIS little book contains three lectures given in April, 1950, at City College, University of London. They were published previously in the "British Journal for the Philosophy of Science."

The "operational" approach to science, of which Professor Bridgman is a leading exponent, is largely a response to the theory of relativity which exposed the need for definition of scientific quantities in terms of the operations involved in obtaining these quantities. In other words, scientific quantities are represented in mathematical processes by symbols which stand for numbers. Since a symbol may, in general, stand for any number, the distinction between different quantities represented by different symbols must lie in the rules describing what is to be counted in order to obtain the numbers. The selection of the things to be counted—the meter sticks which placed end-to-end span a length, or the number of standard weights which balance a mass—and the counting procedures constitute the "operation." It has been suggested by Burchard[2] that philosophers, metaphysicians, and poets seem to have observed the necessity for defining terms long before the physicist.

In the first lecture the author points out that not all physical concepts can be based directly on instrumental operations. For example, the stress inside an elastic body cannot be directly measured. This brings him to consideration of "mental operations" which he subdivides into paper-and-pencil and verbal operations. "Among the paper-and-pencil operations are to be included all manipulation with symbols." Verbal operations include, it seems, manipulation with words and sentences in which the manipulator exhibits compelling patterns of behavior which are part of "a verbal world of his own making."

He discusses the differences between instrumental and mental operations—the haziness or margin of error in the instrumental, the relative sharpness of the paper-and-pencil. He points out that the paper-and-pencil loses its sharpness if pushed to the point of defining identity and recurrence, of assuring ourselves "that we are making the *same* proposition *twice*."

[1] Professor of Mechanical Engineering, Massachusetts Institute of Technology, Cambridge, Mass. Fellow ASME.

[2] "Mid-Century," The Technology Press, Cambridge, Mass., 1950, p. 233.

The justification of the mental operation must always lie in its consistency with the instrumental operation whenever one impinges on the other. This point is discussed in connection with the differential calculus and the concept of field (which was "clothed in mathematical form by Maxwell, and crowned by Einstein in his general relativity theory"). He compares the field concept with "action at a distance" and concludes that "the distinction which physicists actually do make between these two concepts is verbal."

Since a field is something that exists in otherwise empty space, the author considers the concept of empty space in which, he says, we are coming perilously close to an inner contradiction. "For how shall we establish that a purportedly empty space is really empty without going there with an instrument to prove it, and when we have introduced the instrument the space is no longer empty."

In this connection he discusses Ostwald's contention that the concept of atoms is superfluous and points out that the only virtue of the atomic concept is its simplicity. He implies that the operational meaning of reality is closely related to simplicity, and that the operational meaning of understanding is the modern gift of prophecy, the ability to predict.

The second lecture takes up thermodynamics first in the manner of Poincaré in which heat and work are defined first and energy defined in terms of these. He discusses Poincaré's statement that if we were ever confronted with a situation in which conservation of energy apparently failed, we would at once save the situation by inventing a new form of energy. He points out, however, that this device involves "Maxwell relations" which the stresses and strains of the new form of energy must satisfy and that these are subject to verification by instrumental operations.

Conventional thermodynamics implies fluxes of work and heat, the latter being less easily instrumented than the former. He observes that the concept of temperature becomes ambiguous in the presence of large heat flux because temperature is defined in terms of equilibrium states.

He points out that thermodynamics implies that energy can be localized by mental operations—that is, each elementary piece of a system may have an energy associated with it. In electrostatics the energy is localized in the field and its flux through the field can be measured by means of the magnetic field. In gravitation, on the other hand, since no means can be found of identifying such a flux, the energy is localized in the mass rather than in the field. "In fact, the gravitational situation appears to me so repulsive to physical intuition, which I suspect means merely my tacit verbal demands, that it seems to me we may well be on the lookout for a new gravitational effect, analogous to the magnetic field, too small to have yet been detected."

Next, he discusses the problem of the separation of work and heat in the presence of motion. This question introduces current extensions of thermodynamics into essentially irreversible flow phenomena. The author points out that the physical significance of an energy flux must depend upon an instrumental method of detecting the flux independent of the rate of change of localized energy. He says that only recently has it been recognized that "the full thermodynamic picture . . . demands the existence of a flow vector for entropy and also a 'creation function' (as) tools by which certain irreversible processes may be brought within the ambit of thermodynamics."

He discusses entropy creation in various irreversible processes and Tolman and Fine's method of superposition of elementary irreversible processes. He does not discuss the linear relations of coupled flows and the Onsager reciprocal relations. He throws out the suggestion that a thermodynamics of nonequilibrium states, such as states of plastic strain, may be brought within the scope of a generalized thermodynamics the entropy for which will reduce to known values in the limiting case of reversibility. He reports progress in this direction in his studies of some rudimentary processes.

The third lecture deals with electrical phenomena in massive conductors. He discusses the mental operations involved in analyzing the thermocouple process. He tests Heaviside's assumption of a nonfield e.m.f. at the junction of dissimilar metals by applying it to the junction of two identical crystals with crystal axes perpendicular to each other. It has been found since Heaviside's day that such a junction is apparently electrically similar to a junction of dissimilar metals. The author shows, however, that Heaviside's nonfield e.m.f. leads to an absurdity in the case of the crystal. He concludes, therefore, that the nonfield e.m.f. is localized not at the junction but in the body of the metal where there is a temperature gradient. It is thus associated with the Thomson effect rather than with the Peltier effect.

This book is as provocative and stimulating as Bridgman usually is. It is his own up-to-date abstract of his three volumes: "The Logic of Modern Physics," "The Nature of Thermodynamics," and "The Thermodynamics of Electrical Phenomena in Metals."

Physics

THE RISE OF THE NEW PHYSICS (formerly titled "Decline of Mechanism," by A. d'Abro). Dover Publications, Inc., New York, N. Y., second edition, 1951. Two volumes, cloth, 5¼ × 8 in., figs., plates, index, ix and 982 pp., $8 the set.

REVIEWED BY J. ORMONDROYD[1]

THESE two volumes under review discuss the quantum theory of the atom. This requires and receives an adequate outline of the special theory of relativity. The general theory of relativity is dismissed with a few words. The nuclear theory of the atom is omitted entirely. This is not surprising since this work is a revision of an earlier work by the same author entitled "Decline of Mechanism," originally published in 1939 when the nuclear theory was in its nascent state. The first volume is divided into two parts, Part 1, "General Considerations" and Part 2, "Physical Theories of the Classical Period." The first volume is preliminary to the real business of the work which is contained in the second volume. This volume contains Part 3, "The Quantum Theory."

Part 1 is concerned with the history and philosophy of physics and the psychology of physicists. The rise of physics through the stages of observation, experiment, and mathematical theories from the Chaldeans and Egyptians to Newton and the role of assumptions in this process is first discussed. Theoretical physics is shown to have the task of establishing and co-ordinating relationships among observed phenomena and the prediction of phenomena as yet unobserved. "Mathematical simplicity" and "simplicity of assumptions" in physical theories are next discussed. The successive theories of physics are shown to be progressive approximations—climbing up to improved predictive power through the creation of new basic concepts. The old ideas of causality are contrasted to the newer ideas of inherent indeterminancy forced on physics by atomic observations. Four broad types of theories are discussed next—mechanistic theories, field theories, phenomenological theories, and purely mathematical theories. Finally, the psychological preferences of physicists among these types of theories, apparently based mostly on the historical accident of data of birth, are discussed.

Part 2 covers the physical theories developed in the area between Newton and Gibbs. The subjects chosen to illustrate the

[1] Professor of Mechanical Engineering, University of Michigan, Ann Arbor, Mich. Mem. ASME.

classical period are analytical mechanics, the undulatory theory of light, Hamilton's wave mechanics, thermodynamics, and the kinetic theory of gases. The mathematics of function theories, group theory, differential equations, and contract transformations are covered in about half the material in Part 2.

In Part 3 (vol. 2) the historical development of quantum physics is discussed with much more detail than was used in volume one. The works of Planck, Bohr, DeBroglie, Heisenberg, Schrodinger, and Dirac are outlined. Digressions on the theory of vibrations, matrix mathematics, and various types of statistical theories form a good share of Part 3. This part starts with a thoroughgoing discussion of the special theory of relativity.

In both volumes the author satisfies the normal curiosity of his readers by providing portraits (photographs of the moderns) of the great physicists and mathematicians whose works are discussed.

The subject matter in these books is treated at a level intermediate between the purely popular books on modern science and the original treatises and papers of the physicists and mathematicians discussed. For this reason it requires a certain amount of intellectual sophistication in the reader. For a graduate student in the field of atomic physics these two volumes would form a very satisfactory summary of the work of several studious years. The general reader, who might be an engineer, would not learn in detail the subjects discussed; he would learn about them. For instance, after he has read the numerous pages devoted to contact transformations he will not find himself able to make an actual contact transformation. The writing is clear and will make sense to the engineering type of mind.

It is to be regretted that the publishers have given no details on the dust jackets concerning the life of d'Abro. The preface in volume I is not even signed by the author. The repeated use of the words "we" and "our" in this preface makes one wonder if they are used in the editorial sense or whether they indicate the existence of a group of co-operating authors. One would like to know more about the person (or persons) who can give such a clear and lucid outline of the extensive and abstruse subject of atomic physics.

Advanced Mechanics of Materials

ADVANCED MECHANICS OF MATERIALS. By Fred B. Seely and James O. Smith. John Wiley and Sons, Inc., New York, N. Y.; Chapman and Hall, Ltd., London, England, second edition, 1952. Cloth, $5^1/_2 \times 9$ in., 362 figs., references, problems, tables, appendixes, index, xvii and 680 pp., $8.50.

REVIEWED BY NICHOLAS GROSSMAN[1]

THE first edition of this book appeared twenty years ago. It was among the pioneer American texts treating the more advanced phases of the mechanics of materials in a systematic and practical way. This domain of engineering science has been designated by various familiar names such as advanced strength of materials, applied elasticity, resistance of materials. The term mechanics of materials is a happy choice, in the reviewer's opinion, because it correctly reflects that the subject matter has been drawn from both the theoretical treatise and empirical behavior of engineering materials and structural elements. The text is aimed at the advanced undergraduate or early graduate-student level. It is written and arranged to serve the student also as a handy reference book during his future years as a practicing engineer.

The main difference between the first and second editions of the text is the general level of approach; emphasis in engineering education has shifted slowly at first, then accelerated by the impetus of a national emergency and armed conflict. Today's students, both in absolute number and percentagewise, are trained for a more thorough grasping of engineering and science fundamentals, which forms a natural cornerstone for more advanced topics, such as those presented in the present text.

The text is divided into six major groups: (1) Preliminary Considerations, (2) Special Topics on the Strength and Stiffness of Members Subjected to Static Loads, (3) Localized Stress—Stress Concentration, (4) Energy Methods, (5) Influence of Small Inelastic Strains on the Load-Carrying Capacity of Members, (6) Introduction to Instability—Buckling Loads. There are also three appendixes following the afore-mentioned topics: A concise and brief introduction to the Theory of Elasticity; Membrane (Soap-Film) Analogy for Torsion, and Properties of Areas useful in numerical computations.

The first part deals mainly with elementary stress computations, stresses and strains at a point, theories of yielding, and their applications to design. This part serves as a review of the elementary topic required as a background for this book. The second part deals with special topics in beams; flat plates; torsion in noncircular bars, thick-walled tubes, and contact stresses. This last subject then introduces the next major group dealing with localized stresses and stress concentrations. This is a well-written and clearly understandable portion of the text, especially if the reader, not having covered it in the classroom, refers to it on his own. Castigliano's theorem and other energy methods with their applications are treated in part 4. The next part, dealing with the influence of inelastic strains, is rather a specialized and refined method. In the reviewer's opinion, a preferred order would be to place this part last, or even in an appendix. Part 6 treats the buckling of columns and tubes under uniform external pressure.

The text is profusely illustrated with clear and well-labeled figures. Tables are frequently used wherever need arises, which further enhances the value of the book as a reference work. Chapters and sections are followed by completely solved illustrative problems, as well as the customary problems. Ample up-to-date references are listed at the end of the chapters. The neat and crisp appearance of the text adds eye-appeal to the clearly written and descriptive style of the book, which should make it a continued favorite in this field.

Strength of Materials

ADVANCED STRENGTH OF MATERIALS. By J. P. Den Hartog. McGraw-Hill Book Company, Inc., New York, N. Y.; Toronto, Ont., Can.; London, England, 1952. Cloth, $5^3/_4 \times 9$ in., 219 figs, problems, index, ix and 379 pp., $8.50.

REVIEWED BY M. HETÉNYI[1]

AS A text on the intermediate level, this book gives a maximum return for a minimum of introductory study. Assuming that the student would have only one semester's preparation in elementary strength of materials and a smattering of calculus, in the nine chapters of this moderately sized volume the author succeeds in conducting considerable inroads into three major fields of advanced mechanics: the theory of elasticity, the theory of plates and shells, and the theory of elastic stability.

The book starts with a chapter on problems of torsion, including noncircular cross sections, hollow sections, and shafts of variable diameter. In each case the nature of the solution is ex-

[1] Head, Mechanical Development Section, Atomic Energy Division, Sylvania Electric Products, Inc., Bayside, Long Island, N. Y. Mem. ASME.

[1] Walter P. Murphy Professor, The Technological Institute, Northwestern University, Evanston, Ill. Mem. ASME.

plained by means of existing analogies, thus affording a physical insight with the circumvention of mathematical complications. The next chapter deals with the calculation of centrifugal and shrink-fit stresses in circular disks of constant and hyperbolically varying thicknesses, including discussion of the rotating disk of uniform stress.

The third chapter is devoted to the membrane theory of thin shells, with applications to containers, domes, and pressure vessels, including a brief exposition on shells of uniform strength and also treating cases of nonsymmetrical loadings. The bending of flat plates is the subject of the next chapter. After the derivation of the fundamental equations, the method of solution is shown for a uniformly loaded circular plate, while for other cases only the end results are given in a "catalogue" of formulas. The chapter concludes with a discussion of the effect of large deflections.

The fifth chapter deals with the theory of beams on elastic foundation, and its application to the analysis of grillage beams and axially symmetrical flexure of thin shells.

In the sixth chapter an outline is given of the two-dimensional elasticity theory, illustrating its application to the bending of curved bars, and discussing three basic solutions, those by Kirsch for the circular hole, by Flamant for the semi-infinite plane, and by Michell for the diametrically loaded circular disk. The chapter concludes with a discussion of some classical problems of the plasticity theory.

The next two chapters deal with the energy method, its use in the analysis of curved tubes in bending, and a rather extensive treatment of buckling problems involving rings, tubes, arches, plates, and cases of torsional stability in beams, shafts, and columns. The last chapter is devoted to miscellaneous topics, such as Mohr's circle for three dimensions, the torsion of pretwisted thin-walled sections, a theorem by Biezeno on transversely loaded rings, and an application of Mueller-Breslau's solution for arches to the analysis of thermal stresses in pipe lines.

The book is concluded with a collection of 217 well-chosen problems and their answers and an index of subjects treated.

There are two chief characteristics of this book which distinguish it from other publications in this field—an informal conversational tone of presentation and a distinctly intuitive manner of approach in getting to the physical essence of the problems. Both of these features are likely to have considerable appeal to students and teachers alike.

Heat Transfer

INTRODUCTION TO HEAT TRANSFER. By Aubrey I. Brown and Salvatore M. Marco. McGraw-Hill Book Company, Inc., New York, N. Y., second edition, 1951. Cloth, 6 × 9 in., xvii and 267 pp., figures, tables, problems, index, and appendix. $4.50.

REVIEWED BY JOSEPH KAYE[1]

THE major objective of this book is to provide an introduction to heat transfer for undergraduate engineering students. This objective is achieved by almost complete elimination of material requiring the use of advanced calculus, by placing emphasis mainly on physical explanations, and by using detailed illustrative numerical examples. Dimensional analysis is used as a helpful tool in much of the discussion throughout the book, and great care is taken to guide the student through the maze of different units so often encountered in heat transfer and fluid mechanics.

In presenting the elementary material on conduction the utility of the concept of thermal resistance is not emphasized. The chapter on radiation is good from a pedagogical viewpoint and contains interesting historical notes. The material on convection is explained on the basis of the "stagnant" film theory whereas an appeal to the boundary-layer hypothesis of laminar and turbulent flows might be considered as a better way to indoctrinate students without changing the correlation equations used in this section of heat transfer. The state of the art with regard to boiling and condensation is discussed briefly. Practical applications are given in design of feedwater heater, surface condenser, finned coil, and the like, but design based on the economic viewpoint is not given. Transient heat-flow problems are given for the semi-infinite solid, the flat slab, and centers of various bodies, but no discussion is given of solution by relaxation or finite-difference methods. An appendix contains properties of some common fluids encountered in heat-transfer problems.

The book is well written and gives a brief description of the state of the art of heat transfer to students taking this subject for the first time. A teacher might wish to place greater emphasis on one phase of the subject or on another but it appears that he could easily supplement the treatment in the book.

Although great care is evident in the preparation of the text, tables, examples, and so on, two slips were noticed. On page 98 the surface coefficient of heat transfer for forced convection is said to be influenced by the difference in temperature on the two sides of the film, and then this effect is omitted without explanation from the equation which follows. Near the bottom of page 100 the reciprocal of the Prandtl number is incorrectly called the Stanton number.

[1] Associate Professor of Mechanical Engineering, Massachusetts Institute of Technology, Cambridge, Mass. Mem. ASME.

Servomechanism Analysis

SERVOMECHANISM ANALYSIS. By George J. Thaler and Robert G. Brown. McGraw-Hill Book Co., Inc., Electrical and Electronic Engineering Series, New York, N. Y.; Toronto, Ont., Can.; London, England, 1953. Cloth, 5½ × 9 in., figs., problems, tables, appendixes, bibliography, index, xii and 414 pp., $7.50.

REVIEWED BY JOHN A. HRONES[1]

THIS addition to the rapidly growing literature in the servomechanisms field is aimed at the senior—lower graduate level. It is written by electrical engineers who appear quite convinced that everything must be converted to electrical "lingo" to be comprehensible. The book deals largely with techniques and methods for dealing with the solution of linear differential equations with the major emphasis on the frequency-response approach. The selection of system gain and the use of compensation circuits is discussed at some length. Brief treatments of certain commonly used components are included. Considerable stress is placed upon the analogous dynamic behavior of a number of physical systems. Transient analysis is lightly discussed and used, although a limited discussion of root loci is included. There is a brief discussion of relay servomechanisms with a light touch of Kochenburger's method for using frequency-response techniques in handling contactor servos. The problems are largely electrical in character, and emphasize solution techniques rather than basic understanding of dynamical problems in general. What is presented appears to be technically sound but one cannot rate this as a significant work which makes a new and necessary contribution. It is a book which can be used in a number of servo courses as they are now presented, and may be a very useful text at the level for which it is intended. Coverage for the various chapters follows.

The first six chapters cover such phases of the, subject as Laplace transformations, equations of physical systems, transient analysis

[1] Professor of Mechanical Engineering, Massachusetts Institute of Technology, Cambridge, Mass. Mem. ASME.

of servomechanisms, transfer functions with graphical representations. Chapter 7 is devoted to an analysis of servomechanism performance from equations and transfer-function plots. The next four chapters are devoted to design, gain adjustment, series, and parallel compensations.

The last three chapters cover such subjects as logarithmic coordinates in analysis and design, relay servomechanisms, and the root-locus method.

Fatigue and Fracture of Metals

FATIGUE AND FRACTURE OF METALS. Edited by W. M. Murray, with a foreword by J. C. Hunsaker. The Technology Press of the Massachusetts Institute of Technology and John Wiley & Sons, Inc., New York, N. Y., 1952. Cloth, $5^1/_2 \times 9$ in., figs, references, tables, viii and 313 pp. $6.

REVIEWED BY T. J. DOLAN[1]

THE fourteen papers constituting this volume were presented at a special conference at Massachusetts Institute of Technology in June, 1950. They contain a review of the present-day knowledge of material behavior and expert opinions on laboratory experiments commonly used to appraise the resistance of metals to fracture. The collection of papers will prove valuable to engineers whose primary interest is in the selection of materials to resist progressive fracture or fracture induced by suddenly applied loads.

The papers review not only the general phenomenological and statistical aspects of fatigue of metals but also cover several phases of brittle fracture, the concepts of transition temperatures, and factors involved in temper brittleness. Specific applications to service failures and their importance are discussed in some detail for aircraft structures, naval vessels, and machinery.

The book will serve a useful purpose as an up-to-date record of the opinions of experts in the field on the present state of knowledge of the complex nature of fracture and of fatigue failure. Some of the concepts, experimental methods, and interpretations are influenced by the authors' personal opinions; it is unfortunate that the extensive discussions by the several hundred engineers participating in the symposium could not be included in the book. For a complete understanding of the present knowledge of the nature of fracture, it is regrettable that some of the more fundamental work from studies in the modern physics of solids was not covered by any of the papers. In some instances the titles of the papers are somewhat misleading but a general idea of the scope and fields covered may be obtained from the following list of titles and authors included in the book:

1 General Survey of the Problem of Fatigue and Fracture, by M. Gensamer.
2 The Fatigue Problem in Airplane Structures, by H. L. Dryden, R. V. Rhode, and P. Kuhn.
3 Brittle Fracture and Fatigue in Ships, by F. Jonassen.
4 Brittle Fracture and Fatigue in Machinery, by R. E. Peterson.
5 Internal Stresses and Fatigue, by O. J. Horger and H. R. Neifert.
6 Designing for Fatigue, by R. L. Templin.
7 Fundamentals of Brittle Behavior in Metals, by E. Orowan.
8 Experimental Study on Temper Brittleness of Slightly Alloyed Carbon Steel, by P. A. Jacquet and A. R. Weill.
9 The Statistical Aspect of Fatigue Failures and Its Consequences, by W. Weibull.
10 A Review of Cumulative Damage in Fatigue, by N. M. Newmark.
11 Significance of Transition Temperature in Fatigue, by C. W. MacGregor.
12 The Influence of Metallographic Structure on Fatigue, by P. L. Teed.
13 Fatigue at Elevated Temperatures, by N. J. Grant.
14 The Techniques of Physical Metallurgy for Studying Fatigue Damage, by J. T. Norton.

As may be expected, there still remain many unsolved problems in the fracture and fatigue fields, but the reader will be well repaid by the wealth of knowledge and the present-day understanding of the phenomena reviewed in this symposium.

[1] Head of the Department of Theoretical and Applied Mechanics, University of Illinois, Urbana, Ill.

AN ASME PAPER

Its Preparation, Submission and Publication, and Presentation

To a large degree the papers prepared and presented under the ASME sponsorship are evidence by which its professional standing and leadership are judged. It follows, therefore, that to qualify for ASME sponsorship, a paper must not only present suitable subject matter, but it must be well written and conform to recognized standards of good English and literary style.

The pamphlet on "AN ASME PAPER" is designed to aid authors in meeting these requirements and to acquaint them with rules of the Society relating to the preparation and submission of manuscripts and accompanying illustrations. It also includes suggestions for the presentation of papers before Society meetings.

CONTENTS

PREPARATION OF A PAPER—

General Information—Style, Preferred Spelling, Length Limitation, Approvals and Clearances.

Contents of the Paper—Title, Author's Name, Abstract, Body of Paper, Appendixes, Acknowledgments, Bibliographies, Tables, Captions, Photographs, Other Illustrations.

Writing the Paper—Outline Tabulations, Tables, Graphs, Charts for Computation, Drawings, Mathematics, Accuracy, Headings and Numbering, Lantern Slides, Motion Pictures, Typing, Number of Copies.

SUBMISSION AND PUBLICATION OF A PAPER—

Intention to Submit Paper Required in Advance, Meeting Dates, Due Dates for Manuscript, Discussers, Review and Acceptance, Proofs, Advance Copies and Reprints, Discussion and Closure, Publication by Others.

PRESENTATION OF A PAPER—

Time Limit, Addressing Your Audience, Public Address Systems, Use of Slides.

REFERENCES—

References on Writing and Speaking, Engineering Standards.

Price 40¢. No discount allowed. *A remittance must accompany all orders for $5.00 or less. U. S. Postage Stamps are acceptable.*

THE AMERICAN SOCIETY OF MECHANICAL ENGINEERS

29 West 39th Street, New York 18, N. Y.

6 NEW ASME BOOKS

For Mechanical Engineers

1952 ASME TRANSACTIONS

2000 PAGES—CLOTH BOUND
$15 ($7.50 TO ASME MEMBERS)

Nowhere else will you find in a single volume so much tested and adaptable information on major trends and developments throughout the mechanical engineering field. Containing 228 papers and discussions, this massive reference places at your fingertips the experience of 350 experts, each a specialist in his field, with problems associated with fuels, gas turbine power, heat transfer, hydraulics, fluid meters and measurement, industrial instruments, lubrication, machine design, metal cutting, petroleum mechanical engineering, plastics, properties of metals, steam power generation, and applied mechanics.

Additionally, there are carefully prepared bibliographies keyed to many of the articles giving sources for further information; numerous illustrations to help you visualize new developments; and hundreds of tables, graphs, and charts which supplement and clarify the text.

General Discussion ON HEAT TRANSFER

500 PAGES—CLOTH BOUND
$10 TO MEMBERS AND NONMEMBERS

Here is a truly valuable book for those engaged in heat transfer work. Within its pages over 150 eminent engineers of twelve countries review developments in the mechanism of heat transfer and in the design of apparatus relating thereto which have been made in the past ten years . . . consider the numerous engineering applications of heat transfer . . . appraise new fundamental discoveries in the field . . . and discuss modern methods of approach to heat transfer problems.

Coverage includes heat transfer with change of state; heat transfer between fluids and surfaces; conduction in solids and fluids; radiation, instrumentation, measurement techniques and analogies; and special problems such as heat transfer in turbine blade cooling, in liquid metals, in gas turbines, and in piston engines.

The 93 papers and discussions which make up this volume were presented at the IME-ASME Conference held in London, 1951.

PROCEEDINGS of The First U. S. National Congress of Applied Mechanics

1000 PAGES—CLOTH BOUND
$20 ($16 TO ASME MEMBERS)

One hundred and fifty nationally recognized authorities have pooled their knowledge and experience to make possible this record of advances in modern applied mechanics. The coverage embraces many of the significant problems encountered in the following branches of the field: dynamics, vibrations, impact, elasticity, photoelasticity, plate theory, plasticity, behavior of materials, fluid flow, aerodynamics, and heat.

There are 130 papers in the collection and in them research workers and engineers concerned with design and development will find an unequaled amount of reference material for constant consultation.

MANUAL ON THE CUTTING OF METALS

222 PAGES—CLOTH BOUND
$10 ($8 TO ASME MEMBERS)

Held at a practical level for the information of designers, tool engineers, and production executives, this new Second Edition gives the kind of help that cuts costs, steps up production, and standardizes practice. Fabrication methods, chip control, tool chatter and surface quality of work are treated in detail; composition, types, and functions of cutting fluids and the handling of cutting oils are thoroughly discussed; feeds and speeds for machining various metals are given; forces, power, and cutting speeds for specific cutting conditions when turning a variety of metals are recommended; and consideration is given to cost of cutting operations. In addition, there are 330 tables giving data on feeds, speeds, and depths of cut to be used when turning commonly used steels and cast irons.

AUTOBIOGRAPHIES OF Dexter S. Kimball and W. F. Durand

$4 each ($3.20 TO ASME MEMBERS)

REMEMBER, the Autobiography of Dexter S. Kimball, is the vital story of a dynamic era and the equally engrossing story of an intrepid leader in industry, engineering, and education. What Dean Kimball remembers ranges from the San Francisco of the eighties to the college campus of today, and from engineering education to engineering practice. Also reflected is his outstanding work with the War Production Board in Washington, presidency of the ASME, and his guiding role in the expansion of Cornell and its establishment as a great engineering school.

In ADVENTURES in the Navy, in Education, Science, Engineering, and in War, Dr. Durand has recorded what he considers to be the most interesting and important events of his life. They include his part, as a young cadet engineer, in the design of power plants for the first steel ships of the U. S. Navy, his researches at Cornell on the performance of ship propellers, the aeronautical engineering problems encountered at the NACA where he served as its first president and in other capacities for nearly thirty years, and his activities after retirement from Stanford University as consultant on the Hoover Dam and other similar projects, and as a participant in the encyclopedic summary of Aerodynamic Theory.

Published by

THE AMERICAN SOCIETY OF MECHANICAL ENGINEERS
29 West 39th Street New York 18, New York